The influence of high hydrostatic pressure on structure and reactivity of small organic catalysts and the synthesis of ^{15}N-labeled compounds

Dissertation

Zur Erlangung des Doktorgrades der Naturwissenschaften

Dr. rer. nat.

der Fakultät für Chemie und Pharmazie

der Universität Regensburg

vorgelegt von

Martin Hofmann

aus Tübingen

Regensburg 2018

Die Arbeit wurde angeleitet von:	Prof. Dr. Oliver Reiser	
Promotionsgesuch eingereicht am:		08.03.2018
Promotionskolloquium am:		27.04.2018
Prüfungsauschuss:	Vorsitz:	Prof. Dr. Jörg Heilmann
	1. Gutachter:	Prof. Dr. Oliver Reiser
	2. Gutachter:	Prof. Dr. Julia Rehbein
	3. Gutachter:	Prof. Dr. Frank-Michael Matysik

Der experimentelle Teil der vorliegenden Arbeit wurde im Zeitraum von Februar 2014 bis Juni 2017 unter der Anleitung von Prof. Dr. Oliver Reiser am Institut für Organische Chemie der Universität Regensburg angefertigt.

Besonders bedanken möchte ich mich bei Herrn Prof. Dr. Oliver Reiser für die Aufnahme in seinen Arbeitskreis, die Überlassung des interessanten Themas, die anregenden Diskussionen und die stete Unterstützung.

Für meine Familie

“Science, my lad, has been built upon many errors, but they are errors which it was good to fall into, for they led to the truth.”

Jules Verne (1828 – 1905)

Table of contents

A. Introduction 5

1. The high-pressure activation principle – the volume of activation 6
2. Methods to generate high pressures and applications in science and industry 9
3. High pressure in organic chemistry 11

B. Main part 16

1. Covalent Lewis base organocatalysts under pressure 16
   - 1.1 Introduction 16
   - 1.2 Development of the concept and catalyst preparation 19
   - 1.3 Influence of secondary activation modes on reactivity 24
   - 1.4 Influence of secondary activation modes on selectivity 30
2. Peptidic organocatalysts containing cyclic β-amino acids under pressure 39
   - 2.1 Introduction 39
   - 2.2 Synthetic approach to *cis*-β-ACHC 41
   - 2.3 Synthesis of the flexible tripeptides from racemic β-ACHC 43
   - 2.4 Synthesis of the flexible tripeptides from enantiomerically enriched β-ACHC 46
   - 2.5 Synthesis of the rigid peptide H-Pro-Ant-Pro-OH 53
   - 2.6 Identification of the side product obtained in the synthesis of H-Pro-Ant-Pro-OH 55
   - 2.7 Catalysis with tripeptides 59
   - 2.8 Conformational study of H-Pro-(-)-⬢-Pro-OH using HP-NMR 67
3. Synthesis and evaluation of β-ACHC model compounds 71
   - 3.1 Synthesis of the model compounds 72
   - 3.2 Conformational studies of the model compounds in solution using NMR and HP-IR 76
4. Synthesis of ^{15}N-labeled compounds 83
   - 4.1 Synthesis of ^{15}N-TMAO 84
   - 4.2 Synthesis of ^{15}N-methylacetamide 85

C. Summary 88

D. Zusammenfassung 91

E. Experimental Part 94

1. General Information 94
2. Small organocatalysts under pressure 98
   - 2.1. Synthesis of catalyst and starting materials 98
   - 2.2. Catalysis 101
3. Synthesis of tripeptides containing unnatural β-amino acids 107

3.1. Synthesis of racemic β-ACHC 107
3.2. Desymmetrization reactions 109
3.3. Synthesis of peptides containing β-ACHC 112
3.4. Synthesis of peptides containing anthranilic acid 123
4. Catalysis with tripeptides containing unnatural β-amino acids 131
5. Synthesis of β-ACHC model compounds 134
6. Synthesis of ^{15}N-labeled compounds 144
F. References 147
G. Appendix 157
1. Tables 157
2. NMR spectra 160
3. HPLC chromatograms 217
4. X-ray crystallography data 234
5. Curriculum Vitae 254
H. Acknowledgment – Danksagung 256
I. Declaration 258

Abbreviations

Ac	acetyl
ACBC	aminocyclobutylcarboxylic acid
ACC	aminocyclopropylcarboxylic acid
ACHC	aminocyclohexylcarboxylic acid
ACPC	aminocyclopentylcarboxylic acid
Ala	alanine
Ant	anthranilic acid
APAT	ambient pressure / ambient temperature
APCI	atmospheric pressure chemical ionization
aq	aqueous
Asp	asparagine
Bn	benzyl
Boc	*tert*-butyloxycarbonyl
Cbz	carboxybenzyl
CMDMCS	chloromethyldimethylsilyl chloride
COMU	(1-cyano-2-ethoxy-2-oxoethyliden-aminooxy)dimethylamino-morpholino-carbenium hexafluorophosphate
Cys	cysteine
conc.	concentrated
d	day(s)
DABCO	1,4-diazabicyclo[2.2.2]octane
DCM	dichloromethane
DCP	dicumyl peroxide
DIPEA	*N*,*N*-diisopropylethylamine
DMAP	4-dimethylaminopyridine
DMSO	dimethylsulfoxide
DPPA	diphenyl phosphoryl azide
dr	diastereomeric ratio
EDC	1-ethyl-3-(3-dimethylaminopropyl)-carbodiimide
ee	enantiomeric excess
EI	electron ionization
EIC	extracted-ion chromatogram
Eq.	equation
equiv.	equivalent(s)
ESI	electrospray ionization
FEP	fluorinated ethylene propylene
FT	Fourier transform
Glu	glutamic acid
h	hour(s)
HATU	1-[Bis(dimethylamino)methylene]-1*H*-1,2,3-triazolo[4,5-*b*]pyridinium 3-oxid hexafluorophosphate
His	histidine
HMBC	heteronuclear multiple-bond correlation
HMDS	hexamethyldisilazane
HMPA	hexamethylphosphoramide
HOBt	hydroxybenzotriazole
HP	high pressure
HPLC	high performance liquid chromatography
HRMS	high-resolution mass spectrometry
HSQC	heteronuclear single-quantum correlation
HT	high temperature
i-	*iso*-
IR	infrared
JH	Jørgensen-Hayashi
Leu	leucine
m.p.	melting point
Me	methyl
min	minute(s)
MS	mass spectrometry
n-	*normal*-
n/a	not applicable
n.d.	not determined
NMA	*N*-methylacetamide
NMM	*N*-Methylmorpholine
NMR	nuclear magnetic resonance
NOESY	nuclear Overhauser effect spectroscopy
Ph	phenyl
Phe	phenylalanine
PLE	pig liver esterase
ppm	parts per million
Pr	propyl
Pro	proline
PTFE	polytetrafluoroethylene
R	arbitrary residue
R_f	retardiation factor
ref.	reference
rt	room temperature
RT	Raumtemperatur
sat.	saturated
Ser	serine
T3P	*n*-propylphosphonic anhydride
TBAB	tetrabutylammonium bromide
tert	tertiary
Tf	triflyl

TFA	trifluoroacetic acid
THF	tetrahydrofuran
TLC	thin layer chromatography
TMAO	trimethylammonium *N*-oxide
tmm	trimethylene methane
TMS	trimethylsilyl
TPS	triisopropylbenzenesulfonyl
triphos	1,1,1-tris(diphenylphosphinomethyl)-ethane
v/v	volume fraction
wt%	weight percent

A. Introduction

In 2011, Paul Snelgrove, oceanographer and one of the leading members of the international "Census of Marine Life" research program, stated that man's knowledge about the deep sea floor is smaller than the knowledge of the surfaces of the Moon and Mars.[1]*

This is rather astonishing, as the oceans cover more than 70% of the entire planet's surface and encompass more than 90% of the biosphere's volume that supports life. While the photic zone between 0 – 200 m depth (the "light" zone) has been investigated to a larger extent, the aphotic zone of the oceans at depths greater than 200 m (the "dark" zone) remains almost unexplored.[2]

Organisms living in those depths are subjected to rather extreme conditions: not only are they in total darkness with water temperatures not far from the freezing point, they also have to be able to withstand the tremendous forces of the increasing hydrostatic pressure at lower sea levels. As the pressure increases by 1 bar for roughly every 10 m in depth, this means that creatures living 1000 m below the surface of the ocean are already experiencing pressures a hundred times stronger than on land.[3] In the deepest reaches of the sea, pressures exceeding 1000 bar can be reached.[4]

The harsh living conditions and high pressures often lead to bizarre appearances of the animals living in great depths, *e.g.* the Fangtooth fish with its disproportionally large teeth, the bioluminescent Vampire squid or the enormous Giant Spider crab. However, not only do high pressures lead to altered body structures but they also greatly influence the structure and efficacy of biomolecules and their associated biological and chemical processes. For instance, the activity of an enzyme can be significantly de- or increased under elevated pressures.[3–5]

While effects like these can prove dramatic for an organism, requiring it to adapt in order to survive, they are highly interesting from a chemist's point of view. It means that high pressure can act as a tool which can affect chemical and structural equilibria. Therefore, studying how high-pressure conditions influence the outcome of chemical reactions, as well as understanding its effect on the three-dimensional structure of molecules, might aid scientists in the development of more active catalytic systems or even the discovery of new transformations which are not feasible under other conditions.

* "We know more about the surface of the Moon and about Mars than we do about [the deep sea floor], despite the fact that we have yet to extract a gram of food, a breath of oxygen or a drop of water from those bodies."[1]

1. The high-pressure activation principle – the volume of activation

Already in the 19th century, Henry Le Chatelier discovered that a chemical equilibrium can be influenced by changing the reaction conditions.[6] Applying pressure to a chemical system leads to a reduction in volume, bringing it into a compressed state. This results in an increased concentration of the molecules, affecting intermolecular diffusion as well as the rate of molecular collisions (Figure 1).[7] It, therefore, becomes apparent that pressure must also have an impact on the equilibrium of chemical transformations.

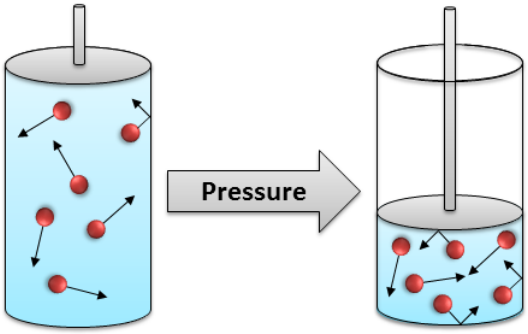

Figure 1: Graphical representation of the effect of compression on a chemical system.

The key thermodynamic parameter that determines how and to which extent a chemical reaction can be influenced by pressure is the volume of activation $\Delta V^{\ddagger}$. Knowing the value of $\Delta V^{\ddagger}$ for a transformation allows the prediction of the pathway and the outcome of the reaction. To evaluate how $\Delta V^{\ddagger}$ relates to pressure, a brief explanation of the underlying thermodynamic correlations is given in this chapter.[7–27]

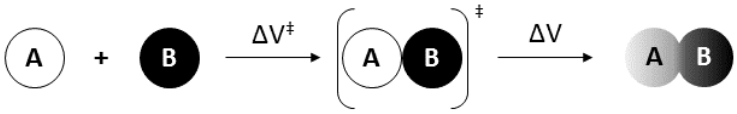

Scheme 1: A standard bimolecular addition reaction proceeding through a transition state. Reproduced from ref. [28] with permission.

Considering a bimolecular addition reaction where A and B react with each other to AB through the formation of a transition state[29] $[AB]^{\ddagger}$ (Scheme 1), the volume of activation is defined as:

$$\Delta V^{\ddagger} = V^{\ddagger}_{[AB]} - (V_A + V_B) \qquad \text{(Eq. 1)}$$

with $V^{\ddagger}_{[AB]}$, V_A and V_B being the partial molar volumes of the transition state $[AB]^{\ddagger}$ and the starting materials A and B. This chemical reaction is inherently accompanied by a change of the Gibbs free energy ΔG, which is expressed in the Gibbs fundamental thermodynamic relation as:

$$\Delta G = \Delta U - T\Delta S + p\Delta V \quad \text{(Eq. 2)}$$

with ΔU being the change of the inner energy and ΔS the change of the entropy. From eq. 2 it can be seen that ΔG has a pressure dependent term $p\Delta V$ which gains in influence with higher pressures and, therefore, larger degrees of compression. At the same time, changes to the chemical equilibrium of the reaction can be described by the van't Hoff equation:

$$\Delta G = -RT \cdot \ln K \quad \text{(Eq. 3)}$$

with K representing the equilibrium constant.

From Eq. 2 and 3, the following connection can be derived for the change of volume ΔV:

$$\Delta V = \left(\frac{\partial \Delta G}{\partial p}\right)_T = -RT \cdot \left(\frac{\partial \ln K_p}{\partial p}\right)_T \quad \text{(Eq. 4)}$$

with K_p beeing the pressure-dependent equilibrium constant of the reaction. Based on transition state theory, Evans and Polyani deduced a similar correlation for the pressure-dependent rate constant k_p and the volume of activation $\Delta V^{\ddagger}$:

$$\Delta V^{\ddagger} = \left(\frac{\partial \Delta G^{\ddagger}}{\partial p}\right)_T = -RT \cdot \left(\frac{\partial \ln k_p}{\partial p}\right)_T \quad \text{(Eq. 5)}$$

where $\Delta G^{\ddagger}$ represents the Gibbs energy of activation.[30]

From Eq. 5 it becomes apparent that a negative volume of activation will lead to an increase in the rate constant. This infers that a chemical reaction is *accelerated* by pressure when $\Delta V^{\ddagger} < 0$ (*i.e.* the transition state is smaller in size than the reactants combined), which is the case for all addition reactions. At the same time, pressure *inhibits* reactions when $\Delta V^{\ddagger} > 0$, *e.g.* dissociations. However, this is only fully valid for homolytic dissociation reactions, as heterolytic reactions are often accompanied with a negative $\Delta V^{\ddagger}$.

The explanation for this conundrum is that the volume of activation is composed of different contributing factors:

$$\Delta V^{\ddagger} = \Delta V^{\ddagger}_{struct} + \Delta V^{\ddagger}_{solv} + \Delta V^{\ddagger}_{steric} \quad \text{(Eq. 6)}$$

While $\Delta V^{\ddagger}_{struct}$ represents the intrinsic volume changes of the reactants during the formation of the transition state, $\Delta V^{\ddagger}_{solv}$ describes the changes in volume as a result of electrostatic solvent-solute interactions.[7–9,11–16,18–28] This relates to the observed contraction of volume of charged species in a dielectric medium (the solvent) which is called *electrostriction* and can be described by the Drude-Nernst equation:

$$\Delta V_e = -\frac{q^2}{2r\varepsilon_r^2} \cdot \left(\frac{\partial \varepsilon_r}{\partial p}\right) \qquad \text{(Eq. 7)}$$

with q being the charge, r the ionic radius and ε_r the relative static permittivity of the solvent.[31]

Electrostriction results from the reordering of charged species (ions, zwitterions or polarized species) and the surrounding solvent molecules which leads to a sharp decrease in volume. This contribution to the volume of activation can be very high (up to -100 cm^3) especially in apolar (uncharged) media,[28] and explains why heterolytic dissociation reactions can be accelerated by pressure (Scheme 2).

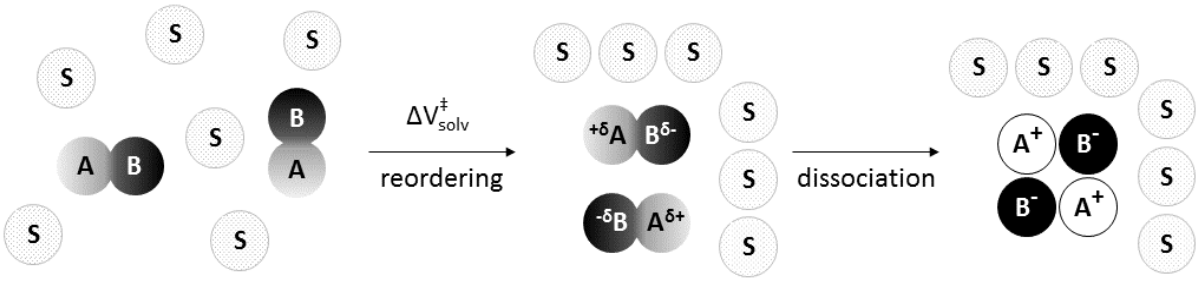

Scheme 2: Graphical representation of electrostriction: Reordering of the dipolar compound AB and the solvent molecules S results in a sharp volume contraction which can lead to complete dissociation of AB under pressure. Adapted from ref. [28] with permission.

Besides $\Delta V^{\ddagger}_{struct}$ and $\Delta V^{\ddagger}_{solv}$, Jenner *et al.* defined a third contributing factor $\Delta V^{\ddagger}_{steric}$, which relates to the steric congestion of the transition state. As pressure forces molecules into close spatial proximity it has a beneficial effect on reactions with sterically hindered substrates, overcoming steric repulsion.[16,18,19,32]

In general, the following conclusions can be drawn for the volume of activation and how it affects the pressure response of a chemical reaction:

(1) If $\Delta V^{\ddagger} < 0$: the reaction is *accelerated* by pressure.

(2) If $\Delta V^{\ddagger} > 0$: the reaction is *hindered* by pressure.

(3) The formation of charged species is positively affected by pressure due to *electrostriction*.[7]

2. Methods to generate high pressures and applications in science and industry

Several methods have been developed to generate and sustain high hydrostatic pressures for scientific and industrial applications (Figure 2). In the following, a small overview of the different devices will be given as well as examples for the use of pressure in scientific and industrial applications.

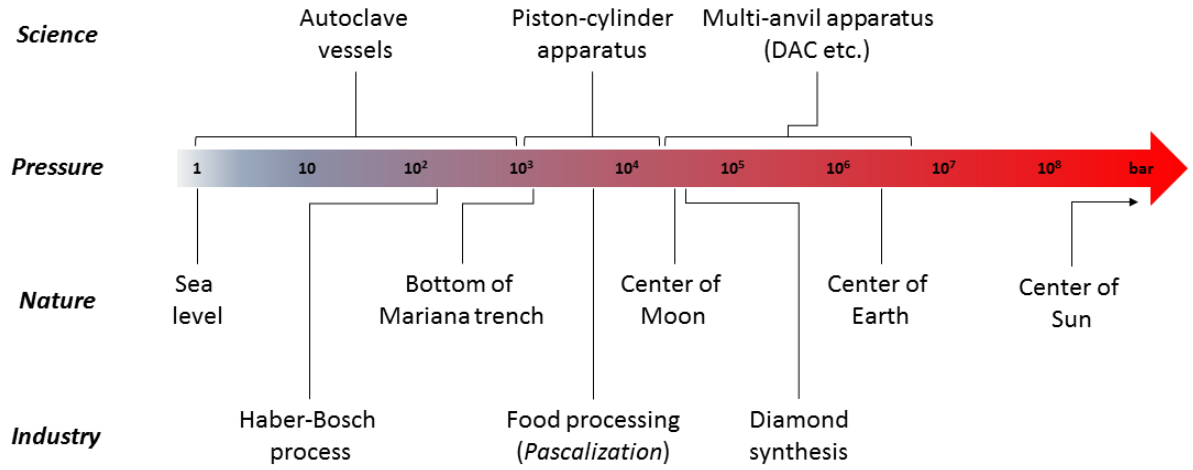

Figure 2: Pressure ranges achievable by man and selected examples from nature and industrial applications for comparison.[25,27,33] DAC = diamond anvil cell.

Lower pressures up to 1 kbar are omnipresent in everyday life: from the air pressure in tires of cars and bicycles to the water pressure generated by water jet cleaners, these pressures can be generated fairly easy by using high-pressure pumps. Industrial applications in this pressure range are quite common and often involves gases.[34] One of the most important chemical processes of all times, the Haber-Bosch process, is carried out under pressures up to 300 bar.[35,36] It is used to fix nitrogen from the atmosphere into ammonia, which is then utilized for the synthesis of fertilizers on a scale of several million tons per year.[36] Furthermore, pressure techniques are employed *e.g.* in the vulcanization of rubbers or in the dyestuff synthesis.[24] For scientific applications, experiments involving pressurized gases are usually carried out in gas-tight autoclave vessels, which are very scalable in terms of size. In medicine, autoclaves are used for the sterilization of medical equipment while in chemistry, these types of vessels are commonly used for *e.g.* hydrogenation reactions or polymerizations.[37]

However, a multitude of chemical reactions, especially in organic chemistry, take place in solution. As these reactions often require pressures exceeding 1 kbar to be significantly influenced, the use of simple autoclave vessels becomes rather limited. This resulted in the invention of the hydraulic piston-cylinder apparatus (Figure 3).

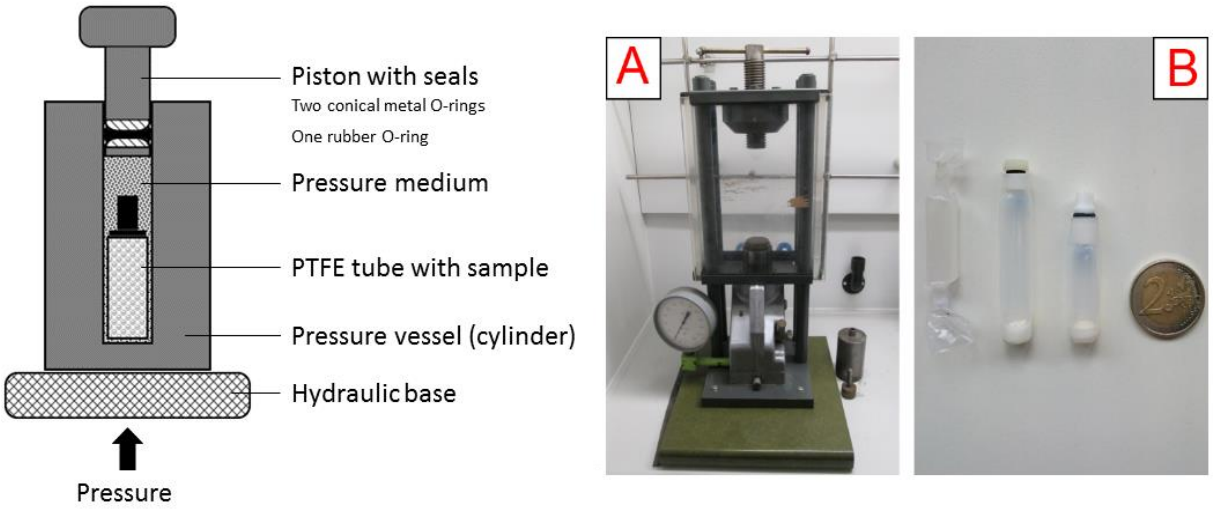

Figure 3: Depiction of the high-pressure apparatus used for high-pressure reactions in the course of making this thesis, capable of generating pressures up to 5 kbar. Left*:* schematic representation of the operation mode of the apparatus. The piston is held into position from the top by a manual screw and the medium-filled vessel is then pressed against the piston from below. Right*:* A) Picture of the high-pressure apparatus. B) Picture of the reaction vessels used: molten PTFE tubes and reusable PTFE/FEP vials of different sizes (2 € coin for size comparison).

Devices of this type typically consist of a hydraulic pump, a pressure vessel (often cylindrical) and a moving piston. The sample is encapsulated air-free into a container (usually made from inert PTFE) and put into the pressure vessel, which is then filled with a pressure medium (*e.g.* oils, hydrocarbons or water/glycol mixtures). The piston is then inserted into the vessel and the medium (which ensures that the built-up pressure is uniformly transferred to the sample) is compressed with force through a manual or automatic pump. While pressures between 5 – 10 kbar can be reached with this setup, using it in combination with a hydraulic pressure intensifier can extend the operational limit up to 40 kbar.[25,34,38] In applications on a laboratory scale, sample volumes are usually in the range of several milliliters, however, devices capable of compressing more than 1000 L have been developed.[34,39] Scientific application of high hydrostatic pressures between 1 – 20 kbar has been growing over the last decades. Besides its usefulness to enable and accelerate a multitude of chemical transformations, utilization of high pressure in combination with spectroscopic methodologies (*e.g.* IR, UV-VIS, NMR) has seen an increasing interest due to the improved availability of suitable equipment.[9,10,23,40,41] These techniques, for instance, allow the study of the conformational behavior of biomolecules found in deep sea fish or the kinetics of aggregation and unfolding of proteins.[42] Industrial applications also exist in this pressure range: in the food industry high-pressure processing (“Pascalization”) is utilized to preserve and sterilize foodstuffs. The process uses pressures up to 6 kbar and has established itself as a viable alternative to thermal pasteurization.[33,43]

Pressures exceeding 50 kbar require the use of multi-anvil devices. Their typical mode of action is that a small sample (< 1 mL) is placed in between two opposing anvils and sealed by a gasket. Through pressing the anvils against each other, extremely high pressures can be generated. Early pioneering

work was carried out by Percy W. Bridgman in the early 20th century, reaching pressures up to 100 kbar by using tungsten carbide anvils.[26,38,44] For his contribution to the field of high-pressure science, he was awarded the Nobel Prize in Physics in 1946. The Bridgman anvil apparatus was improved with the invention of the diamond anvil cell (DAC) in 1958.[44,45] Using two diamonds as anvils allows the generation of pressures up to 7.5 Mbar, which is more than twice the pressure found at the earth's core[46] and enough to compress even the densest metal, osmium.[47] The use of diamond also enables the combined use with optical spectroscopy and X-ray analysis, enabling measurements at extreme pressures.[44] Important findings in this pressure range have been, for instance, new modifications of ice,[48] polymeric nitrogen,[49] high-temperature superconductivity of sulfur hydride at 203 K[50] and the (still debated) metallic hydrogen.[51] Industrial applications using pressures greater than 50 kbar are scarce, as the sample sizes in the devices used to generate such pressures are limited. One notable example, however, is the artificial synthesis of diamond, which has seen increased interest over the last decades.[52]

3. High pressure in organic chemistry

Due to the unique activation principle, high-pressure techniques (> 1 kbar) have also found applications in organic chemistry. Studies on the effect of high hydrostatic pressures on organic reactions can be dated back as far as the early 20th century.[53,54] These early investigations often involved polymerization and cycloaddition reactions, for instance, Bridgman *et al.* who showed that the polymerization of isoprene is greatly accelerated under pressure.[53] As interest in high-pressure research increased, so did the understanding of its effects on thermodynamic parameters improve. Especially the significance of the volume of activation $\Delta V^{\ddagger}$ as an indicator for how compression will affect a reaction was recognized. This sparked the investigation of a multitude of different organic transformations under high pressure conditions between the 1970s and 1990s, which allowed the determination of average $\Delta V^{\ddagger}$ values (Table 1).*

* Several compendia have been published listing volumes of activation for a plethora of organic and inorganic transformations.[8,12,24,27]

Table 1: Average values $\Delta V^{\ddagger}$ for selected transformations.

Reaction type	Average volume of activation $\Delta V^{\ddagger}$ [$cm^3 \cdot mol^{-1}$]	Reference(s)
Radical decompositions	0 to +15	[7]
Radical polymerizations	-10 to -25	[7]
Rearrangement reactions (Cope, Claisen)	-8 to -15	[7]
Diels-Alder reactions	-25 to -50	[7,28]
Michael-type reactions	-20 to -50	[12,55,56]
(Nitro-)Aldol reactions	-20 to -25	[55,56]
Baylis-Hillman reactions	-60 to -80	[57]
Wittig reactions	-20 to -30	[58]
Heck reactions	-10 to -30	[28,59]

In the following, a few examples are given for how pressure can affect the activity as well as selectivity of different organic reactions.

The Diels-Alder reaction is one of the prime examples for the use of high pressures as activation mode to accelerate chemical reactions. The Diels-Alder reaction between dienamines and electron-deficient alkenes is rather sluggish under conventional heating conditions and results in a mixture of several different products.[60] In 1974, Dauben *et al.* demonstrated that high-pressure conditions did not only gave severely improved yields but also led to the exclusive formation of Diels-Alder adducts of the type **3A** (Scheme 3).[61]

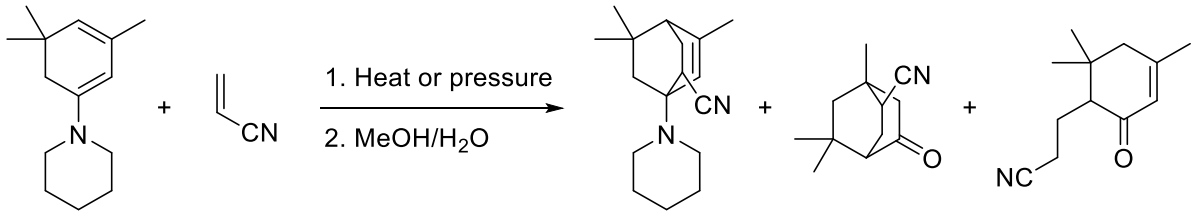

	3A	3B	3C
Heat:	3%	10%	20%
Pressure:	90%	0%	0%

Scheme 3: Example from Dauben *et al.* for the pressure-mediated Diels-Alder reaction of dienamine **1** with acrylonitrile (**2**). Pressure greatly increases reactivity and improves regioselectivity. Reaction conditions: Heat = dioxane, reflux, 1 bar, 7 h; pressure = diethyl ether, 8.4 kbar, rt, 13 h.[60,61]

An example of a practical application of a high-pressure Diels-Alder reaction was published six years later by the same group. The biologically active compound cantharidin (**7**) was conveniently synthesized through a cycloaddition of furan (**4**) with the bicyclic maleic anhydride derivative **5**, followed by a desulfurization-hydrogenation step of cycloadduct **6b** with Raney-Ni (Scheme 4). While the cycloaddition was not feasible under high-temperature conditions, the use of high pressures

resulted in quantitative formation of the cycloadducts, predominantly generating the desired isomer **6b**.[62] A scale-up of this process even enabled the synthesis of cantharidin (**7**) on a multi-gram scale.[63]*

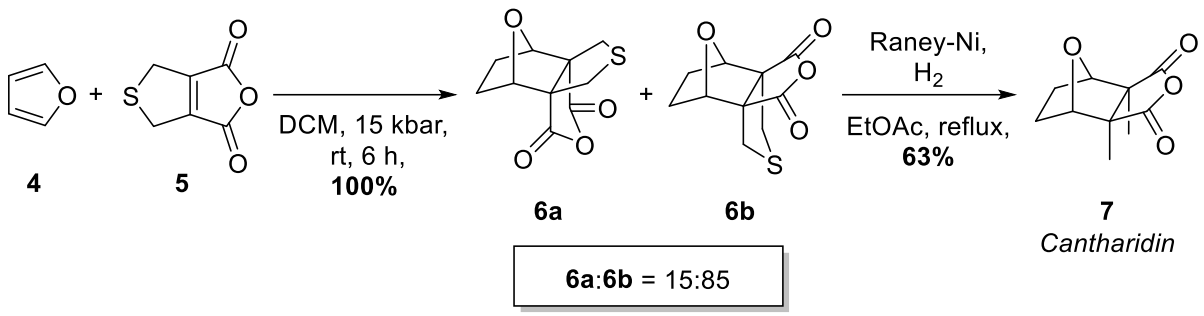

Scheme 4: Total synthesis of cantharidin published by Dauben *et al.* in 1980 using the pressure-induced Diels-Alder reaction between furan (**4**) and maleic anhydride derivative **5** as the key step.[62,63]

However, the scope of transformations that can be influenced by pressure is not limited to cycloadditions. In 1997, Bellassoued *et al.* studied the effects of pressure on the Mukaiyama aldol reaction of benzaldehyde (**8**) with an unsaturated silyl ketene acetal **9** (Scheme 5). Not only did they observe an improved yield, but also a reversal of the regioselectivity of the reaction. While lower pressures (2 kbar) resulted in the predominant formation of the linear γ-adduct **10a**, the preference is shifted towards the branched α-adduct **10b** at 17 kbar, probably due to the fact that the transition state leading to **10b** is more compact than that of **10a** and is thus favored at higher pressures.[66]

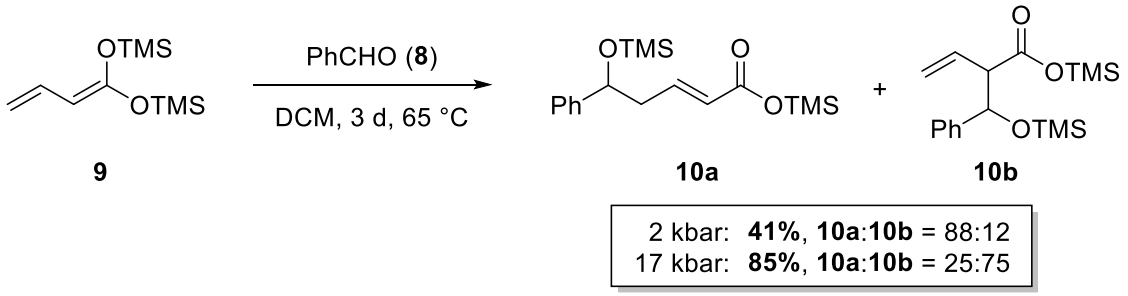

Scheme 5: The Mukaiyama aldol reaction of **8** and **9** under high-pressure conditions published by Bellassoued *et al.* in 1997. The more compact, branched product **10b** is formed preferentially at very high pressures.[66]

The related Henry (nitroaldol) reaction was subject of the investigations of Matsumoto *et al.* in 2002 (Scheme 6). They could demonstrate that chiral α-amino aldehydes react smoothly with nitroalkenes at elevated pressures (8 kbar) without the need of an additional catalyst. No significant racemization of the stereocenters was observed, substantiating that high pressure can act as a "mild" activation mode.[67]

* There are more examples for the use of high pressure-promoted Diels-Alder reactions in the total synthesis of biologically active compounds, *e.g.* kainic acid[64] and (tetrahydro)cannabinol derivatives.[65]

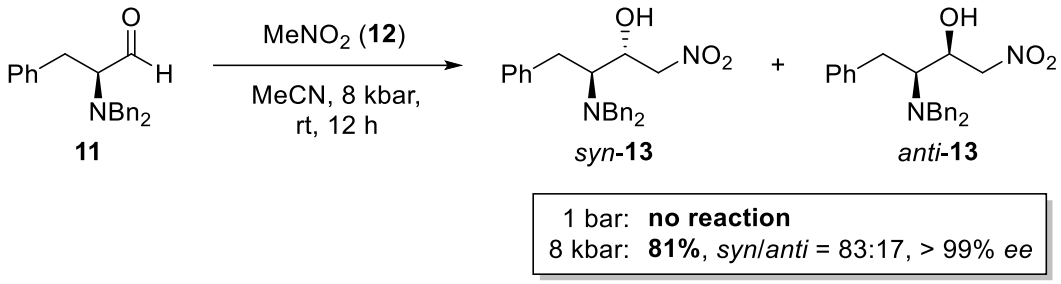

Scheme 6: Example for the high pressure-mediated Henry reaction of an α-amino aldehyde (**11**) with nitromethane (**12**) without catalyst as reported by Matsumoto *et al.* in 2002.[67]

In 2010, Kotsuki *et al.* showed that high-pressure techniques offers the capability to overcome steric strain in uncatalyzed aza-Michael reactions of secondary amines to α,β-unsaturated esters. While the reaction did not perform under reflux conditions at ambient pressures, the use of 14 kbar pressure rendered it possible, allowing the synthesis of highly congested adducts containing an aminated quaternary carbon center (Scheme 7).[68]

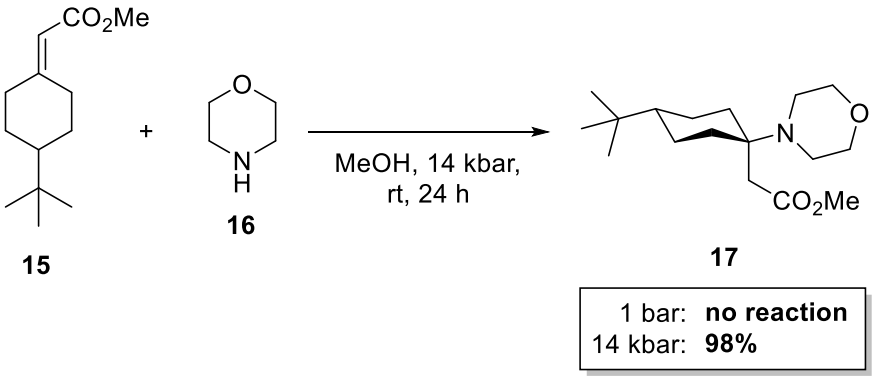

Scheme 7: An example from Kotsuki *et al.* for the high-pressure aza-Michael addition of an amine (**16**) to an α,β-unsaturated ester (**15**). The formed adduct **17** contains a sterically congested quaternary carbon center.[68]

Contributions to the field of high-pressure organic chemistry have also been made by the Reiser group. In 2001, they published a protocol for a high-pressure Domino-Horner-Wadsworth-Emmons-Michael reaction, illustrating that pressure can also be a useful tool for multicomponent reactions (Scheme 8).[69]

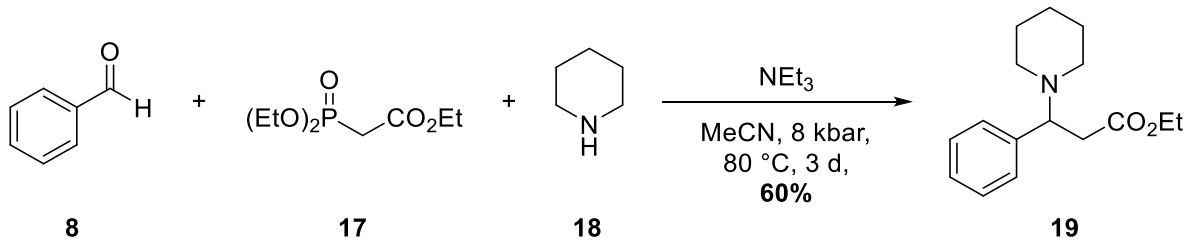

Scheme 8: High-pressure Domino-Horner-Wadsworth-Emmons-Michael reaction of benzaldehyde (**8**), phosphonate **17** and piperidine (**18**) published by Reiser *et al.* in 2001.[69]

Furthermore, they demonstrated that also catalyzed organometallic reactions can be positively influenced by pressure (Scheme 9). The Pd-catalyzed arylation of 2,3-dihydrofuran (**20**) gave vastly improved results under pressure, enabling the use of significantly lowered catalyst loadings (≤ 0.01 mol%).[70] This is a good example that the use of high-pressure conditions can also be beneficial in economical as well as ecological terms, as it allows reducing the amount of costly and potentially harmful chemicals.

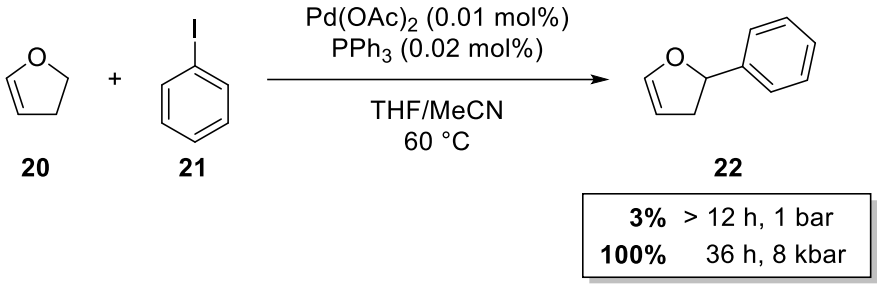

Scheme 9: Reiser *et al.* demonstrated that the Pd-catalyzed Heck reaction of 2,3-dihydrofuran (**20**) with iodobenzene (**21**) is significantly accelerated upon pressurization. The yield of the reaction at 1 bar did not improve with longer reaction times.[70]

While these examples are only a small excerpt of the research done over the last century, they definitely show the advantages high pressure can offer for organic transformations. The studies presented in this thesis were carried out as a part of the FOR 1979 research group "Exploring the Dynamical Landscape of Biomolecular Systems by Pressure Perturbation". Focus was laid on the investigation of small, biologically-relevant compounds as well as biomimetic catalysts and how they are affected by high hydrostatic pressure in terms of reactivity and structure. The results are presented in the following chapters.

B. Main part

1. Covalent Lewis base organocatalysts under pressure

1.1 Introduction

Ever since its "rediscovery" at the turn of the century by the groups of List[71] and MacMillan,[72] organocatalysis has been developing into a non-negligible tool for organic chemistry besides metal- and biocatalysis.[73,74] It provides access to a multitude of chemo-, regio- and stereoselective transformations as well as to completely new activation modes.[73,75,76] In addition, the catalyst systems can often be derived from abundant, non-toxic compounds like amino acids, sugars or alcohols, rendering them inexpensive and safe to use (Scheme 10).[71,74,77] Organocatalytic reactions have therefore gained popularity in the chemical community and have been employed in a variety of applications, *e.g.* in the synthesis of natural products or biologically relevant molecules for medicine.[78]

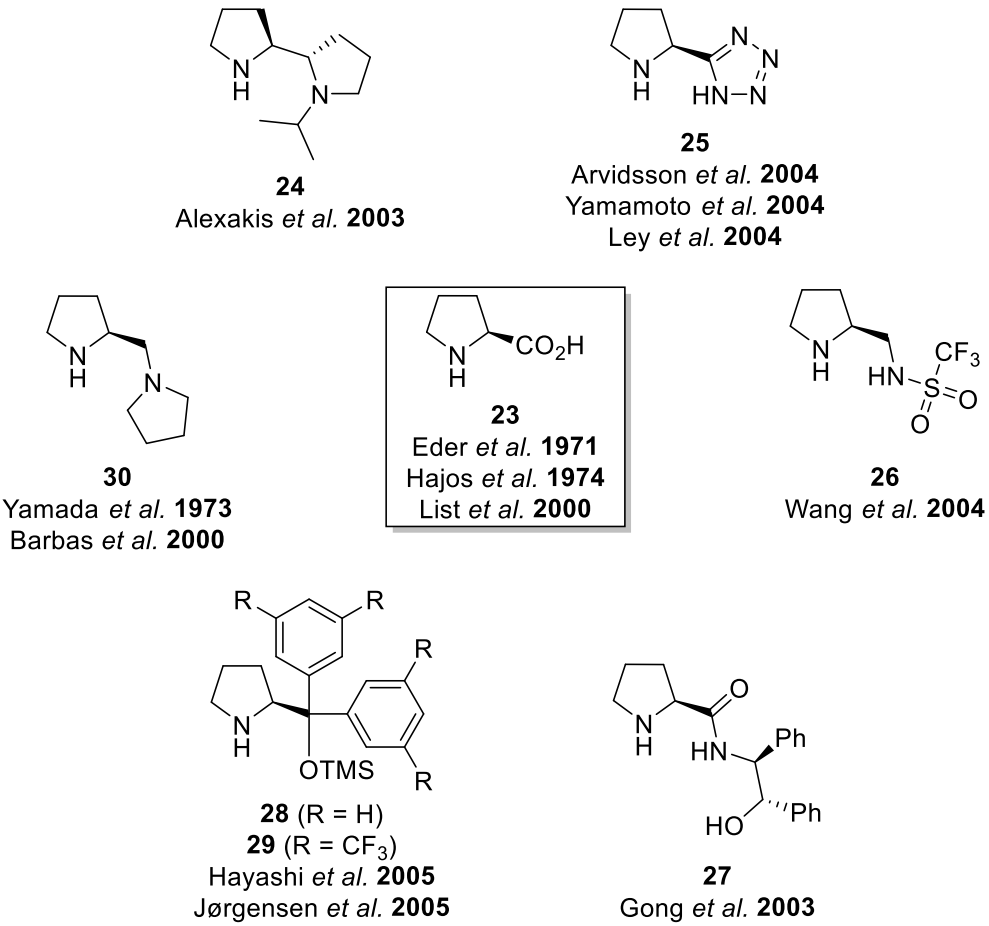

Scheme 10: Overview of different covalent Lewis base organocatalysts and the corresponding research groups, who identified their efficacy in organocatalysis. All compounds contain a chiral pyrrolidine-motif and the majority can be derived directly from the naturally occurring amino acid L-proline (**23**). References: **23**,[71,79] **24**,[80,81] **25**,[82] **26**,[83] **27**,[84] **28** and **29**,[85–87] **30**.[88,89]

Despite these benefits, an often stated common disadvantage of organocatalysts is their rather low reaction rates (especially for covalent Lewis base catalysis),[76] which leads to the requirement of using higher catalyst loadings or prolonged reaction times.[77] A way to counteract these issues is the use of organocatalysts in combination with secondary activation modes. Several methods have been investigated over the years, including microwave irradiation, ultrasonication, ball milling or the use of high hydrostatic pressure.[90]

Curiously, little research has been done on high-pressure activation in combination with organocatalyzed asymmetric reactions, although applications in the field are known since the 1980s. These initial studies were carried out by Matsumoto *et al.*, who investigated the cinchona alkaloid-catalyzed asymmetric addition of nitromethane (**12**) to chalcone (**31**). Using quinidine (**32**), the reaction did not proceed at all in apolar solvents under ambient conditions, however, it proceeded smoothly under high-pressure conditions. Interestingly, the enantioselectivity of the reaction displayed a pressure optimum at 9 kbar (60% *ee*), with lower or higher pressures resulting in diminished selectivities (Scheme 11).[91,92]

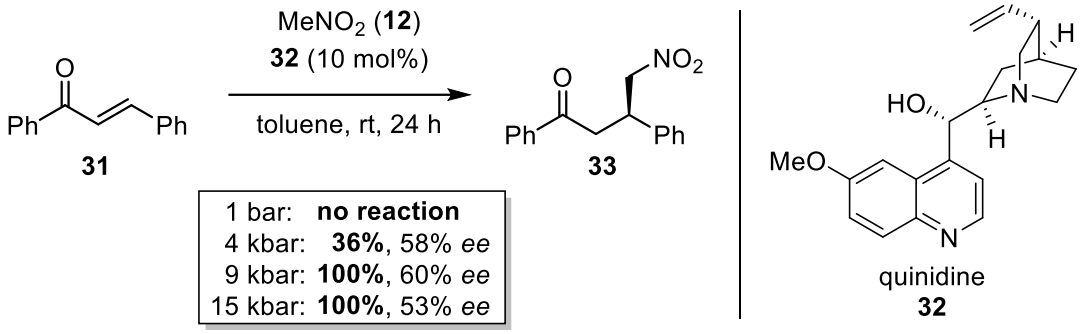

Scheme 11: Matsumoto *et al.* reported the first use of high-pressure conditions in an organocatalyzed reaction. At 9 kbar, the quinine-catalyzed Michael addition of nitromethane (**12**) to chalcone (**33**) performed smoothly giving quantitative yields and fair enantioselectivities.[91,92]

In 1995, Oishi *et al.* demonstrated that chiral DABCO derivatives are efficient catalysts for the condensation of methyl vinyl ketone and 4-nitrobenzaldehyde when submitted to high pressures (5 kbar). Not only did they observe increased reactivity, the enantioselectivity could be increased as well (from 12 to 47% *ee*).[93] Unfortunately, despite these remarkable discoveries, further investigations into the subject were rather scarce.

This changed slightly with the resurgence of organocatalysis in 2000, which sparked an increase in the investigation of organocatalyzed reactions under pressure. Focusing on L-proline (**23**) catalysis, Hayashi *et al.* and Kotsuki *et al.* investigated the effect of high-pressure conditions on the aldol addition between ketones and aldehydes independently. Kotsuki *et al.* performed the reaction without solvent in a piston-cylinder apparatus[94] and Hayashi *et al.* used DMSO and applied pressure by water induced

freezing in a closed autoclave, generating up to 2 kbar of pressure.[95] Both groups observed a significant increase in reactivity, less formation of the aldol condensation side product and slightly improved selectivities when using high-pressure activation (Scheme 12). Further studies of Hayashi *et al.* underlined that high pressure is a viable mode of activation in covalent organocatalysis, expanding the application scope to Baylis-Hillman[96] and direct Mannich reactions.[97] Kotsuki *et al.* also continued to prove the efficacy of high pressure in organocatalyzed Hetero-Diels-Alder[98] and aza-Michael reactions[99] as well as in the desymmetrization of cyclohexadienones.[100]

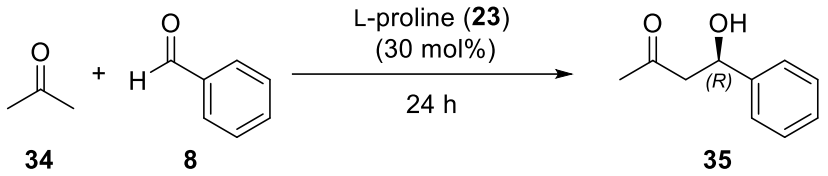

Hayashi *et al.* [ref. 95]:	DMSO, -20 °C	**40%**, 78% *ee* (1 bar) **100%**, 75% *ee* (2 kbar)
Kotsuki *et al.* [ref. 94]:	neat, rt	**90%**, 72% *ee* (2 kbar) **88%**, 63% *ee* (8 kbar)

Scheme 12: High-pressure organocatalytic aldol addition of acetone (**34**) to benzaldehyde (**8**), catalyzed by L-proline (**23**). Both, Hayashi *et al.*[95] and Kotsuki *et al.*[94] obtained improved results in comparison to the same reaction under ambient conditions as reported by List *et al.* in 2000.[71] Note, that this reaction also appears to show a pressure optimum in terms of enantioselectivity.

The initial attempt of Matsumoto *et al.* was eventually picked up in 2011 when Kwiatkowski *et al.* investigated the asymmetric addition of nitroalkenes to sterically congested cycloalkenones catalyzed by cinchona alkaloid derivatives (Scheme 13).

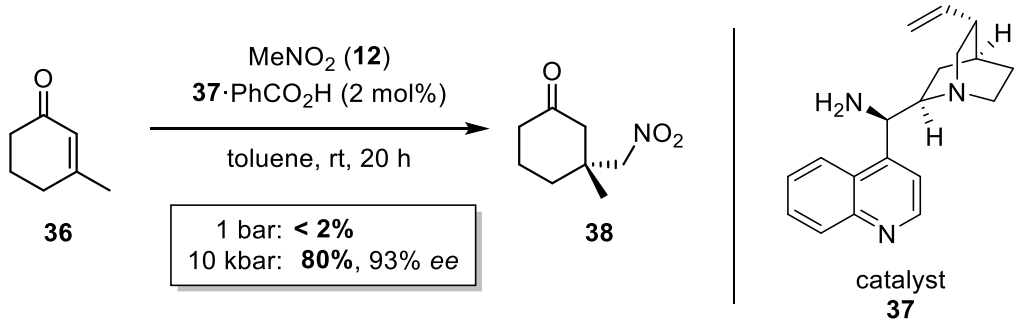

Scheme 13: Example from Kwiatkowski *et al.* in 2011, showing the high-pressure organocatalytic Michael addition of nitromethane (**12**) to 3-methylcyclohex-2-en-1-one (**36**).[101]

While the reaction did not occur at ambient conditions, it proceeded smoothly under elevated pressures up to 10 kbar, successfully generating γ-nitroketones with quaternary stereocenters in good yields (73 - 90%) and excellent selectivities (96 – 99% *ee*).[101] They also improved the original protocol of Matsumoto *et al.* and expand its scope by using a cinchona alkaloid-based thiourea catalyst.[102]

Additionally, they were also able to perform sterically demanding Friedel-Crafts alkylations[103] and hydroxyalkylations of indoles[104] using high-pressure conditions.

1.2 Development of the concept and catalyst preparation

Despite the fact that these examples provided evidence for the high versatility of high-pressure activation, its application in organocatalysis in general (and covalent Lewis base catalysis in particular) has been rather scarce.* Usually, the most commonly used method of activating a not proceeding chemical reaction is through heating the reaction mixture, introducing thermal energy into the system.[105] Although this often leads to improved reactivity, heating might also have detrimental effects, especially with respect to diastereo- and enantioselectivites of the products.† Higher temperatures lead to increased molecular motion, thus complicating the formation of defined transition states which are essential for high selectivities. Here, the use of high pressure can have a decisive advantage: it adds energy into the system while limiting molecular movement through volume constriction at the same time.[19,20,24,26,28] Furthermore, once the pressure is build up and stable it does not require the constant addition of energy unlike heating rendering it more economical.[28] Interestingly, there are almost no comparative studies on how different activation methods influence the outcome of an organocatalyzed reaction.‡ Therefore, a study was conceived to compare the influence of high temperature (HT) and high pressure (HP) on an organocatalyzed reaction. As aforementioned, especially covalent Lewis base organocatalysis is reported to suffer from rather low reactivity, thus making catalysts of this type prime subjects for investigation in combination with a secondary activation mode.[76,77] In search of a suitable test reaction, the conjugate Michael addition between aldehydes (**39a-g**) and *trans*-β-nitrostyrene (**40**) was chosen (Scheme 14).

* This might be attributed to the perceived complexity of performing high pressure reactions and/or lack of equipment, however, with the previously mentioned method developed by Hayashi *et al.*, at least the generation of pressures up to 2 kbar requires nothing more than an autoclave vessel.[95–97]

† Elevated temperatures can also result in thermal decomposition of the reactants.

‡ In 2006, Bolm *et al.* analyzed the thermal effects on the outcome of the organocatalyzed Mannich reaction by comparing results obtained from conventional heating against those using microwave irradiation.[106] In the same year, they published a study on the organocatalyzed aldol reaction, comparing the use of ball milling and conventional mechanical stirring.[107] However, the activation modes employed in these studies have the same underlying principle (temperature and mechanical force); studies with a direct comparison of two or more different activation modes appear to have not been published until now.

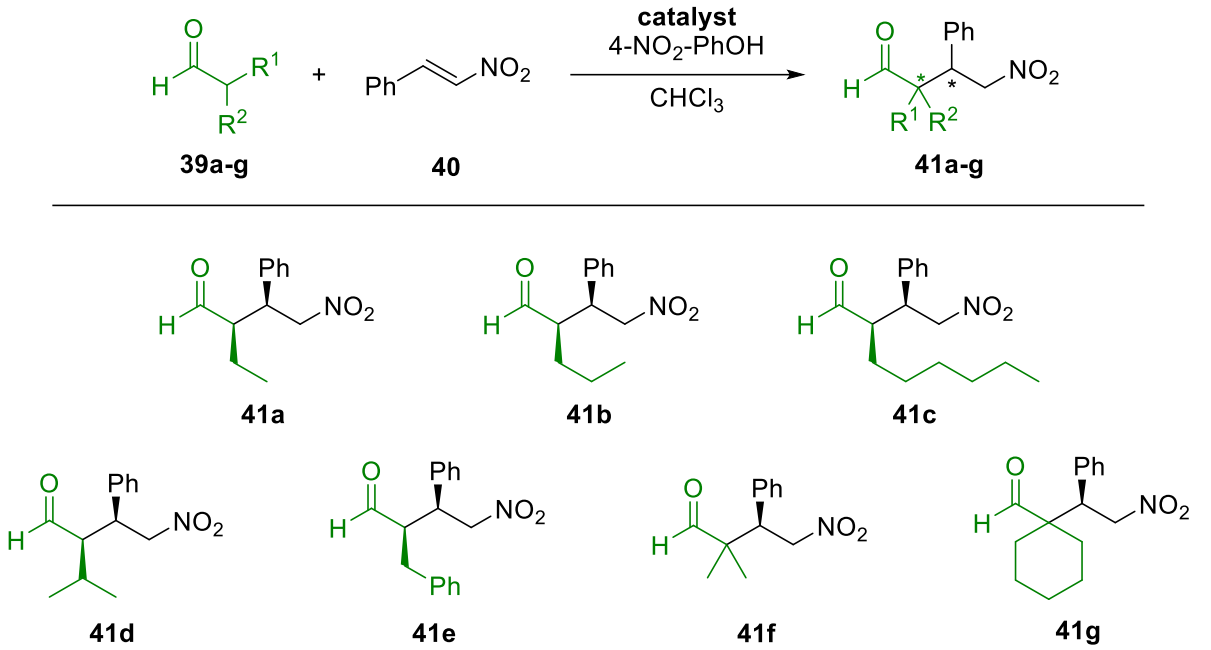

Scheme 14: The conjugate Michael addition of various aldehydes (**39a-g**) to *trans*-β-nitrostyrene (**40**), used as the test reaction in the comparative study of secondary activation modes. Catalysts were pyrrolidine (**42**) and the Jørgensen-Hayashi catalyst (**28**), 4-Nitrophenol was used as acidic cocatalyst.

This transformation has developed into a standard test reaction in organocatalysis over the years and enables the exploration of reactivity as well as diastereo- and enantioselectivity with a broad substrate scope.[85,108,109,110] Furthermore, it has not been investigated with the combination of covalent Lewis base organocatalysis and high-pressure activation until now. Seven different aldehydes were chosen as substrates: while **39a-c** are differing in the alkyl chain length, **39d** and **39e** provide considerable more steric bulk, thus potentially hampering the reaction. **39f** and **39g** were chosen as the most challenging substrates, as they possess only one proton in α-position, thus leading to the formation of products containing quaternary carbon centers.

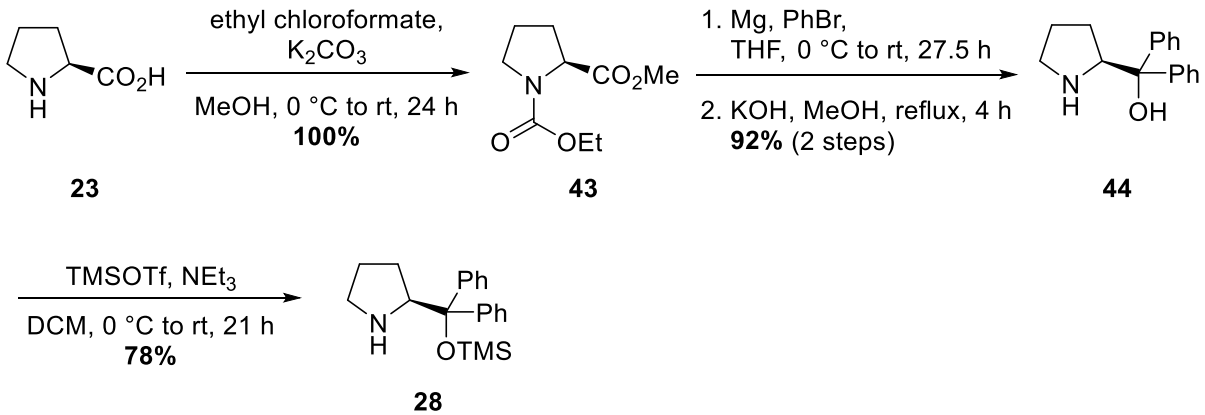

Scheme 15: Synthesis of the Jørgensen-Hayashi catalyst (**28**) from L-proline (**23**).

In terms of catalysts, two substances were picked for the reaction: pyrrolidine (**42**) and the Jørgensen-Hayashi catalyst (JH catalyst, **28**). Pyrrolidine (**42**) represents the simple basic core of all L-proline

derived organocatalysts. As it contains no functional groups which could interfere during the reaction, it is ideal to study pressure and temperature effects, meaning that all changes in yield and diastereoselectivity can be attributed solely to the applied secondary activation mode. The Jørgensen-Hayashi catalyst (**28**) was chosen as an asymmetric variant of a pyrrolidine-based catalyst, in particular, to investigate the effect secondary activation modes can have on the enantioselectivity of the reaction.[85–87,111] It can be conveniently synthesized starting from commercially available L-proline (**23**). Using the established procedure from Kanth *et al.*, the precursor diphenylprolinol (**44**) could be synthesized in 92% yield over 3 steps.[112] TMS protection of the alcohol group then gave rise to the finished catalyst **28** in good yield (Scheme 15).[113]

This sterically bulky, highly versatile catalyst has already been investigated in the chosen Michael addition under ambient conditions (AP/AT) by Hayashi *et al.* in 2005.[85] Since then, the underlying enamine-type reaction mechanism has been explored in detail by various research groups (Scheme 16).[114–121] The aldehyde is activated through formation of the (*E*)-enamine **45-1**[119,122,123] with the catalyst **28**, which then attacks the electron deficient Michael acceptor. This attack can proceed through different pathways: either through a [4+2] cycloaddition forming dihydrooxazine oxide **45-2A**, through a [2+2] cycloaddition forming cyclobutane **45-2B** or the elusive nitronate **45-TS1**.* Interestingly, the direction the reaction takes is dependent on the substrate structure and the reaction conditions. For aldehydes bearing only one α-proton (**39f-g**), only cycle A can lead to product formation. Here, deprotonation of **45-2B** to **45-TS2** is not possible, rendering the cyclobutane an off-cycle side product in parasitic equilibrium with **45-2A** and **45-TS1**. The rate-determining-step is, therefore, considered to be the protonation of **45-2A** (or **45-TS1**), leading to the iminium species **45-4A**, which releases the catalyst **28** and the product **41f-g** upon hydrolysis.[114,116] Using aldehydes with two α-protons, however, opens the reaction to two possible routes as ring opening of **45-2B** is now feasible (cycle B). This leads to the formation of nitronate **45-TS2** which is further protonated to enamine **45-3B** (again, this is considered to be the rate-determining step).[114,116] A second protonation step then leads to **45-4A**, thus reentering cycle A. For aldehydes **39a-e**, both catalytic cycles are viable and are probably occurring simultaneously, which is in so far interesting as the stereoselectivity-inducing steps are different for each pathway. In cycle A, stereochemistry is determined in the initial addition step, in cycle B selectivity must arise from the selective protonation of enamine **45-3B** by

* All three structures appear to be in an equilibrium with each other. While **45-2A** and **45-2B** have both been identified to be intermediates in the reaction mechanism, the occurrence of **45-TS1** is highly debated up until today.[114–121] Seebach *et al.* showed that linear aldehydes (like **39a-c**) form the cyclobutane (**45-2B**) preferentially over the dihydrooxazine oxide (**45-2A**) with *trans*-β-nitrostyrene (**40**) in anhydrous benzene-d_6. They also proved that stability of the cyclic intermediates is highly dependent on the solvent, showing almost immediate ring-opening in DCM-d_2 but high stability in benzene-d_6 under anhydrous conditions.[117]

4-nitrophenol (HA). Due to the complexity of the underlying mechanism, it is not surprising that the reaction is still subject to investigation today.[110,114–121]

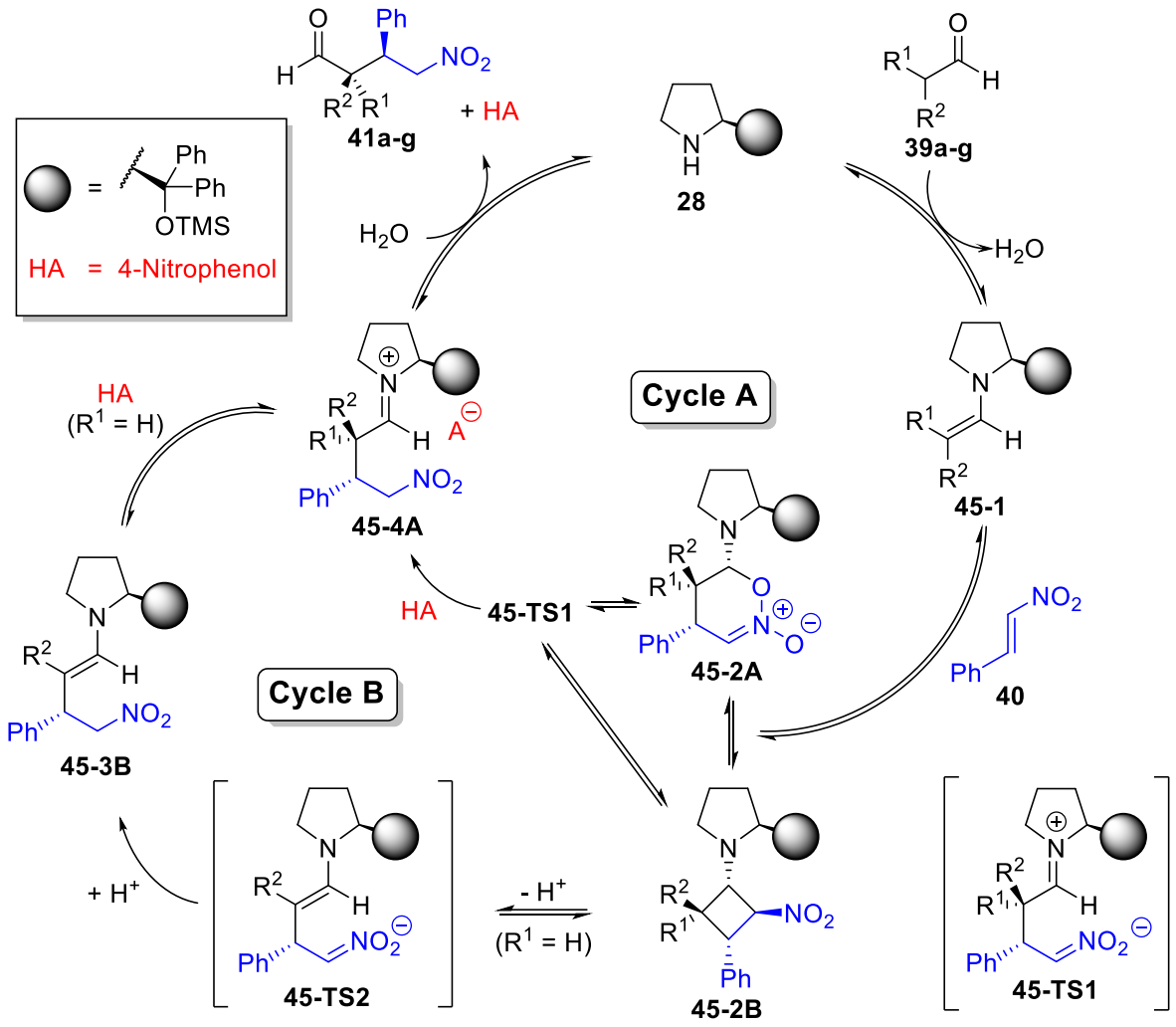

Scheme 16: Proposed reaction mechanism based on the publications of Seebach, Blackmond and Pihko *et al.* for the Michael addition of aldehydes (**39a-g**) to *trans*-β-nitrostyrene (**40**) catalyzed by the Jørgensen-Hayashi catalyst (**28**). While all aldehydes (**39a-g**) can proceed through cycle A, only aldehydes with R^1 = H (**39a-e**) can react through cycle B.[110,114–118,120,121]

In order to facilitate analysis of the reactions, it was chosen to use an NMR standard.* This allowed the fast and accurate determination of yields and diastereomeric ratios in the crude reaction mixture and ensured that errors due to partial loss of product during purification were prevented. Purification was, therefore, only necessary to determine the enantiomeric excess of the products. To achieve comparability throughout the experiment, all reaction parameters were kept constant, varying solely in the use of the different secondary activation modes (Table 2).

* Diphenoxymethane (**46**) was chosen as standard as it generates a reliable signal in a non-crowded part of the spectrum. It has already proven itself to be a good NMR standard in the past, as it fulfills the criteria for a good NMR standard: it is high boiling, easy to handle and, as an ether, unreactive.[124]

Table 2: Conditions of the secondary activation modes used in the comparative study.

Conditions	Abbreviation	Temperature [°C]	Pressure [kbar]
Ambient	AP/AT	22	10^{-3}
High temperature	HT	55	10^{-3}
High pressure	HP	22	4.6

The AP/AT conditions basically represent an unaltered reaction sequence without any additional influences, thus setting benchmark results. Catalyst loadings were customized for each aldehyde under ambient conditions (AP/AT) in order to obtain yields between 30 – 50%. This ensured that changes in both directions could be tracked. This enabled the estimation of the influence of the secondary activation modes on the reaction, allowing the evaluation of basic trends for yields and selectivities.

1.3 Influence of secondary activation modes on reactivity

The first parameter that was investigated was the reactivity (*i.e.* yield) of the reaction and the resulting changes that result from heating or pressurization (Figure 4).

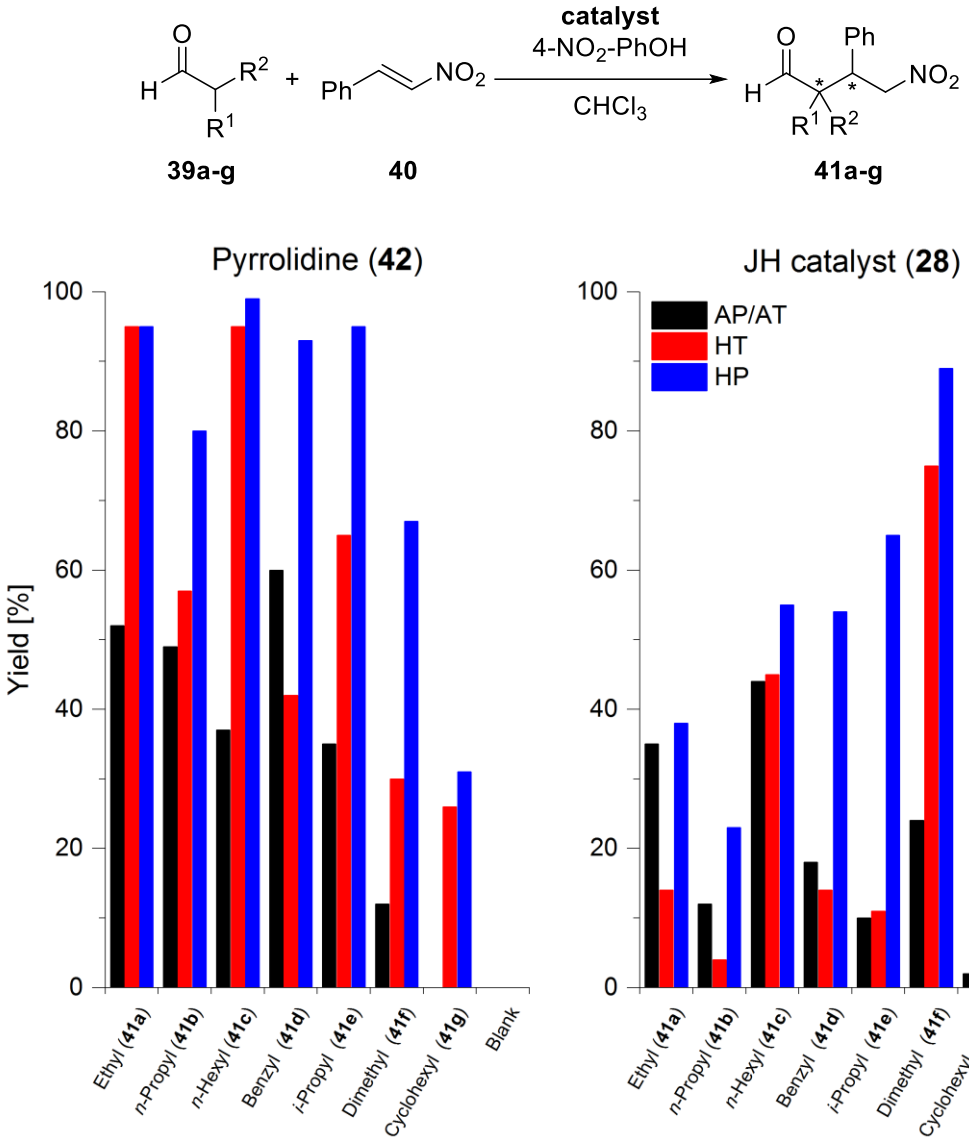

Figure 4: Obtained yields from the Michael reaction catalyzed by pyrrolidine (**42,** left) and the Jørgensen-Hayashi catalyst (**28**, right). Ambient conditions (AP/AT): black, high temperature (HT): red, high pressure (HP): blue. Reaction conditions: **39a-c**: 1 h, 1 mol% **42** or **28**; **39d**: 1 h, 1mol% **42** or 2.5 mol% **28**; **39e:** 1 h, 2.5 mol% **42** or **28**; **39f-g**: 4 h, 10 mol% **42** or **28**. All results and parameters can also be found in tabular form in the appendix (see chapter G.1., Table 7 & Table 8).

Before starting experiments, any occurrence of a background reaction under the applied conditions had to be ruled, as this would falsify the results. Therefore, blank reactions with **39a** using no catalyst were conducted. Only slight conversion of the starting material *trans*-β-nitrostyrene (**40**) and no formation of product **41a** was observed after 45 h, hence proving that the Michael addition only takes

place in the presence of a catalyst. Therefore, the catalyzed reaction could then be performed with the different aldehydes **39a-g** and conditions.

1.3.1 Pyrrolidine-catalyzed reactions

The racemic variant of the reaction, using pyrrolidine (**42**) as catalyst, was performed first (Figure 4, left). Here, the results showed that both linear (**39a-c**) as well sterically more demanding aldehydes (**39d-e**) gave mediocre yields (35-60%) under AP/AT conditions. A clear trend was visible for linear aldehydes (**39a-c**), displaying decreasing reactivity with extended chain lengths (Ethyl > *n*-Propyl > *n*-Hexyl). This was expected, as the probability of effective collisions required for enamine formation should decrease with larger substrates. Interestingly, the most reactive aldehyde of these was the sterically hindered hydrocinnamic aldehyde (**39d**) which gave yields similar to *n*-butanal (**39a**). This might be attributed to the possibility of beneficial π-π-interactions with *trans*-β-nitrostyrene (**40**), guiding it to the enamine.[*] The bulky *i*-pentanal (**39e**) reacted the slowest, residing in the same range as *n*-octanal (**39c**), though requiring higher catalyst loadings (2.5 mol% for **39e** instead of 1 mol% for **39a-d**). This is unsurprising, as the higher steric bulk should hinder the reaction. Finally, the more challenging substrates, containing only one proton in α-position, reacted significantly slower at AP/AT even with 10 mol% of catalyst. While at least small amounts of product could be obtained with *i*-butanal (**39f**), the use of the bulkier cyclohexyl carbaldehyde (**39g**) resulted in no product formation at all. This might be explained by the hampered addition of the bulkier enamine to *trans*-β-nitrostyrene (**40**) or a result of catalyst blockage due to the formation of the parasitic cyclobutane described earlier (Scheme 16, **45-2B**).

Applying secondary activation modes had drastic effects on the outcome of the reactions. Both HT and HP conditions appear to accelerate the reactions, however, to a different extent. This can be related to the different influences of HT and HP on the reaction. Generally, both activation modes increase reactivity by adding extra energy to the system, which is required to overcome activation barriers. HT works through adding kinetic energy to the system which leads to increased molecular motion, and therefore collisions, in a specific amount of time. HP also adds energy, however, by forcing molecules into close proximity to each other, which is advantageous for bond-forming reactions ($\Delta V^{\ddagger} < 0$). The important difference to HT is that HP also constrains the reaction volume and molecular flexibility, thus overcoming activation barriers and steric repulsion at the same time.[19,20,24,26,28] An example for these

[*] However, the reaction with hydrocinnamic aldehyde **39d** was prone to side reactions. The resulting side products unfortunately proved inseparable and could thus not be identified.

beneficial effects are the observations made with the linear aldehydes **39a-c**. The reactions of the short-chained *n*-butanal (**39a**) and the long-chained *n*-octanal (**39c**) could be driven to completion under HT as well as HP conditions, increasing the reaction rate by a factor of at least two (compared to AP/AT). However, the medium-sized *n*-pentanal (**39c**) was less susceptible to activation: while HT only led to slightly better yields, only HP conditions were able to significantly improve the outcome in this case. With the alkyl chain length being the only difference between the aldehydes **39a-c**, it is likely a steric effect that causes the reactivity change. Scheme 17 depicts the transition state for the attack of the (*E*)-enamines[119,122,123] on *trans*-β-nitrostyrene (**40**) leading to the *syn* products, which were predominantly formed (see also chapter 1.4).

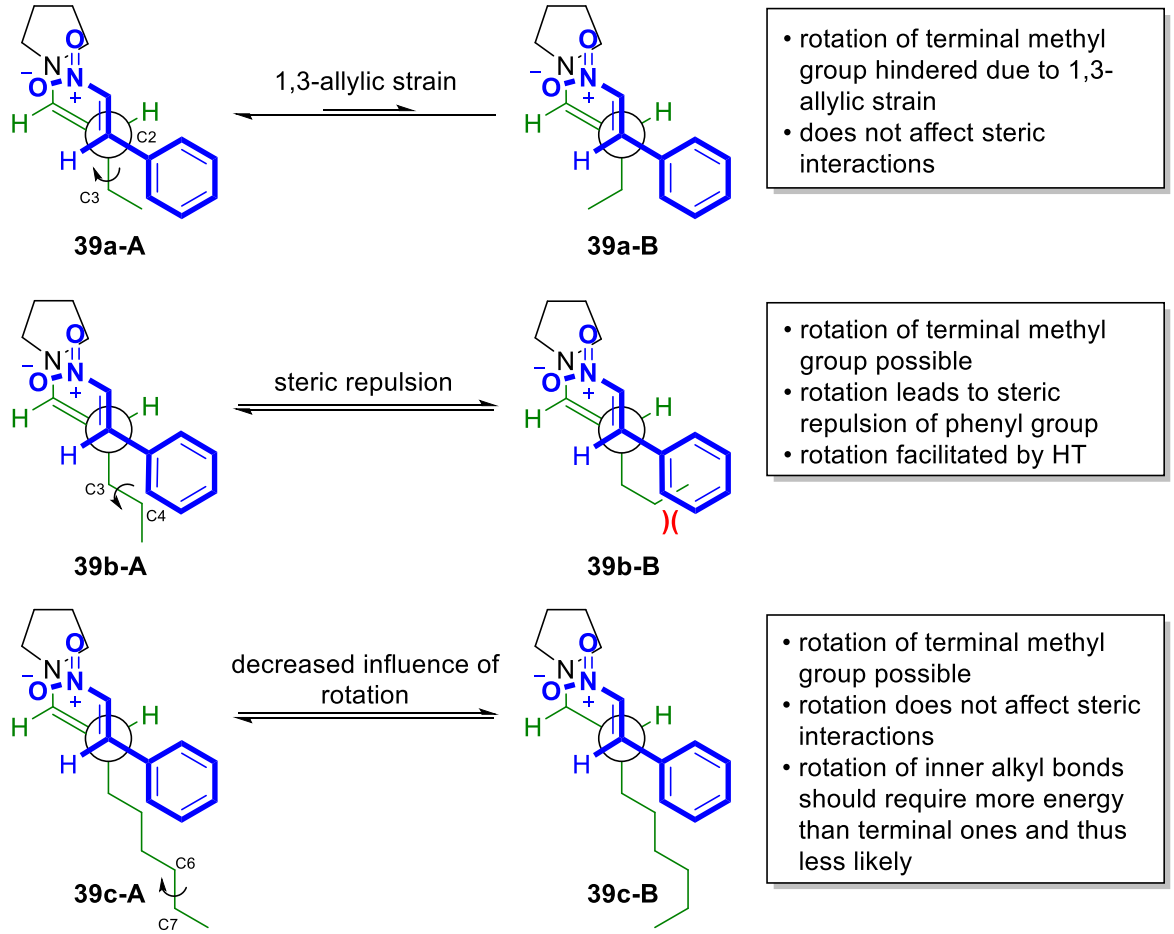

Scheme 17: Possible explanation for the discrepancy in reactivity observed in the HT- and HP-activated reaction with *n*-pentanal **39c**.

Looking at **39b**, it becomes apparent that rotation of the terminal methyl group in enamine **39b-A** can lead to an unfavorable interaction with the nitroalkene (**39b-B**), resulting in steric repulsion. With the shorter **39a**, this interaction should be severely hindered as rotation around the C2-C3 bond of the enamine would lead to 1,3-allylic strain.[125] For the longer **39c**, the terminal methyl group should be too far away to have any influence. Of course, rotation around the inner alkyl bonds can also occur,

although, moving the entire alkyl chain should require more energy than a simple methyl group. Additionally, **39c** has a higher degree of freedom, making it less probable that the rotation occurs selectively at the C3-C4 bond of the enamine (in contrast to **39b** where this displays the only bond rotation that can occur unhindered). Under standard conditions, the alkyl chains are probably arranged in a linear fashion as a result of least amount of steric strain. With the addition of energy, however, rotation of the chains should become more prominent as the rotational barriers can be overcome. Both activation modes add energy to the system, but only HP acts through constraining volume. Therefore, HP should, on the one hand, reduce flexibility of the molecules and, on the other hand, force molecules into spatial proximity despite steric repulsion. While unfavorable rotation and repulsion might still occur, its effect should hence be diminished by the use of HP. In contrast to this, HT only adds energy, which might increase overall reactivity but cannot counteract the rising influence of steric repulsion, thus explaining the observed discrepancy.[*]

The tendency for HP conditions to outperform HT became more prominent with the sterically more demanding aldehydes (**39d-e**). Although the reaction with *i*-pentanal (**39e**) ran almost twice as fast under HT conditions (as there is no steric strain with the catalyst which could be detrimental), it could only be driven to completion with HP (> 3x faster). With hydrocinnamic aldehyde (**39d**), the use of HT even had detrimental effects on the reaction outcome. Increased formation of side products was observed under HT conditions resulting in diminished yields of **41d**. In contrast, HP conditions boosted the activity of the reaction once more reaching complete conversion, while suppressing side product formation at the same time.

The most drastic effects, however, could be observed with the challenging substrates **39f** and **39g** bearing only one α-proton. While the use of HT led to more than doubled yields in the reaction with *i*-butanal (**39f**), HP resulted in an almost six-fold increase in reactivity. As mentioned earlier, an issue for the low conversion under ambient conditions could be the formation of the cyclobutane (**45-2B**) in the conjugate addition step (Scheme 16, cycle B). With aldehydes **39f-g**, this intermediate depicts an off-cycle resting state of the catalyst, as the lack of an abstractable α-proton prevents further transformation. Although these cyclobutanes can be fairly stable, Seebach *et al.* demonstrated that the reverse reaction back to the enamine and *trans*-β-nitrostyrene (**40**) is facilitated by increased temperatures. This means that higher temperatures should release the active catalytic species again if trapped in the cyclobutane species, thus increasing the chances for the reaction to proceed through cycle A and producing product **41f**. While this is a plausible explanation for the improved activity under

[*] This could be also one reason why the *anti* product is formed to larger extent under HT conditions, as the steric hinderance is less prominent in the respective transition state (see chapter 1.4.1).

HT, this rationalization should not apply to HP conditions. Here, another mode of action is more reasonable, namely electrostriction, a result of the interaction between the medium and the reactant. In organic reactions, the occurrence of ionic transition states will lead to an ordering of the charged species, resulting in a tighter packing of the medium (*i.e.* $CHCl_3$) around them. This effect is called electrostriction and is accompanied by a sharp volume decrease, which can have a significant impact on the volume of activation $\Delta V^{\ddagger}$. Therefore, reactions proceeding through highly dipolar or ionic transition states can be significantly accelerated by pressure.[19,20,24,26,28] This explains the increased reactivity under HP conditions for **39f**, as the product-forming cycle A goes through the zwitterionic transition state **45-TS1** and eventually leads to the equally zwitterionic **45-4A**, which should both be formed preferentially under pressure due to electrostriction effects.* Curiously, the bulky cyclohexyl-bearing **39g**, which did not form under AP/AT conditions, gave more or less comparable results for both activation modes. The even higher steric complexity of the enamine and the corresponding intermediates might be the reason that this reaction proceeds rather slowly.

1.3.2 Reactions catalyzed by the Jørgensen-Hayashi catalyst

After analyzing the reactivity with the simple, non-chiral pyrrolidine (**42**), focus was then turned towards the asymmetric Jørgensen-Hayashi catalyst (Figure 4, right). On first glance, it becomes obvious that the overall yields are generally lower than in the racemic reactions. This is not surprising as the catalyst bears a large stereoinducing group which lowers the general accessibility of the active center, thus hampering the reactivity. Although similarities exist to the pyrrolidine-catalyzed reactions regarding reactivity trends, some aldehydes react quite differently. For instance, the linear aldehydes **39a-c** now show the same discrepancy in reactivity already under AP/AT conditions, which was only observed under HT or HP in the racemic reactions. As mentioned earlier, the reason for this is likely to be a steric effect (see Scheme 17). Here, the issue is now further amplified because of the bulky substituent of the catalyst, thus being significant enough to be observed even at AP/AT. Unsurprisingly, HT conditions worsened this problem through increased rotation, leading to diminished yields with the short **39a** and **39b**. In contrast, HP conditions could achieve slightly increased yields, however, not to the same extent as in the pyrrolidine-catalyzed reactions. Interestingly, the longest chain aldehyde **39c** was observed to be the most reactive and the only linear aldehyde, where HT seemed to have no detrimental effect. This might be attributed to its larger size. It makes rotations around bonds which

* This of course should then also be true for all the other HP-activated reactions with aldehydes **39a-g**, making electrostriction an additional accelerating effect that has to be taken into account.

lead to unfavorable interactions stochastically less probable. Additionally, the volume decrease upon bond formation (*i.e.* in the transition state) should be higher than with the smaller sized aldehydes, resulting in a more negative volume of activation ($\Delta V^{\ddagger}$), which in return leads to enhanced reaction rates upon pressurization.[*]

With the sterically more demanding aldehydes (**39d-e**), the results were as expected. Yields were low under AP/AT and HT conditions; a result from the steric strain between the aldehydes and the catalyst (**28**) complicating productive collisions (in contrast to pyrrolidine (**42**), where no spatially demanding groups were present). Here, the benefits of HP activation came to play, as the constriction of volume could effectively bring the reactants into proximity for the reaction to occur. As a result, the use of HP resulted in a 3-fold increase in reactivity for **39d** and a more than 6-fold for **39e**.

The reactions with the challenging substrates **39f** and **39fg**, bearing only one α-proton, again resulted in interesting outcomes. Curiously, *i*-butanal (**39f**) gave even better results with the Jørgensen-Hayashi catalyst (**28**) than with pyrrolidine (**42**). Moreover, both HT and HP conditions had a beneficial impact on the transformation, with HP even reaching complete conversion.[†] A possible explanation for this behavior might be that the earlier mentioned cycle-breaking cyclobutane is less stable with the Jørgensen-Hayashi catalyst (**28**). Its bulky substituent could lead to steric strain with the methyl groups, thus decreasing the amount of cyclobutane being formed and favoring the product-yielding catalytic cycle. However, this might not be the singular reason for this observation, as the other structurally complex aldehyde **39g** showed almost no reactivity under AP/AT and HT conditions. Only HP could generate small amounts of product, indicating that either steric strain of the cyclobutane is not the only factor or that cyclohexyl carbaldehyde **39g** is simply less active (*e.g.* prone to enamine formation) as **39f**.[‡]

At this point, the results nicely demonstrated the overall beneficial effects HP has on the reactivity of the organocatalyzed Michael addition, which are much more constant and reliable than using plain HT activation methods.

[*] The slightly higher yield for **39c** compared to **39a** in the pyrrolidine-catalyzed reaction might also be indicative of this, however, both reactions had reached complete conversion making analysis difficult.

[†] This is interesting as Blackmond *et al.* reported less than 5% yield for **41f** in their investigations, although with benzene-d_6 as solvent and acetic acid as additive.[120] However, Seebach *et al.* demonstrated that solvent and additives can have an significant effect on the reaction and its intermediates.[117,118]

[‡] A possibly activating coordinative effect of the protected or unprotected[126] alcohol moiety of the catalyst **28** can be ruled out under the here employed conditions according to literature.[114–118,120,121]

1.4 Influence of secondary activation modes on selectivity

With the analysis of the reactivity accomplished, the focus then turned to the selectivity of the reaction, as the use of aldehydes **39a-e** led to products containing two stereocenters, resulting in the formation of *syn* and *anti* diastereomers.

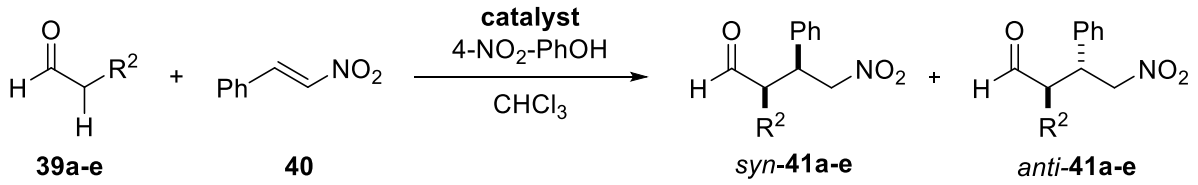

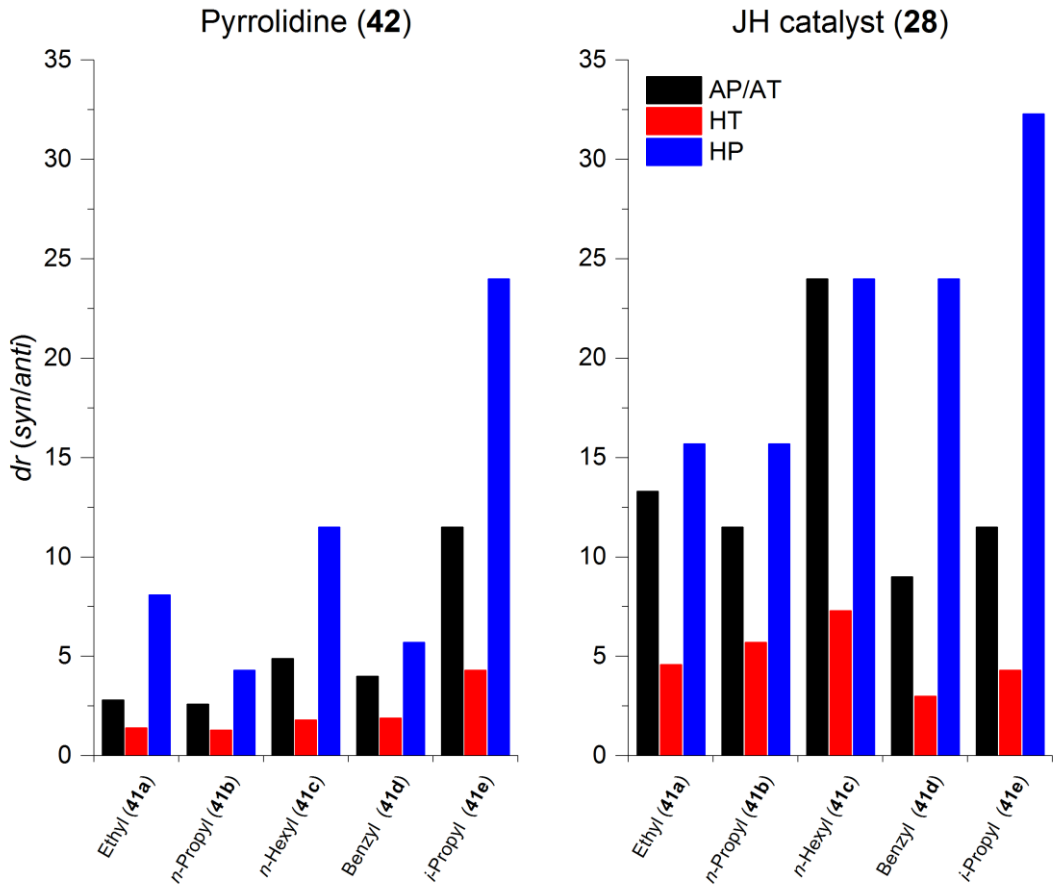

Figure 5: Obtained diastereomeric ratios from the Michael reaction catalyzed by pyrrolidine (**42,** left) and the Jørgensen-Hayashi catalyst (**28**, right). *syn*/*anti* ratios are normalized to *anti* = 1. Ambient conditions (AP/AT): black, high temperature (HT): red, high pressure (HP): blue.

1.4.1 Pyrrolidine-catalyzed reactions

Again, the pyrrolidine-catalyzed reactions are evaluated first. As pyrrolidine (**42**) itself is achiral, all changes in terms of selectivity can be attributed to the interactions between the reactants and the employed activation mode. Taking a first look at the results (Figure 5, left), a clear trend for selectivities in relation to the reaction conditions can be seen, as the formation of the *syn* product was preferential for all aldehydes and conditions. Initially, this might appear to be counterintuitive as no stereodirecting group is present in the catalyst (**42**), however, it becomes clear upon examining the transition states occurring in the reaction (Scheme 18). If the reaction proceeds through the catalytic cycle A (see Scheme 16), the stereochemistry will be defined in the initial addition step (Scheme 18 a)).

Already in 1981, Seebach *et al.* investigated the Michael addition of aldehydes to nitroalkenes using achiral morpholine as catalyst.[127] They stated that the nitro group coordinates to the nitrogen atom of the enamine due to electrostatic interactions. This leads to (*Re*,*Re*)- and (*Si*,*Si*)-approaches, being favored over (*Re*,*Si*)- and (*Si*,*Re*)-approaches, thus explaining the observed selectivity for the *syn* product.[127–129] This hypothesis was later picked up and transferred by Alexakis and Hayashi *et al.* to explain the asymmetric variants of the Michael addition with other Lewis-base catalysts.[81,85]

As mentioned in chapter 1.2, the reaction with aldehydes **39a-e** can also proceed through a second catalytic cycle B. This involves a [2+2]-cycloaddition forming a cyclobutane intermediate whose stereochemistry is similarily influenced by the orientation of the nitroalkene. In Scheme 18 b), it can be seen that the (*Si*,*Si*)-approach of the reactants leads to the formation of the sterically favored *all-trans* cyclobutane (*all-trans*-**45-2B**), while a (*Re*,*Si*)-approach would generate the more strained (thus disfavored) *cis*,*trans*,cis,trans isomer (*cis*,*trans*,*cis*,*trans*-**45-2B**).* Although the stereochemistry of the cyclobutane has no direct influence on the final product (due to deprotonation **45-TS2** in the next step of cycle B), it is also in an equilibrium with species from catalytic cycle A, where the stereochemistry is defined in the initial addition step.[117,118]

* A similar conclusion can be drawn for the dihydrooxazine oxide intermediate **45-2A**. The (*Si*,*Si*)-approach leads to formation of a six-membered ring with all substituents in equatorial position, while the (*Re*,*Si*)-approach requires at least one substituent to be in axial position.

a) Transition states of the conjugate addition leading to all four stereoisomers

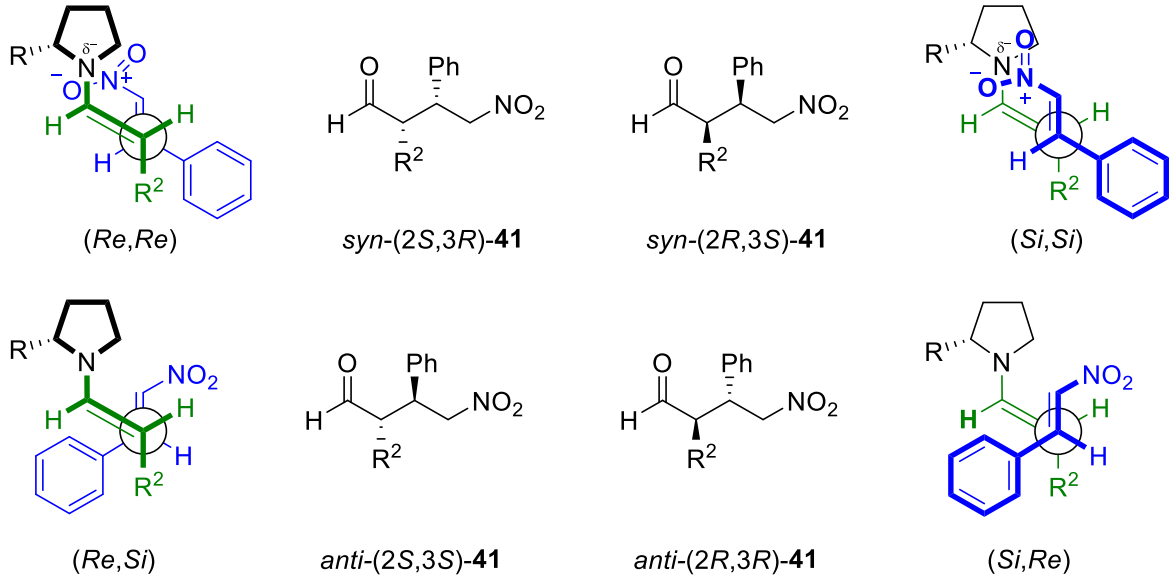

b) Intermediates obtained from [2+2]-cycloaddition

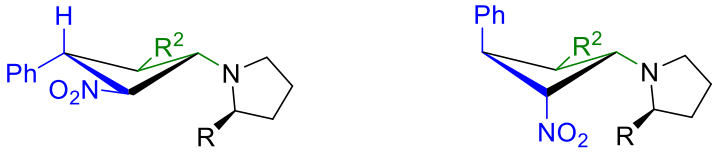

c) Transition states for the stereoselective protonation of enamine **45-3B**

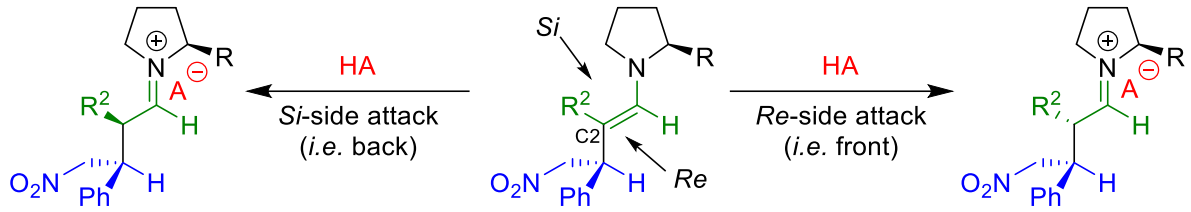

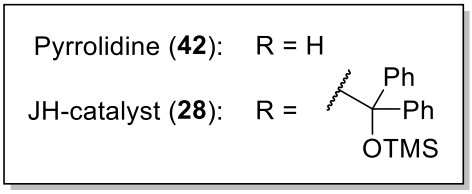

Scheme 18: Evaluation of the different stereoinducing steps which can occur during the Michael addition. a) Transition states of the initial addition step for all stereoisomers, molecules in the front are depicted bold. Preferred outcome is the *syn* adduct through (*Re*,*Re*)- or (*Si*,*Si*)-approach of the enamine and *trans*-β-nitrostyrene (**40**), as this leads to favorable stereoelectronic interaction between the nitro group and the nitrogen on the enamine.[127–129] If the JH catalyst (**28**) is used, the (*Si*,*Si*)-approach is favored due to shielding of the *Re*-side, generating *syn*-(2*R*,3*S*)-**41**.[85] b) Exemplary structures of the cyclobutanes formed by (*Si*,*Si*) or (*Re*,*Si*)-addition.[117,118] With pyrrolidine (**42**) as catalyst, also the not depicted (*Re*,*Re*) or (*Si*,*Re*)-additions are viable. c) Rational analysis of the diastereoselective protonation of enamine **45-3B**, explaining the observed *syn* selectivity for catalytic cycle B. *Re*/*Si*-nomenclature relative to C2. [114,115,117,120] HA = 4-nitrophenol.

In catalytic cycle B, the stereochemistry is defined by the selective protonation of the enamine **45-3B** (assuming *all-trans*-**45-2B** was formed earlier). Scheme 18 c) depicts the two possible pathways this can take place. When using pyrrolidine (**42**) as catalyst, there is no asymmetric substituent which could guide the proton source (4-nitrophenol). However, **45-3B** should be orientated as portrayed in order to reduce 1,3-allylic strain, facing the bulky phenyl group to the *Re*-side (*i.e.* front in Scheme 18 c)).[125] This means that protonation from the *Si*-side (*i.e.* back) should be favored, as it is sterically more accessible, thus again leading to the *syn* product preferentially.[114,115,117,120]

With these explanations, the experimentally determined selectivities and changes can be explained. Under AP/AT conditions, a dependence between the *syn*/*anti* ratio and the steric bulk of the used aldehyde could be observed. While small linear aldehydes (**39a-b**) showed lower selectivities, the larger **39c** gave improved results. On the first look, this seems plausible, as the added steric bulk should lead to the increased differentiation between the different transition states. Rationally, this should be accompanied by a decreased reactivity, however, this was not observed (compare chapter 1.3.1, Scheme 17). An explanation might be that with the linear aldehydes, the [2+2]-cycloadduct **45-2A** is formed initially. While the smaller aldehydes **39a-b** could form both cyclobutanes due to their low size, **39c** should preferentially form the *all-trans*-adduct (*all-trans*-**45-2B**) as it possesses considerable more steric bulk (Scheme 18 b)). The adduct then undergoes ring-opening and the reaction proceeds through catalytic cycle A, explaining the simultaneous high selectivity and reactivity of **39c**. Using the bulky *i*-pentanal (**39e**) led to an expected increase in selectivity, reaching the highest values for all aldehydes under AP/AT conditions (*syn*/*anti* = 92:8 or 11.5:1). Hydrocinnamic aldehyde (**39d**), however, gave selectivities comparable to **39c**, probably due to its higher flexibility than **39e**.

Repeating the same reactions with the use of secondary activation modes resulted in a clear trend. On the one hand, the use of HT conditions led to diminished diastereoselectivities for all aldehydes. This is not surprising, as it is known that the *anti*-products are the thermodynamically more stable products.[114,115,120] The added thermal energy increases molecular motion, leading to a higher probability that also (*Re*,*Si*)- and (*Si*,*Re*)-approaches of the reactants occur (Scheme **18**, a)). Additionally, the increased energy amount should weaken the guiding stereoelectronic coordination of the nitro group to the enamine nitrogen, thus diminishing the preference for the formation of the *syn* product. Another aspect is that diastereoselectivity can erode if the product stays in contact with the catalyst over an extended amount of time, especially near or after complete conversion. Blackmond *et al.* demonstrated that this occurs through equilibration of the iminium species **45-4A** to the enamine **45-3B**, which results in the loss of stereo information at C2 until a *syn*/*anti* ratio of around 60:40 (= 1.5:1) is reached (under AP/AT).[114,115,120] This is very likely to occur under HT conditions, as

equilibration should be facilitated by the higher temperatures and is supported by the fact that *syn*/*anti* ratios of around 60:40 were found for all products except the bulky **41e**.

On the other hand, HP conditions had the complete opposite effect, as all diastereoselectivities were enhanced, reaching *syn*/*anti* ratios up to 96:4 (= 24:1). As with the reactivity study, this can be explained by the unique activation mechanism high pressure provides.[19,20,24,26,28] Through constraining the reaction volume and forcing the reactants into close spatial proximity, steric repulsion can be overcome. Transition states of smaller volume will be formed preferentially as their volume of activation ($\Delta V^{\ddagger}$) is lower, hence increasing the yield of the sterically more constrained *syn* product. Additionally, HP stabilizes zwitterionic intermediates through electrostriction, thus effectively canceling out the erosion of stereoinformation through equilibration between the charged iminium species **45-4A** and the uncharged enamine **45-3B**. Interestingly, the discrepancy of the linear aldehydes, which was already observed in the reactivity studies (chapter 1.3.1), could also be observed here, as *n*-pentanal (**39b**) was less susceptible to pressurization as **39a** and **39c**. This might be attributed to a unfavorable rotation of the terminal methyl group, which hinders the (*Re*,*Re*)- or (*Si*,*Si*)-approach (see Scheme 17). This issue is not as prominent with the (*Re*,*Si*) and (*Si*,*Re*)-approach of the reactants leading to the *anti* product. Indeed, the reaction with **39b** resulted in an increased formation of the *anti* diastereomer, which is indicative that the explanation made earlier is correct.

1.4.2 Reactions catalyzed by the Jørgensen-Hayashi catalyst

Unsurprisingly, using the asymmetric Jørgensen-Hayashi catalyst (**28**) had a large impact on the diastereoselectivity of the reaction. The bulky stereoinducing group is shielding the *Re*-side of the enamines. This effectively blocks the (*Re*,*Re*)-approach of the reactants, leaving the (*Si*,*Si*)-transitions state as the favored one.[*] At the same time, the propensity of the reaction to proceed through the (*Re*,*Si*)-transition state (and to a smaller degree the (*Si*,*Re*)- approach as well) is decreased. In these cases, the phenyl group of *trans*-β-nitrostyrene (**40**) is adjacent to the asymmetric substituent of the catalyst **28**, resulting in steric strain and, therefore, diminished formation of the *anti* products (see Scheme 18 a)). Additionally, the catalyst **28** shielding the *Re*-side of the intermediary enamine **45-3B** also improves the stereocontrol in the selective protonation step leading to *syn*-**45-4A**, explaining the

[*] Reducing the available transition states from four to only one of course should have an effect on the reactivity, thus partially explaining the decrease in reactivity compared to the pyrrolidine-catalyzed reactions (see chapter 1.4.1).

overall tendency to form *syn* adducts (see Scheme 18 c)).

Under AP/AT conditions, this led to an increase of selectivity over the pyrrolidine-catalyzed reactions with almost all aldehydes. All aldehydes gave *syn* selectivities greater than 90:10 (= 9:1), with the linear aldehydes profiting more from the use of an asymmetric catalyst. With the sterically demanding aldehydes **39d-e** the influence was less prominent: while a reasonable increase in diastereoselectivity could be observed in the reaction with the moderately flexible hydrocinnamic aldehyde (**39d**), the use of *i*-pentanal (**39e**) resulted in unchanged values. Due to their steric bulk and inflexibility, these aldehydes (**39d-e**) cannot evade steric strain completely. Therefore, the propensity for the formation of the more stable, less strained *anti*-product is slightly higher compared to the reactions with the more flexible linear aldehydes **39a-c**.

The HT reactions catalyzed by the Jørgensen-Hayashi catalyst (**28**) behaved similarly to the thermally activated, pyrrolidine-catalyzed reactions. Compared to AP/AT, heating resulted in a severe drop of *syn* diastereoselectivity for all aldehydes (**39a-e**), as the formation of the thermodynamically favored *anti* products became more prominent. Again, the increased equilibration of the iminium species **45-4A** to the enamine **45-3B** as well as the increased molecular motion leading to more (*Re*,*Si*)- and (*Si*,*Re*)-approaches of the reactants might be the main reason for this to occur. However, it is important to note that selectivities were considerably better than with achiral pyrrolidine (**42**).

In contrast to these findings, using HP conditions also improved the stereoinduction for the asymmetric version of the reaction, reaching excellent *syn* selectivities for all aldehydes (≥ 94:6 or 15.7:1). This time, the diastereoselectivity of the linear aldehydes **39a-c** were less respondent to pressurization than in the racemic reactions. The bulky aldehydes **39d-e**, however, benefit clearly from the increased pressure. This fits well with the observations made in the AP/AT reactions: the steric repulsion, which led to lower selectivities of **39d-e** under ambient conditions, now is overcome as HP forces the molecules closer together, constraining the reaction volume. It is therefore not surprising that the best overall selectivity ratio was observed with the bulkiest aldehyde **39e** (*syn*/*anti* = 97:3 or 32.3:1).

With the use of the asymmetric Jørgensen-Hayashi catalyst, the enantiopurity of the products also became a point of investigation. It is important that a secondary activation mode does not interfere with the enantioinduction of the catalyst. Lower enantioinduction is usually detrimental as it leads to the requirement of tedious workup procedures (*e.g.* crystallization, chiral HPLC, etc.) to obtain the product in enantiopure form.

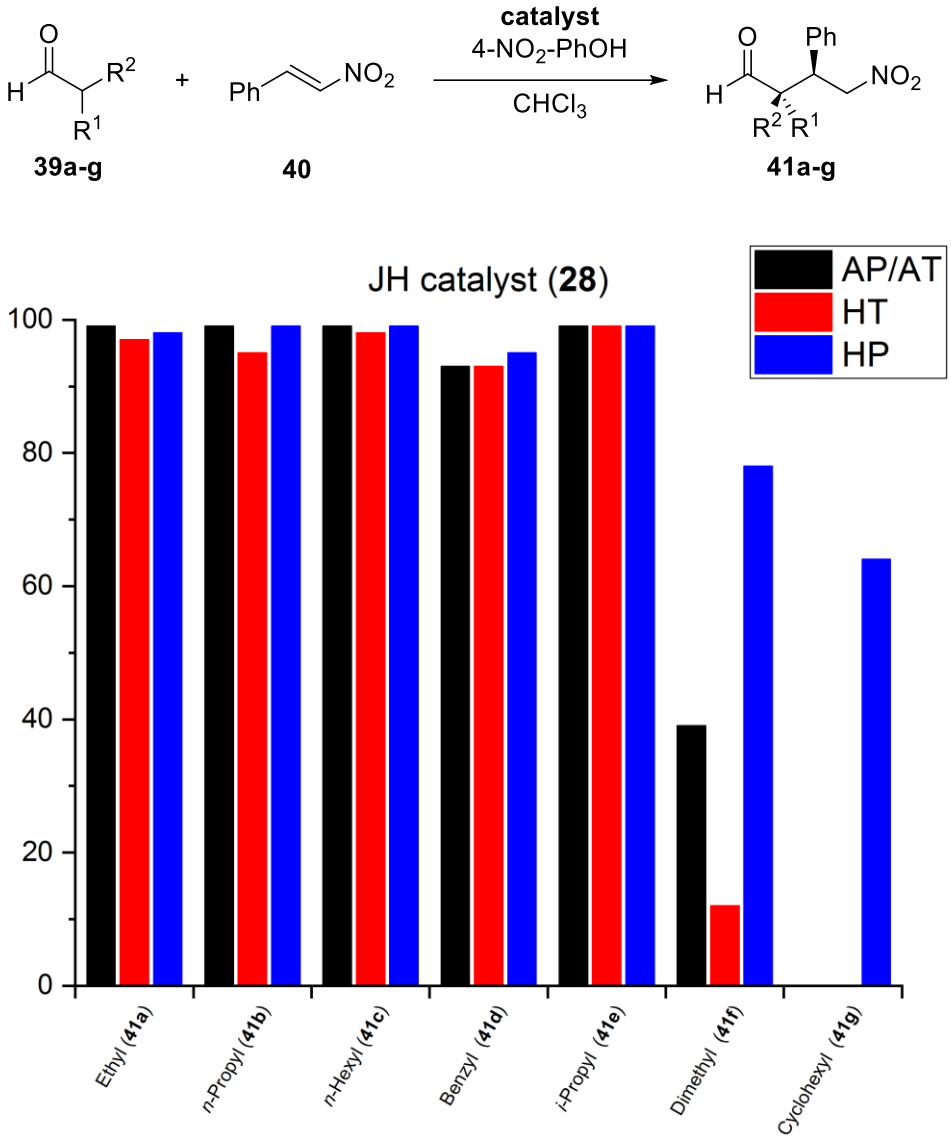

Figure 6: Obtained enantiomeric excesses from the asymmetric Michael reactions catalyzed by the Jørgensen-Hayashi catalyst (**28**).

With the use of an asymmetric catalyst, the enantiopurity of the products also became a point of investigation. It is important that a secondary activation mode does not interfere with the enantioinduction of the catalyst. Lower enantiomeric excess is usually detrimental as it leads to the requirement of tedious workup procedures (*e.g.* crystallization, chiral HPLC etc.) to obtain the product in enantiopure form. Therefore, the enantiopurities of all *syn* compounds obtained from the asymmetric reaction with **28** were determined (Figure 6).

For aldehydes **39a-e**, the use of a secondary activation mode appeared to have almost no influence on the enantioselectivity of the Jørgensen-Hayashi catalyst (**28**). While AP/AT and HP gave constantly excellent enantioselectivities, slightly decreased *ee* values were detected for the linear aldehydes **39a-c** under HT conditions, however, changes were marginal. This underlines, that the earlier

described (*Si*,*Si*)-approach of the reactants should lead to the most stable transition state with the Jørgensen-Hayashi catalyst (**28**), generating the *syn*-(2*R*,3*S*)-products **41a-e** (see Scheme 18 a)).*

As these results proved to be uneventful, the focus was then turned on **39f** and **39g**. These symmetrical aldehydes bear only one α-proton, thus generating no diastereomers but a quaternary carbon center at C2 (**41f** and **41g**). The use of **39f** led to an interesting discovery, as the products enantioselectivity was highly dependent on the reaction conditions. Under ambient conditions, (*R*)-**41f** was obtained in only moderate excess (39% ee). However, a sharp increase in enantioselectivity was observed under HP conditions, yielding (*R*)-**41f** with 78% *ee*. In contrast, heating led to a diminished enantioinduction, generating (*R*)-**41f** with poor 12% *ee*.

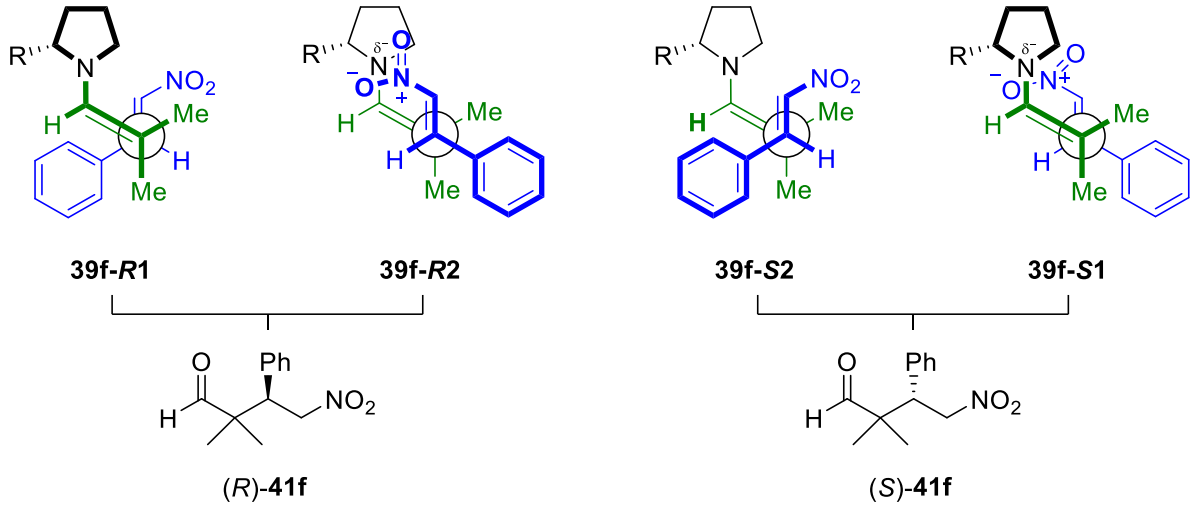

Scheme 19: Depiction of the transition state leading to the two enantiomers of **41f**. R = Ph_2(C)OTMS.

As the aldehyde **39f** is symmetric, two possible transition states exist for the formation of each enantiomer (Scheme 19). For **39f-*R*1** and **39f-*S*1**, *trans*-β-nitrostyrene (**40**) approaches from the side the bulky substituent of the Jørgensen-Hayashi catalyst (**28**) is facing, therefore, these should be disfavored at AP/AT and can be ruled negligible. This means that the preferentially formed (*R*)-enantiomer (*R*)-**41f** is probably generated through **39f-*R*2**, as it allows the stereoelectronic interaction of the nitro group and the nitrogen on the enamine.† However, as the (*S*)-enantiomer (*S*)-**41f** is also formed in considerable amount, this means that the reaction should also proceed through **39f-*S*2**. This can be explained by the structure of the enamine: as it bears two methyl groups, the **39f-*R*2** approach should generate considerable steric strain with the phenyl group of **28**. Transition state **39f-*S*2** avoids this partially, however, sacrificing the extra stabilization through the electronic interaction. This should also explain the observed changes upon heating and pressurization. The more thermal energy is added,

* The *anti* products were only formed to a minor extent and could, therefore, not be investigated in detail for each adduct, however, analysis of residual traces revealed them to be almost racemic.

† This is in analogy to (*Si*,*Si*)-approach which is favored in the reaction with aldehydes **39a-e**.[85]

the higher the molecular motion becomes. This leads to less ordered transition states and makes steric repulsion more decisive, thus decreasing the overall enantioselectivity as the reaction is forced to proceed through **39f-*S*2** as well. In contrast, high pressures lead to volume constriction, overcoming steric strain and stabilizing ionic interactions due to electrostriction. Therefore, the reaction proceeds preferentially through **39f-*R*2**, resulting in the increased formation of (*R*)-**41f** as observed. The last aldehyde investigated was the challenging **39g**. As only HP conditions led to the formation of significant amounts of product, no comparison to the other activation modes could be drawn. The product (*R*)-**41g** was obtained with fair 64% *ee*, slightly lower than in the analogous (*R*)-**41f**, probably due to increased steric strain.

Overall, it can be clearly seen that HP conditions vastly improve the *syn* selectivity for racemic and asymmetric reactions, surpassing both AP/AT and HT conditions significantly. In contrast, the use of HT led to an increase in the formation of *anti* products. This might open up interesting synthetic strategies, as the *syn*/*anti* ratio can be directly influenced by using the appropriate activation mode. In the asymmetric reactions, the use of a secondary activation mode had only little effect on the enantioselectivity for aldehydes **39a-e**. However, symmetric aldehydes bearing only one α-proton (**39f-g**) were decisively influenced by the reaction conditions. Again, HP conditions improved enantioinduction while HT led to erosion of the stereochemistry.

2. Peptidic organocatalysts containing cyclic β-amino acids under pressure

2.1 Introduction

The last chapter demonstrated the efficacy of using amino acid derivatives as catalysts in organocatalytic asymmetric reactions. While these compounds account for a significant amount of catalysts in the field of organocatalysis, it is not limited to only using those. An important subset of organocatalysts is formed by short synthetic peptides, which can be seen as a link between small organic molecule organocatalysis and biocatalysis (using enzymes).

The use of peptides offers several potential advantages. Catalysts can be conveniently designed in a modular fashion using peptide coupling methodologies, allowing for the selective introduction of functional groups through the choice of appropriate amino acids. This allows for the design of structurally diverse, highly active catalysts which are able to adapt to certain transformations and substrates. At the same time, the reduced molecular size of the peptide can improve solubility in organic solvents compared to an equivalent enzyme.[130]

The use of short peptides to catalyze organic reactions is known for several decades, *e.g.* Thr-Ala-Cys-His-Asp in the hydrolysis of 4-nitrophenyl acetate (1968),[131] *poly*-Leu in the Juliá-Colonna epoxidation of olefins (1980),[132] and *cyclo*-Phe-Ser in the asymmetric hydrocyanation of aldehydes (1990).[133]* However, research on the subject was not picked up to a greater extent until 2000, with the "rediscovery" of organocatalysis[74,134] as an independent field in asymmetric catalysis.

Over the last years, several research groups have made significant contributions to the field of modern peptide organocatalysis. Especially the work of Miller *et al.* can be seen as pioneering, demonstrating the efficacy and versatility of short peptide-based catalysts in a wide range of applications, *e.g.* in asymmetric azidation-cycloadditions,[135] Stetter[136] and Baylis-Hillman[137] reactions, Baeyer-Villiger oxidations,[138] kinetic resolutions of alcohols[139] or as tools for site-selective modifications of natural products.[140] Besides studying their catalytic properties, Miller *et al.* also conducted structural investigations on the relationship between flexibility and secondary structure elements of peptides and the resulting implications on catalysis.[141]

* Note that in this thesis all amino acids which are abbreviated with the conventional three letter code and do not contain stereodescriptors are in the naturally occurring L-configuration. Exceptions are highlighted.

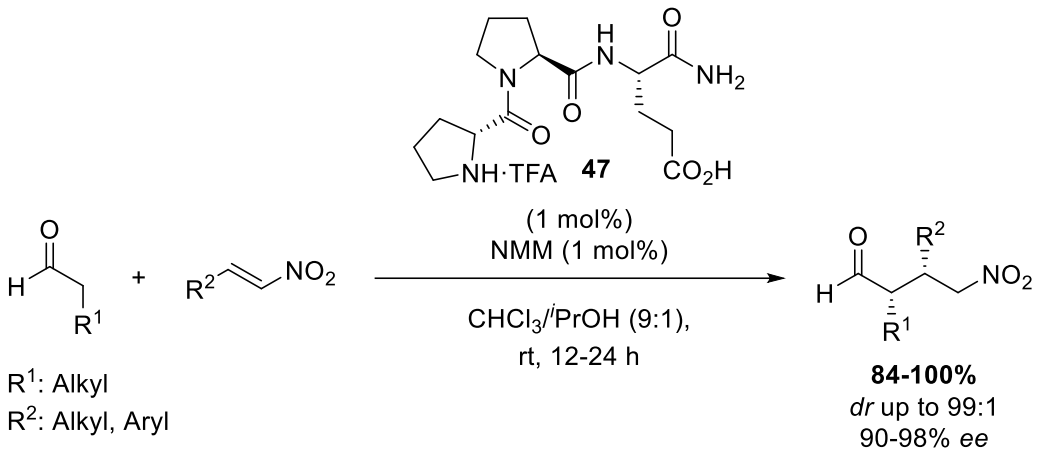

Scheme 20: Michael addition of aldehydes to nitroalkenes catalyzed by the synthetic tripeptide H-D-Pro-Pro-Glu-NH_2 (**47**) as published by Wennemers *et al*.[142] NMM = *N*-methylmorpholine.

Other important discoveries were made by Wennemers *et al.*, who discovered the catalytic efficiency of two privileged tripeptides, H-D-Pro-Pro-Glu-NH_2 (**47**) and H-Pro-Pro-Asp-NH_2 (**48**) While **47** proved to be remarkably active in asymmetric Michael reactions,[143,144,145] **48** showed excellent activity in asymmetric aldol additions (Scheme 20).[146,147]With complementary studies, they were able to determine functional group requirements for effective catalysis, *e.g.* demonstrating that amine (NH) and acid (CO_2H) groups in close spatial proximity are required to obtain optimal results.[142,147,148] Based on these discoveries, immobilized variants of the catalysts were developed which could even be employed in a microreactor setup under flow conditions.[149] Finally, supplementary investigations revealed in-depth information about the conformational behavior of the tripeptides[150] and the underlying mechanisms and intermediates of the reactions.[151,152]

In order to investigate the use of other than the natural α-amino acids, Reiser *et al.* introduced structurally confined *cis*-β-aminocyclopropane carboxylic acid (β-ACC, ▲) into their peptide catalysts.[153] This was done to ensure proper spatial arrangement of the functional groups, as cyclic β-amino acids are known to stabilize secondary structures.[154] From a library of several di-, tri- and tetrapeptides, H-Pro-▲-Pro-OH (**49**) turned out to be the best catalyst, efficiently catalyzing intra- and intermolecular aldol reactions with very good yields and good selectivities.[153] In 2014, Pilsl could show that the activity of the catalyst **49** could be significantly improved by using high-pressure conditions, without erosion of enantioselectivity.[155] These promising results initiated further research on the effect cyclic β-amino acids have when incorporated into tripeptides and how this influences the catalytic performance. Herein, special focus was laid upon the relationship between pressure activation and ring size of the β-amino acid, as larger rings increase the conformational freedom (and therefore flexibility) of the catalyst (Scheme 21). Peptides containing larger rings should be more susceptible to pressurization and conformational change, which could influence catalysis.

In cooperation with Botines[156] and Ortuño *et al.*,[157] *cis*-β-aminocyclobutane carboxylic acid (β-ACBC, ■) was introduced into the tripeptides and analyzed, while Ertl from the Reiser group investigated the corresponding *cis*-β-aminocyclopentane carboxylic acid (β-ACPC, ⬟)-containing peptides. [158] In this thesis, ultimately, the incorporation of *cis*-β-aminocyclohexane carboxylic acid (β-ACHC, ⬢) into tripeptides is discussed, thus generating the most flexible catalysts of the sequence (**52** and *ent*-**52**). Furthermore, a more rigid analog containing anthranilic acid (Ant), **53**, was synthesized. The efficacy of these catalysts was then evaluated in different organocatalytic reactions and compared to the other peptides, **49**, **50** and **51**.

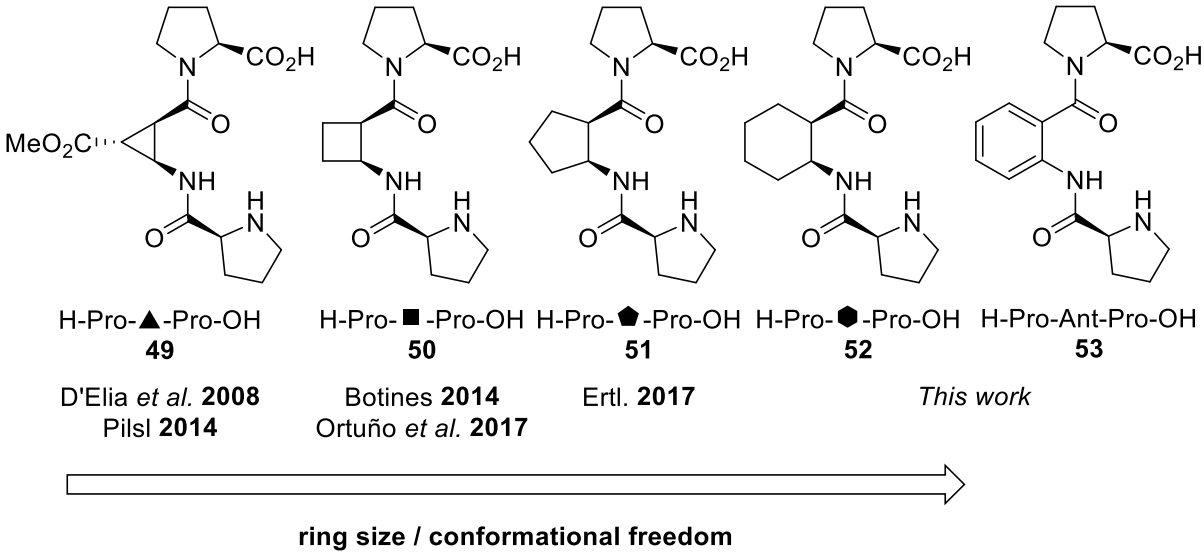

Scheme 21: Different tripeptides with the structural motif H-Pro-Xxx-Pro-OH containing cyclic β-amino acids of various ring size synthesized by Reiser *et al.* and Ortuno *et al.* In most cases, both *cis*-diastereomers of the catalysts were synthesized (Prolyl configuration was always L).

2.2 Synthetic approach to *cis*-β-ACHC

The synthesis of the *cis*-β-ACHC-containing tripeptides can be roughly divided into two parts: the synthesis of the unnatural cyclic amino acid and the peptide couplings with protected L-proline, followed by the deprotection of the tripeptide. As orthogonally protected L-proline derivatives are commercially available and due to the fact that a large variety of peptide coupling methodologies exist, the main focus of this work laid upon the reliable synthesis of the unnatural cyclic amino acid.

There are several literature known approaches to obtain protected *cis*-β-ACHC derivatives, in a racemic as well as a stereoselective manner.[159–161] In the following, three methodologies and their advantages and disadvantages will be elaborated to give an overview about potential synthetic approaches (see Scheme 22).

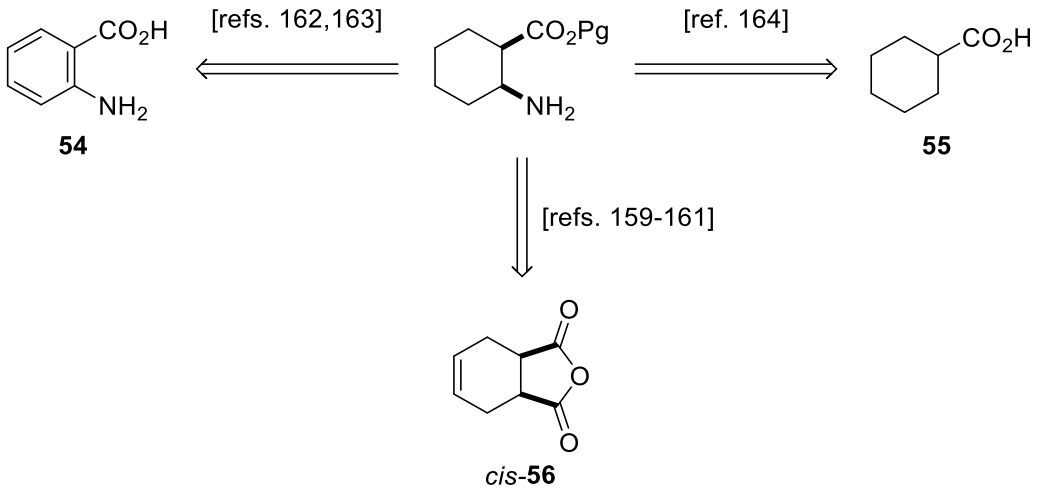

Scheme 22: Three potential starting materials for the synthesis of *cis*-β-ACHC derivatives.

Probably the shortest and most convenient route is the hydrogenation of anthranilic acid (**54**). Due to the mechanism involved, it usually also leads to the (in this case desirable) exclusive formation of the racemic *cis* adduct in 60% yield.[162] However, as is common with the hydrogenation of aromatic compounds, the use of rather harsh conditions and expensive catalysts like rhodium is required, to overcome the significant aromatic stabilization.[163] Furthermore, at this point there are no known asymmetric variants for this particular transformation, limiting its usefulness even more.

A second approach, which is more flexible in terms of stereoselectivity, is a methodology developed by Davies *et al.* from 1994.[164] Herein, cyclohexanecarboxylic acid (**55**) was used as starting material, transformed into the α,β-unsaturated *tert*-butyl ester and then subjected to a conjugate addition with a sterically demanding homochiral lithium amide. Changing the stereochemistry of the lithium amide and using low-temperature conditions enabled the selective synthesis of both *cis* adducts with excellent diastereomeric excess (> 95%). However, a major drawback was the efficiency of the process. The generation of the conjugate acceptor alone resulted in only 30% yield, after the conjugate addition, it dropped even further to just 21% overall yield. This, combined with the fact that the experimental procedure is rather elaborate, rendered this not the method of choice for the β-ACHC synthesis.

The third approach is based on the fact that six-membered rings can be conveniently generated through [4+2]-cycloaddition reactions (the Diels-Alder reaction). The diastereoselectivity of these reactions is based on the structure of the reactants, allowing facile access to exclusively *cis*-disubstituted products. In the synthesis of β-ACHC, the key compound is *cis*-4-Cyclohexene-1,2-dicarboxylic anhydride (*cis*-**56**) which is obtained through a Diels-Alder reaction of 1,3-butadiene and maleic anhydride. The anhydride *cis*-**56** can then be desymmetrizied and the resulting hemiester transformed into the orthogonally protected β-ACHC by the use of the Curtius reaction.[159–161]

This pathway was chosen for the tripeptide synthesis and will be elucidated later in the upcoming chapter. With a suitable way identified to synthesize the β-ACHC, the focus then turned to the actual diastereo- and enantioselective synthesis of the tripeptides.

2.3 Synthesis of the flexible tripeptides from racemic β-ACHC

As mentioned earlier, the concept of cyclic *cis*-β-amino acid-containing tripeptides as organocatalysts is not a new one. In their original approach from 2008, Reiser *et al.* coupled racemic β-ACC (*rac*-**57**) with commercially available *N*-Boc-L-Proline (**58**), resulting in a diastereomeric mixture of the protected dipeptide. Fortunately, the two diastereomers, Boc-Pro-▲-OMe (**59**) and Boc-Pro-▼-OMe (**60**), could be cleanly separated by column chromatography. This simplified the synthetic process, as no extra step had to be employed to obtain the β-ACC in an enantiopure form, hence generating both desired dipeptides in a one-pot fashion, rather than having to synthesize them in separate processes.[153] For these reasons, this approach was also chosen for the preparation of the peptides containing β-ACHC, first synthesizing the cyclic amino acid, then coupling it with *N*-Boc-L-Proline (**57**) and separating the resulting diastereomeric dipeptides.

The Diels-Alder reaction was chosen as the go-to method to obtain the required *cis*-disubstituted cyclohexane derivatives, in this case, *cis*-4-Cyclohexene-1,2-dicarboxylic anhydride (*cis*-**56**).[159–161] *cis*-**56** can be formally obtained by reacting maleic anhydride (**61**) with 1,3-butadiene.[165] However, rather than using gaseous 1,3-butadiene, solid 3-sulfolene (**62**) was chosen as the 1,3-butadiene source. 3-Sulfolene (**62**) is a shelf-stable, easy to handle solid and, upon heating, readily undergoes a [4+1]-Retro-Diels-Alder reaction, releasing 1,3-butadiene and sulfur dioxide.[166–168] Using the thermally induced reaction of **62** with maleic anhydride (**61**), *cis*-4-Cyclohexene-1,2-dicarboxylic anhydride (*cis*-**56**) was successfully synthesized on a 500 mmol scale, achieving a very good yield and purity.[168,169] As predicted from the Diels-Alder reaction mechanism involved, no formation of the *trans* product could be observed. The next step was the ring opening of the anhydride in such a fashion, that one of the resulting carboxylic acid moieties remained unchanged, while the other had to be protected. The introduction of a methyl ester group was chosen, as it provides orthogonality to the Boc-group which was about to be introduced later in the peptide coupling. This was accomplished by simply refluxing the anhydride in methanol, and gave rise to the racemic methyl hemiester *rac*-**63** in quantitative yield. The next step towards the cyclic β-amino acid now required the conversion of the free carboxylic acid moiety into an amine functionality. A useful way to achieve this is by using the Curtius rearrangement. It involves the preparation of an acyl azide, which thermally rearranges to the isocyanate. Subsequent

trapping with a nucleophile then generates a substituted amine (often an amide).[170] One of the first implementations of this strategy for the synthesis of β-ACHC was done by Kobayashi *et al.* in 1990.[171] However, older protocols for this process are somewhat tedious, as they require several individual steps (activation of the carboxylic acid, azidation, rearrangement) and the use of hazardous and even potentially explosive compounds, *e.g.* NaN_3 and the intermediary acyl azides.[172] Fortunately, by using diphenyl phosphoryl azide (DPPA) these issues can be circumvented and the complete rearrangement can be performed in a one-pot protocol.[173] Following the procedure from Timpano *et al.,*[174] and using benzyl alcohol as trapping reagent, enabled the direct synthesis of racemic, Cbz-protected β-ACHC *cis*-**64** in good yield.* The final step before peptide coupling consisted of hydrogenolysis of the Cbz group and the hydrogenation of the double bond. Both could be achieved simultaneously, giving rise to the racemic β-ACHC methyl ester, H-(±)-⬢-OMe (*rac*-**65**), in 52% yield over four steps.

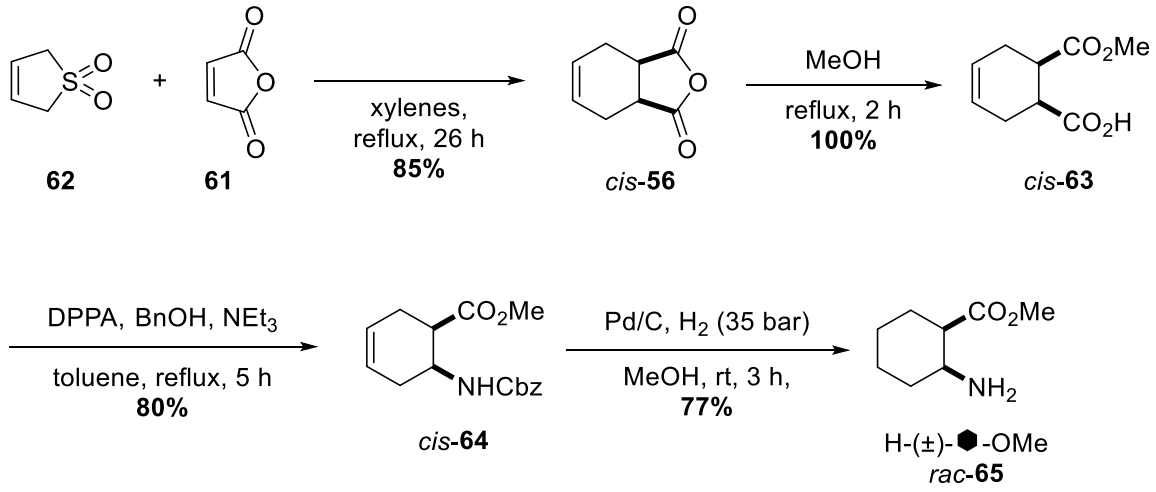

Scheme 23: Synthesis of racemic H-(±)-⬢-OMe (*rac*-**65**).

After successful synthesis of the racemic building block, the next step involved the coupling with *N*-Boc-L-proline (**58**), which was accomplished with a standard protocol using EDC hydrochloride (EDC·HCl).[153,155] The diastereomeric mixture Boc-Pro-(±)-⬢-OMe (*rac*-**66**) was obtained in good yield (72%). However, in contrast to the β-ACC-containing dipeptides of Reiser *et al.*, separation of the two diastereomers of the β-ACHC-dipeptide *rac*-**66** was unsatisfactory. To improve separability, the synthesis was continued further to the tripeptide stage. This required the selective deprotection of the methyl ester using LiOH,[176] followed by the second peptide coupling with L-Proline benzyl ester (**67**),

* The Cbz-group was chosen again with consideration to orthogonality, as it could be easily cleaved through hydrogenation. The purification of the crude product proved to be tedious, as BnOH was difficult to separate from the product due to similar R_f values. This issue was addressed by Gellman *et al.* in 2000. By skipping the purification of the Curtius product and performing the hydrogenolysis immediately afterwards this could be solved, as the BnOH could then be easily removed by extraction.[175] For similar reasons, this process was later also used in the synthesis of the β-ACHC containing tripeptides.

again using the EDC hydrochloride protocol.[153,155] Diastereomer separation was reattempted but unfortunately led to similar negative results as before. As further reaction steps only included the deprotection of the tripeptide (*rac*-**68**), a third and final attempt was made there. The first step, the Boc deprotection, was performed with HCl in ethyl acetate, a process already used by Reiser *et al*.[153,177] The resulting free amine moiety led to an increased polarity of the compound which was thought to aid the separation, however, even this was not sufficient. Despite this, the synthesis was still completed with the hydrogenolysis of the Cbz group, giving rise to the finished tripeptide in 23% overall yield from maleic anhydride (**61**), albeit as a diastereomeric mixture.

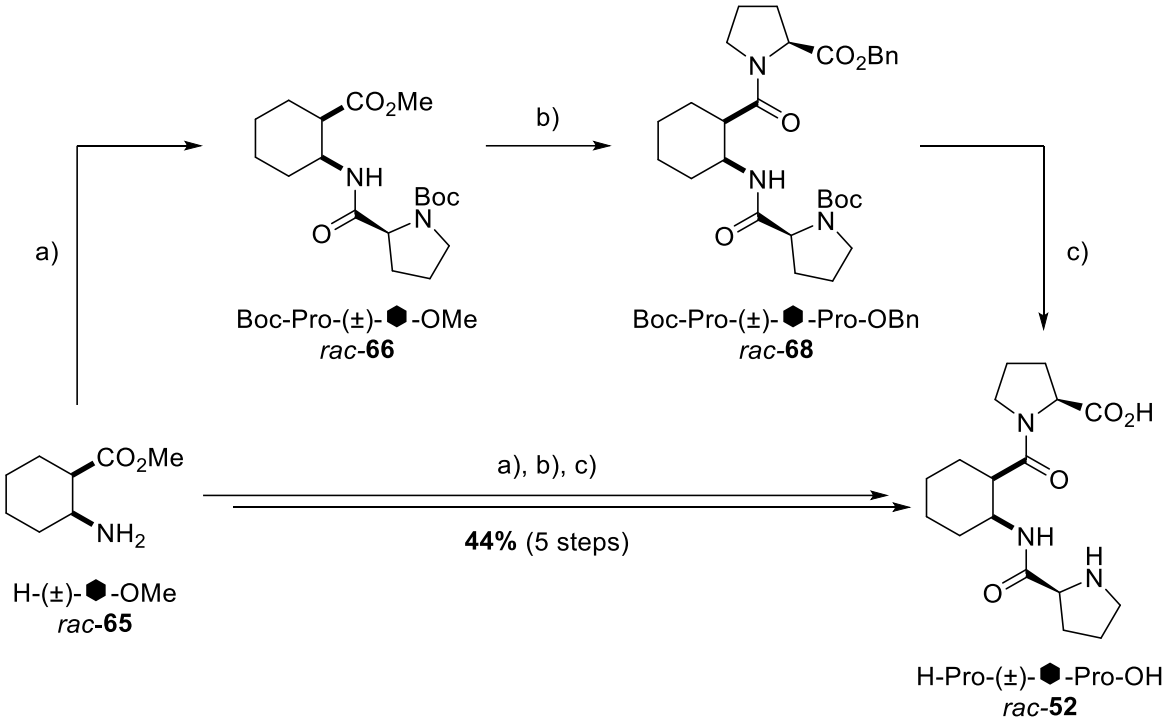

Scheme 24: Synthesis of the diastereomeric mixture H-Pro-(±)-⬢-Pro-OH (***rac*-52**). Reaction conditions: a) *N*-Boc-Pro-OH (**58**), EDC·HCl, NEt_3, DCM, rt, 22 h, 72%; b) 1.) LiOH, THF/H_2O, 0 °C to rt, 2 h, 2.) H-Pro-OBn·HCl (**67·HCl**), EDC·HCl, NEt_3, DCM, rt, 46 h, 79% (2 steps); c) 1.) HCl/EtOAc, 0 °C, 3 h, 2.) Pd/C, H_2 (1 bar), MeOH, rt, 1 h, 77% (2 steps).

The poor separability of the diastereomers might be attributed to the presence of the cyclohexane ring, as it allows the peptides a higher degree of conformational freedom compared to the rigid cyclopropane ring present in the β-ACC-peptides. The increased conformational ambiguity of the β-ACHC diastereomers could be the reason for their higher chemical similarity and, therefore, hampers their separation in chromatography. To still arrive at diastereomerically (and enantiomerically) pure β-ACHC-containing tripeptides, another pathway had to be found.

2.4 Synthesis of the flexible tripeptides from enantiomerically enriched β-ACHC

While synthesizing the tripeptides from racemic β-ACHC turned out to be unfeasible, a viable option appeared to be the use of enantiomerically enriched β-ACHC. This would eliminate the need to separate the diastereomers after peptide coupling.

Several methods to achieve this goal have already been mentioned in chapter 2.2.[159–161] However, rather than changing the complete procedure, it was decided to stick to the initial approach of using the Diels-Alder reaction to build up the core cyclohexane scaffold. Hence, a process had to be found which allowed the enantioselective synthesis of one of the intermediates in this procedure. When looking at the aforementioned synthetic route (Scheme 23), it quickly becomes clear that there are only two steps which have an impact on the stereochemical outcome of the products: the initial Diels-Alder reaction or the subsequent generation of the hemiester **63-Pg**.* While there are literature protocols for racemic synthesis through Diels-Alder reactions,[178] enantioselective routes are rather scarce, especially for unsubstituted, monocyclic β-ACHC. The intramolecular 1,3-dipolar cycloaddition of unsaturated nitrones fused with chiral auxiliaries, which then generate isoxazolidines, has been successfully used in the synthesis of the homologous β-ACPC.[179] A transfer of the procedure to β-ACHC through chain elongation of the starting material could be feasible, however, the required chemicals are expensive and the synthetic effort demanding. This, overall, renders the use of an enantioselective Diels-Alder reaction a rather unsuitable approach.

Fortunately, the subsequent reaction intermediate, hemiester **63-Pg**, is significantly easier to obtain in enantiopure form. Over the last decades, a variety of different methods and procedures have been developed to address this particular problem, with the majority revolving around one common theme: the desymmetrization of *meso* compounds.[180,181] A small overview of the available methods is depicted in Scheme 25.

* The other transformations (*i.e.* the Curtius reaction and the Cbz deprotection) do not alter the stereocenters and are, therefore, uncapable of changing the stereochemistry of the product.

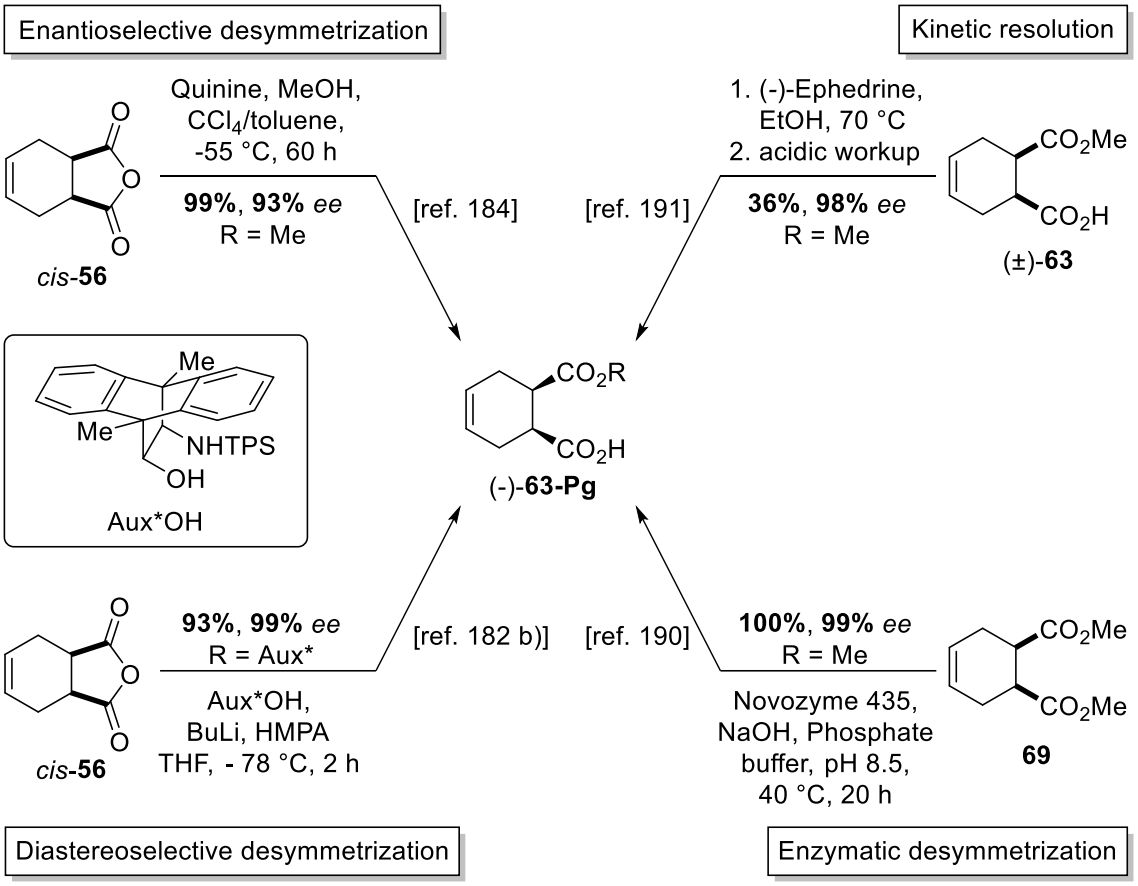

Scheme 25: Literature examples of different approaches to the enantioselective synthesis of hemiesters (-)-**63-Pg**.

Anhydride *cis*-**56** belongs to this group and is often used as a common starting point in a number of approaches. In order to achieve desymmetrization, the anhydride *cis*-**56** is opened using either a diastereoselective or an enantioselective ring opening reaction.

The diastereoselective route usually involves the use of nucleophiles bearing chiral auxiliaries to open the anhydride. This leads to the formation of diastereomers, which then have to be separated. While these processes can be highly efficient, they also often rely on very elaborate chiral auxiliaries which can be very expensive and tedious to synthesize or require hazardous chemicals. Additionally, the auxiliaries must be removed to allow for subsequent transformations, which might be complicated (especially when using N-nucleophiles as auxiliaries).[182]

In the enantioselective desymmetrization route, a chiral compound acts as stereoinducing mediator for other nucleophiles. Through creating a well-defined complex with the substrate they only allow the attack of nucleophiles from certain directions, thus directly generating the enantioenriched product.[180] Over the years, many compounds have been used to achieve stereoinduction: Lewis acids (*e.g.* Ti-TADDOLates[183]), Lewis bases (*e.g.* cinchona alkaloids,[184–187] thiourea organocatalysts[188,189]) or enzymes[190–193]. Especially with enzymes, the use of *meso* diester **69** instead of anhydride *cis*-**56** gave considerably better results.[190]

Besides the desymmetrization approach, the kinetic resolution of the methyl hemiester *cis*-**63** is also feasible. Several different chiral amines have been known to form diastereomeric salts with *cis*-**63** (*e.g.* (-)-ephedrine,[191] (+)-dehydroabietylamine[191] or cinchonidine[194]). Nearly enantiopure product can be obtained after recrystallization and acidic extraction. As with every kinetic resolution, the maximum achievable yield of the enantiomers is limited to 50% when starting from the racemic material.

After careful consideration, three different approaches were chosen to obtain both enantiomers of the methyl hemiester *cis*-**63** (Scheme 26).

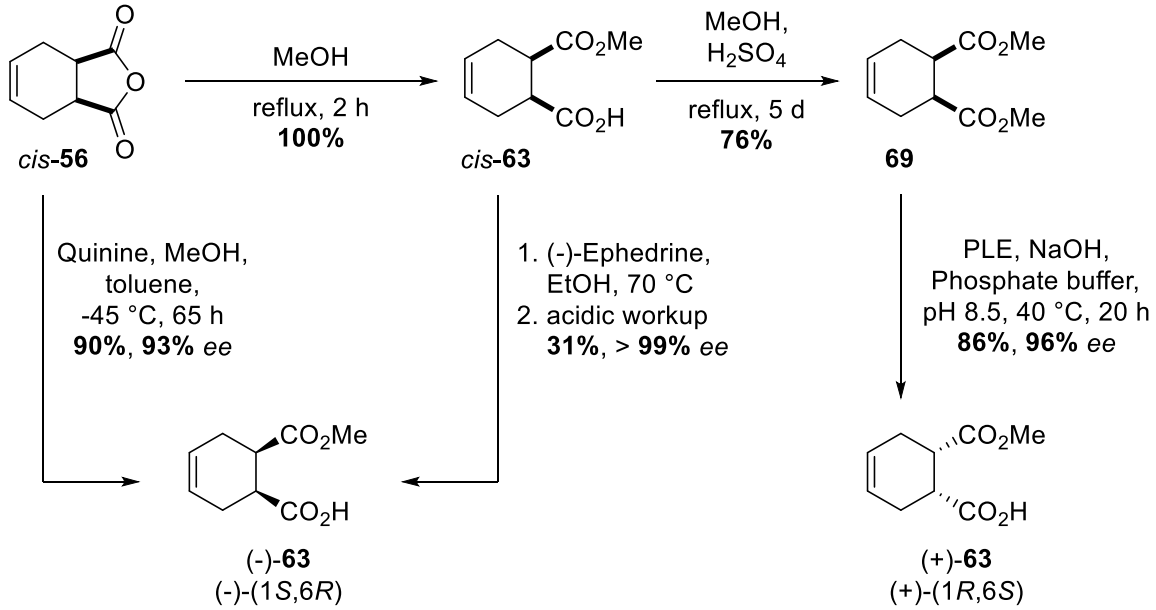

Scheme 26: Desymmetrization of meso anhydride (*cis*-**56**) to obtain both enantiomers of hemiester **63**. PLE = pig liver esterase.

The first attempt at generating enantiopure (-)-**63** was conducted using the quinine mediated desymmetrization of *meso* anhydride *cis*-**56** first published by Bolm *et al.* in 1999 (see Scheme 25, upper left).[186] The original protocol was, however, slightly modified. The reaction performed equally well in pure toluene, thus avoiding the use of hazardous CCl_4.* Additionally, the temperature could be increased to -45 °C without having detrimental effects on the enantioselectivity. While the method required stoichiometric amounts of quinine and long reaction times at low temperatures, it gave hemiester (-)-**63** in very good yield (90%) and satisfying enantiopurity (93% *ee*). As recrystallization of (-)-**63** itself, in order to improve enantiopurity, is complicated due to its low melting point and tendency to form oils, the second approach was the kinetic resolution of the racemic hemiester *cis*-**63**. In 1986,

* This was already discovered by Bolm *et al.* in a follow-up publication in 2000, as they tested the desymmetrization of various *meso* anhydrides in pure toluene rather than in the CCl_4/toluene mixture. They concluded that very similar results could be obtained with most substrates, although it required lower concentrations of the anhydrides.[184]

Gais *et al.* successfully separated the racemate *cis*-**63** by forming the diastereomeric salt with (-)-ephedrine and subsequent recrystallization.[191] Utilizing this procedure gave access to enantiopure hemiester (-)-**63** (> 99% *ee*) after recrystallizing the salt three times, although, in rather limited yields (31%). However, this issue could be mitigated as the process itself was easy to scale up, resulting in several grams of enantiopure material.*

As both methods to obtain (-)-**63** required the use of stoichiometric amounts of chiral compounds (although recovery was possible in both cases), a third method was chosen to synthesize the other enantiomer, (+)-**63**. In 1983, Mohr *et al.* first published the use of pig liver esterase (PLE) for the selective saponification of symmetrical diesters, including the synthesis of (+)-**63** from *meso* diester **69** in 95% yield with 85% *ee*.[193] This process was picked up quickly by other researchers and many iterations with slightly changed conditions were published over the last decades.[171,190–192] Using a slightly modified procedure from Kobayashi *et al.*,[171] the hemiester (+)-**63** could be obtained with very good yields and good enantiopurity (96% *ee*). Both enantiomers in hand, the diastereomerically pure synthesis of the β-ACHC-containing tripeptides could now be reattempted (Scheme 27).

The hemiesters were again subjected to the Curtius rearrangement. As previously mentioned, the required excess of BnOH complicated the purification of the product. The resulting Cbz-protected β-ACHCs were, therefore, not purified, but immediately subjected to hydrogenolysis. The resulting, slightly volatile, free amines were conveniently separated by extraction and then directly coupled with *N*-Boc-L-Proline (**58**) to obtain the respective dipeptides. For the synthesis of Boc-Pro-(-)-⬢-OMe (**66**), the previously described EDC hydrochloride protocol was used again, as it gave good results earlier in the preparation of the diastereomeric mixture *rac*-**66**. This time, however, due to the use of enantioenriched β-ACHC, almost no other diastereomer was formed, meaning the successful synthesis of pure Boc-Pro-(-)-⬢-OMe (**66**) from (-)-**63** in 34% yield over three steps. Following the route used earlier, the methyl ester of the dipeptide **66** was saponified and the free carboxylic acid coupled with H-Pro-OBn with EDC·HCl,[153,155] eventually giving rise to the diastereomerically pure tripeptide and Boc-Pro-(-)-⬢-Pro-OBn (**68**) in 90% yield over two steps. Two-step deprotection using first EtOAc/HCl[153,177] for Boc- and secondly hydrogenolysis for Bn-deprotection finally gave rise to enantio- and diastereomerically pure H-Pro-(-)-⬢-Pro-OH (**52**) in 28% overall yield from enantioenriched (-)-**63**.

* This method could also allow for the isolation of the other enantiomer, (+)-**63**, from the mother liquor after recrystallization. Gais *et al.* were able to obtain highly enantioenriched (+)-**63** (98% *ee*) through inverse recrystallization. After liberating the free acid from the residue of the mother liquor, they added seed crystals of (±)-**63** to the enantioenriched solution, which led to an increase of the *ee* in the solution.[191] Similar attempts were made, however, 76% *ee* for (+)-**63** was the highest level of enantioinduction which could be achieved.

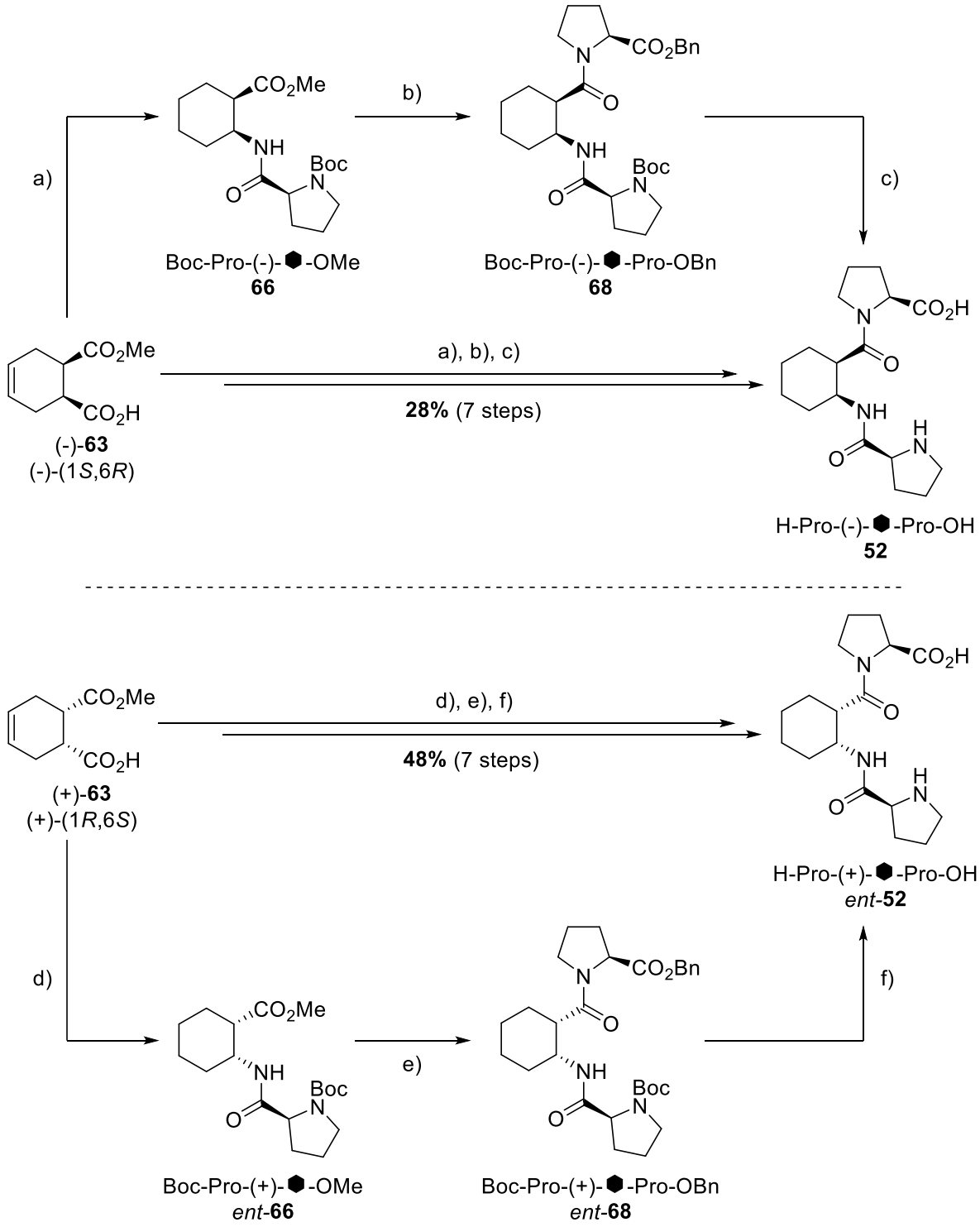

Scheme 27: Synthesis of diastereomeric H-Pro-(-)-⬢-Pro-OH (**52**) and H-Pro-(+)-⬢-Pro-OH (*ent*-**52**). Reaction conditions: a) 1.) DPPA, BnOH, NEt_3, toluene, reflux, 4 h, 2.) Pd/C, H_2 (30 bar), rt, 4 h, 3.) *N*-Boc-Pro-OH (**58**), EDC·HCl, NEt_3, DCM, rt, 22 h, 34% (3 steps); b) 1.) LiOH, THF/H_2O, 0 °C to rt, 3 h; 2.) H-Pro-OBn·HCl (**67·HCl**), EDC·HCl, NEt_3, DCM, rt, 24 h, 90% (2 steps); c) 1.) HCl/EtOAc, 0 °C, 3.5 h; 2.) Pd/C, H_2 (1 bar), MeOH, rt, 3 h, 92% (2 steps); d) 1.) DPPA, BnOH, NEt_3, toluene, reflux, 4 h, 2.) Pd/C, H_2 (45 bar), rt, 19 h, 3.) *N*-Boc-Pro-OH (**58**), T3P, pyridine, EtOAc, -10 °C to rt, 20 h, 64% (3 steps); e) 1.) LiOH, THF/H_2O, 0 °C to rt, 21.5 h; 2.) H-Pro-OBn·HCl (**67·HCl**), T3P, pyridine, NEt_3, -10 °C to rt, 48 h, 82% (2 steps); f) 1.) HCl/EtOAc, 0 °C to rt, 22 h; 2.) Pd/C, H_2 (1 bar), MeOH, rt, 20 h, 91% (2 steps).

The synthesis of the diastereomer, H-Pro-(+)-⬢-Pro-OH (*ent*-**52**), was conducted in a similar fashion.

However, minor changes were made for the peptide couplings. As the EDC hydrochloride mediated coupling often gave varying and sometimes sluggish results, another reagent, *n*-propylphosphonic anhydride (T3P), was tested. T3P was introduced by Dunetz *et al.* and shown to be a reliable, easy-to-handle coupling reagent, outperforming EDC·HCl in terms of epimerization.[195] With T3P, the pure dipeptide Boc-Pro-(+)-⬢-OMe (*ent*-**66**) was successfully synthesized from (+)-**63** after using the Curtius/hydrogenolysis/peptide coupling sequence, this time in 64% yield. The subsequent methyl ester deprotection and second peptide coupling (again using T3P) gave rise to pure Boc-Pro-(+)-⬢-Pro-OBn (*ent*-**68**) in 82%.

The synthesis was again completed by the deprotection of the Boc- and Bn-groups, this time giving rise to enantio- and diastereomerically pure H-Pro-(+)-⬢-Pro-OH (*ent*-**52**) in 48% overall yield from enantioenriched (+)-**63**.

The diastereomeric purity of both peptides could be proven at the protected dipeptide and tripeptide stage using chiral HPLC analysis. In contrast to the β-ACC-containing tripeptides from Reiser *et al.*,[155] it was possible to crystallize H-Pro-(-)-⬢-Pro-OH (**52**) from methanol and obtain suitable crystal for X-ray analysis (Figure 7).

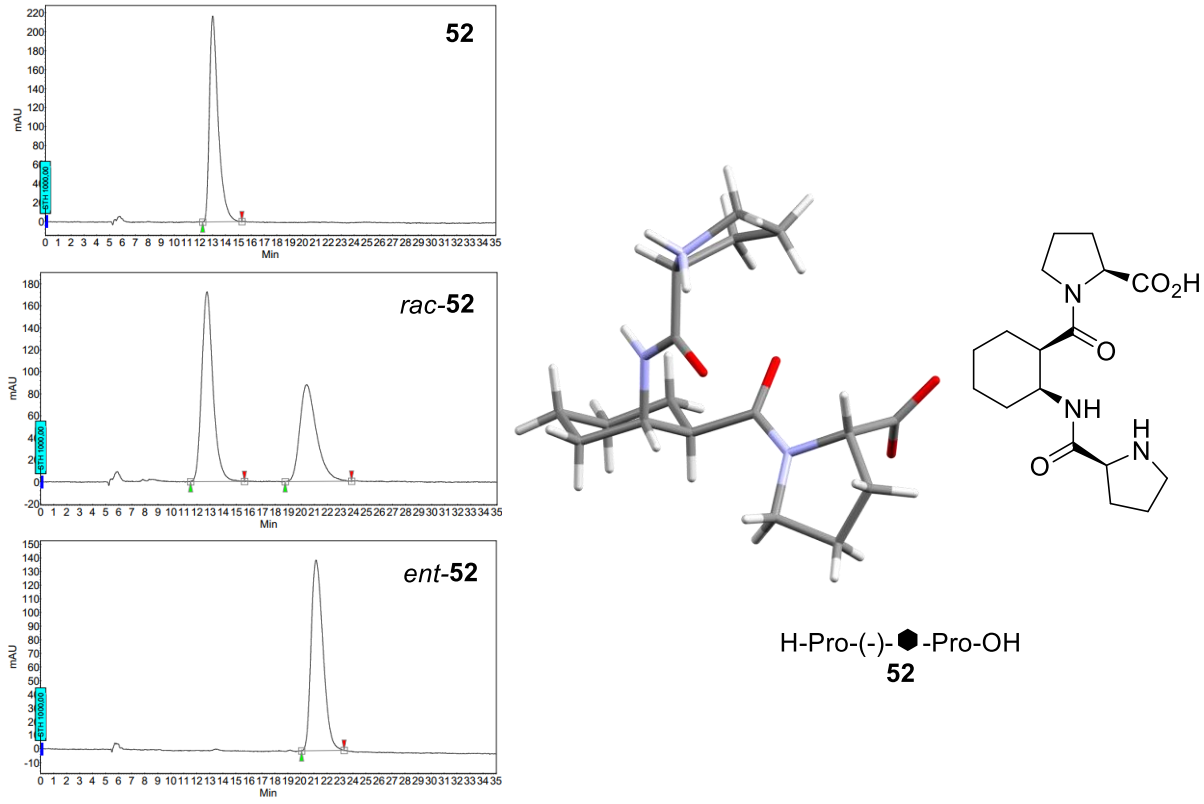

Figure 7: Left: chiral HPLC chromatograms from the Boc/Bn-protected tripeptides. Upper left: pure **52**, center left: diastereomeric mixture *rac*-**52**, bottom left: pure *ent*-**52**. Right: crystal structure from H-Pro-(-)-⬢-Pro-OH (**52**), proving the *cis*-configuration of the β-ACHC in the final product. As expected, the peptide exists in zwitterionic form.

The crystal structure not only proved the successful synthesis of H-Pro-(-)-⬢-Pro-OH (**52**), but also confirmed the *cis*-configuration of the β-ACHC. As expected, the peptide appears to reside in a zwitterionic form. Interestingly, the two charged functional groups, the amine and the carboxylic acid, do not form an intramolecular ionic bond and pointed away from each other. They tend to form intermolecular interactions between another molecule of **52** and incorporated solvent molecules (MeOH). This was rather concerning, as Pilsl and Reiser *et al.* reported the importance of spatial proximity of the functional groups in order to catalyze organic reactions in an effective and selective manner.[153,155] However, the orientation of functional groups in a solid crystal structure does not directly translate into a similar behavior in the liquid phase, where molecules usually exhibit a much higher flexibility and often very different bonding properties.

In a combined effort with Ertl[158] to further simplify the reaction sequence, the use of *N*-Cbz-L-Proline (**70**) instead of *N*-Boc-L-Proline (**58**) was considered. This would allow the complete deprotection of the tripeptides in only one step *via* hydrogenolysis. Test reactions gave Cbz-protected tripeptide *ent*-**72** in diastereomerically pure form. Hydrogenolysis of *ent*-**72** resulted in quantitative amounts of the deprotected tripeptide *ent*-**52**, proving the viability of this synthetic route.

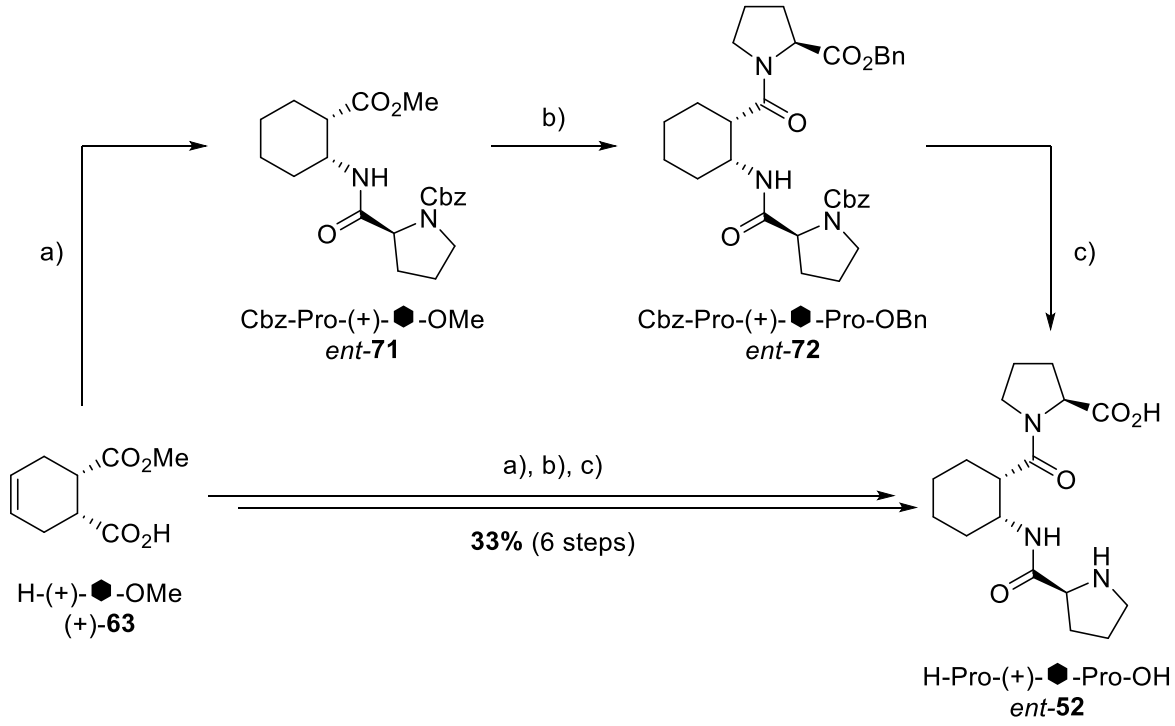

Scheme 28: Alternative synthetic route towards H-Pro-(+)-⬢-Pro-OH (**52**) using *N*-Cbz-L-Proline (**70**). Reaction conditions: a) 1.) DPPA, BnOH, NEt_3, toluene, reflux, 4 h, 2.) Pd/C, H_2 (45 bar), rt, 16 h, 3.) *N*-Cbz-Pro-OH (**70**), T3P, pyridine, EtOAc, -10 °C to rt, 65 h, 44% (3 steps); b) 1.) LiOH, THF/H_2O, 0 °C to rt, 21.5 h, 2.) H-Pro-OBn·HCl (**67·HCl**), T3P, pyridine, NEt_3, EtOAc, -10 °C to rt, 48 h, 74% (2 steps); c) Pd/C, H_2 (40 bar), MeOH, rt, 25 h, 100%.

2.5 Synthesis of the rigid peptide H-Pro-Ant-Pro-OH

After the flexible tripeptides **52** and *ent*-**52** had been successfully obtained in diastereomerically pure form, the focus now turned to the synthesis of a counterpart containing a rigid β-amino acid. Such a system with low conformational freedom would then serve as a reference point in the upcoming catalytic evaluation of the β-ACHC-tripeptides.

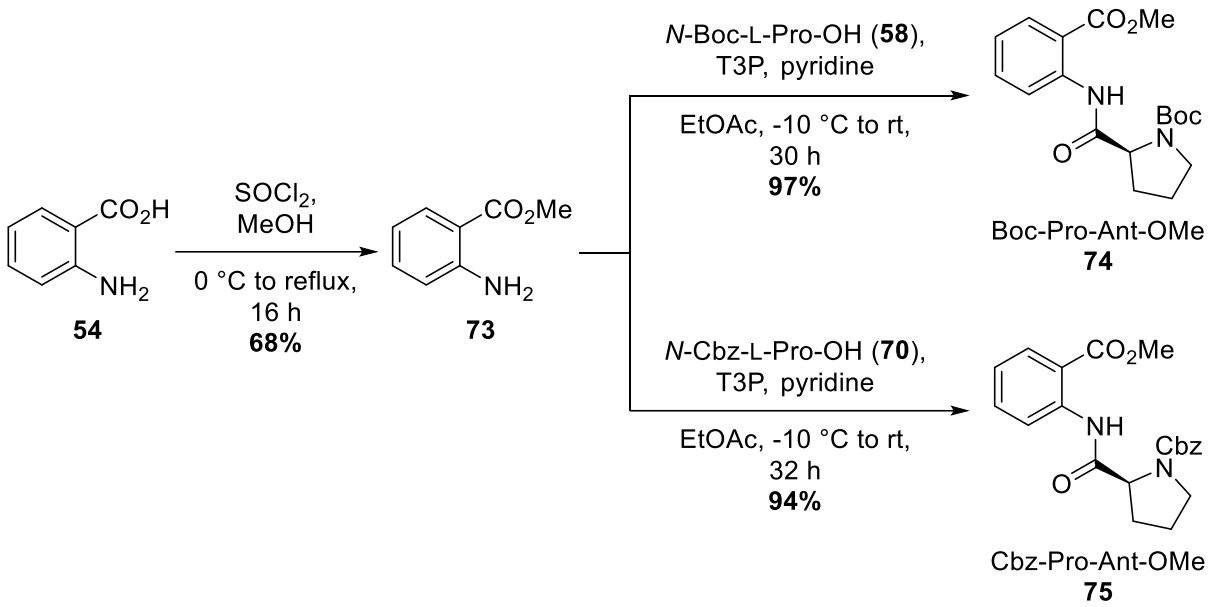

Scheme 29: Synthesis of Boc-Pro-Ant-OMe (**74**) and Cbz-Pro-Ant-OMe (**75**).

The obvious β-amino acid to choose was anthranilic acid (Ant, **54**). Its structure is closely related to β-ACHC and its core is, due to its aromatic character, completely inflexible. Literature procedures for the synthesis of the protected tripeptides Boc-Pro-Ant-Pro-OBn (**77**) and Cbz-Pro-Ant-Pro-OBn (**78**) are known, using commercially available anthranilic acid **53** as starting material.[196,197] These procedures have a high resemblance to the protocols used for the generation of the flexible peptides, requiring the formation of the methyl ester **73** as the first step as well. **73** was obtained in fair yield (68%) using standard thionyl chloride activation.[198] It was then subjected to the first peptide coupling and both, the Boc- and the Cbz-protected dipeptide (**74**[196,199] & **75**[200]), could be prepared in excellent yields (Scheme 29). Continuing on, the methyl esters were saponified with LiOH and the now deprotected dipeptides coupled with H-Pro-OBn. However, the reaction turned out to be rather sluggish. Standard conditions with T3P as coupling reagent provided only very poor yields: 21% for Boc-Pro-Ant-Pro-OBn (**77**)[197] and 15% for Cbz-Pro-Ant-Pro-OBn (**78**). A small study with Boc-Pro-Ant-OH (**76**) was, therefore, conducted to examine whether different coupling reagents could result in improved yields (Table 3).

Table 3: Various reaction conditions tested for the synthesis of Boc-Pro-Ant-Pro-OBn (**80**).

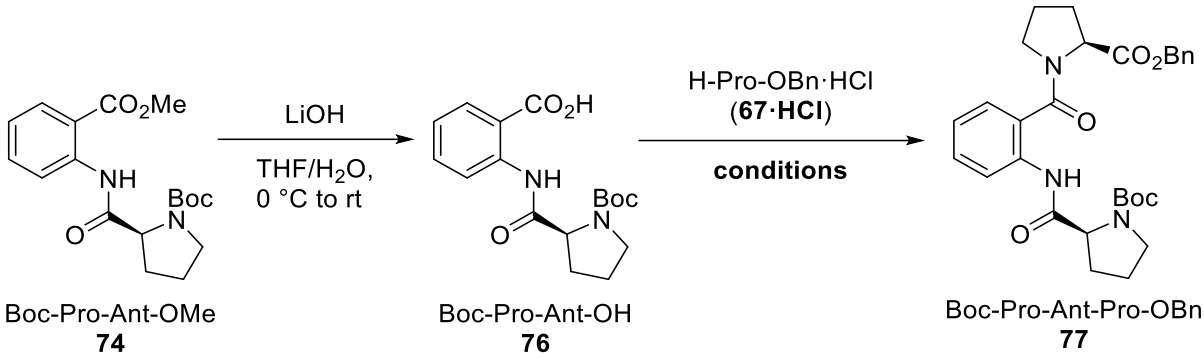

Boc-Pro-Ant-OMe **74** | Boc-Pro-Ant-OH **76** | Boc-Pro-Ant-Pro-OBn **77**

Entry	Conditions	Isolated yield (over 2 steps)	Remarks
1	T3P, pyridine, NEt_3, EtOAc, -10 °C to rt, 100 h	21%	SM partially recovered alongside side product
2	EDC·HCl, NEt_3, DCM, 0 °C to rt, 50 h	-	Inseparable mixture
3	EDC·HCl, HOBt, NEt_3, DCM, rt, 22 h	36%	SM partially recovered
4	COMU, DIPEA, DCM, 0 °C to rt, 4 h	30%	SM partially recovered

The first attempt was made with previously mentioned EDC·HCl. Unfortunately, this only led to the formation of a complex, inseparable mixture and no product could be isolated. A second attempt was made by using the more effective combination of EDC·HCl and HOBt. This method was successfully employed by Vijayadas *et al.* in their synthesis of several di- and tripeptides with a Pro-Ant motif, and apparently resulted in very good yields (86%) of Boc-Pro-Ant-Pro-OBn (**77**).[197] With additional HOBt, it was actually possible to obtain **77**, although only in poor yield (36%), yet still better than with T3P. As a final test, another coupling reagent was used: COMU, an uronium-type combined coupling- and activation reagent of the Oxyma family. Over the past years, COMU proved to be a valid, less dangerous alternative to benzotriazole-based coupling reagents like HATU, with a similar or even better performance.[201] While the COMU-mediated coupling of **76** with H-Pro-OBn (**67**) was significantly faster than with the other coupling reagents, still only 30% of **77** could be isolated in pure form. The overall poor performance of all applied reaction conditions triggered a small investigation for possible causes and could be traced to severe side product formation, which will be elucidated in a separate chapter (see chapter 2.6).

Although all reaction conditions worked poorly, pure Boc-Pro-Ant-Pro-OBn (**77**) could eventually be synthesized in a sufficiently large quantity which made progression of the synthesis possible. Boc-/Bn-deprotection was accomplished in analogy to the β-ACHC-tripeptides and H-Pro-Ant-Pro-OH (**53**) was finally obtained in 22% overall yield over six steps (Scheme 30).

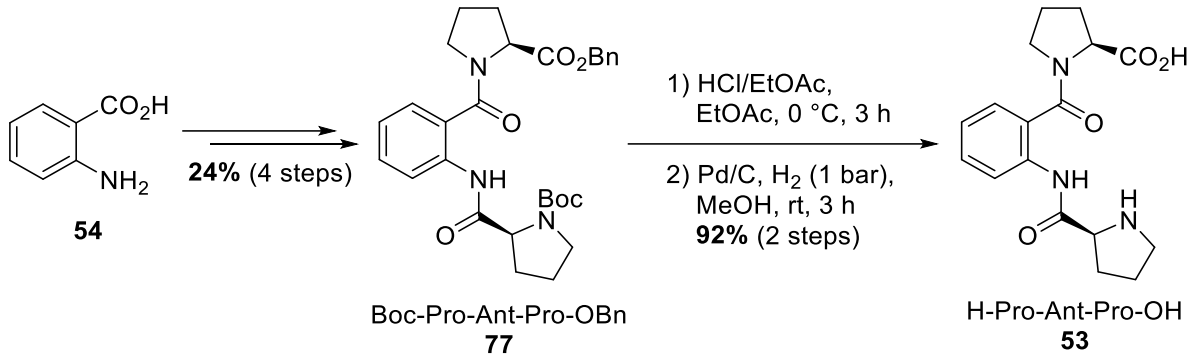

Scheme 30: Final steps in the synthesis of H-Pro-Ant-Pro-OH (**53**) from **54**.

With all three tripeptides in hand, evaluation of the catalytic activity was examined to gain more insight into the relationship between conformational freedom, catalyst performance and high-pressure conditions (chapter 2.7).

2.6 Identification of the side product obtained in the synthesis of H-Pro-Ant-Pro-OH

As mentioned in the previous chapter, the synthesis of H-Pro-Ant-Pro-OH (**53**) was severely hampered by the extremely poor outcomes of the second peptide coupling, a problem that persisted even when using various different coupling strategies. In order to understand the probable causes, the reaction was analyzed in more detail.

An initial point was an observation made with all conditions in the test reactions with the Boc-dipeptide **76**. The TLC analysis clearly showed the formation of a second product, with higher R_f values than the actual product. However, isolation of this side product was more difficult than expected, as it was always accompanied by another compound, the starting material **76**. This was especially odd, as **76** should have either been completely consumed during the reaction or (if not completely converted) retain on the silica column due to its high polarity caused by the free carboxylic acid group. Therefore, it was considered that **76** must have formed during or after purification (or even as late as during TLC analysis) and that the side product must be rather unstable. While the side product derived from Boc-Pro-Ant-OH (**77**) could not be obtained in pure form,[196] a crude mass spectrum gave new insight. Two mass peaks were found, one belonging to the starting material **76** (MH^+ = 335.2), the other to a compound with a mass of MH^+ = 317.1. As the new compound was 18 u lighter than **76**, its formation could be explained as the elimination of water from **76**. This gave the first hint into possible reaction paths and several theoretically possible structures were proposed (Scheme 31).

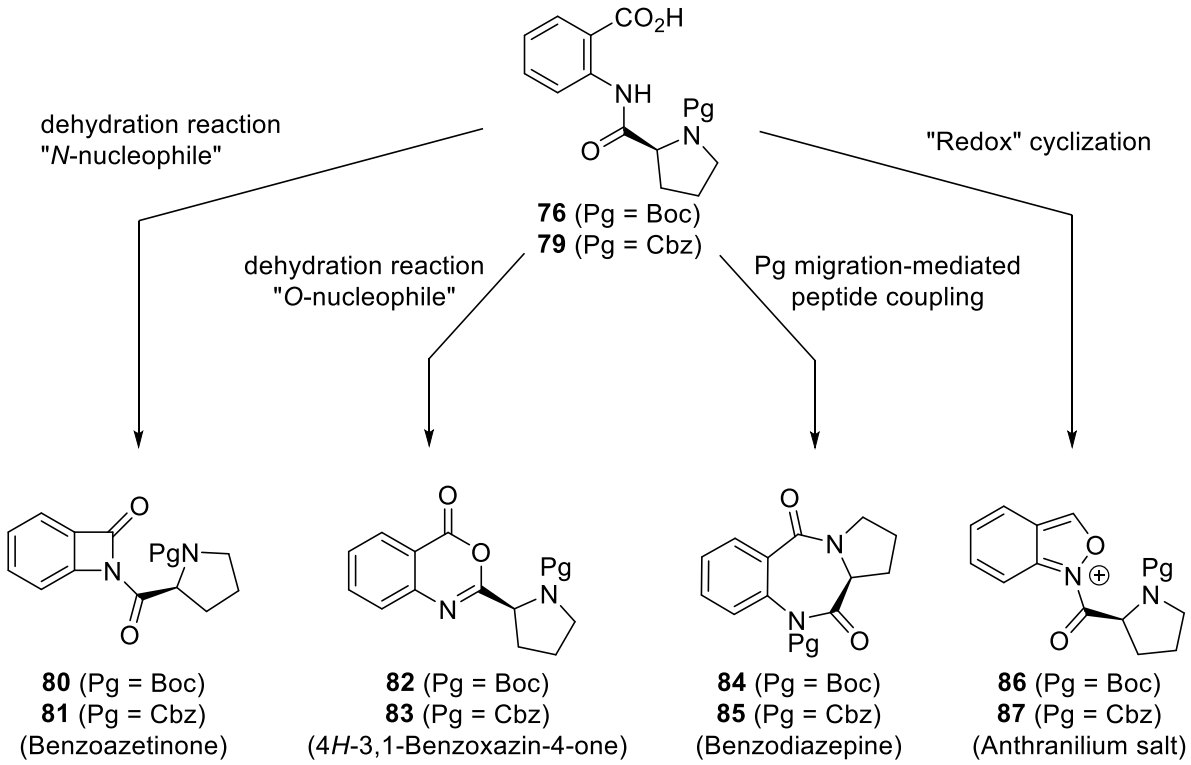

Scheme 31: Theoretically possible side product structures, based on the mass spectra obtained from the unknown compounds. Pg = protecting group.

All of these compounds are in accordance with the observed mass, however, the anthranilium salt **86** was excluded very quickly, as this should be highly unstable and there are no literature precedents in which a comparable substance was successfully isolated.* However, an unambiguous identification of the correct structure required the side product to be analyzed in more detail, for which pure material was needed. While this was not achievable with the Boc-derivative, the analogous side product could be isolated in 76% yield through careful workup in the synthesis of the related Cbz-tripeptide **78**. With pure compound in hand, a full analysis of the compound was possible. NMR analysis underlined that the anthranilium salt **87** was not formed. The formal reduction of the carboxylic acid moiety of **79** would have added an extra CH signal in the DEPT-135 and DEPT-90 spectra, which was not observed.

The focus then turned to the Benzodiazepine **85**. The formation from **79** was considered questionable, as it should be a stable compound and not be prone to hydrolysis. Furthermore, the formation would actually require the migration of the Cbz group from the proline moiety to the highly unreactive amide. The migration of Cbz-groups is not unprecedented, although, it usually requires special circumstances to take place[208] and no example for the here required transformation has been published.

* While *N*-alkylated anthranilium salts are known and have been isolated,[202–206] *N*-acylated derivatives have not been synthesized and were only once postulated in literature as a possible intermediate in a reaction sequence[207]. *N*-alkylated anthranilium salts have been successfully transformed into the corresponding *N*-alkylated benzoazetinones.[202–206]

Fortunately, **85** had already been synthesized by Nagasaka *et al.* in the course of their Tilivalline total synthesis.[209] By comparing NMR and IR data, it could be shown that the side product was not the benzodiazepine **85**.*

The differentiation between benzoazetinone **81** and 4*H*-3,1-benzoxazin-4-one **83**, however, was more complicated: NMR (1D & 2D COSY, HSQC, HMBC) and IR analysis were not sufficient to differentiate between both with absolute certainty. This stems from the fact that both compounds are closely related to each other, as they are basically isomeric intramolecular anhydrides of *N*-acylated anthranilic acid. Interestingly, the literature on this topic is complex. Although the compound class itself was known since 1883,[211] the determination of the structure of *N*-acylated anthranilic acid anhydrides had been a subject of a long-lasting debate in the scientific community.† Today, the 4*H*-3,1-benzoxazin-4-one structure is widely accepted in the scientific community.[215,219–223,226] A literature search for **83** showed that it had already been published once by Spencer *et al.* in 1986,[227] however, neither an experimental procedure nor analytical data were provided, rendering a determination through comparison of data impossible (the synthesis of the analogous Boc-derivative was published three times[196,228]). Due to the fact that even today there are publications claiming to have synthesized *N*-acyl benzoazetinone type compounds (the most recent being from Ansary *et al.* in 2017[229] it appeared necessary to provide evidence for the 4*H*-3,1-benzoxazin-4-one structure, preferably using X-ray crystallography. Unfortunately, no crystalline material could be obtained as the compound is an oily substance at room temperature. Therefore, a simple derivative, *N*-acetyl anthranilic acid (**88**), was

* Although, benzodiazepine **85** should be possible to generate from a very similar compound as **79**: H-Ant-Pro-OBn. Rather than coupling the N-terminus of anthranilic acid first, this would require the initial coupling to happen on the *C*-terminus. The resulting "inverse" dipeptide could then react to benzodiazepine **85**, as the nucleophilic free amine would readily attack the activated ester. There are several literature reports which describe this kind of benzodiazepine formation.[199,210]

† This topic was actually only a subplot of a bigger discussion around the turn of the 19th century, which involved the determination of the structure of anthranil.[212] Anthranil was found to be exactly 18 u lighter than anthranilic acid and was, therefore, considered to be its internal anhydride.[211,212] Several different structures were proposed, one of them being the β-lactam (or benzoazetinone).[211,213–218] As analytical methods like X-ray diffraction or NMR had just been invented or simply did not exist at that time, structural determination of compounds basically relied on elemental analysis and observations made during derivatization reactions of the analyte. One of these derivatizations was the *N*-acylation of anthranil.[211,213–215,217,219] Supporters of the benzoazetinone structure defined this to be simply the *N*-acylated β-lactam, to further substantiate their claim on the β-lactam structure of anthranil.[211–213,217] However, other scientists were more skeptical and concluded that the high steric strain made the presence of a β-lactam rather unlikely.[215,219,220] Through additional experiments they could prove that the acyl carbonyl group can actually partake in reactions rather than it being assumed "inert".[219] This resulted in the postulation of the 4*H*-3,1-benzoxazin-4-one structure[220] (also sometimes termed "acylanthranil"[221–223]). In the end, this turned out to be correct and was later proven by X-ray diffraction.[224] The original debate concerning the structure of anthranil itself was laid to rest in 1924 by Auwers,[218,225] confirming it to be 2,1-benzisoxazole, again disproving the β-lactam theory.[218,225]

synthesized[230,231] and then subjected to similar reaction conditions as used in the peptide coupling of **79**. Although resulting only in 8% of pure material, a single crystal of the product **89** could be isolated and analyzed by X-ray diffraction (Scheme 32).

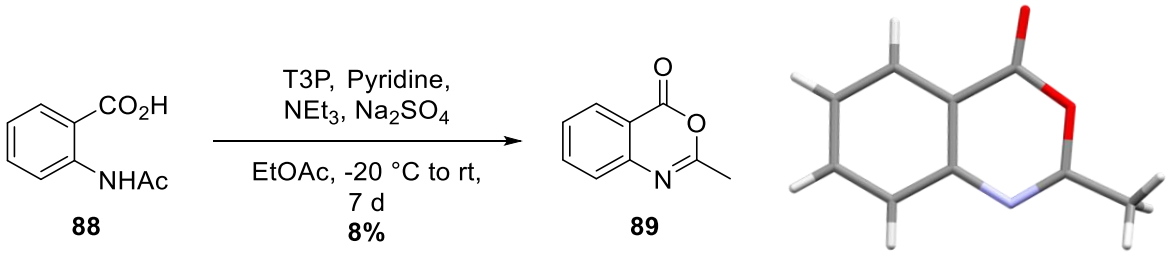

Scheme 32: Synthesis (left) and X-ray structure (right) of **89**.

As can bee seen, the X-ray structure nicely proves the presence of a 4*H*-3,1-benzoxazin-4-one-type structure. Although this is not direct evidence for the structure of the side product, it, paired together with literature precedents, underlines the validity of the assumption that the side product obtained in the peptide coupling is actually **83** (or **82** for the analogous Boc-derivative).

Curiously, **83** is rather unstable[196,232,233] (as observed with its tendency to hydrolyze) and should, in theory, be able to react with H-Pro-OBn (**67**) to the desired tripeptide over time. However, the rather demanding steric bulk of **67** might hamper this reaction, a point that could be underlined in a short study in relation to the hydrolytic stability of **83** (Appendix, Table 9). Besides proving the rapid hydrolysis of **83** under basic and acidic conditions,[232] it could be shown that **83** can, in fact, react smoothly with secondary amines, however, only if the amine does not possess sterically demanding substituents (Scheme 33).

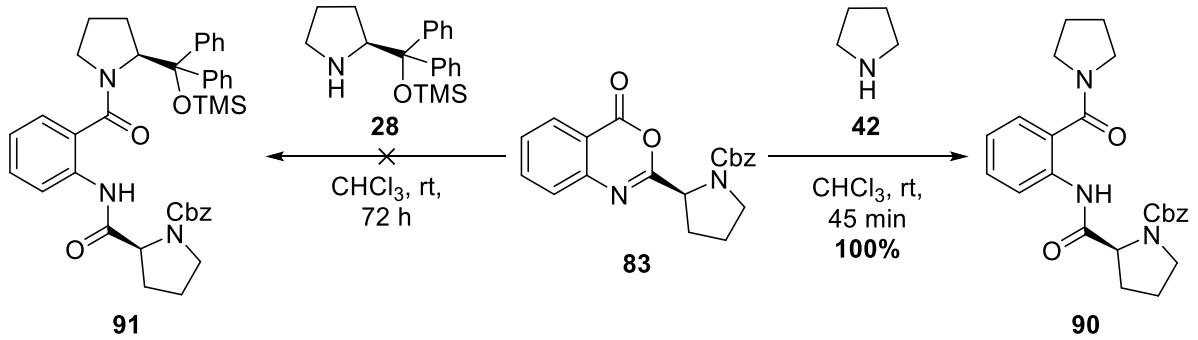

Scheme 33: Test reactions with **83** in a reactivity study. While **83** reacted fast and clean with unsubstituted pyrrolidine (**42**) to give **90**, the use of sterically demanding Jørgensen-Hayashi (**28**) catalyst did not lead to any product (**91**) at all, even after prolonged reaction times.

This explains that the side product was the preferred outcome of the peptide coupling reaction and implies that the formation of **83** must be significantly faster, a point which is supported by the fact that

intramolecular processes usually occur quicker than intermolecular ones.[6] Additionally, the aromatic core structure should provide a good alignment of the functional groups involved, facilitating the formation of **83** even further (Scheme 34).[199]

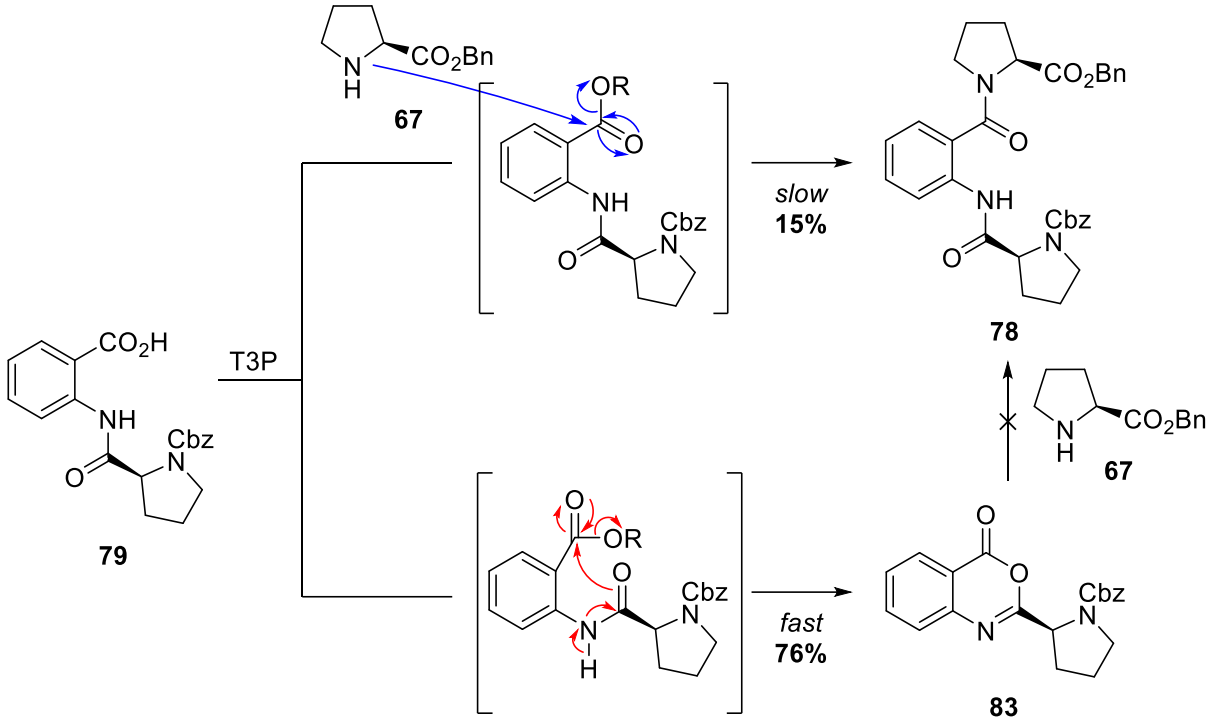

Scheme 34: Proposed reaction mechanism of the different reaction pathways that can occur during peptide coupling of **79**. R = T3P phosphonic ester.

2.7 Catalysis with tripeptides

Having all tripeptides successful synthesized, the focus could now be turned on the evaluation of their organocatalytic abilities. As the underlying activation mechanism of the tripeptides should be similar to L-proline catalysis (*i.e.* enamine catalysis), the test reactions were chosen accordingly.*

The aldol reaction between 4-nitrobenzaldehyde (**92**) and acetone (**34**) was the benchmark reaction investigated, as it was the subject of ongoing research in the Reiser group in order to gain insight into the relationship between structural flexibility and catalytic performance of small organocatalysts. Therefore, the catalytic activity of several tripeptides containing β-amino acids of varying ring size, including cyclopropyl- (**49**),[153,155] cyclobutyl- (**50**),[156,157,234] and cyclopentyl (**51**)[158] derivatives, were

* Besides a multitude of examples under ambient (AP/AT) conditions, there are currently only two examples for the L-proline catalyzed aldol reaction under high pressure (HP) conditions.[94,95]

evaluated. Additionally, catalyzed reactions were carried out under high pressure (HP) conditions in order to investigate correlations between pressure and catalyst flexibility. As a higher degree of conformational freedom should make the catalyst more susceptible to pressure effects, pressurization could trigger a change in the spatial orientation of the active functional groups. This, in return, could then lead to improved activity and/or selectivity. In this connection, the synthesized β-ACHC-tripeptides **52** and *ent*-**52** would represent the most flexible systems, while the Ant-tripeptide **53** would act as a rigid reference model to which the results could be compared to.

In a first test run, a small solvent screening of the aldol reaction was conducted to identify the most suitable system for all future investigations (Figure 8 & Appendix Table 10). Reiser *et al.* had already reported that acetone/water mixtures turned out to be very suitable for the tripeptide-catalyzed aldol reaction.[153] Additionally, a second solvent system consisting of chloroform and isopropanol was evaluated, as this had been proven to be the most effective in the study of Wennemers *et al.* with their tripeptide organocatalysts.[143,145] The results indicated, that the acetone/water mixtures gave far superior results in comparison to the chloroform/isopropanol mixtures. Interestingly, highest activity required a specific amount of water to be present, with the optimum revolving around 10% (v/v). Decreasing or increasing the water amount led to significantly reduced yields.

This might, on the one hand, be explained through the reaction mechanism: while small amounts of water could positively affect reprotonation, facilitate the release of the product and lead to a faster catalyst turnover, higher amounts might push the equilibrium of the initial enamine formation towards the starting materials, thus effectively canceling out the reaction.[157] On the other hand, the spatial arrangement of the functional groups of the catalyst could be influenced by the solvent. Here, it appears that polar aprotic solvents (like acetone) are the most suited in stabilizing an “active” conformation. As proximity of the amine and the carboxylic acid group is essential for catalytic activity,[147,155] the presence of a water molecule could aid this by acting as a mediator, bridging the functional groups through hydrogen-bonds, thus bringing them closer together and rigidifying the catalyst. If water levels are decreased or a non-polar solvent is used (*e.g.* chloroform), this mediating effect might be negated leading to more flexibility, while increased amounts of water or polar solvents (*e.g.* isopropanol) would lead to an increased interaction of the functional groups with the solvent molecules, rather than with each other. This can be somewhat underlined by the observations made in the X-ray analysis of **52**.

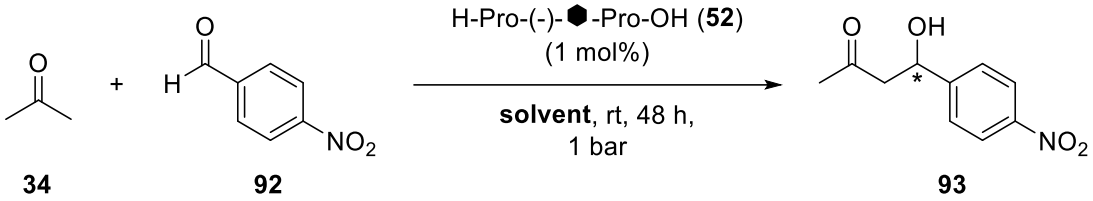

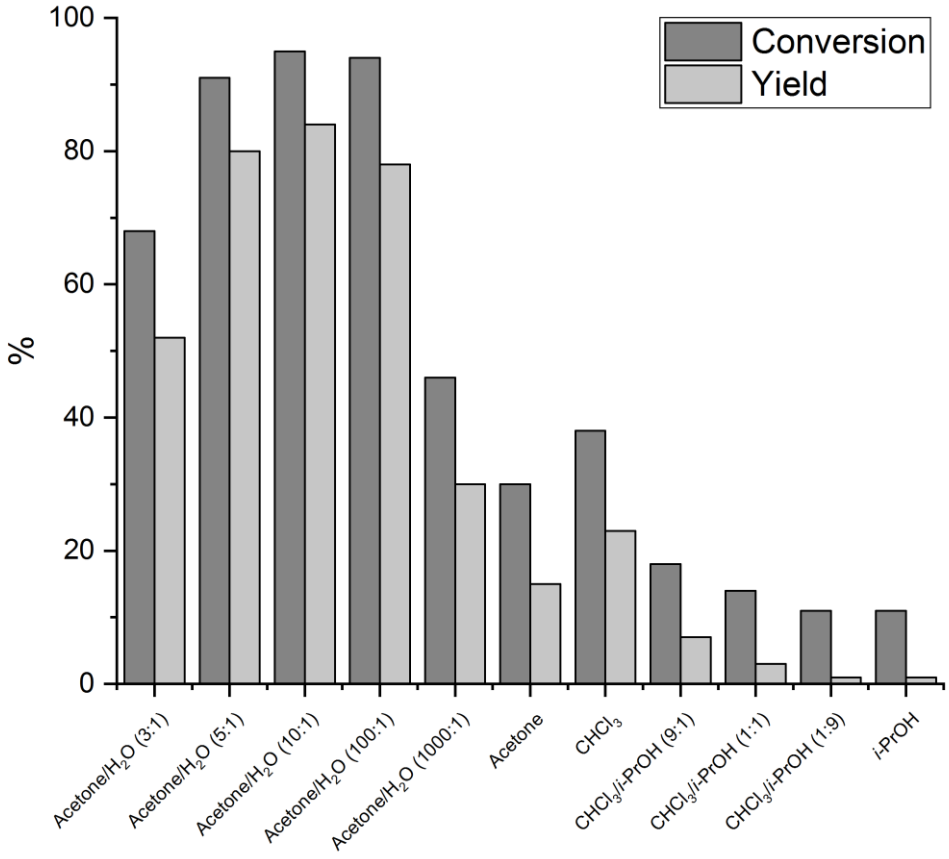

Figure 8: Solvent screening of the benchmark aldol reaction catalyzed by tripeptide **52**. Conditions: 1.00 mmol 4-nitrobenzaldehyde (**92**), 10 equiv. acetone (**34**) (if not present as solvent), 2 mL solvent. Conversion and yield determined by NMR using diphenoxymethane (**46**) as internal standard.

Having settled for acetone/water 10:1 (v/v) as solvent, focus was moved on evaluating the catalytic activity of the tripeptides under AP/AT and HP conditions (Table 4). Blank reactions were carried out first, in order to rule out the occurrence of a background reaction. Slight conversion of the aldehyde was observed (similar to the Michael reaction described in the previous chapter), however, no product formation could be detected under AP/AT as wells as HP conditions (entries 1&2). First reactions were carried out with 10 mol% of **52** at AP/AT (entry 5), reproducing the conditions used by Pilsl with the β-ACC-tripeptide **49** (entry 3).[155] The more flexible catalyst **52** led to improved yields after 24 h (from 73% to 84%), however, the increased conformational freedom led to drastic losses of selectivity (69% to 19% *ee*). The reaction was repeated with a decreased catalyst load of only 1 mol% (entry 6) and, remarkably, **52** retained it's high reactivity, achieving similar yields as **49** but requiring only one-tenth

of the catalyst amount.* With less catalyst, however, a slight drop of (the already low) enantioselectivity could be observed (19% to 13% *ee*). Using the diastereomeric catalyst *ent*-**52** gave similar reactivity (64% yield), but this time led to no enantioinduction at all (entry 9), indicating that the spatial arrangement of the functional groups is slightly better in **52**. The best enantioselectivity could be achieved with the rigidified catalyst **53** (29% *ee*), although, this resulted in diminished reactivity (47% yield, entry 11). The *R*-enantiomer of **93** was formed exclusively with all catalysts, which is in accordance with the observations made with the other tripeptides bearing the same structural motif.[153,155,158]

Table 4: Results of the catalyst evaluation of the aldol reaction.

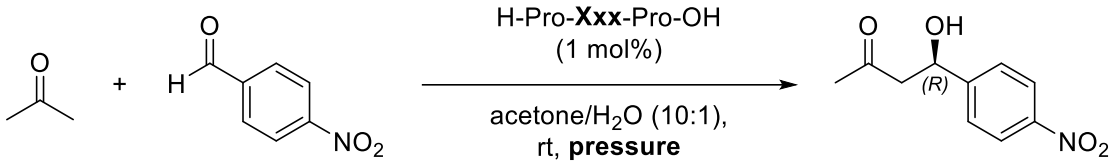

34 **92** **93**

Entry	Catalyst [Xxx]	catalyst loading [mol%]	Time [h]	Pressure [kbar]	Conversion [%][a)]	Yield [%][b)]	*ee* (*R*) [%][c)]
1	-	-	24	10^{-3}	9	0	-
2	-	-	7	4.8	12	0	-
3[d)]	(-)-▲ (**49**)	10	24	10^{-3}	84	68[e)]	69
4[d)]	(-)-▲ (**49**)	10	4	4.8	97	73[e)]	67
5	(-)-⬢ (**52**)	10	24	10^{-3}	n.d.	84[e)]	19
6	(-)-⬢ (**52**)	1	24	10^{-3}	n.d.	71[e)]	13
7	(-)-⬢ (**52**)	1	7	10^{-3}	47	42	11
8	(-)-⬢ (**52**)	1	7	4.8	87	74	22
9	(+)-⬢ (*ent*-**52**)	1	24	10^{-3}	75	64	0
10	(+)-⬢ (*ent*-**52**)	1	7	4.8	93	69	9
11	Ant (**53**)	1	24	10^{-3}	61	47	29
12	Ant (**53**)	1	7	4.8	79	77	28

Reaction conditions: 1.00 mmol 4-nitrobenzaldehyde (**92**), 2 mL solvent. a) Determined by crude NMR using diphenoxymethane (**46**) as internal standard or through recovered starting material. b) Determined by crude NMR using diphenoxymethane (**46**) as internal standard. c) Determined using chiral HPLC (AS-H). d) From ref. [155], 0.2 mmol scale. e) Isolated yield.

When comparing the reaction outcomes under AP/AT conditions, it became apparent that there seemed to be a correlation between the flexibility of the catalyst on the one hand, and the resulting reactivity and selectivity on the other hand. While the more flexible catalysts **52** and *ent*-**52** gave improved yields, selectivity appeared to be positively influenced by the structural rigidity of **53**. The increased flexibility allows the catalyst to better adapt to the reactants, bringing the active functional

* Neither Reiser *et al.*,[153] nor Pilsl[155] attempted to use less than 10 mol% of catalyst, therefore, it cannot be ruled out that the reaction would also occur with 1 mol% of **49**. This is likely to be the case, as the reaction ran with all other tripeptide catalysts under these conditions (Table 5).

groups into proximity. However, the higher conformational ambiguity probably makes the transition state in the stereoinducing step of the reaction less stable, which leads to lower selectivities.

To tackle this dilemma, the use of high-pressure conditions was considered, as HP forces molecules into more rigid, tightly-packed conformations while acting as activation mode at the same time. All tests were, therefore, rerun under HP conditions. Leading with **52**, the reaction reached similar yields after only 7 hours under HP conditions (entry 8) compared to the same reaction under AP/AT conditions after 24 h (entry 6). Interestingly, enantioinduction was slightly increased as well (22% *ee*). The reaction was repeated under AP/AT conditions and 7 h (entry 7), which affirmed that the reaction indeed proceeded faster and more selective under HP conditions by a factor of two. The diastereomer *ent*-**52** behaved similar, also achieving comparable yields and slightly increased enantioinduction (although only to a small degree) after just 7 h under HP conditions (entries 9&10). The reaction with the rigidified catalyst **53** profited most from the use of HP. It reached similar yields as the equally constrained β-ACC catalyst (entry 4) and the flexible catalysts under the same conditions, without erosion of enantioselectivity (entry 12). This indicated, that the accelerating effect of HP probably stems from it being a general activation method by the means of adding energy to the system and shifting the equilibrium, rather than through drastically influencing the conformation. Otherwise, the reaction catalyzed by the rigid **53** should not have shown such a drastic increase in yield when pressurized. However, HP appears to stabilize conformations and, therefore, transition states to a certain degree. This leads to a more defined, less flexible catalyst-substrate complex, which in return results in improved enantioinduction in the product, as was observed with the flexible catalysts.

As mentioned before, the aldol reaction was also subject of a comparative study with tripeptide catalysts containing β-amino acids of varying ring size.[155,156,158,234] **52** represents the most flexible of all catalysts and the obtained results fit well in the series (Table 5).

Selectivity-wise, a clear trend is observable. Enantioselectivity decreases steadily with increasing ring size of the β-amino acid. This underlines that a stereoselective reaction environment requires rigidity (*i.e.* low conformational freedom), in order to develop a well-defined catalyst-substrate complex with these types of compounds. The use of constraining HP conditions, therefore, has little effect on the selectivity of already inflexible systems (cyclopropyl and –butyl derivatives **49** & **50**, entries 2&4). However, more flexible systems are positively influenced to a small extent (cyclopentyl and –hexyl derivatives **51** & **52**, entries 6&8).

Table 5: Comparison of results obtained with tripeptide catalysts containing β-amino acids of varying ring size.

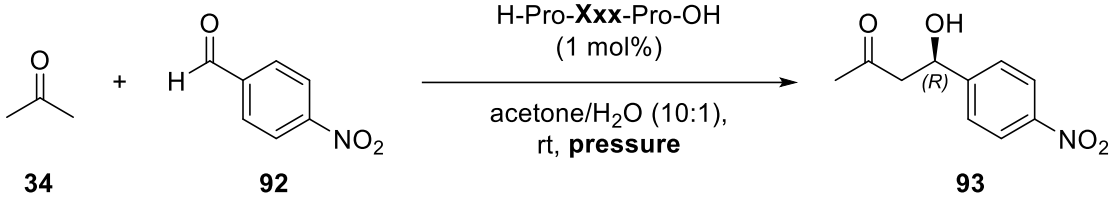

34 **92** **93**

Entry	Catalyst [Xxx]	Catalyst loading [mol%]	Time [h]	Pressure [kbar]	Isolated yield [%]	*ee* (*R*) [%][a)]
1[b)]	(-)-▲ (**49**)	10	24	10^{-3}	68	69
2[b)]	(-)-▲ (**49**)	10	4	4.8	73	67
3[c)]	(-)-■ (**50**)	1	24	10^{-3}	45	47
4[c)]	(-)-■ (**50**)	1	7	5.0	66	41
5[d)]	(-)-⬟ (**51**)	1	24	10^{-3}	82	31
6[d)]	(-)-⬟ (**51**)	1	6	4.6	57	41
7	(-)-⬢ (**52**)	1	24	10^{-3}	71	13
8	(-)-⬢ (**52**)	1	7	4.8	65	22

Reaction conditions: 1.00 mmol 4-nitrobenzaldehyde (**92**), 2 mL solvent. a) Determined using chiral HPLC (AS-H). b) From ref. [155], 0.2 mmol scale. c) From refs. [156,234]. d) From ref. [158].

In terms of reactivity, the results are a little more diverse. Under AP/AT conditions, the catalysts performed similar, with the exception of the slightly less active cyclobutyl analogue **50**. Under HP conditions and shorter time periods, however, **50** (in comparison) achieved higher yields, while the cyclopentyl analogue **51** gave diminished yields. The HP reactions with the cyclopropyl and –hexyl derivatives gave comparable results to the standard AP/AT conditions. Due to this ambiguous behavior, it is difficult to draw a conclusion on the relation between ring-size-induced flexibility and reactivity. This might be attributed to the slightly different orientation of the catalytically active prolyl moieties in each catalyst. The dihedral angle between the two substituents of the β-amino acids is dependent on ring size,[235] thus changing the spatial arrangement of the functional groups for every catalyst, making a direct comparison impossible.*

Although the overall accelerating effect of HP conditions on the tripeptide catalyzed aldol reactions might not be directly correlated to conformational changes, compression clearly has an observable impact on the reaction outcome. In this case, HP probably acts more as a general activation mode through addition of energy and the fact that Aldol reactions (as most reactions which are accompanied by entropy decrease) have a negative volume of activation $\Delta V^{\ddagger}$ and, therefore, benefit from the use

* To further extend this point, simple *cis*-dimethyl cycloalkanes were drawn in Chem3D® (Perkin Elmer), subjected to the implemented energy minimization protocol (using MM2 default parameters) and the dihedral bond angle of the methyl substituents were calculated. Cyclopropyl: 0°, Cyclobutyl: 23.1°, Cyclopentyl: 45.8°, Cyclohexyl: 54.2°.

of HP conditions.[236]

To broaden the scope of applications, it was decided to test the synthesized catalysts in a second benchmark reaction, the conjugate Michael-type addition between acetone (**34**) and *trans*-β-nitrostyrene (**40**). The reaction had, again, been reported to proceed with L-proline (**23**) as catalyst under AP/AT conditions,* reassuring that it could be catalyzed by the tripeptides as well (Table 6).[237] Blank reactions again ruled out the occurrence of a background reaction forming product (entries 1&2). Some conversion of starting material could be observed, however, this was to be expected from earlier studies.[124]

Table 6: Results of the catalyst evaluation of the Michael reaction.

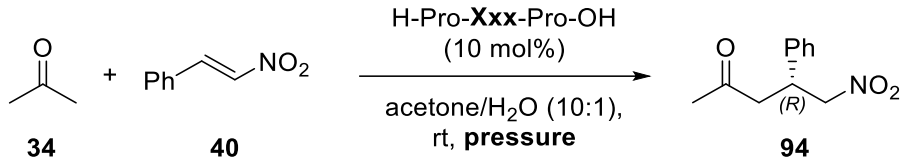

34 **40** **94**

Entry	Catalyst [Xxx]	Time [h]	Pressure [kbar]	Conversion [%][a)]	Yield [%][a)]	*ee* (*R*) [%][b)]
1	-	48	10^{-3}	10	0	-
2	-	16	4.8	21	0	-
3	(-)-⬢ (**52**)	48	10^{-3}	92	91	13
4	(-)-⬢ (**52**)	4	10^{-3}	25	23	12
5	(-)-⬢ (**52**)	16	4.8	98	79	9
6	(-)-⬢ **(52)**	4	4.8	80	64	10
7	(+)-⬢ (*ent*-**52**)	48	10^{-3}	63	60	14
8	(+)-⬢ (*ent*-**52**)	16	4.8	100	88	18
9	Ant (**53**)	48	10^{-3}	39	33	24
10	Ant (**53**)	16	4.8	94	85	24

Reaction conditions: **52** and *ent*-**52**: 0.50 mmol *trans*-β-nitrostyrene (**40**), 2 mL solvent, **53**: 0.25 mmol *trans*-β-nitrostyrene (**40**), 1 mL solvent. a) Determined by crude NMR using diphenoxymethane (**46**) as internal standard. b) Determined using chiral HPLC (AS-H).

In contrast to the aldol reaction, 1 mol% of catalyst did not lead to any significant conversion after 24 h, thus requiring the use of 10 mol%. After 48 h under AP/AT conditions, **52** gave excellent yield (91%, entry 3), however, enantioinduction was equally poor as in the aldol reaction. Interestingly, the diastereomeric *ent*-**52** reached only fair yield (60%, entry 7), contrasting the results of the aldol reaction where both flexible catalysts performed similar under AP/AT conditions. The use of the more rigid **53**, however, led to similar results as in the aldol reaction: poor yield (33%) but highest selectivity of all (24% *ee*, entry 9). The significantly divergent results of the diastereomeric flexible catalysts indicated that, in the Michael addition, proper conformational alignment is probably more important

* There are currently no examples for the Michael reaction under HP conditions *via* covalent enamine-type catalysis.

to achieve good reactivity. This might be related to the different transition state the reaction proceeds through, which **52** can apparently stabilize to a higher extent. (Figure 9).

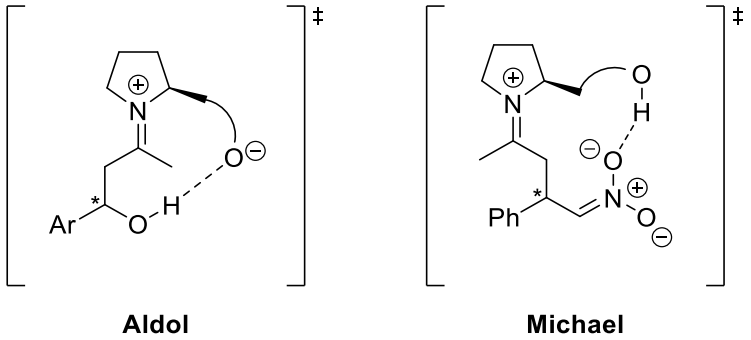

Figure 9: Simplified transition states of the aldol and Michael reaction catalyzed by the tripeptide catalysts, demonstrating their different structure and size. The transition states were originally proposed by Wennemers *et al.*[148,152]

To once again analyze the implications the use of high pressure has on the catalyst systems, all reactions were run under HP conditions. With **52**, a slightly lower yield (79%, entry 5) than under AP/AT was obtained, however, the reaction time could be reduced to only 16 h. To see if this could be pushed even further, reaction times were once more reduced to 4 h. While under AP/AT conditions the reaction had only proceeded to a small amount (23% yield, entry 4), the analogous HP reaction had already reached a fair yield (64%, entry 6), which equates roughly to a tripled turnover number. Surprisingly, the diastereomeric catalyst *ent*-**52** gave even an improved yield under HP conditions, leading to an almost six times faster reaction. The rigid **53** also gave a vastly improved yield under HP conditions (85%, entry 10), actually achieving a more than seven times faster reaction under HP than under ambient conditions. While high pressure had a clearly positive influence on reactivity, this time selectivity remained almost unchanged with both, flexible and rigid tripeptides. The increase in reactivity under high pressure, again, is most likely caused by the action of HP as a general activation mode through the addition of energy into the system. Whether the enantioselectivity is influenced by HP or not is probably dependent on the transition state of the catalyst-substrate complex and its stability, rather than on the flexibility of the catalyst in general.

In conclusion, the results of this catalytic study neatly demonstrate that, in peptide organocatalysis, HP conditions positively affect reactivity, while retaining (or even improving) selectivity of reactions. This underlines the viability of HP as secondary activation mode in organocatalyzed reactions.

2.8 Conformational study of H-Pro-(-)-⬢-Pro-OH using HP-NMR

Reiser *et al.* described the presence of two distinct conformations in the NMR of H-Pro-▲-Pro-OH (**49**) at ambient pressure in a 3:1 ratio, which arose from the (literature known) *cis*/*trans* isomerism of the C-terminal proline moiety.[153] Pilsl further investigated **49** under HP-NMR conditions, demonstrating that conformations could be severely influenced by high pressure. Combining the results with theoretical calculations, he proposed that the functional groups were aligned best in the *cis*-conformer, thus it represents the catalytically most active and selective structure.[155] Interestingly, in the closely related H-Pro-(-)-■-Pro-OH (**50**), only the *trans*-conformer could be identified.[156] In both rigid peptides, no significant isomerism of the N-terminal proline could be detected. However, measurements of **49** and **50** were conducted in MeOH-d_3 and not in the actual solvent system used for catalysis.

Initial ^{1}H- and ^{13}C-NMR measurements in $CDCl_3$ of H-Pro-(-)-⬢-Pro-OH (**52**) at ambient pressure indicated that **52** resides in at least two distinct conformational states, as the spectra showed clear signs of signal doubling, especially with the amide proton signal. It was unclear whether this stemmed from the *cis*/*trans* isomerism observed earlier with **49** or had a different origin. In order to gain insight into the conformational behavior of the flexible peptide, **52** was analyzed in a collaborative project within the FOR 1979 high-pressure research group using HP-NMR, as HP-NMR is a helpful tool for identifying rare conformational states.[238] The studies were carried out in the biophysical department of the University of Regensburg by Ertinger in the group of Kalbitzer and Kremer as a collaborative project.[239]

To remain close to the catalytic conditions, the peptide was supposed to be measured in the solvent system used for catalysis, acetone-d_6/D_2O (10:1), utilizing one-dimensional ^{1}H, ^{13}C, DEPT and NOESY, as well as the two-dimensional COSY, HSQC and TOCSY experiments. However, **52** had to be measured in H_2O/D_2O (10:1) first to assign all signals, as directly measuring in acetone-d_6/D_2O proved to be complicated due to the large residual solvent signals. Overlaying the assigned spectra then allowed the successful identification of the respective signals in acetone-d_6/D_2O (10:1) and an NMR pressure series was recorded (Figure 11). Plotting the chemical shift values against the pressure allowed the extraction of thermodynamic parameters (ΔG_i, ΔV_i), which in return gave information on the conformations.[239]

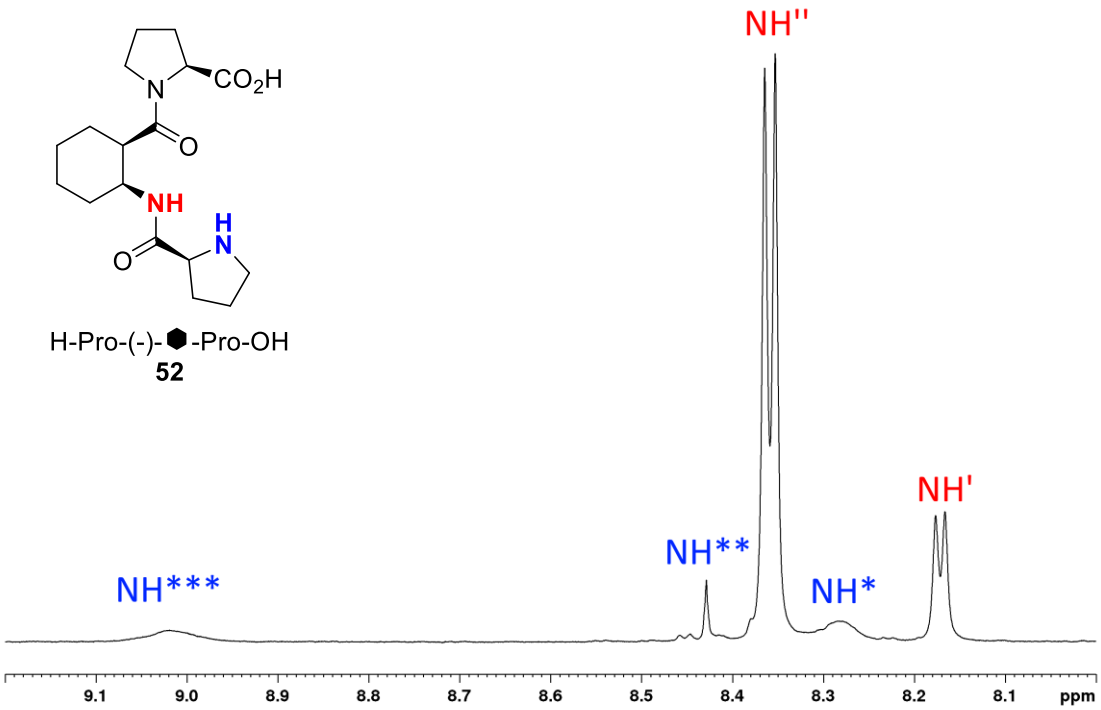

Figure 10: 800 MHz NMR spectrum of **52** in H_2O/D_2O (10:1) at ambient pressure and 275 K, clearly showing several resonances of amine and amide protons correlating to different conformations being present.[239] The NH'/NH'' ratio is approximately 1:4.

The measurements revealed that even at ambient temperature several conformers of **52** exist simultaneously (Figure 10). Two of them are associated to the cyclohexyl ring (seen by the two amide proton signals, NH'' and NH' in a 4:1 ratio) and three with the N-terminal proline (NH*, NH** and NH***) (Scheme 35). The two cyclohexyl conformations (**52-A** and **52-B**) are probably caused by ring inversion of the cyclohexyl scaffold of the *trans*,*trans*-configured peptide, as trans amide bonds are known to be more stable.[240,241] The fact that both cyclohexyl conformations are detectable by NMR shows that they must (at least) be meta-stable and interconvert rather slowly. This hints on some sort of stabilization (probably through H-bonding of the amide proton and the amide carbonyl group), although one conformation should be favored due to the observed 4:1 peak integral ratio.

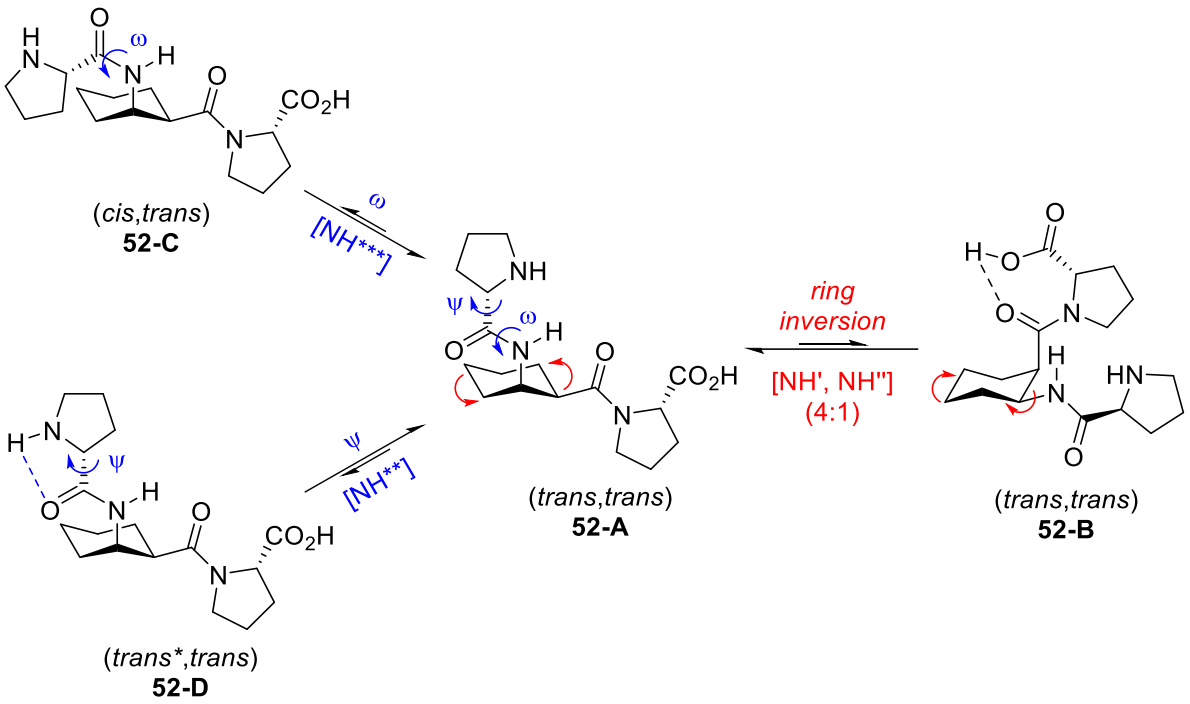

Scheme 35: Proposed conformations of H-Pro-(-)-⬢-Pro-OH (**52**) identified by HP-NMR.[239] The central **52-A** represents the closest resemblance to the structure obtained from X-ray analysis and is probably the most stable. While depicted in **52-B**, the hydrogen bond responsible for locking the rotation of the C-terminal proline is omitted in the other structures for reasons of clarity.

The other conformations can be tracked to rotation of the N-terminal proline. While one amine signal stems from the stable *trans*,*trans*-isomer, isomerization of the amide bond leads to the *cis*,*trans*-conformer **52-C** (isomerisation of prolyl amides is more common as with other amino acids due to the increased steric bulk[240,241]). The other conformer **52-D** is probably formed by rotation of the prolyl moiety around the bond adjacent to the carbonyl group (bond angle ψ). This, supported by the fact that the corresponding NMR signal is rather sharp, indicates the formation of a hydrogen bond that stabilizes the conformation. Interestingly, analysis of the obtained thermodynamic parameters showed that the C-terminal proline resides in only one conformation, stabilized through a hydrogen bond between the proton of the carboxyl group and the adjacent carbonyl group of the amide bond.[239] A similar observation was made for the cyclobutyl derivative **50**.[156]

With increasing pressure, it appeared that almost all conformations became less populated. Although high pressure can weaken intramolecular interactions,[242] this might be traced to the solvent system acetone-d_6/D_2O, which is not entirely inert in combination with the tripeptide. In analogy to the catalysis experiments, **52** can form an iminium ion with acetone (**34**),* which is facilitated under high

* Recently, Ortuño *et al.* reported the identification of iminium ion intermediates in acetone-d_6 with tripeptides containing γ-cyclobutyl amino acids.[157]

pressure. This leads to the generation of new competing species that further complicates the interpretation of the spectra.[239]

To facilitate the investigation of the cyclohexyl scaffold of β-ACHC in particular, simplified model compounds were synthesized which do not bear all the functional groups of the catalyst **52**. The results are discussed in detail in the following chapter.

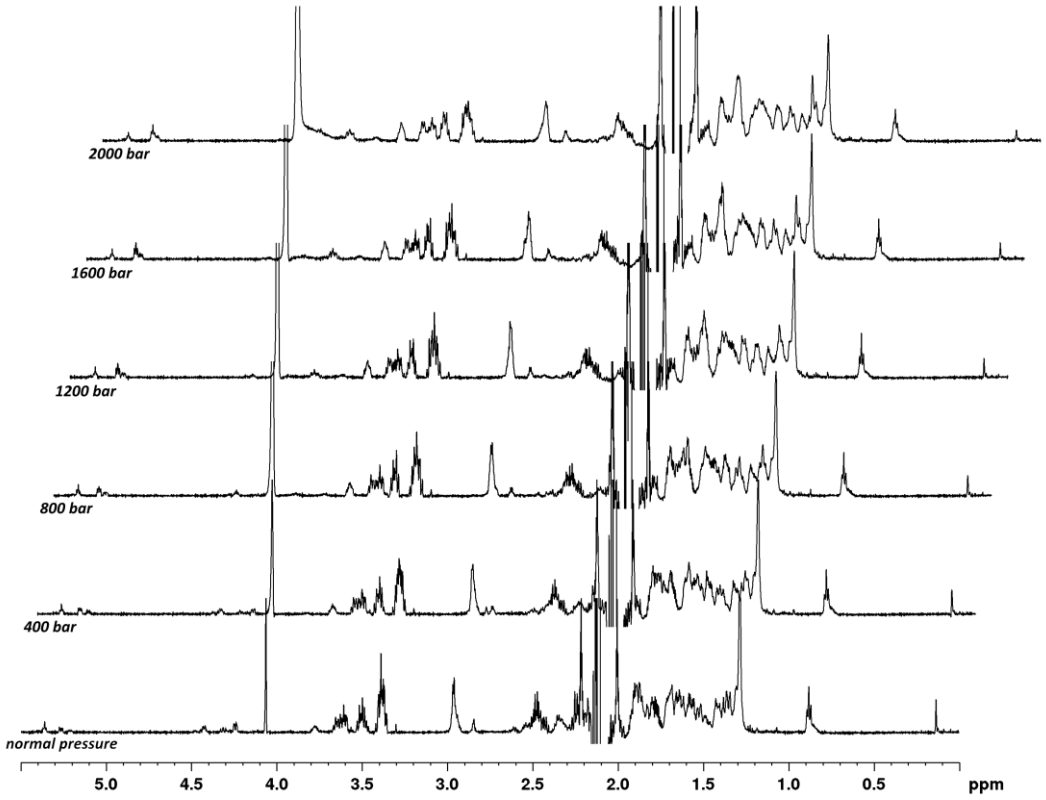

Figure 11: Stacked plot of 600 MHz ^{1}H-NMR spectra of **52** obtained at various pressures at 275 K in acetone-d_6/D_2O.[239] An indication for the formation of the iminium ion is the increasing signal of the residual water (around 4.1 ppm) and acetone (2.1 ppm), which is likely to be caused through isotope exchange with acetone-d_6.

3. Synthesis and evaluation of β-ACHC model compounds

The HP-NMR studies of the H-Pro-(-)-⬢-Pro-OH (**52**) revealed high conformational freedom making the tripeptide catalyst highly flexible,[239] which is believed to be a major contributing factor to the poor enantioselectivities in the catalytic test reactions. Amongst others, one observed behavior was the assumed ring inversion of the central *cis*-β-amino acid scaffold. The high flexibility and functional group density of **52**, however, severely complicated the interpretability of the acquired data. In order to gain more insight into the matter, it became reasonable to analyze *cis*-β-ACHC independently, as its conformational behavior could prove useful for understanding that of the entire peptide **52**.

This idea was based on the studies of Gellman *et al.* in the 1990s, who used small, linear or cyclic model compounds that were structurally related to α-, β- and γ-amino acids. Analyzing these molecules with NMR and IR spectroscopy as well as theoretical calculations allowed them to obtain general information on the conformational behavior of different amino acids and their hydrogen-bonding (H-bonding) patterns.[243,244] Similar investigations have been carried out for cyclic β-amino acids, *e.g.* in the Reiser group for β-ACC[245,246] or by Ortuno *et al.* for β-ACBC.[247]

Therefore, the synthesis of Ac-⬢-NMe_2 (*cis*-**95**) was conceived, as it represented a structural analog to the *cis*-β-ACHC in the tripeptide **52,** containing the entirety of the amino acid scaffold but omitted the large, substituted prolyl residues of **52** which would interfere and complicate the spectroscopic analysis (Figure 12). Besides *cis*-**95** the corresponding *trans*-compound *trans*-**95** was synthesized as well. It should not display ring inversion, as this would leave both substituents in the energetically disfavored *all*-axial orientation, rendering it a reference to compare results to. Both model compounds were then investigated using NMR spectroscopy and, in cooperation with the TU Dortmund, with HP-IR spectroscopy in order to learn more about their conformational properties and the influence of high-pressure conditions.

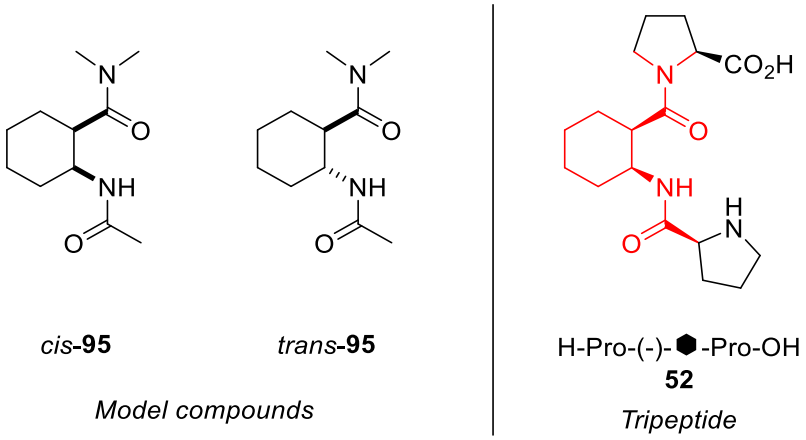

Figure 12: Chemical structures of the synthesized model compounds (left) for the investigation of the conformational behavior of the central β-amino acid in the tripeptide H-Pro-(-)-⬢-Pro-OH (**52**) (right).

3.1 Synthesis of the model compounds

As the final products are not literature known, a synthetic pathway had to be developed. Building on the approach used for the tripeptides (see Scheme 23), a slightly modified synthetic route was conceived to gain access to the model compounds. As the conformational analysis should not be influenced by the absolute stereochemistry of the molecules, this meant that only the relative stereochemistry (*cis* & *trans*) had to be introduced. This can be achieved conveniently in the initial Diels-Alder reaction and makes the kinetic resolution step (which was essential in the peptide synthesis) redundant. The opening of the resulting anhydrides (*cis*- & *trans*-**56**) with dimethylamine would then result in the formation of the hemi-amides (*cis*- & *trans*-**96**), which are subsequently subjected to Curtius rearrangement to convert the free carboxylic acid moieties into the protected amines (*cis*- & *trans*-**97**). As final steps, hydrogenation followed by simple *N*-acetylation would result in the final model compounds (*cis*- & *trans*-**95**).

The synthesis was started with the same Diels-Alder reaction already employed in the tripeptide synthesis, using 3-sulfolene (**62**) as 1,3-butadiene precursor.[166–168] As the *cis* adduct *cis*-**56** had already been obtained, only *trans* adduct *trans*-**56** had to be synthesized. As direct generation was impossible (the corresponding "fumaric anhydride" does not exist), the equivalent diacid *trans*-**99** had to be formed first with fumaric acid (**98**) as dienophile, following the procedure developed by Reddy *et al.* in 2014.[248] Treatment with acetic anhydride then led to the successful formation of the *trans* anhydride (*trans*-**56**) in 82% yield over two steps (Scheme 36).[249]

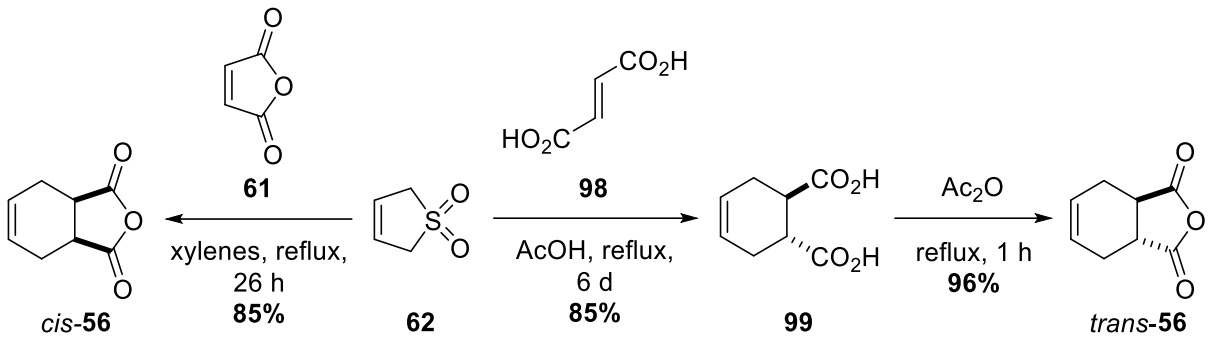

Scheme 36: Synthesis of the *cis*- and *trans*-cycloadducts *cis*-**56** and *trans*-**56**.

With both anhydrides available, the next step was the ring-opening amidation using *in situ* generated dimethylamine (Scheme 37). In this reaction, the isomers displayed quite different properties as *trans*-**56** showed a higher reactivity than its *cis* counterpart, probably a result of the decreased stability of the *trans*-anhydride. Unfortunately, the subsequent Curtius reaction did not proceed as planned. For reasons unknown, both diastereomers reacted extremely sluggish, providing almost no rearranged products (*cis*- & *trans*-**97**). This is probably related to the presence of the adjacent amide moiety, as previous reports exist describing this particular issue. Hibbs *et al.* experienced similar difficulties while synthesizing a structurally related amino acid containing a norbornene scaffold, proving that the use of DPPA as azide-transfer agent fails when an amide group is adjacent to the carboxylic acid.[250]

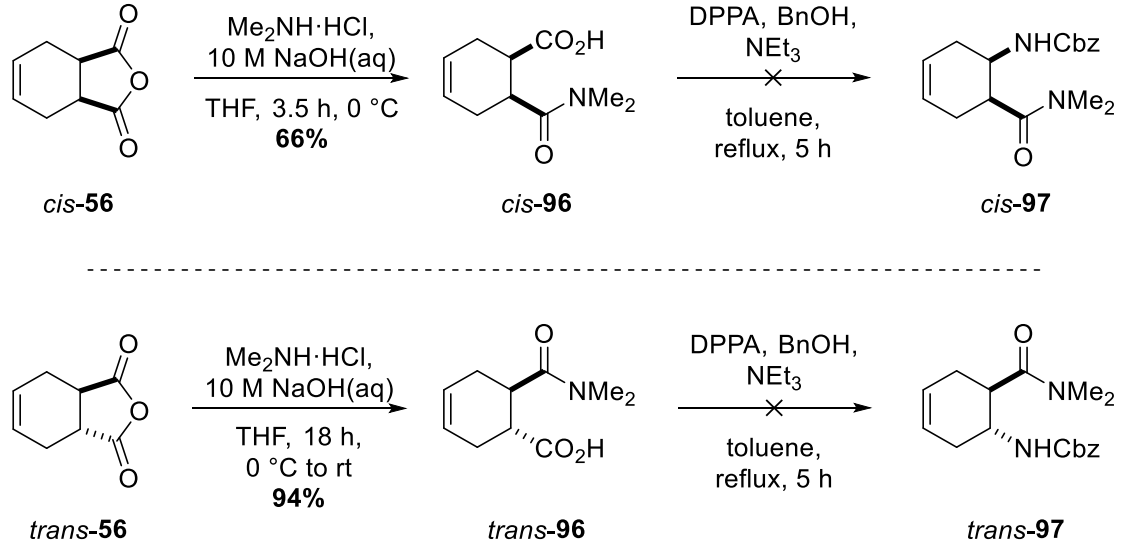

Scheme 37: Initial synthetic strategy for the synthesis of the model compounds starting through ring-opening amidation.

Therefore, this approach was rendered impractical and the route was changed to the strategy that had already been used to synthesize *cis*-β-ACHC for the tripeptides. Although this made the reaction longer and more elaborate, this sequence (including the Curtius reaction) had already proven to work reliably.

Again starting from the cycloadducts (*cis*-**56** and *trans*-**56**), both were reacted with methanol to obtain the corresponding hemiesters *cis*- and *trans*-**63** in quantitative yield. With those in hands, the DPPA-

mediated Curtius reaction with BnOH worked smoothly, introducing the Cbz-protected amine functionalities.[174] The crude product[175] was submitted to hydrogenolysis, cleaving the protecting group and hydrogenating the double bond. The now free amine was then reacted with acetyl chloride, yielding amides *cis*-**100** in 46% and *trans*-**100** in 50% yield over three steps. After saponification of the methyl ester,[176] only the final amidation of the carboxylic group with dimethylamine was left to be performed for both isomers. Two different approaches were attempted. The first included the generation of the acid chloride using thionyl chloride, which was subsequently treated with a freshly prepared 1.26 M solution of dimethylamine in THF. The second attempt was a one-pot procedure where activation and amidation proceeded simultaneously, using T3P as activating agent and the same dimethylamine solution.[195] In the end, the one-pot procedure turned out to be more effective, as it was easier to work up, resulted in higher yields and was less prone to side product formation.

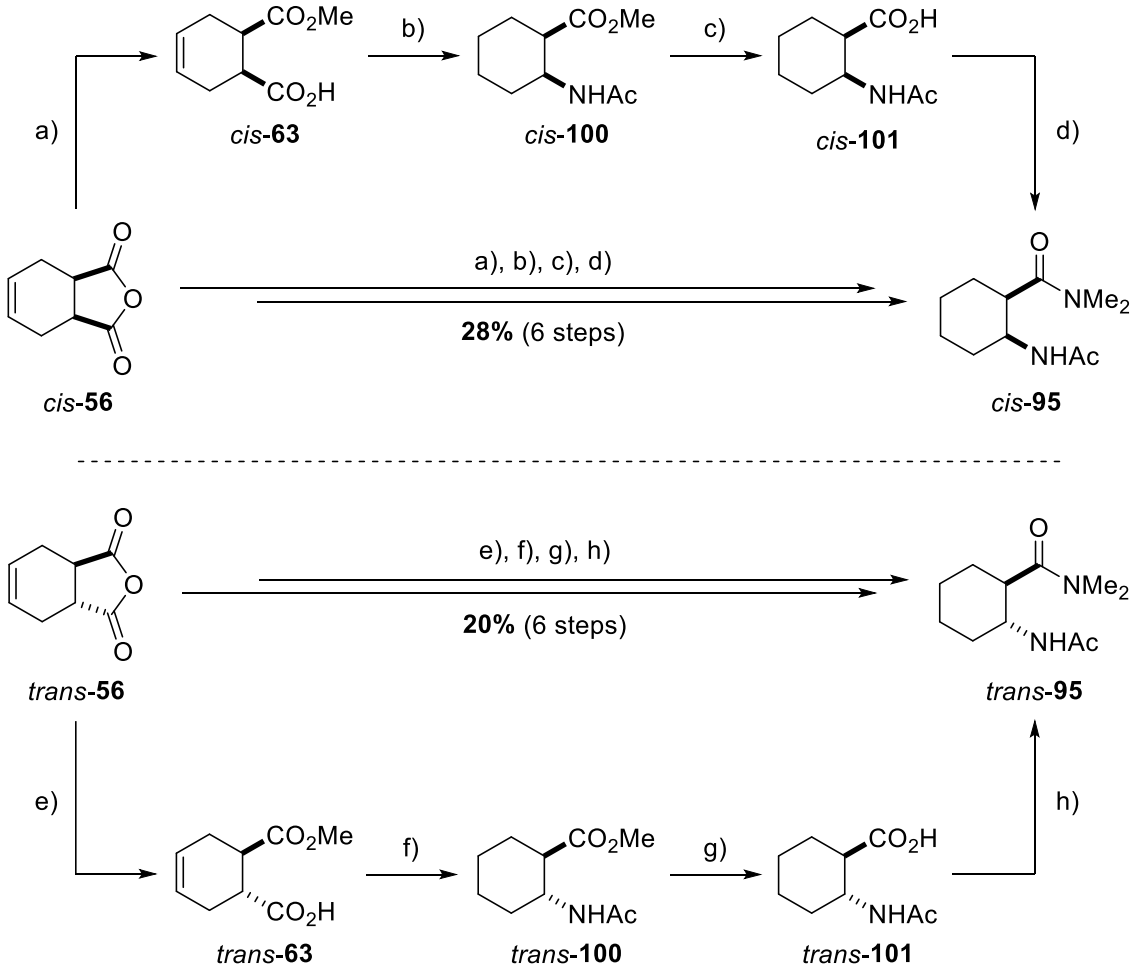

Scheme 38: Synthesis of the model compounds *cis*- and *trans*-**95**. Reaction conditions: a) MeOH, reflux, 2 h, 100%; b) 1.) DPPA, BnOH, NEt_3, toluene, reflux, 18.5 h, 2.) Pd/C, H_2 (40 bar), rt, 17 h, 3.) AcCl, DCM, 0 °C to rt, 17.5 h, 46% (3 steps); c) LiOH, THF/H_2O, 0 °C to rt, 18 h, 95%; d) 1.26 M $HNMe_2$ in THF, T3P, pyridine, THF/DMF, -10 °C to rt, 46 h, 66%; e) MeOH, reflux, 0.5 h, 95%; f) 1.) DPPA, BnOH, NEt_3, toluene, reflux, 19 h, 2.) Pd/C, H_2 (40 bar), rt, 16 h, 3.) AcCl, DCM, 0 °C to rt, 0.5 h, 50% (3 steps); g) LiOH, THF/H_2O, 0 °C to rt, 20 h, 81%; h) 1.26 M $HNMe_2$ in THF, T3P, pyridine, THF/DMF, -10 °C to rt, 46 h, 52%.

With this procedure, *cis*-**95** was obtained with 25% yield over seven steps and *trans*-**95** with 16% yield over eight steps, both starting from the cycloaddition of 3-sulfolene (**62**) respectively (Scheme 38). The two isomers could be recrystallized and the obtained crystals were subjected to X-ray analysis which confirmed their structures. A closer look at the crystal structures gives a first insight into their conformational behavior and already reveals several differences between both diastereomers (Figure 13). Model compound *cis*-**95**, which resembles the building block present in the tripeptides, features two molecules forming a well-defined dimer. Hydrogen bonding occurs between the amide and carbonyl functionality located at the cyclohexyl ring of the respective molecules. The external carbonyl of the acetyl group does not partake in any kind of coordinative action. In contrast, *trans*-**95** behaves very differently. Rather than forming dimers like *cis*-**95**, *trans*-**95** appears to order itself into a stacked, chain-like multimer through H-bonding. While these results of course only resemble the solid state case, the difference in the spatial arrangement of the molecules and H-bonding has observable effects. For instance, the melting point of *trans*-**95** is around 20 °C higher than that of *cis*-**95**. This might be explained through the H-bonding pattern: while *cis*-**95** forms only dimers, *trans*-**95** is able to generate larger coherent H-bond networks, thus stabilizing the crystal lattice and increasing the required amount of energy to melt the molecule. However, to get more insight into the actual behavior in the liquid phase, more experiments had to be conducted in solution using NMR and HP-IR spectroscopy.

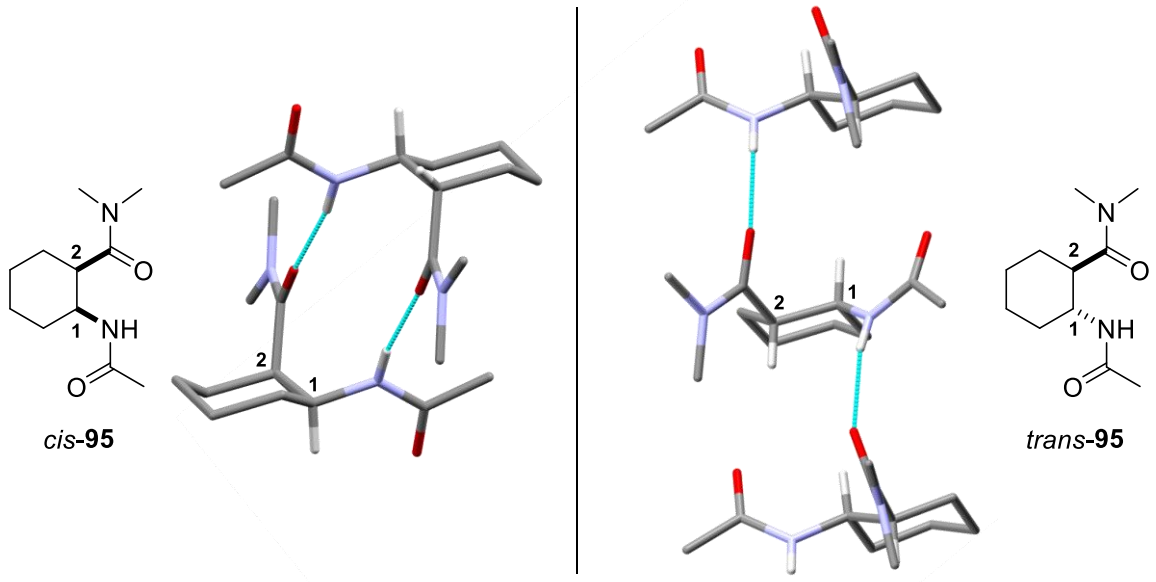

Figure 13: X-ray single crystal structures obtained from *cis*-**95** (left) and *trans*-**95** (right). Non-essential hydrogen atoms are omitted for the sake of clarity, H-bonds are depicted in cyan. The substituent-bearing carbon atoms of the cyclohexyl ring are numbered to facilitate comparison between chemical and X-ray structure.

3.2 Conformational studies of the model compounds in solution using NMR and HP-IR

3.2.1 Conformational analysis with NMR spectroscopy

After successful synthesis and preliminary investigation of the solid state properties, conformational analysis of *cis*- and *trans*-**95** in solution was carried out with NMR spectroscopy. In order to minimize solvent-solute interactions that would influence the conformational behavior, both compounds were measured in $CDCl_3$ at room temperature. A full set of 1D- and 2D-spectra were recorded, including ^{1}H, ^{13}C + DEPT, COSY, HSQC, HMBC and 2D-NOESY-experiments, allowing the unambiguous assignment of all relevant signals.

Against expectations, NMR spectra of *cis*-**95** displayed a single set of signals, indicating that it resided in only one conformation under the investigated conditions.* Evaluation of the spectroscopic data revealed that the NHAc moiety is likely to be in axial position, leaving the $C(O)NMe_2$ group in an equatorial position of the cyclohexane chair (Figure 14). The lack of ring inversion might be explained by a fixed spatial orientation of the substituents due to a stabilizing intramolecular H-bond between the carbonyl- and the amide groups. It is worth mentioning that this conformation is directly opposite to the one found in the crystal structure of *cis*-**95** (see Figure 13), but exactly resembles the one in the tripeptide **52** (see Figure 7). This leads to the assumption that the observed flexibility of the tripeptide **52** should be a result of the additional inter- and intramolecular interactions of the Prolyl-residues, rather than it being an intrinsic property of β-ACHC.

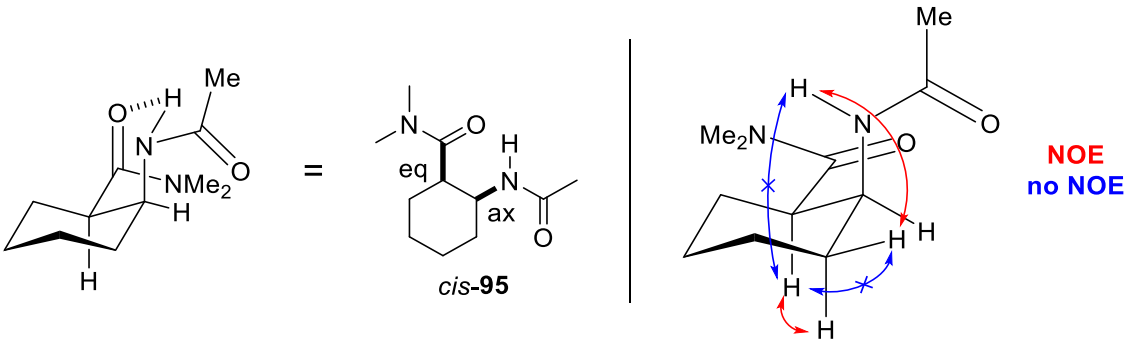

Figure 14: Depiction of the proposed conformation for *cis*-**95** based on NMR data (ax = axial, eq = equatorial, NOE = signal present in NOESY).

The investigation of the corresponding *trans*-isomer *trans*-**95** again led to unexpected findings. Here, the existence of two distinct conformations in a 5:1 ratio could be detected. The occurrence of ring inversion is highly unlikely, as this would lead an *all*-axial orientation of the substituents, which is highly

* It is also conceivable that it resides in two (or more) conformations which are rapidly interconverting. However, this should lead to significant line broadening in the NMR spectrum, which was not observed.

disfavored energetically. Furthermore, the formation of a stabilizing intramolecular H-bond is only possible in the *all*-equatorial configuration. Analysis of the ^3J(H,H)-coupling constants of the proton located at the same carbon center as the C(O)NMe$_2$-group (proton H^d, Scheme 39) proved that no ring flip occurs.* Unfortunately, the low abundance of the second conformer and the large signal overlap made structure determination rather difficult. However, the spectral data indicated that the conformational ambiguity probably stems from the *N*-acetyl moiety and two possible explanations were proposed (Scheme 39).

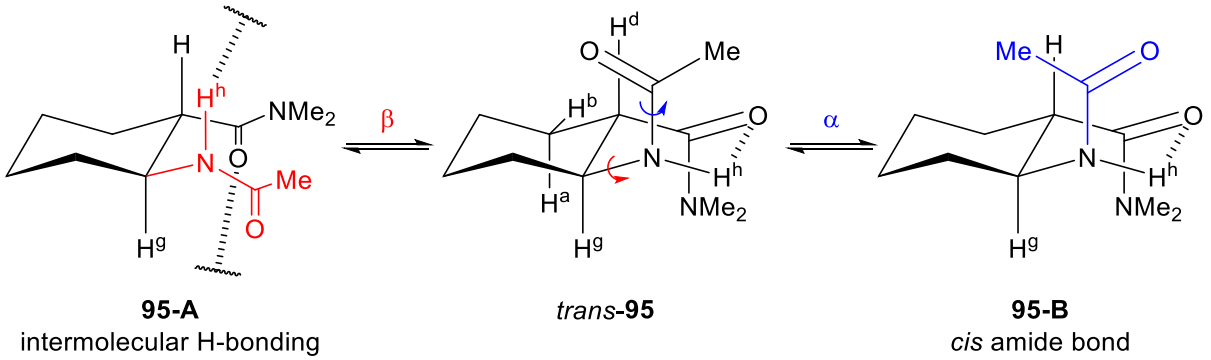

95-A
intermolecular H-bonding

trans-**95**

95-B
cis amide bond

Scheme 39: Possible structures of the minor conformer observed for *trans*-**95**. The protons are labeled in accordance with the assignment of the NMR spectra found in the appendix and are mentioned in the text.

The first one is the occurrence of an isomerization of the amide bond, leading to the (disfavored) *cis* amide **95-B**. This is supported by literature reports as it was also observed for structurally related compounds.[253] The second one is the breaking of the *intra*molecular H-bond in favor of an *inter*molecular one, as observed in the crystal structure (see Figure 13). The fact that the coupling constant of the amide proton is different for both conformers substantiates this assumption. While the main conformer (^3J(H^g,H^h) = 6.2 Hz) indicates a dihedral angle θ(H^g,H^h) of 60°, the minor conformer has a higher coupling constant (^3J(H^g,H^h) = 10.4 Hz), hinting on θ(H^g,H^h) = 180° which would resemble **95-A**.[251,252]

The tendency of intermolecular H-bonds being formed is highly dependent on the concentration of the compound and increases with higher concentrations. Whether this occurs or not can be determined

* In cyclohexanes, the ^3J(H,H) coupling constant is dependent on the dihedral angle θ(H,H) between the hydrogen atoms on adjacent carbon centers. This dependence can be described by the Karplus equation. Dihedral angles of around 60° (*i.e.* an axial-equatorial or equatorial-equatorial orientation of the adjacent protons, like H^d↔H^b in Scheme 39) leads to ^3J = 2 - 5 Hz. Angles of 180° (*i.e.* axial-axial orientation, like H^d↔H^g in Scheme 39) results in ^3J = 8 - 15 Hz. In an *all*-axial conformation of the substituents, proton H^d would be in equatorial position. This would result in θ(H,H) = 60° for all adjacent protons, meaning that the ^3J coupling constants should all be rather small. However, proton H^d gave similar coupling constants for both conformers: ^3J = 3.5 & 11.3 Hz (major) and *J* = 3.3, 10.3 Hz (minor), which is only possible for the all-equatorial conformation (as θ(H,H) = 60° and 180°). Therefore, the presence of the all-axial conformation was ruled out.[251,252]

by analyzing NMR spectra at variable concentrations, as the chemical shift of the amide proton is sensitive to hydrogen bonding. If H-bonded, the N-H bond is weakened, therefore, the proton should resonate at lower fields.[245] Hence, NMR spectra of both *cis*- and *trans*-**95** were measured at concentrations of 1 mM, 5mM, 10 mM and 50 mM (Figure 15).

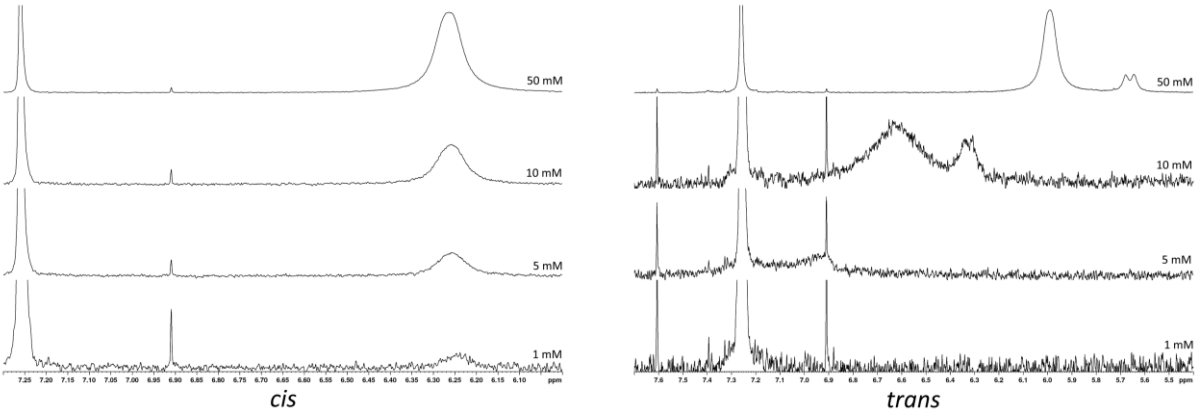

Figure 15: Excerpts of 300 MHz ^{1}H-NMR spectra of *cis*-**95** (left) and *trans*-**95** (right) at variable concentrations in $CDCl_3$ at 293 K, in order to determine the presence of intermolecular H-bonds. The large signal on the left of both spectra is from the $CDCl_3$ signal, acting as reference. Both compounds were measured with 64 scans, however, in case of *trans*-**95**, the signal-to-noise ratio is rather poor, which is probably attributed to the presence of two conformers which lowers the effective concentration. At 1 mM, the signal of the main conformer of *trans*-**95** disappears under the $CDCl_3$ signal; the minor conformer could not be traced at concentrations lower than 10 mM.

The *cis*-**95** showed no shift over the complete concentration range, indicating that it forms an intramolecular hydrogen bond, as previously proposed. Curiously, *trans*-**95** displayed a significant downfield shift of the amide proton at higher concentrations. This is odd as it would mean a weakening of the H-bonding in more concentrated solutions, potentially due to a rearrangement of the hydrogen bond network. At the same time, this decreases the likelihood of intermolecular hydrogen bonds (**95-A**) being the cause for the observation of the minor conformer in the NMR spectra and tips the scale in favor of **95-B**.

3.2.2 Conformational analysis with high-pressure infrared spectroscopy (HP-IR)

The NMR analysis revealed, that it was worthwhile to further elucidate the hydrogen bonding behavior of *cis*- and *trans*-**95**. Infrared spectroscopy measurements are an ideal tool for identifying hydrogen-bonded states, as H-bonding leads to a weakening of the bond strengths of the donor and acceptor groups. This is observable as a shift to lower wavenumbers in the IR spectrum of the respective vibrational modes. Analysis of three important vibrational bands, amide A (N-H stretching), amide I (C=O stretching) and amide II (C-N stretching and N-H bending), will provide information on the hydrogen bonding state of the model compounds (Figure 16).[254]

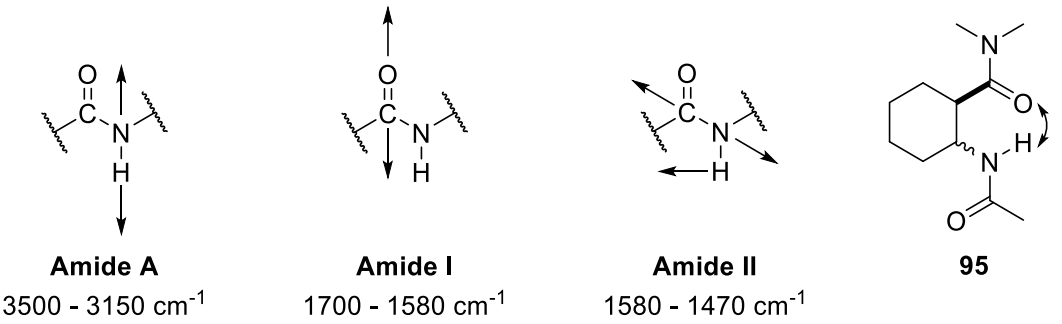

Figure 16: Investigated vibrational modes of the model compounds.

As the influence of elevated pressure is known to affect hydrogen bonding,[40,41,242,255] this investigation became a cooperative project within the FOR 1979 high-pressure research group. This enabled the measurement of HP-IR spectra of *cis*- and *trans*-**95** in collaboration with Winter *et al.* at the TU Dortmund. Spectra were recorded at relatively high concentrations, meaning that intra- as well as intermolecular hydrogen bonding (if present) would be observed, while the use of $CHCl_3$ made sure that solvent-solute interactions remained minimal.*

The HP-IR spectra of *cis*-**95** appeared to be rather simple (Figure 17). At low pressures, the amide A band showed two peaks, a narrow one at 3427 cm^{-1}, which is considered to arise from a non-hydrogen bonded state, and a broad one at 3338 cm^{-1} as a result of hydrogen bonding. As no concentration dependence of the amide proton was observed in the NMR experiments (see Figure 15), both states should be rapidly interconverting.

* Recording spectra at lower concentrations (which would eliminate the intermolecular contribution) was not possible due to technical limitations in the experiment setup.

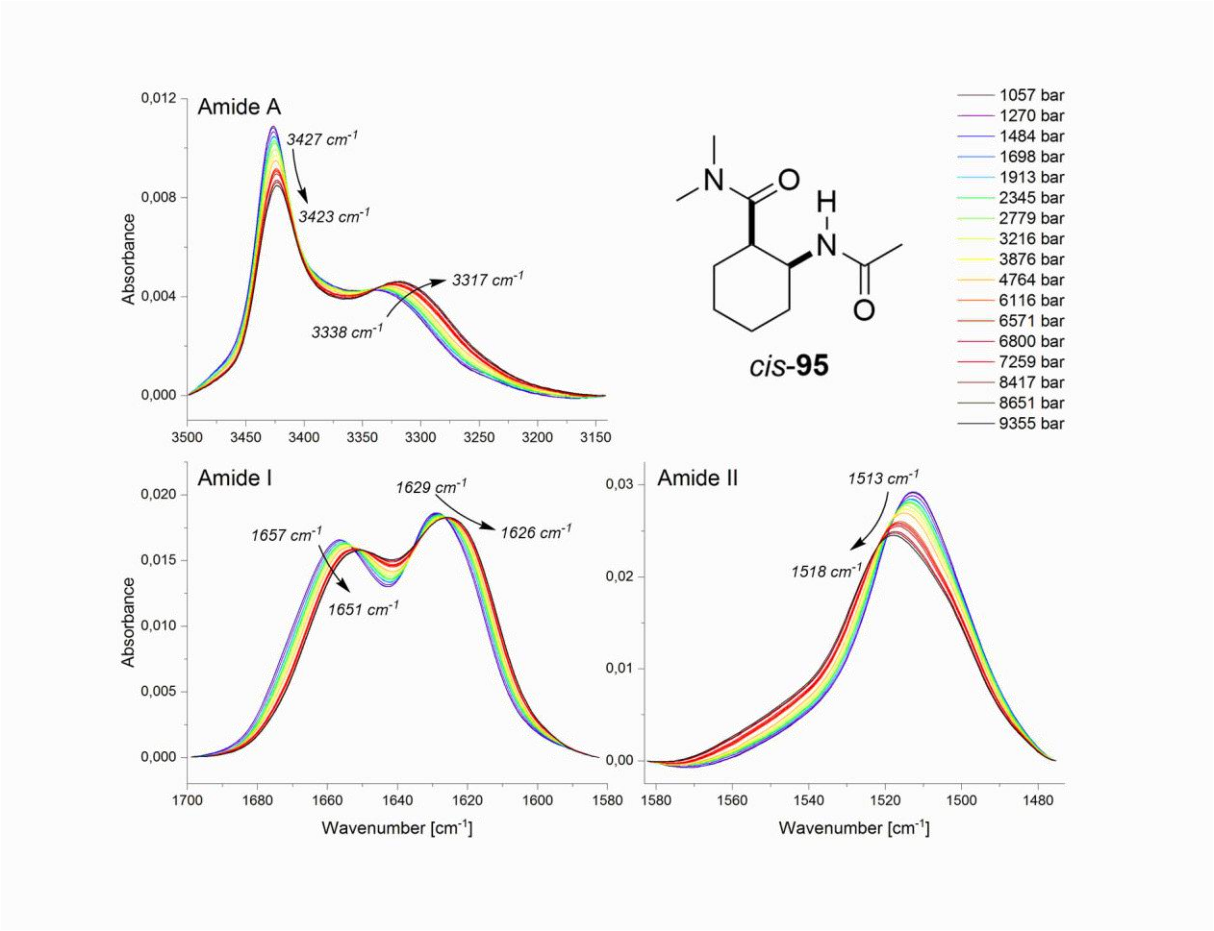

Figure 17: Normalized HP-IR spectra of *cis*-**95** in $CHCl_3$ (236 mM) at 298 K.

This indicates that the H-bond is rather weak, which is presumably caused by the non-linearity of the N-H···O bond angle and the non-planarity of the N-C=O···H torsional angle in an intramolecular H-bond.[244]* Upon pressurization, the intensity of the non-bonded state decreased while the bonded state increased, and both peaks shifted to lower wavenumbers (3423 and 3317 cm^{-1}). These observations correspond to a strengthening of the hydrogen bond of *cis*-**95** as well as an increase in its tendency to form under pressure. This appears to be a logical consequence when the volume is confined and is in agreement with literature reports on the influence of pressure on H-bonding.[40,41,242,255] Analyzing the Amide I band, it has to be considered that the molecule contains two carbonyl groups from which only one ($C(O)NMe_2$) is involved in effective hydrogen bonding, explaining the two relatively narrow peaks at 1657 and 1629 cm^{-1}. The band at 1657 cm^{-1} displayed a higher susceptibility to pressurization (shifting to 1651 cm^{-1}) than the band at 1629 cm^{-1} (which only

* Studies of Gellman *et al.*, investigating hydrogen bonding patterns in relation to their ring sizes, revealed a similar behavior for linear model compounds of comparable structure. The compound with a six-membered hydrogen bond did also display a bonded and a non-bonded state, with a prevalence for the bonded state. They attributed the observed stability of the hydrogen bond to the lack of torsional strain and a minimal entropic barrier during formation.[244]

shifted to 1626 cm^{-1}). As the C=O bond is weakened by H-bonding and the observations for the amide A band indicated that H-bonding increases with pressure, this indicates that the band at 1657 cm^{-1} originates from the carbonyl group that is involved in hydrogen bonding ($C(O)NMe_2$). The amide II band is rather broad with only one visible maximum at 1513 cm^{-1}. Here, pressurization leads to a shift to higher wavenumbers (1518 cm^{-1}), corresponding to a stronger C-N bond as a result of both, the N-H and C=O bonds, being weakened by increased H-bonding.[256] Overall, *cis*-**95** was found to reside in one conformer, which is stabilized partially by a weak hydrogen bond which strengthens upon pressurization.*

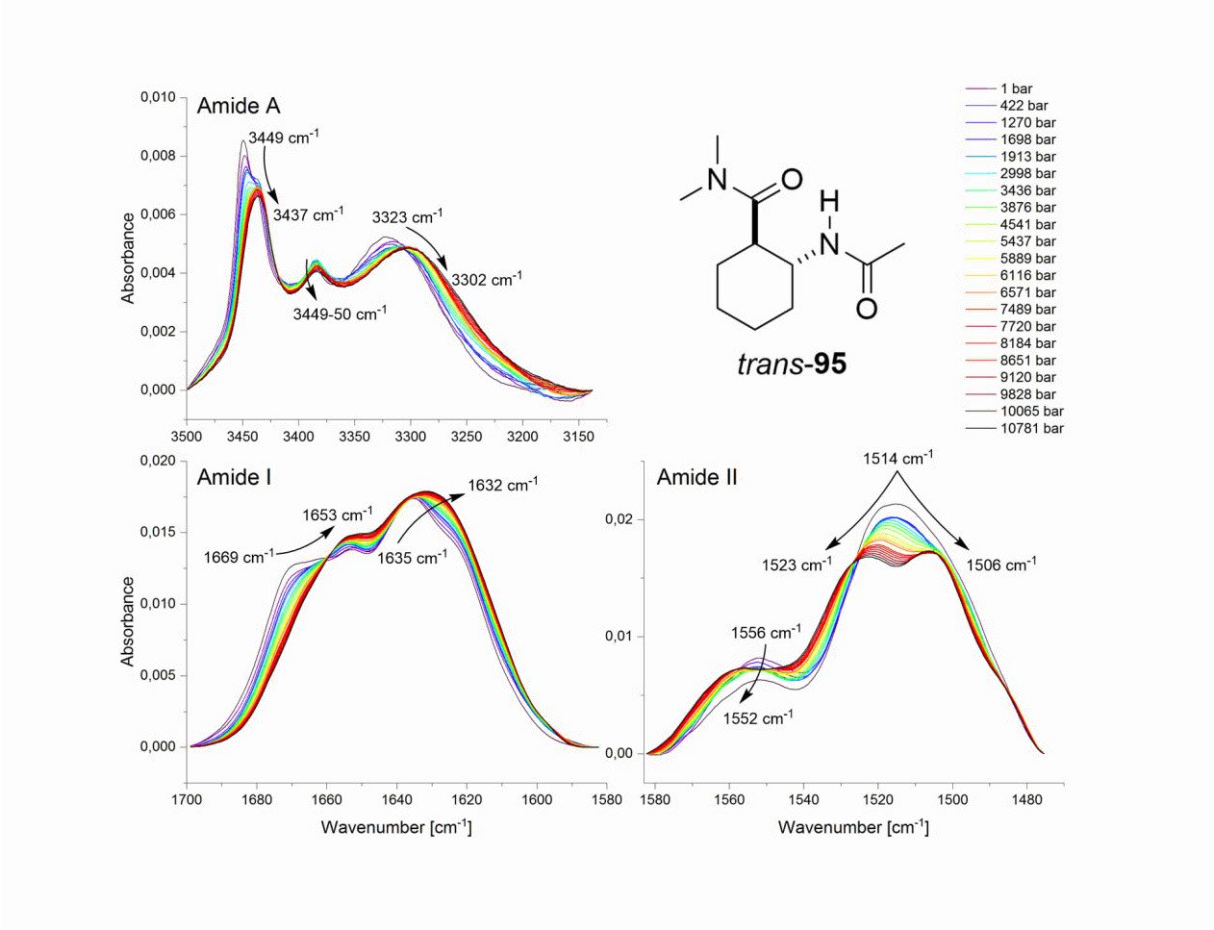

Figure 18: Normalized HP-IR spectra of *trans*-**95** in $CHCl_3$ (236 mM) at 298 K.

The data obtained from *trans*-**95** proved to be more complex than for *cis*-**95** (Figure 18). The amide A band showed three major bands at ambient pressure. The narrow one at 3449 cm^{-1} should again represent the non-hydrogen bonded N-H, however, the presence of a shoulder to the right side of the

* In the last chapter, it was discovered that the enantioselectivity of the β-ACHC-tripeptide-catalyzed aldol reaction improved under HP conditions. It was argued that pressurization should result in rigidification, leading to a more defined catalyst structure (see chapter 2.7). The increased tendency of hydrogen bond formation of *cis*-**95** under higher pressures might be an important contributing factor to this conformer stabilization.

peak indicates that there should be at least two different non-bonded states. Interestingly, there are two separate bands which probably associate with some sort of hydrogen-bonded state, the broad peak at 3323 cm^{-1} and the small peak at 3385 cm^{-1}. Due to the high sample concentration, intermolecular H-bonding could not be ruled out, which means that the second peak could also arise from this (see **95-A** in Scheme 39). However, the appearance of a third peak like the one at 3385 cm^{-1} was also reported by Gellman *et al.*, who analyzed their (comparable) model compounds at low concentrations (1 mM) where an intermolecular contribution could be ruled out. They indicated that the peak might arise from a weak H-bonding of the amide proton with the π-system of the dimethylamide moiety.[244] The pressure response of the system is comparable to *cis*-**95**: while the non-bonded state decreases (3437 cm^{-1}), the H-bonded state becomes more populated at higher pressures and the strength of the H-bond increases (3302 cm^{-1}). The third, weakly-bonded state is barely influenced at all (3384 cm^{-1}). Analysis of the amide I band gave little to interpret, as the spectrum at ambient pressure showed several overlapping peaks (1669, 1653, 1635 cm^{-1}) and shoulders in a small area. Upon pressurization, the spectrum became simpler as several peaks converged and shifted to lower wavenumbers, leaving only two peaks (1653 and 1632 cm^{-1}). The amide II band provided more information. While only two bands were observed at 1 bar (1552 cm^{-1} and 1514 cm^{-1}), the high-pressure spectra showed a split-up of the signal at 1514 cm^{-1} into two separate maxima at 1523 cm^{-1} and 1506 cm^{-1}. As the amide II band is partially associated with the C-N stretching vibration, this might provide evidence for the *cis*-*trans* isomerization of the amide bond (see **95-B**), as intermolecular hydrogen bonding should not lead to the observed splitting but rather lead to a general shift to higher wavenumbers (as in *cis*-**95**).[*] This is underlined by investigations from Sahai *et al.* who demonstrated that the amide II band of a *cis* amide bond is shifted to lower wavenumbers than the corresponding *trans* amide.[257] Comparing this to the observed peak splitting of *trans*-**95** provides strong evidence for the *cis*-*trans* isomerization of the amide bond (see **95-B**) and nicely demonstrates the usefulness of high pressure as a tool for stabilizing and identifying rare conformational states.

In conclusion, the investigation of the model compound revealed that even small cyclic model compounds can possess a high conformational ambiguity. Therefore, the model compounds should be further investigated in the FOR 1979 research group, by using other spectroscopic methods (*e.g.* HP-NMR), analyzing them in more polar solvents (*e.g.* acetone/H_2O) and through complementary theoretical calculations to determine low energy conformers.

[*] However, this only disproves that the intermolecular hydrogen bonded system is the cause behind the second conformer observed in the NMR. It does not disprove the existence of intermolecular hydrogen bonds in general, which are still very likely to form.

4. Synthesis of ^{15}N-labeled compounds

The development of NMR spectroscopy methods has advanced rapidly since their establishment in the 1950s.[258,259] From non-invasive body imaging in medicine[260] to the analysis of complex physical, chemical and biological processes and compounds it plays a vital role as a versatile analytical tool in modern science.[258,259] Especially in the field of structure determination of large biological macromolecules like, *e.g.* proteins it plays a pivotal role, as it is one of few experimental methods capable of determining the conformation in solutions.[261]

NMR spectroscopy requires the presence of respondent nuclei with a nonzero spin.[259] Besides hydrogen and carbon, nitrogen nuclei are probably one of the most important for measuring biological compounds, due to the high presence of nitrogen in biomolecules like DNA, RNA, or peptides. Measuring nitrogen's main isotope ^{14}N (99.6%) is hampered by the fact that it is a quadrupole which leads to extremely broadened, hard to interpret signals.[259,262] Using the naturally occurring isotope ^{15}N counteracts these problems, however, its abundance is only around 0.4%.[263] Coupled with a rather low sensitivity, recording natural abundance ^{15}N spectra would be immensely time-consuming, especially when only limited amounts of sample are available.[259,262] Therefore, the most viable way to approach this problem is by using isotopically enriched compounds.

In the FOR 1979 high-pressure research group, two molecules are of high interest: trimethylammonium *N*-oxide (TMAO, **102**) and *N*-methylacetamide (NMA, **103**). Both are currently investigated in detail, especially in relationship with pressure effects.

The challenge in synthesizing both ^{15}N-labeled derivatives was, besides the requirement of analytically pure samples in sufficient amounts (> 500 mg), the limitation to a common, commercially available starting material: $^{15}NH_4Cl$ (**^{15}N-104**). This was chosen primarily due to economic reasons. As mentioned above, the natural abundance of ^{15}N is very low, therefore, ^{15}N-labeled compounds are usually very costly. $^{15}NH_4Cl$ (**^{15}N-104**) is used routinely in minimal bacterial growth media in biology for the expression of isotopically enriched proteins and DNA, it is widely available and rather inexpensive.* Moreover, as an inorganic salt, it can be easily handled and stored without deterioration. However, this also posed complications, as its inorganic nature renders it almost non-reactive in organic reactions. Special focus had to be laid upon ensuring that no inseparable byproducts (*e.g.* salts) were formed to preserve the analytical purity of the final product. Preliminary test experiments were carried

* Prices for 1 g of compound (>98% ^{15}N) from Sigma Aldrich (19.02.2018): $^{15}NH_4Cl$ (**^{15}N-104**): 75.50 €. $^{15}NMe_3{\cdot}HCl$ (**^{15}N-105**, intermediate in the ^{15}N-TMAO synthesis): 551.00 €. ^{15}N-acetamide (**^{15}N-106**, intermediate in the ^{15}N-NMA synthesis): 385.00 €.

out using non-labeled NH_4Cl to develop reliable synthetic routes which could then be transferred to the actual syntheses using the labeled $^{15}NH_4Cl$ (**^{15}N-104**).

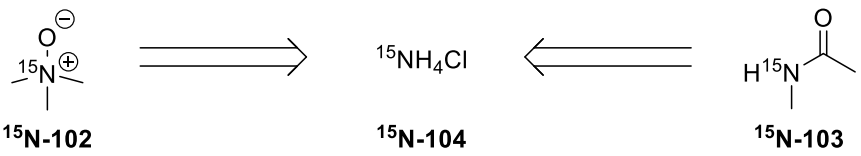

^{15}N-102 **^{15}N-104** **^{15}N-103**

Scheme 40: The two ^{15}N-labeled target molecules which had to be synthesized from $^{15}NH_4Cl$ (**^{15}N-104**): ^{15}N-TMAO (**^{15}N-102**) and ^{15}N-NMA (**^{15}N-103**).

4.1 Synthesis of ^{15}N-TMAO

Trimethylammonium *N*-oxide (**102**) is a naturally occurring osmolyte found in saltwater organisms. As an osmolyte, TMAO (**102**) serves as a stabilizing agent for proteins against external influences like temperature fluctuations and salinities. It preserves the proteins folded structure, and therefore functional state, thus preventing undesired denaturation and subsequent loss of functionality. Interestingly, the TMAO concentration in the tissue of deepwater fish increases the lower their natural habitat is located. Therefore, TMAO (**102**) appears to also play a major role in protein stabilization against high hydrostatic pressures. It also appears in the human body as a metabolite and elevated TMAO levels are believed to be linked to a higher risk of cardiovascular attacks.[264] This makes TMAO (**102**) a primary research subject of the FOR 1979 research group.

As ^{15}N-labeled TMAO (**^{15}N-102**) is not commercially available, it had to be synthesized. The idea for the straightforward synthesis of ^{15}N-TMAO (**^{15}N-102**) from $^{15}NH_4Cl$ (**^{15}N-104**) was to perform a triple *N*-methylation, *N*-oxidation sequence. This required a reliable protocol for the selective triple methylation, rendering standard conditions using MeI and base useless, as they result in low selectivities and tend to lead to quaternization. In 2016, Beydoun *et al.* published an efficient protocol for the selective catalytic N-methylation of ammonium chloride with CO_2 and H_2 in dioxane/water.[265] Although the use of CO_2 as a methylating agent is interesting, especially in terms of using waste products as reactants, the process required the use of a non-commercial ruthenium catalyst [Ru(triphos)(tmm)].

A more convenient approach was the utilization of the Eschweiler-Clarke reaction. Herein, an aldehyde reacts with the amine generating an imine, which is subsequently reduced by the acts of a reductant, usually formic acid. Already in 1921, Adams *et al.* published the highly selective synthesis of trimethylamine hydrochloride (**105**) from NH_4Cl (**104**) with the use of paraformaldehyde.[266] This simple process does not require the use of an additional reductant and can be performed completely

without solvent and worked smoothly (Scheme 41). Considering that the next step would involve the liberation of gaseous trimethylamine followed by *N*-oxidation, purification of the obtained crude trimethylamine hydrochloride (**105**) was deemed to be unnecessary. The *N*-oxidation would then be achieved by leading the trimethylamine directly into a cooled solution of hydrogen peroxide. This procedure ensured that no other impurities were introduced into the final product, especially inorganic salts which would have been very difficult to separate otherwise. Following this route, non-labeled TMAO (**102**) could be synthesized as the dihydrate in 72% yield in analytically pure form. Therefore, the chosen reaction sequence was transferred to the synthesis of ^{15}N-TMAO (**^{15}N-102**), which could be obtained as the dihydrate in 67% yield in analytically pure form (Scheme 41).

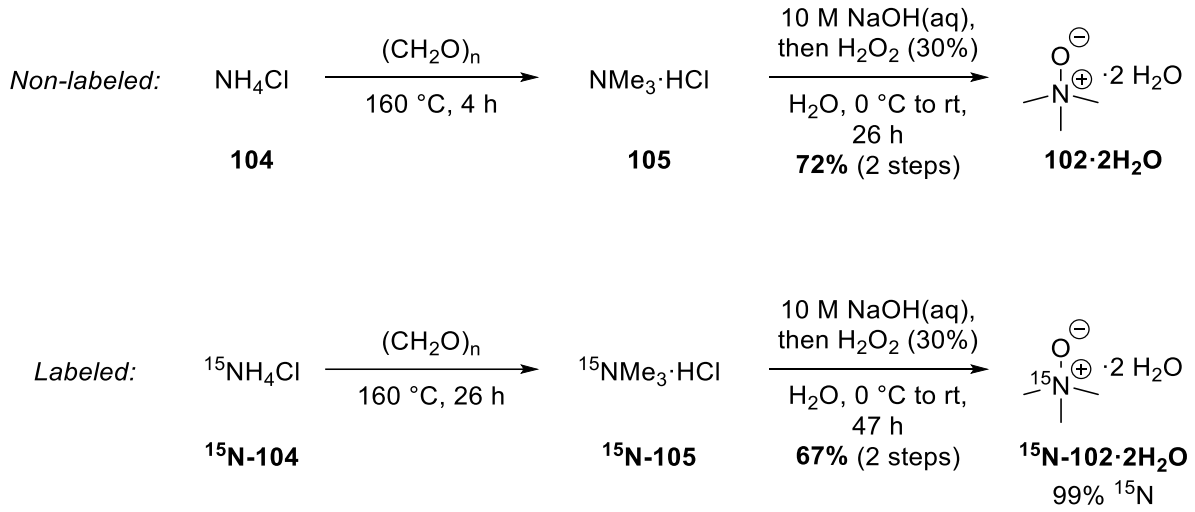

Scheme 41: Synthesis of labeled and non-labeled TMAO dihydrate (**102·2H$_2$O**).

This describes the first successful chemical synthesis of ^{15}N-TMAO (**^{15}N-102**). It was handed over to the biophysical department of the University of Regensburg and is currently being analyzed and used in further experiments in collaborative work within the FOR 1979 research group.

4.2 Synthesis of ^{15}N-methylacetamide

N-methylacetamide (**103**) represents a prototypical amide bond and can thus act as a model compound for the protein amide backbone in spectroscopic and computational methods.[267] In particular, high-pressure NMR spectroscopy (HP-NMR) proved to be a powerful tool in the analysis and determination of rare, low-populated protein conformation states.[238] Detailed knowledge of these conformations allows a better understanding of the behavior of proteins in solution, which itself might lead to the development of new, more selective drugs.[268] Identification of these rare states is accomplished by plotting chemical shift values against pressure and subsequent extrapolation of relevant

thermodynamic parameters using a polynomial fit function.[269] However, due to the high complexity of protein NMR spectra, the in-depth analysis of all data sets is often tedious and time-consuming. Furthermore, the correct interpretation of the obtained parameters requires the knowledge about whether the observed shifts are due to the pressure itself or simply because of the changing electronic properties of the solvent under pressure.[267] Here, computational models are often a helpful tool for additional input. Within the research group FOR 1979, Kast *et al.* from the TU Dortmund developed the "Embedded Cluster Reference Interaction Site Model" (EC-RISM) computational method.[270] It allows the prediction of NMR shifts with respect to high-pressure influences, using *N*-methylacetamide (**103**) as a model for the prototypical amide backbone.[267,271] However, to verify the validity of the method it needed to be compared to experimental data. Therefore, HP-NMR experiments were conducted which required the synthesis of ^{15}N-labeled *N*-methylacetamide (**^{15}N-103**).

There are several methods known how to synthesize NMA (**103**) on a laboratory scale. Common synthetic methods include, *e.g.* the Beckmann rearrangement of acetone oxime,[272] the acetylation of methylamine[272] or the thermal decomposition of methylammonium acetate.[273] These methods, however, are impractical if the choice of starting materials is limited to ammonium chloride. They would require either hydroxylamine or methylamine, which both are tedious to synthesize on a small scale. Therefore, a different approach was pursued. It was considered to first synthesize acetamide (**106**) from ammonia and then do a subsequent *N*-methylation. Morgan *et al.* already published a synthesis of ^{15}N-labeled acetamide (**^{15}N-106**) in 1991, using an aqueous ammonia solution in combination with 2,2,2-trifluoroethyl acetate (**107**) as acetylating agent. While 2,2,2-trifluoroethyl acetate (**107**) could be readily synthesized from 2,2,2-trifluoroethanol and acetyl chloride,[274] an aqueous ammonia solution was generated from heating a solid mixture of NH_4Cl (**104**) and $Ca(OH)_2$ and transferring the gas into cooled water. The reaction between the ammonia solution and 2,2,2-trifluoroethyl acetate (**107**) was successful, giving rise to non-labeled acetamide (**106**) in 56% yield (Scheme 42).

The next step, the *N*-monomethylation of acetamide (**106**), proved to be rather complicated. A first attempt was made to use a modified Eschweiler-Clarke reaction published by Rosenau *et al.*, in analogy to the TMAO synthesis.[275] Unfortunately, the reaction failed as no conversion of the starting material was detectable. This is probably due to the fact that the amide is too unreactive to form the imine, which is crucial for the reaction to perform. A second attempt was made by using a procedure published by Bassindale *et al.* in 2000.[276] Herein, they reported the use of chloromethyldimethylsilyl chloride (CMDMCS), hexamethyldisilazane (HMDS) and cesium fluoride to efficiently synthesize *N*-methylpropanamide from propanamide. Application of these conditions, however, gave only unsatisfactory results as only traces of product were formed.

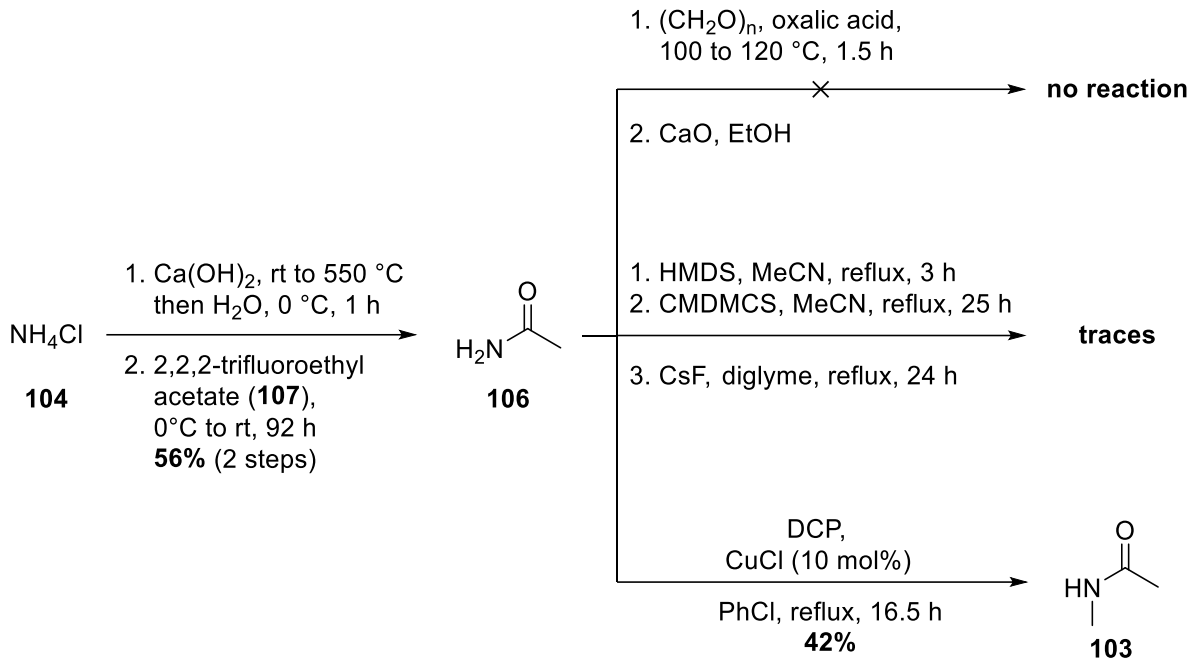

Scheme 42: Synthetic approach to non-labeled *N*-methylacetamide (**103**). DCP = dicumyl peroxide.

In 2013, Xia *et al.* were able to methylate a variety of aromatic and non-aromatic amides with dicumyl peroxide (DCP) in combination with copper catalysis.[277] They provided evidence for a radical mechanism in which a methyl radical from the DCP was transferred to the amide. With this process, acetamide (**106**) could be successfully methylated to *N*-methylacetamide (**103**), although it required an elaborate purification process. The complete reaction sequence in hand now enabled the synthesis of ^{15}*N*-methylacetamide (**^{15}N-103**) starting from $^{15}NH_4Cl$ (**^{15}N-104**). ^{15}N-Acetamide (**^{15}N-106**) and ^{15}*N*-methylacetamide (**^{15}N-103**) were both synthesized successfully in analytically pure form, giving access to ^{15}*N*-methylacetamide (**^{15}N-103**) in 37% overall yield starting from **^{15}N-104** (Scheme 43).

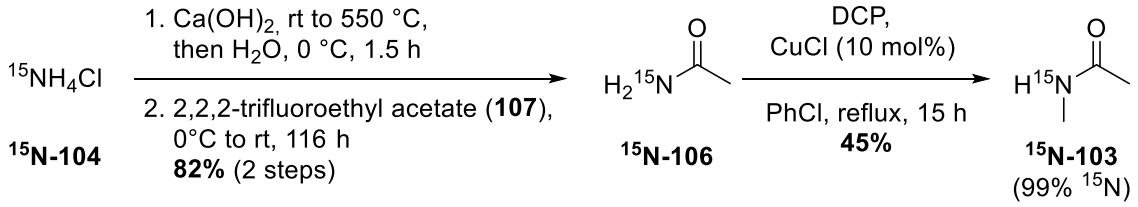

Scheme 43: Synthesis of ^{15}*N*-methylacetamide (**^{15}N-103**). DCP = dicumyl peroxide.

The ^{15}N-labeled compound **^{15}N-103** was investigated in detail under HP NMR conditions by Kalbitzer and Kremer *et al.* in the biophysical department of the University of Regensburg. Pressure dependent ^{1}H-, ^{13}C- and ^{15}N-spectra were recorded and all relevant thermodynamic parameters determined. Comparison of the empirical results with the ones obtained with computation revealed that the computational model delivered quite accurate results for ^{1}H and ^{13}C, although the ^{15}N predictions still require further optimization.[267] This work is currently further pursued within the FOR 1979 network.

C. Summary

Over the last century, the use of high hydrostatic pressure has established itself as a valuable tool in chemistry, either as activation mode for chemical reactions or in combination with spectroscopic methods in order to investigate the structural and conformational behavior of (bio-)molecules.

The first chapter of this thesis compares the influence of high-temperature and high-pressure conditions on the Lewis base-organocatalyzed Michael addition of aldehydes (**39a-g**) to *trans*-β-nitrostyrene (**40**), using a racemic (**42**) as well as an asymmetric catalyst (**28**) (Scheme 44).

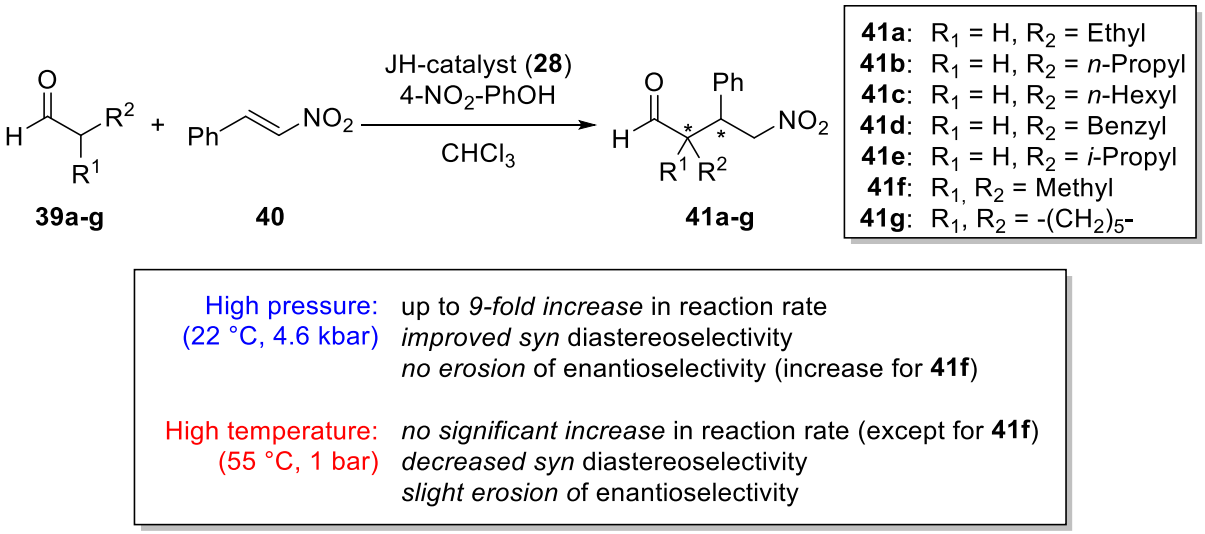

Scheme 44: Organocatalytic asymmetric Michael addition using the Jørgensen-Hayashi catalyst (**28**) under high pressure and high-temperature conditions.

The investigations demonstrated that pressurization clearly outperforms conventional heating as secondary activation mode. Compression provided higher reactivities and vastly improved diastereoselectivities compared to ambient conditions and led to no erosion of enantioselectivity in the asymmetric reactions. These results illustrate the viability of the high-pressure technique as a mild and powerful alternative to the established heating procedure.

The second chapter describes the synthesis of three different tripeptide organocatalysts containing unnatural β-amino acids and the evaluation of their catalytic as well as structural behavior under pressure. Key step for the synthesis of the flexible tripeptides **52** and *ent*-**52** was the desymmetrization of *meso* anhydride *cis*-**56** in order to obtain the enantiopure β-amino acids. For the rigidified **53**, anthranilic acid (**54**) could be used as starting material (Scheme 45).

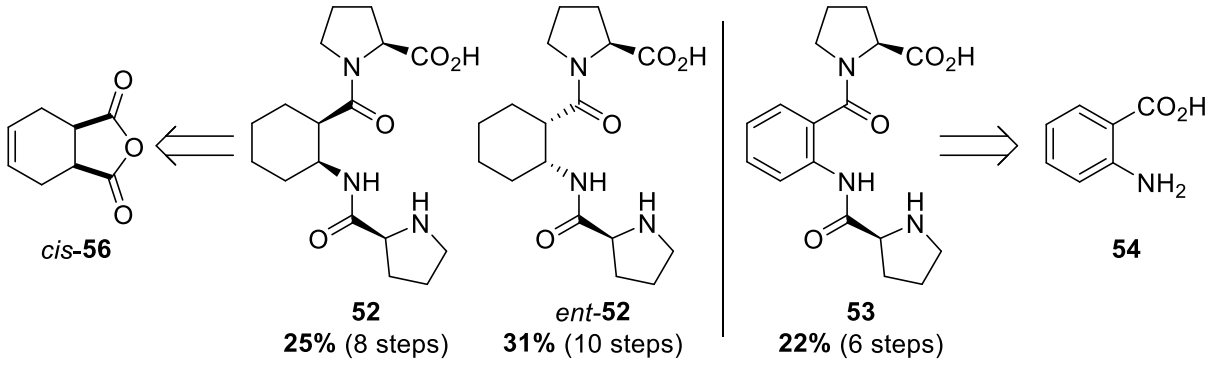

Scheme 45: Synthesized tripeptide catalysts containing unnatural β-amino acids.

Their catalytic abilities were subsequently put to the test in an intermolecular aldol and a Michael addition under ambient as well as high-pressure conditions. In both transformations, the catalysts exhibited significantly increased reaction rates at elevated pressures. While the rigidified tripeptide **53** proved to be the most susceptible to pressure in terms of reactivity, the flexible catalysts **52** and *ent*-**52** displayed a slight increase in enantioselectivity in the aldol reaction upon pressurization (Scheme 46).

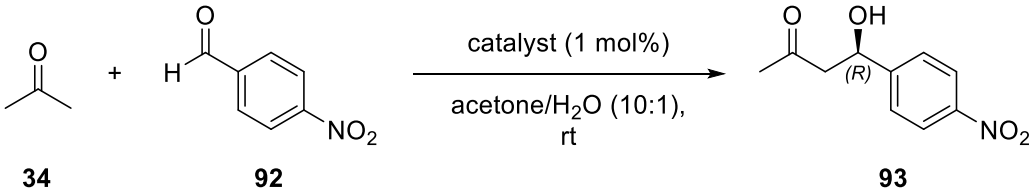

	Pressure effect (1 bar to 4.8 kbar)
Flexible catalysts: (**52** & *ent*-**52**)	more than *3-fold increase* in reaction rate *slightly improved* enantioselectivity
Rigidified catalyst: (**53**)	more than *5-fold increase* in reaction rate *unchanged* enantioselectivity

Scheme 46: Tripeptide-catalyzed aldol reaction under high-pressure conditions.

As this observation might be linked to a pressure-induced conformational change, it was decided to further investigate the structural behavior of catalyst **52**. High-pressure NMR studies in acetone-d_6/D_2O (10:1) revealed that the tripeptide **52** resides in at least three different conformations. These are probably caused by ring inversion of the central β-amino acid and rotations around the peptide bond of the N-terminal prolyl moiety.

Since the high structural ambiguity of **52** complicated the conformational analysis, two model compounds were synthesized in order to solely investigate the behavior of the central β-amino acid. The findings are described in the third chapter. Both molecules were synthesized from their respective

meso anhydrides: *cis*-**95** representing the structural analog to **52** and *trans*-**95** as a reference which does not undergo ring inversion (Scheme 47). NMR- as well as high pressure IR-spectroscopy in chloroform revealed that *cis*-**95** resides in only one conformation which is stabilized by an intramolecular hydrogen bond. The isomeric *trans*-**95**, however, resides in two conformations, which are probably caused by a *cis*-*trans*-isomerism of the peptide bond of the *N*-acetyl moiety.

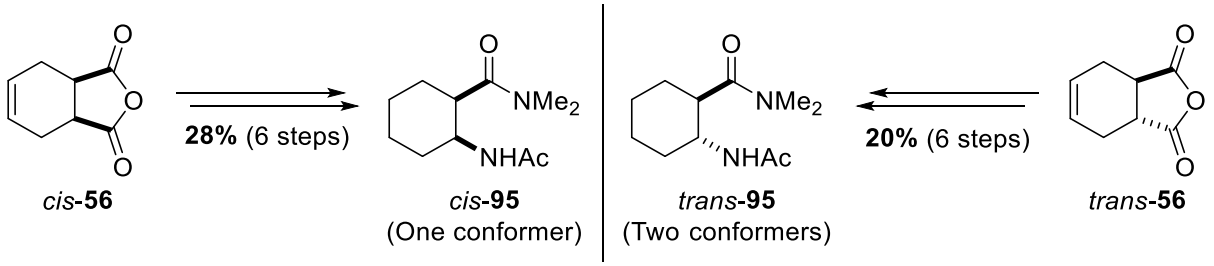

Scheme 47: Synthesis of β-ACHC derivatives used as model compounds for conformational analyses.

The final chapter describes the synthesis of two ^{15}N-labeled compounds for investigations with NMR spectroscopy. Both molecules, ^{15}N-TMAO (**^{15}N-102**) and ^{15}N-NMA (**^{15}N-103**), were obtained from inorganic, affordable $^{15}NH_4Cl$ (**^{15}N-104**) in analytically pure form and have been used in an ongoing collaborative research project within the FOR 1979 high-pressure research group (Scheme 48). TMAO (**102**) represents a naturally occurring osmolyte that stabilizes proteins of deep sea fish against high pressures, making it a relevant research subject. The synthesis ^{15}N-NMA (**^{15}N-103**) became necessary in order to enable validation of a computational model for the prediction of NMR shifts under pressure developed by Kast *et al.* with actual empiric data. First promising results have already been published, with further investigations still ongoing within the research group.

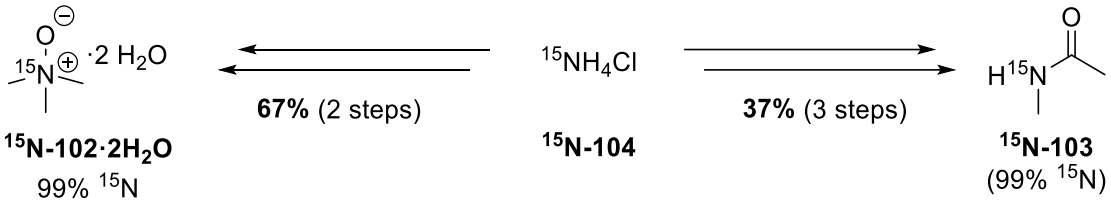

Scheme 48: Synthesis of ^{15}N-labeled TMAO dihydrate (**^{15}N-102·2H$_2$O**) and NMA (**^{15}N-103**) from affordable $^{15}NH_4Cl$ (**^{15}N-104**).

D. Zusammenfassung

Über das letzte Jahrhundert hat sich die Verwendung von hohem hydrostatischen Druck als wertvolles Werkzeug in der Chemie etabliert, entweder als Aktivierungsmethode für chemische Reaktionen oder in Kombination mit spektroskopischen Methoden um das strukturelle und konformelle Verhalten von (Bio-)Molekülen zu untersuchen.

Das erste Kapitel dieser Arbeit vergleicht den Einfluss von Hochtemperatur- und Hochdruckbedingungen auf die Lewis-Base-organokatalysierte Michael-Addition von Aldehyden (**39a-g**) an *trans*-β-Nitrostyrol (**40**), unter Verwendungen eines racemischen (**42**) und eines asymmetrischen Katalysators (**28**) (Schema 1).

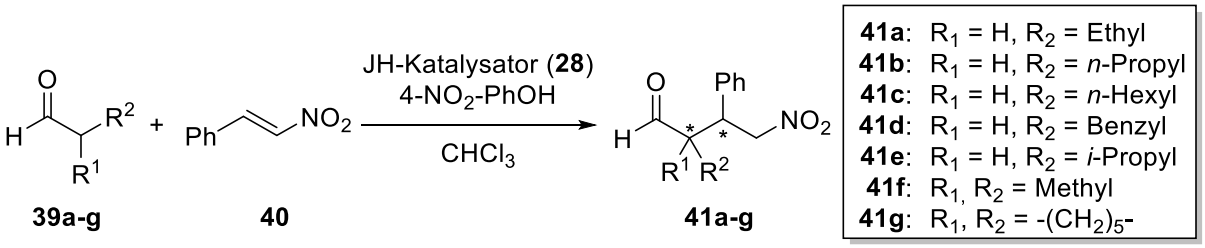

Schema 1: Organokatalytische Michael-Addition unter Hochtemperatur- und Hochdruckbedingungen.

Die Untersuchungen zeigten, dass Druckbeaufschlagung als sekundäre Aktivierungsmethode das konventionelle Heizen klar übertrifft. Kompression führte zu höherer Reaktivität und erheblich verbesserter Diastereoselektivität im Vergleich zu Normalbedingungen und führte zu keiner Abnahme der Enantioselektivität in den asymmetrischen Reaktionen. Diese Ergebnisse verdeutlichen die Wirksamkeit der Hochdruckmethodik als eine milde und zugleich leistungsfähige Alternative zum konventionellen Aufheizen der Reaktionsmischung.

Das zweite Kapitel beschreibt die Synthese von drei verschiedenen Tripeptidorganokatalysatoren, welche unnatürliche β-Aminosäuren enthalten, und die Evaluierung ihres katalytischen sowie strukturellen Verhaltens unter Druck. Den Schlüsselschritt für die Synthese der flexiblen Tripeptide **52** und *ent*-**52** stellte die Desymmetrisierung des *meso*-Anhydrids *cis*-**56** dar, um die enantiomerenreinen

β-Aminosäuren zu erhalten. Für das rigidere **53** konnte Anthranilsäure (**54**) als Startmaterial verwendet werden (Schema 2).

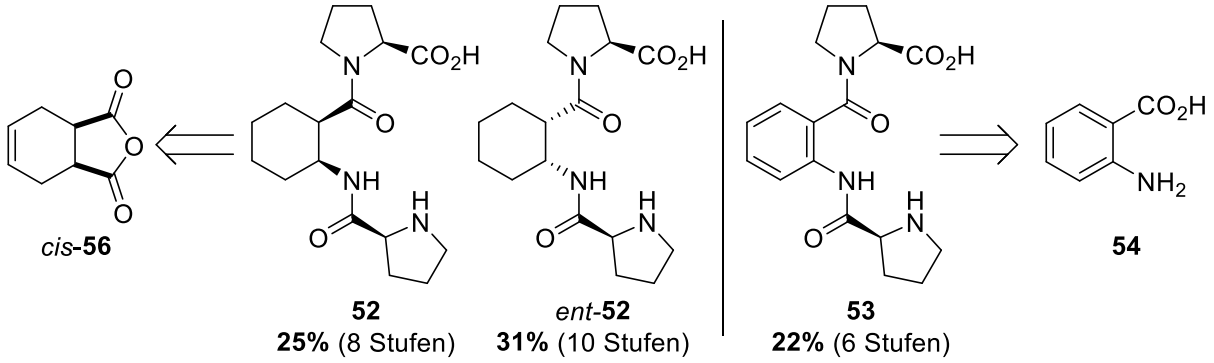

Schema 2: Synthetisierte, β-Aminosäure-enthaltende Tripeptidkatalysatoren.

Ihre katalytischen Fähigkeiten wurden anschließend in einer intermolekularen Aldol- sowie einer Michael-Addition unter Normal- sowie Hochdruckbedingungen getestet. In beiden Reaktionen zeigten die Katalysatoren signifikant gesteigerte Reaktionsgeschwindigkeiten unter erhöhtem Druck. Während der Druck den deutlichsten Einfluss auf die Reaktivität des rigideren Tripeptids **53** hatte, zeigten die flexibleren Katalysatoren **52** und *ent*-**52** eine leicht erhöhte Enantioselektivität in der Aldolreaktion bei Druckbeaufschlagung (Schema 3).

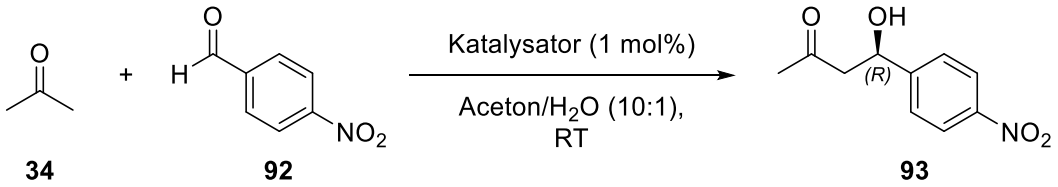

	Druckeffekt (von 1 bar auf 4.8 kbar)
Flexible Katalysatoren: (**52** & *ent*-**52**)	mehr als *3-fache Steigerung* der Reaktionsgeschwindigkeit *leicht verbesserte* Enantioselektivität
Rigider Katalysator: (**53**)	mehr als *5-fache Steigerung* der Reaktionsgeschwindigkeit *unveränderte* Enantioselektivität

Schema 3: Tripeptidkatalysierte Aldolreaktion unter Hochdruckbedingungen.

Da diese Beobachtung mit einer druckinduzierten Konformationsänderung zusammenhängen könnte, wurde entschieden das strukturelle Verhalten des Katalysators **52** weiter zu untersuchen. Hochdruck-NMR-Studien in Aceton-d_6/D_2O (10:1) zeigten, dass das Tripeptid **52** in mindestens drei verschiedenen Konformationen vorliegt. Diese werden vermutlich durch Ringinversion der zentralen β-Aminosäure sowie durch Rotationen um die Peptidbindung des N-terminalen Prolylrests verursacht.

Nachdem die strukturelle Vieldeutigkeit von **52** die konformelle Analyse erschwerte, wurden zwei Modellverbindungen synthetisiert, um allein das Verhalten der zentralen β-Aminosäure studieren zu können. Die Ergebnisse werden im dritten Kapitel beschrieben. Beide Moleküle wurden ausgehend von den entsprechenden *meso*-Anhydriden synthetisiert: *cis*-**95** als strukturelles Analogon zu **52** und *trans*-**95** als eine Referenzverbindung, welche keine Ringinversion zeigt (Schema 4). NMR- sowie Hochdruck-IR-Spektroskopie in Chloroform zeigte, dass *cis*-**95** in nur einer Konformation vorliegt, welche durch eine intramolekulare Wasserstoffbrückenbindung stabilisiert wird. Das isomere *trans*-**95** hingegen liegt in zwei Konformationen vor, welche vermutlich von einer *cis*-*trans*-Isomerie der Peptidbindung des *N*-Acetylrests hervorgerufen werden.

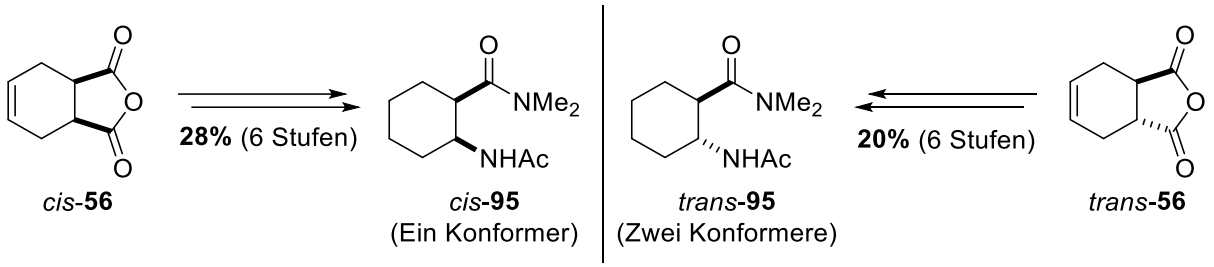

Schema 4: Synthese der für die konformelle Analyse als Modellverbindungen genutzten β-ACHC-Derivate.

Das letzte Kapitel beschreibt die Synthese von zwei ^{15}N-markierten Verbindungen für NMR-Untersuchungen. Beide Moleküle, ^{15}N-TMAO (**^{15}N-102**) und ^{15}N-NMA (**^{15}N-103**), wurden aus anorganischem, kostengünstigen $^{15}NH_4Cl$ (**^{15}N-104**) in analysenreiner Form hergestellt und in gruppenübergreifenden Projekten innerhalb der FOR 1979 Hochdruckforschergruppe verwendet (Schema 5). TMAO (**102**) stellt einen natürlich vorkommenden Osmolyt dar, welcher Proteine von Tiefseefischen gegen hohe Drücke stabilisiert, was es zu einem relevanten Forschungsobjekt macht. Die Synthese von ^{15}N-NMA (**^{15}N-103**) war notwendig, um ein von Kast *et al.* entwickeltes Computermodell zur Vorhersage von NMR-Verschiebungen unter Druck mithilfe von empirischen Daten validieren zu können. Erste vielversprechende Ergebnisse wurden bereits publiziert und weitere Untersuchungen werden innerhalb der Forschergruppe fortgeführt.

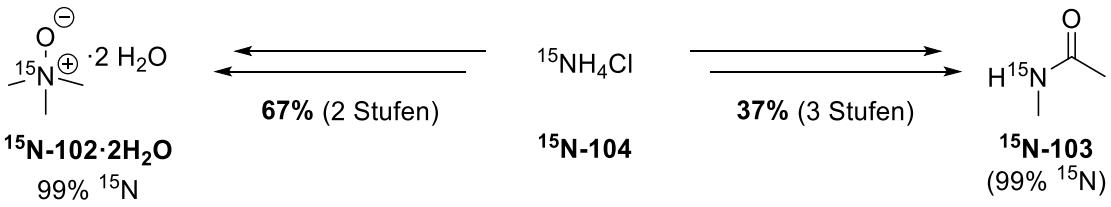

Schema 5: Synthese von ^{15}N-markiertem TMAO-Dihydrat (**^{15}N-102·2H$_2$O**) und NMA (**^{15}N-103**) ausgehend von kostengünstigem $^{15}NH_4Cl$ (**^{15}N-104**).

E. Experimental Part

1. General Information

^{1}H-NMR spectroscopy

^{1}H-NMR spectra were recorded on a Bruker Avance 300 (300 MHz), a Bruker Avance 400 (400 MHz) and a Bruker Avance III HD 600 spectrometer (600 MHz) at ambient temperatures unless otherwise noted. The spectra were recorded in $CDCl_3$, CD_2Cl_2, CD_3OD, $(CD_3)_2SO$ and D_2O. Chemical shifts are reported as δ, parts per million (ppm), relative to the center of the residual solvent signals: $CDCl_3$ = 7.26 ppm, CD_2Cl_2 = 5.32 ppm, CD_3OD = 3.31 ppm, $(CD_3)_2SO$ = 2.50 ppm, D_2O = 4.79 ppm. Spectra were evaluated in first order and coupling constants (*J*) are given Hertz (Hz). The multiplicity of the signals is given as follows: s = singlet, bs = broad singlet, d = doublet, t = triplet, q = quartet, quint = quintet, m = multiplet, dd = doublet of doublets, ddd = doublet of doublets of doublets, dt = doublet of triplets, dq = doublet of quartets, td = triplet of doublets, tt = triplet of triplets, pt = pseudo triplet. The integrals display the relative number of hydrogen atoms associated with the signals.

^{19}F-NMR spectroscopy

^{19}F-NMR spectra were recorded on a Bruker Avance 300 (300 MHz) spectrometer at ambient temperatures. All spectra were recorded in $CDCl_3$. Chemical shifts are reported as δ, parts per million (ppm). Spectra were evaluated in first order and coupling constants (*J*) are given Hertz (Hz). The integrals display the relative number of fluorine atoms associated with the signals.

^{13}C-NMR spectroscopy

^{13}C-NMR spectra were recorded on a Bruker Avance 300 (75.5 MHz), a Bruker Avance 400 (101 MHz) and a Bruker Avance III HD 600 spectrometer (151 MHz) at ambient temperatures unless otherwise noted. The spectra were recorded in $CDCl_3$, CD_2Cl_2, CD_3OD, $(CD_3)_2SO$ and D_2O. Chemical shifts are reported as δ, parts per million (ppm), relative to the center of the residual solvent signals: $CDCl_3$ = 77.16 ppm, CD_2Cl_2 = 53.84 ppm, CD_3OD = 49.00 ppm, $(CD_3)_2SO$ = 39.52 ppm. If necessary, DEPT 135 and DEPT 90 spectra were recorded to determine the number of hydrogen atoms attached to each carbon atom (DEPT: distortionless enhancement by polarization transfer). Signals are therefore stated as either + for a primary or tertiary carbon atom (positive DEPT signal), - for a secondary carbon atom (negative DEPT signal) or C_q for a quaternary carbon atom (no DEPT signal).

2D-NMR spectroscopy

Two-dimensional NMR spectra (COSY, HSQC, HMBC, 2D-NOESY) were recorded on a Bruker Avance 400 (400 MHz) and a Bruker Avance III HD 600 spectrometer (600 MHz) at ambient temperature in $CDCl_3$. Chemical shifts are reported as δ, parts per million (ppm).

Chiral high-performance liquid chromatography (chiral HPLC)

Chiral HPLC was performed on a Varian LC-902 Liquid Chromatograph using a Chiralpak AS-H column (4.6 × 250 mm, 10 µm), as well as Phenomenex Lux Cellulose-1 and Cellulose-2 columns (4.6 × 250 mm, 5 µm). The absolute configuration of the product was determined through comparison with literature values.

Column chromatography

(Flash-) Column chromatography was performed using Merck Gerduran 60 (0.063 – 0.200 mm) or Merck flash (0.040 – 0.063 mm) silica gel.

High-pressure infrared spectroscopy (HP-IR)

High-pressure infrared spectra were measured at the TU Dortmund on a Thermo Nicolet 6700 FT IR with a custom built pressure cell. The sample was measured as a 236 mM solution in $CHCl_3$ at ambient temperatures, using $BaSO_4$ as a pressure sensor.

High-pressure NMR spectroscopy (HP-NMR)

High-pressure NMR spectra were measured on a Bruker Avance 600 (600 MHz) and a Bruker Avance 800 (800 MHz) at 275 K using a custom-built high-pressure system and a ceramic high-pressure cell in the biophysical department of the University Regensburg.[278] The sample concentrations were 14.8 mM (H_2O/D_2O 10:1, v/v) and 3.2 mM (acetone-d_6/D_2O, 10:1, v/v), 4,4-dimethyl-4-silapentane-1-sulfonic acid was used as reference material. Water suppression was accomplished by using appropriate pulse sequences.[239]

High-pressure reactions

High-pressure reactions up to 5 kbar were performed using a custom-built hydraulic high-pressure apparatus from Unipress (Warsaw). Either melted PTFE tubes or reusable self-made PTFE/FEP vials were used as reaction vessels. The apparatus used a 1:1 (v/v) mixture of decahydronaphthalene (mixture of cis & trans) and 2,2,4-trimethylpentane as pressurizing medium. The pressurization and depressurizations step usually took no more than 5 min individually.

Infrared spectroscopy (IR)

Infrared spectra were recorded on a Bio-Rad Excalibur FTS 3000 MX equipped with a Specac Golden Gate Diamond Single Reflection ATR-System and an Agilent Cary 630 FT-IR spectrometer. Both solid and liquid compounds were measured neat. The wavenumbers are reported as cm^{-1}.

Mass spectrometry (MS)

Mass spectrometry was performed in the Analytical Department of the University of Regensburg ("Zentrale Analytik") on a Jeol AccuTOF GCX, a Finnigan MAT SSQ 710 A, a Finnigan ThermoQuest TSQ 7000 and an Agilent Q-TOF 6540 UHD.

Melting points

Melting points were determined using an SRS MPA 100 OptiMelt apparatus with a silicon oil bath and are thus uncorrected.

Optical rotation

Optical rotation values were determined using a Perkin Elmer 241 polarimeter at a wavelength of 589 nm (sodium-*d*-line) in a 1.0 dm cell with an inner volume of approximately 1 mL.

pH measurements

pH measurements have been performed using Hanna Instruments HI 991001 portable pH meter.

Solvents and chemicals

All commercially available chemicals were purchased in high quality and used without further purification unless otherwise noted. EtOAc, hexanes (60/40) and DCM were freshly distilled before usage. Anhydrous solvents were prepared *via* established procedures.[279] If necessary, chloroform was filtrated through basic aluminum oxide in order to remove acidic impurities.

Maleic anhydride (**61**) was purified by dissolving in $CHCl_3$ or DCM and filtering off the remaining solid. Aldehydes (**39a-g**) were purified prior to use according to established procedures, if necessary.[280]

Isotopically enriched $^{15}NH_4Cl$ (99% ^{15}N, **^{15}N-104**) was purchased from Cambridge Isotope Laboratories Inc. and was used as received.

Thin layer chromatography (TLC)

Thin layer chromatography was performed on silica gel coated aluminium plates (Merck silica gel 60 F_{254} and Macherey-Nagel ALUGRAM® Xtra SIL G/UV_{254}). Visualization was accomplished with UV light (λ = 254 nm) and through the use of TLC stains, *e.g.* $KMnO_4$, vanillin/sulfuric acid, phosphomolybdic acid, bromocresol green, Mostain and ninhydrin solutions, followed by heating.

X-ray crystallography

X-ray crystallography was performed in the analytical department of the University of Regensburg ("Zentrale Analytik") on an Agilent Technologies SuperNova, an Agilent Technologies Gemini R Ultra, an Agilent GV 50 and a Rigaku GV 50.

2. Small organocatalysts under pressure

2.1. Synthesis of catalyst and starting materials

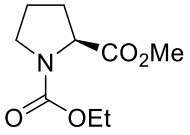

_N_-Ethoxycarbonyl-L-proline methyl ester (43)[112]

L-proline (3.45, 30.0 mmol, 1 equiv., **23**) was filled into a flame-dried 100 mL Schlenk flask and dissolved in dry MeOH (60 mL). K_2CO_3 (4.15 g, 30.0 mmol, 1 equiv.) was added to the solution and the flask sealed with a rubber septum. Subsequently, ethyl chloroformate (6.3 mL, 7.15 g, 65.9 mmol, 2.2 equiv.) was added dropwise over 5 min at 0 °C. The resulting slurry was then stirred at 0 °C for 8 h, followed by stirring at ambient temperature for further 16 h. After completion, all volatiles were removed by distillation and the residue transferred into a separating funnel with H_2O (30 mL). The aqueous phase was extracted with DCM (4x 40 mL) and the combined organic phases washed with sat. NaCl solution (80 mL). The extract was dried over Na_2SO_4, filtered, the solvent evaporated and the residue dried under high vacuum. Colorless oil (6.03 g, 30.0 mmol, 100%).

$\mathbf{R_f}$ = 0.30 (hexanes/EtOAc 4:1); **^{1}H-NMR** (300 MHz, $CDCl_3$) δ_H (ppm) = 4.40 – 4.22(1 H, m), 4.21 – 3.98 (2 H, m), 3.70 (3 H, d, *J* = 4.9 Hz), 3.63 – 3.35 (2 H, m), 2.30 – 2.06 (1 H, m), 2.05 – 1.80 (3 H, m), 1.21 (3 H, dt, *J* = 21.3, 7.1Hz); **^{13}C-NMR** (75 MHz, $CDCl_3$) δ_C (ppm) = 173.54 (C_q), 173.40 (C_q), 155.26 (C_q), 154.70 (C_q), 61.44 (-, CH_2), 61.31 (-, CH_2), 59.11 (+, CH), 58.89 (+, CH), 52.30 (+, CH_3), 52.22 (+, CH_3), 46.81 (-, CH_2), 46.41 (-, CH_2), 30.99 (-, CH_2), 30.01 (-, CH_2), 24.44 (-, CH_2), 23.63 (-, CH_2), 14.79 (+, CH_3), 14.74 (+, CH_3) (signal doubling due to rotamers).

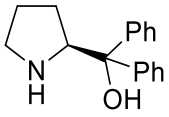

(2*R*)-α,α-Diphenyl-2-pyrrolidinemethanol (44)[112]

A flame-dried 50 mL two-necked Schlenk flask equipped with dropping funnel and reflux condenser was charged with Mg (1.94 g, 80.0 mmol, 4.0 equiv.), dry THF (15 mL) and a catalytic amount of I_2. PhBr (4.2 mL, 40 mmol, 2.0 equiv.) was filled into the dropping funnel and diluted with dry THF (15 mL). Subsequently, a small amount of the PhBr solution was added to the Mg suspension without stirring and heated gently. After the Grignard reaction had started, the rest of the solution was added dropwise while stirring in such a fashion that the reaction proceeded not to violently (only slight reflux). After complete addition, the now brownish slurry was stirred for another 10 min at ambient temperature.

During this time, a second 100 mL Schlenk flask was charged with **43** (2.01 g, 10.0 mmol, 1.0 equiv.) and dry THF (20 mL). The flask was sealed with a rubber septum, cooled down to 0 °C with an ice bath and the freshly prepared PhMgBr solution was added dropwise using a syringe. Once the addition was completed, the mixture was stirred for 3.5 h at 0°C, followed by 24 h at ambient temperature. The greyish-green reaction was quenched with sat. NH_4Cl solution (20 mL), resulting in the precipitation of a white solid. The overstanding yellowish solution was decanted off, the solid dissolved in H_2O and extracted with $CHCl_3$ (2x 20 mL). All organic phases were combined, dried over $MgSO_4$, filtered, evaporated and dried under high vacuum. The yellowish oil was redissolved in dry MeOH (20 mL) and KOH (5.73 g, 102 mmol, 10 equiv.) added. The mixture was refluxed for 4 h, the solvent evaporated and the residue transferred into a separating funnel with H_2O (10 mL). The aqueous phase was extracted with $CHCl_3$ (4x 15 mL), the combined organic extracts dried over $MgSO_4$, filtered and all volatiles distilled off. The crude product was purified by column chromatography (hexanes/EtOAc 3:1 + 1% NEt_3). Slight yellow solid (2.34 g, 9.24 mmol, 92%).

R_f = 0.13 (hexanes/EtOAc 3:1 + 1% NEt_3); **^{1}H-NMR** (300 MHz, $CDCl_3$) δ_H (ppm) = 7.60 – 7.58(2 H, m), 7.53 – 7.48 (2 H, m), 7.33 – 7.24 (4 H, m), 7.20 – 7.13 (2 H, m), 4.26 (1 H, t, *J* = 7.5 Hz), 3.08 – 2.89 (2 H, m), 1.80 – 1.50 (4 H, m); **^{13}C-NMR** (75 MHz, $CDCl_3$) δ_C (ppm) = 148.28 (C_q), 145.52 (C_q) 128.36 (+, CH), 128.10 (+, CH), 126.59 (+, CH), 126.48 (+, CH), 125.98 (+, CH), 125.65 (+, CH), 77.22 (C_q), 64.59 (+, CH), 46.89 (-, CH_2), 26.41 (-, CH_2), 25.64 (-, CH_2).

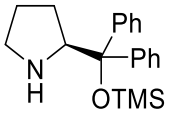

(2*S*)-2-[Diphenyl[(trimethylsilyl)oxy]methyl]pyrrolidine (28)[113]

A flame-dried 50 mL Schlenk was charged with **44** (1.06 g, 4.18 mmol, 1.0 equiv.) and of dry DCM (25 mL). Dry triethylamine (0.83 mL, 4.6 mmol, 1.1 equiv.) was added and the solution cooled down to 0 °C in an ice bath. Subsequently, TMSOTf (0.64 mL, 4.6 mmol, 1.1 equiv.) was added dropwise and the mixture stirred at ambient temperature. After 21 h, the reaction was quenched with H_2O, transferred into a separating funnel and extracted with DCM (3x). The combined organic extracts were washed with sat. NaCl solution, dried over Na_2SO_4, filtered, the solvent evaporated and the residue dried under high vacuum. The crude product was purified by flash column chromatography (hexanes/EtOAc 9:1 + 0.5% NEt_3). Yellow oil (1.06 g, 3.26 mmol, 78%).

R_f = 0.15 (hexanes/EtOAc 9:1 + 1% NEt_3); **^{1}H-NMR** (300 MHz, $CDCl_3$) δ_H (ppm) = 7.48 – 7.43(2 H, m), 7.38 – 7.32 (2 H, m), 7.30 – 7.17 (6 H, m), 7.20 – 7.13 (6 H, m), 4.06 – 4.00 (1 H, m), 2.89 – 2.75

(2 H, m), 1.69 (1 H, bs), 1.63 – 1.50 (3 H, m), 1.45 – 1.30 (1 H, m), -0.09 (9 H, s); **^{13}C-NMR** (75 MHz, $CDCl_3$) δ_C (ppm) = 146.98 (C_q), 145.93 (C_q) 128.57 (+, CH), 127.74 (+, CH), 127.71 (+, CH), 127.66 (+, CH), 127.03 (+, CH), 126.86 (+, CH), 83.31 (C_q), 65.55 (+, CH), 47.30 (-, CH_2), 27.64 (-, CH_2), 25.19 (-, CH_2), 2.33 (+, CH_3).

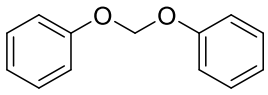

Diphenoxymethane (46)[281]

KOH (118.9 g, 2.119 mol, 14.5 equiv.) was added to a 500 mL round bottom flask equipped with a reflux condenser and dissolved in H_2O (100 mL) while cooling to 0 °C. After complete dissolution, phenol (25.24 g, 268.2 mmol, 1.0 equiv.), TBAB (10.37 g, 32.18 mmol, 0.1 equiv.) and DCM (250 mL) were added successively and the mixture stirred vigorously at 40 °C for 24 h. The solution was transferred into a separating funnel, the aqueous phase was discarded and the organic phase washed with H_2O (3x), sat. $NaHCO_3$ (5x) and sat. NaCl solution (5x). The organic phase was then dried over Na_2SO_4, filtered, all volatiles distilled off and the residue dried under high vacuum. Colorless, slightly oily liquid (26.08 g, 130.3 mmol, 97%).

R_f = 0.73 (hexanes/EtOAc 9:1); **^{1}H-NMR** (300 MHz, $CDCl_3$) δ_H (ppm) = 7.38 – 7.28(4 H, m), 7.18 – 7.11 (4 H, m), 7.10 – 7.01 (2 H, s), 5.76 (2 H, s); **^{13}C-NMR** (75 MHz, $CDCl_3$) δ_C (ppm) = 157.11 (C_q), 129.69 (+, CH), 122.55 (+, CH), 116.57 (+, CH), 91.24 (-, CH_2).

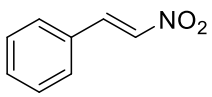

***trans*-β-Nitrostyrene (40)[282]**

A 250 mL three-necked round bottom flask equipped with an internal thermometer and a dropping funnel was charged with benzaldehyde (10.2 mL, 10.6 g, 100 mmol, 1.0 equiv.), nitromethane (5.40 mL, 6.16 g, 101 mmol, 1.0 equiv.) and EtOH (20 mL) and then cooled to 0 °C in an ice bath. Subsequently, 2 M NaOH (55 mL, 4.40 g, 110 mmol, 1.1 equiv.) was added dropwise in a fashion that the internal temperature did not rise above 10 °C. After complete addition, the mixture was stirred further for 1 h, diluted with H_2O (50 mL) and then poured slowly into a 250 mL Erlenmeyer flask filled with 50 g ice and conc. HCl (16 mL, 37wt%, 1.9 equiv.). An orange solid precipitated which was filtered off and rinsed twice with ice-cold H_2O (10 mL). The crude product (11 g) was recrystallized from EtOH (9 mL). Yellow needles (5.83 g, 39.1 mmol, 39%).

R_f = 0.50 (hexanes/EtOAc 9:1); **^{1}H-NMR** (300 MHz, $CDCl_3$) δ_H (ppm) = 8.01 (1 H, d, *J* = 13.7 Hz), 7.59 (1 H, d, *J* = 13.7 Hz), 7.58 – 7.41 (5 H, m); **^{13}C-NMR** (75 MHz, $CDCl_3$) δ_C (ppm) = 139.23, 137.22, 132.29, 130.17, 129.53, 129.28.

2.2. Catalysis

Both, racemic and asymmetric reactions have been performed under the exact same conditions, using stock solutions of the respective catalysts **28** and **42** in $CHCl_3$. The general procedures are written using the reaction of *n*-butanal (**39a**) catalyzed by **28** as an example.

General procedure for reactions under ambient conditions (GP-1)

A 10 mL round bottom flask was charged with *trans*-β-nitrostyrene (149 mg, 1.00 mmol, 1.0 equiv., **40**) and 4-nitrophenol (1.4 mg, 10 µmol, 1 mol%). The solids were dissolved in 2 mL of a 5.0 mM stock solution of catalyst **28** in $CHCl_3$ (3.3 mg of **28**, 10 µmol, 1 mol%) and spiked with the internal standard diphenoxymethane (180 µL, 200 mg, 1.00 mmol, 1.0 equiv., **46**). The reaction was started through the addition of *n*-butanal (360 µL, 4.00 mmol, 4.0 equiv., **39a**) and stirred for 1 h at ambient temperature (22 °C). Subsequently, the volatiles were evaporated, the residue dissolved in $CDCl_3$ and a ^{1}H-NMR measured immediately. For HPLC analysis, the crude mixture was purified *via* flash column chromatography, using hexanes/EtOAc as eluent.

General procedure for high-temperature reactions (GP-2)

A 10 mL pressure tube was charged with *trans*-β-nitrostyrene (149 mg, 1.00 mmol, 1.0 equiv., **40**) and 4-nitrophenol (1.4 mg, 10 µmol, 1 mol%). The solids were dissolved in 2 mL of a 5.0 mM stock solution of catalyst **28** in $CHCl_3$ (3.3 mg of **28**, 10 µmol, 1 mol%) and spiked with the internal standard diphenoxymethane (180 µL, 200 mg, 1.00 mmol, 1.0 equiv., **46**). The reaction was started through the addition of *n*-butanal (360 µL, 4.00 mmol, 4.0 equiv., **39a**), the tube sealed and stirred for 1 h at 60 °C. Subsequently, the volatiles were evaporated, the residue dissolved in $CDCl_3$ and a ^{1}H-NMR measured immediately. For HPLC analysis, the crude mixture was purified *via* flash column chromatography, using hexanes/EtOAc as eluent.

General procedure for high-pressure reactions (GP-3)

A 5 mL snap cap vial was charged with *trans*-β-nitrostyrene b(149 mg, 1.00 mmol, 1.0 equiv., **40**) and 4-nitrophenol (1.4 mg, 10 µmol, 1 mol%). The solids were dissolved in 2 mL of a 5.0 mM stock solution of catalyst **28** in $CHCl_3$ (3.3 mg of **28**, 10 µmol, 1 mol%) and spiked with the internal standard diphenoxymethane (180 µL, 200 mg, 1.00 mmol, 1.0 equiv., **46**). n-Butanal (360 µL, 4.00 mmol, 4.0 equiv., **39a**) was added, the mixture stirred for a few seconds until it became homogeneous and then transferred into a high-pressure vial. The vial was sealed, inserted into the apparatus and pressurized with 4.6 kbar for 1 h at ambient temperature (22 °C). Subsequently, the pressure was released, the mixture transferred into a round bottom flask and the volatiles were evaporated. The residue was dissolved in $CDCl_3$ and a ^{1}H-NMR measured immediately. For HPLC analysis, the crude mixture was purified *via* flash column chromatography, using hexanes/EtOAc as eluent.

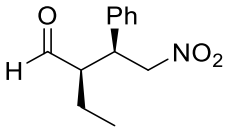

(2*R*,3*S*)-2-Ethyl-4-nitro-3-phenylbutanal (41a)[85,108]

Prepared by using *n*-butanal (0.36 mL, 4.0 mmol, **39a**). Colorless oil (88.1 mg, 398 µmol, 40%).

Syn diastereomer:

R_f = 0.33 (hexanes/EtOAc 6:1); **^{1}H-NMR** (400 MHz, $CDCl_3$) δ_H (ppm) = 9.72 (1 H, d, *J* = 2.6 Hz), 7.38 – 7.27 (3 H, m), 7.20 – 7.15 (2 H, m), 4.72 (1 H, dd, *J* = 12.7, 5.0 Hz), 4.63 (1 H, dd, *J* = 12.7, 9.6 Hz), 3.79 (1 H, td, *J* = 9.8, 5.0 Hz), 2.72 – 2.64 (1 H, m), 1.56 – 1.47 (2 H, m), 0.84 (3 H, t, *J* = 7.5 Hz); **^{13}C-NMR** (101 MHz, $CDCl_3$) δ_C (ppm) = 203.32 (+, CH), 136.94 (C_q), 129.25 (+, CH), 128.28 (+, CH), 128.14 (+, CH), 78.68 (-, CH_2), 55.15 (+, CH), 42.86 (+, CH), 20.51 (-, CH_2), 10.81 (+, CH_3).

Anti diastereomer:

^{1}H-NMR (400 MHz, $CDCl_3$) δ_H (ppm) = 9.49 (1 H, d, *J* = 2.9 Hz), 7.38 – 7.27 (3 H, m), 7.20 – 7.15 (2 H, m), 4.81 (1 H, dd, *J* = 12.9, 6.2 Hz), 4.78 – 4.72 (1 H, m), 3.85 – 3.75 (1 H, m), 2.61 – 2.54 (1 H, m), 1.79 – 1.56 (2 H, m), 0.99 (3 H, t, *J* = 7.4 Hz); **^{13}C-NMR** (101 MHz, $CDCl_3$) δ_C (ppm) = 203.44 (+, CH), 136.43 (C_q), 129.23 (+, CH), 128.37 (+, CH), 128.35 (+, CH), 78.07 (-, CH_2), 55.07 (+, CH), 44.28 (+, CH), 20.75 (-, CH_2), 11.62 (+, CH_3).

Chiral HPLC performed on Chiralcel Phenomenex Lux Cellulose-1 (*n*-heptane/*i*-PrOH = 70:30, λ = 215 nm, 0.5 mL/min). *Syn* diastereomer: t_r(major) = 24.8 min, t_r(minor) = 20.1 min; enantiomeric excess: 98%. *Anti* diastereomer: t_r(major) = 36.7 min, t_r(minor) = 21.6 min.

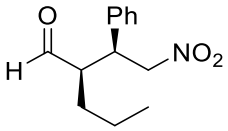

(*R*)-2-((*S*)-2-Nitro-1-phenylethyl)pentanal (41b)[85]

Prepared by using *n*-pentanal (0.43 mL, 4.0 mmol, **39b**). Colorless oil (54.4 mg, 398 µmol, 23%).

Syn diastereomer:

R_f = 0.40 (hexanes/EtOAc 6:1); **^{1}H-NMR** (400 MHz, $CDCl_3$) δ_H (ppm) = 9.71 (1 H, d, *J* = 2.8 Hz), 7.38 – 7.27 (3 H, m), 7.20 – 7.14 (2 H, m), 4.70 (1 H, dd, *J* = 12.7, 5.3 Hz), 4.64 (1 H, dd, *J* = 12.7, 9.4 Hz), 3.77 (1 H, td, *J* = 9.5, 5.4 Hz), 2.74 – 2.67 (1 H, m), 1.75 – 1.10 (4 H, m), 0.80 (3 H, t, *J* = 7.1 Hz); **^{13}C-NMR** (101 MHz, $CDCl_3$) δ_C (ppm) = 203.36 (+, CH), 136.95 (C_q), 129.27 (+, CH), 128.30 (+, Ph), 128.14 (+, CH), 78.56 (-, CH_2), 53.97 (+, CH), 43.33 (+, CH), 29.63 (-, CH_2), 19.92 (-, CH_2), 14.07 (+, CH_3).

Anti diastereomer:

^{1}H-NMR (400 MHz, $CDCl_3$) δ_H (ppm) = 9.48 (1 H, d, *J* = 3.0 Hz), 7.38 – 7.27 (3 H, m), 7.20 – 7.14 (2 H, m), 4.82 (1 H, dd, *J* = 13.0, 6.2 Hz), 4.75 (1 H, dd, *J* = 13.0, 9.0 Hz), 3.83 – 3.74 (1 H, m), 2.67 – 2.59 (1 H, m), 1.75 – 1.10 (4 H, m), 0.93 (3 H, t, *J* = 7.3 Hz); **^{13}C-NMR** (101 MHz, $CDCl_3$) δ_C (ppm) = 203.51 (+, CH), 136.39 (C_q), 129.24 (+, CH), 128.38 (+, CH), 128.36 (+, CH), 78.03 (-, CH_2), 53.42 (+, CH), 44.63 (+, CH), 29.79 (-, CH_2), 20.48 (-, CH_2), 14.12 (+, CH_3).

Chiral HPLC performed on Chiralcel Phenomenex Lux Cellulose-1 (*n*-Heptane/*i*-PrOH = 70:30, λ = 215 nm, 0.5 mL/min). *Syn* diastereomer: t_r(major) = 24.3 min, t_r(minor) = 18.4 min; enantiomeric excess: 99%. *Anti* diastereomer: t_r(major) = 33.5 min, t_r(minor) = 21.2 min.

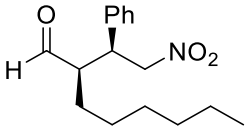

(*R*)-2-((*S*)-2-Nitro-1-phenylethyl)octanal (41c)[283]

Prepared by using *n*-octanal (0.63 mL, 4.0 mmol, **39c**). Slightly yellow oil (132 mg, 474 µmol, 47%).

Syn diastereomer:

R_f = 0.45 (hexanes/EtOAc 6:1); **^{1}H-NMR** (400 MHz, $CDCl_3$) δ_H (ppm) = 9.70 (1 H, d, *J* = 2.8 Hz), 7.37 – 7.27 (3 H, m), 7.19 – 7.15 (2 H, m), 4.71 (1 H, dd, *J* = 12.7, 5.2 Hz), 4.64 (1 H, dd, *J* = 12.7, 9.5 Hz), 3.79 (1 H, td, *J* = 9.6, 5.3 Hz), 2.73 – 2.65 (1 H, m), 1.56 – 1.01 (10 H, m), 0.82 (3 H, t, *J* = 7.0 Hz); **^{13}C-NMR** (101 MHz, $CDCl_3$) δ_C (ppm) = 203.39 (+, CH), 136.95 (C_q), 129.25 (+, CH), 128.29 (+, CH), 128.14 (+, CH), 78.58 (-, CH_2), 54.06 (+, CH), 43.28 (+, CH), 31.47 (-, CH_2), 29.18 (-, CH_2), 27.48 (-, CH_2), 26.49 (-, CH_2), 22.54 (-, CH_2), 14.08 (+, CH_3).

Anti diastereomer:

^{1}H-NMR (400 MHz, $CDCl_3$) δ_H (ppm) = 9.47 (1 H, d, *J* = 3.0 Hz), 7.37 – 7.27 (3 H, m), 7.19 – 7.15 (2 H, m), 4.81 (1 H, dd, *J* = 12.9, 6.2 Hz), 4.75 (1 H, dd, *J* = 12.8, 9.1 Hz), 3.83 – 3.73 (1 H, m), 2.65 – 2.58 (1 H, m), 1.76 – 1.01 (10 H, m), 0.87 (3 H, t, *J* = 6.8 Hz); **^{13}C-NMR** (101 MHz, $CDCl_3$) δ_C (ppm) = 203.55 (+, CH), 136.41 (C_q), 129.24 (+, CH), 128.38 (+, CH), 128.36 (+, CH), 78.05 (-, CH_2), 53.63 (+, CH), 44.61 (+, CH), 31.62 (-, CH_2), 29.31 (-, CH_2), 27.68 (-, CH_2), 27.16 (-, CH_2), 22.64 (-, CH_2), 14.13 (+, CH_3).

Chiral HPLC performed on Chiralcel Phenomenex Lux Cellulose-1 (*n*-heptane/*i*-PrOH = 70:30, λ = 215 nm, 0.5 mL/min). *Syn* diastereomer: t_r(major) = 20.4 min, t_r(minor) = 16.1 min; enantiomeric excess: 99%. *Anti* diastereomer: t_r(major) = 27.7 min, t_r(minor) = 17.2 min.

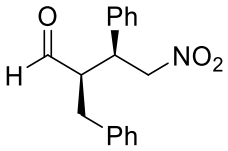

(2*R*,3*S*)-2-Benzyl-4-nitro-3-phenylbutanal (41d)[118]

Prepared by using 3-phenylpropanal (0.53 mL, 4.0 mmol, **39d**). Yellow oil. This product could not be completely purified by chromatography or other methods and contained several unidentifiable side products.

Syn diastereomer:

R_f = 0.38 (hexanes/EtOAc 5:1); **^{1}H-NMR** (400 MHz, $CDCl_3$) δ_H (ppm) = 9.72 (1 H, d, *J* = 2.3 Hz), 7.42 – 7.10 (8 H, m), 7.06 – 7.00 (2 H, m), 4.73 (1 H, d, *J* = 1.3 Hz), 4.71 (1 H, d, *J* = 3.7 Hz), 3.83 (1 H, td, *J* = 8.7, 6.2 Hz), 3.16 – 3.08 (1 H, m), 2.78 (1 H, d, *J* = 4.4 Hz), 2.76 (1 H, d, *J* = 1.4 Hz); **Chiral HPLC** performed on Chiralcel AS-H (*n*-heptane/*i*-PrOH = 95:5, λ = 215 nm, 0.5 mL/min). *Syn* diastereomer: t_r(major) = 28.6 min, t_r(minor) = 26.9 min; enantiomeric excess: 95%.

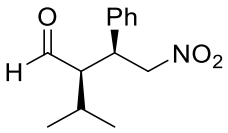

(2*R*,3*S*)-2-Isopropyl-4-nitro-3-phenylbutanal (41e)[85,108]

Prepared by using 3-methylbutanal (0.42 mL, 4.0 mmol, **39e**). Slightly yellow oil (108 mg, 457 µmol, 46%).

Syn diastereomer:

R_f = 0.35 (hexanes/EtOAc 6:1); **^{1}H-NMR** (400 MHz, $CDCl_3$) δ_H (ppm) = 9.93 (1 H, d, *J* = 2.4 Hz), 7.37 – 7.27 (3 H, m), 7.21 – 7.14 (2 H, m), 4.67 (1 H, dd, *J* = 12.6, 4.4 Hz), 4.58 (1 H, dd, *J* = 12.5, 9.9 Hz), 3.90 (1 H, td, *J* = 4.4, 10.3 Hz), 2.77 (1 H, ddd, *J* = 10.7, 4.1, 2.5 Hz), 1.79 – 1.66 (1 H, m), 1.10 (3 H, d, *J* = 7.2 Hz), 0.89 (3 H, d, *J* = 7.0 Hz); **^{13}C-NMR** (101 MHz, $CDCl_3$) δ_C (ppm) = 204.48 (+, CH), 137.25 (C_q), 129.31 (+, CH), 128.24 (+, CH), 128.10 (+, CH), 79.13 (-, CH_2), 58.93 (+, CH), 42.09 (+, CH), 28.06 (+, CH), 21.88 (+, CH_3), 17.13 (+, CH_3).

Anti diastereomer:

^{1}H-NMR (400 MHz, $CDCl_3$) δ_H (ppm) = 9.48 (1 H, d, *J* = 4.2 Hz), 7.37 – 7.27 (3 H, m), 7.21 – 7.14 (2 H, m), 4.77 (1 H, dd, *J* = 12.9, 6.1 Hz), 4.66 (1 H, dd, *J* = 12.7, 9.2 Hz), 3.97 (1 H, dt, *J* = 9.0, 6.6 Hz), 2.36 (1 H, td, *J* = 7.2, 4.2 Hz), 2.09 – 1.96 (1 H, m), 1.16 (3 H, d, *J* = 6.8 Hz), 1.00 (3 H, d, *J* = 6.8 Hz); **^{13}C-NMR** (101 MHz, $CDCl_3$) δ_C (ppm) = 204.52 (+, CHO), 135.99 (C_q), 129.27 (+, CH), 128.53 (+, CH), 128.40 (+, CH), 78.63 (-, CH_2), 59.17 (+, CH), 42.92 (+, CH), 27.09 (+, CH), 21.06 (+, CH_3), 19.26 (+, CH_3).

Chiral HPLC performed on Chiralcel AS-H (*n*-heptane/*i*-PrOH = 95:5, λ = 215 nm, 0.5 mL/min). *Syn* diastereomer: t_r(major) = 31.8 min, t_r(minor) = 30.5 min; enantiomeric excess: 99%. *Anti* diastereomer: t_r(major) = 39.4 min, t_r(minor) = 35.9 min.

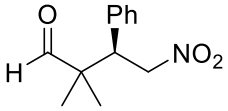

(*R*)-2,2-Dimethyl-4-nitro-3-phenylbutanal (41f)[85]

Prepared by using 2-methylpropanal (0.37 mL, 4.0 mmol, **39f**). Slightly yellow oil (190 mg, 857 µmol, 86%).

R_f = 0.10 (hexanes/EtOAc 9:1); **^{1}H-NMR** (400 MHz, $CDCl_3$) δ_H (ppm) = 9.53 (1 H, s), 7.37 – 7.27 (3 H, m), 7.23 – 7.17 (2 H, m), 4.86 (1 H, dd, *J* = 13.0, 11.2 Hz), 4.69 (1 H, dd, *J* = 13.1, 4.2 Hz), 3.78 (1 H, dd, *J* = 11.2, 4.2 Hz), 1.14 (3 H, s), 1.01 (3 H, s); **^{13}C-NMR** (101 MHz, $CDCl_3$) δ_C (ppm) = 204.22 (+, CH), 135.35

(C_q, CH), 129.08 (+, CH), 128.73 (+, CH), 128.17 (+, CH), 76.33 (-, CH_2), 48.51 (+, CH), 48.23 (C_q), 21.70 (+, CH_3), 18.92 (+, CH_3); **Chiral HPLC** performed on Chiralcel Phenomenex Lux Cellulose-1 (*n*-heptane/*i*-PrOH = 90:10, λ = 215 nm, 1.0 mL/min). t_r(major) = 16.5 min, t_r(minor) = 23.8 min; enantiomeric excess: 78%; $[\alpha]_D^{22}$: +6.8 (c = 1.01, $CHCl_3$).

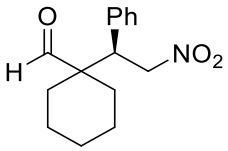

(*R*)-1-(2-Nitro-1-phenylethyl)cyclohexane-1-carbaldehyde (41g)[89]

Prepared by using cyclohexane carbaldehyde (0.48 mL, 4.0 mmol, **39g**). Yellow oil (56 mg, 214 µmol, 21%).

R_f = 0.21 (hexanes/EtOAc 19:1); **^{1}H-NMR** (300 MHz, $CDCl_3$) δ_H (ppm) = 9.55 (1 H, s), 7.36 – 7.27 (3 H, m), 7.17 – 7.08 (2 H, m), 4.80 (1 H, dd, *J* = 13.1, 10.8 Hz), 4.73 (1 H, dd, *J* = 13.2, 4.9 Hz), 3.54 (1 H, dd, *J* = 10.8, 4.8 Hz), 2.15 – 2.00 (1 H, m), 1.94 – 1.80 (1 H, m), 1.75 – 1.50 (3 H, m), 1.48 – 1.32 (1 H, m), 1.31 – 1.03 (4 H, m); **^{13}C-NMR** (75 MHz, $CDCl_3$) δ_C (ppm) = 207.49 (+, CH), 135.01 (C_q), 129.21 (+, CH), 128.84 (+, CH), 128.32 (+, CH), 76.22 (-, CH_2), 51.36 (C_q), 50.62 (+, CH), 31.20 (-, CH_2), 29.88 (-, CH_2), 25.22 (-, CH_2), 22.82 (-, CH_2), 22.70 (-, CH_2); **Chiral HPLC** performed on Chiralcel Phenomenex Lux Cellulose-1 (*n*-heptane/*i*-PrOH = 90:10, λ = 215 nm, 1.0 mL/min). t_r(major) = 27.9 min, t_r(minor) = 12.2 min; enantiomeric excess: 64%; $[\alpha]_D^{22}$: -15.9 (c = 1.00, $CHCl_3$).

3. Synthesis of tripeptides containing unnatural β-amino acids

3.1. Synthesis of racemic β-ACHC

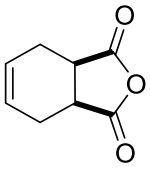

***cis*-4-Cyclohexene-1,2-dicarboxylic acid anhydride (*cis*-56)[169]**

A 500 mL round bottom flask was charged with freshly powdered 3-sulfolene (80.4 g, 680 mmol, 1.36 equiv., **62**) and maleic anhydride (49.0 g, 500 mmol, 1.00 equiv., **61**). Dry xylenes (35 mL) were added and the flask equipped with a reflux condenser and bubble counter. The mixture was stirred at ambient temperature for 5 min and then gently heated up to 130 °C in such a manner that the only weak gas evolution occurred. After 9 h, another batch of freshly powdered 3-sulfolene (10.0 g, 86.6 mmol, 0.17 equiv., **62**) was added, the bubble counter exchanged for a $CaCl_2$ filled drying tube and the mixture stirred further for 18 h at 130 °C. The now deep brown reaction was then stopped, diluted with dry xylenes (250 mL) and mixed with 3 g of fine powdered activated charcoal. The resulting slurry was then stirred for 20 min at 70 °C, immediately filtered hot and washed with xylenes. Upon cooling, a colorless solid started to precipitate from the yellowish solution. The already crashed out solid was redissolved by heating the filtrate in a water bath and cyclohexane (100 mL) added. The solution was then stirred for 1 h in an ice bath. During this time, the product crystallized from the solution. The solid was filtered off and washed with small amounts of ice-cold toluene and cyclohexane and then dried in a desiccator over silica gel. A second crop of product was obtained through further cooling the mother liquor and filtration. White solid (64.8 g, 426 mmol, 85%).

^{1}H-NMR (300 MHz, $CDCl_3$) δ_H (ppm) = 6.01 – 5.96 (2 H, m), 3.41 – 3.35 (2 H, m), 2.68 – 2.56 (2 H, m), 2.36 – 2.24 (2 H, m); **^{13}C-NMR** (75 MHz, $CDCl_3$) δ_C (ppm) = 174.38, 127.74, 38.63, 23.42.

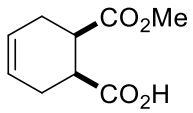

cis-2-Methoxycarbonyl-4-cyclohexene-1-carboxylic acid (_cis_-63)[184]

A 25 mL round bottom flask equipped with a reflux condenser was charged with *cis*-**56** (2.94 g, 19.4 mmol, 1.0 equiv.) and MeOH (10 mL) and the mixture was refluxed for 2 h. All volatiles were evaporated and the residue was dried under high vacuum. White solid (3.52 g, 19.1 mmol, 99%).

^{1}H-NMR (400 MHz, $CDCl_3$) δ_H (ppm) = 10.22 (1 H, bs), 5.68 (2 H, s), 3.69 (3 H, s), 3.11 – 3.02 (2 H, m), 2.64 – 2.50 (2 H, m), 2.42 – 2.31 (2 H, m); **^{13}C-NMR** (75 MHz, $CDCl_3$) δ_C (ppm) = 179.88 (C_q), 173.81 (C_q), 125.29 (+, CH), 125.16 (+, CH), 52.08 (+, CH_3), 39.69 (+, CH), 39.54 (+, CH), 25.83 (-, CH_2), 25.64 (-, CH_2).

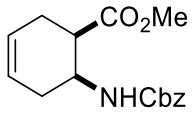

Methyl _cis_-6-(((benzyloxy)carbonyl)amino)cyclohex-3-ene-1-carboxylate (_cis_-64)[174]

A flame-dried two-necked Schlenk flask equipped with a reflux condenser, bubble counter and septum was charged with *cis*-**63** (1.54 g, 8.35 mmol, 1.0 equiv.), NEt_3 (1.2 mL, 8.7 mmol, 1.0 equiv.) and dry toluene (30 mL). DPPA (2.30 g, 8. 35 mmol, 1.0 equiv.) was added dropwise to the stirred mixture, followed by BnOH (1.8 mL, 17.3 mmol, 2.1 equiv.). The reaction was heated to 120 °C and stirred for 5 h (gas evolution was observed). Subsequently, the mixture was allowed to cool to ambient temperature, transferred into a separating funnel and diluted with EtOAc (1x 30 mL). The organic phase was washed consecutively with 2 M HCl (1x 60 mL), sat. $NaHCO_3$ (1x 60 mL) and sat. NaCl solutions (1x 60 mL), then dried over $MgSO_4$, filtered, all volatiles evaporated and the residue dried under high vacuum. The crude product was purified by flash column chromatography (DCM/MeOH 9:1). Yellowish oil (1.93 g, 6.67 mmol, 80%).

R_f = 0.63 (DCM/MeOH 200:1); **^{1}H-NMR** (300 MHz, $CDCl_3$) δ_H (ppm) = 7.40 – 7.28 (5 H, m), 5.72 – 5.55 (2 H, m), 5.43 (1 H, d, *J* = 9.4 Hz), 5.08 (2 H, dd, *J* = 14.4, 12.3 Hz), 4.36 – 4.17 (1 H, m), 3.68 (3 H, s), 2.88 – 2.74 (1 H, m), 2.61 – 2.12 (4 H, m); **^{13}C-NMR** (75 MHz, $CDCl_3$) δ_C (ppm) = 173.89 (C_q), 155.91 (C_q), 136.56 (C_q), 128.61 (+, CH), 128.23 (+, CH), 128.21 (+, CH), 125.05 (+, CH), 124.78 (+, CH), 66.78 (-, CH_2), 52.02 (+, CH_3), 46.85 (+, CH), 42.10 (+, CH), 30.69 (-, CH_2), 25.57 (-, CH_2).

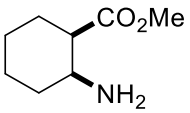

Methyl *cis*-2-aminocyclohexane-1-carboxylate (*rac*-65)[284]

cis-**46** (2.32 g, 8.02 mmol, 1.0 equiv.) was transferred into an autoclave vessel with MeOH (10 mL) and 120 mg Pd/C (10 wt% Pd) added. The mixture was hydrogenated for 6 h with 30 bar H_2. After the reaction was completed, the slurry was filtered* and the solvent removed carefully on a rotatory evaporator (the free amine tends to be volatile). The residue was diluted with H_2O (40 mL) and transferred into a separating funnel, then acidified with 2 M HCl to approximately pH 3 and extracted with diethyl ether (2x). The aqueous phase was then basified with sat. Na_2CO_3 to pH 9 and extracted with DCM (5x), until TLC control showed no more remaining product. The combined organic phases were dried over Na_2SO_4, filtered and the solvent removed carefully on a rotatory evaporator. Yellowish liquid (973 mg, 6.19 mmol, 77%).

R_f = 0.08 (DCM/MeOH 100:1); **^{1}H-NMR** (400 MHz, $CDCl_3$) δ_H (ppm) =3.64 (3 H, s), 3.29 – 3.20 (1 H, m), 2.51 (1 H, dt, *J* = 9.9, 3.8 Hz), 1.84 – 1.19 (10 H, m); **^{13}C-NMR** (101 MHz, $CDCl_3$) δ_C (ppm) = 175.04(C_q), 51.45 (+, CH_3), 48.52 (+, CH), 47.29 (+, CH), 33.03 (-, CH_2), 24.28 (-, CH_2), 23.80 (-, CH_2), 20.92 (-, CH_2)

3.2. Desymmetrization reactions

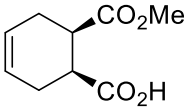

(1*S*,6*R*)-6-(Methoxycarbonyl)cyclohex-3-ene-1-carboxylic acid ((-)-63)

Pathway A - Kinetic resolution using (1*R*,2*S*)-(-)-ephedrine[191]

In separate flasks, racemic *cis*-**63** (22.63 g, 122.9 mmol, 1.0 equiv.) and (1*R*,2*S*)-(-)-ephedrine (20.30 g, 122.9 mmol, 1.0 equiv.) were each dissolved in EtOH (60 mL) and heated to 70 °C. The hot ephedrine solution was then added to the *cis*-**63** solution in one portion and the resulting yellow mixture was allowed to reach ambient temperature. After 2 h, a white solid had precipitated, was filtered off and washed with small amounts of hexanes.† The salt was recrystallized from EtOH three times, after which the enantiomeric excess was estimated to be >99%. The white solid (9.33 g) was dissolved in ice-cold

* Two paper filters were used to ensure that no palladium was washed into the filtrate.

† Estimation of the enantiopurity was achieved using ^{1}H-NMR, as the diastereomeric salts display slightly shifted resonances for the methyl ester groups (3.59 vs 3.61 ppm).

1 M H_2SO_4 (25 mL) and extracted with diethyl ether (6x 25 mL) The combined organic extracts were washed with 1 M H_2SO_4 (50 mL) and H_2O (50 mL), dried over Na_2SO_4, filtered, the solvent evaporated off and the residue dried under high vacuum. Yellowish oil (4.78 g, .26.0 mmol, 42%).

Analytical data is similar to *cis*-**63**. Enantiomeric excess was determined by derivatization according to **GP-4** and subsequent chiral HPLC analysis, >99% *ee*.

Pathway B - Desymmetrization using quinine[184–186]

A flame-dried three-necked round bottom flask equipped with a septum and nitrogen inlet was charged with racemic *cis*-**56** (1.52 g, 10.0 mmol, 1.0 equiv.) and quinine (3.57 g, 11.0, 1.1 equiv.) and evacuated for 3 h to remove remaining traces of humidity. The solids were suspended in dry toluene (100 mL) under a nitrogen atmosphere and the slurry was cooled down to -45 °C. Dry MeOH (1.3 mL, 32.1 mmol, 3.2 equiv.) was added dropwise using a syringe and the mixture was stirred for 65 h at -45 °C. Subsequently, the now clear solution was allowed to warm up to ambient temperature and all volatiles were removed under reduced pressure. The residue was transferred into a separating funnel with small amounts of EtOAc and 2 M HCl. The organic phase was separated and the aqueous phase extracted with EtOAc. The combined organic extracts were dried over $MgSO_4$, filtered, the solvent was distilled off and the product dried under high vacuum. Yellowish oil (1.66 g, 9.03 mmol, 90%).

Analytical data is similar to *cis*-**63**. $[\alpha]_D^{22}$: -10.2 (c = 1.32, $CHCl_3$). Enantiomeric excess was determined by derivatization according to **GP-4** and subsequent chiral HPLC analysis, 93% *ee*.

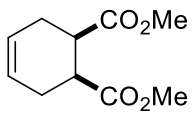

***cis*-Dimethyl cyclohex-4-ene-1,2-dicarboxylate (69)[285]**

In a 100 mL round bottom flask, racemic *cis*-**63** (8.02 g, 43.5 mmol, 1.0 equiv.) was dissolved in MeOH (40 mL) and conc. H_2SO_4 (3 mL, 96 wt%) was added carefully while stirring. Subsequently, the mixture was refluxed for 5 d. After the reaction was complete, the solvent was distilled off, transferred into a separating funnel with H_2O and extracted with MTBE (3x). The combined organic extracts were washed successively with H_2O, sat. $NaHCO_3$ solution and again H_2O, then dried over Na_2SO_4, filtered and all volatiles removed by rotatory evaporation. The crude product was purified by distillation under reduced pressure (75 °C, 0.9 mbar). Colorless oil (6.55 g, 33.0 mmol, 76%).

R_f = 0.58 (hexanes/EtOAc 4:1); **^{1}H-NMR** (300 MHz, $CDCl_3$) δ_H (ppm) = 5.66 (2 H, s), 3.68 (6 H, s), 3.08 – 2.98 (2 H, m), 2.61 – 2.47 (4 H, m); **^{13}C-NMR** (75 MHz, $CDCl_3$) δ_C (ppm) = 173.89 (C_q), 125.23 (+, CH), 51.98 (+, CH_3), 39.80 (+, CH), 25.83 (-, CH_2).

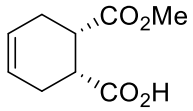

(1*R*,6*S*)-6-(Methoxycarbonyl)cyclohex-3-ene-1-carboxylic acid ((+)-63)[171]

69 (4.00 g, 20.18 mmol, 1.0 equiv.) was suspended in 50 mM pH 8.0 phosphate buffer (100 mL) in a 250 mL Erlenmeyer flask equipped with a pH meter. 2000 U PLE (111.1 mg, 18 U/mg, Aldrich) were added in one portion and the resulting yellowish slurry was stirred at 30 °C. The pH was monitored carefully, using 1 M NaOH to maintain a slightly basic pH (7.5 – 8.0). After 5 h and the total addition of 20 mL 1 M NaOH (20 mmol, 1.0 equiv.), the reaction was aborted and filtered through a plug of Celite. The aqueous filtrate was extracted with diethyl ether (3x), then acidified to pH 2 using conc. HCl and extracted once more. The extraction process was hampered by excessive formation of foam and partial gelification/emulsification of the organic phase. The combined, gel-like organic extracts were pre-dried over Na_2SO_4 and then filtered off. As a consequence, the emulsion broke up, resulting in a distinct organic and aqueous phase. The organic phase was separated off, dried once more over Na_2SO_4, filtered, the solvent evaporated off and the product dried under high vacuum. Yellowish oil (3.21 g, 17.5 mmol, 86%).

Analytical data is similar to *cis*-**63**. Enantiomeric excess was determined by derivatization according to **GP-4** and subsequent chiral HPLC analysis, 96% *ee*.

General procedure for the derivatization of hemiesters for HPLC analysis (GP-4)[188]

A 10 mL round bottom flask was charged with hemiester (+)-**63** (50.0 mg, 271 µmol, 1.0 equiv.), 4-Br-PhOH (47.0 mg, 271 µmol, 1.0 equiv.) and DCM (3 mL). The solution was cooled to 0 °C in an ice bath and DCC (56.0 mg, 271 µmol, 1.0 equiv.) and DMAP (8.3 mg, 68 µmol, 25 mol%) were added successively. The mixture was stirred for 25 h at ambient temperature, during which a white solid precipitated. The precipitate was removed by filtration and the solvent was removed with a rotatory evaporator. The crude product was purified by flash column chromatography (hexanes/EtOAc 9:1). White solid (69.4 mg, 205 µmol, 75%).

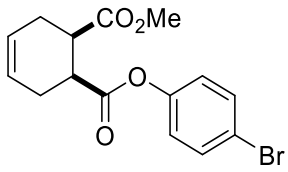

***cis*-1-(4-Bromophenyl) 2-methyl cyclohex-4-ene-1,2-dicarboxylate (108)[188]**

White solid.

R_f = 0.30 (hexanes/EtOAc 9:1); **^{1}H-NMR** (300 MHz, $CDCl_3$) δ_H (ppm) = 7.52 – 7.44 (2 H, m), 7.01 – 6.93 (m, 2 H), 5.78 – 5.67 (2 H, s), 3.74 – 3.68 (3 H, s), 3.28 – 3.18 (2 H, m), 2.73 – 2.55 (2 H, m), 2.55 – 2.35 (2 H, m); **^{13}C-NMR** (75 MHz, $CDCl_3$) δ_C (ppm) = 173.60 (C_q), 171.82 (C_q), 149.92 (C_q), 132.62 (+, CH), 132.52 (+, CH), 125.30 (+, CH), 124.99 (+, CH), 123.46 (+, CH), 118.95 (C_q), 52.15 (+, CH_3), 40.01 (+, CH), 26.00 (-, CH_2), 25.52 (-, CH_2); **Chiral HPLC** performed on Chiralcel Phenomenex Lux Cellulose-2 (*n*-heptane/*i*-PrOH = 95:5, λ = 215 nm, 0.5 mL/min). t_r = 15.2 min (1*S*,2*R*), t_r = 18.2 min (1*R*,2*S*).

3.3. Synthesis of peptides containing β-ACHC

General procedure for the deprotection of methyl esters (GP-5)[176]

A 25 mL round bottom flask was charged with a methyl ester (1.0 mmol, 1.0 equiv.), dissolved in THF (5 mL) and cooled to 0 °C in an ice bath. Meanwhile, a solution of LiOH (5.0 mmol, 5.0 equiv.) in H_2O (5 mL) was prepared in a second flask, chilled to 0 °C as well and then added dropwise to the THF solution. After complete addition, the slightly turbid mixture was allowed to warm up to ambient temperature and stirred until TLC showed complete conversion. The reaction mixture was then transferred into a separating funnel with small amounts of H_2O, acidified to pH 2 using 1 M HCl and then extracted with EtOAc (4x). The combined organic phases were dried over Na_2SO_4, filtered, all volatiles removed by rotatory evaporation and the product dried under high vacuum.

General procedure for the consecutive Boc/Bn deprotection (GP-6)

A 25 mL round bottom flask was charged with **68** (264 mg, 501 µmol, 1.0 equiv.) and EtOAc (5 mL, pre-dried over K_2CO_3) and cooled to 0 °C. A 4.2 M solution of HCl in EtOAc (5.0 mL, 21 mmol, 42 equiv.) was added carefully and the mixture stirred for 3.5 h at 0°C, until complete conversion was detected by TLC. Subsequently, the solvent was removed directly under high vacuum, the residue diluted in H_2O (15 mL) and transferred into a separating funnel. The aqueous phase was washed with diethyl ether (2x), then basified with sat. Na_2CO_3 to pH 9 and extracted with DCM (4x), until TLC control showed no

more remaining product in the extract. The combined organic phases were dried over Na_2SO_4, filtered and the solvent removed carefully on a rotatory evaporator.

The white foam-like solid was transferred into a Schlenk flask filled with 50 mg Pd/C (10 wt% Pd) using MeOH (10 mL). The slurry was flushed with H_2 and hydrogenated for 3 h until complete conversion was detected by TLC. The crude mixture was filtered through a plug of Celite and washed thoroughly with MeOH. The solvent was evaporated and the remaining product was dried under high vacuum. White solid (155 mg, 460 µmol, 92%).

General procedure for the simultaneous Bn/Cbz deprotection (GP-7)

50 mg Pd/C (10 wt% Pd) were filled into an autoclave vessel and suspended carefully with MeOH (1 mL) under a nitrogen atmosphere. *ent*-**72** (217 mg, 386 µmol, 1.0 equiv.) was transferred into the vessel with MeOH (5 mL) and the mixture was hydrogenated for 25 h with 40 bar H_2 until complete conversion was observed with TLC. The crude mixture was filtered through a plug of Celite and washed thoroughly with MeOH. The solvent was evaporated off and the remaining product was dried under high vacuum. White solid (130 mg, 385 µmol, 100%).

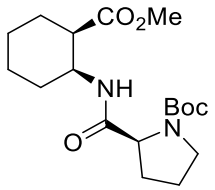

***tert*-Butyl (*S*)-2-(((1*S*,2*R*)-2-(methoxycarbonyl)cyclohexyl)carbamoyl)pyrrolidine-1-carboxylate (Boc-Pro-(-)-⬢-OMe, 66)[155,174]**

A flame-dried two-necked Schlenk flask equipped with a reflux condenser, bubble counter and septum was charged with (-)-**63** (1.66 g, 9.03 mmol, 1.0 equiv.), NEt_3 (1.3 mL, 9.4 mmol, 1.0 equiv.) and dry toluene (30 mL). DPPA (2.49 g, 9.03 mmol, 1.0 equiv.) was added dropwise to the stirred mixture, followed by BnOH (1.9 mL, 18.3 mmol, 2.0 equiv.). The reaction was heated to 120 °C and stirred for 4 h (gas evolution was observed). Subsequently, the mixture was allowed to cool to ambient temperature, transferred into a separating funnel and diluted with EtOAc (1x 30 mL). The organic phase was washed consecutively with 2 M HCl (1x 60 mL), sat. $NaHCO_3$ (1x 60 mL) and sat. NaCl solutions (1x 60 mL), then dried over $MgSO_4$, filtered, all volatiles evaporated and the residue dried under high vacuum.

The yellow oil was transferred into an autoclave vessel with MeOH (10 mL) and 140 mg Pd/C (10 wt% Pd) added. The mixture was hydrogenated for 4 h with 30 bar H_2. After the reaction was completed, the slurry was filtered* and the solvent removed carefully on a rotatory evaporator (the free amine tends to be volatile). The residue was diluted with H_2O (20 mL) and transferred into a separating funnel, then acidified with 2 M HCl to approximately pH 3 and extracted with diethyl ether (2x). The aqueous phase was then basified with sat. Na_2CO_3 to pH 9 and extracted with DCM (15x), until TLC control showed no more remaining product. The combined organic phases were dried over Na_2SO_4, filtered and the solvent removed carefully on a rotatory evaporator.

The yellowish liquid (1.29 g) was then diluted in dry DCM (5 mL) and cooled to 0 °C. Meanwhile, a cooled solution of *N*-Boc-L-Pro-OH (1.85 g, 8.60 mmol, 1.1 equiv., **58**) in dry DCM (25 mL) was preactivated with EDC·HCl (1.65 g, 8.60 mol, 1.1 equiv.) for 60 min and then added dropwise to the crude amine. Subsequently, a cooled solution of triethylamine (1.4 mL, 10.2 mmol, 1.3 equiv.) in dry DCM (20 mL) was added as well. The reaction mixture was allowed to warm to ambient temperature and stirred for 20 h. The mixture was quenched with H_2O (50 mL) and the solution acidified to pH 3 with 1 M $KHSO_4$. The solution was transferred into a separating funnel and the aqueous phase extracted with DCM (4x). The combined organic phases were washed successively with sat. $NaHCO_3$ (1x) and sat. NaCl solutions (1x), then dried over Na_2SO_4, filtered, all volatiles evaporated off and the residue dried under high vacuum. The crude product was purified by flash column chromatography (hexanes/ EtOAc 1:1). White solid (1.10 g, 3.09 mmol, 34% over 3 steps).

R_f = 0.40 (hexanes/EtOAc 1:1); **^{1}H-NMR** (400 MHz, CD_2Cl_2, 300 K): δ_H (ppm) =7.36 (0.6 H, bs), 6.88 (0.4 H, bs), 4.12 (2 H, bs), 3.65 (3 H, s), 3.50 – 3.25 (2 H, m), 2.71 (1 H, bs), 2.26 – 1.20 (21 H, m); **^{13}C-NMR** (101 MHz, CD_2Cl_2, 233 K): δ_C (ppm) = 171.46 (C_q), 174.30 (C_q), 171.52 (C_q), 171.13 (C_q), 154.42 (C_q), 79.98 (C_q), 79.77 (C_q), 61.16 (+, CH), 60.06 (+, CH), 52.04 (+, CH_3), 51.92 (+, CH_3), 47.20 (-, CH_2), 46.95 (-, CH_2), 44.31 (+, CH), 31.30 (-, CH_2), 29.45 (-, CH_2), 28.08 (+, CH_3), 27.96 (+, CH_3), 24.66 (-, CH_2), 23.67 (-, CH_2), 22.20 (-, CH_2) (signal doubling due to rotamers); **IR** (neat): $\tilde{\nu}$ = 3300, 2936, 2864, 1734, 1689, 1654, 1540, 1389, 1363, 1310, 1245, 1159, 1118, 1036, 980, 924, 858, 771, 650, 590, 538; **MS** (+ESI, 120 V): *m/z* (%) = 255.2 (36) [(MH_2-Boc)$^+$], 355.2 (100) [(M+H)$^+$], 377.2 (37) [(M+Na)$^+$], 731.4 (26) [(2M+Na)$^+$]. **HRMS** (+ESI, 120 V): 355.2233 ($C_{18}H_{31}N_2O_5$ [(M+H)$^+$]: calc. 355.2227). $[\alpha]_D^{22}$: -115.2 (c = 1.01, $CHCl_3$); **Chiral HPLC** performed on Chiralpak AS-H (*n*-heptane/*i*-PrOH = 90:10, λ = 215 nm, 1.0 mL/min): t_r(major) = 34.1 min; diastereomeric excess: >99%; **m.p.** 94 – 98 °C.

* Two paper filters were used to ensure that no palladium was washed into the filtrate.

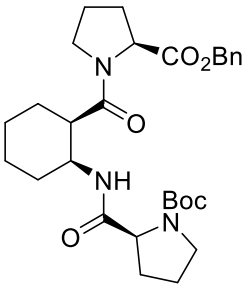

***tert*-Butyl (*S*)-2-(((1*S*,2*R*)-2-((*S*)-2-((benzyloxy)carbonyl)pyrrolidine-1-carbonyl)cyclohexyl)-carbamoyl)-pyrrolidine-1-carboxylate (Boc-Pro-(-)-⬢-Pro-OBn, 68)[155]**

The starting material **66** (640 mg, 1.81 mmol, 1.0 equiv.) was dissolved in THF (10 mL) and deprotected according to **GP-5** using LiOH (216 mg, 9.03 mmol, 5.0 equiv.) in H_2O (10 mL).

The resulting white solid was dissolved in dry DCM (25 mL), charged with EDC·HCl (382 mg, 1.99 mmol, 1.1 equiv.) and preactivated for 30 min at ambient temperature. To this mixture, H-L-Pro-OBn·HCl (525 mg, 2.17 mmol, 1.2 equiv., **67·HCl**) and NEt_3 (300 µL, 2.17 mmol, 1.2 equiv.) were added and the resulting slurry stirred for 24 h at ambient temperature. The mixture was quenched with H_2O (20 mL) and the solution acidified to pH 2 with 1 M $KHSO_4$. The crude mixture was transferred into a separating funnel and the organic phase washed successively with sat. $NaHCO_3$ (1x) and sat. NaCl solutions (1x). The organic phase was dried over Na_2SO_4, filtered, all volatiles evaporated off and the residue dried under high vacuum. The crude product was purified using flash column chromatography (DCM/MeOH 50:1). White solid (860 g, 1.63 mmol, 90% over 2 steps).

$\mathbf{R_f}$ = 0.30 (DCM/MeOH 50:1); **^{1}H-NMR** (300 MHz, $CDCl_3$): δ_H (ppm) =7.40 – 7.28 (5 H, m), 7.07 (0.6 H, bs) + 6.61 (0.4 H, bs), 4.12 (2 H, bs), 5.25 – 5.01 (2 H, m), 4.55 – 4.48 (1 H, m), 4.30 – 4.02 (2 H, m), 3.70 – 3.22 (4 H, m), 2.95 – 2.83 (1 H, m), 2.30 – 1.72 (11 H, m), 1.71 – 1.27 (14 H, m); **^{13}C-NMR** (101 MHz, CD_2Cl_2): δ_C (ppm) = 172.83 (C_q), 172.02 (C_q), 155.75 (C_q), 154.72 (C_q), 136.62 (C_q), 128.96 (+, CH), 128.61 (+, CH), 128.47 (+, CH), 80.19 (C_q), 80.04 (C_q), 66.97 (-, CH_2), 61.45 (+, CH), 60.88 (+, CH), 59.40 (-, CH_2), 47.62 (-, CH_2), 47.39 (-, CH_2), 43.10 (+, CH), 31.87 (-, CH_2), 31.77 (-, CH_2), 29.62 (-, CH_2), 29.47 (-, CH_2), 28.66 (+, CH_3), 26.38 (-, CH_2), 25.99 (-, CH_2), 25.59 (-, CH_2), 25.01 (-, CH_2), 24.09 (-, CH_2), 23.79 (-, CH_2), 23.15 (-, CH_2), 22.82 (-, CH_2) (signal doubling due to rotamers); **IR** (neat): $\tilde{\nu}$ = 2932, 2873, 1742, 1692, 1638, 1509, 1430, 1389, 1246, 1161, 1121, 1090, 1031, 982, 921, 737, 698; **MS** (+ESI, 120 V): *m/z* (%) = 428.3 (6) [(MH_2-Boc)$^+$], 528.3 (100) [(M+H)$^+$], 550.3 (25), [(M+Na)$^+$], 1077.6 (20) [(2M+Na)$^+$]; **HRMS** (+ESI, 120 V): 528.3071 ($C_{29}H_{42}N_3O_6$ [(M+H)$^+$]: calc. 528.3068); $[\alpha]_D^{22}$: -135.1 (c = 0.53, $CHCl_3$); **Chiral HPLC** performed on Chiralcel Phenomenex Lux Cellulose-2 (*n*-heptane/*i*-PrOH = 70:30, λ = 215 nm, 0.5 mL/min): t_r(major) = 13.0 min; diastereomeric excess: >99%; **m.p.** 51 – 74 °C.

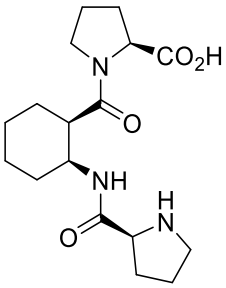

((1*R*,2*S*)-2-((*S*)-Pyrrolidine-2-carboxamido)cyclohexane-1-carbonyl)-L-proline (H-Pro-(-)-⬢-Pro-OH, 52)[155]

Synthesized from **68** (264 mg, 501 µmol, 1.0 equiv.) according to **GP-6**. White solid (155 mg, 460 µmol, 92%). A crystal for X-ray analysis was obtained by recrystallization from MeOH.

R_f = 0.03 (DCM/MeOH 4:1); **^{1}H-NMR** (400 MHz, $CDCl_3$, 300 K): δ_H (ppm) =8.47 – 5.20 (1 H, bs), 7.87 (0.4 H, d, *J* = 8.6 Hz) + 7.27 (0.6 H, bs), 4.43 – 3.85 (3 H, m), 3.70 – 3.39 (3 H, m), 3.34 – 3.11 (2 H, m), 2.88 – 2.70 (1 H, m), 2.44 – 1.69 (10 H, m), 1.69 – 1.28 (6 H, m); **^{13}C-NMR** (101 MHz, $CDCl_3$): δ_C (ppm) = 178.43 (C_q), 176.31 (C_q), 173.18 (C_q), 172.38 (C_q), 170.67 (C_q), 169.04 (C_q), 62.26 (+, CH), 61.10 (+, CH), 60.33 (+, CH), 59.51 (+, CH), 48.26 (+, CH), 47.68 (+, CH), 46.59 (-, CH_2), 45.86 (-, CH_2), 43.04 (+, CH), 41.76 (+, CH), 31.94 (-, CH_2), 31.15 (-, CH_2), 29.60 (-, CH_2), 29.51 (-, CH_2), 29.33 (-, CH_2), 28.79 (-, CH_2), 25.98 (-, CH_2), 25.40 (-, CH_2), 25.32 (-, CH_2), 24.74 (-, CH_2), 23.19 (-, CH_2),.22.29 (-, CH_2), 22.43 (-, CH_2) (signal doubling due to rotamers); **IR** (neat): $\tilde{\nu}$ = 3346, 2934, 2872, 1664, 1604, 1444, 1387, 1366, 1294, 1253, 1195, 1130, 1093, 1042, 923, 856, 680; **MS** (+ESI, 120 V): *m/z* (%) = 338.2 (100) [$(M+H)^+$], 675.4 (1) [$(2M+H)^+$]; **HRMS** (+ESI, 120 V): 338.2080 ($C_{17}H_{28}N_3O_4$ [$(M+H)^+$]: calc. 338.2074); $[\alpha]_D^{22}$: -96.6 (c = 0.97, $CHCl_3$); **m.p.** 127 °C (decomposition).

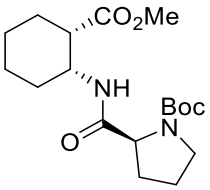

***tert*-Butyl (*S*)-2-(((1*R*,2*S*)-2-(methoxycarbonyl)cyclohexyl)carbamoyl)pyrrolidine-1-carboxylate (Boc-Pro-(+)-⬢-OMe, *ent*-66)[155,174]**

A flame-dried two-necked Schlenk flask equipped with a reflux condenser, bubble counter and septum was charged with (+)-**63** (1.00 g, 5.43 mmol, 1.0 equiv.), dry NEt_3 (0.78 mL, 5.6 mmol, 1.0 equiv.) and dry toluene (20 mL). DPPA (1.53 g, 5.57 mmol, 1.0 equiv.) was added dropwise to the stirred mixture, followed by BnOH (1.1 mL, 10.6 mmol, 2.0 equiv.). The reaction was heated to 120 °C and stirred for 4 h (gas evolution was observed). Subsequently, the mixture was allowed to cool to ambient temperature, transferred into a separating funnel and diluted with EtOAc (10 mL). The organic phase

was washed consecutively with 2 M HCl (1x 30 mL), sat. $NaHCO_3$ (1x 30 mL) and sat. NaCl solutions (1x 30 mL), then dried over Na_2SO_4, filtered, all volatiles removed and the residue dried under high vacuum.

The yellow oil was transferred into an autoclave vessel with MeOH (10 mL) and 200 mg Pd/C (10 wt% Pd) added. The mixture was hydrogenated for 19 h at 45 bar H_2. After the reaction was completed, the slurry was filtered and the solvent was removed carefully on a rotatory evaporator (the free amine tends to be volatile). The residue was diluted with H_2O (10 mL) and transferred into a separating funnel, then acidified with 2 M HCl to approximately pH 3 and extracted with diethyl ether (2x). The aqueous phase was then basified with sat. Na_2CO_3 to pH 9 and extracted with DCM (12x), until TLC control showed no more remaining product in the extract. The combined organic phases were dried over Na_2SO_4, filtered and the solvent removed carefully on a rotatory evaporator.

The yellowish liquid was then diluted with EtOAc (15 mL) and charged with pyridine (1.3 mL, 16.3 mmol, 3.0 equiv.) and *N*-Boc-L-Pro-OH (1.23 g, 5.70 mmol, 1.1 equiv., **58**). The slurry was cooled to -10 °C and T3P (50 wt% in EtOAc) (6.91 g, 10.91 mmol, 2.0 equiv.) added dropwise. The reaction mixture was allowed to warm up to ambient temperature and stirred for 20 h. The mixture was transferred into a separating funnel and diluted with H_2O (25 mL). The organic phase was separated off, the aqueous phase extracted with EtOAc (3x) and the combined organic phases dried over Na_2SO_4. The drying agent was filtered off, all volatiles evaporated off and the residue dried under high vacuum. The crude product was purified by flash column chromatography (hexanes/ EtOAc 2:1 → 1:1). Colorless oil (1.23 g, 3.48 mmol, 64% over 3 steps).

R_f = 0.35 (hexanes/EtOAc 1:1); **^{1}H-NMR** (400 MHz, $CDCl_3$): δ_H (ppm) =7.22 (0.5 H, bs) + 6.79 (0.5 H, bs), 4.21 – 3.90 (2 H, m), 3.49 (3 H, s), 3.41 – 3.04 (2 H, m), 2.55 (1 H, bs), 2.29 – 1.03 (21 H, m); **^{13}C-NMR** (101 MHz, $CDCl_3$): δ_C (ppm) = 174.54 (C_q), 173.78 (C_q), 171.52 (C_q), 171.02 (C_q), 155.30 (C_q), 154.90 (C_q), 154.31 (C_q), 153.74 (C_q), 80.03 (C_q), 79.39 (C_q), 61.16 (+, CH), 60.00 (+, CH), 58.73 (+, CH), 58.60 (+, CH), 51.34 (+, CH_3), 47.14 (+, CH), 46.66 (-, CH_2), 46.47 (-, CH_2), 46.04 (-, CH_2), 44.45 (+, CH), 44.16 (+, CH), 30.94 (-, CH_2), 30.67 (-, CH_2), 29.32 (-, CH_2), 28.12 (+, CH), 26.41 (-, CH_2), 25.03 (-, CH_2), 24.07 (-, CH_2), 23.36 (-, CH_2), 22.95 (-, CH_2), 22.23 (-, CH_2) (signal doubling due to rotamers); **IR** (neat): $\tilde{\nu}$ = 3421, 3332, 2975, 2940, 2870, 1729, 1685, 1664, 1536, 1449, 1400, 1360, 1313, 1163, 1119, 1085, 1039, 987, 918, 885, 846, 776, 753; **MS** (+ESI, 120 V): *m/z* (%) = 355.2 (100) [$(M+H)^+$], 377.2 (20) [$(M+Na)^+$], 731.4 (20) [$(2M+Na)^+$]; **HRMS** (+ESI, 120 V): 355.2230 ($C_{18}H_{31}N_2O_5$ [$(M+H)^+$]: calc. 355.2227); $[\alpha]_D^{22}$: -54.5 (c = 1.05, $CHCl_3$); **m.p.** 42 – 55 °C; **Chiral HPLC** performed on Chiralpak AS-H (*n*-heptane/*i*-PrOH = 90:10, λ = 215 nm, 1.0 mL/min): t_r(major) = 19.2 min; diastereomeric excess: >99%.

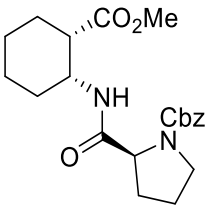

Benzyl (*S*)-2-(((1*R*,2*S*)-2-(methoxycarbonyl)cyclohexyl)carbamoyl)pyrrolidine-1-carboxylate (Cbz-Pro-(+)-⬢-OMe, *ent*-71)[174,195]

A flame-dried two-necked Schlenk flask equipped with a reflux condenser, bubble counter and septum was charged with (+)-**63** (1.00 g, 5.43 mmol, 1.0 equiv.), dry NEt_3 (0.78 mL, 5.6 mmol, 1.0 equiv.) and dry toluene (20 mL). DPPA (1.53 g, 5.57 mmol, 1.0 equiv.) was added dropwise to the stirred mixture, followed by BnOH (1.1 mL, 10.6 mmol, 2.0 equiv.). The reaction was heated to 120 °C and stirred for 4 h (gas evolution was observed). Subsequently, the mixture was allowed to cool to ambient temperature, transferred into a separating funnel and diluted with EtOAc (10 mL). The organic phase was washed consecutively with 2 M HCl (1x 30 mL), sat. $NaHCO_3$ (1x 30 mL) and sat. NaCl solutions (1x 30 mL), then dried over Na_2SO_4, filtered, all volatiles removed and the residue dried under high vacuum.

The yellow oil was transferred into an autoclave vessel with MeOH (10 mL) and 200 mg Pd/C (10 wt% Pd) added. The mixture was hydrogenated for 16 h at 45 bar H_2. After the reaction was completed, the slurry was filtered and the solvent was removed carefully on a rotatory evaporator (the free amine tends to be volatile). The residue was diluted with H_2O (10 mL) and transferred into a separating funnel, then acidified with 2 M HCl to approximately pH 3 and extracted with diethyl ether (2x). The aqueous phase was then basified with sat. Na_2CO_3 to pH 9 and extracted with DCM (10x), until TLC control showed no more remaining product. The combined organic phases were dried over Na_2SO_4, filtered and the solvent removed carefully on a rotatory evaporator.

The yellowish liquid (653 mg) was then diluted with EtOAc (15 mL) and charged with pyridine (1.0 mL, 12.5 mmol, 3.0 equiv.) and *N*-Cbz-L-Pro-OH (1.09 g, 4.36 mmol, 1.1 equiv., **70**). The slurry was cooled to -10 °C and T3P (50 wt% in EtOAc) (5.29 g, 8.31 mmol, 2.0 equiv.) added dropwise. The reaction mixture was allowed to warm up to ambient temperature and stirred for 65 h. The mixture was transferred into a separating funnel and diluted with H_2O (25 mL). The organic phase was separated off, the aqueous phase extracted with EtOAc (3x) and the combined organic phases dried over Na_2SO_4. The drying agent was filtered off, all volatiles evaporated and the residue dried under high vacuum. The crude product was purified using flash column chromatography (hexanes/ EtOAc 1:1). Colorless oil (929 mg, 2.39 mmol, 44% over 3 steps).

R_f = 0.23 (hexanes/EtOAc 1:1); **^{1}H-NMR** (300 MHz, $CDCl_3$): δ_H (ppm) =7.57 – 6.43 (6 H, m), 5.30 – 4.77 (2 H, m), 4.38 – 3.78 (2 H, m), 3.41 – 3.04 (5 H, m), 2.54 (1 H, bs), 2.34 – 0.80 (12 H, m); **^{13}C-NMR** (75 MHz, $CDCl_3$): δ_C (ppm) = 173.58 (C_q), 170.78 (C_q), 170.28 (C_q), 155.47 (C_q), 154.54 (C_q), 136.21 (C_q), 128.02 (+, CH), 127.58 (+, CH), 127.43 (+, CH), 66.69 (-, CH_2), 60.67 (+, CH), 60.30 (+, CH), 51.08 (+, CH_3), 46.98 (+, CH), 46.68 (+, CH), 46.37, 44.26 (+, CH), 43.78 (+, CH), 30.69 (-, CH_2), 29.17 (-, CH_2), 28.78 (-, CH_2), 28.05 (-, CH_2), 26.03 (-, CH_2), 25.11 (-, CH_2), 23.94 (-, CH_2), 23.01 (-, CH_2), 22.65 (-, CH_2), 22.20 (-, CH_2) (signal doubling due to rotamers); **IR** (neat): $\tilde{\nu}$ = 3418, 3329, 2937, 2863, 1677, 1513, 1450, 1409, 1357, 1238, 1170, 1115, 1088, 1036, 984, 917, 883, 749, 697; **MS** (+ESI, 120 V): *m/z* (%) = 389.2 (100) [$(M+H)^+$], 411.2 (34) [$(M+Na)^+$], 799.4 (1) [$(2M+Na)^+$]; **HRMS** (+ESI, 120 V): 389.2075 ($C_{21}H_{29}N_2O_5$ [$(M+H)^+$]: calc. 389.2071); $[\alpha]_D^{22}$: -45.8 (c = 1.03, $CHCl_3$); **Chiral HPLC** performed on Chiralcel Phenomenex Lux Cellulose-2 (*n*-heptane/*i*-PrOH = 90:10, λ = 215 nm, 1.0 mL/min): t_r(major) = 36.2 min; diastereomeric excess: >99%.

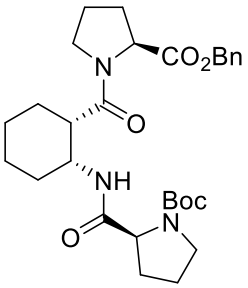

***tert*-Butyl (S)-2-(((1*R*,2*S*)-2-((*S*)-2-((benzyloxy)carbonyl)pyrrolidine-1-carbonyl)cyclohexyl)-carbamoyl)-pyrrolidine-1-carboxylate (Boc-Pro-(+)-⬢-Pro-OBn, *ent*-68)[155]**

The starting material *ent*-**66** (400 mg, 1.13 mmol, 1.0 equiv.) was dissolved in THF (10 mL) and deprotected according to **GP-5** using LiOH (135 mg, 5.64 mmol, 5.0 equiv.) in H_2O (10 mL).

The resulting white solid was dissolved in EtOAc (10 mL) and charged with pyridine (0.37 mL, 4.58 mmol, 4.1 equiv.), H-L-Pro-OBn·HCl (300 mg, 1.24 mmol, 1.1 equiv., **67·HCl**) and NEt_3 (175 µL, 1.26 mmol, 1.1 equiv.). The slurry was cooled to -10 °C and T3P (50 wt% in EtOAc) (1.44 g, 2.26 mmol, 2.0 equiv.) added dropwise. The reaction mixture was allowed to warm up to ambient temperature and stirred for 48 h. The mixture was transferred into a separating funnel and diluted with H_2O (20 mL). The organic phase was separated off, the aqueous phase extracted with EtOAc (3x) and the combined organic phases washed with sat. NH_4Cl, sat. $NaHCO_3$ and sat. NaCl solutions. The organic phase was dried over Na_2SO_4, filtered, all volatiles evaporated off and the residue dried under high vacuum. The crude product was purified using flash column chromatography (hexanes/ EtOAc 1:2 → 1:4). White foam-like solid (489 mg, 926 µmol, 82% over 2 steps).

R_f = 0.25 (hexanes/EtOAc 1:4); **^{1}H-NMR** (400 MHz, $CDCl_3$): δ_H (ppm) =7.58 – 6.51 (6 H, m), 5.19 – 4.93 (2 H, m), 4.52 – 4.28 (1 H, m), 4.24 – 3.91 (2 H, m), 3.76 – 3.10 (4 H, m), 2.82 (1 H, bs), 2.44 – 1.07 (25 H, m); **^{13}C-NMR** (101 MHz, $CDCl_3$): δ_C (ppm) = 171.57 (C_q), 171.24 (C_q), 171.07 (C_q), 170.83 (C_q), 153.55 (C_q), 134.66 (+, CH), 134.13 (+, CH), 127.59 (+, CH), 127.52 (+, CH), 127.42 (+, CH), 127.30 (+, CH), 127.09 (+, CH), 126.91 (+, CH), 78.87 (C_q), 78.54 (C_q), 66.10 (-, CH_2), 65.50 (-, CH_2), 60.58 (+, CH), 59.89 (+, CH), 58.00 (+, CH), 57.62 (+, CH), 46.30 (+, CH), 46.00 (-, CH_2), 45.80 (-, CH_2), 45.28 (-, CH_2), 44.69 (-, CH_2), 42.30 (+, CH), 41.13 (+, CH), 30.20 (-, CH_2), 28.90 (-, CH_2), 28.46 (-, CH_2), 27.82 (-, CH_2), 27.76 (-, CH_2), 27.26 (+, CH_3), 25.03 (-, CH_2), 24.27 (-, CH_2), 22.98 (-, CH_2), 22.52 (-, CH_2), 22.29 (-, CH_2), 21.49 (-, CH_2), 21.24 (-, CH_2), 20.82 (-, CH_2) (signal doubling due to rotamers); **IR** (neat): $\tilde{\nu}$ = 3392, 2978, 2930, 2863, 1741, 1696, 1673, 1618, 1513, 1439, 1383, 1267, 1234, 1167, 1118, 857, 775, 731, 697; **MS** (+ESI, 120 V): *m/z* (%) = 528.3 (100) [$(M+H)^+$], 550.3 (62) [$(M+Na)^+$], 1077.6 (11) [$(2M+Na)^+$]; **HRMS** (+ESI, 120 V): 528.3079 ($C_{29}H_{42}N_3O_6$ [$(M+H)^+$]: calc. 528.3068); $[\alpha]_D^{22}$: -83.1 (c = 1.00, $CHCl_3$); **Chiral HPLC** performed on Chiralcel Phenomenex Lux Cellulose-2 (*n*-heptane/*i*-PrOH = 70:30, λ = 215 nm, 0.5 mL/min): t_r(major) = 21.2 min; diastereomeric excess: >99%; **m.p.** 106 – 112 °C.

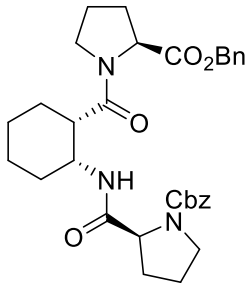

Benzyl (*S*)-2-(((1*R*,2*S*)-2-((*S*)-2-((benzyloxy)carbonyl)pyrrolidine-1-carbonyl)cyclohexyl)carbamoyl)-pyrrolidine-1-carboxylate (Cbz-Pro-(+)-⬢-Pro-OBn, *ent*-72)[195]

The starting material *ent*-**71** (401 mg, 1.03 mmol, 1.0 equiv.) was dissolved in THF (10 mL) and deprotected according to **GP-5** using LiOH (124 mg, 5.16 mmol, 5.0 equiv.) in H_2O (10 mL).

The resulting white solid was dissolved in EtOAc (10 mL) and charged with pyridine (0.34 mL, 4.21 mmol, 4.1 equiv.), H-L-Pro-OBn·HCl (275 mg, 1.14 mmol, 1.1 equiv., **67·HCl**) and NEt_3 (160 µL, 1.15 mmol, 1.1 equiv.). The slurry was cooled to -10 °C and T3P (50 wt% in EtOAc) (1.31 g, 2.06 mmol, 2.0 equiv.) added dropwise. The reaction mixture was allowed to warm up to ambient temperature and stirred for 48 h. The mixture was transferred into a separating funnel and diluted with H_2O (20 mL). The organic phase was separated off, the aqueous phase extracted with EtOAc (3x) and the combined organic phases washed with sat. NH_4Cl (1x), sat. $NaHCO_3$ (1x) and sat. NaCl solutions (1x). The organic phase was dried over Na_2SO_4, filtered, all volatiles evaporated and the residue dried under high

vacuum. The crude product was purified by flash column chromatography (hexanes/ EtOAc 1:1 → 1:4). Colorless oil (430 mg, 765 µmol, 74% over 2 steps).

R_f = 0.30 (hexanes/EtOAc 1:4); **^{1}H-NMR** (400 MHz, $CDCl_3$): δ_H (ppm) =7.63 – 6.99 (10 H, m), 6.87 (0.5 H, d, *J* = 6.5 Hz) + 6.71 (0.5 H, d, *J* = 7.0 Hz), 5.31 – 4.85 (4 H, m), 4.57 – 4.36 (1 H, m), 4.32 – 3.89 (2 H, m), 3.86 – 3.22 (4 H, m), 2.99 – 2.70 (1 H, m), 2.61 – 0.85 (16 H, m); **^{13}C-NMR** (101 MHz, $CDCl_3$): δ_C (ppm) = 172.81 (C_q), 172.65 (C_q), 172.22 (C_q), 172.10 (C_q), 171.76 (C_q), 171.42 (C_q), 155.08 (C_q), 136.79 (C_q), 136.53 (C_q), 135.62 (C_q), 135.17 (C_q), 128.65 (+, CH), 128.58 (+, CH), 128.49 (+, CH), 128.37 (+, CH), 127.90 (+, CH), 127.80 (+, CH), 67.16 (-, CH_2), 66.99 (-, CH_2), 66.87 (-, CH_2), 66.59 (-, CH_2), 61.20 (+, CH), 59.10 (+, CH), 58.68 (+, CH), 47.43 (+, CH), 47.26 (-, CH_2), 46.99 (-, CH_2), 46.83 (-, CH_2), 46.34 (-, CH_2), 43.19 (+, CH), 41.76 (+, CH), 31.23 (-, CH_2), 30.05 (-, CH_2), 29.34 (-, CH_2), 28.79 (-, CH_2), 25.91 (-, CH_2), 24.74 (-, CH_2), 24.11 (-, CH_2), 23.47 (-, CH_2), 23.01 (-, CH_2), 22.28 (-, CH_2), 21.97 (-, CH_2) (signal doubling due to rotamers); **IR** (neat): $\tilde{\nu}$ = 3403, 3332, 2933, 2878, 1744, 1703, 1700, 1633, 1513, 1435, 1405, 1267, 1238, 1167, 1115, 1030, 977, 917, 738, 697; **MS** (+ESI, 120 V): *m/z* (%) = 562.3 (100) [$(M+H)^+$], 584.3 (44) [$(M+Na)^+$], 1145.6 (19) [$(2M+Na)^+$]; **HRMS** (+ESI, 120 V): 562.2921 ($C_{32}H_{40}N_3O_6$ [$(M+H)^+$]: calc. 562.2912); $[\alpha]_D^{22}$: -64.5 (c = 1.01, $CHCl_3$); **Chiral HPLC** performed on Chiralcel Phenomenex Lux Cellulose-2 (*n*-heptane/*i*-PrOH = 50:50, λ = 215 nm, 0.5 mL/min): t_r(major) = 29.2 min; diastereomeric excess: >99%.

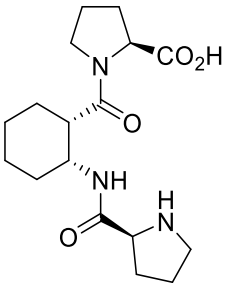

((1*S*,2*R*)-2-((*S*)-Pyrrolidine-2-carboxamido)cyclohexane-1-carbonyl)-L-proline (H-Pro-(+)-⬢-Pro-OH, *ent*-52)[155]

Synthesized from *ent*-**68** (202 mg, 383 µmol, 1.0 equiv.) according to **GP-6**. White solid (118 mg, 349 µmol, 91%).

Also synthesized from *ent*-**72** (217 mg, 386 µmol, 1.0 equiv.) according to **GP-7**. White solid (130 mg, 385 µmol, 100%).

R_f = 0.07 (DCM/MeOH 10:1); **^{1}H-NMR** (300 MHz, $CDCl_3$): δ_H (ppm) = 9.27 (1 H, d, *J* = 9.0 Hz), 9.06 (1 H, s), 8.76 (1 H, bs), 7.47 (1 H, bs), 5.42 – 4.79 (1 H, m), 4.78 – 4.43 (1 H, m), 4.42 – 3.84 (1 H, m), 3.83 – 0.96 (20 H, m); **^{13}C-NMR** (75 MHz, $CDCl_3$): δ_C (ppm) = 177.98 (C_q), 172.15 (C_q), 168.44 (C_q), 61.14 (+, CH),

59.01 (+, CH), 47.29 (-, CH_2), 47.16 (-, CH_2), 44.77 (+, CH), 44.07 (+, CH), 31.66 (-, CH_2), 28.88 (-, CH_2), 28.56 (-, CH_2), 25.74 (-, CH_2), 24.80 (-, CH_2), 24.65 (-, CH_2), 22.96 (-, CH_2), 20.06 (-, CH_2) (signal doubling due to rotamers); **IR** (neat): $\bar{\nu}$ = 3216, 3049, 2930, 2858, 1667, 1611, 1577, 1441, 1378, 1357, 1287, 1243, 1194, 1120, 1088, 1038, 975, 918, 846, 725; **MS** (+ESI, 120 V): *m/z* (%) = 338.2 (100) [$(M+H)^+$], 675.4 (1) [$(2M+H)^+$]; **HRMS** (+ESI, 120 V): 338.2078 ($C_{17}H_{28}N_3O_4$ [$(M+H)^+$]: calc. 338.2074); $[\alpha]_D^{22}$: -43.7 (c = 1.01, $CHCl_3$); **m.p.** 111 °C (decomposition).

3.4. Synthesis of peptides containing anthranilic acid

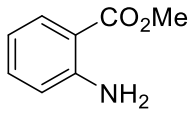

Methyl 2-aminobenzoate (73)[198]

Anthranilic acid (4.00 g, 29.2 mmol, 1.0 equiv., **54**) was dissolved in MeOH (100 mL, 2.47 mol, 85 equiv.) and the dark yellow solution was cooled to 0°C. $SOCl_2$ (8.50 mL, 13.9 g, 117.2 mmol, 4.0 equiv.) was added dropwise at 0°C with a syringe pump over 30 min under tarnishing of the solution. The solution was heated under reflux for 16 h. The solvent was then removed under reduced pressure yielding a light pink solid. The crude product was transferred into a separating funnel with sat. $NaHCO_3$ solution. The aqueous phase was extracted with EtOAc (1x 60 mL), the organic layer washed with sat. $NaHCO_3$ (1x) and sat. NaCl solutions (1x), dried over Na_2SO_4, filtered and the solvent removed under reduced pressure. The resulting brown suspension was filtered and concentrated *in vacuo*. Brown liquid (3.02 g, 20.0 mmol, 68%).

^{1}H-NMR (300 MHz, $CDCl_3$): δ_H (ppm) = 7.86 (1 H, dd, J = 8.1 Hz, 1.4 Hz), 7.30 – 7.23 (1 H, m), 6.69 – 6.62 (2 H, m), 3.87 (3 H, s); **^{13}C-NMR** (75 MHz, $CDCl_3$) δ_C (ppm) = 168.68 (C_q), 150.39 (C_q), 134.20 (+, CH), 131.32 (+, CH), 116.85 (+, CH), 116.47 (+, CH), 110.91 (C_q), 51.65 (+, CH_3).

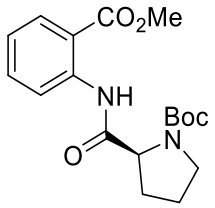

***tert*-Butyl (*S*)-2-((2-(methoxycarbonyl)phenyl)carbamoyl)pyrrolidine-1-carboxylate (Boc-Pro-Ant-OMe, 74)**[155,199]

Methyl 2-aminobenzoate (759 mg, 5.02 mmol, 1.0 equiv., **73**) was dissolved in EtOAc (10 mL) and charged with pyridine (1.2 mL, 15.1 mmol, 3.0 equiv.) and *N*-L-Boc-Pro-OH (1.13 g, 5.27 mmol, 1.1 equiv., **58**). The slurry was cooled to -10 °C and T3P (50 wt% in EtOAc) (6.39 g, 10.0 mmol, 2.0 equiv.) added dropwise. The reaction mixture was allowed to warm up to ambient temperature and stirred for 30 h. The mixture was transferred into a separating funnel and diluted with H_2O (25 mL). The organic phase was separated off and the aqueous phase extracted with EtOAc (3x). The combined organic phases were dried over Na_2SO_4, filtered, all volatiles evaporated and the residue dried under

high vacuum. The crude product was purified by flash column chromatography (hexanes/ EtOAc 4:1 → 3:1). Orange oil (1.70 g, 4.89 mmol, 97%).

R_f = 0.18 (hexanes/EtOAc 6:1); **^{1}H-NMR** (400 MHz, $CDCl_3$): δ_H (ppm) = 11.56 (0.4 H, bs) + 11.45 (0.6 H, bs) 8.80 – 8.71 (1 H, m), 8.07 – 7.95 (1 H, m), 7.59 – 7.47 (1 H, m), 7.14 – 7.01 (1 H, m), 4.50 – 4.22 (1 H, m), 3.90 (3 H, m), 3.76 – 3.40 (2 H, m), 2.38 – 2.05 (2 H, m), 2.04 – 1.80 (2 H, m), 1.57 – 1.26 (9 H, m); **^{13}C-NMR** (101 MHz, $CDCl_3$): δ_C (ppm) = 172.55 (C_q), 172.07 (C_q), 168.34 (C_q), 155.19 (C_q), 154.37 (C_q), 141.28 (C_q), 141.06 (C_q), 134.69 (+, CH), 131.07 (+, CH), 130.82 (+, CH), 122.79 (+, CH), 120.41 (+, CH), 120.20 (+, CH), 115.46 (C_q), 80.39 (C_q), 80.23 (C_q), 62.84 (+, CH), 62.25 (+, CH), 52.57 (+, CH), 52.25 (+, CH), 47.26 (-, CH_2), 46.93 (-, CH_2), 31.67 (-, CH_2), 30.64 (-, CH_2), 28.56 (+, CH_3), 28.34 (+, CH_3), 24.46 (-, CH_2), 23.94 (-, CH_2) (signal doubling due to rotamers); **IR** (neat): $\tilde{\nu}$ = 3269, 2974, 2881, 1689, 1588, 1513, 1450, 1368, 1297, 1260, 1159, 1088, 951, 921, 880, 753; **MS** (+ESI, 120 V): *m/z* (%) = 249.1 [(MH_2-Boc)$^+$] (77), 293.1 [(MH-C_4H_8)$^+$] (61), 349.2 (100) [(M+H)$^+$], 371.2 (60) [(M+Na)$^+$], 719.3 (52) [(2M+Na)$^+$]; **HRMS** (+ESI, 120 V): 333.1769 ($C_{21}H_{23}N_2O_5$ [(M+H)$^+$]: calc. 349.1758); $[\alpha]_D^{22}$: -121.4 (c = 1.10, $CHCl_3$).

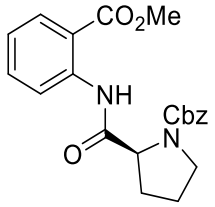

Benzyl (*S*)-2-((2-(methoxycarbonyl)phenyl)carbamoyl)pyrrolidine-1-carboxylate (Cbz-Pro-Ant-OMe, 75)[195,200]

Methyl 2-aminobenzoate (1.08 g, 7.12 mmol, 1.0 equiv., **73**) was dissolved in EtOAc (15 mL) and charged with pyridine (1.7 mL, 21.4 mmol, 3.0 equiv.) and *N*-L-Boc-Pro-OH (1.86 g, 7.47 mmol, 1.1 equiv., **58**). The slurry was cooled to -10 °C and T3P (50 wt% in EtOAc) (9.06 g, 14.2 mmol, 2.0 equiv.) added dropwise. The reaction mixture was allowed to warm up to ambient temperature and stirred for 32 h. The mixture was transferred into a separating funnel and diluted with H_2O (25 mL). The organic phase was separated off and the aqueous phase extracted with EtOAc (3x). The combined organic phases were dried over Na_2SO_4, filtered, all volatiles evaporated and the residue dried under high vacuum. The crude product was purified by flash column chromatography (hexanes/ EtOAc 4:1 → 1:1). Orange oil (2.55 g, 6.67 mmol, 94%).

R_f = 0.30 (hexanes/EtOAc 1:2); **^{1}H-NMR** (400 MHz, $CDCl_3$): δ_H (ppm) = 11.60 (0.5 H, bs) + 11.46 (0.5 H, bs), 8.74 (1 H, dd, J = 19.1, 8.4 Hz), 8.04 – 7.96 (1 H, m), 7.53 (1 H, pt, *J* = 7.8 Hz), 7.48 – 7.27 (2 H, m),

7.25 – 7.00 (4 H, m), 5.28 – 4.95 (2 H, m), 4.57 – 4.38 (1 H, m), 3.88 – 3.73 (4 H, m), 3.69 – 3.51 (1 H, m), 2.38 – 2.14 (2 H, m), 2.06 – 1.88 (2 H, m); **^{13}C-NMR** (101 MHz, $CDCl_3$): δ_C (ppm) = 171.88 (C_q), 171.44 (C_q), 168.57 (C_q), 168.21 (C_q), 155.65 (C_q), 154.84 (C_q), 141.14 (C_q), 140.93 (C_q), 136.82 (C_q), 136.45 (C_q), 134.61 (+, CH), 130.96 (+, CH), 130.88 (+, CH), 128.50 (+, CH), 128.23 (+, CH), 128.04 (+, CH), 127.92 (+, CH), 127.81 (+, CH), 122.82 (+, CH), 120.39 (+, CH), 120.20 (+, CH), 115.49 (C_q), 67.36 (-, CH_2), 67.19 (-, CH_2), 62.60 (+, CH), 62.48 (+, CH), 52.43 (+, CH_3), 52.32 (+, CH_3), 47.51 (-, CH_2), 47.07 (-, CH_2), 31.63 (-, CH_2), 30.53 (-, CH_2), 24.43 (-, CH_2), 23.79 (-, CH_2) (signal doubling due to rotamers); **IR** (neat): $\tilde{\nu}$ = 3265, 3064, 3034, 2952, 2881, 1685, 1588, 1517, 1450, 1402, 1353, 1260, 1163, 1115, 1088, 984, 917, 753, 697; **MS** (+ESI, 120 V): *m/z* (%) = 383.2 (100) [(M+H)$^+$], 405.1 (38) [(M+Na)$^+$], 787.3 (26) [(2M+Na)$^+$]; **HRMS** (+ESI, 120 V): 333.1612 ($C_{21}H_{23}N_2O_5$ [(M+H)$^+$]: calc. 383.1601); $[\alpha]_D^{22}$: -106.3 (c = 1.11, $CHCl_3$).

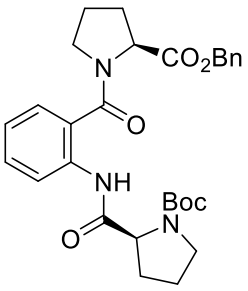

***tert*-Butyl (*S*)-2-((2-((*S*)-2-((benzyloxy)carbonyl)pyrrolidine-1-carbonyl)phenyl)carbamoyl)-pyrrolidine-1-carboxylate (Boc-Pro-Ant-Pro-OBn, 77)[155,197]**

The starting material **74** (1.17 g, 3.35 mmol, 1.0 equiv.) was dissolved in THF (7.5 mL) and deprotected according to **GP-5** using LiOH (402 mg, 16.8 mmol, 5.0 equiv.) in H_2O (7.5 mL).

The now deprotected dipeptide **76** (334 mg, 1.00 mmol, 1.0 equiv.) was dissolved in dry DCM (25 mL) and EDC·HCl (230 mg, 1.20 mmol, 1.2 equiv.), HOBt·H_2O (162 mg, 1.20 mmol, 1.2 equiv.), and H-Pro-OBn·HCl (290 mg, 1.20 mmol, 1.2 equiv., **67·HCl**) were added at ambient temperature. Subsequently, NEt_3 (1.0 mL, 7.5 mmol, 1.1 equiv.) was added and the reaction mixture stirred for 22 h. The pale yellow solution was transferred into a separating funnel and acidified with 1 M $KHSO_4$ to pH 2. The organic layer was washed with sat. $NaHCO_3$ (1x) and sat. NaCl solutions (1x), dried over Na_2SO_4, filtered and the solvent removed under reduced pressure, yielding an orange oil. The resulting crude product was purified by flash column chromatography (DCM/MeOH 50:1). White solid (191 mg, 365 µmol, 36% over 2 steps).

R_f = 0.25 (DCM/MeOH 50:1); **^{1}H-NMR** (400 MHz, $CDCl_3$): δ_H (ppm) = 9.84 – 9.54 (0.9 H, m) + 9.19 – 9.00 (0.1 H, m), 8.55 – 8.28 (0.9 H, m) + 8.16 – 8.00 (0.1 H, m), 7.61 – 6.76 (8 H, m),5.31 – 4.82 (2 H, m), 4.80 – 4.61 (1 H, m), 4.37 (0.5 H, bs) + 4.21 (0.5 H, bs), 3.83 – 3.27 (4 H, m), 2.43 – 1.70 (8 H, m), 1.43 (4.5 H, s) + 1.33 (4.5 H, s); **^{13}C-NMR** (101 MHz, $CDCl_3$): δ_C (ppm) = 171.93 (C_q), 171.57 (C_q), 168.40 (C_q), 154.95 (C_q), 153.99 (C_q), 136.89 (C_q), 136.27 (C_q), 135.53 (C_q), 131.19 (+, CH), 130.80 (+, CH), 128.39 (+, CH), 128.34 (+, CH), 128.25 (+, CH), 127.95 (+, CH), 127.34 (+, CH), 127.14 (+, CH), 126.44 (+, CH), 124.67 (C_q), 123.57 (+, CH), 123.01 (+, CH), 122.72 (+, CH), 121.61 (+, CH), 120.92 (+, CH), 79.78 (C_q), 66.85, 62.16 (+, CH), 61.59 (+, CH), 61.34 (+, CH), 58.96 (+, CH), 50.04 (-, CH_2), 49.70 (-, CH_2), 47.05 (-, CH_2), 46.64 (-, CH_2), 31.31 (-, CH_2), 30.16 (-, CH_2), 29.12 (-, CH_2), 28.38 (+, CH_3), 28.21 (+, CH_3), 25.12 (-, CH_2), 24.28 (-, CH_2), 23.73 (-, CH_2), 22.60 (-, CH_2) (signal doubling due to rotamers); **IR** (neat): $\bar{\nu}$ = 3310, 2974, 2881, 1744, 1689, 1625, 1588, 1517, 1454, 1383, 1297, 1249, 1159, 1118, 1088, 1040, 984, 954, 861, 749; **MS** (+ESI, 120 V): *m/z* (%) = 422.2 (16) [(M-C_4H_8-CO_2)$^+$], 522.3 (100) [(M+H)$^+$], 544.2 (12) [(M+Na)$^+$], 1065.5 (18) [(2M+Na)$^+$]; **HRMS** (+ESI, 120 V): 522.2605 ($C_{29}H_{36}N_3O_6$ [(M+H)$^+$]: calc. 522.2599); $[\alpha]_D^{22}$: - 109.6 (c = 0.75, $CHCl_3$); **m.p.** 36 – 50 °C.

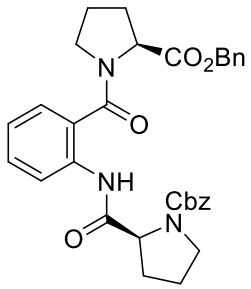

Benzyl (*S*)-2-((2-((*S*)-2-((benzyloxy)carbonyl)pyrrolidine-1-carbonyl)phenyl)carbamoyl)pyrrolidine-1-carboxylate (Cbz-Pro-Ant-Pro-OBn, 78)[195]

The starting material **75** (1.20 g, 3.14 mmol, 1.0 equiv.) was dissolved in THF (7.5 mL) and deprotected according to **GP-5** using LiOH (376 mg, 15.7 mmol, 5.0 equiv.) in H_2O (7.5 mL).

The resulting white solid (1.07 g) was dissolved in EtOAc (10 mL) and charged with pyridine (0.91 mL, 8.8 mmol, 3.0 equiv.), H-L-Pro-OBn·HCl (712 mg, 2.94 mmol, 1.0 equiv., **67·HCl**) and NEt_3 (320 µL, 2.95 mmol, 1.0 equiv.). The slurry was cooled to -20 °C and T3P (50 wt% in EtOAc) (3.71 g, 5.83 mmol, 2.0 equiv.) added dropwise. The reaction mixture was allowed to warm up to ambient temperature and stirred for 48 h. The mixture was transferred into a separating funnel and diluted with H_2O (20 mL). The organic phase was separated off, the aqueous phase extracted with EtOAc (3x) and the combined organic phases washed with sat. NH_4Cl (1x), sat. $NaHCO_3$ (1x) and sat. NaCl solutions (1x). The organic phase was dried over Na_2SO_4, filtered, all volatiles evaporated off and the residue dried under high

vacuum. The crude product was purified by flash column chromatography (hexanes/ EtOAc 1:1 → 1:4). Colorless oil (258 mg, 465 µmol, 15% over 2 steps).

R_f = 0.33 (hexanes/EtOAc 1:2); **^{1}H-NMR** (300 MHz, $CDCl_3$): δ_H (ppm) = 9.84 – 9.56 (0.9 H, m) + 9.25 – 9.10 (0.1 H, m), 8.54 – 8.32 (0.9 H, m) + 8.18 – 8.03 (0.1 H, m), 7.68 – 6.83 (13 H, m), 5.36 – 4.86 (4 H, m), 4.85 – 4.57 (1 H. m), 4.56 – 4.30 (1 H, m), 3.92 – 3.12 (4 H, m), 2.51 – 1.53 (8 H, m); **^{13}C-NMR** (101 MHz, $CDCl_3$): δ_C (ppm) = 172.00 (C_q), 171.20 (C_q), 170.84 (C_q), 168.23 (C_q), 168.09 (C_q), 155.21 (C_q), 154.36 (C_q), 136.47 (C_q), 136.19 (C_q), 135.94 (C_q), 135.35 (C_q), 130.78 (+, CH), 130.67 (+, CH), 128.38 (+, CH), 128.23 (+, CH), 128.10 (+, CH), 127.77 (+, CH), 127.71 (+, CH), 127.65 (+, CH), 127.42 (+, CH), 127.18 (+, CH), 126.87 (+, CH), 124.66 (C_q), 124.06 (C_q), 123.03 (-, CH_2), 122.89 (-, CH_2), 121.40 (-, CH_2), 120.85 (-, CH_2), 66.94 (-, CH_2), 66.84 (-, CH_2), 66.70 (-, CH_2), 61.57 (+, CH), 61.42 (+, CH), 58.89 (+, CH), 58.75 (+, CH), 49.59 (-, CH_2), 49.37 (-, CH_2), 47.21 (-, CH_2), 46.75 (-, CH_2), 31.17 (-, CH_2), 30.01 (-, CH_2), 29.09 (-, CH_2), 28.92 (-, CH_2), 25.00 (-, CH_2), 24.84 (-, CH_2), 24.11 (-, CH_2), 23.47 (-, CH_2) (signal doubling due to rotamers); **IR** (neat): $\tilde{\nu}$ = 3310, 3064, 3034, 2956, 2881, 1741, 1700, 1625, 1588, 1517, 1402, 1349, 1297, 1163, 1115, 1088, 1029, 984, 913, 880, 738, 697; **MS** (+ESI, 120 V): *m/z* (%) = 556.2 (100) [$(M+H)^+$], 578.2 (20) [$(M+Na)^+$], 1133.5 (34) [$(2M+Na)^+$]; **HRMS** (+ESI, 120 V): 556.2444 ($C_{32}H_{34}N_3O_6$ [$(M+H)^+$]: calc. 556.2442); $[\alpha]_D^{22}$: -109.3 (c = 0.99, $CHCl_3$).

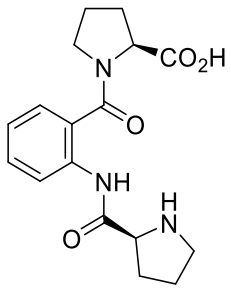

(*S*)-1-(2-((*S*)-Pyrrolidine-2-carboxamido)benzoyl)pyrrolidine-2-carboxylic acid (H-Pro-Ant-Pro-OH, 53)[155]

Synthesized from **77** (190 mg, 365 µmol, 1.0 equiv.) according to **GP-6**. White solid (112 mg, 338 µmol, 92%).

R_f = 0.03 (DCM/MeOH 15:1); **^{1}H-NMR** (300 MHz, $CDCl_3$): δ_H (ppm) = 10.73 (1 H, s), 8.22 (1 H, d, *J* = 7.8 Hz), 8.12 – 6.10 (5 H, m + bs), 5.17 – 4.06 (2 H, m), 4.06 – 2.81 (4 H, m), 2.81 – 1.42 (8 H, m); **^{13}C-NMR** (101 MHz, $CDCl_3$): δ_C (ppm) = 178.01 (C_q), 169.37 (C_q), 167.48 (C_q), 134.38 (C_q), 130.07 (+, CH), 128.46 (C_q), 126.25 (+, CH), 124.90 (+, CH), 121.48 (+, CH), 60.82 (+, CH), 58.95 (+, CH), 48.85 (-, CH_2), 46.55 (-, CH_2), 31.83 (-, CH_2), 30.24 (-, CH_2), 25.00 (-, 2x CH_2); **IR** (neat): $\tilde{\nu}$ = 2971, 2878, 1696, 1618,

1588, 1551, 1454, 1420, 1379, 1290, 1252, 1204, 1088, 1040, 984, 951, 917, 872, 846, 749; **MS** (+ESI, 120 V): *m/z* (%) = 332.2 (100) [(M+H)$^+$]; **HRMS** (+ESI, 120 V): 332.1612 ($C_{17}H_{22}N_3O_4$ [(M+H)$^+$]: calc. 332.1605); $[\alpha]_D^{30}$: -150.8 (c = 1.01, $CHCl_3$); **m.p.** 154 °C (decomposition).

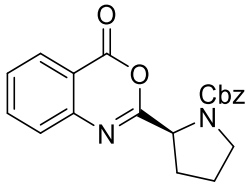

Benzyl (*S*)-2-(4-oxo-4H-benzo[d][1,3]oxazin-2-yl)pyrrolidine-1-carboxylate (83)[227]

Obtained as a side product in the synthesis of **78**. Colorless oil (700 mg, 2.00 mmol, 64% over 2 steps).

R_f = 0.75 (hexanes/EtOAc 1:2); **^{1}H-NMR** (400 MHz, $CDCl_3$): δ_H (ppm) =8.14 – 8.04 (1 H, m), 7.76 – 7.68 (1 H, m), 7.56 – 7.39 (2 H, m), 7.37 – 7.22 (2 H, m), 7.08 – 6.92 (3 H, m), 5.22 – 5.14 (0.5 H, m) + 4.89 – 4.82 (0.5 H, m), 5.11 (1 H, s), 4.78 – 4.64 (1 H, m), 3.78 – 3.67 (1 H, m), 3.65 – 3.51 (1 H, m), 2.41 – 2.24 (1 H, m), 2.20 – 2.00 (2 H, m), 2.00 – 184 (1 H, m); **^{13}C-NMR** (101 MHz, $CDCl_3$): δ_C (ppm) = 162.08 (C_q), 161.78 (C_q), 159.22 (C_q), 158.89 (C_q), 146.09 (C_q), 145.89 (C_q), 136.57 (C_q), 136.34 (+, CH), 136.30 (+, CH), 136.09 (C_q), 128.33 (+, CH), 128.28 (+, CH), 128.20 (+, CH), 128.03 (+, CH), 127.83 (+, CH), 127.64 (+, CH), 127.59 (+, CH), 127.47 (+, CH), 126.87 (+, CH), 126.72 (+, CH), 116.94 (C_q), 116.72 (C_q), 66.85 (-, CH_2), 66.77 (-, CH_2), 59.72 (+, CH), 59.19 (+, CH), 47.05 (-, CH_2), 46.62 (-, CH_2), 31.63 (-, CH_2), 30.73 (-, CH_2), 24.05 (-, CH_2), 23.27 (-, CH_2) (signal doubling due to rotamers); **IR** (neat): $\bar{\nu}$ = 3064, 3034, 2956, 2881, 1756, 1700, 1644, 1607, 1469, 1409, 1353, 1260, 1215, 1163, 1111, 1036, 1006, 772, 738, 693; **MS** (+ESI, 120 V): *m/z* (%) = 351.1 (100) [(M+H)$^+$] 373.1 (26) [(M+Na)$^+$], 723.2 (13) [(2M+Na)$^+$]; **HRMS** (+ESI, 120 V): 353.1341 ($C_{20}H_{19}N_2O_4$ [(M+H)$^+$]: calc. 353.1339); $[\alpha]_D^{22}$: -127.1 (c = 1.19, $CHCl_3$).

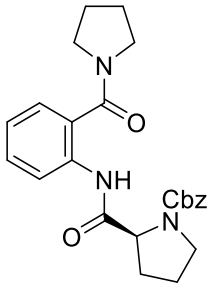

Benzyl (*S*)-2-((2-(pyrrolidine-1-carbonyl)phenyl)carbamoyl)pyrrolidine-1-carboxylate (90)

83 (100 mg, 286 µmol, 1.0 equiv.) was filled into a snap cap vial and dissolved in 1 mL of deactivated $CHCl_3$ (previously filtered through basic Al_2O_3). Pyrrolidine (30 µL, 337 µmol, 1.2 equiv.) was added and

the solution stirred for 45 min. The crude mixture was filtered through a short silica plug ($CHCl_3$/MeOH 50:1), all volatiles were evaporated and the product dried under high vacuum. Colorless oil (120 mg, 285 µmol, 100%).

R_f = 0.23 (hexanes/EtOAc 1:2); **^{1}H-NMR** (400 MHz, $CDCl_3$): δ_H (ppm) =10.12 – 9.96 (1 H, m), 8.36- 8.22 (1 H, m), 7.46 – 7.02 (8 H, m), 5.27 – 5.04 (2 H, m), 4.50 – 4.31 (1 H, m), 3.80 – 3.16 (6 H, m), 2.33 – 1.53 (8 H, m); **^{13}C-NMR** (101 MHz, $CDCl_3$): δ_C (ppm) = 171.11 (C_q), 170.59 (C_q), 168.41 (C_q), 168.31 (C_q), 155.57 (C_q), 154.56 (C_q), 136.54 (C_q), 136.47 (C_q), 130.84 (+, CH), 130.68 (+, CH), 128.43 (+, CH), 128.33 (+, CH), 127.97 (+, CH), 127.88 (+, CH), 127.70 (+, CH), 127.46 (+, CH), 127.34 (+, CH), 127.25 (+, CH), 125.31 (C_q), 124.79 (C_q), 122.98 (+, CH), 121.91 (+, CH), 121.67 (+, CH), 67.22 (-, CH_2), 66.84 (-, CH_2), 61.95 (+, CH), 49.90 (-, CH_2), 47.36 (-, CH_2), 46.97 (-, CH_2), 46.26 (-, CH_2), 31.31 (-, CH_2), 30.01 (-, CH_2), 26,35 (-, CH_2), 24.32 (-, CH_2), 23.63 (-, CH_2) (signal doubling due to rotamers); **IR** (neat): $\tilde{\nu}$ = 3276, 2956, 2878, 1692, 1621, 1588, 1513, 1454, 1405, 1342, 1297, 1252, 1174, 1115, 1085, 1029, 984, 917, 876, 746, 697; **MS** (+ESI, 120 V): *m/z* (%) = 422.2 (100) [$(M+H)^+$], 865.4 (19) [$(2M+Na)^+$]; **HRMS** (+ESI, 120 V): 422.2081 ($C_{24}H_{28}N_3O_4$ [$(M+H)^+$]: calc. 422.2074); $[\alpha]_D^{22}$: -91.8 (c = 0.97, $CHCl_3$).

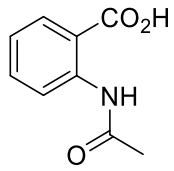

2-Acetamidobenzoic acid (88)[230,231]

A 25 mL round bottom flask was charged with anthranilic acid (5.00 g, 36.5 mmol, 1.0 equiv., **54**), AcOH (7.5 mL, 0.13 mol, 3.6 equiv.) and Ac_2O (7.5 mL, 79 mmol, 2.2 equiv.). The mixture was refluxed at 120 °C, whereby the initially formed slurry turned into a yellow solution. After 3 h, the still hot reaction mixture was poured onto 20 g of ice in a 100 mL beaker and cooled in an ice bath. After 15 min, a yellowish solid started to crash out of the solution. The precipitate was filtered off and washed with ice-cold H_2O (10 mL). The crude product was purified by recrystallization from EtOH/H_2O (1:1). Slightly yellow solid (5.53 g, 30.9 mmol, 85%).

H-NMR (300 MHz, CD_3OD): δ_H (ppm) =8.53 (1 H, d, *J* = 8.4 Hz), 8.06 (1 H, d, *J* = 8.0 Hz), 7.53 (1 H, t, *J* = 7.9 Hz), 7.12 (1 H, t, *J* = 7.6 Hz), 2.20 (3 H, s); **^{13}C-NMR** (75 MHz, CD_3OD): δ_C (ppm) = 171.39 (C_q), 171.24 (C_q), 142.32 (C_q), 135.13 (+, CH), 132.45 (+, CH), 123.90 (+, CH), 121.28 (+, CH), 117.30 (C_q), 25.05 (+, CH_3).

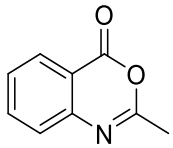

2-Methyl-4*H*-benzo[d][1,3]oxazin-4-one (89)[231,286]

88 (2.00 g, 11.2 mmol, 1.0 equiv.) and pyridine (2.7 mL, 34 mmol, 3.0 equiv.) were suspended in EtOAc (10 mL) and chilled to -20 °C. NEt_3 (1.6 mL, 12 mmol, 1.0 equiv.) was added, followed by the dropwise addition of T3P (50 wt% in EtOAc) (14.2 g, 22.3 mmol, 2.0 equiv.). The mixture was allowed to reach ambient temperature and stirred for 4 d. Na_2SO_4 (5 g) was added and the mixture stirred for a further 3 d. The yellowish solution was transferred into a separating funnel and diluted with H_2O (25 mL). The organic phase was separated, the aqueous phase extracted with EtOAc (3x). The combined organic phases were washed with sat. NH_4Cl (1x), sat. $NaHCO_3$ (1x), and sat. NaCl solutions (1x), dried over Na_2SO_4, filtered and all volatiles evaporated off. The crude product was purified by flash column chromatography (hexanes/EtOAc 1:2). Slightly yellow solid (147 mg, 911 µmol, 8%). A crystal for X-ray analysis was obtained by recrystallization from hexanes/EtOAc.

R_f = 0.73 (hexanes/EtOAc 1:2); **^{1}H-NMR** (300 MHz, $CDCl_3$): δ_H (ppm) =8.16 – 8.10 (1 H, m), 7.80 – 7.71 (1 H, m), 7.53 – 7.42 (2 H, m), 2.44 – 2.43 (3 H, m); **^{13}C-NMR** (75 MHz, $CDCl_3$): δ_C (ppm) = 160.27 (C_q), 159.71 (C_q), 146.44 (C_q), 136.61 (+, CH), 128.47 (+, CH), 128.25 (+, CH), 126.42 (+, CH), 116.66 (C_q), 21.43 (+, CH_3); **m.p.** 74 – 77 °C.

4. Catalysis with tripeptides containing unnatural β-amino acids

General procedure for aldol reactions under ambient conditions (GP-8)

A snap cap vial was charged with 4-nitrobenzaldehyde (151 mg, 1.00 mmol, 1.0 equiv., **92**) and the catalyst **52** (3.3 mg, 10 µmol, 1 mol%). The reaction was started *via the* addition of an acetone/H_2O mixture (2 mL, 10:1, v/v) and stirred for 24 h at ambient temperature (22 °C). At the end of the reaction, the mixture was spiked with the internal standard diphenoxymethane (180 µL, 200 mg, 1.00 mmol, 1.0 equiv., **46**), the volatiles evaporated, the residue dissolved in $CDCl_3$ and a ^{1}H-NMR spectrum measured immediately. For HPLC analysis, the crude mixture was purified *via* flash column chromatography, using hexanes/EtOAc as eluent (hexanes/ EtOAc 3:1 → EtOAc).

General procedure for high-pressure aldol reactions (GP-9)

A PTFE tube (ø = 0.5 cm, ↕ = 10 cm) was sealed off on one side using heated crucible tongs and charged with 4-nitrobenzaldehyde (151 mg, 1.00 mmol, 1.0 equiv.). The reaction was started by the addition of a freshly mixed solution of the catalyst **52** (3.3 mg, 10 µmol, 1 mol%) in an acetone/H_2O mixture (2 mL, 10:1, v/v). The PTFE tube was then completely sealed, all reactants mixed thoroughly through shaking and the tube inserted into the pressure vessel. The vessel was filled with the pressurizing medium, inserted into the high-pressure apparatus and pressurized for 7 h. After depressurization, the mixture was filled into a round bottom flask and spiked with the internal standard diphenoxymethane (180 µL, 200 mg, 1.00 mmol, 1.0 equiv., **46**). All volatiles were evaporated off, the residue was dissolved in $CDCl_3$ and a ^{1}H-NMR spectrum measured immediately. For HPLC analysis, the crude mixture was purified *via* flash column chromatography, using hexanes/EtOAc as eluent (hexanes/ EtOAc 3:1 → EtOAc).

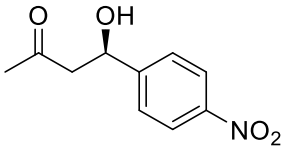

(*R*)-4-Hydroxy-4-(4-nitrophenyl)butan-2-one (93)[153,155]

Slightly yellow solid (136 mg, 650 µmol, 65%).

R_f = 0.19 (hexanes/EtOAc 2:1); **^{1}H-NMR** (300 MHz, $CDCl_3$): δ_H (ppm) =8.20 (2 H, d, *J* = 8.7 Hz), 7.53 (2 H, d, *J* = 8.7 Hz), 5.26 (1 H, dd, *J* = 7.4, 4.9 Hz), 3.63 (1 H, bs), 2.86 (1 H, s), 2.84 (1 H, d, *J* = 3.2 Hz), 2.22 (3 H, s); **^{13}C-NMR** (75 MHz, $CDCl_3$): δ_C (ppm) = 208.69, 150.07, 147.42, 126.54, 123.90, 69.02, 51.62,

30.85; **Chiral HPLC** performed on Chiralcel AS-H (*n*-heptane/*i*-PrOH = 70:30, λ = 254 nm, 0.5 mL/min): t_r = 23.5 min (*R*), t = 28.7 min (*S*).

General procedure for Michael reactions under ambient conditions (GP-10)

A snap cap vial was charged with *trans*-β-nitrostyrene (74.6 mg, 500 µmol, 1.0 equiv., **40**) and the catalyst **52** (16.9 mg, 50.0 µmol, 10 mol%). The reaction was started *via the* addition of an acetone/H_2O mixture (2 mL, 10:1, v/v) and stirred for 48 h at ambient temperature (22 °C). At the end of the reaction, the mixture was spiked with the internal standard diphenoxymethane (90 µL, 0.10 g, 0.50 mmol, 1.0 equiv., **46**), the volatiles evaporated, the residue dissolved in $CDCl_3$ and a ^{1}H-NMR measured immediately. For HPLC analysis, the crude mixture was transferred into a separating funnel and washed with H_2O (1x 2 mL, 1x 1 mL). The organic phase was dried over Na_2SO_4, filtered, all volatiles evaporated off and the residue purified by flash column chromatography, using hexanes/EtOAc as eluent (hexanes/ EtOAc 4:1).

General procedure for high-pressure Michael reactions (GP-11)

A PTFE tube (ø = 0.5 cm, ↕ = 10 cm) was sealed off on one side using heated crucible tongs and charged with *trans*-β-nitrostyrene (74.6 mg, 500 µmol, 1.0 equiv., **40**). The reaction was started *via the* addition of a freshly mixed solution of the catalyst **52** (16.9 mg, 50.0 µmol, 10 mol%) in an acetone/H_2O mixture (2 mL, 10:1, v/v). The PTFE tube was then completely sealed, all reactants mixed thoroughly through shaking and the tube inserted into the pressure vessel. The vessel was filled with the pressurizing medium, inserted into the high-pressure apparatus and pressurized for 7 h. After depressurization, the mixture was filled into a round bottom flask and spiked with the internal standard diphenoxymethane (90 µL, 0.10 g, 0.50 mmol, 1.0 equiv., **46**). All volatiles were evaporated off, the residue was dissolved in $CDCl_3$ and a ^{1}H-NMR measured immediately. For HPLC analysis, the crude mixture was transferred into a separating funnel and washed with H_2O (1x 2 mL, 1x 1mL). The organic phase was dried over Na_2SO_4, filtered, all volatiles evaporated off and the residue purified *via* flash column chromatography, using hexanes/EtOAc as eluent (hexanes/ EtOAc 4:1). The catalyst could be recovered by evaporation of the aqueous phase.

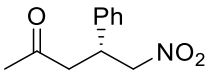

(*R*)-5-Nitro-4-phenylpentan-2-one (94)[124,287]

White solid (85.5 mg, 413 µmol, 83%).

R_f = 0.20 (hexanes/EtOAc 4:1); **^{1}H-NMR** (400 MHz, $CDCl_3$): δ_H (ppm) =7.38 – 7.18 (5 H, m), 4.69 (1 H, dd, *J* = 12.3, 6.8 Hz), 4.59 (1 H, dd, *J* = 12.4, 7.7 Hz), 4.00 (1 H, quint, *J* = 7.0 Hz), 2.91 (2 H, d, *J* = 7.0 Hz), 2.11 (3 H, s); **^{13}C-NMR** (101 MHz, $CDCl_3$): δ_C (ppm) = 205.48 (C_q), 138.95 (C_q), 129.08 (+, CH), 127.91 (+, CH), 127.44 (+, CH), 79.51 (-, CH_2), 46.16 (-, CH_2), 39.09 (+, CH), 30.38 (+, CH_3); **Chiral HPLC** performed on Chiralcel AS-H (*n*-heptane/*i*-PrOH = 65:35, λ = 215 nm, 0.5 mL/min): t_r = 19.7 min (*S*), t = 25.5 min (*R*).

5. Synthesis of β-ACHC model compounds

Preparation of a solution of dimethylamine in dry THF

A 100 mL flame-dried Schlenk tube, the receiving flask, was filled with dry THF (50 mL), and a Pasteur pipette was inserted through a bored rubber stopper into the solution. A second Schlenk flask, the producing flask, containing pre-dried dimethylamine hydrochloride (9.79 g, 120 mmol, 1.0 equiv.), was sealed with a rubber septum. The producing flasks Schlenk valve and the Pasteur pipette were connected using rubber tubing, with a drying tube filled with KOH set in between (to dry the $HNMe_2$). The receiving flask was cooled to 0 °C and the Schlenk valve was connected to two wash bottles, the first one empty, the second one filled with 1 M HCl. Using a syringe pump, an 18 M NaOH solution (7.50 mL, 5.40 g, 135 mmol, 1.1 equiv.) was slowly added to the dimethylamine hydrochloride over 1 h, using a gentle stream of nitrogen to bubble the developing $HNMe_2$ into the THF. After complete addition, another 2.5 mL of the 18 M NaOH solution (1.80 g, 45.0 mmol, 0.4 equiv.) was added and the producing flask was heated in a water bath to 60 °C for 1 h to ensure complete conversion.

In order to determine the concentration, 0.5 mL of the prepared solution were transferred into a 10 mL pear flask and diluted with 1 mL H_2O. One drop of a bromothymol blue solution (17.7 mg in 18 mL EtOH/H_2O (1:1)) was added as pH indicator and the blue solution titrated against 1 M HCl until it turned yellow. The concentration was determined to be 1.64 M.

General procedure for the acetylation with thionyl chloride (GP-12)

A 25 mL round bottom flask was charged with *cis*-**101** (166.6 mg, 899.5 µmol, 1.0 equiv.), dry DCM (10 mL) and DMF (5 µL), then sealed with a rubber septum. The slurry was cooled to 0 °C and thionyl chloride (0.33 mL, 4.6 mmol, 5.1 equiv.) was added dropwise. Thereby, the reaction became homogeneous. The septum was exchanged for a bubble counter and the mixture was stirred for 9.5 h at ambient temperature. Afterwards, all volatiles from the now pink solution were removed by directly applying high vacuum for 30 min. The brownish foam-like solid was then redissolved in dry THF (5 mL) and cooled to 0 °C. A 1.64 M solution of diethylamine in THF (2.2 mL, 3.6 mmol, 4.0 equiv.) was then added dropwise and the resulting brownish solution was stirred for 2 h at ambient temperature. The solvent was distilled off and the residue was transferred in a separating funnel with H_2O (20 mL). The aqueous phase was extracted with DCM (4x), the combined organic extracts dried over Na_2SO_4, filtered, the solvent evaporated and the crude product dried under high vacuum. Purification was

accomplished by recrystallization from DCM/diethyl ether, followed by flash column chromatography (DCM/MeOH 50:1). Slight yellow solid (93.8 mg, 442 µmol, 49% over 2 steps).

General procedure for acetylation with T3P (GP-13)[195]

In a 25 mL round bottom flask, *cis*-**101** (305.0 mg, 1.65 mmol, 1.0 equiv.) was suspended in EtOAc (10 mL, pre-dried over K_2CO_3) and dry DMF (1.5 mL) and cooled to -15 °C. To the chilled slurry, pyridine (0.40 mL, 5.0 mmol, 3.0 equiv.), a 1.26 M solution of dimethylamine in THF (3.9 mL, 4.9 mmol, 3.0 equiv.) and T3P (50 wt% in EtOAc) (2.10 g, 3.29 mmol, 2.0 equiv.) were added in succession and the resulting mixture was stirred at ambient temperature for 21 h. The reaction was then transferred into a separating funnel and quenched with H_2O (30 mL). The organic phase was separated off and the aqueous phase was extracted with DCM (5x). The combined organic extracts were dried over Na_2SO_4, filtered and all volatiles evaporated. The residue was redissolved in toluene and evaporated twice to remove residual DMF and then dried under high vacuum. The crude product was purified by flash column chromatography (DCM/MeOH 15:1). White solid (318 mg, 1.50 mmol, 91%).

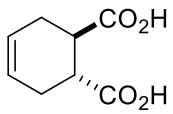

***trans*-Cyclohex-4-ene-1,2-dicarboxylic acid (99)[248]**

A flame-dried 250 mL two-necked Schlenk flask was equipped with fumaric acid (6.30 g, 54.3 mmol, 1.0 equiv., **98**), 3-sulfolene (10.0 g, 84.6 mmol, 1.6 equiv., **62**) and 65 mL glacial acetic acid, stirred for 15 min and then heated to 110 °C. After 48 h, an additional batch of 3-sulfolene (2.00 g, 16.9 mmol, 0.3 equiv., **62**) was added and stirred until TLC showed complete conversion. The still warm mixture was charged with 1 g fine powdered activated charcoal and then allowed to cool to ambient temperature while stirring. The yellowish solution was filtered off, the charcoal washed with small amounts of acetic acid and the solvent evaporated off on a rotatory evaporator. The resulting white solid was transferred into a 50 mL flask, treated with EtOAc (10 mL) and stirred for 1 h at 50 °C. After this washing step, the solid was filtered off, washed with small amounts of ice-cold EtOAc and dried under high vacuum. Off-white solid (7.82 g, 46.0 mmol, 85%).

^{1}H-NMR (300 MHz, $(CD_3)_2SO$) δ_H (ppm) = 12.26 (2 H, s), 5.70 – 5.64 (2 H, m), 2.61 – 2. 53 (2 H, m), 2.39 – 2.26 (2 H, m), 2.11 – 1.97 (2 H, m); **^{13}C-NMR** (75 MHz, $(CD_3)_2SO$) δ_C (ppm) = 175.98 (C_q), 125.20 (+, CH), 40.84 (+, CH), 27.52 (-, CH_2).

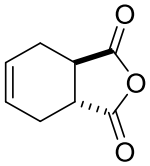

***trans*-4-Cyclohexene-1,2-dicarboxylic acid anhydride (*trans*-56)**[249]

A 50 mL round bottom flask was charged with **99** (2.00 g, 11.8 mmol, 1.0 equiv.) and acetic anhydride (20.0 mL, 212 mmol, 18 equiv.) and the mixture was refluxed for 45 min. The reaction was allowed to cool to ambient temperature, upon which a solid crystallized from the solution. The precipitate was filtered off, washed with ice-cold *n*-pentane and dried under high vacuum. White solid (566 mg, 3.72 mmol, 32%). A second batch of product was isolated through complete evaporation of the mother liquor. Off-white solid (1.15 g, 7.56 mmol, 64%).

^{1}H-NMR (300 MHz, $CDCl_3$) δ_H (ppm) = 5.83 – 5.77 (2 H, m), 2.94 – 2. 85 (2 H, m), 2.65 – 2.52 (2 H, m), 2.49 – 2.35 (2 H, m); **^{13}C-NMR** (75 MHz, $CDCl_3$) δ_C (ppm) = 170.47 (C_q), 126.13 (+, CH), 42.99 (+, CH), 25.36 (-, CH_2).

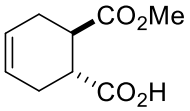

***trans*-2-Methoxycarbonyl-4-cyclohexene-1-carboxylic acid (*trans*-63)**[288]

A 50 mL round bottom flask equipped with a reflux condenser was charged with *trans*-**56** (2.78 g, 18.3 mmol, 1.0 equiv.) and MeOH (20 mL) and the mixture was refluxed for 30 min. All volatiles were evaporated and the residue was dried under high vacuum. Yellowish solid (3.19 g, 17.3 mmol, 95%).

^{1}H NMR (300 MHz, $CDCl_3$) δ_H (ppm) = 10.18 (1 H, bs), 5.70 (2 H, d, *J* = 2.7 Hz), 3.71 (3 H, s), 2.97 – 2.77 (2 H, m), 2.54 – 2.37 (2 H, m), 2.30 – 2.11 (2 H, m); **^{13}C NMR** (75 MHz, $CDCl_3$) δ_C (ppm) = 181.05 (C_q), 175.38 (C_q), 125.06 (+, CH), 124.89 (+, CH), 52.18 (+, CH_3), 41.11 (+, CH), 40.94 (+, CH), 27.85 (-, CH_2).

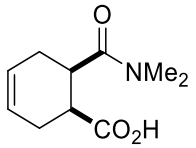

***cis*-6-(Dimethylcarbamoyl)cyclohex-3-ene-1-carboxylic acid (*cis*-96)**

A flame-dried 50 mL Schlenk flask was charged with *cis*-**56** (2.00 g, 13.1 mmol, 1.0 equiv.) and the solid dissolved in dry THF (25 mL). A Pasteur pipette was inserted through a bored rubber stopper into the solution. The Schlenk valve was connected to two wash bottles, the first one empty, the second one filled with 1 M HCl. A second Schlenk flask, the $HNMe_2$-producing flask, was filled with dimethylamine hydrochloride (3.22 g, 39.4 mmol, 3.0 equiv.) and sealed with a rubber septum. The producing flasks Schlenk valve and the Pasteur pipette were connected with a rubber tube. The whole system was flushed with nitrogen and the THF solution was cooled to 0 °C with an ice bath. Using a syringe pump, a 10 M NaOH solution (6.6 mL, 2.6 g, 66 mmol, 5.0 equiv.) was slowly added to the dimethylamine hydrochloride over 30 min. The generated gaseous $HNMe_2$ was bubbled into the THF solution with the aid of a gentle stream of nitrogen. After complete addition, the mixture was stirred for 2 h at 0°C, during which a white solid started to precipitate from the solution. The producing flask was then exchanged for a new one, containing another 3.22 g of dimethylamine hydrochloride (39.4 mmol, 3.0 equiv.). Again, a 10 M NaOH solution (6.6 mL, 2.63 g, 65.7 mmol, 5.0 equiv.) was added to the fresh dimethylamine hydrochloride over 30 min. After stirring for further 30 min, the THF was removed using a rotatory evaporator. The white residue was dissolved in sat. $NaHCO_3$ solution and transferred into a separating funnel (pH 8). The aqueous phase was washed with diethyl ether (2x), then acidified to pH 2 by the use of 1 M HCl. The now acidic aqueous phase was extracted with DCM (4x). The combined organic phases were dried over Na_2SO_4, filtered and the solvent evaporated. The crude product was then purified by column chromatography (DCM/MeOH 50:1). White solid (1.72 g, 13.2 mmol, 66%).

R_f = 0.25 (DCM/MeOH 25:1); **^{1}H-NMR** (300 MHz, $CDCl_3$): δ_H (ppm) = 14.18 (1 H, bs), 5.83 – 5.59 (2 H, m), 3.26 – 3.17 (1 H, m), 3.14 (3 H, s), 3.09 – 2.93 (4 H, m), 2.88 – 2.76 (m, 1 H), 2.41 – 2.10 (m, 3 H); **^{13}C-NMR** (75 MHz $CDCl_3$): δ_C (ppm) = 176.89 (C_q), 173.29 (C_q), 127.29 (+, CH), 124.51 (+, CH), 40.59 (+, CH), 39.33 (+, CH), 38.24 (+, CH_3), 36.66 (+, CH_3), 29.20 (-, CH_2), 26.28 (-, CH_2); **IR** (neat): $\bar{\upsilon}$ = 3027, 2971, 2941, 2907, 2840, 2639, 1692, 1633, 1502, 1402, 1342, 1305, 1256, 1144, 1059, 947, 917, 801, 760; **MS** (+ESI, 120 V): *m/z* (%) = 180.1 (24) [$(M+H)^+$-H_2O], 198.1 (100) [$(M+H)^+$], 417.2 (2) [$(2M+Na)^+$]; **HRMS** (+ESI, 120 V): 198.1128 ($C_{10}H_{16}NO_3$ [$(M+H)^+$]: calc. 198.1125); **m.p.** 110 – 118 °C.

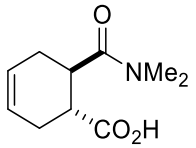

***trans*-6-(Dimethylcarbamoyl)cyclohex-3-ene-1-carboxylic acid (*trans*-96)**

A flame-dried 50 mL Schlenk flask was charged with *trans*-**56** (1.34 g, 8.81 mmol, 1.0 equiv.) and the solid dissolved in dry THF (25 mL). A Pasteur pipette was inserted through a bored rubber stopper into the solution. The Schlenk valve was connected to two wash bottles, the first one empty, the second one filled with 1 M HCl. A second Schlenk flask, the $HNMe_2$-producing flask, was filled with dimethylamine hydrochloride (2.16 g, 26.5 mmol, 3.0 equiv.) and sealed with a rubber septum. The producing flasks Schlenk valve and the Pasteur pipette were connected using a rubber tube. The whole system was flushed with nitrogen and the THF solution was cooled to 0 °C with an ice bath. Using a syringe pump, a 10 M NaOH solution (4.4 mL, 1.8 g, 44 mmol, 5.0 equiv.) was slowly added to the dimethylamine hydrochloride over 30 min. The generated gaseous $HNMe_2$ was bubbled into the THF solution with the aid of a gentle stream of nitrogen. After complete addition, the mixture was stirred for a further 2 h at 0°C, the solution remained clear. The producing flask was then exchanged for a new one, containing another 2.16 g of dimethylamine hydrochloride (26.5 mmol, 3.0 equiv.). Again, a 10 M NaOH solution (4.4 mL, 1.77 g, 44.2 mmol, 5.0 equiv.) was added to the fresh dimethylamine hydrochloride over 30 min. After further stirring for 15 h at ambient temperature, the THF was distilled off using a rotatory evaporator. The white residue was taken up in sat. $NaHCO_3$ solution and transferred into a separating funnel (pH 8). The aqueous phase was washed with diethyl ether (2x), then acidified to pH 2 by the use of 1 M HCl. The now acidic aqueous phase was extracted with DCM (4x), the combined organic phases dried over Na_2SO_4, filtered and the solvent evaporated. The product was dried under high vacuum. White solid (1.63 g, 8.28 mmol, 94%).

^{1}H NMR (300 MHz, $CDCl_3$): δ_H (ppm) = 10.86 (1 H, bs), 5.69 (2 H, bs), 3.10 (3 H, s), 3.06 – 2.97 (2 H, m), 2.95 (3 H, s), 2.58 – 2.41 (1 H, m), 2.29 – 2.03 (3 H, m); **^{13}C-NMR** (75 MHz, $CDCl_3$): δ_C (ppm) = 179.72 (C_q), 175.57 (C_q), 125.26 (+, CH), 41.91 (+, CH), 38.46 (+, CH), 37.60 (+, CH_3), 36.02 (+, CH_3), 28.53 (-, CH_2), 27.93 (-, CH_2); **IR** (neat): $\bar{\upsilon}$ = 3030, 2974, 2915, 2844, 2646, 1741, 1595, 1510, 1435, 1364, 1252, 1190, 1159, 1070, 973, 869, 760; **MS** (+ESI, 120 V): *m/z* (%) = 180.1 (36) [$(MH\text{-}H_2O)^+$], 198.1 (100) [$(M+H)^+$], 395.2 (10) [$(2M+H)^+$]; **HRMS** (+ESI, 120 V): 198.1129 ($C_{10}H_{16}NO_3$ [$(M+H)^+$]: calc. 198.1125); **m.p.** 136 – 139 °C.

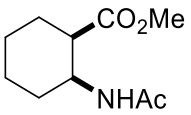

***cis*-2-(Acetylamino)cyclohexanecarboxylic acid methyl ester (*cis*-100)[289]**

A 100 mL flame-dried two-necked Schlenk flask equipped with a reflux condenser with bubble counter was charged with *cis*-**63** (2.00 g, 10.9 mmol, 1.0 equiv.) and dry toluene (40 mL). Dry triethylamine (1.55 mL, 11.2 mmol, 1.0 equiv.) was added to the solution and the flask sealed with a rubber septum. DPPA (3.02 g, 11.0 mmol, 1.0 equiv.) and benzyl alcohol (2.3 mL, 22 mmol, 2.0 equiv.) were added dropwise in succession using a syringe and the mixture was refluxed for 18.5 h. The reaction was then allowed to cool to ambient temperature, transferred into a separating funnel and diluted with EtOAc (30 mL). The aqueous phase was discarded and the organic phase washed with 2 M HCl (1x), sat. $NaHCO_3$ (1x) and sat. NaCl solutions (1x). The organic phase was dried over $MgSO_4$, filtered, the solvent evaporated and the residue dried under high vacuum. The remaining oil was transferred with MeOH (10 mL) into an autoclave vessel filled with 200 mg Pd/C (10 wt% Pd). The mixture was hydrogenated for 17 h at 40 bar H_2. After the reaction was completed, the slurry was filtered and the solvent removed carefully on a rotatory evaporator (the free amine tends to be volatile). The residue was transferred into a separating funnel using H_2O (10 mL), acidified with 2 M HCl to approximately pH 3 and extracted with diethyl ether (2x). The aqueous phase was then basified with sat. Na_2CO_3 (pH 9) and extracted with DCM (10x), until TLC control showed no more remaining product in the extract. The combined organic phases were dried over $MgSO_4$, filtered and the solvent removed carefully on a rotatory evaporator. The yellowish liquid (1.07 g, 6.80 mmol, 1.0 equiv.) was then diluted in DCM (10 mL), charged with triethylamine (0.95 mL, 6.9 mmol, 1.0 equiv.) and cooled to 0 °C. Subsequently, acetyl chloride (0.49 mL, 6.9 mmol, 1.0 equiv.) was added dropwise and the reaction was stirred for 18 h at ambient temperature. Upon completion, the mixture was transferred into a separating funnel and washed successively with 1 M HCl (1x), sat. $NaHCO_3$ (1x) and sat. NaCl (1x) solutions. The organic phase was dried over Na_2SO_4, filtered, all volatiles evaporated off and the residue dried under high vacuum. The crude yellow oil was purified by column chromatography (hexanes/ EtOAc 9:1 → EtOAc). White solid (999 mg, 5.01 mmol, 46% over 3 steps).

$\mathbf{R_f}$ = 0.20 (hexanes/ EtOAc 1:1); **^{1}H NMR** (400 MHz, $CDCl_3$): δ_H (ppm) = 6.39 (1 H, bs), 4.12 (1 H, tt, *J* = 9.7, 4.1 Hz), 3.69 (3 H, s), 2.80 (q, *J* = 4.6 Hz, 1 H), 2.18 – 2.00 (1 H, m), 1.95 (3 H, s), 1.80 – 1.55 (4 H, m), 1.54 – 1.32 (2 H, m), 1.29 – 1.15 (1 H, m); **^{13}C-NMR** (75 MHz, $CDCl_3$): δ_C (ppm) = 174.85 (C_q), 169.33 (C_q), 51.78 (+, CH_3), 47.87 (+, CH), 44.37 (+, CH), 29.32 (-, CH_2), 27.46 (-, CH_2), 24.29 (-, CH_2), 23.72 (+, CH_3), 22.46 (-, CH_2); **IR** (neat): $\bar{\upsilon}$ = 3332, 2933, 2851, 1733, 1648, 1539, 1468, 1435, 1372, 1338, 1297, 1223, 1189, 1133, 1036, 977, 943, 895, 682; **MS** (+APCI, 120 V): *m/z* (%) = 168.1 (22) [(MH-MeOH)$^+$], 200.1

(100) [(M+H)$^+$], 399.2 (2) [(2M+H)$^+$]; **HRMS** (+APCI, 120 V): 200.1285 ($C_{10}H_{18}NO_3$ [(M+H)$^+$]: calc. 200.1281); **m.p.** 73 – 76 °C.

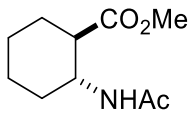

***trans*-2-(Acetylamino)cyclohexanecarboxylic acid methyl ester (*trans*-100)[289]**

A 100 mL flame-dried two-necked Schlenk flask equipped with a reflux condenser with bubble counter was charged with *trans*-**63** (2.00 g, 10.9 mmol, 1.0 equiv.) and dry toluene (40 mL). Dry triethylamine (1.55 mL, 11.2 mmol, 1.0 equiv.) was added to the solution under stirring and the flask sealed with a rubber septum. DPPA (3.02 g, 11.0 mmol, 1.0 equiv.) and benzyl alcohol (2.3 mL, 22 mmol, 2.0 equiv.) were added dropwise in succession using a syringe and the mixture was refluxed for 16 h. The reaction was then allowed to cool to ambient temperature, transferred into a separating funnel and diluted with EtOAc (30 mL). The aqueous phase was discarded and the organic phase washed with 2 M HCl (1x), sat. $NaHCO_3$ (1x) and sat. NaCl solutions (1x). The organic phase was dried over $MgSO_4$, filtered, the solvent distilled off using a rotatory evaporator and dried under high vacuum. The oily residue was transferred into an autoclave vessel with MeOH (10 mL) and 200 mg Pd/C (10 wt% Pd) added. The mixture was hydrogenated for 16 h at 40 bar H_2. After the reaction was completed, the slurry was filtered and the solvent was removed carefully on a rotatory evaporator (the free amine tends to be volatile). The residue was transferred into a separating funnel using 10 mL H_2O, acidified with 2 M HCl to approximately pH 3 and extracted with diethyl ether (2x). The aqueous phase was then basified with sat. Na_2CO_3 (pH 9) and extracted with DCM (10x), until TLC control showed no more remaining product in the extract. The combined organic phases were dried over $MgSO_4$, filtered and the solvent removed carefully on a rotatory evaporator. The yellowish liquid (1.49 g, 9.47 mmol, 1.0 equiv.) was diluted in DCM (10 mL), charged with triethylamine (1.35 mL, 9.74 mmol, 1.0 equiv.) and cooled to 0 °C. Subsequently, acetyl chloride (0.68 mL, 9.5 mmol, 1.0 equiv.) was added dropwise and the reaction was stirred for 30 min at 0 °C. Upon completion, the mixture was transferred into a separating funnel and washed successively with 1 M HCl (1x), sat. $NaHCO_3$ (1x) and sat. NaCl (1x) solutions. The organic phase was dried over Na_2SO_4, filtered, all volatiles evaporated off and the residue dried under high vacuum. The crude yellow oil was purified using column chromatography (hexanes/ EtOAc 1:2 → EtOAc). White solid (1.07 g, 5.38 mmol, 50% over 3 steps).

R_f = 0.22 (hexanes/ EtOAc 1:2); **^{1}H NMR** (300 MHz, $CDCl_3$): δ_H (ppm) = 5.58 (1 H, bs), 4.05 – 3.84 (1 H, m), 3.65 (3 H, s), 2.31 – 2.17 (1 H, m), 2.10 – 1.98 (1 H, m), 1.97 – 1.84 (4 H, m), 1.80 - 1.05 (6 H, m). **^{13}C-NMR** (75 MHz, $CDCl_3$): δ_C (ppm) = 174.40 (C_q), 169.43 (C_q), 52.01 (+, CH_3), 50.17 (+, CH), 50.04

(+, CH), 32.88 (-, CH_2), 28.56 (-, CH_2), 24.71 (-, CH_2), 24.54 (-, CH_2), 23.53 (+, CH_3). **IR** (neat): $\bar{\upsilon}$ = 3267, 3079, 2937, 2855, 1737, 1640, 1554, 1429, 1372, 1316, 1249, 1167, 1126, 1029, 969, 902, 846, 723; **MS** (+APCI, 120 V): *m/z* (%) = 168.1 (23) [(MH-MeOH)$^+$], 200.1 (100) [(M+H)$^+$], 399.2 (1) [(2M+H)$^+$]; **HRMS** (+APCI, 120 V): 200.1283 ($C_{10}H_{18}NO_3$ [(M+H)$^+$]: calc. 200.1281); **m.p.** 104 – 107 °C.

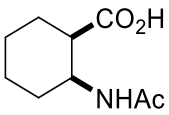

***cis*-2-Acetamidocyclohexane-1-carboxylic acid (*cis*-101)[290,291]**

Synthesized according to general procedure **GP-5** using *cis*-**100** (204 mg, 1.02 mmol, 1.0 equiv.) in THF (5 mL) and LiOH (123 mg, 5.12 mmol, 5.0 equiv.) in H_2O (5 mL). White solid (181 mg, 976 µmol, 95%).

^{1}H NMR (300 MHz, CD_3OD): δ_H (ppm) = 4.30 – 4.12 (1 H, m), 2.81 – 2.65 (1 H, m), 2.12 – 1.33 (11 H, m); **^{13}C-NMR** (75 MHz, CD_3OD): δ_C (ppm) = 176.98 (C_q), 172.58 (C_q), 48.89(+, CH), 45.37 (+, CH), 30.46 (-, CH_2), 26.47 (-, CH_2), 24.15 (-, CH_2), 23.70 (-, CH_2), 22.61 (+, CH_3); **IR** (neat): $\bar{\upsilon}$ = 3321, 2922, 2859, 2803, 2583, 2486, 1685, 1610, 1547, 1439, 1383, 1275, 1129, 1044, 984, 962, 895, 753, 701; **MS** (+ESI, 120 V): *m/z* (%) = 168.1 (32) [(M+H)$^+$-MeOH], 186.1 (100) [(M+H)$^+$], 371.2 (19) [(2M+H)$^+$]; **HRMS** (+ESI, 120 V): 186.1125 ($C_9H_{16}NO_3$ [(M+H)$^+$]: calc. 186.1125); **m.p.** 151 – 153 °C.

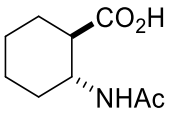

***trans*-2-Acetamidocyclohexane-1-carboxylic acid (*trans*-101)[290,291]**

Synthesized according to general procedure **GP-5** using *trans*-**100** (277 mg, 1.39 mmol, 1.0 equiv.) in THF (8 mL) and LiOH (166.2 mg, 6.938 mmol, 5.0 equiv.) in H_2O (8 mL). White solid (208 mg, 1.13 mmol, 81%).

^{1}H NMR (300 MHz, CD_3OD): δ_H (ppm) = 3.92 (1 H, td, *J* = 11.1, 4.1 Hz), 2.36 – 2.24 (1 H, m), 2.05 – 1.83 (5 H, m), 1.82 – 1.64 (2 H, m), 1.62 – 1.12 (4 H, m); **^{13}C-NMR** (75 MHz, CD_3OD): δ_C (ppm) = 177.81 (C_q), 172.32 (C_q), 50.91 (+, CH), 50.17 (+, CH), 33.33 (-, CH_2), 30.35 (-, CH_2), 25.83 (-, CH_2), 25.74 (-, CH_2) 22.65 (+, CH_3); **IR** (neat): $\bar{\upsilon}$ = 3295, 3101, 2937, 2855, 2710, 2661, 2587, 2546, 2490, 1722, 1692, 1607, 1566, 1439, 1379, 1323, 1256, 1208, 1126, 1040, 992, 954, 854, 794, 693; **MS** (+ESI, 120 V): *m/z* (%) = 168.1 (37) [(M+H)$^+$-MeOH], 186.1 (100) [(M+H)$^+$], 371.2 (13) [(2M+H)$^+$]; **HRMS** (+ESI, 120 V): 186.1128 ($C_9H_{16}NO_3$ [(M+H)$^+$]: calc. 186.1125); **m.p.** 208 – 211 °C.

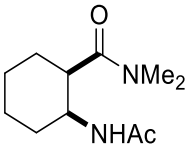

***cis*-2-Acetamido-*N*,*N*-dimethylcyclohexane-1-carboxamide (*cis*-95)**

Synthesized *via* **GP-12** using *cis*-**101** (166.6 mg, 899.5 µmol, 1.0 equiv.), thionyl chloride (0.33 mL, 4.6 mmol, 5.1 equiv.) and a 1.64 M solution of diethylamine in THF (2.2 mL, 3.6 mmol, 4.0 equiv.). The crude product was purified by recrystallization from DCM/diethyl ether, followed by flash column chromatography (DCM/MeOH 50:1). Slight yellow solid (93.8 mg, 442 µmol, 49% over 2 steps).

Synthesized *via* **GP-13** using *cis*-**101** (305 mg, 1.65 mmol, 1.0 equiv.), pyridine (0.40 mL, 5.0 mmol, 3.0 equiv.), a 1.26 M solution of dimethylamine in THF (3.9 mL, 4.9 mmol, 3.0 equiv.) and T3P (50 wt% in EtOAc) (2.10 g, 3.29 mmol, 2.0 equiv.). The crude product was purified by flash column chromatography (DCM/MeOH 15:1). White solid (318 mg, 1.50 mmol, 91%).

A crystal for X-ray analysis was obtained by recrystallization from acetone/hexanes.

R_f = 0.22 (DCM/MeOH 50:1); **^{1}H NMR** (600 MHz, $CDCl_3$): δ_H (ppm) = 6.25 (1 H, d, *J* = 4.5 Hz), 4.10 – 4.02 (1 H, m), 3.01 (3 H, s), 2.99 – 2.95 (1 H, m), 2.89 (3 H, s), 2.26 – 2.18 (1 H, m), 1.92 (3 H, s), 1.86 – 1.78 (1 H, m), 1.64 – 1.54 (2 H, m), 1.53 – 1.43 (2 H, m), 1.42 – 1.33 (m, 2 H); **^{13}C-NMR** (151 MHz, $CDCl_3$): δ_C (ppm) = 173.79 (C_q), 169.80 (C_q), 47.37 (+, CH), 40.90 (+, CH), 37.51 (+, CH_3), 35.59 (+, CH_3), 29.29 (-, CH_2), 26.19 (-, CH_2), 23.72 (+, CH_3), 23.00 (-, CH_2), 22.71 (-, CH_2); **IR** (neat): $\bar{\upsilon}$ = 3340, 3068, 2926, 2855, 1670, 1621, 1543, 1506, 1446, 1420, 1362, 1256, 1133, 1059, 947, 913, 779, 723, 682; **MS** (+APCI, 120 V): *m/z* (%) = 168.1 (26) [$(MH\text{-}HNMe_2)^+$], 213.2 (100) [$(M+H)^+$]; **HRMS** (+APCI, 120 V): 213.1601 ($C_{11}H_{21}N_2O_2$ [$(M+H)^+$]: calc. 213.1598); **m.p.** 134 – 138 °C.

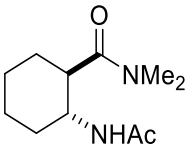

***trans*-2-Acetamido-*N*,*N*-dimethylcyclohexane-1-carboxamide (*trans*-95)**

Synthesized *via* **GP-12** using *trans*-**101** (199 mg, 1.08 mmol, 1.0 equiv.), thionyl chloride (0.39 mL, 5.4 mmol, 5.0 equiv.) and a 1.64 M solution of diethylamine in THF (2.6 mL, 4.3 mmol, 4.0 equiv.). The crude product was purified by flash column chromatography (DCM/MeOH 20:1). Slight yellow solid (69.9 mg, 329 µmol, 31% over 2 steps).

Synthesized *via* **GP-13** using *trans*-**101** (100 mg, 540 µmol, 1.0 equiv.), pyridine (130 µL, 1.62 mmol, 3.0 equiv.), a 1.26 M solution of dimethylamine in THF (0.86 mL, 1.1 mmol, 2.0 equiv.), T3P (50 wt% in EtOAc) (687 mg, 1.08 mmol, 2 equiv.) and 1 mL dry DMF. The crude product was purified by recrystallization from hexanes/EtOAc. White solid (59.8 mg, 282 µmol, 52%).

A crystal for X-ray analysis was obtained by recrystallization from acetone/hexanes.

R_f = 0.23 (DCM/MeOH 20:1); Major conformer: **^{1}H NMR** (400 MHz, $CDCl_3$): δ_H (ppm) = 6.15 (1 H, d, *J* = 6.2 Hz), 3.61 – 3.49 (1 H, m), 3.30 – 2.18 (1 H, td, *J* = 11.3, 3.5 Hz), 3.04 (3 H, s), 2.91 (3 H, s), 1.97 – 1.64 (5 H, m), 1.84 (3 H, s), 1.44 – 1.09 (3 H,m); **^{13}C-NMR** (101 MHz, $CDCl_3$): δ_c (ppm) = 174.45 (C_q), 170.07 (C_q), 52.66 (+, CH), 43.97 (+, CH), 37.38 (+, CH_3), 35.74 (-, CH_3), 30.73 (-, CH_2), 29.33 (-, CH_2), 25.26 (-, CH_2), 24.93 (-, CH_2), 23.90 (+, CH_3): Minor conformer: **^{1}H NMR** (400 MHz, $CDCl_3$): δ_H (ppm) = 6.06 (1 H, d, *J* = 10.4 Hz), 3.71 – 3.61 (1 H, m), 3.02 (3 H, s), 2.89 (3 H, s), 2.57 – 2.50 (1 H, td, *J* = 10.3, 3.3 Hz), 2.04 (3 H, s), 1.97 – 1.64 (5 H, m), 1.55 – 1.09 (3 H, m); **^{13}C-NMR** (101 MHz, $CDCl_3$): δ_C (ppm) = 173.65 (C_q), 173.05 (C_q), 54.03 (+, CH), 46.74 (+, CH), 37.34 (+, CH_3), 35.86 (-, CH_3), 33.98 (-, CH_2), 29.09 (-, CH_2), 25.03 (-, CH_2), 24.74 (-, CH_2), 20.26 (+, CH_3); **IR** (neat): $\bar{\nu}$ = 3291, 3071, 2933, 2855, 16670, 1618, 1547, 1502, 1428, 1275, 1211, 1163, 1062, 954, 902, 813, 716; **MS** (+APCI, 120 V): *m/z* (%) = 168.1 (20) [$(M+H)^+$-$HNMe_2$], 213.2 (100) [$(M+H)^+$], 425.3 (1) [$(2M+H)^+$]; **HRMS** (+APCI, 120 V): 213.1597 ($C_{11}H_{21}N_2O_2$ [$(M+H)^+$]: calc. 213.1598); **m.p.** 153 – 155 °C.

6. Synthesis of ^{15}N-labeled compounds

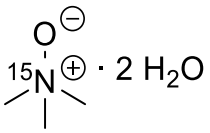

Trimethylamine ^{15}N-oxide dihydrate (^{15}N-102·2H$_2$O)[266,292]

In a 25 mL Schlenk flask equipped with magnetic stirring bar and reflux condenser with bubble counter, $^{15}NH_4Cl$ (2.00 g, 36.7 mmol, 1.0 equiv., **^{15}N-104**) and paraformaldehyde (5.05 g, 168 mmol, 4.6 equiv.) were added. The mixture was carefully heated to 115 °C under gentle stirring. At that point, the mixture liquefied and gas evolution observed. Heating of the resulting yellow solution was continued at 115 °C in such a manner that gas evolution did not become too violent. After 1.5 h, gas evolution ceased almost completely and the mixture was heated at 160 °C for another 1.5 h. The mixture was allowed to cool to ambient temperature and a white solid started crystallizing, being ^{15}N-trimethylamine hydrochloride (**^{15}N-105**). The reflux condenser was removed, and the Schlenk flask was sealed with a rubber septum.

A 10 mL Schlenk tube with magnetic stirring bar and bubble counter was filled with 30 wt% H_2O_2 (4.20 mL, 41.1 mmol, 1.1 equiv.) and diluted with H_2O (7 mL). A Pasteur pipette was inserted through a bored rubber stopper into the solution, and the tube was cooled to 0 °C with an ice bath. The Schlenk flask containing the crude trimethylamine hydrochloride was connected to the Schlenk tube containing the H_2O_2 solution with a rubber tube. A nitrogen inlet was attached to the Schlenk flask and the system was flushed with nitrogen. Subsequently, 10 M NaOH (4.20 mL, 42.0 mmol, 1.1 equiv.) was added constantly to the crude trimethylamine hydrochloride over 30 min using a syringe pump, causing the evolution of gaseous trimethylamine. After complete addition, the Schlenk flask was heated to 60 °C for 30 min to ensure the complete transfer of trimethylamine to the H_2O_2 solution. After gas evolution had ceased completely, the Pasteur pipette was removed, the Schlenk tube was sealed, and the mixture was stirred at ambient temperature for 47 h. The crude solution was transferred into a 50 mL round bottom flask and excess H_2O was distilled off under reduced pressure (90 °C, 200 mbar). The product was further dried under high vacuum, giving yield to the crude product as a white solid (3.36 g). Recrystallization from MeCN afforded the pure compound. White solid (2.74 g, 24.5 mmol, 67%).

^{1}H NMR (400 MHz, D_2O) δ_H (ppm) = 3.25 (9 H, s); **^{13}C NMR** (101 MHz, D_2O) δ_C (ppm) = 59.49 (+, CH_3, d, J = 7.2 Hz); **IR** (neat): $\tilde{\nu}$ = 3332, 2952, 2289, 1685, 1469, 1398, 1230, 1126, 939, 857, 757 cm^{-1};

MS (+EI, 70 eV): 76.1 (100) [$(M)^{+\cdot}$], 61.1 (29) [$(M\text{-}CH_3)^{+\cdot}$], 60.2 (52) [$(M\text{-}O)^{+\cdot}$], 59.1 (67) [$(M\text{-}OH)^{+\cdot}$]; **HMRS** (+ESI, 120 V): 77.0730 ($C_3H_{10}{}^{15}NO$ [$(M+H)^+$]: calc. 77.0727); **m.p.** 92 °C.

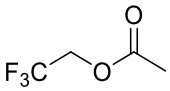

2,2,2-Trifluoroethyl acetate (107)[274]

A flame-dried 50 mL Schlenk flask was filled with 2,2,2-trifluoroethanol (25.0 mL, 33.1 g, 331 mmol, 1.0 equiv.), sealed with a rubber septum and cooled down to 0 °C with an ice bath. The flask was connected to two wash bottles, the first one empty, the second one filled with a diluted sodium hydroxide solution. To the cooled solution, acetyl chloride (25.0 mL, 27.5 g, 350 mmol, 1.1 equiv.) was added dropwise with a syringe at 0 °C. After complete addition, the mixture was allowed to reach ambient temperature and then stirred for 20 h. The solution was then transferred into a separating funnel and washed with H_2O (2x 50 mL), the organic phase dried over Na_2SO_4 and filtered off. Colorless liquid (37.8 g, 266 mmol, 80%).

^{1}H NMR (300 MHz, $CDCl_3$) δ_H (ppm) = 4.41 (2 H, d, *J* = 8.5 Hz), 2.10 (3 H, s); **^{19}F NMR** (283 MHz, $CDCl_3$) δ_F (ppm) = -74.7 (3 F, s); **^{13}C NMR** (75 MHz, $CDCl_3$) δ_C (ppm) = 169.40 (C_q), 123.11 (CF_3, q, *J* = 277 Hz), 60.36 (- , CH_2, q, *J* = 36.6 Hz), 20.19 (+, CH_3).

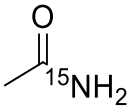

^{15}N-Acetamide (**^{15}N-106**)[267,293]

A 10 mL Schlenk tube with magnetic stirring bar and bubble counter was filled with H_2O (2 mL), a Pasteur pipette was inserted through a bored rubber stopper into the solution, and the tube was cooled down to 0 °C with an ice bath. To this setup, a 25 mL Schlenk flask with magnetic stirring bar and nitrogen inlet, containing a well-dispersed mixture of $^{15}NH_4Cl$ (2.02 g, 37.1 mmol, 1.0 equiv., **^{15}N-104**) and $Ca(OH)_2$ (3.30 g, 44.5 mmol, 1.2 equiv.) was connected using a rubber tube. The mixture was then heated gradually up to 550 °C with a heat gun, leading to the evolution of $^{15}NH_3$ which was then trapped in the cooled H_2O. To ensure complete conversion of $^{15}NH_4Cl$ (**^{15}N-104**), a small amount of H_2O (0.5 mL) was added to the solid mixture after the gas evolution had ceased, and the mixture was heated to 550 °C again. This procedure was repeated two more times. After gas evolution had ceased completely, the Pasteur pipette was removed from the aqueous $^{15}NH_3$ solution, and 2,2,2-Trifluoroethyl acetate (4.60 mL, 40.8 mmol, 1.1 equiv., **107**) was added. The biphasic mixture was

stirred vigorously at ambient temperature for 116 h. The volatiles were distilled of at reduced pressure (75 °C, 100 mbar). The residue was redissolved in MeOH and distilled off again (50 °C, 100 mbar), leaving a colorless solution which solidified after several hours at high vacuum. The compound was further dried in a desiccator over silica gel. White solid (1.82 g, 30.2 mmol, 82%).

R_f = 0.13 (DCM/MeOH 20:1); **^{1}H NMR** (300 MHz, $CDCl_3$) δ_H (ppm) = 5.48 (2 H, d, *J* = 88.4 Hz), 2.02 (3 H, d, *J* = 1.1 Hz); **^{13}C NMR** (75 MHz, $CDCl_3$) δ_C (ppm) = 173.49 (C_q), 22.67 (+, CH_3, d, *J* = 8.7 Hz); **IR** (neat): $\tilde{\nu}$ = 3336, 3150, 2806, 1737, 1644, 1461, 1387, 1148, 1047, 1006, 872, 828 cm^{-1}; **MS** (+EI, 70 eV): 60.0 (100) [$(M)^{+\cdot}$], 45.0 (95) [$(M\text{-}CH_3)^{+\cdot}$]; **HMRS** (+EI, 70 eV): 60.0333 ($C_2H_5{}^{15}NO$ [$(M)^{+\cdot}$]: calc. 60.0336); **m.p.** 70 – 72 °C.

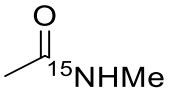

^{15}N-Methylacetamide (**^{15}N-103**)[267,277]

In a flame-dried 50 mL two-necked Schlenk flask equipped with magnetic stirring bar and reflux condenser with bubble counter, ^{15}N-Acetamide (1.00 g, 16.7 mmol, 1.0 equiv., **^{15}N-106**), dicumyl peroxide (9.00 g, 33.3 mmol, 2.0 equiv.), and CuCl (165 mg, 1.67 mmol, 10 mol%) were added under nitrogen and the apparatus was flushed with nitrogen for several minutes. Chlorobenzene (15 mL) was added and the mixture was refluxed for 15 h. During this time, the initially green mixture turned into a deep brown solution. The solution was allowed to cool to ambient temperature, filtered and the volatiles removed *in vacuo*. Initial purification was performed by flash chromatography on silica gel (DCM/MeOH 20:1), giving rise to a brown liquid. The compound was then further purified by micro-distillation under reduced pressure (45 °C, 0.3 mbar), using a liquid nitrogen bath to cool the receiving Schlenk flask. Colorless liquid (553 mg, 7.47 mmol, 45%) which solidified slowly upon standing in the refrigerator.

R_f = 0.19 (DCM/MeOH 20:1); **^{1}H NMR** (400 MHz, $CDCl_3$) δ_H (ppm) = 6.28 (1 H, dq, *J* = 91.6, 4.8 Hz), 2.73 (3 H, d, *J* = 4.5 Hz), 1.93 (3 H, d, *J* = 1.1 Hz); **^{13}C NMR** (101 MHz, $CDCl_3$) δ_C (ppm) = 171.12 (d, *J* = 14.7 Hz), 26.35 (d, *J* = 11.2 Hz), 23.00 (d, *J* = 8.6 Hz); **IR** (neat): $\tilde{\nu}$ = 3276, 3086, 2948, 1629, 1543, 1439, 1413, 1372, 1297, 1156, 1085, 1044, 992 cm^{-1}; **MS** (+EI, 70 eV): 74.0 (100) [$M^{+\cdot}$], 59.0 (45) [$(M\text{-}CH_3)^{+\cdot}$], 43.0 (81) [$(CH_3CO)^{+\cdot}$], 31.0 (54) [$(M\text{-}CH_3CO)^{+\cdot}$]; **HMRS** (+EI, 70 eV): 74.0491 ($C_3H_7{}^{15}NO$ [$(M)^{+\cdot}$]: calc. 74.0439).

F. References

[1] P. V. R. Snelgrove, *A census of the ocean*. *Presentation at TEDGlobal 2011,* can be found under https://www.ted.com/talks/paul_snelgrove_a_census_of_the_ocean (checked 28.02.2018).

[2] a) R. Danovaro, C. Corinaldesi, A. Dell'Anno, P. V. R. Snelgrove, *Curr. Biol.* **2017**, *27*, R461-R465; b) C. L. Prosser in *Comparative Animal Physiology (Fourth Edition)* (Ed.: C. L. Prosser), Wiley-Liss, New York, **1991**, pp. 167–205; c) P. V. R. Snelgrove, *Planta Med.* **2016**, *82*, 790.

[3] G. N. Somero, *Am. Zool.* **1990**, *30*, 123.

[4] R. Jaenicke, *Naturwissenschaften* **1983**, *70*, 332.

[5] G. N. Somero, *Annu. Rev. Physiol.* **1992**, *54*, 557.

[6] P. Y. Bruice, O. Reiser, *Organische Chemie (Fünfte Auflage)*, Pearson Studium, München, **2007**.

[7] G. Jenner, *Angew. Chem. Int. Ed. Engl.* **1975**, *14*, 137.

[8] T. Asano, W. J. Le Noble, *Chem. Rev.* **1978**, *78*, 407.

[9] F. Benito-López, R. J.M. Egberink, D. N. Reinhoudt, W. Verboom, *Tetrahedron* **2008**, *64*, 10023.

[10] D. Bieniek, F. Korte, *Naturwissenschaften* **1972**, *59*, 529.

[11] L. P. Christmann, *Dissertation*, Universität Bielefeld, Bielefeld, **2001**.

[12] A. Drljaca, C. D. Hubbard, R. van Eldik, T. Asano, M. V. Basilevsky, W. J. Le Noble, *Chem. Rev.* **1998**, *98*, 2167.

[13] S. D. Hamann, *Annu. Rev. Phys. Chem.* **1964**, *15*, 349.

[14] S. Has-Becker, *Dissertation*, Universität Regensburg, Regensburg, **2001**.

[15] N. S. Isaacs, *Tetrahedron* **1991**, *47*, 8463.

[16] G. Jenner, *J. Chem. Soc., Faraday Trans. 1* **1985**, *81*, 2437.

[17] G. Jenner, *Tetrahedron* **2002**, *58*, 5185.

[18] G. Jenner, *Tetrahedron* **2005**, *61*, 3621.

[19] G. Jenner in *Advances in Organic Synthesis (Volume 1)* (Ed.: Atta-ur-Rahman), Bentham Science Publishers, Sharjah, **2005**, pp. 25–80.

[20] F.-G. Klärner, F. Wurche, *J. Prakt. Chem.* **2000**, *342*, 609.

[21] W. J. Le Noble in *Progress in Physical Organic Chemistry*, *Vol. 5* (Eds.: A. Streitwieser, R. W. Taft), Wiley, New York, **1967**, pp. 207–330.

[22] W. J. Le Noble, *J. Chem. Educ.* **1967**, *44*, 729.

[23] W. J. Le Noble, *Chem. Unserer Zeit* **1983**, *17*, 152.

[24] K. Matsumoto, H. Hamana, H. Iida, *Helv. Chim. Acta* **2005**, *88*, 2033.

[25] K. Matsumoto, A. Sera, T. Uchida **1985**, 1.

[26] V. Schettino, R. Bini, *Chem. Soc. Rev.* **2007**, *36*, 869.

[27] R. van Eldik, T. Asano, W. J. Le Noble, *Chem. Rev.* **1989**, *89*, 549.

[28] O. Reiser, *Top. Catal.* **1998**, *5*, 105.

[29] H. Eyring, *J. Chem. Phys.* **1935**, *3*, 107.

[30] a) Volume of activation in *IUPAC Compendium of Chemical Terminology* (Eds.: M. Nič, J. Jirát, B. Košata, A. Jenkins, A. McNaught), IUPAC, Research Triagle Park, NC, **2009**; b) M. G. Evans, M. Polanyi, *Trans. Faraday Soc.* **1935**, *31*, 875.

[31] a) P. Drude, W. Nernst, *Z. Phys. Chem.* **1894**, *15*, 79; b) Drude–Nernst equation in *IUPAC Compendium of Chemical Terminology* (Eds.: M. Nič, J. Jirát, B. Košata, A. Jenkins, A. McNaught), IUPAC, Research Triagle Park, NC, **2009**.

[32] G. Jenner, M. Kellou, *Tetrahedron* **1981**, *37*, 1153.

[33] S. Chakraborty, N. Kaushik, P. S. Rao, H. N. Mishra, *Compr. Rev. Food Sci. Food Saf.* **2014**, *13*, 578.

[34] V. V. Brazhkin, *High Press. Res.* **2007**, *27*, 333.

[35] V. Smil, *Nature* **1999**, *400*, 415.

[36] D. Stoltzenberg, *Chem. Unserer Zeit* **1999**, *33*, 359.
[37] a) H. A. Cassar, *Ind. Eng. Chem. Anal. Ed.* **1931**, *3*, 197; b) D. B. Gooch, *Ind. Eng. Chem.* **1943**, *35*, 927.
[38] X.-Y. Liu in *Modern Inorganic Synthetic Chemistry (Second Edition)* (Eds.: R. Xu, Y. Xu), Elsevier, Amsterdam, Oxford, Cambridge, MA, **2017**, pp. 105–141.
[39] M. Groß, *Nachr. Chem. Tech. Lab.* **1992**, *40*, 1236.
[40] V. V. Mozhaev, K. Heremans, J. Frank, P. Masson, C. Balny, *Proteins* **1996**, *24*, 81.
[41] W. Dzwolak, M. Kato, Y. Taniguchi, *Biochim. Biophys. Acta, Protein Struct. Mol. Enzymol.* **2002**, *1595*, 131.
[42] a) C. E. Munte, M. Beck Erlach, W. Kremer, J. Koehler, H. R. Kalbitzer, *Angew. Chem. Int. Ed. Engl.* **2013**, *52*, 8943; b) P. T.T. Wong, D. J. Siminovitch, H. H. Mantsch, *Biochim. Biophys. Acta, Rev. Biomembr.* **1988**, *947*, 139; c) Y. O. Kamatari, R. Kitahara, H. Yamada, S. Yokoyama, K. Akasaka, *Methods* **2004**, *34*, 133.
[43] A. de Roeck, T. Duvetter, I. Fraeye, I. van der Plancken, D. N. Sila, A. van Loey, M. Hendrickx, *Food Chem.* **2009**, *115*, 207.
[44] A. Jayaraman, *Rev. Sci. Instrum.* **1986**, *57*, 1013.
[45] G. J. Piermarini, *J. Res. Natl. Inst. Stand. Technol.* **2001**, *106*, 889.
[46] R. M. Hazen, F. P. Bundy, *Phys. Today* **2000**, *53*, 58.
[47] L. Dubrovinsky, N. Dubrovinskaia, E. Bykova, M. Bykov, V. Prakapenka, C. Prescher, K. Glazyrin, H.-P. Liermann, M. Hanfland, M. Ekholm *et al*., *Nature* **2015**, *525*, 226.
[48] a) A. F. Goncharov, V. V. Struzhkin, M. S. Somayazulu, R. J. Hemley, H. K. Mao, *Science* **1996**, *273*, 218; b) C. G. Salzmann, P. G. Radaelli, E. Mayer, J. L. Finney, *Phys. Rev. Lett.* **2009**, *103*, 105701.
[49] a) M. I. Eremets, A. G. Gavriliuk, I. A. Trojan, D. A. Dzivenko, R. Boehler, *Nat. Mater.* **2004**, *3*, 558; b) C. Mailhiot, L. H. Yang, A. K. McMahan, *Phys. Rev. B* **1992**, *46*, 14419.
[50] A. P. Drozdov, M. I. Eremets, I. A. Troyan, V. Ksenofontov, S. I. Shylin, *Nature* **2015**, *525*, 73.
[51] M. I. Eremets, I. A. Troyan, *Nat. Mater.* **2011**, *10*, 927.
[52] a) R. Abbaschian, H. Zhu, C. Clarke, *Diam. Relat. Mater.* **2005**, *14*, 1916; b) H. Sumiya, S. Satoh, *Diam. Relat. Mater.* **1996**, *5*, 1359.
[53] P. W. Bridgman, J. B. Conant, *Proc. Natl. Acad. Sci. U.S.A.* **1929**, *15*, 680.
[54] a) J. B. Conant, W. R. Peterson, *J. Am. Chem. Soc.* **1932**, *54*, 628; b) J. B. Conant, C. O. Tongberg, *J. Am. Chem. Soc.* **1930**, *52*, 1659; c) E. W. Fawcett, R. O. Gibson, *J. Chem. Soc.* **1934**, 386; d) E. W. Fawcett, R. O. Gibson, *J. Chem. Soc.* **1934**, 396; e) B. Raistrick, R. H. Sapiro, D. M. Newitt, *J. Chem. Soc.* **1939**, 1761; f) B. Raistrick, R. H. Sapiro, D. M. Newitt, *J. Chem. Soc.* **1939**, 1770.
[55] G. Jenner, *J. Phys. Org. Chem.* **2002**, *15*, 1.
[56] G. Jenner, *New J. Chem.* **1999**, *23*, 525.
[57] J. S. Hill, N. S. Isaacs, *Tetrahedron Lett.* **1986**, *27*, 5007.
[58] N. S. Isaacs, O. H. Abed, *Tetrahedron Lett.* **1986**, *27*, 995.
[59] M. Buback, T. Perković, S. Redlich, A. d. Meijere, *Eur. J. Org. Chem.* **2003**, *2003*, 2375.
[60] H. Nozaki, T. Yamaguti, S. Ueda, K. Kondô, *Tetrahedron* **1968**, *24*, 1445.
[61] W. G. Dauben, A. P. Kozikowski, *J. Am. Chem. Soc.* **1974**, *96*, 3664.
[62] W. G. Dauben, C. R. Kessel, K. H. Takemura, *J. Am. Chem. Soc.* **1980**, *102*, 6893.
[63] W. G. Dauben, J. M. Gerdes, D. B. Smith, *J. Org. Chem.* **1985**, *50*, 2576.
[64] A. Orellana, S. K. Pandey, S. Carret, A. E. Greene, J.-F. Poisson, *J. Org. Chem.* **2012**, *77*, 5286.
[65] a) E. Ballerini, L. Minuti, O. Piermatti, *J. Org. Chem.* **2010**, *75*, 4251; b) L. Minuti, A. Temperini, E. Ballerini, *J. Org. Chem.* **2012**, *77*, 7923.
[66] M. Bellassoued, E. Reboul, F. Dumas, *Tetrahedron Lett.* **1997**, *38*, 5631.
[67] Y. Misumi, K. Matsumoto, *Angew. Chem.* **2002**, *114*, 1073.

[68] A. Y. Rulev, S. Azad, H. Kotsuki, J. Maddaluno, *Eur. J. Org. Chem.* **2010**, *2010*, 6423.
[69] S. Has-Becker, K. Bodmann, R. Kreuder, G. Santoni, T. Rein, O. Reiser, *Synlett* **2001**, 1395.
[70] S. Hillers, S. Sartori, O. Reiser, *J. Am. Chem. Soc.* **1996**, *118*, 2087.
[71] B. List, R. A. Lerner, C. F. Barbas, *J. Am. Chem. Soc.* **2000**, *122*, 2395.
[72] K. A. Ahrendt, C. J. Borths, D. W. C. MacMillan, *J. Am. Chem. Soc.* **2000**, *122*, 4243.
[73] E. N. Jacobsen, D. W. C. MacMillan, *Proc. Natl. Acad. Sci. U.S.A.* **2010**, *107*, 20618.
[74] D. W. C. MacMillan, *Nature* **2008**, *455*, 304.
[75] a) S. Bertelsen, K. A. Jørgensen, *Chem. Soc. Rev.* **2009**, *38*, 2178; b) P. I. Dalko, L. Moisan, *Angew. Chem. Int. Ed. Engl.* **2004**, *43*, 5138.
[76] J. Seayad, B. List, *Org. Biomol. Chem.* **2005**, *3*, 719.
[77] J. G. Hernández, E. Juaristi, *Chem. Commun.* **2012**, *48*, 5396.
[78] a) J. Alemán, S. Cabrera, *Chem. Soc. Rev.* **2013**, *42*, 774; b) M. Waser, *Asymmetric Organocatalysis in Natural Product Syntheses*, Springer Vienna, Vienna, **2012**.
[79] a) Z. G. Hajos, D. R. Parrish, *J. Org. Chem.* **1974**, *39*, 1612; b) Z. G. Hajos, D. R. Parrish, *J. Org. Chem.* **1974**, *39*, 1615; c) U. Eder, G. Sauer, R. Wiechert, *Angew. Chem. Int. Ed. Engl.* **1971**, *10*, 496.
[80] a) O. Andrey, A. Alexakis, G. Bernardinelli, *Org. Lett.* **2003**, *5*, 2559; b) S. Mossé, A. Alexakis, *Org. Lett.* **2005**, *7*, 4361.
[81] O. Andrey, A. Alexakis, A. Tomassini, G. Bernardinelli, *Adv. Synth. Catal.* **2004**, *346*, 1147.
[82] a) A. J. Cobb, D. M. Shaw, S. V. Ley, *Synlett* **2004**, 558; b) A. Hartikka, P. I. Arvidsson, *Tetrahedron: Asymmetry* **2004**, *15*, 1831; c) N. Momiyama, H. Torii, S. Saito, H. Yamamoto, *Proc. Natl. Acad. Sci. U.S.A.* **2004**, *101*, 5374.
[83] a) W. Wang, H. Li, J. Wang, L. Liao, *Tetrahedron Lett.* **2004**, *45*, 8229; b) W. Wang, J. Wang, H. Li, *Tetrahedron Lett.* **2004**, *45*, 7243; c) W. Wang, J. Wang, H. Li, L. Liao, *Tetrahedron Lett.* **2004**, *45*, 7235.
[84] a) H.-M. Guo, L.-F. Cun, L.-Z. Gong, A.-Q. Mi, Y.-Z. Jiang, *Chem. Commun.* **2005**, 1450; b) Z. Tang, F. Jiang, X. Cui, L.-Z. Gong, A.-Q. Mi, Y.-Z. Jiang, Y.-D. Wu, *Proc. Natl. Acad. Sci. U.S.A.* **2004**, *101*, 5755; c) Z. Tang, F. Jiang, L.-T. Yu, X. Cui, L.-Z. Gong, A.-Q. Mi, Y.-Z. Jiang, Y.-D. Wu, *J. Am. Chem. Soc.* **2003**, *125*, 5262.
[85] Y. Hayashi, H. Gotoh, T. Hayashi, M. Shoji, *Angew. Chem. Int. Ed. Engl.* **2005**, *44*, 4212.
[86] J. Franzén, M. Marigo, D. Fielenbach, T. C. Wabnitz, A. Kjaersgaard, K. A. Jørgensen, *J. Am. Chem. Soc.* **2005**, *127*, 18296.
[87] M. Marigo, T. C. Wabnitz, D. Fielenbach, K. A. Jørgensen, *Angew. Chem. Int. Ed. Engl.* **2005**, *44*, 794.
[88] a) K. Sakthivel, W. Notz, T. Bui, C. F. Barbas, *J. Am. Chem. Soc.* **2001**, *123*, 5260; b) T. Sone, K. Hiroi, S. Yamada, *Chem. Pharm. Bull.* **1973**, *21*, 2331; c) T. Bui, C. F. Barbas, *Tetrahedron Lett.* **2000**, *41*, 6951.
[89] N. Mase, R. Thayumanavan, F. Tanaka, C. F. Barbas, *Org. Lett.* **2004**, *6*, 2527.
[90] a) A. Bruckmann, A. Krebs, C. Bolm, *Green Chem.* **2008**, *10*, 1131; b) P. Chauhan, S. S. Chimni, *Beilstein J. Org. Chem.* **2012**, *8*, 2132; c) M. Hosseini, N. Stiasni, V. Barbieri, C. O. Kappe, *J. Org. Chem.* **2007**, *72*, 1417; d) P. Kwiatkowski, K. Dudziński, D. Łyżwa in *Comprehensive Enantioselective Organocatalysis*. *Catalysts, reactions, and applications* (Ed.: P. I. Dalko), Wiley-VCH, Weinheim, **2013**, pp. 579–615.
[91] A. Sera, K. Takagi, H. Katayama, H. Yamada, K. Matsumoto, *J. Org. Chem.* **1988**, *53*, 1157.
[92] K. Matsumoto, T. Uchida, *Chem. Lett.* **1981**, *10*, 1673.
[93] T. Oishi, H. Oguri, M. Hirama, *Tetrahedron: Asymmetry* **1995**, *6*, 1241.
[94] Y. Sekiguchi, A. Sasaoka, A. Shimomoto, S. Fujioka, H. Kotsuki, *Synlett* **2003**, 1655.
[95] Y. Hayashi, W. Tsuboi, M. Shoji, N. Suzuki, *Tetrahedron Lett.* **2004**, *45*, 4353.

[96] Y. Hayashi, K. Okado, I. Ashimine, M. Shoji, *Tetrahedron Lett.* **2002**, *43*, 8683.
[97] Y. Hayashi, W. Tsuboi, M. Shoji, N. Suzuki, *J. Am. Chem. Soc.* **2003**, *125*, 11208.
[98] a) K. Mori, T. Yamauchi, J. Maddaluno, K. Nakano, Y. Ichikawa, H. Kotsuki, *Synlett* **2011**, 2080; b) K. Mori, J. Maddaluno, K. Nakano, Y. Ichikawa, H. Kotsuki, *Synlett* **2009**, 2346; c) H. Kotsuki, K. Nakano, Y. Ichikawa, *Heterocycles* **2010**, *80*, 799.
[99] S. Azad, T. Kobayashi, K. Nakano, Y. Ichikawa, H. Kotsuki, *Tetrahedron Lett.* **2009**, *50*, 48.
[100] N. Miyamae, N. Watanabe, M. Moritaka, K. Nakano, Y. Ichikawa, H. Kotsuki, *Org. Biomol. Chem.* **2014**, *12*, 5847.
[101] P. Kwiatkowski, K. Dudzinski, D. Lyzwa, *Org. Lett.* **2011**, *13*, 3624.
[102] P. Kwiatkowski, A. Cholewiak, A. Kasztelan, *Org. Lett.* **2014**, *16*, 5930.
[103] D. Łyżwa, K. Dudziński, P. Kwiatkowski, *Org. Lett.* **2012**, *14*, 1540.
[104] A. Kasztelan, M. Biedrzycki, P. Kwiatkowski, *Adv. Synth. Catal.* **2016**, *358*, 2962.
[105] J. Clayden, N. Greeves, S. Warren, P. Wothers (Eds.) *Organic Chemistry*, Oxford Univ. Press, Oxford, **2001**.
[106] B. Rodríguez, C. Bolm, *J. Org. Chem.* **2006**, *71*, 2888.
[107] a) B. Rodríguez, A. Bruckmann, C. Bolm, *Chemistry* **2007**, *13*, 4710; b) B. Rodríguez, T. Rantanen, C. Bolm, *Angew. Chem.* **2006**, *118*, 7078.
[108] J. M. Betancort, C. F. Barbas, *Org. Lett.* **2001**, *3*, 3737.
[109] a) L.-q. Gu, G. Zhao, *Adv. Synth. Catal.* **2007**, *349*, 1629; b) P. Kotrusz, S. Toma, H.-G. Schmalz, A. Adler, *Eur. J. Org. Chem.* **2004**, *2004*, 1577; c) D. Lu, Y. Gong, W. Wang, *Adv. Synth. Catal.* **2010**, *352*, 644.
[110] L. G. Donadío, M. A. Galetti, G. Giorgi, M. Rasparini, M. J. Comin, *J. Org. Chem.* **2016**, *81*, 7952.
[111] a) B. S. Donslund, T. K. Johansen, P. H. Poulsen, K. S. Halskov, K. A. Jørgensen, *Angew. Chem. Int. Ed. Engl.* **2015**, *54*, 13860; b) K. L. Jensen, G. Dickmeiss, H. Jiang, L. Albrecht, K. A. Jørgensen, *Acc. Chem. Res.* **2012**, *45*, 248.
[112] J. V. Bhaskar Kanth, M. Periasamy, *Tetrahedron* **1993**, *49*, 5127.
[113] S. Kobayashi, T. Kinoshita, H. Uehara, T. Sudo, I. Ryu, *Org. Lett.* **2009**, *11*, 3934.
[114] J. Burés, A. Armstrong, D. G. Blackmond, *J. Am. Chem. Soc.* **2011**, *133*, 8822.
[115] J. Burés, A. Armstrong, D. G. Blackmond, *Acc. Chem. Res.* **2016**, *49*, 214.
[116] G. Sahoo, H. Rahaman, A. Madarász, I. Pápai, M. Melarto, A. Valkonen, P. M. Pihko, *Angew. Chem. Int. Ed. Engl.* **2012**, *51*, 13144.
[117] D. Seebach, X. Sun, M.-O. Ebert, W. B. Schweizer, N. Purkayastha, A. K. Beck, J. Duschmalé, H. Wennemers, T. Mukaiyama, M. Benohoud *et al.*, *Helv. Chim. Acta* **2013**, *96*, 799.
[118] K. Patora-Komisarska, M. Benohoud, H. Ishikawa, D. Seebach, Y. Hayashi, *Helv. Chim. Acta* **2011**, *94*, 719.
[119] T. Földes, Á. Madarász, Á. Révész, Z. Dobi, S. Varga, A. Hamza, P. R. Nagy, P. M. Pihko, I. Pápai, *J. Am. Chem. Soc.* **2017**, *139*, 17052.
[120] J. Burés, A. Armstrong, D. G. Blackmond, *J. Am. Chem. Soc.* **2012**, *134*, 6741.
[121] D. Seebach, X. Sun, C. Sparr, M.-O. Ebert, W. B. Schweizer, A. K. Beck, *Helv. Chim. Acta* **2012**, *95*, 1064.
[122] M. H. Haindl, J. Hioe, R. M. Gschwind, *J. Am. Chem. Soc.* **2015**, *137*, 12835.
[123] M. B. Schmid, K. Zeitler, R. M. Gschwind, *Angew. Chem. Int. Ed. Engl.* **2010**, *49*, 4997.
[124] M. Hofmann, *Master Thesis*, Universität Regensburg, Regensburg, **2013**.
[125] R. W. Hoffmann, *Chem. Rev.* **1989**, *89*, 1841.
[126] M. H. Haindl, M. B. Schmid, K. Zeitler, R. M. Gschwind, *RSC Adv.* **2012**, *2*, 5941.
[127] D. Seebach, J. Goliński, *Helv. Chim. Acta* **1981**, *64*, 1413.
[128] S. J. Blarer, D. Seebach, *Chem. Ber.* **1983**, *116*, 3086.
[129] D. Seebach, A. K. Beck, J. Goliński, J. N. Hay, T. Laube, *Helv. Chim. Acta* **1985**, *68*, 162.

[130] a) S. J. Miller, *Acc. Chem. Res.* **2004**, *37*, 601; b) E. R. Jarvo, S. J. Miller, *Tetrahedron* **2002**, *58*, 2481; c) E. A. C. Davie, S. M. Mennen, Y. Xu, S. J. Miller, *Chem. Rev.* **2007**, *107*, 5759; d) A. Berkessel, *Curr. Opin. Chem. Biol.* **2003**, *7*, 409; e) R. T. Raines, H. Wennemers, *Acc. Chem. Res.* **2017**, *50*, 2419.

[131] I. Photaki, V. Bardakos, A. W. Lake, G. Lowe, *J. Chem. Soc. C* **1968**, 1860.

[132] a) S. Juliá, J. Masana, J. C. Vega, *Angew. Chem. Int. Ed. Engl.* **1980**, *19*, 929; b) S. Juliá, J. Guixer, J. Masana, J. Rocas, S. Colonna, R. Annuziata, H. Molinari, *J. Chem. Soc., Perkin Trans. 1* **1982**, 1317; c) P. A. Bentley, M. W. Cappi, R. W. Flood, S. M. Roberts, J. A. Smith, *Tetrahedron Lett.* **1998**, *39*, 9297.

[133] K. Tanaka, A. Mori, S. Inoue, *J. Org. Chem.* **1990**, *55*, 181.

[134] a) P. I. Dalko, L. Moisan, *Angew. Chem. Int. Ed. Engl.* **2001**, *40*, 3726; b) P. G. Cozzi, Y. Hayashi, *ChemCatChem* **2012**, *4*, 887.

[135] D. J. Guerin, S. J. Miller, *J. Am. Chem. Soc.* **2002**, *124*, 2134.

[136] S. M. Mennen, J. T. Blank, M. B. Tran-Dubé, J. E. Imbriglio, S. J. Miller, *Chem. Commun.* **2005**, 195.

[137] J. E. Imbriglio, M. M. Vasbinder, S. J. Miller, *Org. Lett.* **2003**, *5*, 3741.

[138] M. W. Giuliano, C.-Y. Lin, D. K. Romney, S. J. Miller, E. V. Anslyn, *Adv. Synth. Catal.* **2015**, *357*, 2301.

[139] a) G. T. Copeland, S. J. Miller, *J. Am. Chem. Soc.* **2001**, *123*, 6496; b) A. E. Hurtley, E. A. Stone, A. J. Metrano, S. J. Miller, *J. Org. Chem.* **2017**, *82*, 11326; c) E. R. Jarvo, G. T. Copeland, N. Papaioannou, P. J. Bonitatebus, S. J. Miller, *J. Am. Chem. Soc.* **1999**, *121*, 11638; d) S. J. Miller, G. T. Copeland, N. Papaioannou, T. E. Horstmann, E. M. Ruel, *J. Am. Chem. Soc.* **1998**, *120*, 1629; e) B. R. Sculimbrene, A. J. Morgan, S. J. Miller, *J. Am. Chem. Soc.* **2002**, *124*, 11653.

[140] a) C. A. Lewis, S. J. Miller, *Angew. Chem. Int. Ed. Engl.* **2006**, *45*, 5616; b) C. R. Shugrue, S. J. Miller, *Chem. Rev.* **2017**, *117*, 11894.

[141] A. J. Metrano, N. C. Abascal, B. Q. Mercado, E. K. Paulson, A. E. Hurtley, S. J. Miller, *J. Am. Chem. Soc.* **2017**, *139*, 492.

[142] M. Wiesner, M. Neuburger, H. Wennemers, *Chem. Eur. J.* **2009**, *15*, 10103.

[143] J. Duschmalé, H. Wennemers, *Chem. Eur. J.* **2012**, *18*, 1111.

[144] a) R. Kastl, H. Wennemers, *Angew. Chem. Int. Ed. Engl.* **2013**, *52*, 7228; b) T. Schnitzer, H. Wennemers, *Synlett* **2017**, *28*, 1282.

[145] M. Wiesner, J. D. Revell, H. Wennemers, *Angew. Chem. Int. Ed. Engl.* **2008**, *47*, 1871.

[146] P. Krattiger, R. Kovasy, J. D. Revell, S. Ivan, H. Wennemers, *Org. Lett.* **2005**, *7*, 1101.

[147] J. D. Revell, H. Wennemers, *Adv. Synth. Catal.* **2008**, *350*, 1046.

[148] J. D. Revell, H. Wennemers, *Tetrahedron* **2007**, *63*, 8420.

[149] a) Y. Arakawa, H. Wennemers, *ChemSusChem* **2013**, *6*, 242; b) Y. Arakawa, M. Wiesner, H. Wennemers, *Adv. Synth. Catal.* **2011**, *353*, 1201; c) P. Krattiger, R. Kovàsy, J. D. Revell, H. Wennemers, *QSAR Comb. Sci.* **2005**, *24*, 1158; d) J. D. Revell, D. Gantenbein, P. Krattiger, H. Wennemers, *Biopolymers* **2006**, *84*, 105.

[150] T. Schnitzer, H. Wennemers, *J. Am. Chem. Soc.* **2017**, *139*, 15356.

[151] a) F. Bächle, J. Duschmalé, C. Ebner, A. Pfaltz, H. Wennemers, *Angew. Chem. Int. Ed. Engl.* **2013**, *52*, 12619; b) M. Wiesner, G. Upert, G. Angelici, H. Wennemers, *J. Am. Chem. Soc.* **2010**, *132*, 6.

[152] J. Duschmalé, J. Wiest, M. Wiesner, H. Wennemers, *Chem. Sci.* **2013**, *4*, 1312.

[153] V. D'Elia, H. Zwicknagl, O. Reiser, *J. Org. Chem.* **2008**, *73*, 3262.

[154] a) D. Seebach, P. E. Ciceri, M. Overhand, B. Jaun, D. Rigo, L. Oberer, U. Hommel, R. Amstutz, H. Widmer, *Helv. Chim. Acta* **1996**, *79*, 2043; b) D. Seebach, J. L. Matthews, *Chem. Commun.* **1997**, 2015.

[155] L. K. A. Pilsl, *Dissertation*, Universität Regensburg, Regensburg, **2015**.
[156] C. R. Botines, *Master Thesis*, Universitat Autònoma de Barcelona, Barcelona, **2014**.
[157] O. Illa, O. Porcar-Tost, C. Robledillo, C. Elvira, P. Nolis, O. Reiser, V. Branchadell, R. M. Ortuño, *J. Org. Chem.* **2018**, *83*, 350.
[158] T. Ertl, *Dissertation*, Universität Regensburg, Regensburg, **2017**.
[159] F. Fülöp, *Chem. Rev.* **2001**, *101*, 2181.
[160] F. Fülöp, T. A. Martinek, G. K. Tóth, *Chem. Soc. Rev.* **2006**, *35*, 323.
[161] L. Kiss, F. Fülöp, *Chem. Rev.* **2014**, *114*, 1116.
[162] a) E. E. Smissman, M. Steinman, *J. Med. Chem.* **1966**, *9*, 455; b) N. A. LeBel, M. E. Post, J. J. Whang, *J. Am. Chem. Soc.* **1964**, *86*, 3759.
[163] a) F. Glorius, *Org. Biomol. Chem.* **2005**, *3*, 4171; b) Y.-G. Zhou, *Acc. Chem. Res.* **2007**, *40*, 1357.
[164] S. G. Davies, O. Ichihara, I. Lenoir, I. A. S. Walters, *J. Chem. Soc., Perkin Trans. 1* **1994**, *2*, 1411.
[165] E. F. Jenkins, E. J. Costello, *J. Am. Chem. Soc.* **1946**, *68*, 2733.
[166] O. Grummitt, A. E. Ardis, J. Fick, *J. Am. Chem. Soc.* **1950**, *72*, 5167.
[167] J. M. McIntosh, *Encyclopedia of Reagents for Organic Synthesis*. "3-Sulfolene", **2001**, John Wiley & Sons, New York.
[168] T. E. Sample, L. F. Hatch, *J. Chem. Educ.* **1968**, *45*, 55.
[169] S. Hünig, P. Kreitmeier, G. Märkl, J. Sauer, R. Sustmann, *Integriertes Organisch-chemisches Praktikum (I.O.C.-Praktikum)*. *Mit den Praktikumsversuchen auf CD-ROM*, Lehmanns Media, Berlin, **2007**.
[170] a) T. Curtius, *J. Prakt. Chem.* **1894**, *50*, 275; b) T. Curtius, *Ber. Dtsch. Chem. Ges.* **1890**, *23*, 3023.
[171] S. Kobayashi, K. Kamiyama, M. Ohno, *Chem. Pharm. Bull.* **1990**, *38*, 350.
[172] S. Bräse, C. Gil, K. Knepper, V. Zimmermann, *Angew. Chem. Int. Ed. Engl.* **2005**, *44*, 5188.
[173] T. Shioiri, K. Ninomiya, S. Yamada, *J. Am. Chem. Soc.* **1972**, *94*, 6203.
[174] G. Timpano, G. Tabarani, M. Anderluh, D. Invernizzi, F. Vasile, D. Potenza, P. M. Nieto, J. Rojo, F. Fieschi, A. Bernardi, *ChemBioChem* **2008**, *9*, 1921.
[175] D. H. Appella, P. R. LePlae, T. L. Raguse, S. H. Gellman, *J. Org. Chem.* **2000**, *65*, 4766.
[176] J. D. White, P. Hrnciar, F. Stappenbeck, *J. Org. Chem.* **1999**, *64*, 7871.
[177] C. Bubert, C. Cabrele, O. Reiser, *Synlett* **1997**, 827.
[178] S. Choi, R. B. Silverman, *J. Med. Chem.* **2002**, *45*, 4531.
[179] a) V. K. Aggarwal, S. Roseblade, R. Alexander, *Org. Biomol. Chem.* **2003**, *1*, 684; b) R. Hanselmann, J. Zhou, P. Ma, P. N. Confalone, *J. Org. Chem.* **2003**, *68*, 8739.
[180] I. Atodiresei, I. Schiffers, C. Bolm, *Chem. Rev.* **2007**, *107*, 5683.
[181] a) Díaz de Villegas, María D., J. A. Gálvez, P. Etayo, R. Badorrey, P. López-Ram-de-Víu, *Chem. Soc. Rev.* **2011**, *40*, 5564; b) E. García-Urdiales, I. Alfonso, V. Gotor, *Chem. Rev.* **2005**, *105*, 313; c) E. García-Urdiales, I. Alfonso, V. Gotor, *Chem. Rev.* **2011**, *111*, PR110-80.
[182] a) N. Hashimoto, S. Kawamura, T. Ishizuka, T. Kunieda, *Tetrahedron Lett.* **1996**, *37*, 9237; b) H. Imado, T. Ishizuka, T. Kunieda, *Tetrahedron Lett.* **1995**, *36*, 931; c) Y. Suda, S. Yago, M. Shiro, T. Taguchi, *Chem. Lett.* **1992**, *21*, 389.
[183] D. Seebach, G. Jaeschke, Y. M. Wang, *Angew. Chem. Int. Ed. Engl.* **1995**, *34*, 2395.
[184] C. Bolm, I. Schiffers, C. L. Dinter, A. Gerlach, *J. Org. Chem.* **2000**, *65*, 6984.
[185] C. Bolm, I. Schiffers, I. Atodiresei, C. P.R. Hackenberger, *Tetrahedron: Asymmetry* **2003**, *14*, 3455.
[186] C. Bolm, A. Gerlach, C. L. Dinter, *Synlett* **1999**, 195.
[187] Y. Chen, S.-K. Tian, L. Deng, *J. Am. Chem. Soc.* **2000**, *122*, 9542.
[188] R. Manzano, J. M. Andrés, M.-D. Muruzábal, R. Pedrosa, *J. Org. Chem.* **2010**, *75*, 5417.
[189] S. H. Oh, H. S. Rho, J. W. Lee, J. E. Lee, S. H. Youk, J. Chin, C. E. Song, *Angew. Chem. Int. Ed. Engl.* **2008**, *47*, 7872.

[190] A. Goswami, T. P. Kissick, *Org. Process Res. Dev.* **2009**, *13*, 483.
[191] H.-J. Gais, K. L. Lukas, W. A. Ball, S. Braun, H. J. Lindner, *Liebigs Ann. Chem.* **1986**, *1986*, 687.
[192] H.-J. Gais, K. L. Lukas, *Angew. Chem.* **1984**, *96*, 140.
[193] P. Mohr, N. Waespe-Šarčević, C. Tamm, K. Gawronska, J. K. Gawronski, *Helv. Chim. Acta* **1983**, *66*, 2501.
[194] N. Tamura, H. Natsugari, Y. Kawano, Y. Matsushita, K. Yoshioka, M. Ochiai, *Chem. Pharm. Bull.* **1987**, *35*, 996.
[195] J. R. Dunetz, Y. Xiang, A. Baldwin, J. Ringling, *Org. Lett.* **2011**, *13*, 5048.
[196] V. H. Thorat, T. S. Ingole, K. N. Vijayadas, R. V. Nair, S. S. Kale, V. V. E. Ramesh, H. C. Davis, P. Prabhakaran, R. G. Gonnade, R. L. Gawade *et al*., *Eur. J. Org. Chem.* **2013**, *2013*, 3529.
[197] K. N. Vijayadas, R. V. Nair, R. L. Gawade, A. S. Kotmale, P. Prabhakaran, R. G. Gonnade, V. G. Puranik, P. R. Rajamohanan, G. J. Sanjayan, *Org. Biomol. Chem.* **2013**, *11*, 8348.
[198] R. Nirogi, A. R. Mohammed, I. Ahmad, P. Jayarajan, N. V. Kandikere, A. K. Shinde, R. S. Kambhampati, G. Bhyrapuneni, J. Ravula, S. M. Patnala *et al*., WO2011030349 A1, **2011**.
[199] P. Prabhakaran, S. S. Kale, V. G. Puranik, P. R. Rajamohanan, O. Chetina, J. A. K. Howard, H.-J. Hofmann, G. J. Sanjayan, *J. Am. Chem. Soc.* **2008**, *130*, 17743.
[200] R. L. Sutar, N. N. Joshi, *Tetrahedron: Asymmetry* **2013**, *24*, 43.
[201] a) R. Subirós-Funosas, L. Nieto-Rodriguez, K. J. Jensen, F. Albericio, *J. Pept. Sci.* **2013**, *19*, 408; b) R. Subirós-Funosas, R. Prohens, R. Barbas, A. El-Faham, F. Albericio, *Chem. Eur. J.* **2009**, *15*, 9394; c) A. El-Faham, R. Subirós Funosas, R. Prohens, F. Albericio, *Chem. Eur. J.* **2009**, *15*, 9404; d) A. El-Faham, F. Albericio, *J. Pept. Sci.* **2010**, *16*, 6.
[202] R. A. Olofson, D. S. Morrison, A. Banerji, *J. Org. Chem.* **1984**, *49*, 2652.
[203] R. A. Olofson, R. K. Vander Meer, *J. Org. Chem.* **1984**, *49*, 3377.
[204] R. A. Olofson, R. K. Vander Meer, D. H. Hoskin, M. Y. Bernheim, S. Stournas, D. S. Morrison, *J. Org. Chem.* **1984**, *49*, 3367.
[205] R. A. Olofson, R. K. Vander Meer, S. Stournas, *J. Am. Chem. Soc.* **1971**, *93*, 1543.
[206] R. K. Vander Meer, R. A. Olofson, *J. Org. Chem.* **1984**, *49*, 3373.
[207] N. F. Haley, *J. Org. Chem.* **1978**, *43*, 1233.
[208] L. Bunch, P.-O. Norrby, K. Frydenvang, P. Krogsgaard-Larsen, U. Madsen, *Org. Lett.* **2001**, *3*, 433.
[209] a) T. Nagasaka, Y. Koseki, *J. Org. Chem.* **1998**, *63*, 6797; b) T. Nagasaka, Y. Koseki, F. Hamaguchi, *Tetrahedron Lett.* **1989**, *30*, 1871.
[210] a) I. Z. Siemion, T. Wieland, K.-H. Pook, *Angew. Chem.* **1975**, *87*, 712; b) M. Feigel, G. Lugert, J. Manero, M. Bremer, *Z. Naturforsch.* **1990**, *45b*, 258.
[211] P. Friedländer, S. Wleügel, *Ber. Dtsch. Chem. Ges.* **1883**, *16*, 2227.
[212] P. Friedländer, R. Henriques, *Ber. Dtsch. Chem. Ges.* **1882**, *15*, 2105.
[213] R. Anschütz, O. Schmidt, *Ber. Dtsch. Chem. Ges.* **1902**, *35*, 3463.
[214] E. Bamberger, *Ber. Dtsch. Chem. Ges.* **1903**, *36*, 819.
[215] E. Bamberger, *Ber. Dtsch. Chem. Ges.* **1909**, *42*, 1647.
[216] J. W. Brühl, *Ber. Dtsch. Chem. Ges.* **1903**, *36*, 1305.
[217] G. Heller, *J. Prakt. Chem.* **1908**, *77*, 145.
[218] G. Speroni in *The chemistry of heterocyclic compounds*, *17th volume* (Eds.: A. Quilico, G. Speroni, L. C. Behr, R. L. McKee, R. H. Wiley), Interscience Publishers, New York, **1962**, pp. 177–222.
[219] O. Mumm, H. Hesse, *Ber. Dtsch. Chem. Ges.* **1910**, *43*, 2505.
[220] A. Angeli, F. Angelico, *Gazz. Chim. Ital.* **1900**, *30*, 268.
[221] D. T. Zentmyer, E. C. Wagner, *J. Org. Chem.* **1949**, *14*, 967.
[222] G. M. Coppola, *J. Heterocyclic Chem.* **1999**, *36*, 563.

[223] L. A. Errede, *J. Org. Chem.* **1976**, *41*, 1763.
[224] a) M. Gütschow, U. Neumann, J. Sieler, K. Eger, *Pharm. Acta Helv.* **1998**, *73*, 95; b) A. Verma, S. Kumar, *Org. Lett.* **2016**, *18*, 4388.
[225] K. v. Auwers, *Justus Liebigs Ann. Chem.* **1924**, *437*, 63.
[226] a) A. El-Mekabaty, *Int. J. Modern Org. Chem.* **2013**, *2*, 81; b) H. M. F. Madkour, *Arkivoc* **2004**, 36.
[227] R. W. Spencer, L. J. Copp, B. Bonaventura, T. F. Tam, T. J. Liak, R. J. Billedeau, A. Krantz, *Biochem. Biophys. Res. Commun.* **1986**, *140*, 928.
[228] a) D. K. Mohapatra, A. Datta, *Bioorganic & Medicinal Chemistry Letters* **1997**, *7*, 2527; b) D. Bose, M. Chary, *Synthesis* **2010**, *2010*, 643.
[229] a) I. Ansary, A. Das, P. S. Sen Gupta, A. K. Bandyopadhyay, *Synth. Comm.* **2017**, *47*, 1375; b) C. L. Cioffi, N. Dobri, E. E. Freeman, M. P. Conlon, P. Chen, D. G. Stafford, D. M. C. Schwarz, K. C. Golden, L. Zhu, D. B. Kitchen *et al*., *J. Med. Chem.* **2014**, *57*, 7731.
[230] O. Erez, P. Nakache, WO 2011064657 A2, **2011**.
[231] R. Giri, J. K. Lam, J.-Q. Yu, *J. Am. Chem. Soc.* **2010**, *132*, 686.
[232] M. C. Etter, Z. U. Lipkowska, C. Decoret, J. Royer, F. Bayard, J. Vicens, *Mol. Cryst. Liq. Cryst.* **1988**, *161*, 43.
[233] J. Vicens, C. Decoret, J. Royer, M. C. Etter, *Isr. J. Chem.* **1985**, *25*, 306.
[234] C. R. Botines, *Unpublished results*.
[235] V. Dragojlovic, *ChemTexts* **2015**, *1*, 337.
[236] M. C. Pirrung, *Chem. Eur. J.* **2006**, *12*, 1312.
[237] a) D. Enders, A. Seki, *Synlett* **2002**, 26; b) B. List, P. Pojarliev, H. J. Martin, *Org. Lett.* **2001**, *3*, 2423.
[238] J. Jonas, A. Jonas, *Annu. Rev. Biophys. Biomol. Struct.* **1994**, *23*, 287.
[239] B. Ertinger, *Bachelor Thesis*, Universität Regensburg, Regensburg, **2016**.
[240] T. Reid Alderson, J. H. Lee, C. Charlier, J. Ying, A. Bax, *ChemBioChem* **2017**.
[241] W. J. Wedemeyer, E. Welker, H. A. Scheraga, *Biochemistry* **2002**, *41*, 14637.
[242] B. B. Boonyaratanakornkit, C. B. Park, D. S. Clark, *Biochim. Biophys. Acta, Protein Struct. Mol. Enzymol.* **2002**, *1595*, 235.
[243] a) D. T. McQuade, S. L. McKay, D. R. Powell, S. H. Gellman, *J. Am. Chem. Soc.* **1997**, *119*, 8528; b) G. B. Liang, J. M. Desper, S. H. Gellman, *J. Am. Chem. Soc.* **1993**, *115*, 925; c) Gardner, Robb R., S. H. Gellman, *J. Am. Chem. Soc.* **1995**, *117*, 10411; d) E. A. Gallo, S. H. Gellman, *Tetrahedron Lett.* **1992**, *33*, 7485; e) G. P. Dado, S. H. Gellman, *J. Am. Chem. Soc.* **1994**, *116*, 1054; f) G. P. Dado, S. H. Gellman, *J. Am. Chem. Soc.* **1993**, *115*, 4228; g) G. P. Dado, S. H. Gellman, *J. Am. Chem. Soc.* **1992**, *114*, 3138; h) D. H. Appella, L. A. Christianson, I. L. Karle, D. R. Powell, S. H. Gellman, *J. Am. Chem. Soc.* **1996**, *118*, 13071; i) S. H. Gellman, B. R. Adams, *Tetrahedron Lett.* **1989**, *30*, 3381.
[244] S. H. Gellman, G. P. Dado, G. B. Liang, B. R. Adams, *J. Am. Chem. Soc.* **1991**, *113*, 1164.
[245] C. Zorn, *Dissertation*, Universität Regensburg, Regensburg, **2001**.
[246] De Pol, Silvia, *Dissertation*, Universität Regensburg, Regensburg, **2006**.
[247] a) E. Gorrea, G. Pohl, P. Nolis, S. Celis, K. K. Burusco, V. Branchadell, A. Perczel, R. M. Ortuño, *J. Org. Chem.* **2012**, *77*, 9795; b) A. Sorrenti, O. Illa, R. M. Ortuño, R. Pons, *Langmuir* **2016**, *32*, 6977; c) A. Sorrenti, O. Illa, R. Pons, R. M. Ortuño, *Langmuir* **2015**, *31*, 9608.
[248] A. V. Reddy, A. R. Mitra, A. K. Dubey, P. R. Reddy, WO2014102808 A1, **2014**.
[249] K. Alder, M. Schumacher, *Liebigs Ann. Chem.* **1949**, *564*, 96.
[250] D. E. Hibbs, M. B. Hursthouse, I. G. Jones, W. Jones, K. M. Abdul Malik, M. North, *J. Org. Chem.* **1998**, *63*, 1496.
[251] A. A. Bothner-By, *Adv. Magn. Reson.* **1965**, *1*, 195.

[252] H. J. Reich, "Structure Determination Using NMR", can be found under https://www.chem.wisc.edu/areas/reich/chem605/ (checked 28.02.18).
[253] a) J. S. Laursen, J. Engel-Andreasen, P. Fristrup, P. Harris, C. A. Olsen, *J. Am. Chem. Soc.* **2013**, *135*, 2835; b) X. Hu, W. Zhang, I. Carmichael, A. S. Serianni, *J. Am. Chem. Soc.* **2010**, *132*, 4641.
[254] L. J. Bellamy in *The Infra-red Spectra of Complex Molecules* (Ed.: L. J. Bellamy), Springer Netherlands, Dordrecht, **1975**, pp. 231–262.
[255] R. C. Dougherty, *J. Chem. Phys.* **1998**, *109*, 7372.
[256] N. S. Myshakina, Z. Ahmed, S. A. Asher, *J. Phys. Chem. B* **2008**, *112*, 11873.
[257] M. A. Sahai, M. Szöri, B. Viskolcz, E. F. Pai, I. G. Csizmadia, *J. Phys. Chem. A* **2007**, *111*, 8384.
[258] K. Wüthrich, *Nat. Struct. Biol.* **2001**, *8*, 923.
[259] T. D.W. Claridge, *High-Resolution NMR Techniques in Organic Chemistry (Third Edition)*, Elsevier, Amsterdam, Oxford, **2016**.
[260] I. L. Pykett, *Sci. Am.* **1982**, *246*, 78.
[261] G. M. Clore, A. M. Gronenborn, *Crit. Rev. Biochem. Mol. Biol.* **1989**, *24*, 479.
[262] W. von Philipsborn, R. Müller, *Angew. Chem. Int. Ed. Engl.* **1986**, *25*, 383.
[263] A. F. Holleman, E. Wiberg, N. Wiberg, *Lehrbuch der Anorganischen Chemie (102. Auflage)*, de Gruyter, Berlin, New York, **2007**.
[264] a) M. Ufnal, A. Zadlo, R. Ostaszewski, *Nutrition* **2015**, *31*, 1317; b) M. T. Velasquez, A. Ramezani, A. Manal, D. S. Raj, *Toxins* **2016**, *8*; c) S. H. Zeisel, M. Warrier, *Annu. Rev. Nutr.* **2017**.
[265] K. Beydoun, K. Thenert, E. S. Streng, S. Brosinski, W. Leitner, J. Klankermayer, *ChemCatChem* **2016**, *8*, 135.
[266] R. Adams, C. S. Marvel, *Org. Synth.* **1921**, *1*, 79.
[267] R. Frach, P. Kibies, S. Böttcher, T. Pongratz, S. Strohfeldt, S. Kurrmann, J. Koehler, M. Hofmann, W. Kremer, H. R. Kalbitzer *et al.*, *Angew. Chem. Int. Ed. Engl.* **2016**, *55*, 8757.
[268] H. R. Kalbitzer, I. C. Rosnizeck, C. E. Munte, S. P. Narayanan, V. Kropf, M. Spoerner, *Angew. Chem. Int. Ed. Engl.* **2013**, *52*, 14242.
[269] N. Kachel, W. Kremer, R. Zahn, H. R. Kalbitzer, *BMC Struct. Biol.* **2006**, *6*, 16.
[270] T. Kloss, J. Heil, S. M. Kast, *J. Phys. Chem. B* **2008**, *112*, 4337.
[271] R. Frach, S. M. Kast, *J. Phys. Chem. A* **2014**, *118*, 11620.
[272] H. Sato, H. Yoshioka, Y. Izumi, *J. Mol. Catal. A: Chem.* **1999**, *149*, 25.
[273] M. Rubina, M. Rubin, *Encyclopedia of Reagents for Organic Synthesis*. "N-Methylacetamide", **2001**, John Wiley & Sons, New York.
[274] O. Khersonsky, D. S. Tawfik, *Biochemistry* **2005**, *44*, 6371.
[275] T. Rosenau, A. Potthast, J. Röhrling, A. Hofinger, H. Sixta, P. Kosma, *Synth. Comm.* **2002**, *32*, 457.
[276] A. R. Bassindale, D. J. Parker, P. Patel, P. G. Taylor, *Tetrahedron Lett.* **2000**, *41*, 4933.
[277] Q. Xia, X. Liu, Y. Zhang, C. Chen, W. Chen, *Org. Lett.* **2013**, *15*, 3326.
[278] M. Reinhard Arnold, H. Robert Kalbitzer, W. Kremer, *J. Magn. Reson.* **2003**, *161*, 127.
[279] S. Hünig, *Arbeitsmethoden in der organischen Chemie (Zweite Auflage)*. *(mit Einführungspraktikum)*, Lehmanns Media, Berlin, **2008**.
[280] W. L. F. Armarego, C. L. L. Chai, *Purification of Laboratory Chemicals (Fifth Edition)*, Butterworth - Heinemann Elsevier, Amsterdam, **2003**.
[281] H.-S. Wu, S.-H. Jou, *J. Chem. Technol. Biotechnol.* **1995**, *64*, 325.
[282] a) D. E. Worrall, *Org. Synth.* **1929**, *9*, 66; b) P. Kreitmeier, "V. 5.9 - Synthese trans-β-Nitrostyrol", can be found under http://www-oc.chemie.uni-regensburg.de/img_/docs/LA_5_9_Nitrostyrol.pdf (checked 28.02.18), **2017**; c) A. K. Sinhababu, R. T. Borchardt, *J. Label. Compd. Radiopharm.* **1983**, *20*, 1027.
[283] Q. Tao, G. Tang, K. Lin, Y.-F. Zhao, *Chirality* **2008**, *20*, 833.

[284] M. Sathe, R. Ghorpade, M. P. Kaushik, *Chem. Lett.* **2006**, *35*, 1004.
[285] P. Süss, S. Illner, J. von Langermann, S. Borchert, U. T. Bornscheuer, R. Wardenga, U. Kragl, *Org. Process Res. Dev.* **2014**, *18*, 897.
[286] M. Penhoat, P. Bohn, G. Dupas, C. Papamicaël, F. Marsais, V. Levacher, *Tetrahedron: Asymmetry* **2006**, *17*, 281.
[287] R. Rasappan, O. Reiser, *Eur. J. Org. Chem.* **2009**, 1305.
[288] I. N. Naaarov, V. F. Kucherov, *Russ. Chem. Bull.* **1954**, *3*, 269.
[289] G. Molander, *Tetrahedron* **1997**, *53*, 8887.
[290] G. Göndös, L. Gera, G. Dombi, G. Bernáth, *Monatsh. Chem.* **1996**, *127*, 1167.
[291] G. Bernáth, L. Gera, G. Göndös, I. Pánovics, Z. Ecsery, *Acta. Chim. Acad. Sci. Hung.* **1976**, *89*, 61.
[292] a) A. J. Walker, WO2007063327 A1, **2007**; b) A. J. Pearson, Y. Yamamoto, *Encyclopedia of Reagents for Organic Synthesis*. "Trimethylamine *N*-Oxide", **2001**, John Wiley & Sons, New York.
[293] D. R. Morgan, H. C. Dorn, *J. Label. Compd. Radiopharm.* **1991**, *29*, 777.

G. Appendix

1. Tables

Table 7: Results of the Michael reactions using pyrrolidine (**42**) as catalyst.

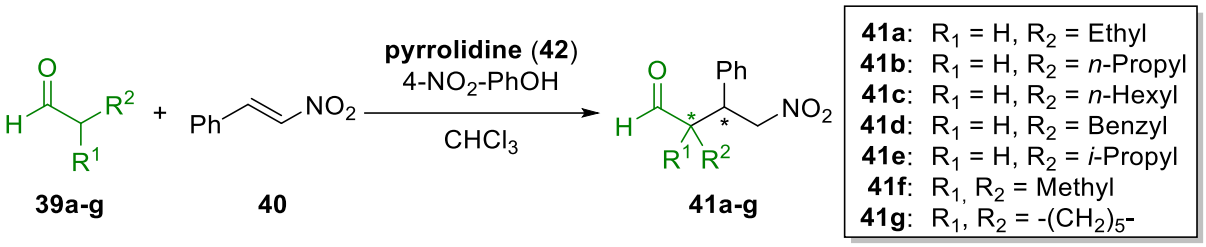

Entry	Substrate	Product	Catalyst loading [mol%]	Time [h]	Conditions	Conversion [%]	Yield [%]	*dr* (*syn*/*anti*)
1	**39a**	**41a**	-	45	AP/AT	7	0	n/a
					HT	11	0	
					HP	6	0	
2	**39a**	**41a**	1	1	AP/AT	59	52	2.8:1
					HT	100	95	1.4:1
					HP	100	95	8.1:1
3	**39b**	**41b**	1	1	AP/AT	56	49	2.6:1
					HT	63	57	1.3:1
					HP	89	80	4.3:1
4	**39c**	**41c**	1	1	AP/AT	41	37	4.9:1
					HT	100	95	1.8:1
					HP	100	99	11.5:1
5	**39d**	**41d**	1	1	AP/AT	61	60	4.0:1
					HT	44	42	1.9:1
					HP	42	93	5.7:1
6	**39e**	**41e**	2.5	1	AP/AT	44	35	11.5:1
					HT	69	65	4.3:1
					HP	100	95	24.0:1
7	**39f**	**41f**	10	4	AP/AT	26	12	n/a
					HT	47	30	
					HP	85	67	
8	**39g**	**41g**	10	4	AP/AT	18	0	n/a
					HT	44	26	
					HP	46	31	

Conditions: 1.00 mmol trans-β-nitrostyrene (**40**), 4 equiv. aldehyde (**39a-g**), 4-NO_2-PhOH equimolar to catalyst, 2 mL solvent. Conversion, yield and *dr* determined by NMR using 1.00 mmol diphenoxymethane (**46**) as internal standard.

Table 8: Results of the Michael reactions using the Jørgensen-Hayashi catalyst (**28**).

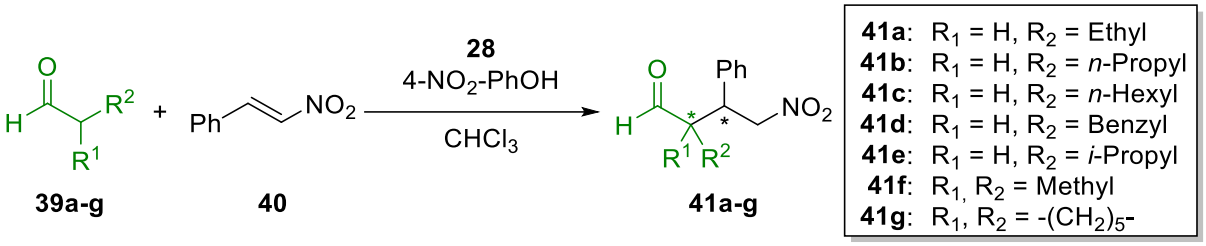

Entry	Substrate	Product	Catalyst loading [mol%]	Time [h]	Conditions	Conversion [%]	Yield [%]	*dr* (*syn*/*anti*)	*ee* [%]
1	**39a**	**41a**	1	1	AP/AT	40	35	13.3:1	99
					HT	21	14	4.6:1	97
					HP	43	38	15.7:1	98
2	**39b**	**41b**	1	1	AP/AT	18	12	11.5:1	99
					HT	12	9	5.7:1	95
					HP	28	23	15.7:1	99
3	**39c**	**41c**	1	1	AP/AT	44	44	24.0:1	99
					HT	50	45	7.3:1	98
					HP	58	55	24.0:1	99
4	**39d**	**41d**	2.5	1	AP/AT	19	18	9.0:1	93
					HT	16	14	3.0:1	93
					HP	59	54	24.0:1	95
5	**39e**	**41e**	2.5	1	AP/AT	15	10	11.5:1	99
					HT	18	11	4.3:1	99
					HP	71	65	32.3:1	99
6	**39f**	**41f**	10	4	AP/AT	30	24		39
					HT	84	74	n/a	12
					HP	100	78		78
7	**39g**	**41g**	10	4	AP/AT	8	2		n.d.
					HT	9	2	n/a	n.d.
					HP	30	18		64

Conditions: 1.00 mmol trans-β-nitrostyrene (**40**), 4 equiv. aldehyde (**39a-g**), 4-NO_2-PhOH equimolar to catalyst, 2 mL solvent. Conversion, yield and *dr* determined by NMR using 1.00 mmol diphenoxymethane (**46**) as internal standard, *ee* determined by chiral HPLC.

Table 9: Examination of the hydrolytic stability of the 4*H*-3,1-benzoxazin-4-one **83**.

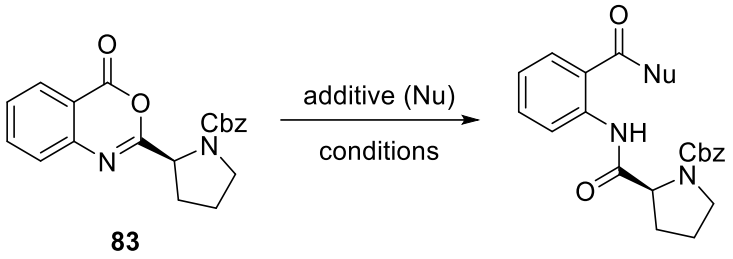

83

Entry	Solvent	Additive (Nu)	Result	Time
1	$CHCl_3$	-	partial hydrolysis	> 24 h
2	$CHCl_3$	solvent filtered over basic Al_2O_3	no change	> 24 h
3	$CHCl_3$	EtOH (dry)	no change	30 min
4	$CHCl_3$	EtOH (dry) + AcOH	partial hydrolysis	> 24 h
5[a)]	$CHCl_3$	pyrrolidine (**42**)	**90** (100%)	45 min
6[b)]	$CHCl_3$	JH catalyst (**28**)	no change	> 72 h
7	acetone	6 M HCl(aq)	complete hydrolysis	5 min
8	acetone	1 M NaOH(aq)	complete hydrolysis	15 min
9	MeOH	6 M HCl(aq)	complete hydrolysis	5 min
10	MeOH	NaOH(s)	complete hydrolysis	45 min
11[c)]	MeOH	Pd/C, H_2 (50 bar)	complex mixture	20 h

Reaction conditions: 10 mg of **83**, 0.5 mL solvent. One drop of additive (30 - 60 µL) for liquids, 30 mg for solids. All reactions carried out at room temperature. a) **83** (100 mg, 286 µmol), **42** (30 µL, 337 µmol, 1.2 equiv.), 1 mL $CHCl_3$; b) **83** (11 mg, 32 µmol), 2.5 mL 12.5 µM **28** in $CHCl_3$ (1.0 equiv.); c) **83** (114 mg, 325 µmol), 50 mg Pd/C, 1 mL MeOH. Hydrolysis leads to formation of **79**.

Table 10: Solvent Screening of the tripeptide-catalyzed aldol reaction.

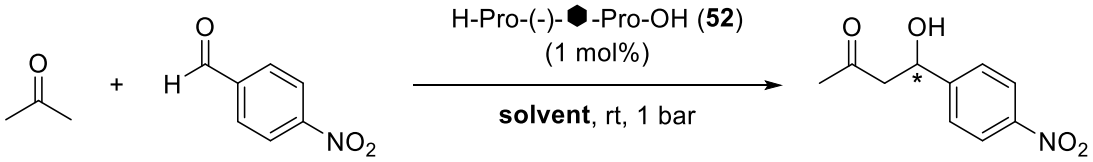

34 **92** **93**

Entry[a)]	solvent (v/v)	24 h		48 h	
		Conversion [%]	Yield [%]	Conversion [%]	Yield [%]
1	Acetone/H_2O (3:1)	44	36	68	52
2	Acetone/H_2O (5:1)	69	58	91	80
3	Acetone/H_2O (10:1)	74	62	95	84
4	Acetone/H_2O (100:1)	73	66	94	78
5	Acetone/H_2O (1000:1)	41	25	46	30
6	Acetone	27	12	30	19
7	$CHCl_3$	28	14	38	23
8	$CHCl_3$/*i*-PrOH (9:1)	14	4	18	7
9	$CHCl_3$/*i*-PrOH (1:1)	13	2	14	3
10	$CHCl_3$/*i*-PrOH (1:9)	11	1	11	1
11	*i*-PrOH	11	1	11	1

Reaction conditions: 1.00 mmol 4-Nitrobenzaldehyde (**92**), 10 equiv. acetone (**34**) (if not present as solvent), 2 mL solvent. a) Conversion and yield determined by NMR using diphenoxymethane (**46**) as internal standard.

2. NMR spectra

^{1}H NMR spectra upper image

^{13}C NMR spectra lower image

Frequency, solvent and temperature (if not ambient) are noted at the top of the spectra.

(2*S*)-2-[Diphenyl[(trimethylsilyl)oxy]methyl]pyrrolidine (28)

^{1}H NMR (300 MHz, $CDCl_3$)

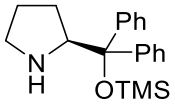

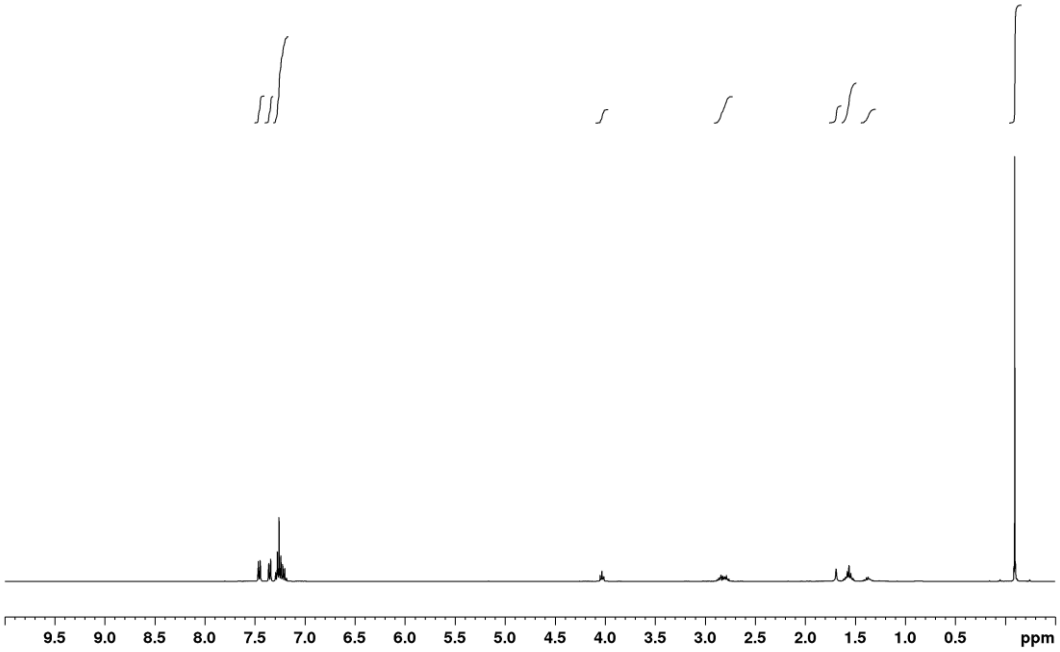

^{13}C NMR (75 MHz, $CDCl_3$)

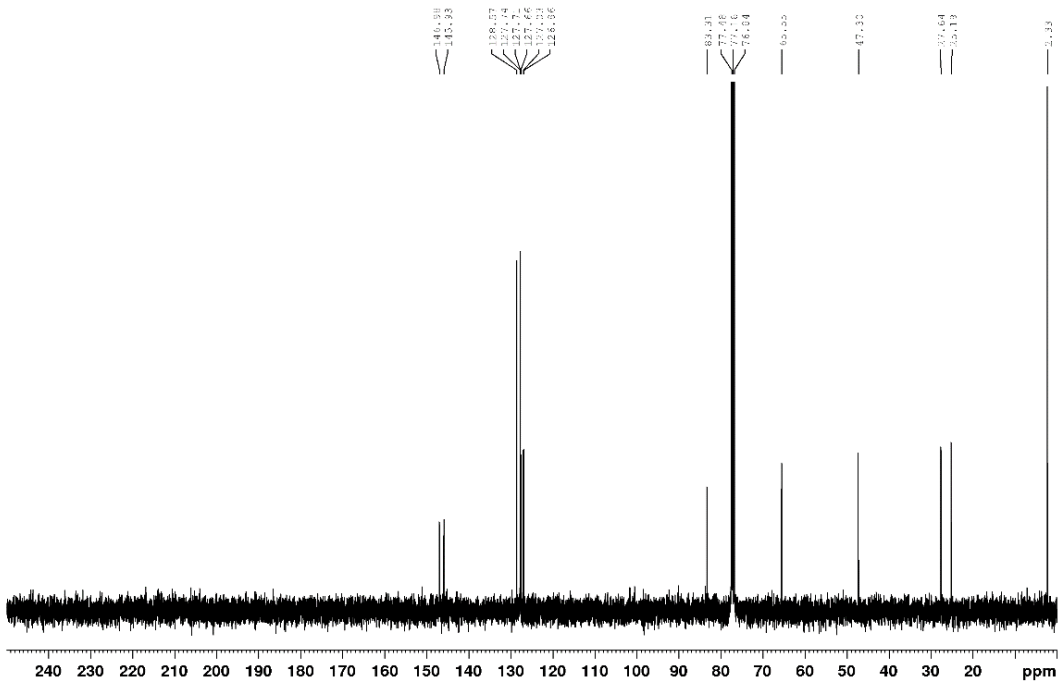

***trans*-β-Nitrostyrene (40)**

^{1}H NMR (300 MHz, $CDCl_3$)

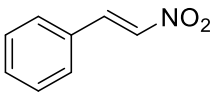

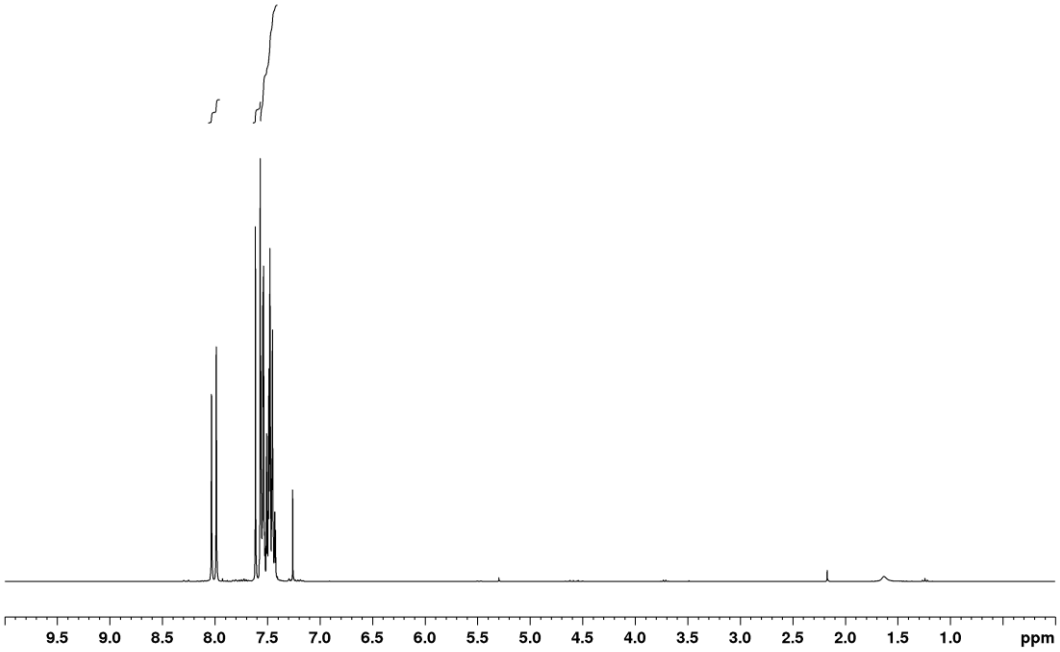

^{13}C NMR (75 MHz, $CDCl_3$)

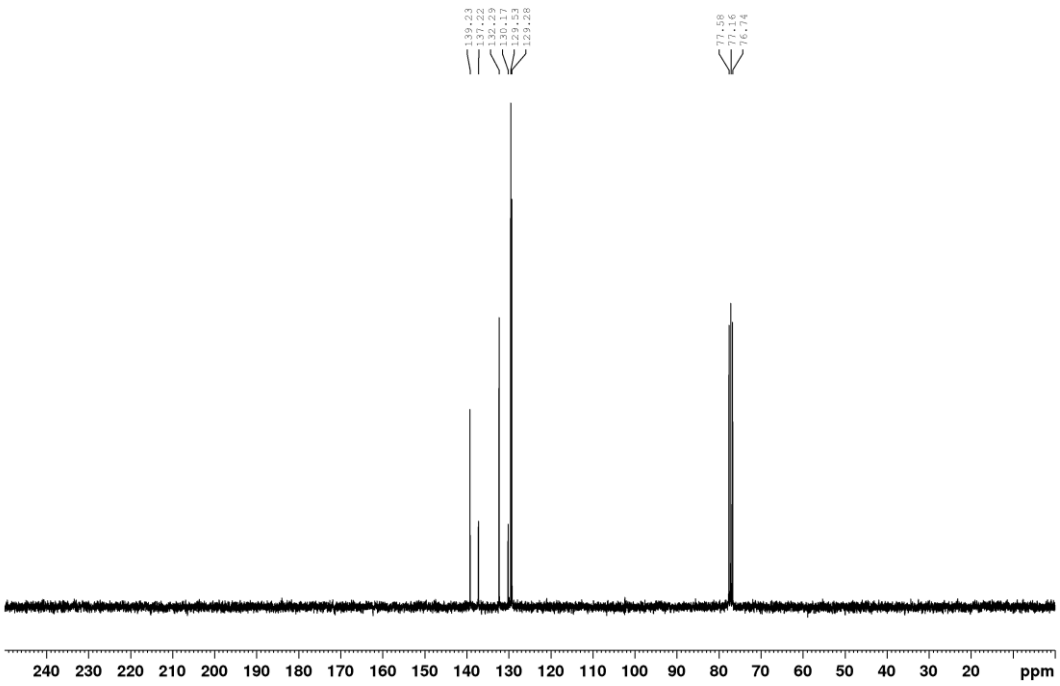

(2*R*,3*S*)-2-Ethyl-4-nitro-3-phenylbutanal (41a)

^{1}H NMR (400 MHz, $CDCl_3$) (*syn*/*anti* = 1.7:1.0)

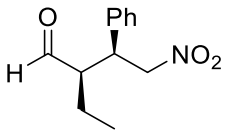

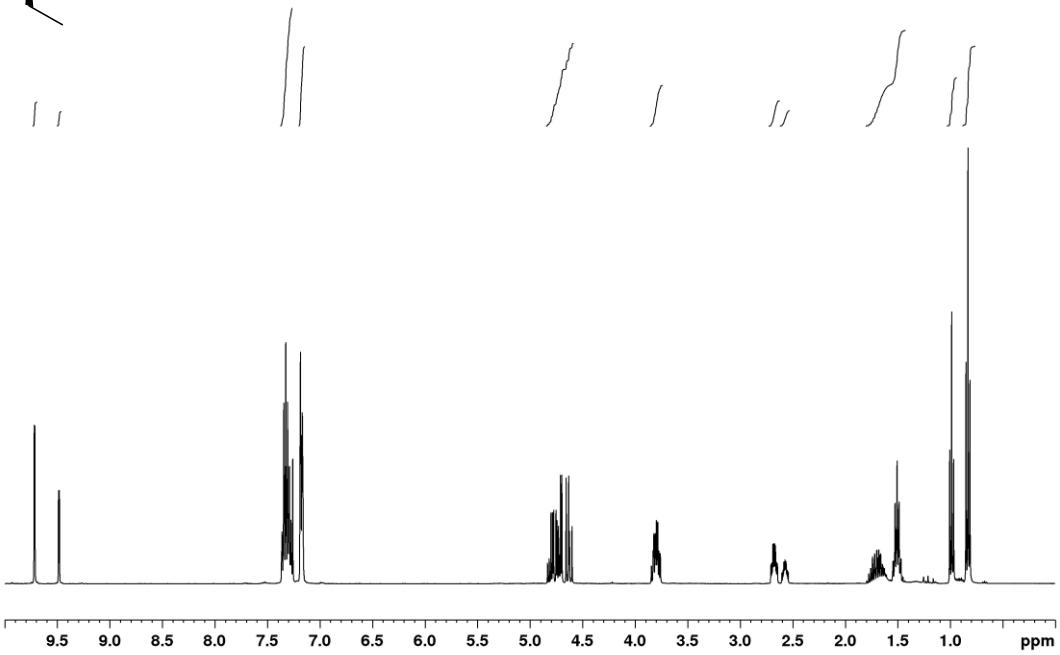

^{13}C NMR (101 MHz, $CDCl_3$)

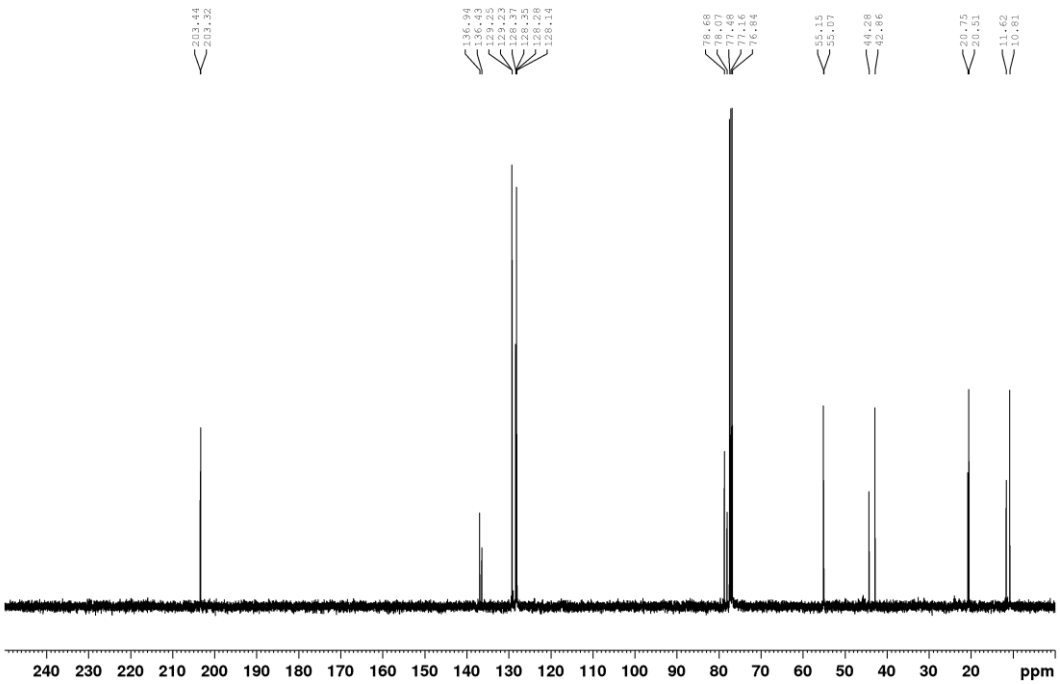

(*R*)-2-((*S*)-2-Nitro-1-phenylethyl)pentanal (41b)

^{1}H NMR (400 MHz, $CDCl_3$) (*syn*/*anti* = 1.5:1.0)

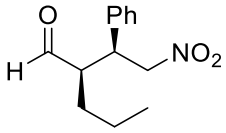

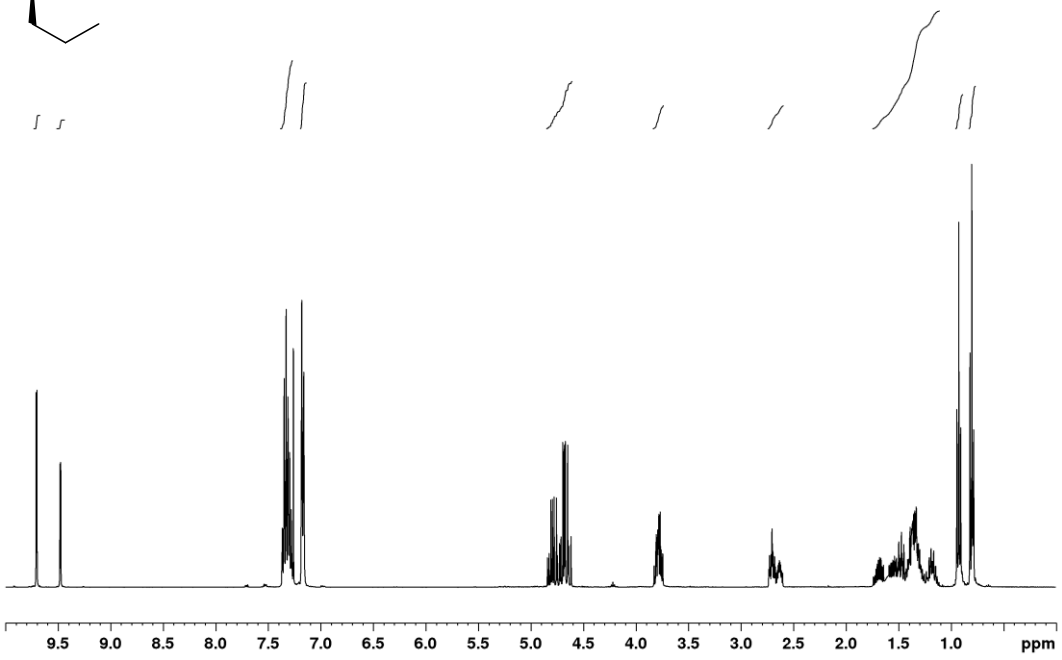

^{13}C NMR (101 MHz, $CDCl_3$)

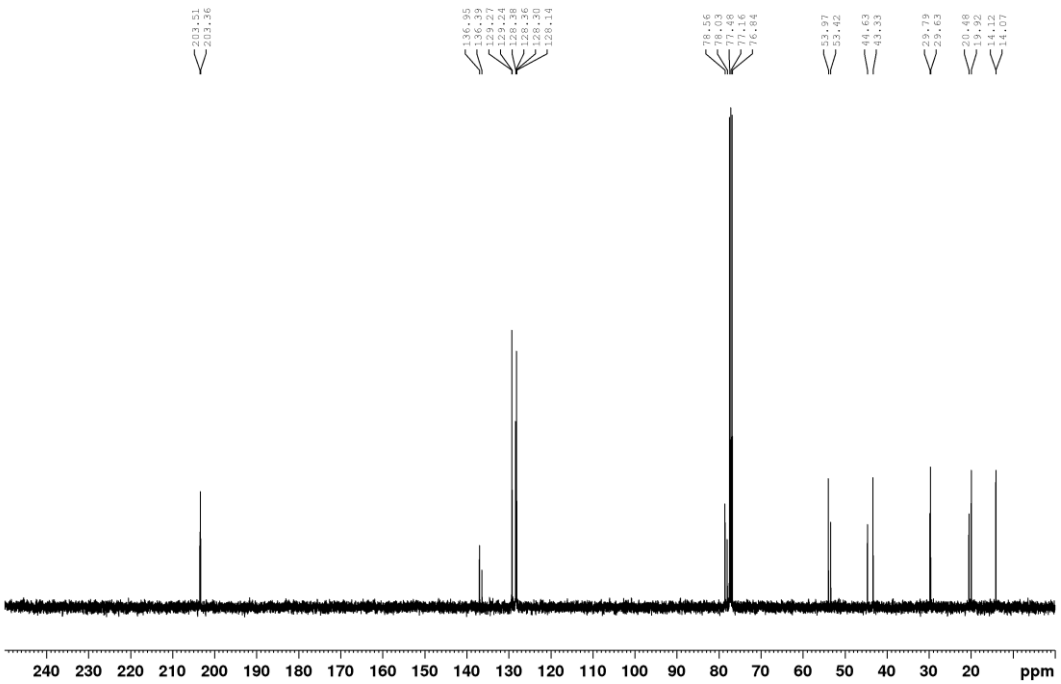

(*R*)-2-((*S*)-2-Nitro-1-phenylethyl)octanal (41c)

^{1}H NMR (400 MHz, $CDCl_3$) (*syn*/*anti* = 51.3:1.0)

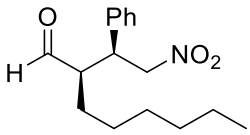

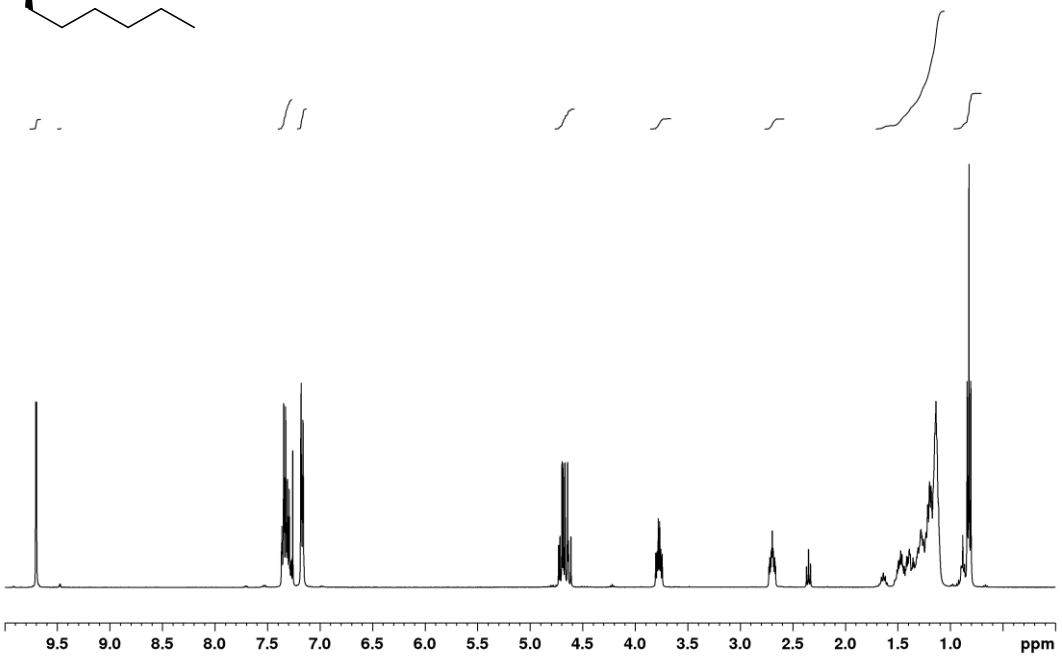

^{13}C NMR (101 MHz, $CDCl_3$)

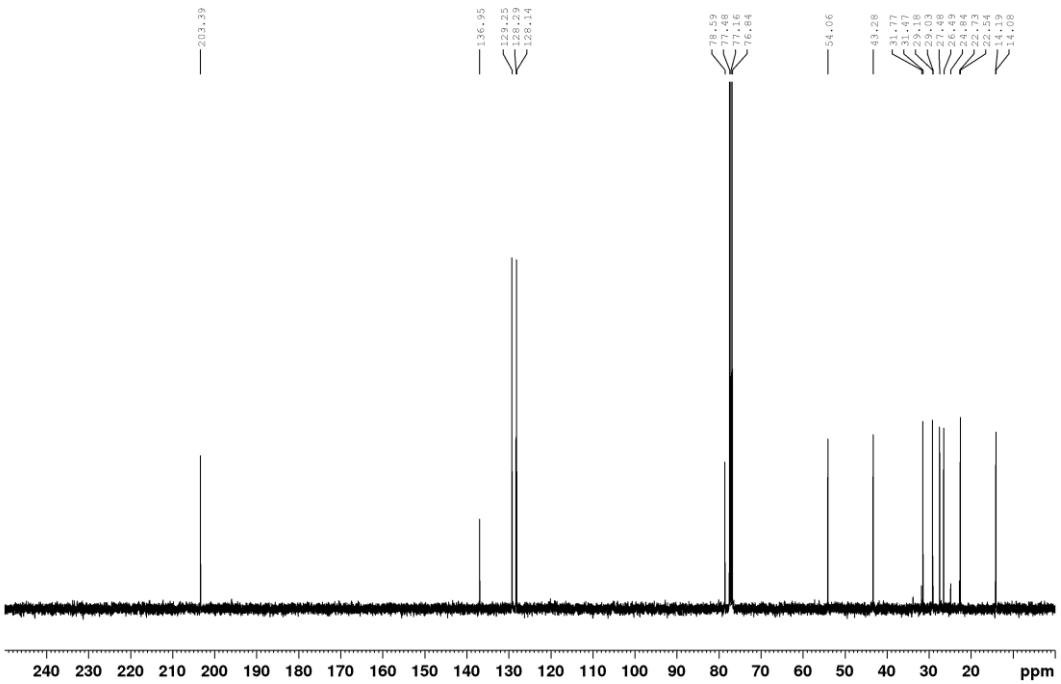

(2*R*,3*S*)-2-Isopropyl-4-nitro-3-phenylbutanal (41e)

^{1}H NMR (400 MHz, $CDCl_3$) (*syn*/*anti* = 2.5:1.0)

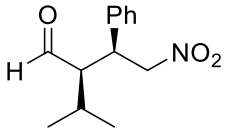

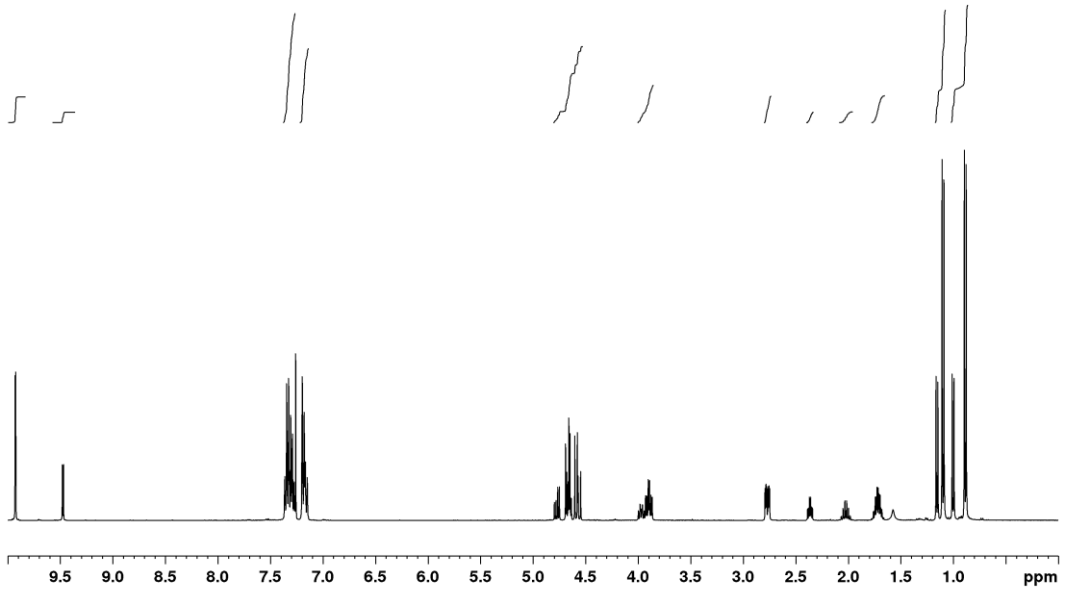

^{13}C NMR (101 MHz, $CDCl_3$)

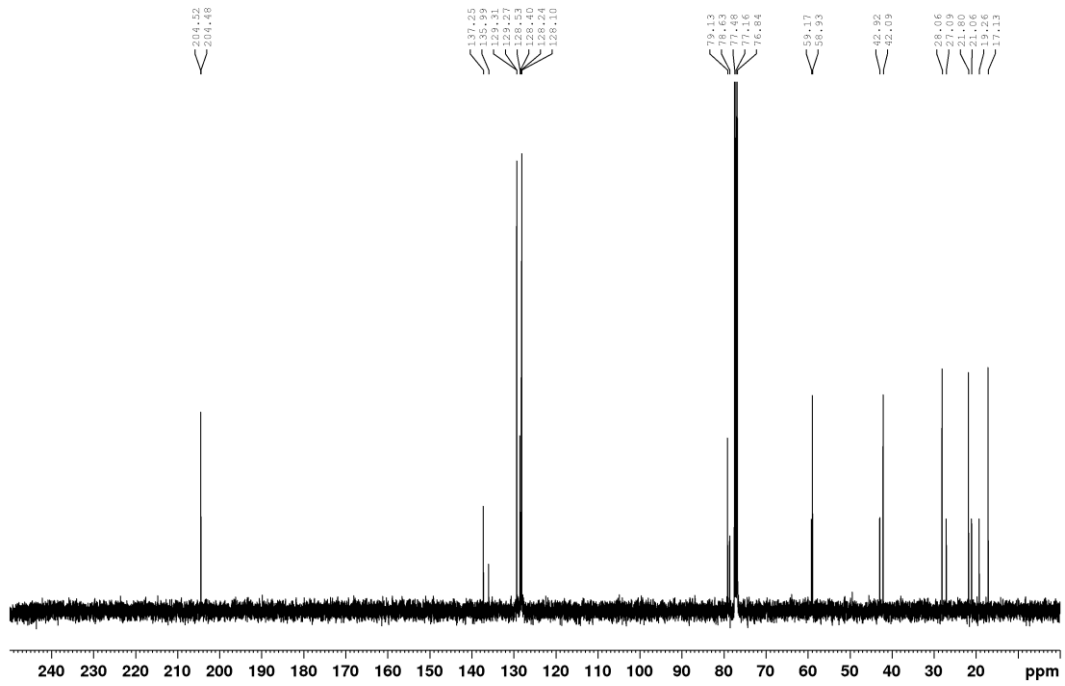

(*R*)-2,2-Dimethyl-4-nitro-3-phenylbutanal (41f)

^{1}H NMR (400 MHz, $CDCl_3$)

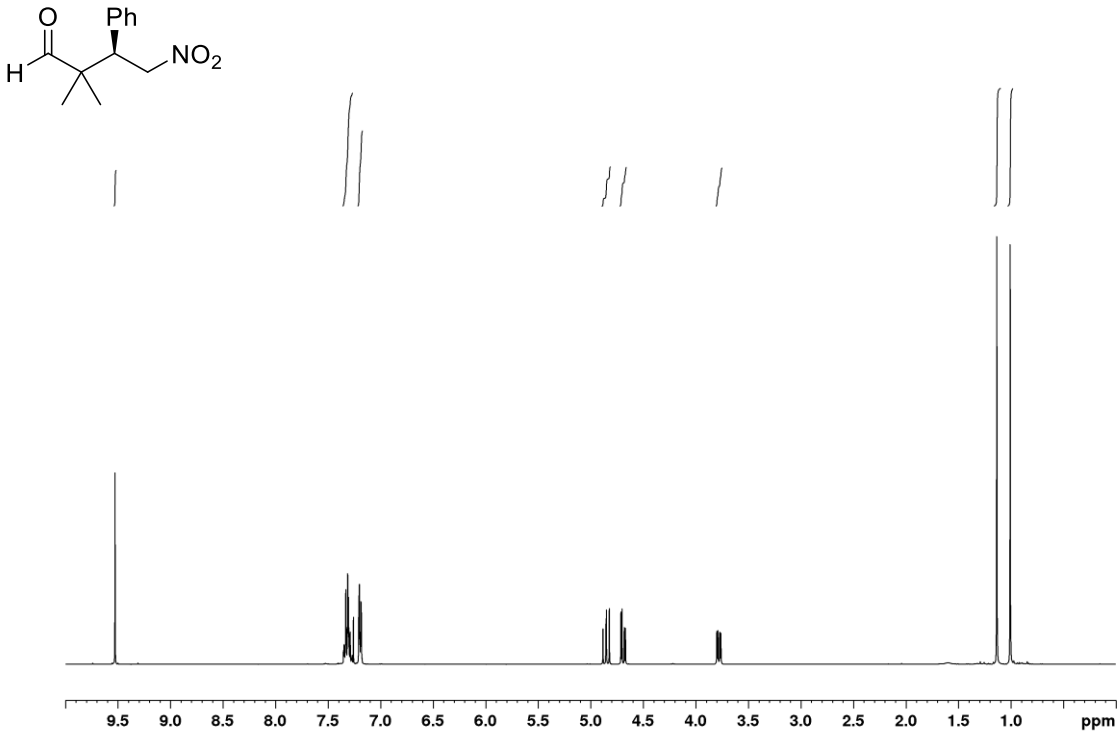

^{13}C NMR (101 MHz, $CDCl_3$)

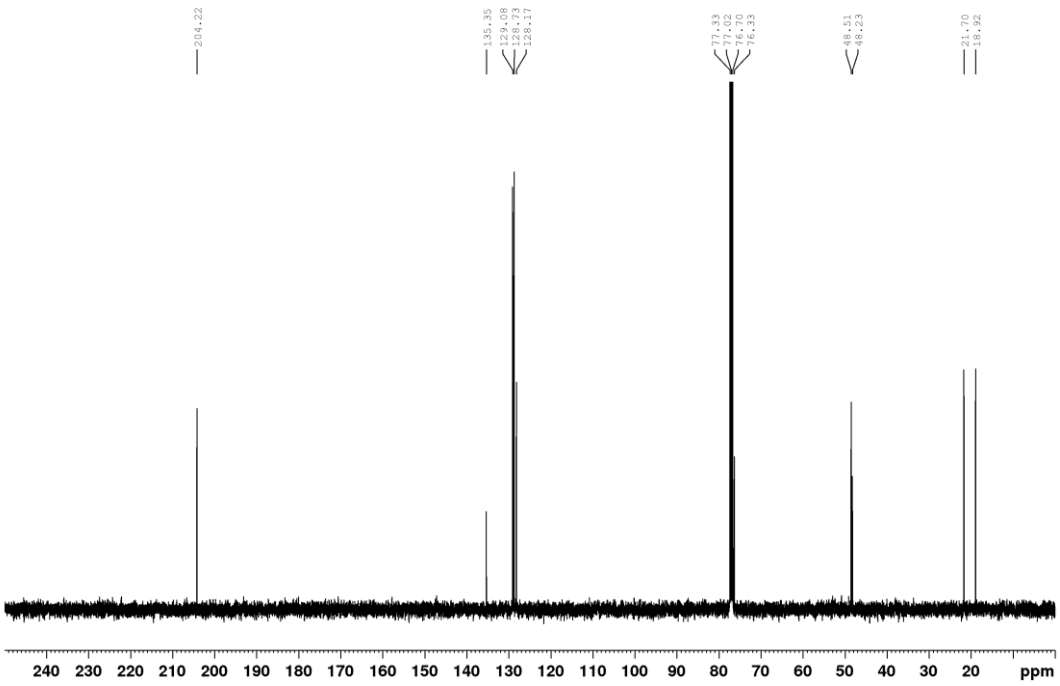

(*R*)-1-(2-Nitro-1-phenylethyl)cyclohexane-1-carbaldehyde (41g)

^{1}H NMR (400 MHz, $CDCl_3$)

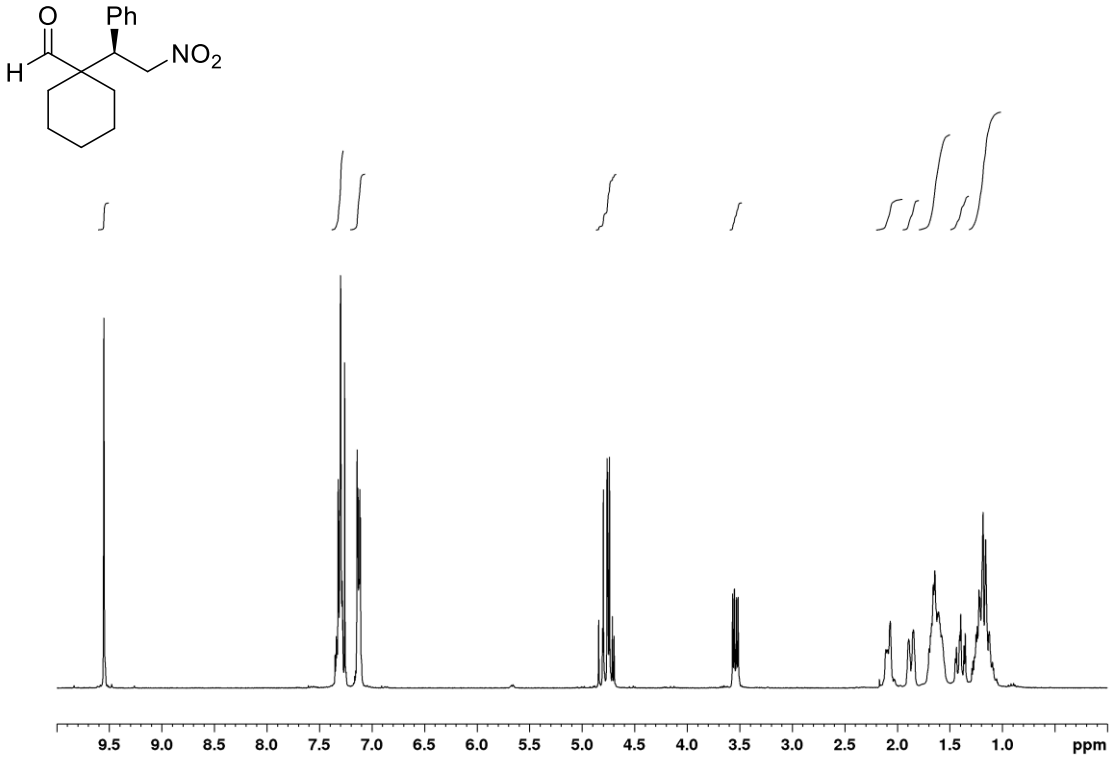

^{13}C NMR (101 MHz, $CDCl_3$)

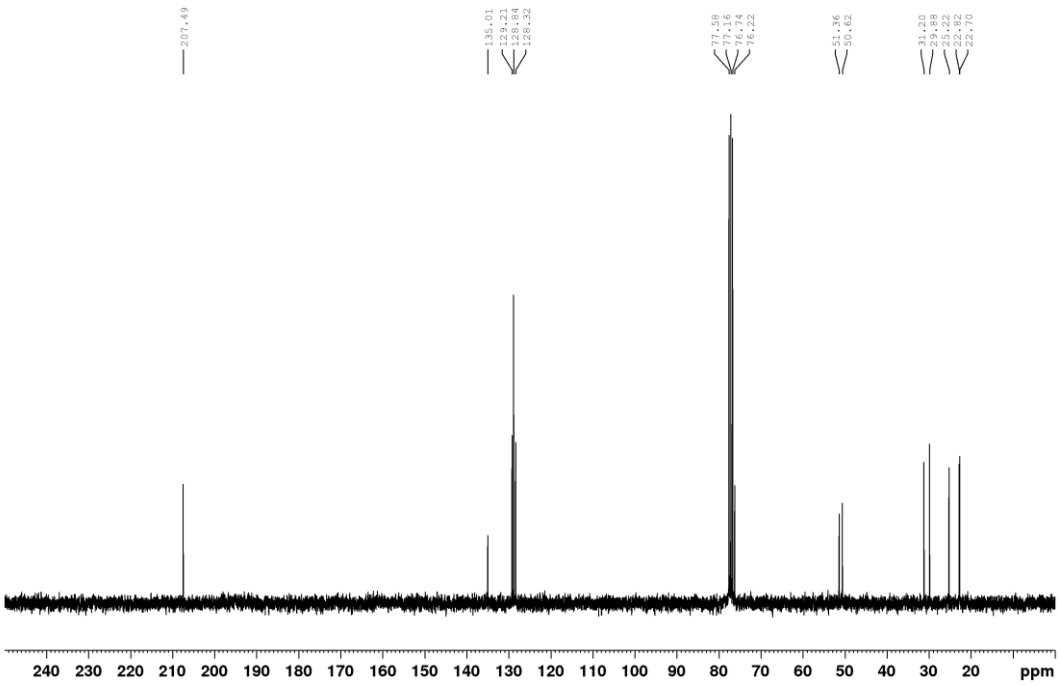

***N*-Ethoxycarbonyl-L-proline methyl ester (43)**

^{1}H NMR (300 MHz, $CDCl_3$)

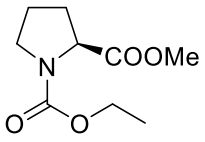

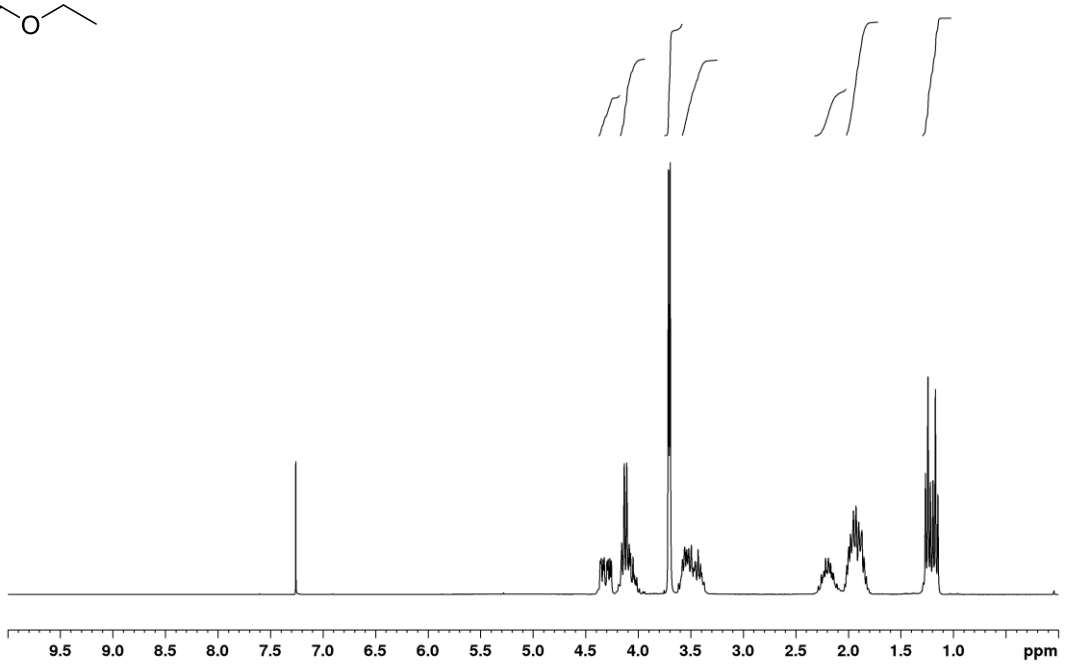

^{13}C NMR (75 MHz, $CDCl_3$)

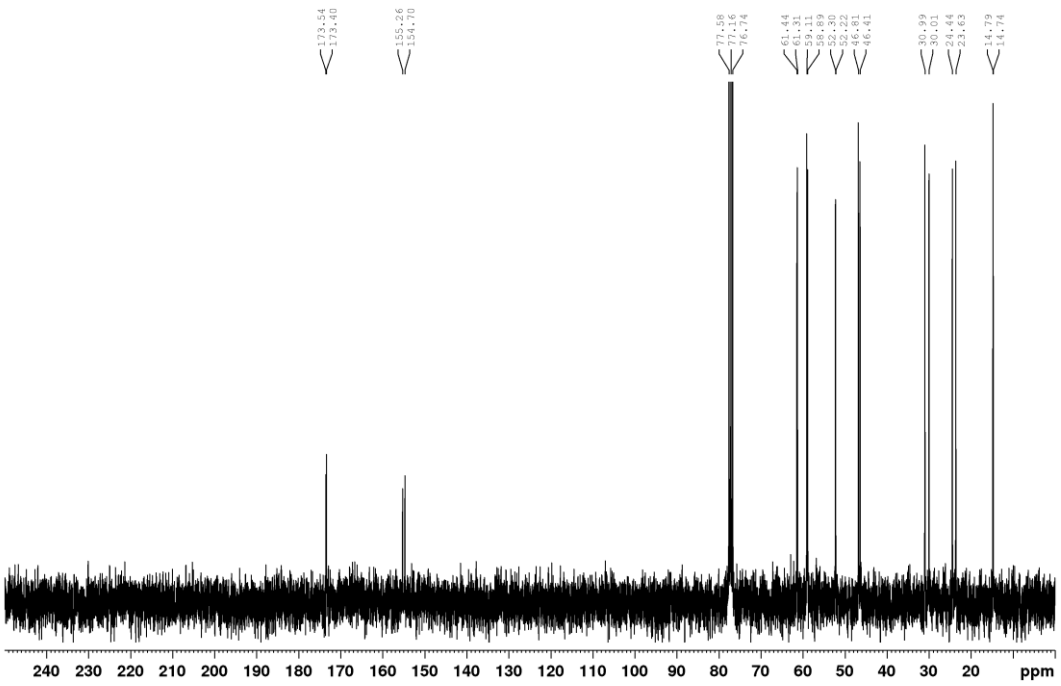

(2*R*)-α,α-Diphenyl-2-pyrrolidinemethanol (44)

^{1}H NMR (300 MHz, $CDCl_3$)

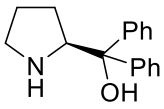

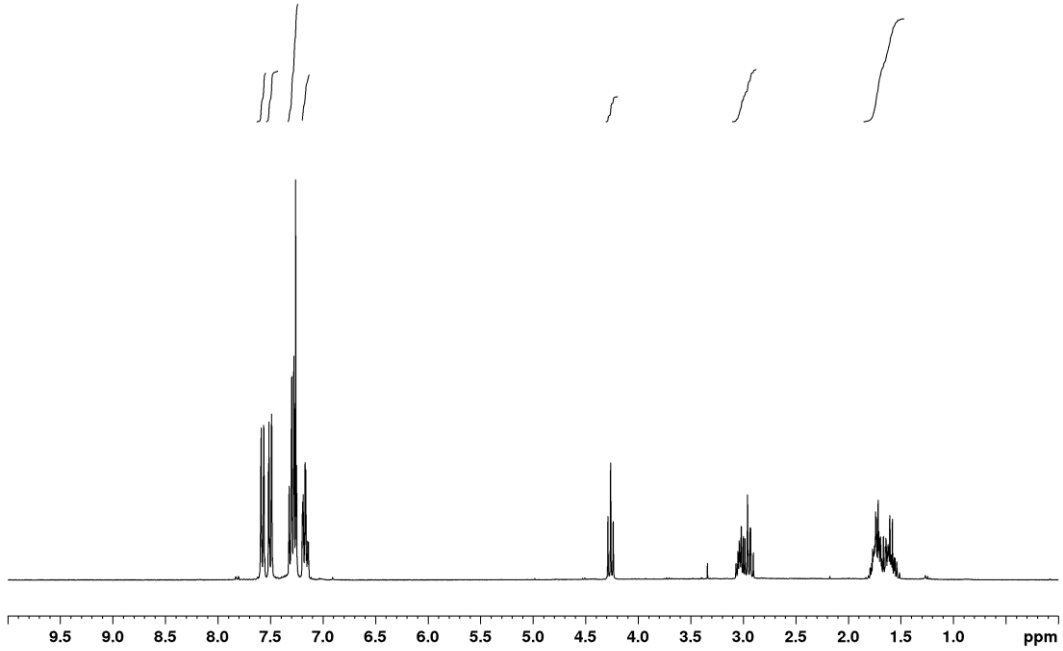

^{13}C NMR (75 MHz, $CDCl_3$)

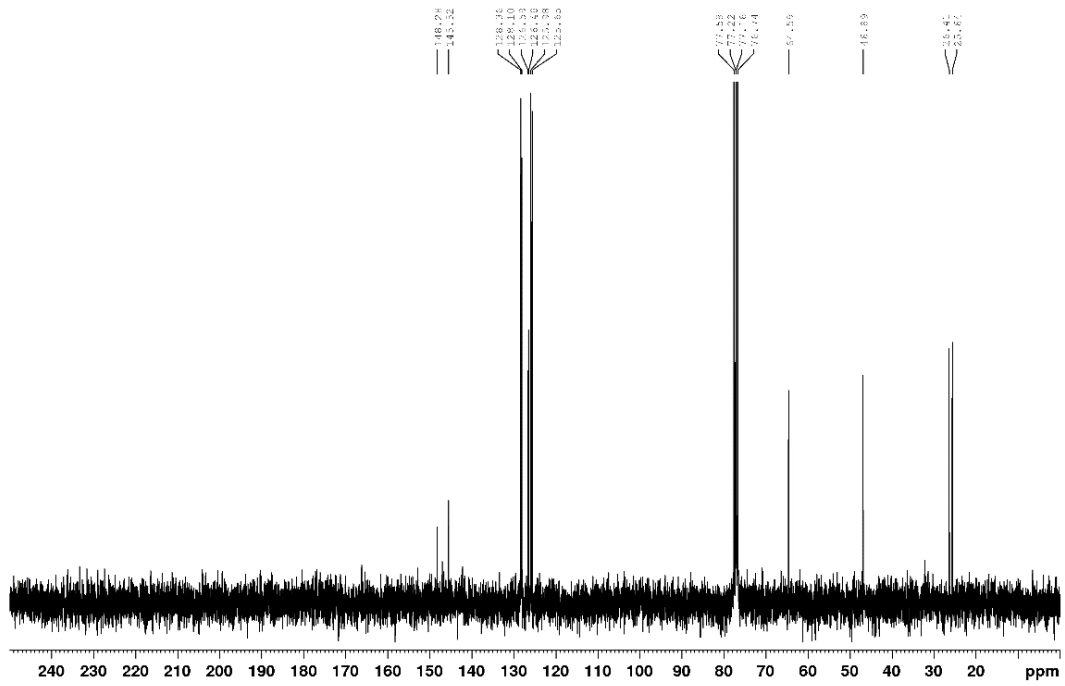

Diphenoxymethane (46)

^{1}H NMR (300 MHz, $CDCl_3$)

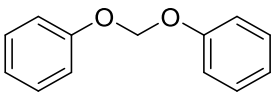

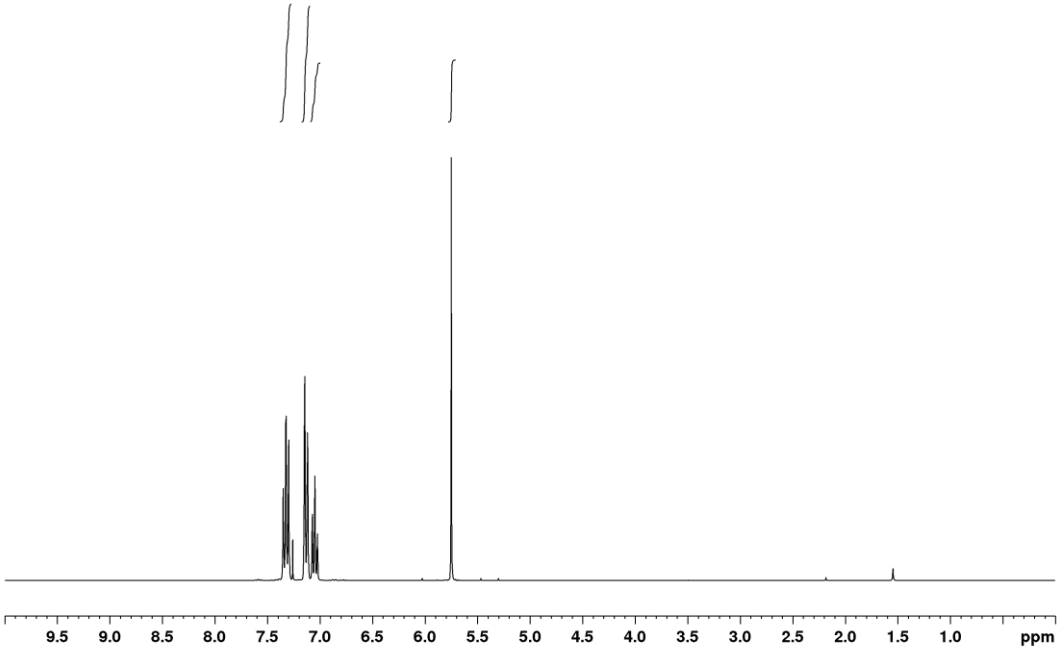

^{13}C NMR (75 MHz, $CDCl_3$)

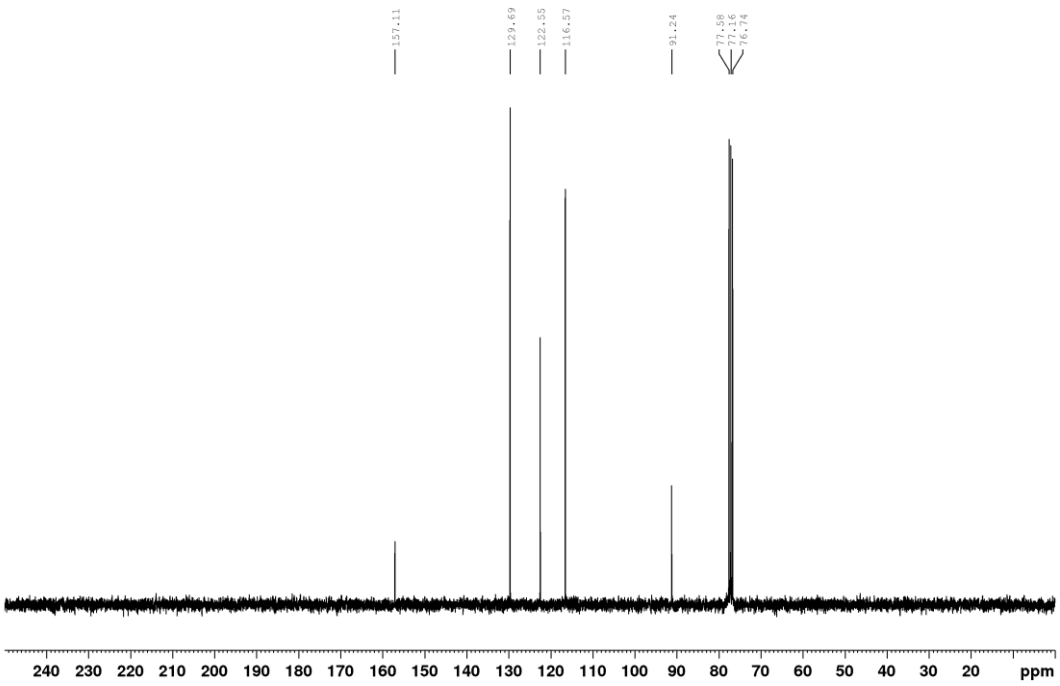

H-Pro-(-)-⬢-Pro-OH (52)

^{1}H NMR (400 MHz, $CDCl_3$, 300 K)

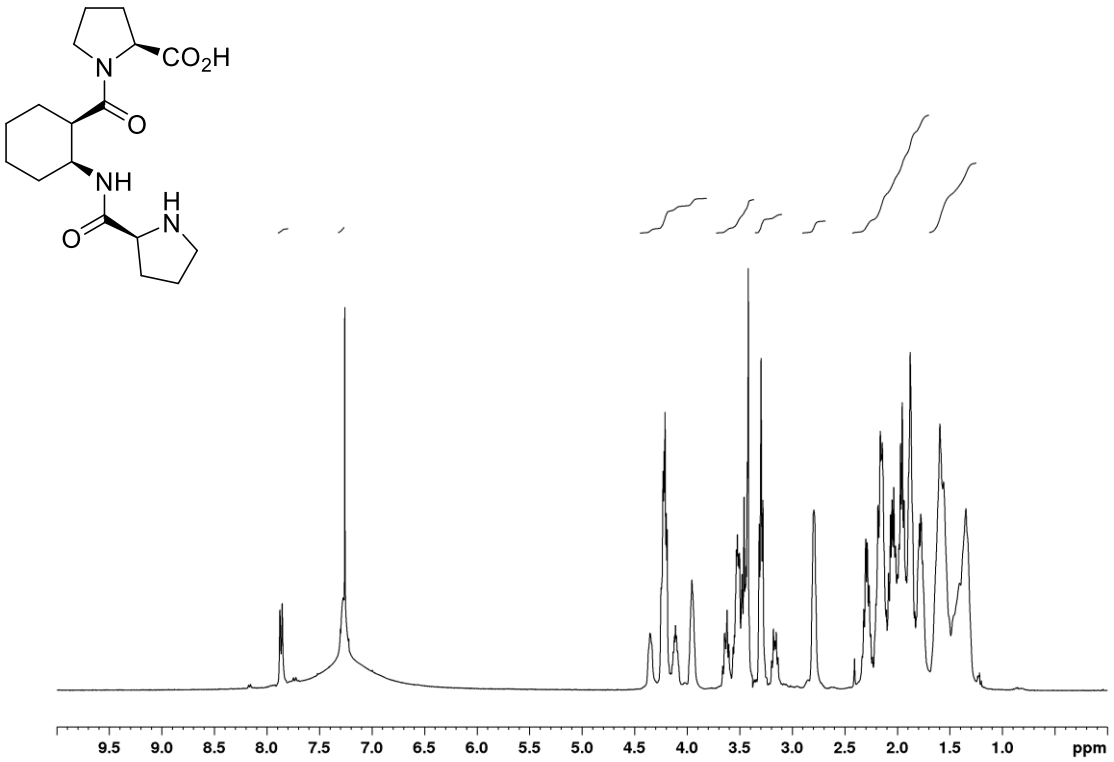

^{13}C NMR (101 MHz, $CDCl_3$)

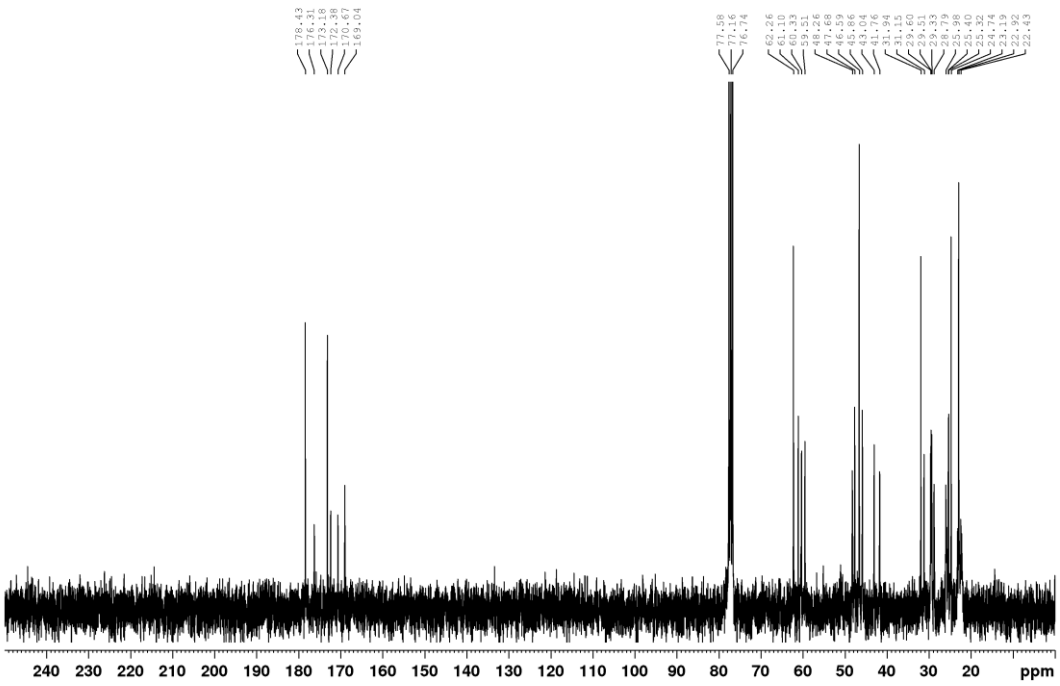

H-Pro-(+)-⬢-Pro-OH (*ent*-52)

^{1}H NMR (400 MHz, $CDCl_3$)

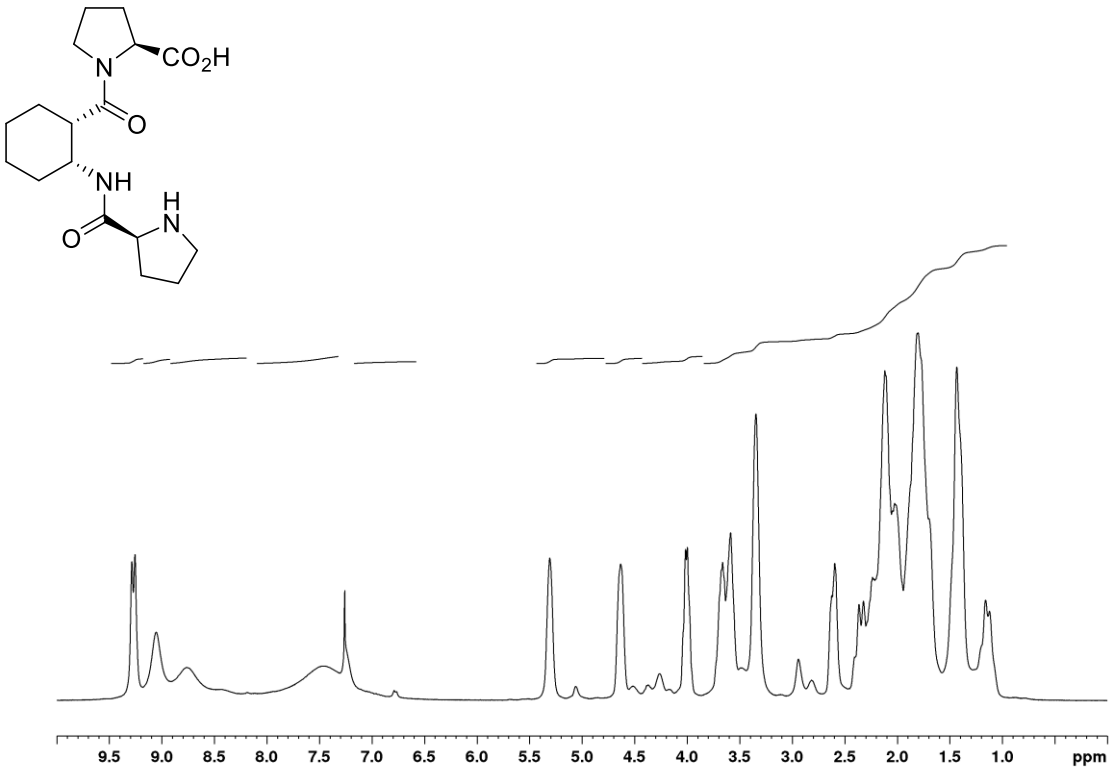

^{13}C NMR (101 MHz, $CDCl_3$)

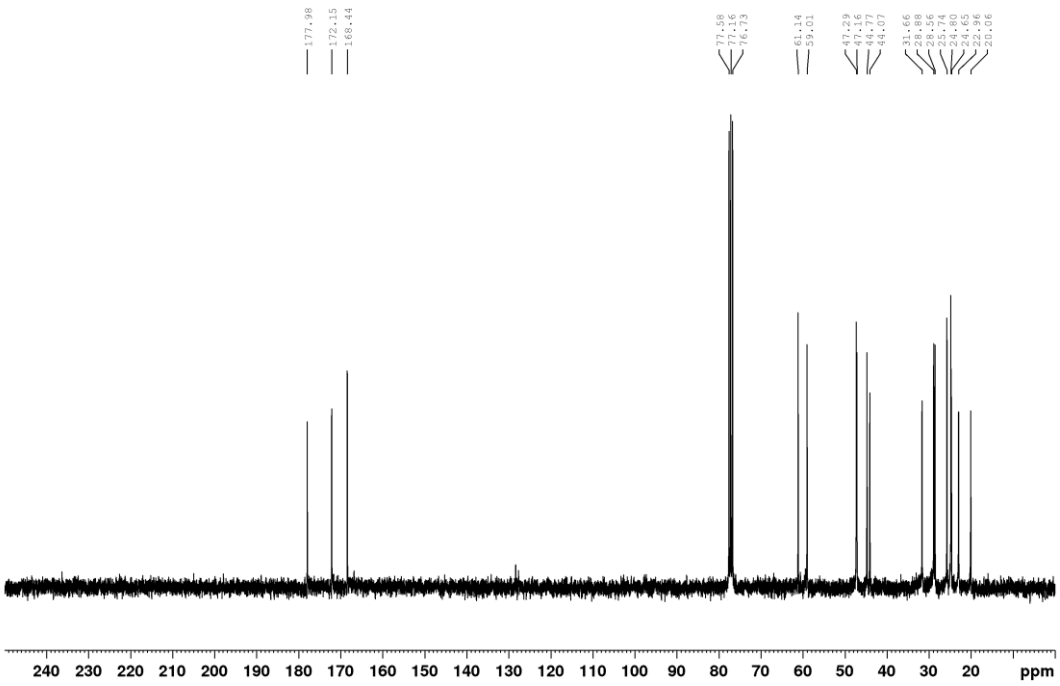

H-Pro-Ant-Pro-OH (53)

^{1}H NMR (300 MHz, $CDCl_3$)

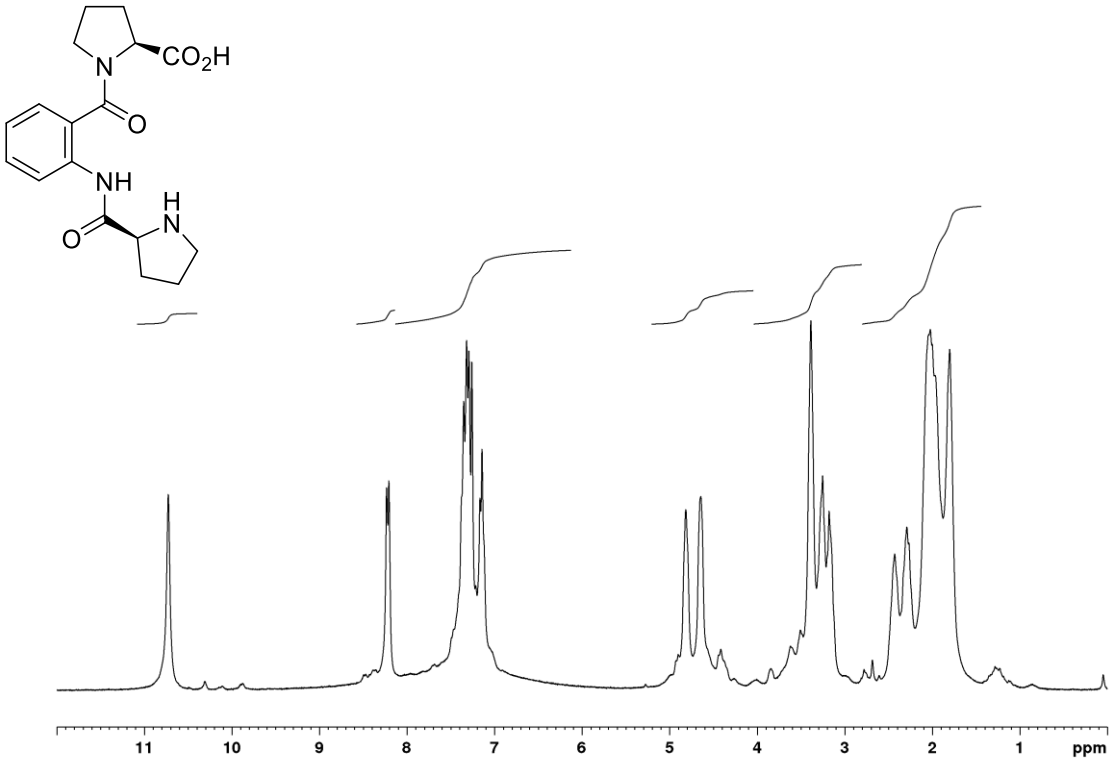

^{13}C NMR (75 MHz, $CDCl_3$)

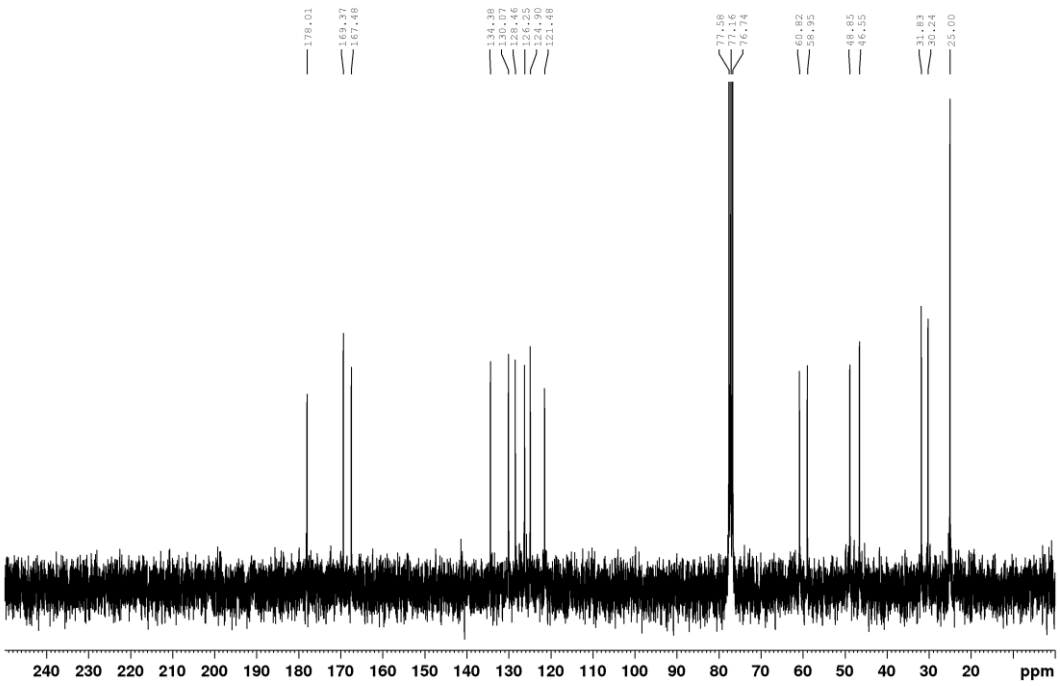

***cis*-4-Cyclohexene-1,2-dicarboxylic acid anhydride (*cis*-56)**

^{1}H NMR (300 MHz, $CDCl_3$)

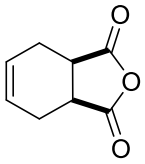

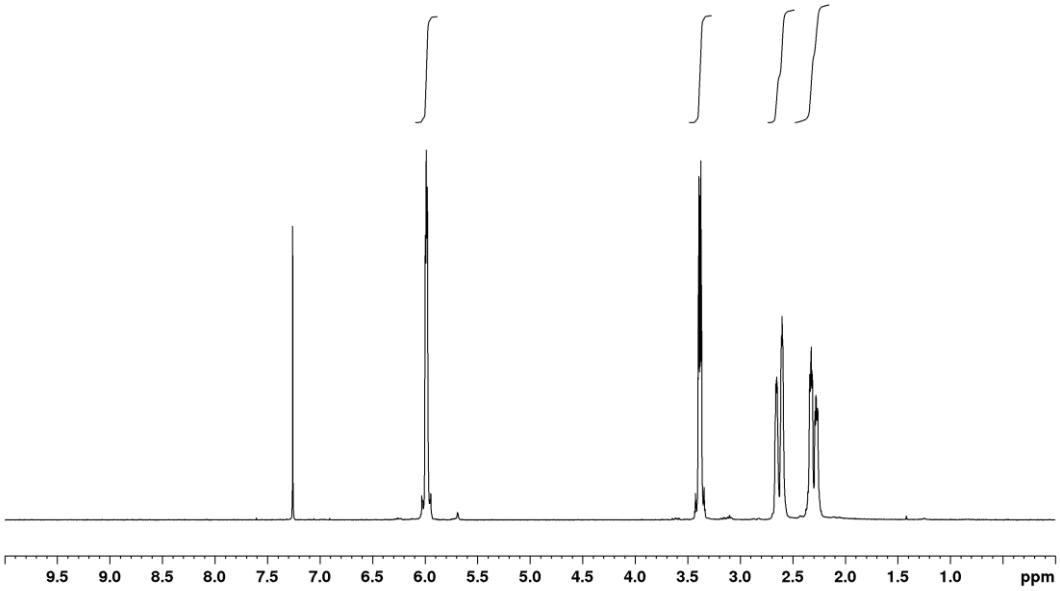

^{13}C NMR (75 MHz, $CDCl_3$)

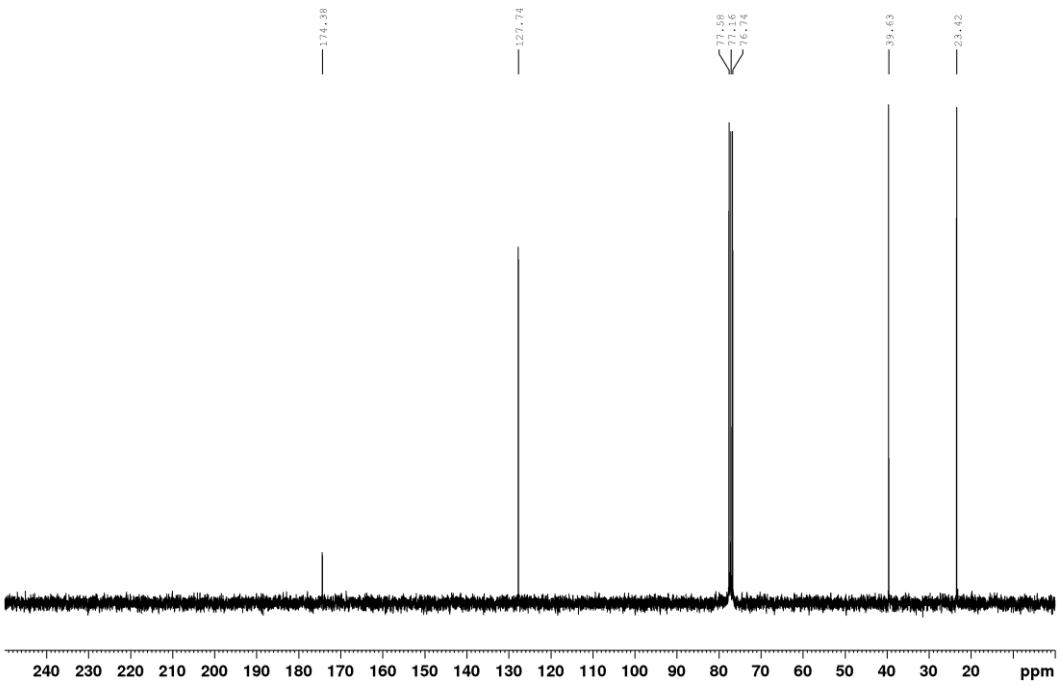

***trans*-4-Cyclohexene-1,2-dicarboxylic acid anhydride (*trans*-56)**

^{1}H NMR (300 MHz, $CDCl_3$)

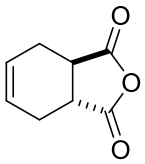

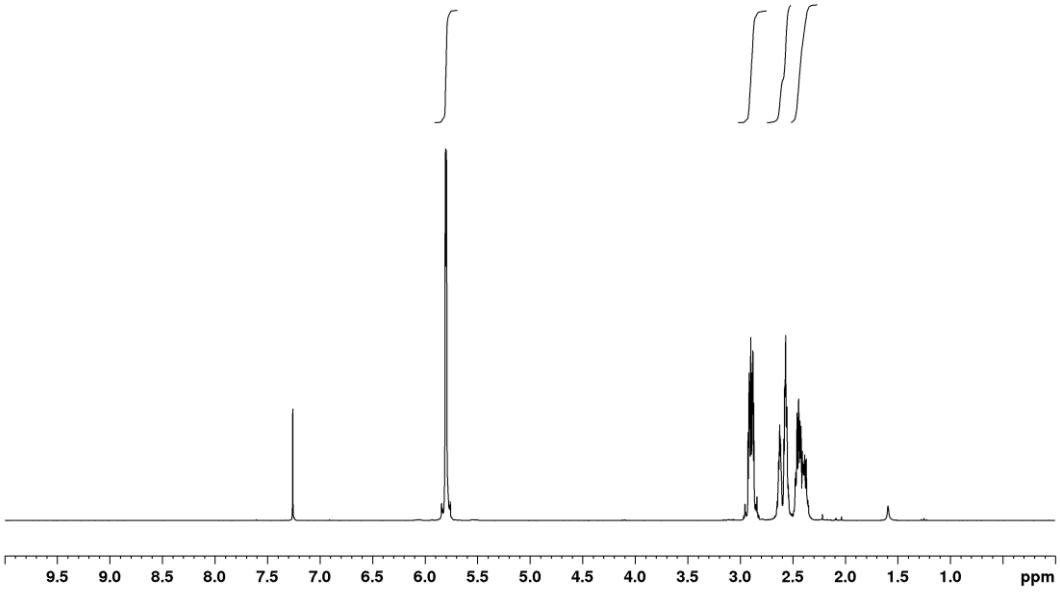

^{13}C NMR (75 MHz, $CDCl_3$)

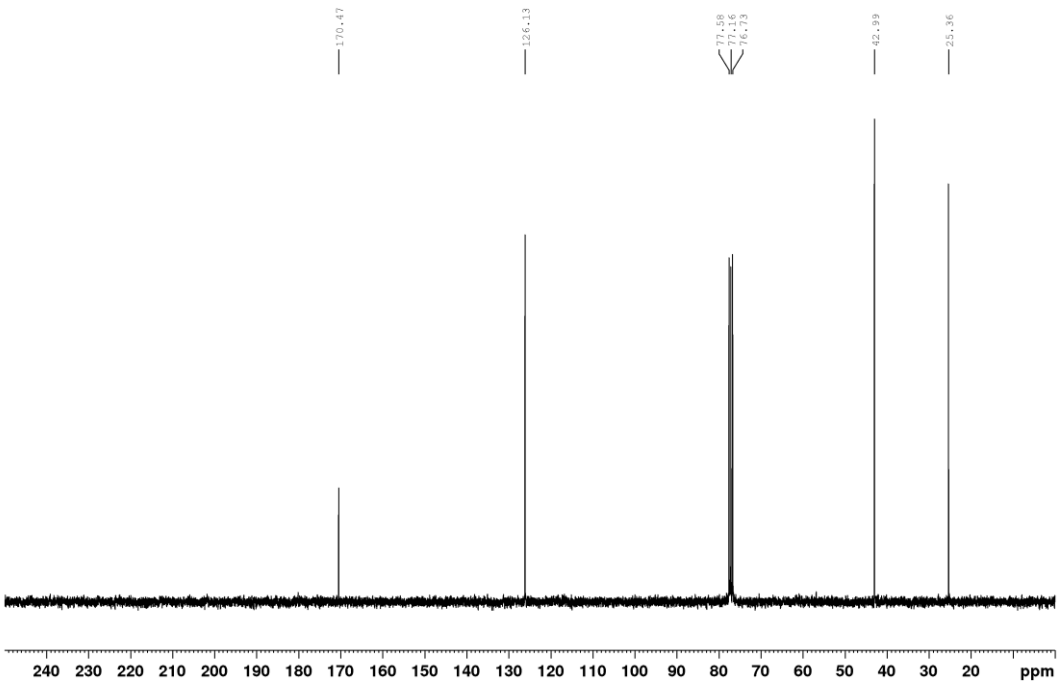

***cis*-2-Methoxycarbonyl-4-cyclohexene-1-carboxylic acid (*cis*-63)**

^{1}H NMR (300 MHz, $CDCl_3$)

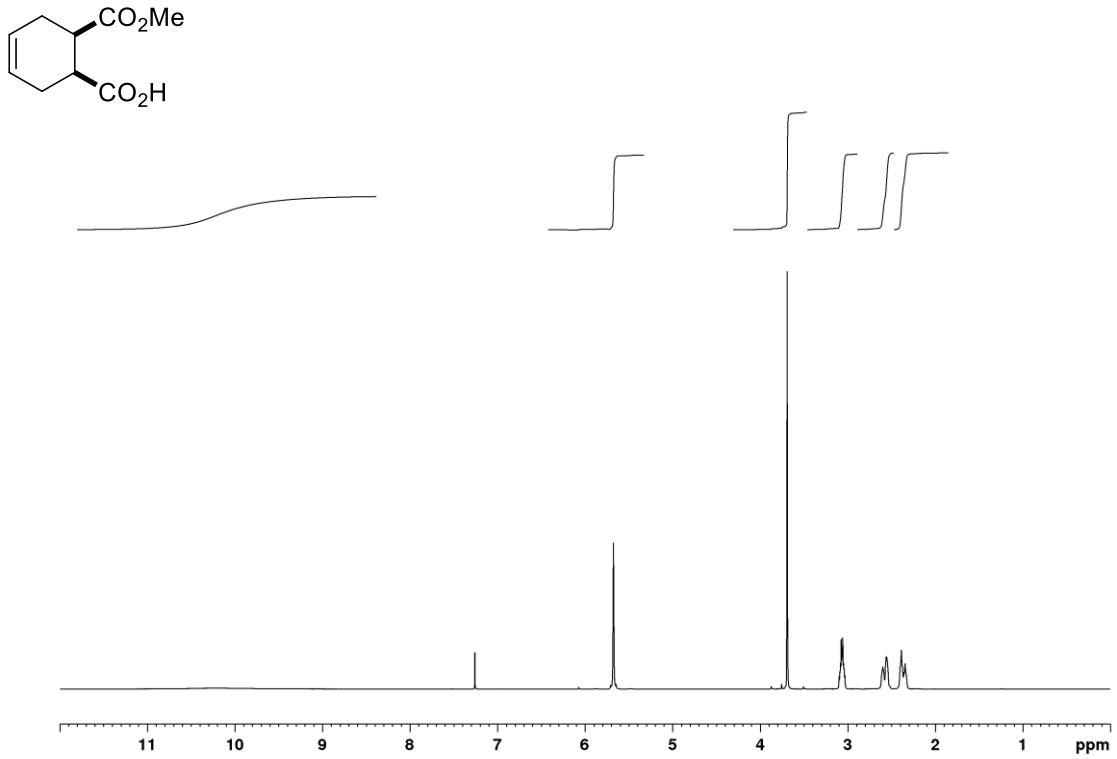

^{13}C NMR (75 MHz, $CDCl_3$)

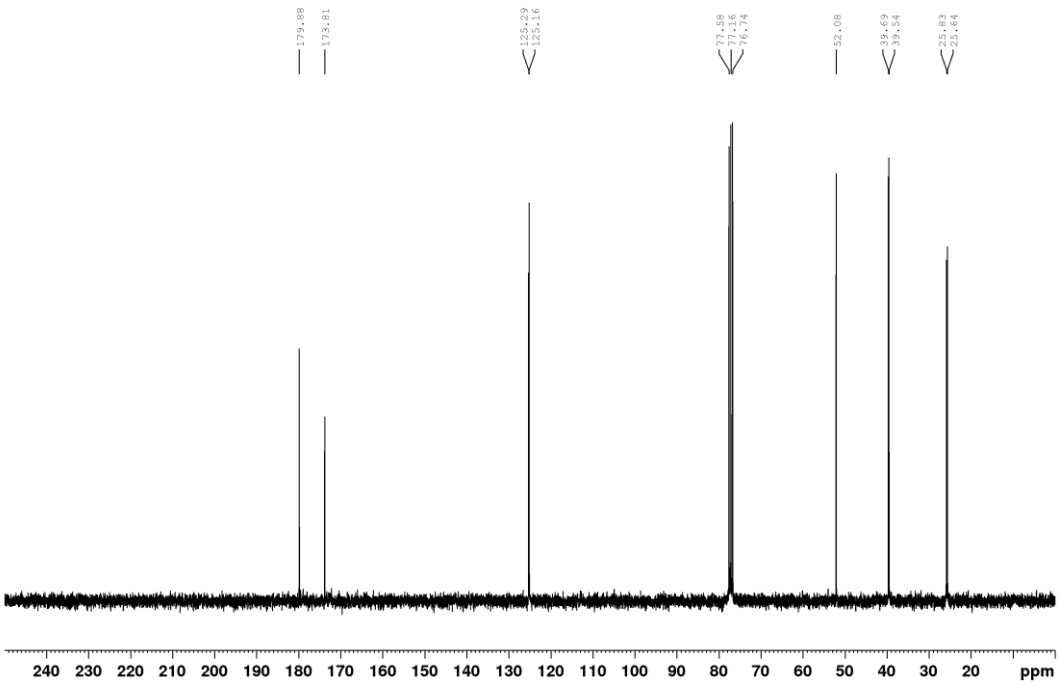

***trans*-2-Methoxycarbonyl-4-cyclohexene-1-carboxylic acid (*trans*-63)**

^{1}H NMR (300 MHz, $CDCl_3$)

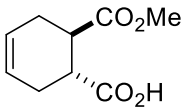

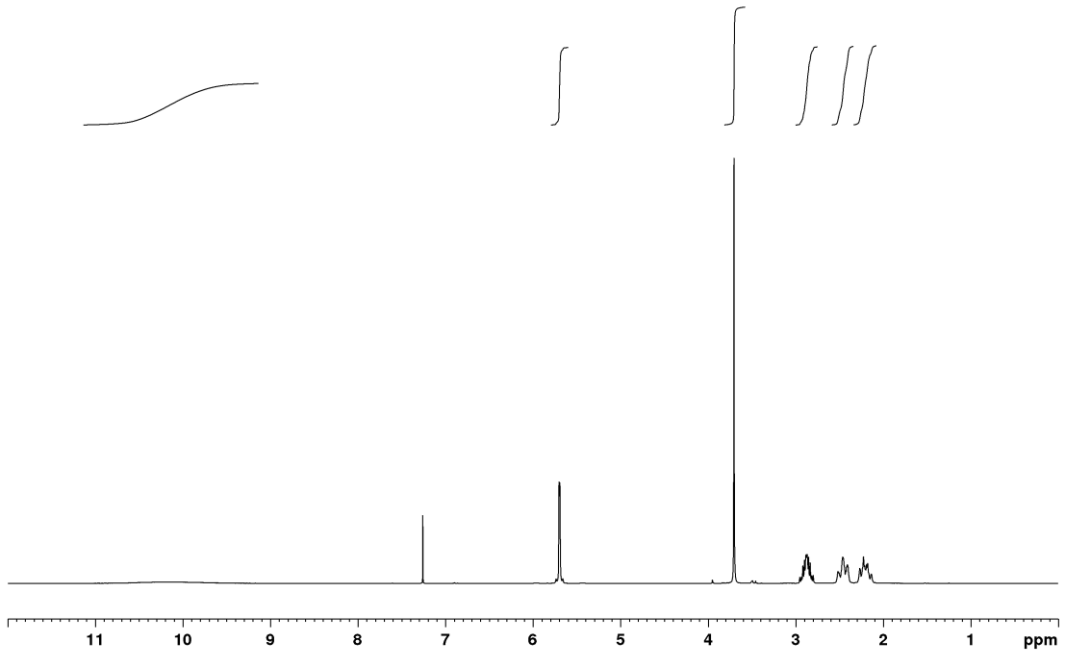

^{13}C NMR (75 MHz, $CDCl_3$)

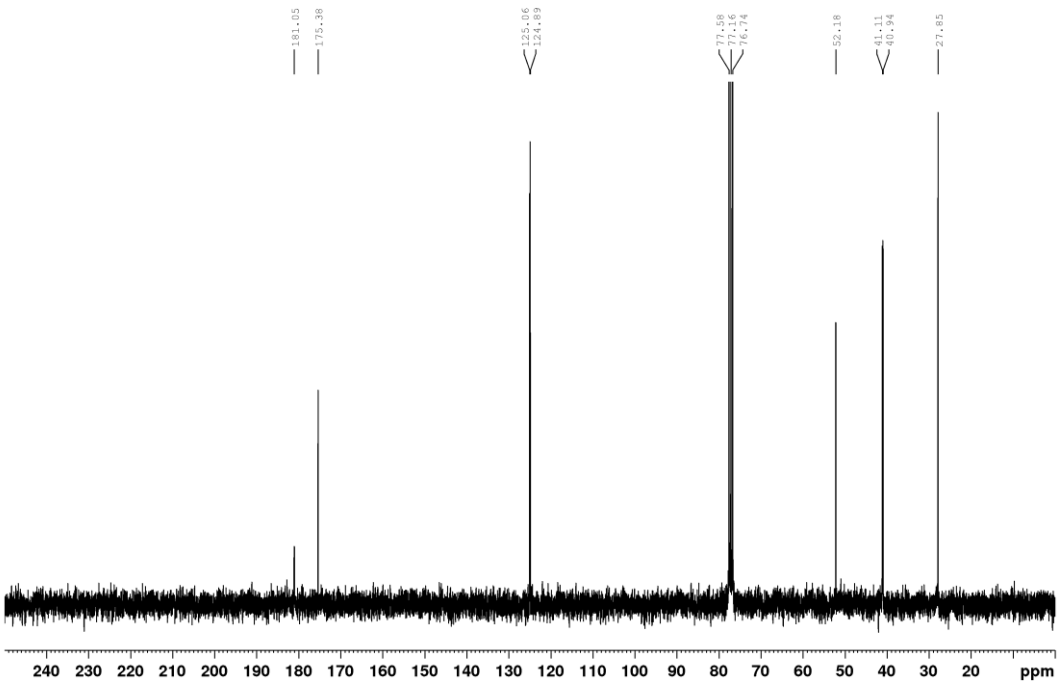

Methyl *cis*-6-(((benzyloxy)carbonyl)amino)cyclohex-3-ene-1-carboxylate (*cis*-64)

^{1}H NMR (300 MHz, $CDCl_3$)

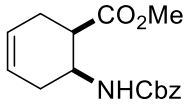

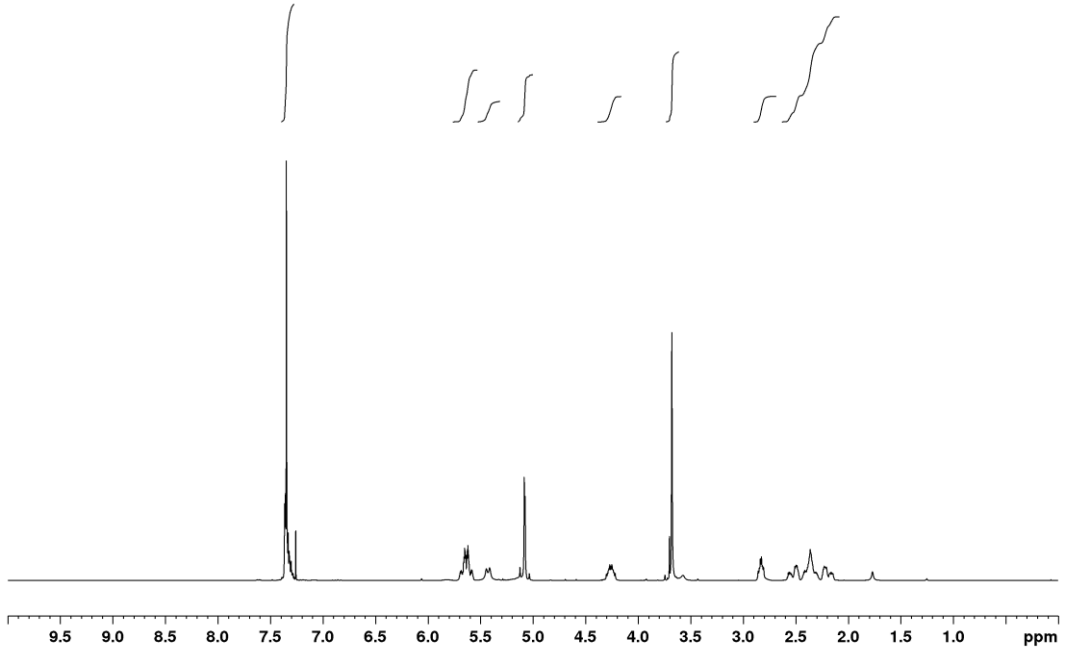

^{13}C NMR (75 MHz, $CDCl_3$)

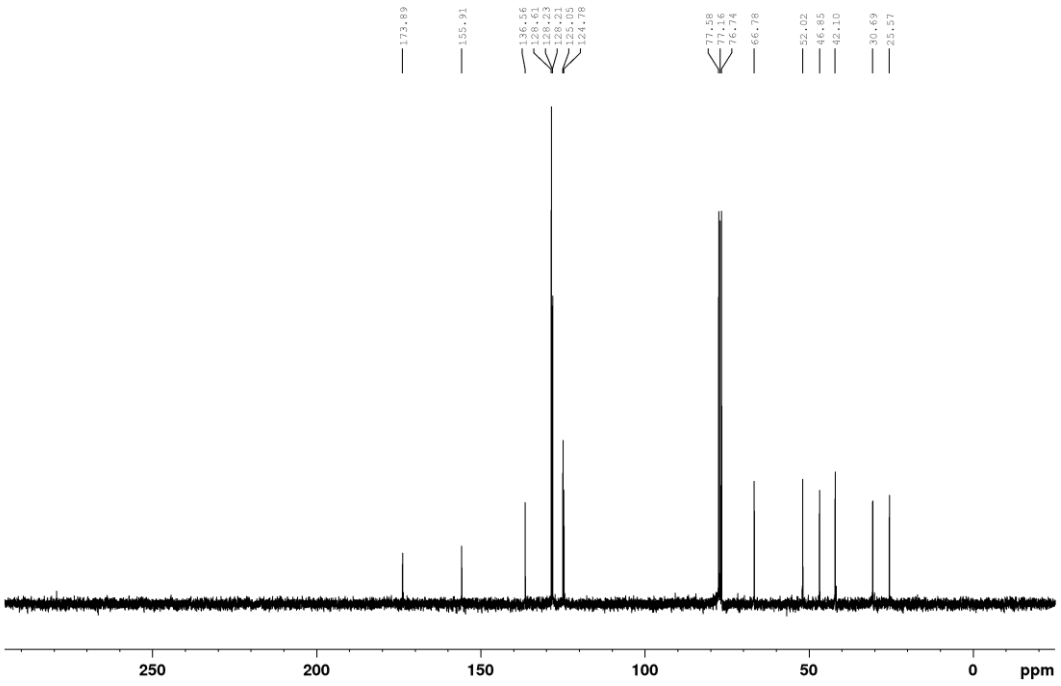

Methyl *cis*-2-aminocyclohexane-1-carboxylate (*rac*-65)

^{1}H NMR (400 MHz, $CDCl_3$)

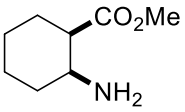

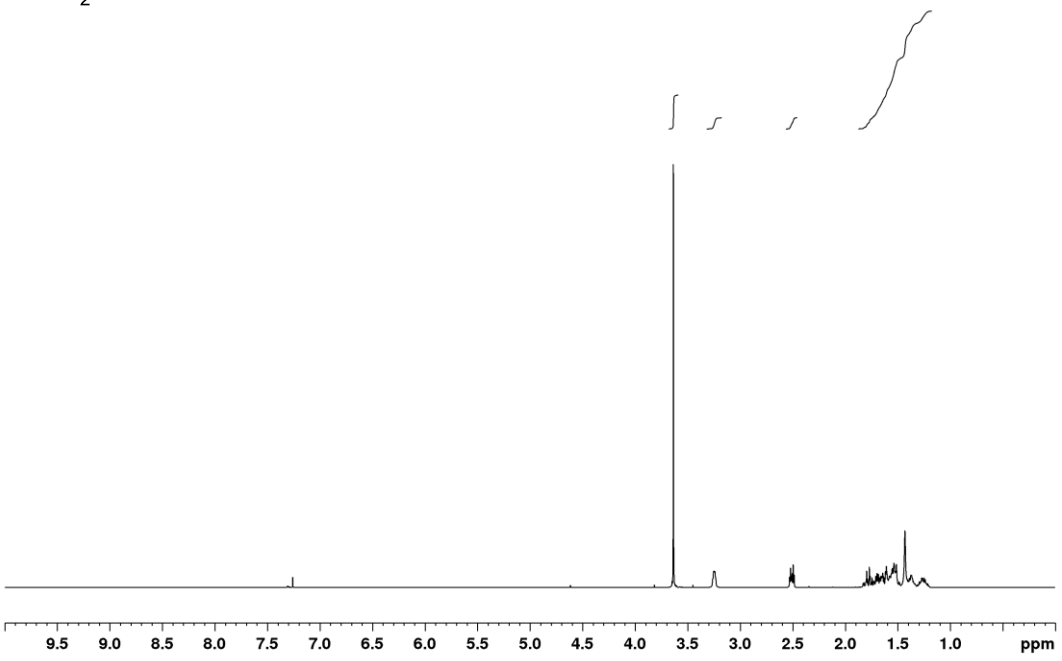

^{13}C NMR (101 MHz, $CDCl_3$)

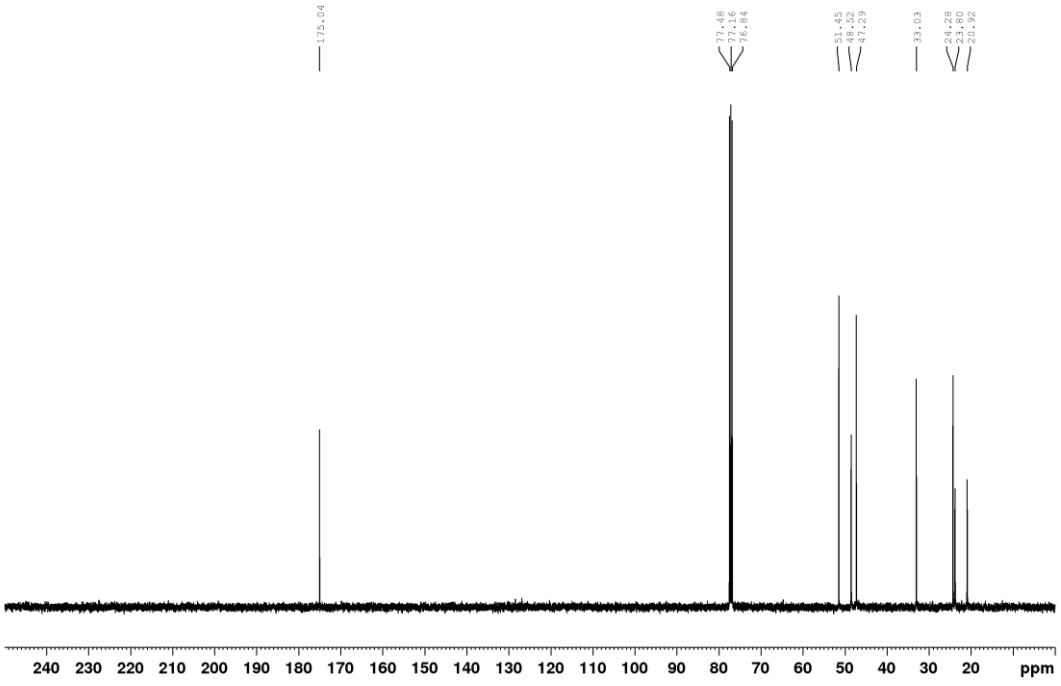

Boc-Pro-(-)-⬢-OMe (66)

^{1}H NMR (400 MHz, $CDCl_3$, 300 K)

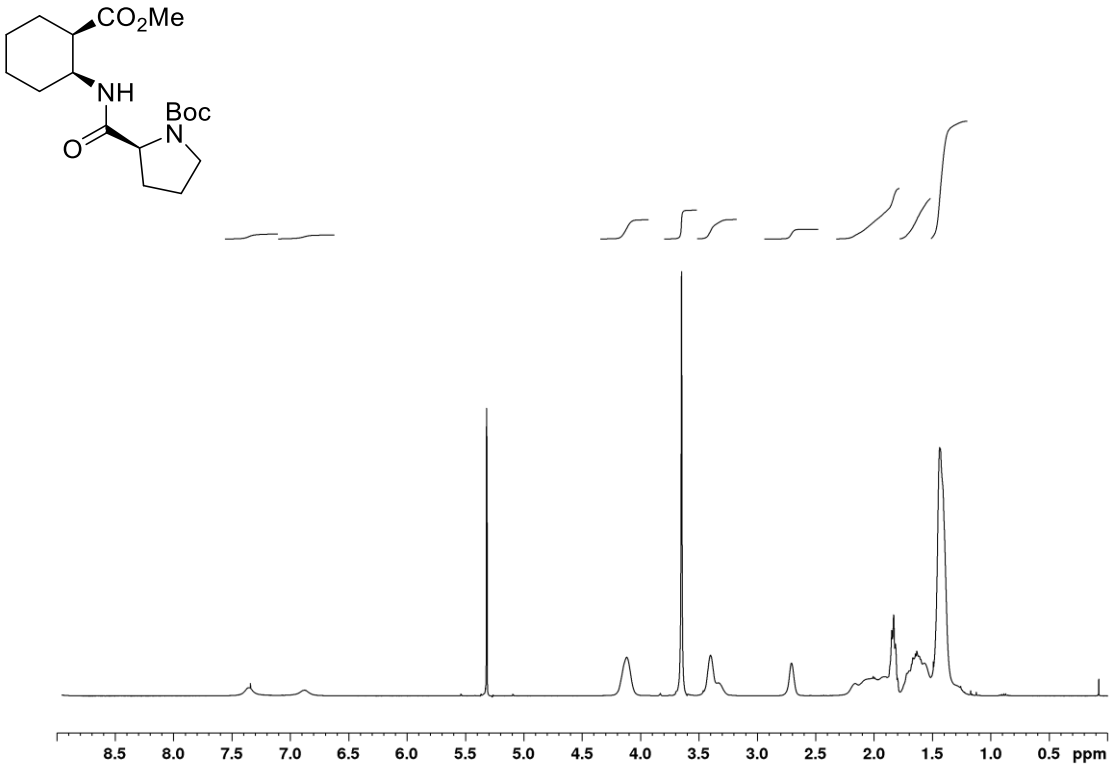

^{13}C NMR (101 MHz, $CDCl_3$, 233 K)

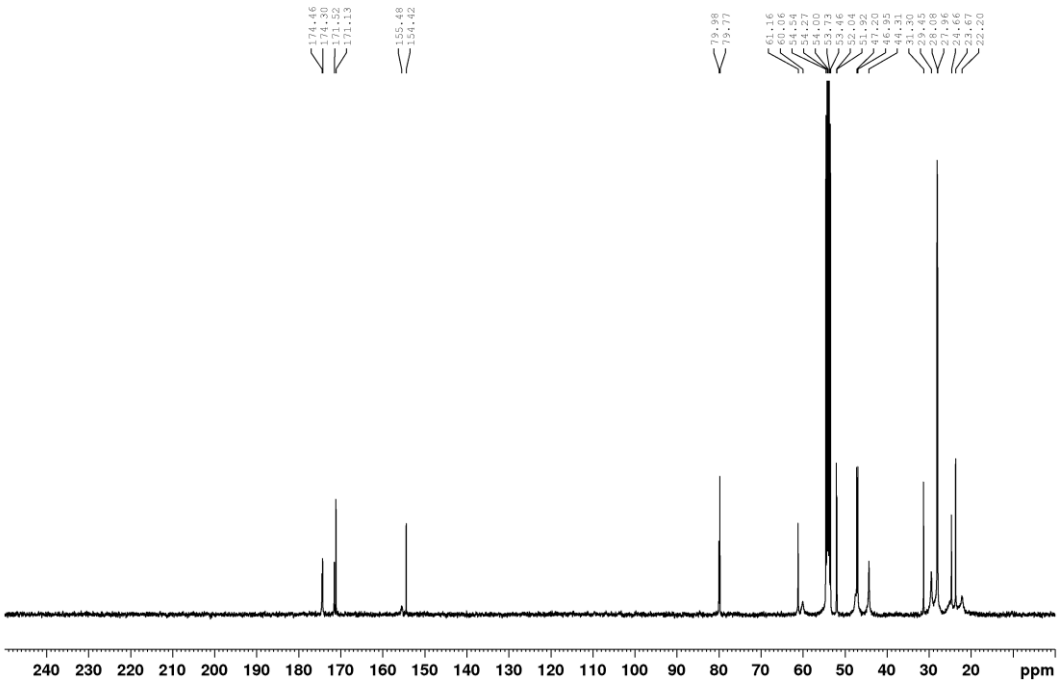

Boc-Pro-(+)-⬢-OMe (*ent*-66)

^{1}H NMR (400 MHz, $CDCl_3$)

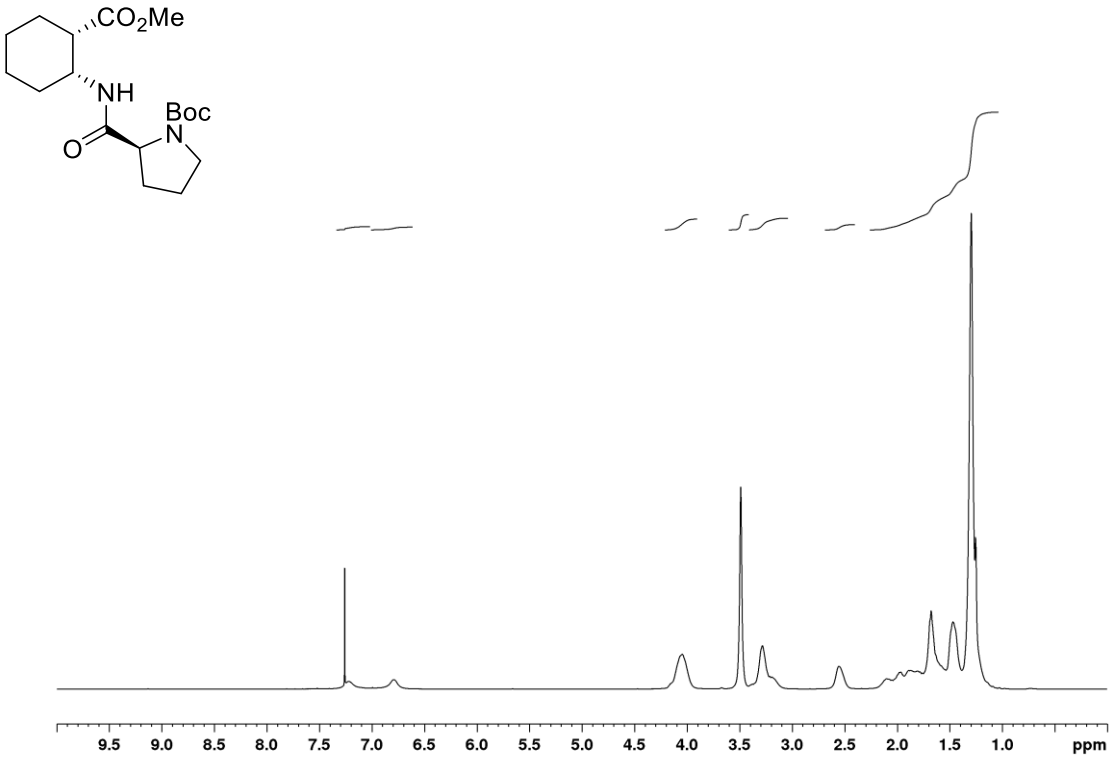

^{13}C NMR (101 MHz, $CDCl_3$)

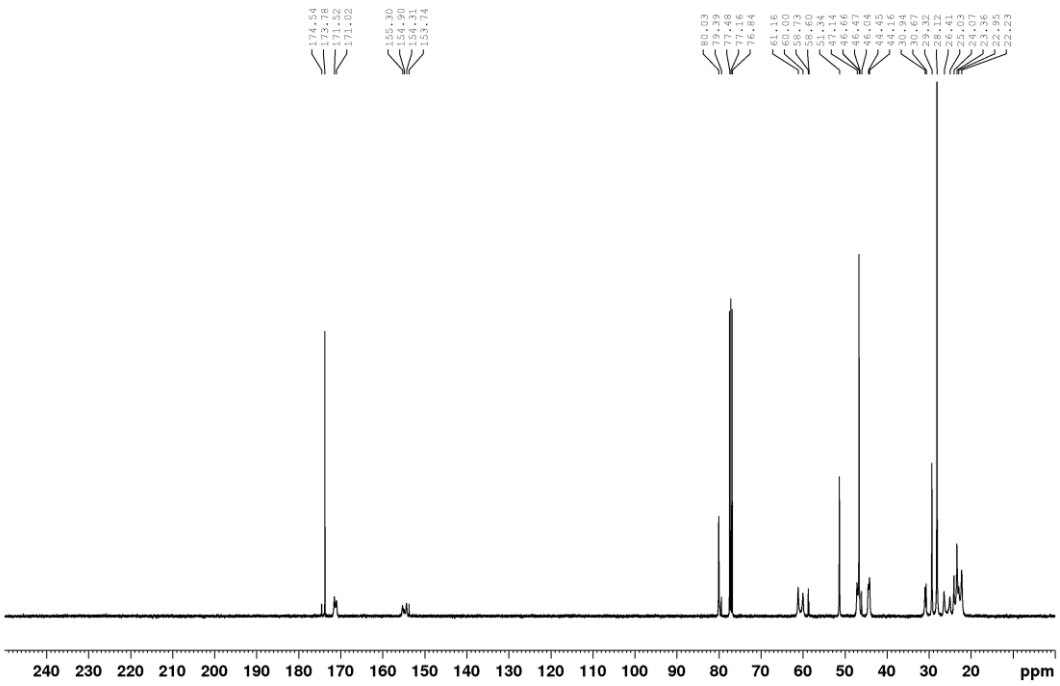

Boc-Pro-(-)-⬢-Pro-OBn (68)

^{1}H NMR (300 MHz, $CDCl_3$)

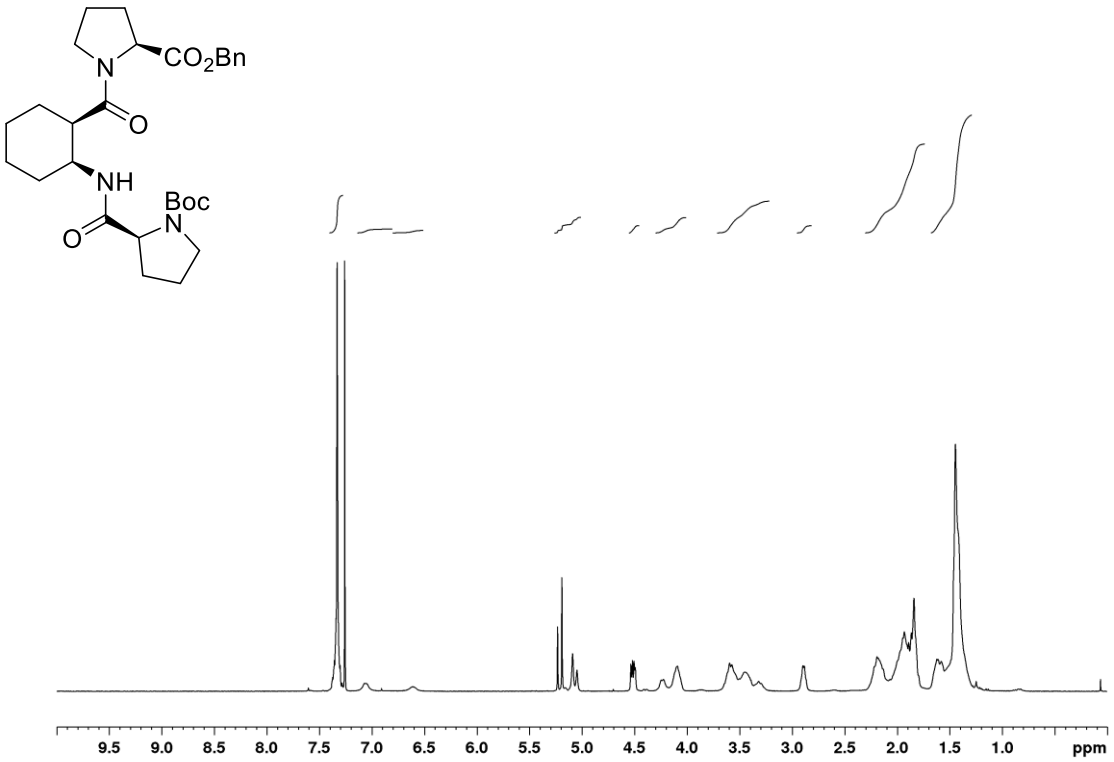

^{13}C NMR (101 MHz, $CDCl_3$)

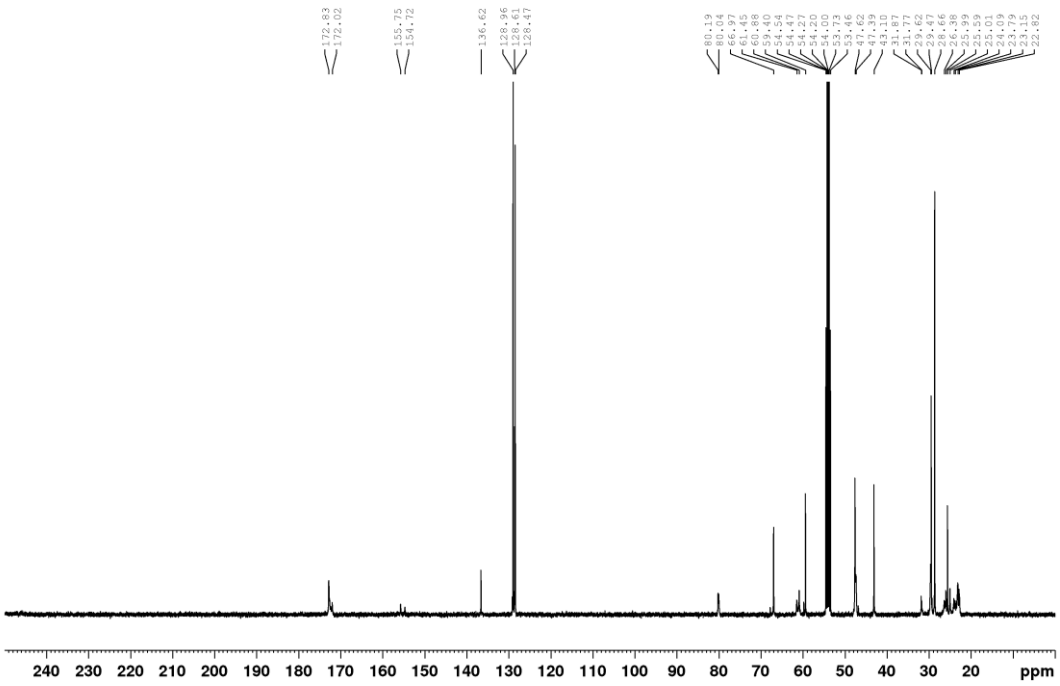

Boc-Pro-(+)-⬢-Pro-OBn (*ent*-68)

^{1}H NMR (400 MHz, $CDCl_3$)

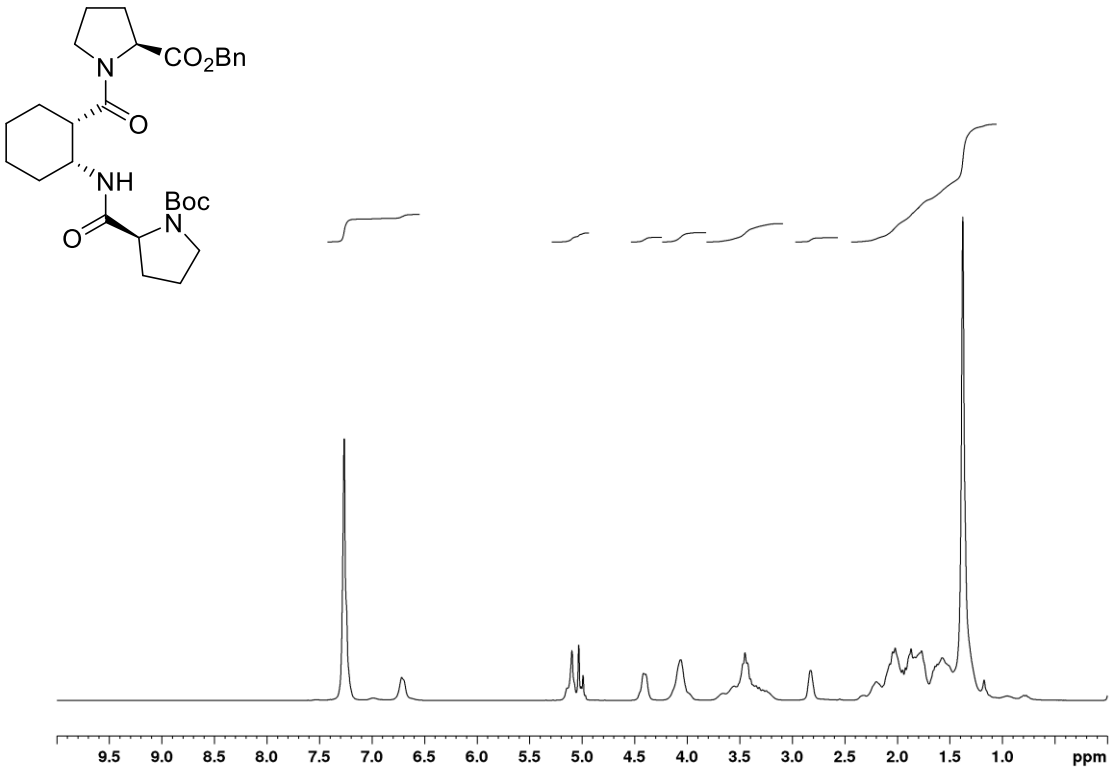

^{13}C NMR (101 MHz, $CDCl_3$)

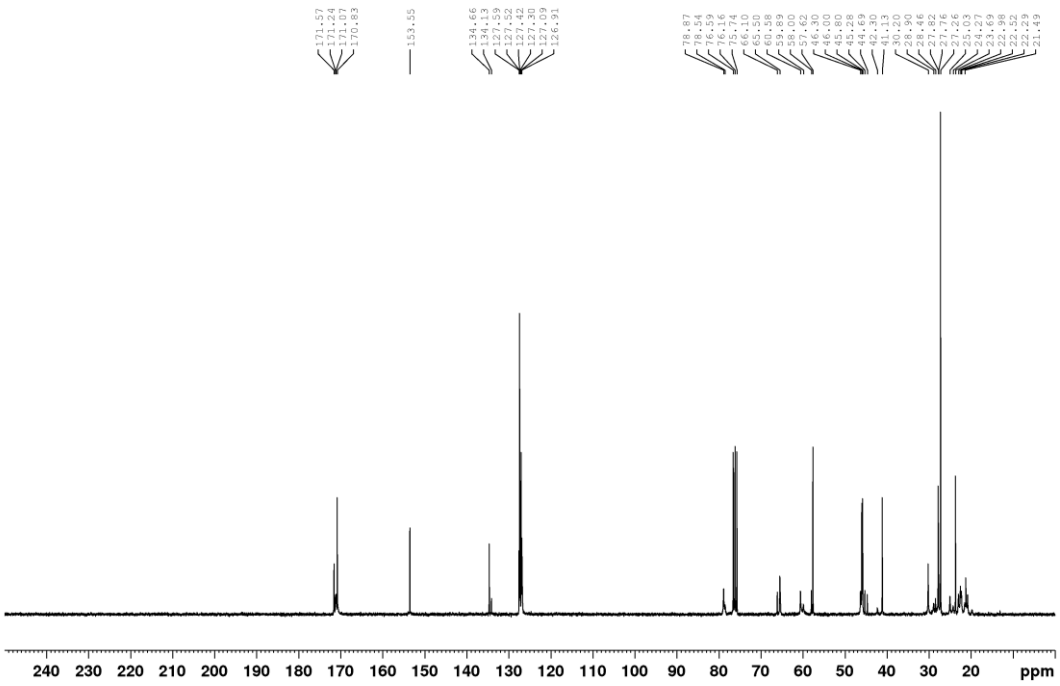

***cis*-Dimethyl cyclohex-4-ene-1,2-dicarboxylate (69)**

^{1}H NMR (300 MHz, $CDCl_3$)

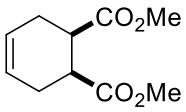

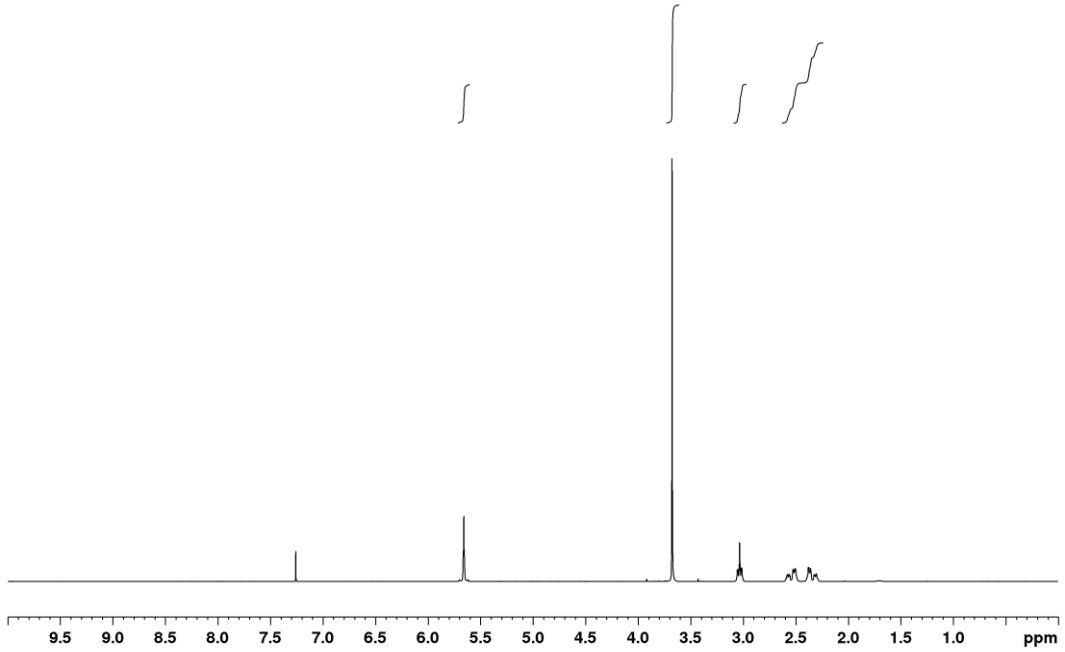

^{13}C NMR (75 MHz, $CDCl_3$)

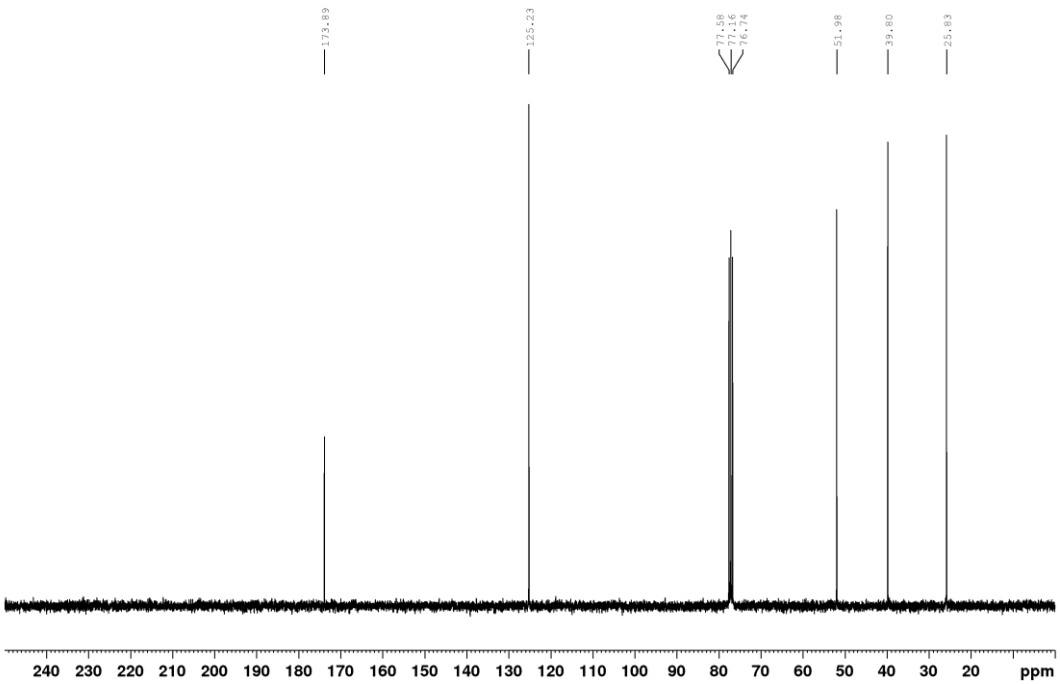

Cbz-Pro-(+)-⬢-OMe (*ent*-71)

^{1}H NMR (300 MHz, $CDCl_3$)

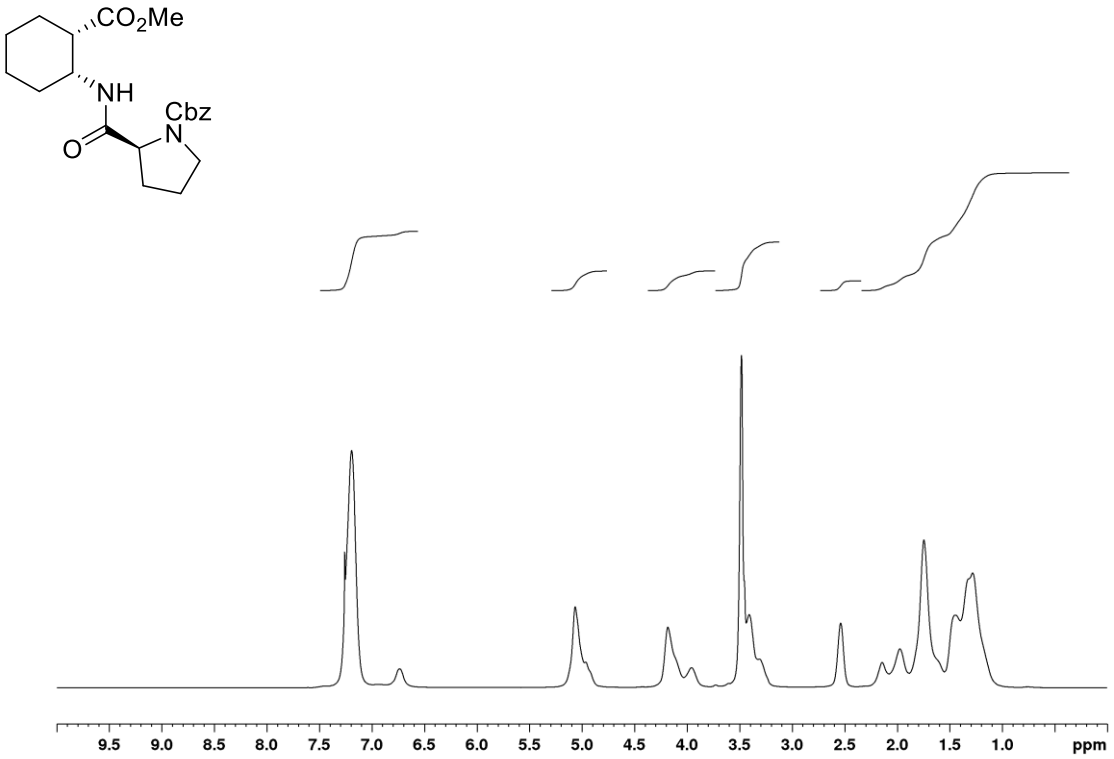

^{13}C NMR (75 MHz, $CDCl_3$)

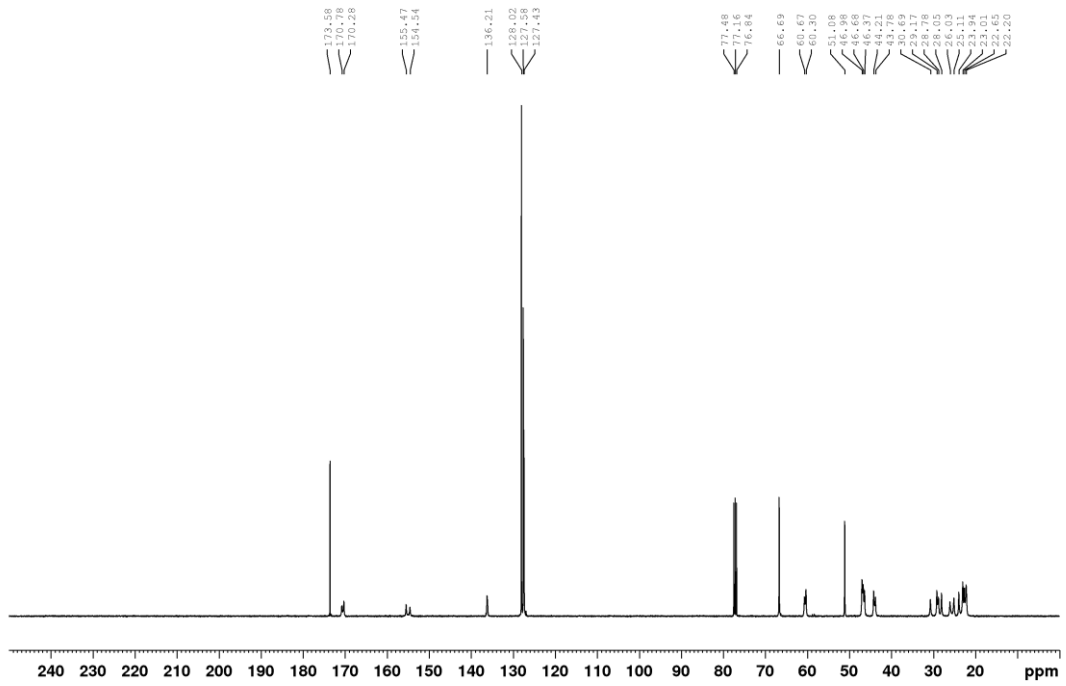

Cbz-Pro-(+)-⬢-Pro-OBn (*ent*-72)

^{1}H NMR (400 MHz, $CDCl_3$)

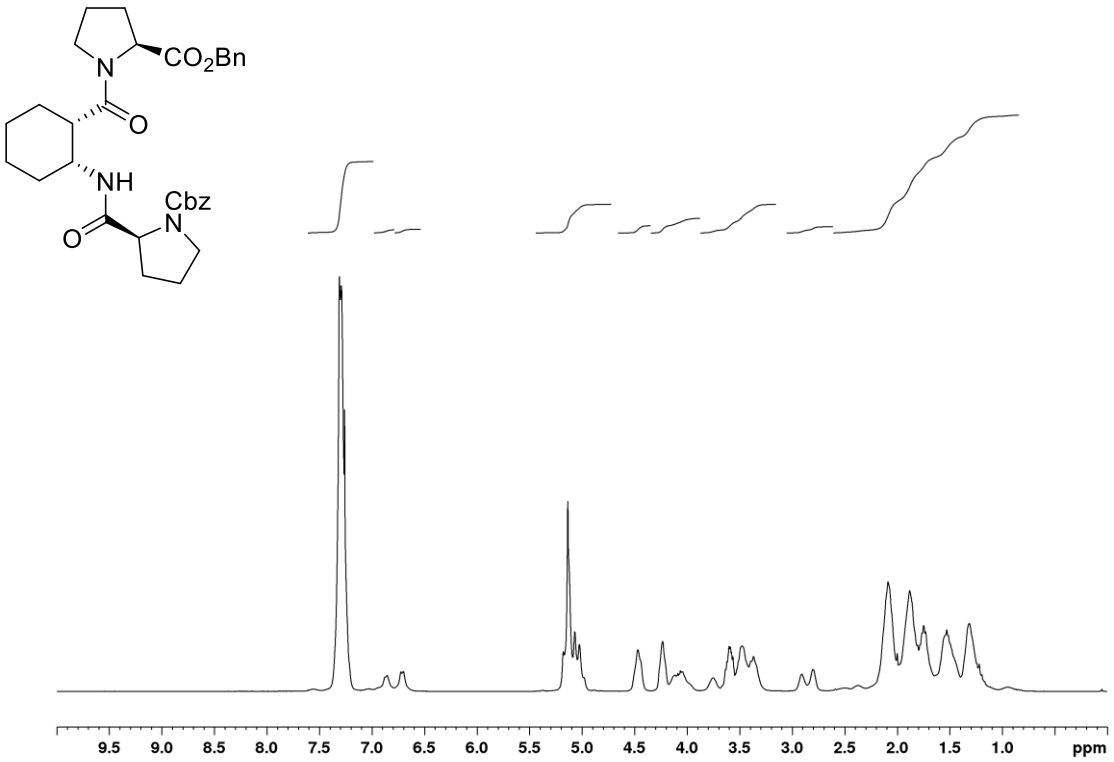

^{13}C NMR (101 MHz, $CDCl_3$)

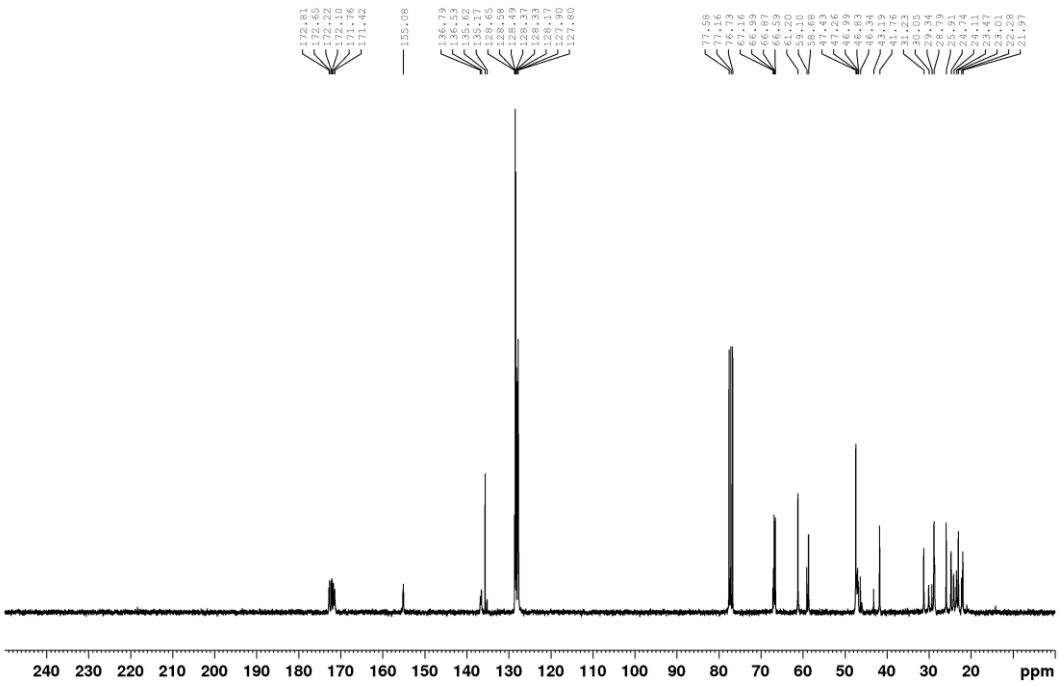

Methyl 2-aminobenzoate (73)

^{1}H NMR (300 MHz, $CDCl_3$)

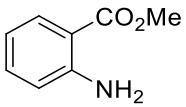

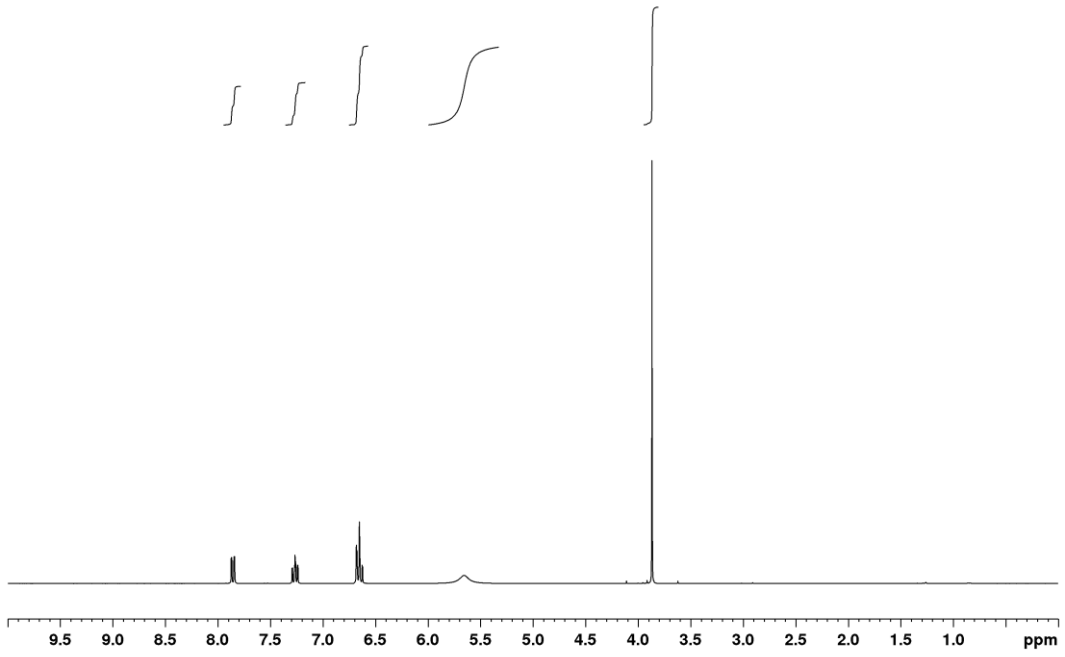

^{13}C NMR (75 MHz, $CDCl_3$)

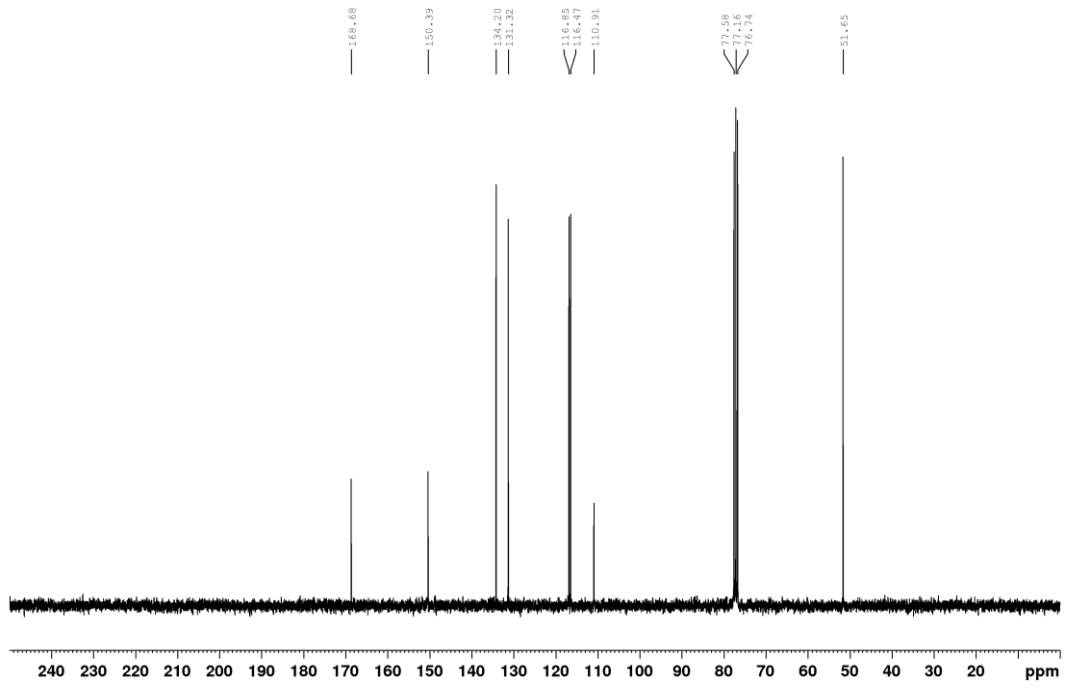

Boc-Pro-Ant-OMe (74)

^{1}H NMR (400 MHz, $CDCl_3$)

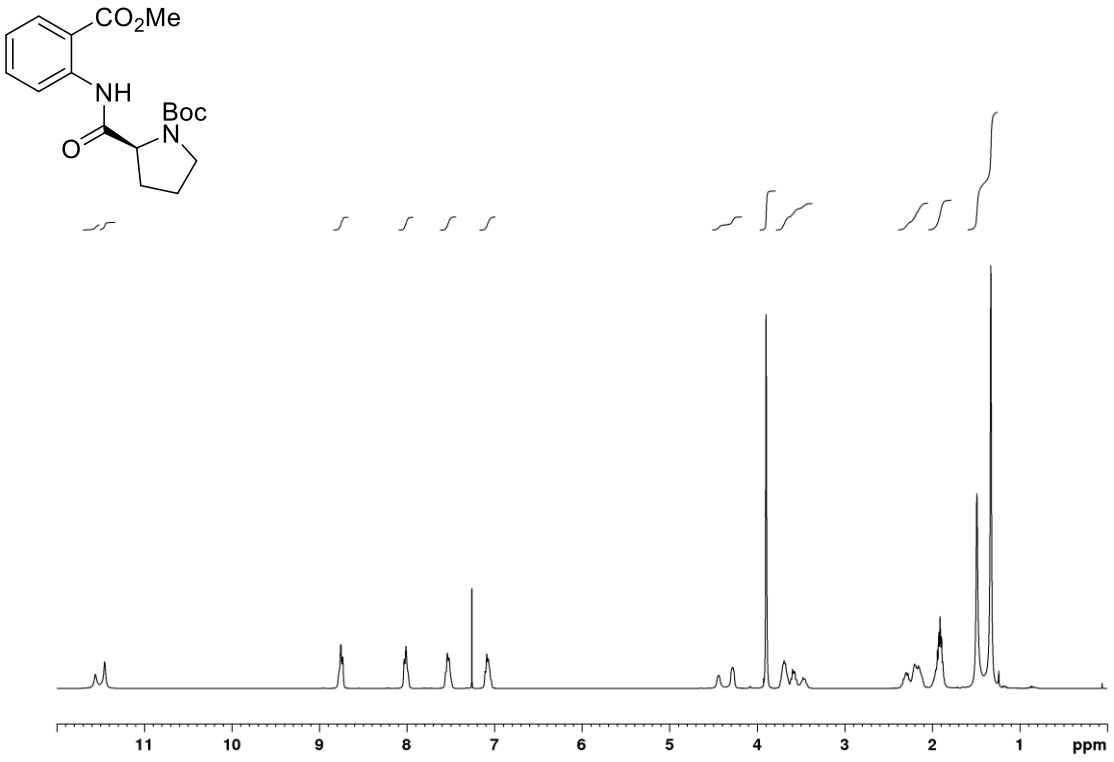

^{13}C NMR (101 MHz, $CDCl_3$)

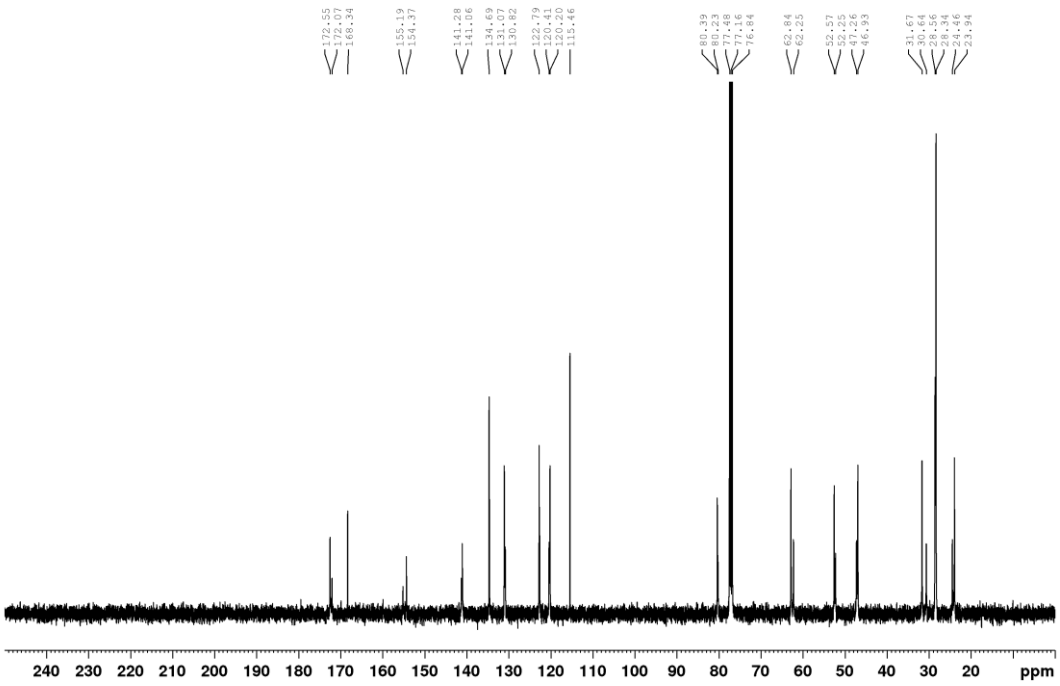

Cbz-Pro-Ant-OMe (75)

^{1}H NMR (400 MHz, $CDCl_3$)

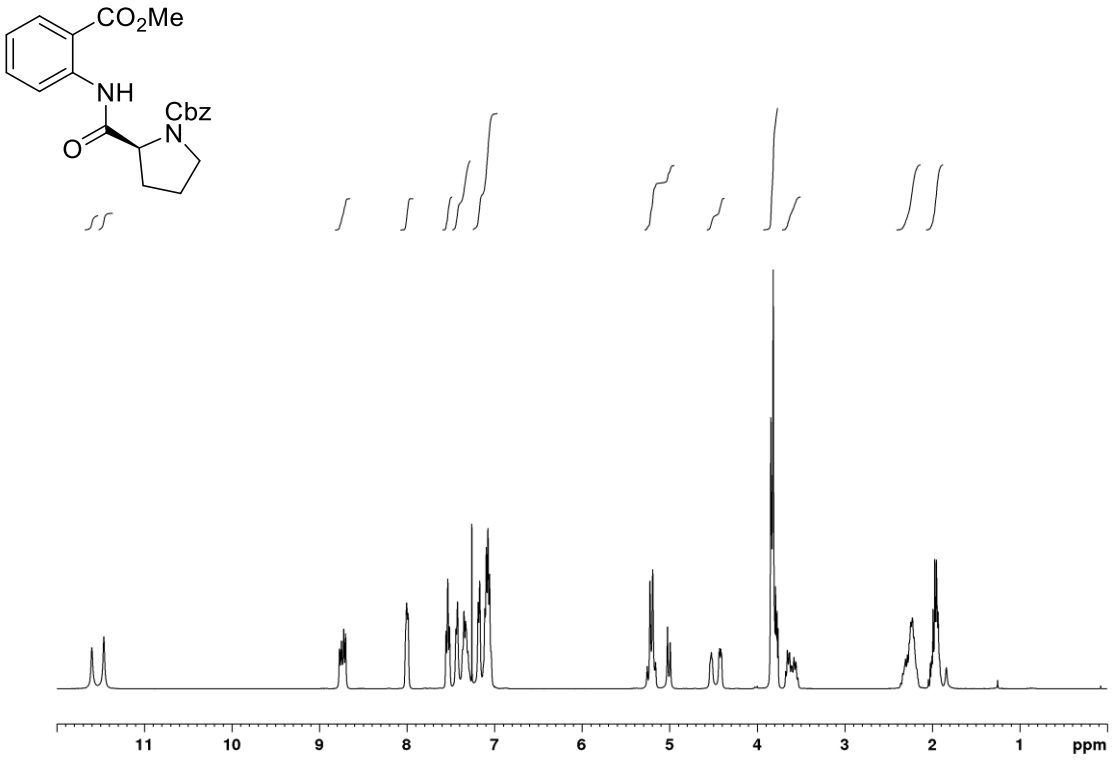

^{13}C NMR (101 MHz, $CDCl_3$)

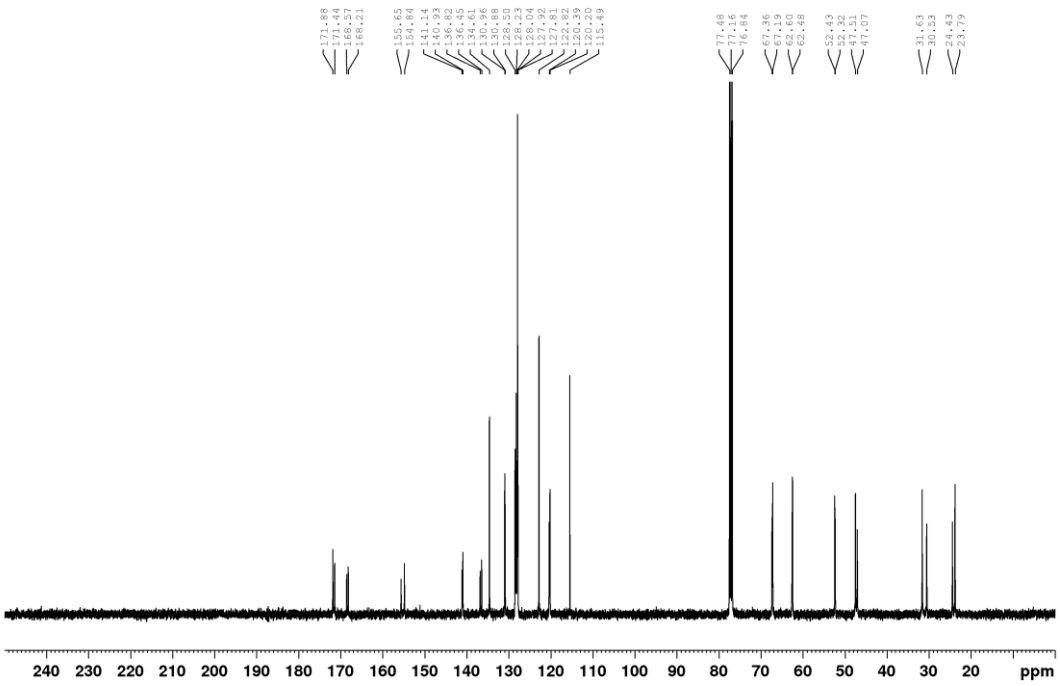

Boc-Pro-Ant-Pro-OBn (77)

^{1}H NMR (400 MHz, $CDCl_3$)

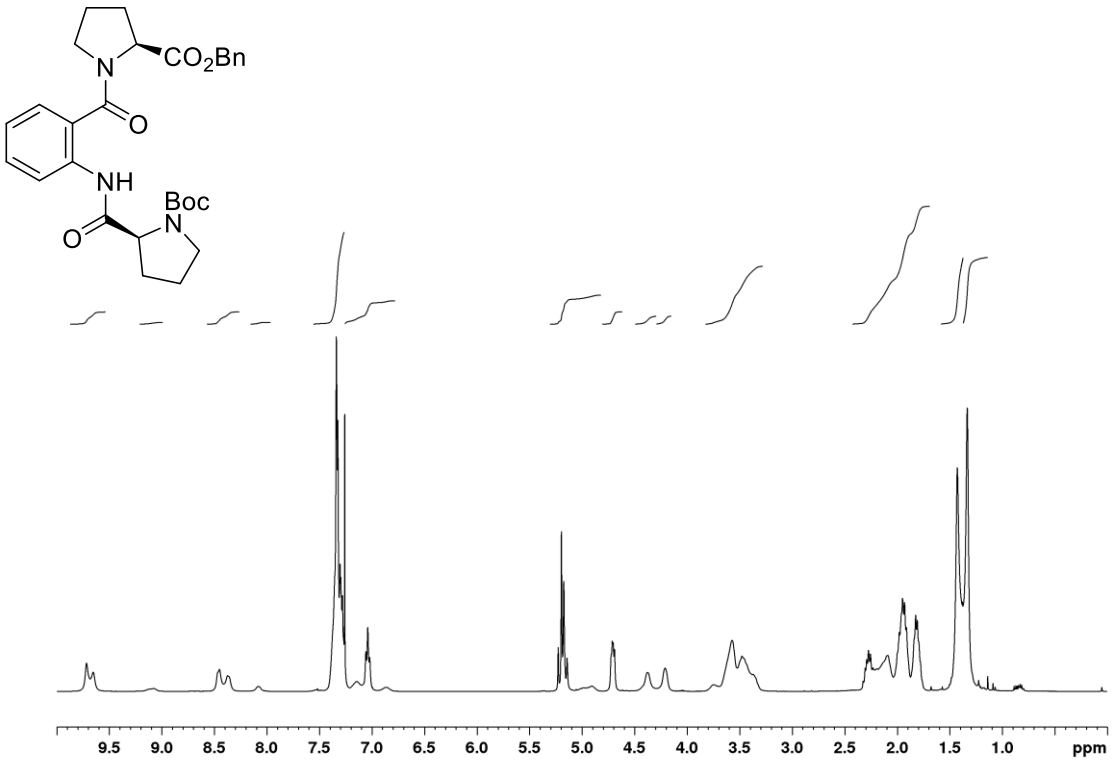

^{13}C NMR (101 MHz, $CDCl_3$)

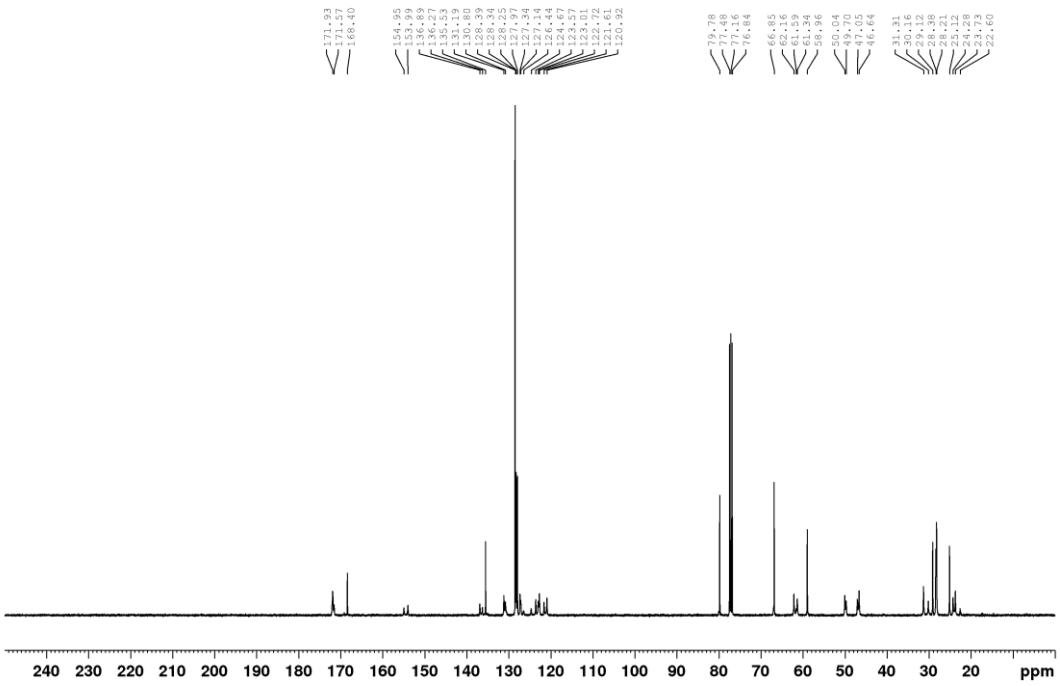

Cbz-Pro-Ant-Pro-OBn (78)

^{1}H NMR (400 MHz, $CDCl_3$)

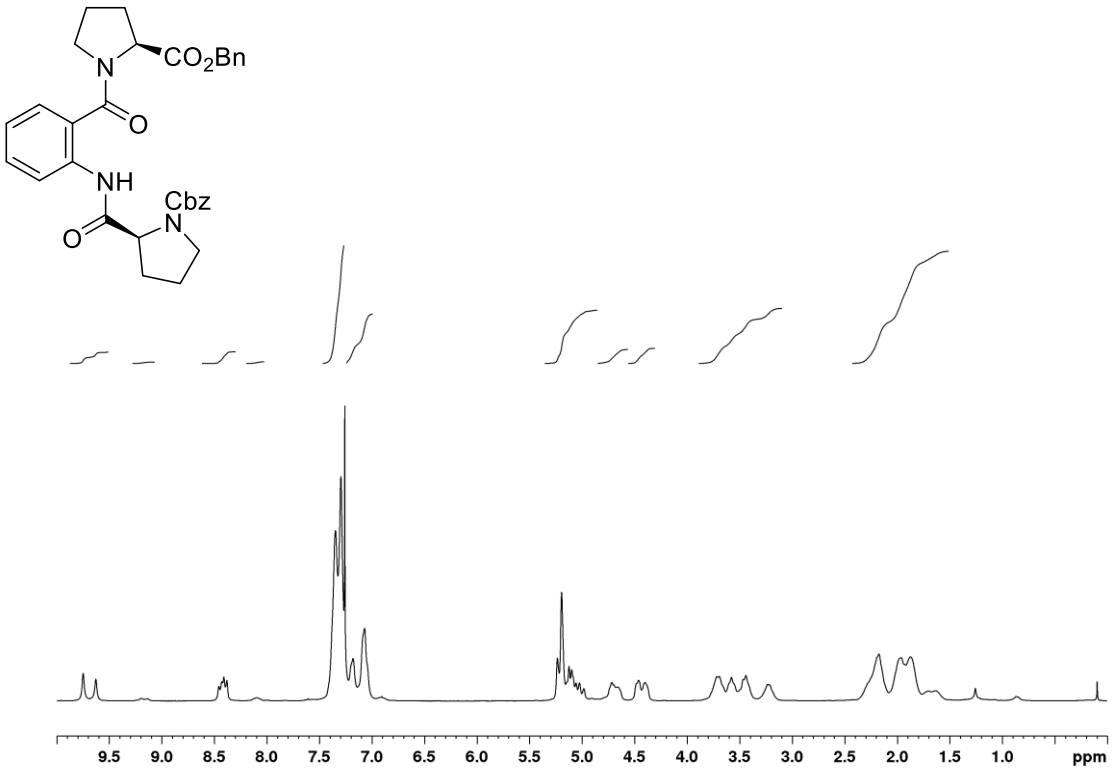

^{13}C NMR (101 MHz, $CDCl_3$)

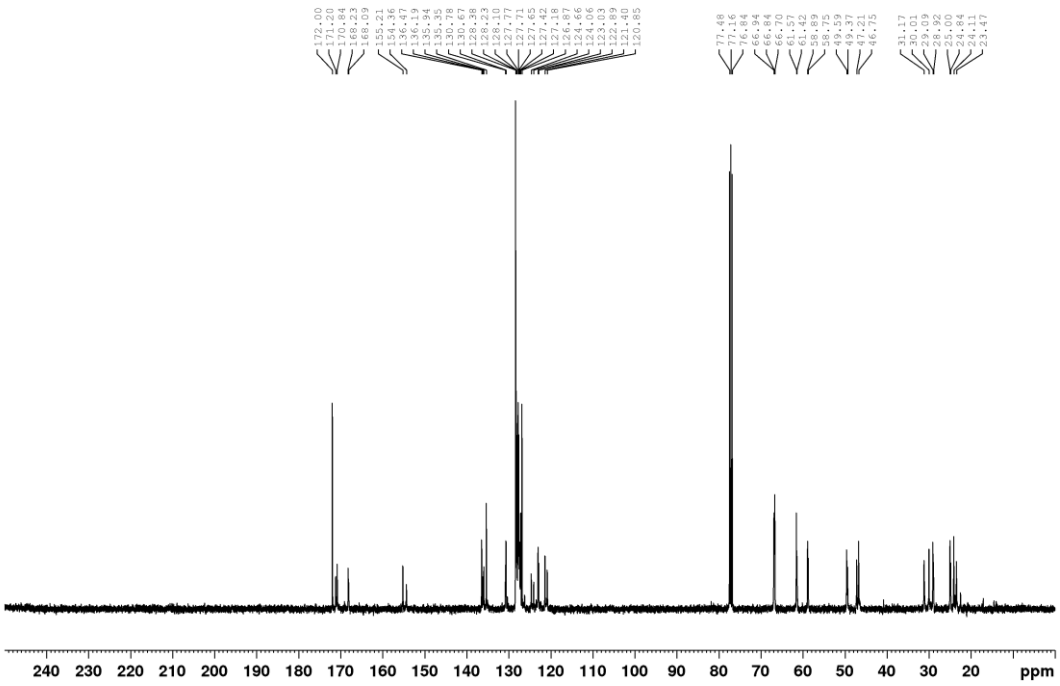

Benzyl (*S*)-2-(4-oxo-4H-benzo[d][1,3]oxazin-2-yl)pyrrolidine-1-carboxylate (83)

^{1}H NMR (400 MHz, $CDCl_3$)

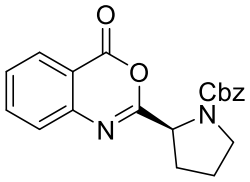

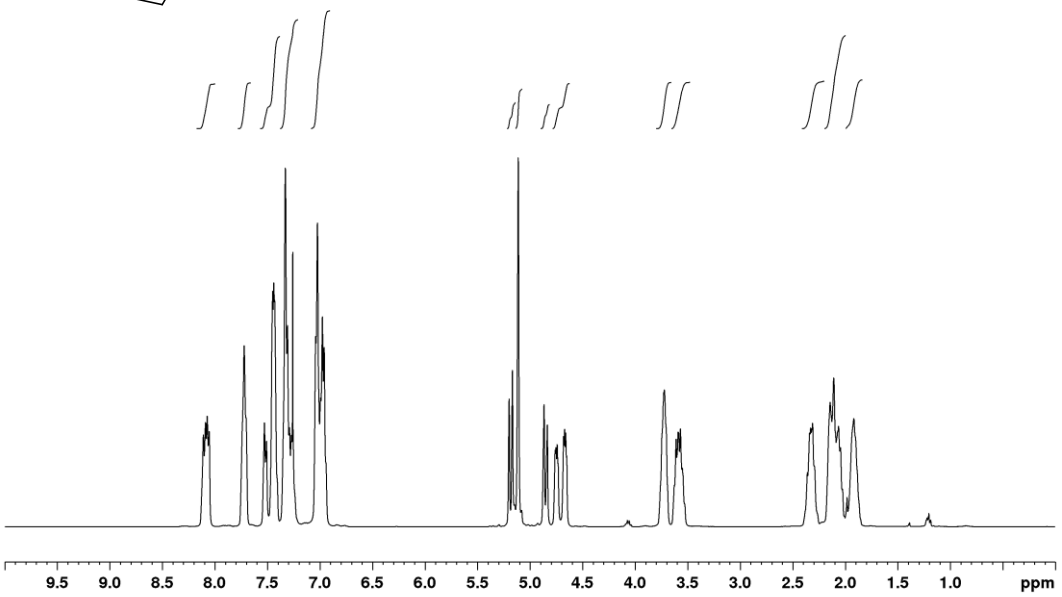

^{13}C NMR (101 MHz, $CDCl_3$)

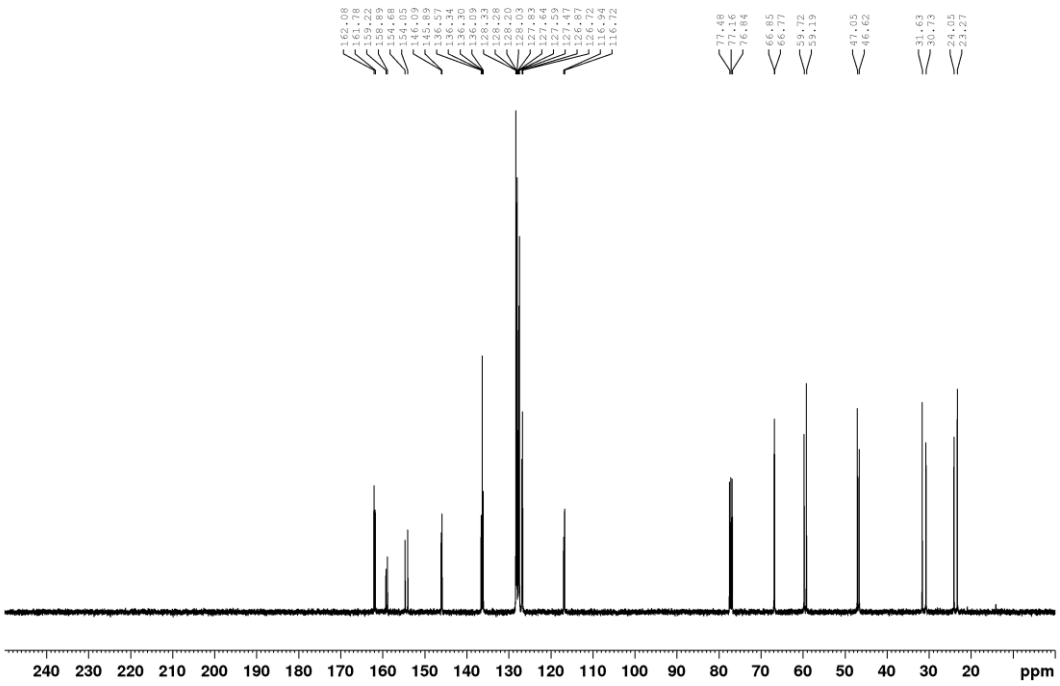

2-Acetamidobenzoic acid (88)

^{1}H NMR (300 MHz, CD_3OD)

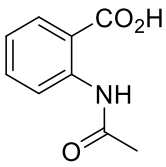

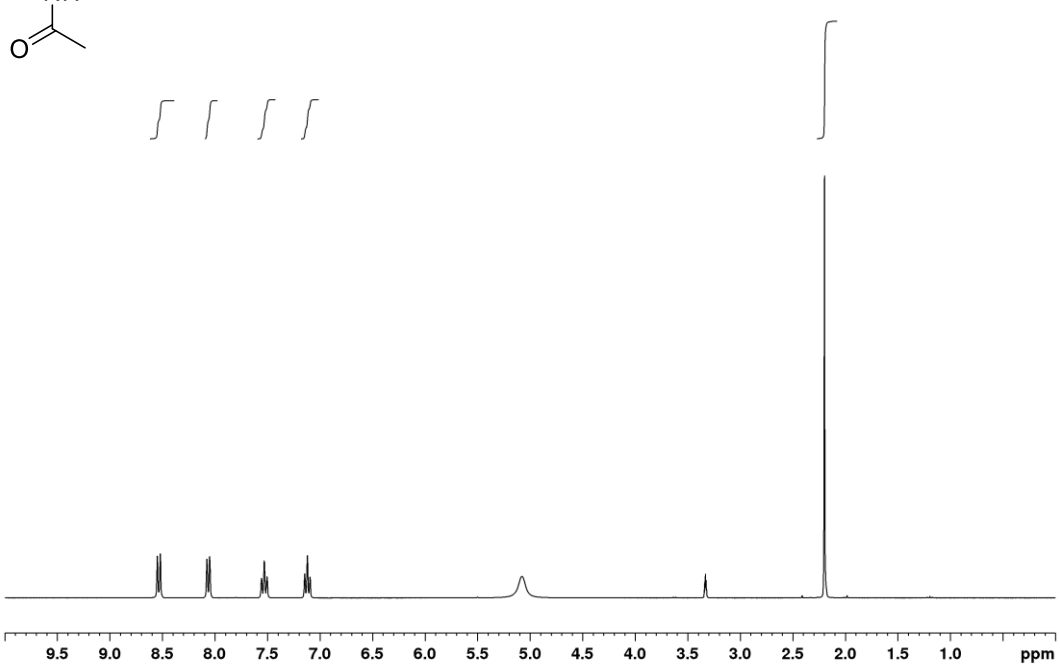

^{13}C NMR (75 MHz, CD_3OD)

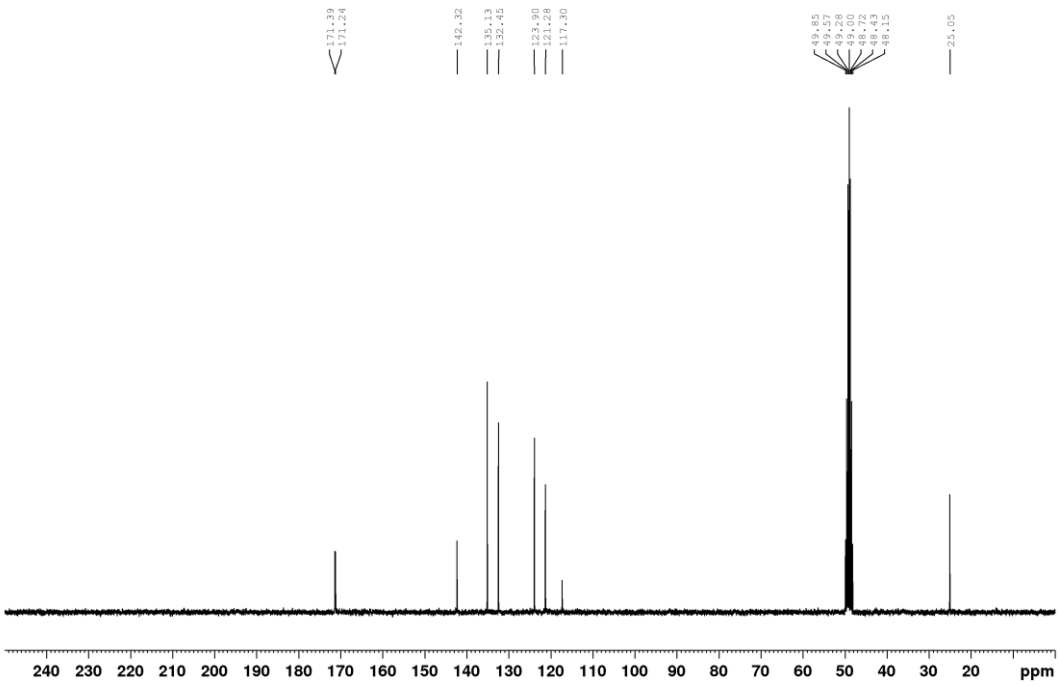

2-Methyl-4*H*-benzo[d][1,3]oxazin-4-one (89)

^{1}H NMR (300 MHz, $CDCl_3$)

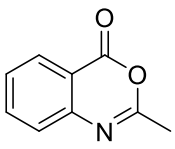

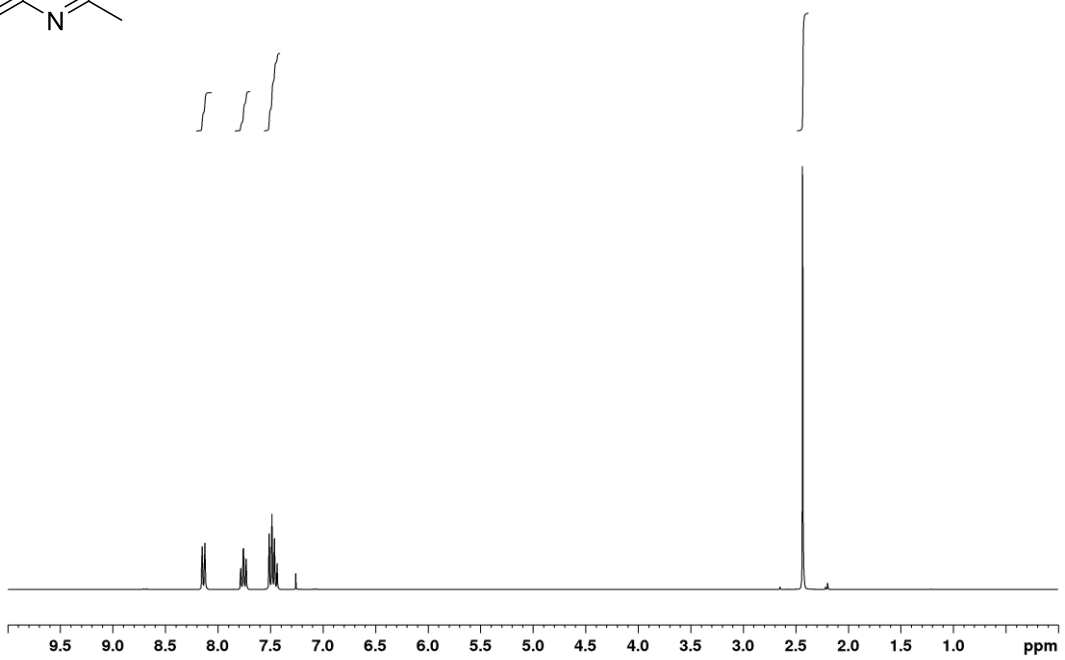

^{13}C NMR (75 MHz, $CDCl_3$)

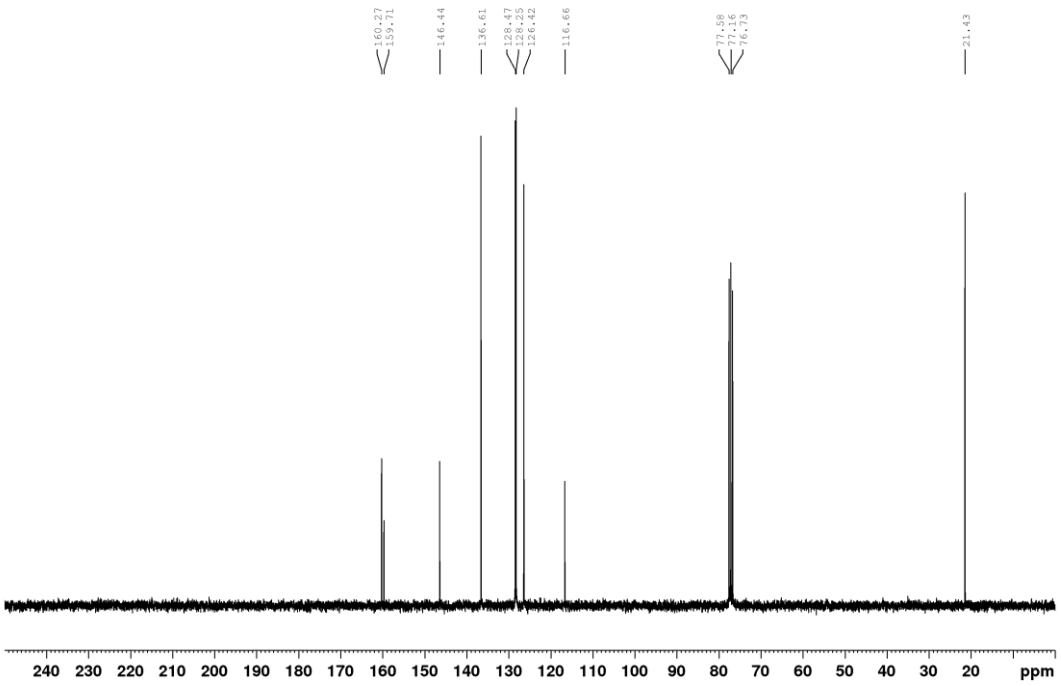

Benzyl (*S*)-2-((2-(pyrrolidine-1-carbonyl)phenyl)carbamoyl)pyrrolidine-1-carboxylate (90)

^{1}H NMR (400 MHz, $CDCl_3$)

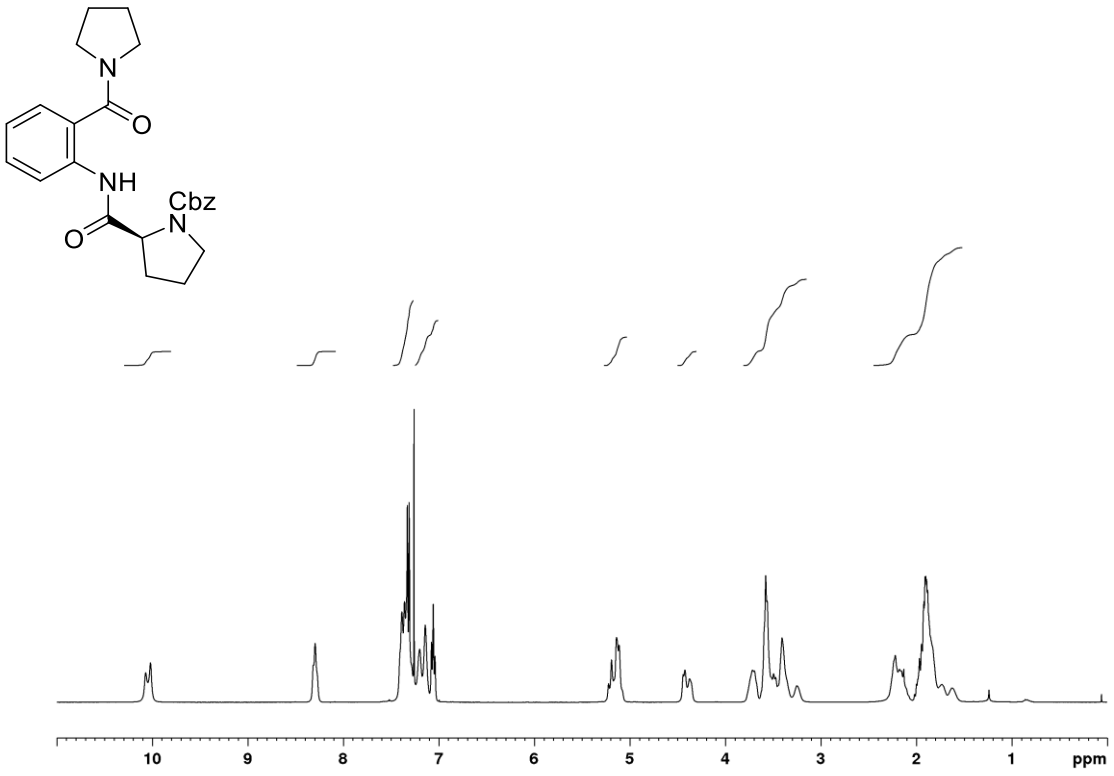

^{13}C NMR (101 MHz, $CDCl_3$)

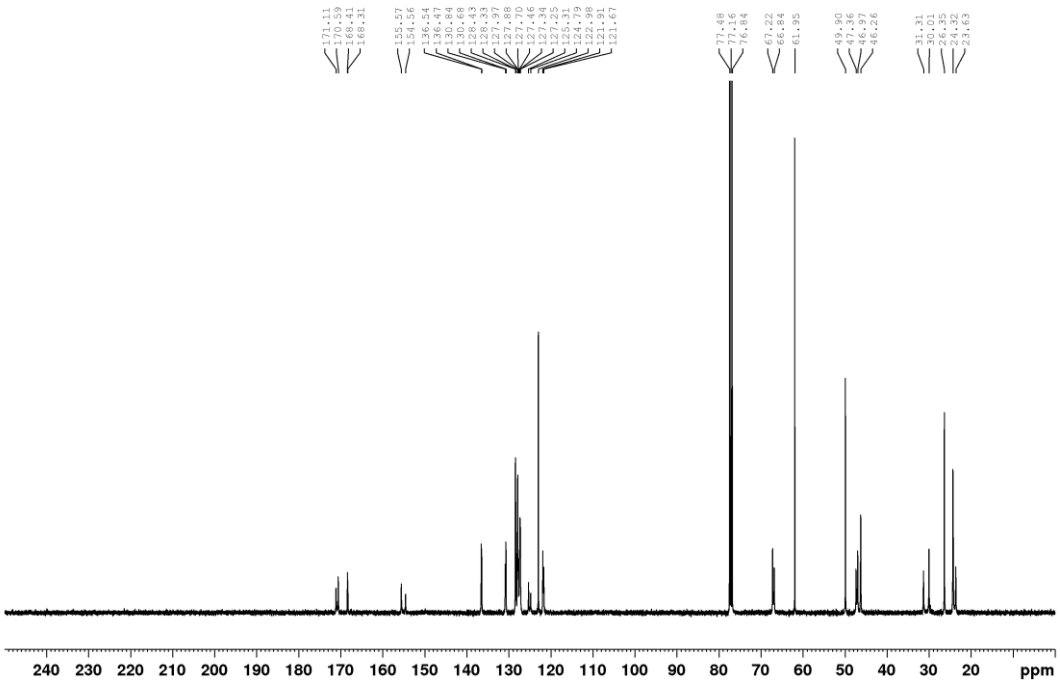

(*R*)-4-Hydroxy-4-(4-nitrophenyl)butan-2-one (93)

^{1}H NMR (300 MHz, $CDCl_3$)

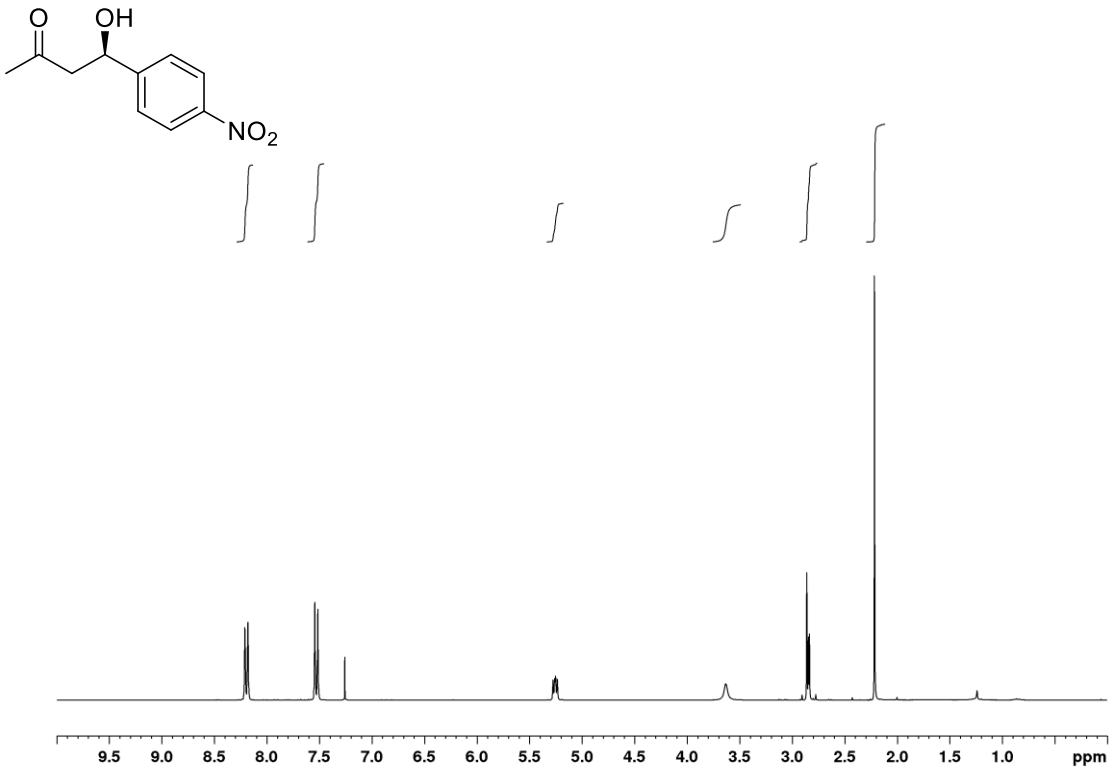

^{13}C NMR (75 MHz, $CDCl_3$)

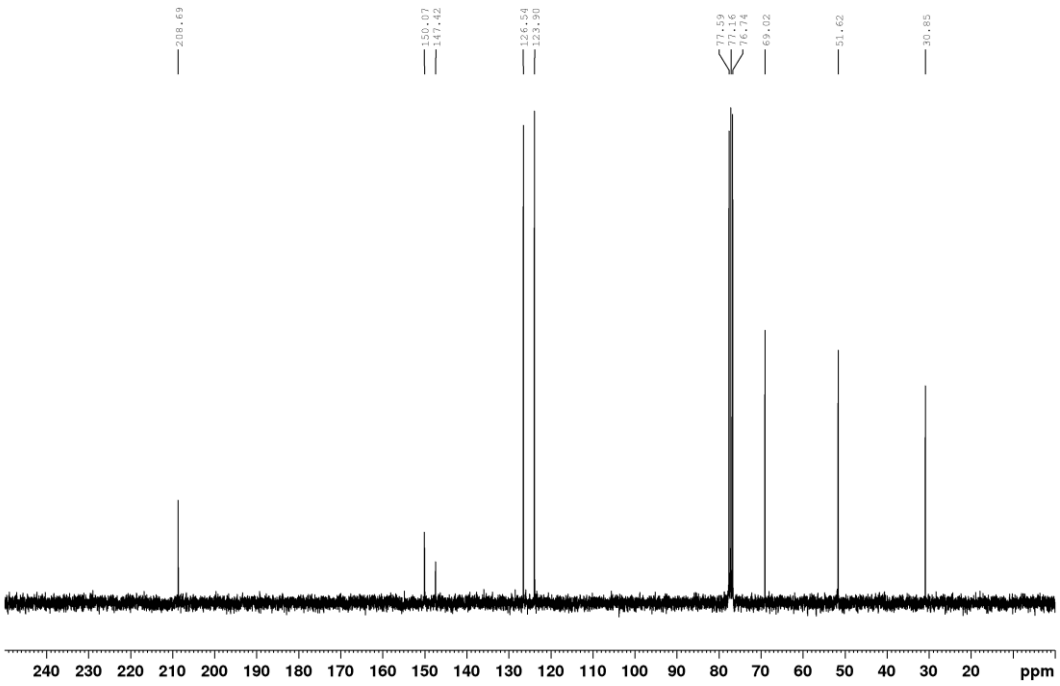

(*R*)-5-Nitro-4-phenylpentan-2-one (94)

^{1}H NMR (400 MHz, $CDCl_3$)

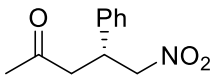

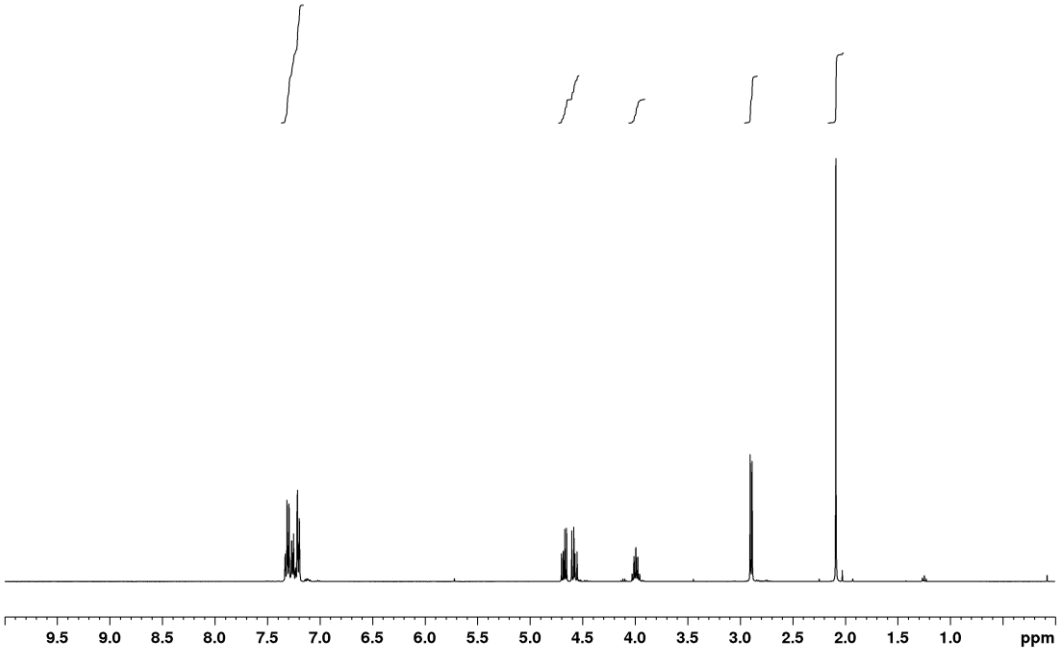

^{13}C NMR (101 MHz, $CDCl_3$)

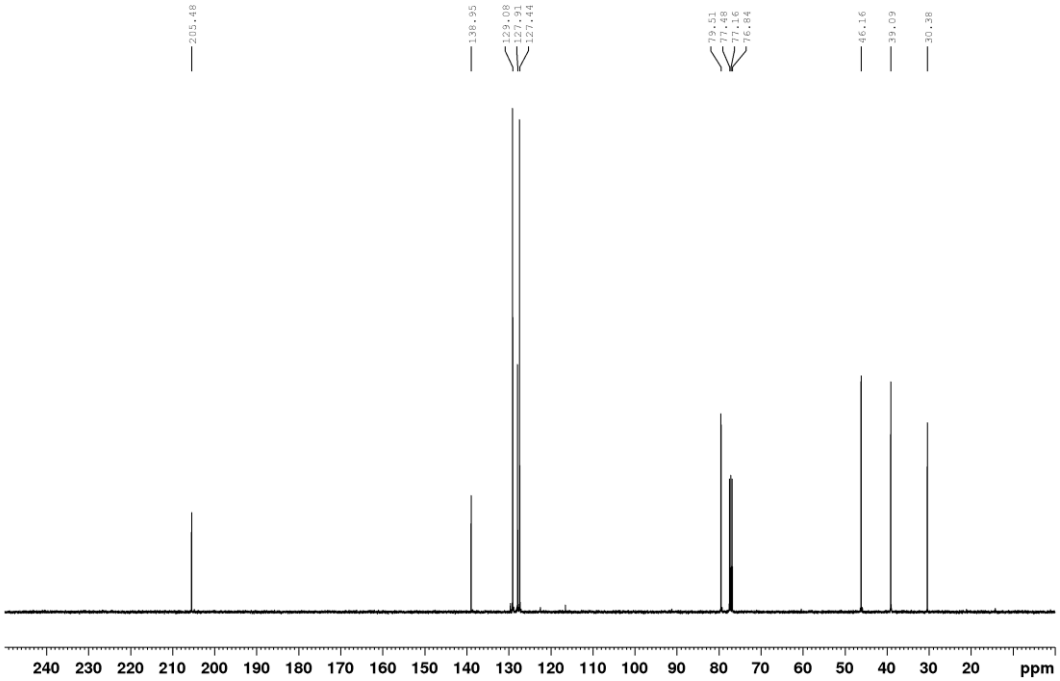

***cis*-2-Acetamido-*N*,*N*-dimethylcyclohexane-1-carboxamide (*cis*-95)**

^{1}H NMR (600 MHz, $CDCl_3$)

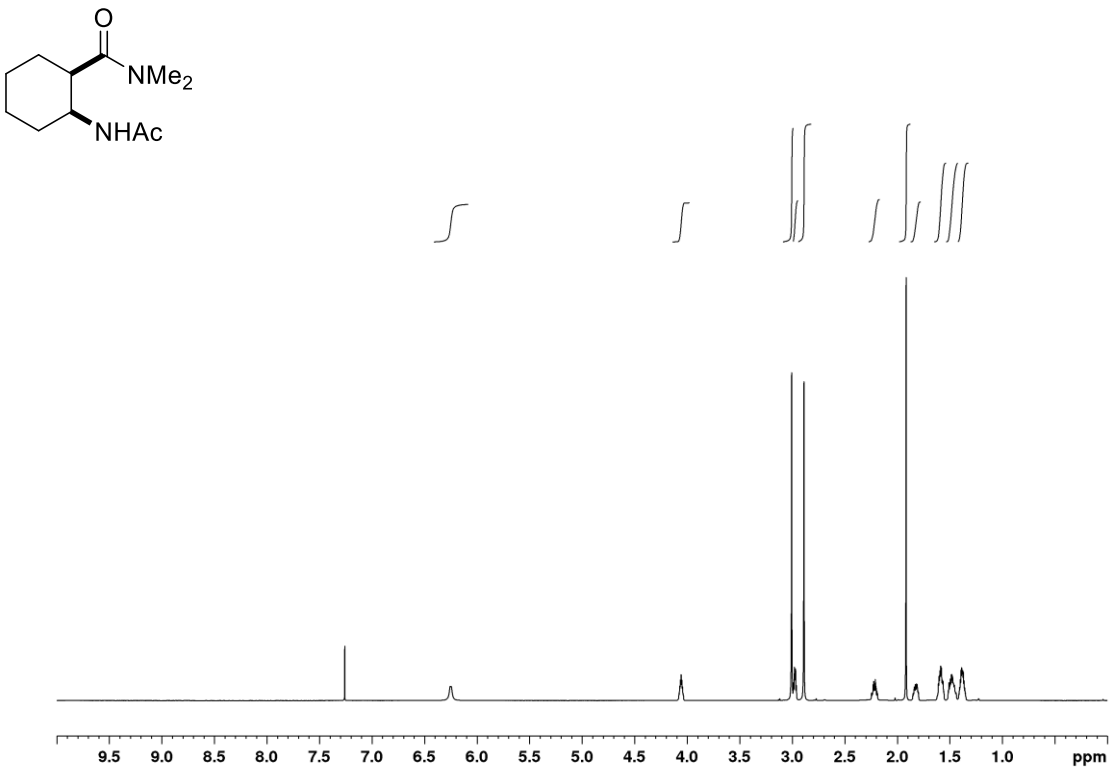

^{13}C NMR (151 MHz, $CDCl_3$)

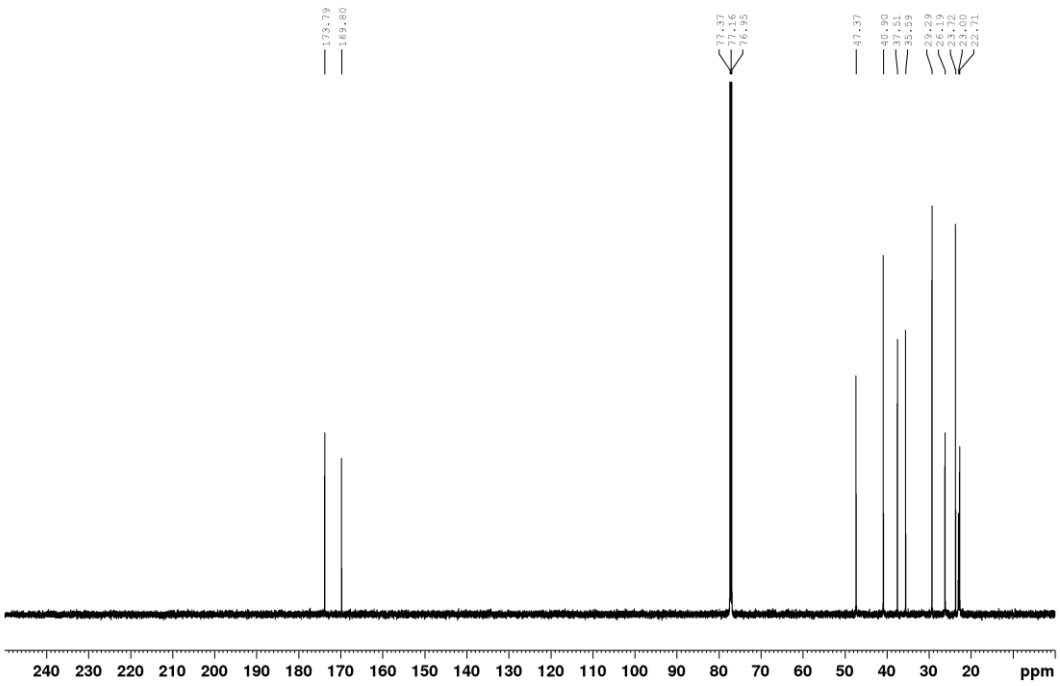

COSY (600 MHz, $CDCl_3$)

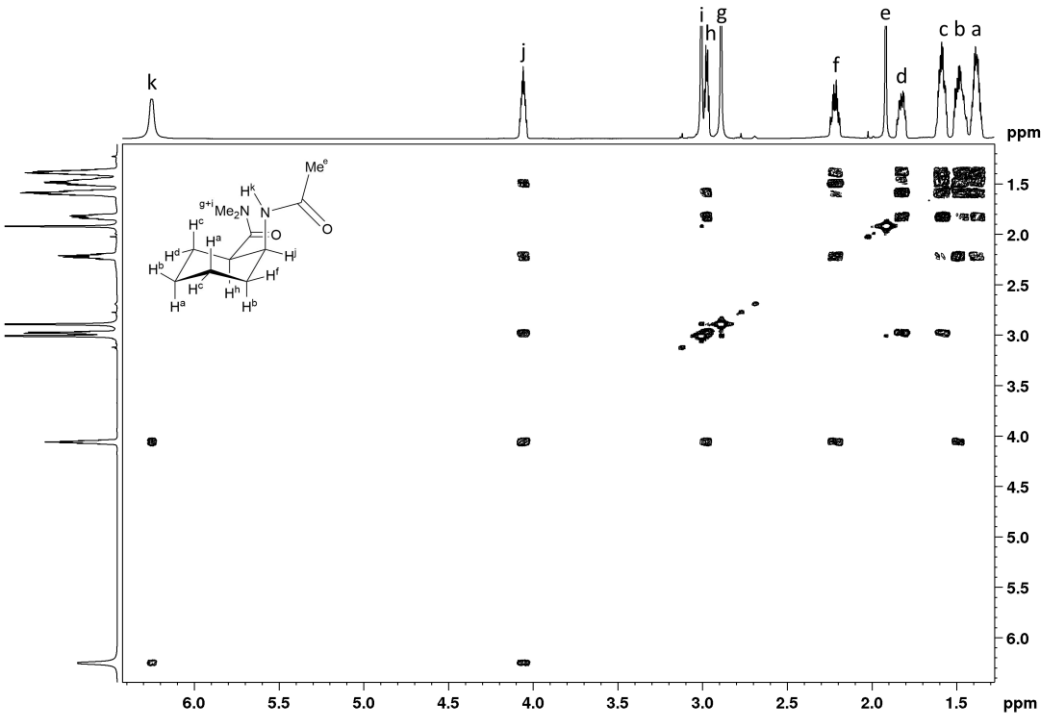

^{1}H,^{13}C-HSQC (600 MHz, $CDCl_3$)

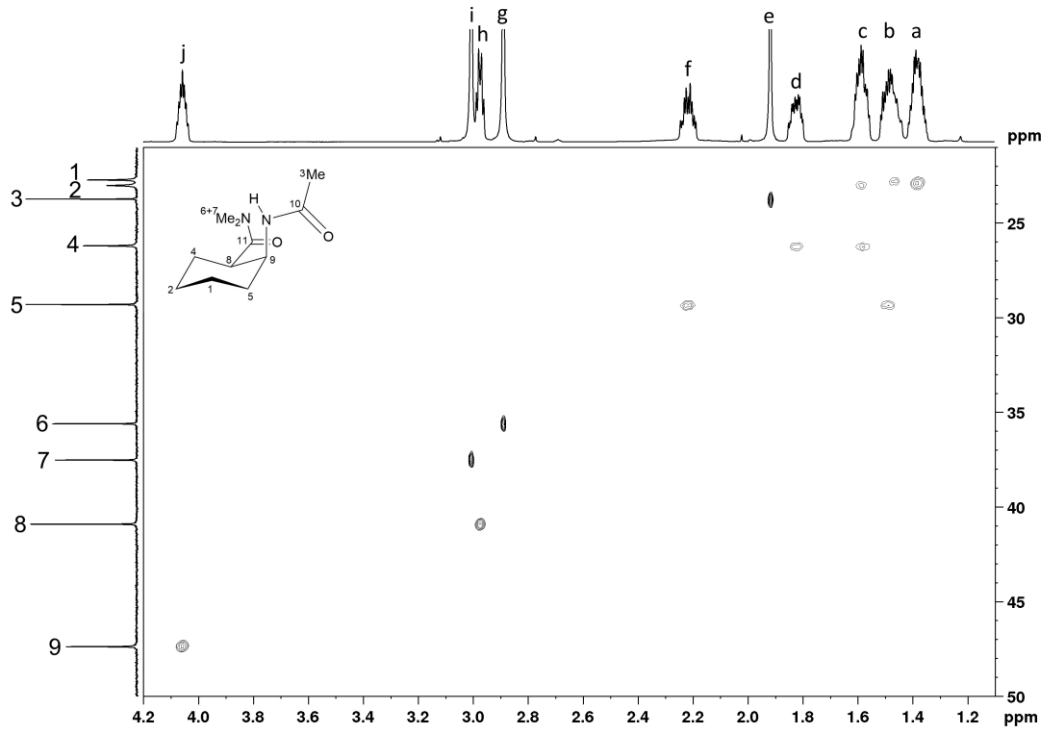

^{1}H,^{13}C-HMBC (600 MHz, $CDCl_3$)

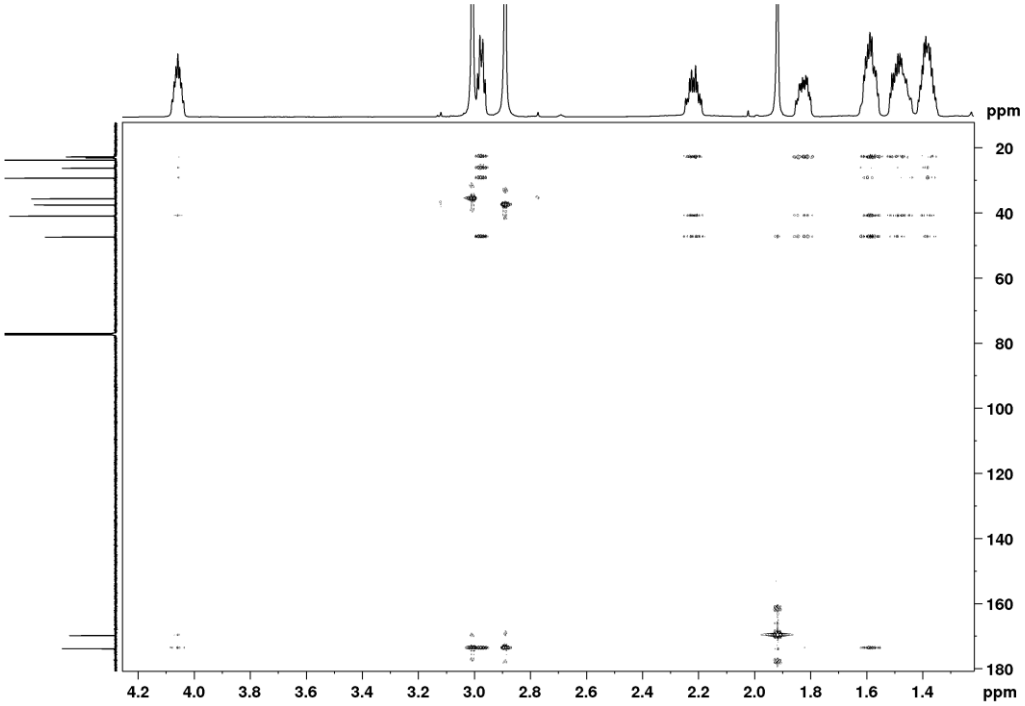

2D-NOESY (600 MHz, $CDCl_3$)

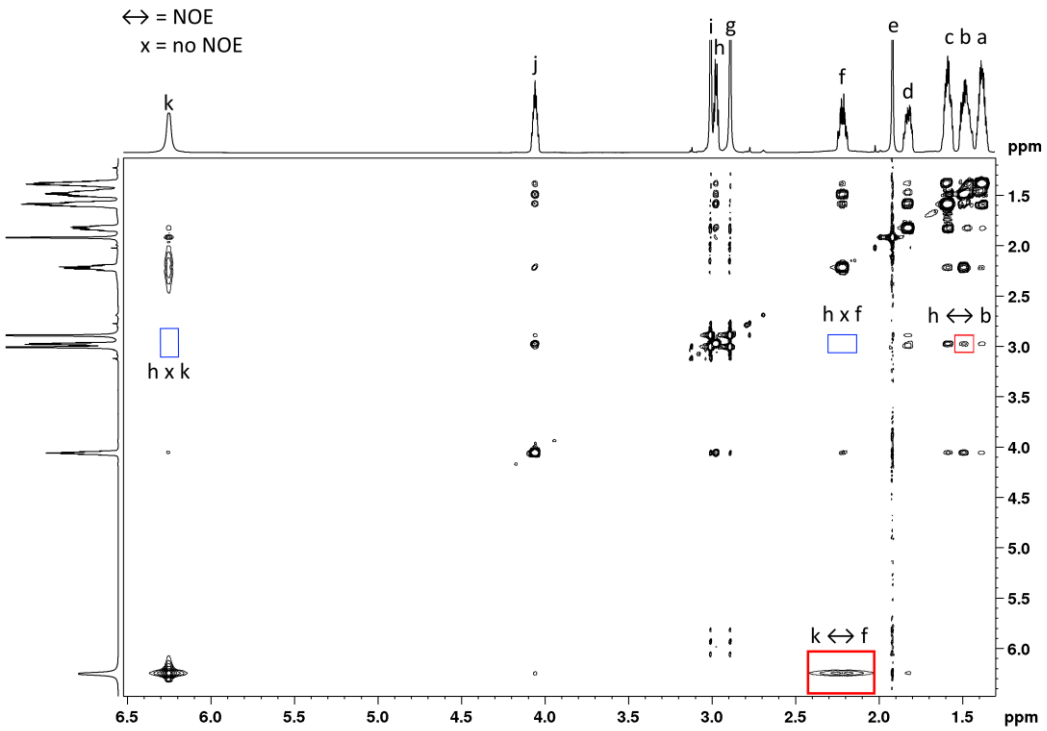

***trans*-2-Acetamido-*N*,*N*-dimethylcyclohexane-1-carboxamide (*trans*-95)**

^{1}H NMR (400 MHz, $CDCl_3$)

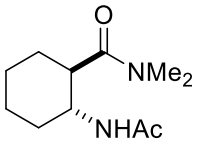

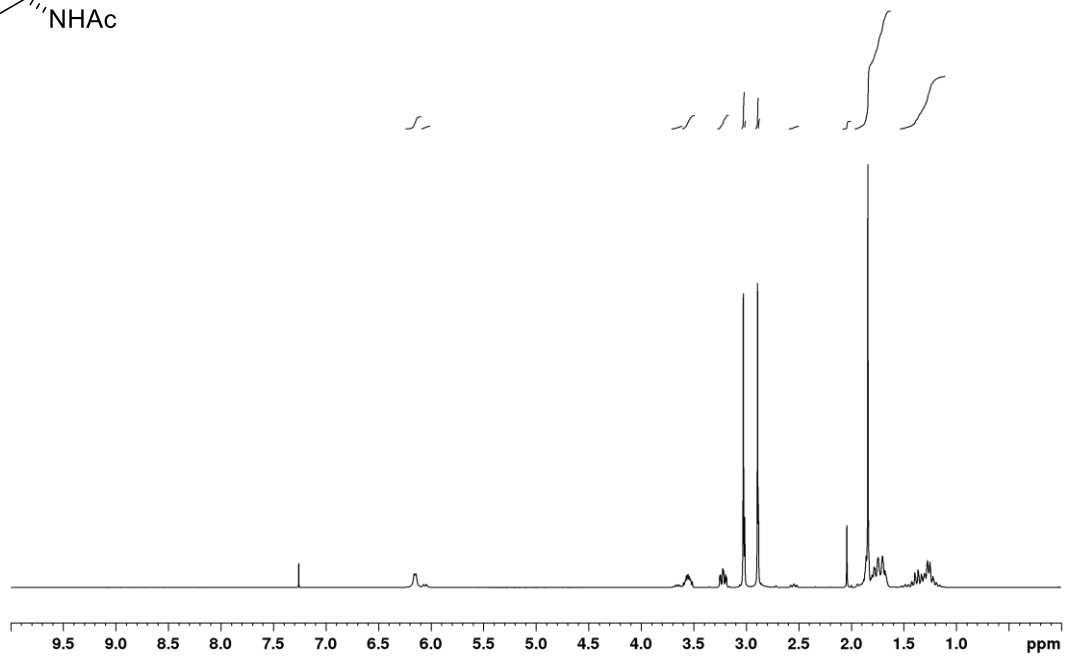

^{13}C NMR (101 MHz, $CDCl_3$)

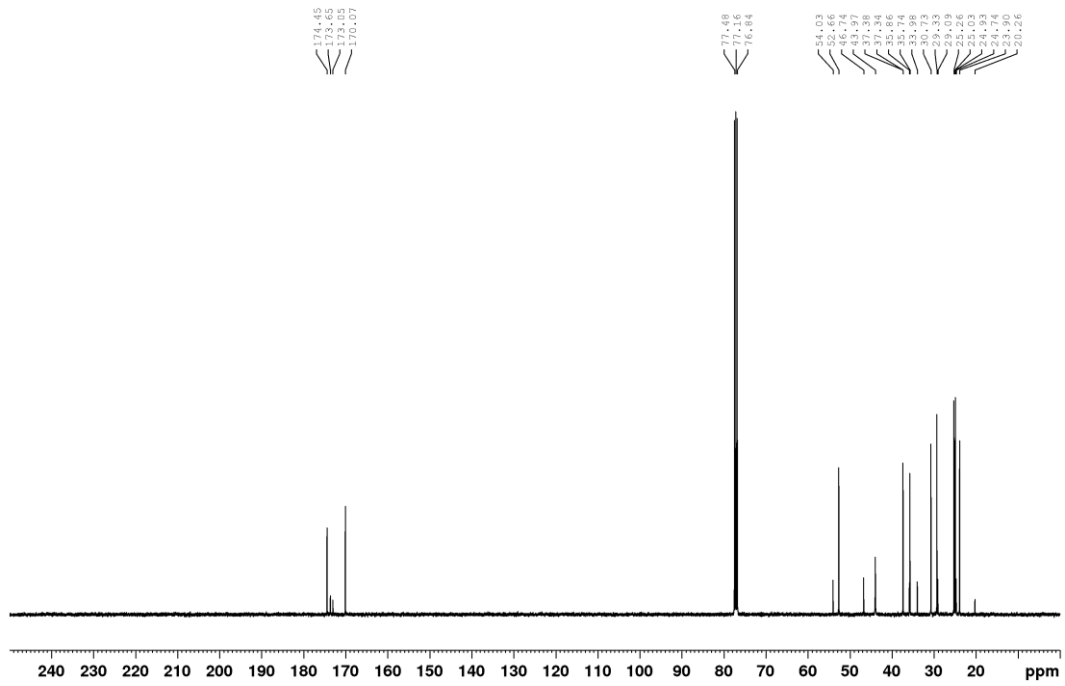

COSY (400 MHz, $CDCl_3$)

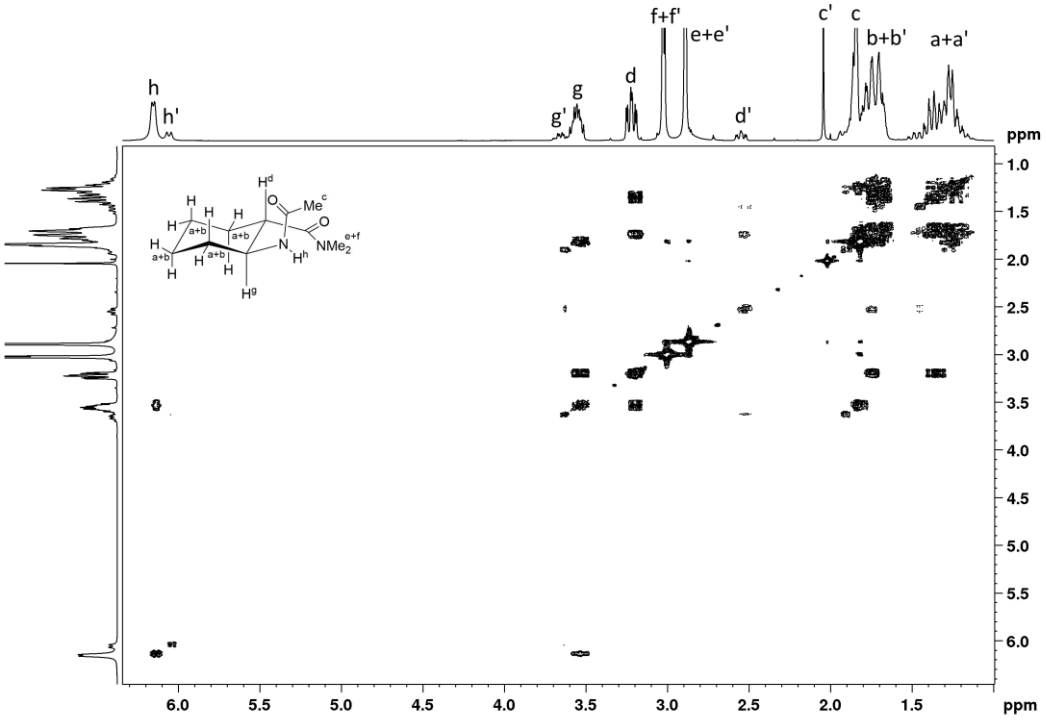

^{1}H,^{13}C-HSQC (400 MHz, $CDCl_3$)

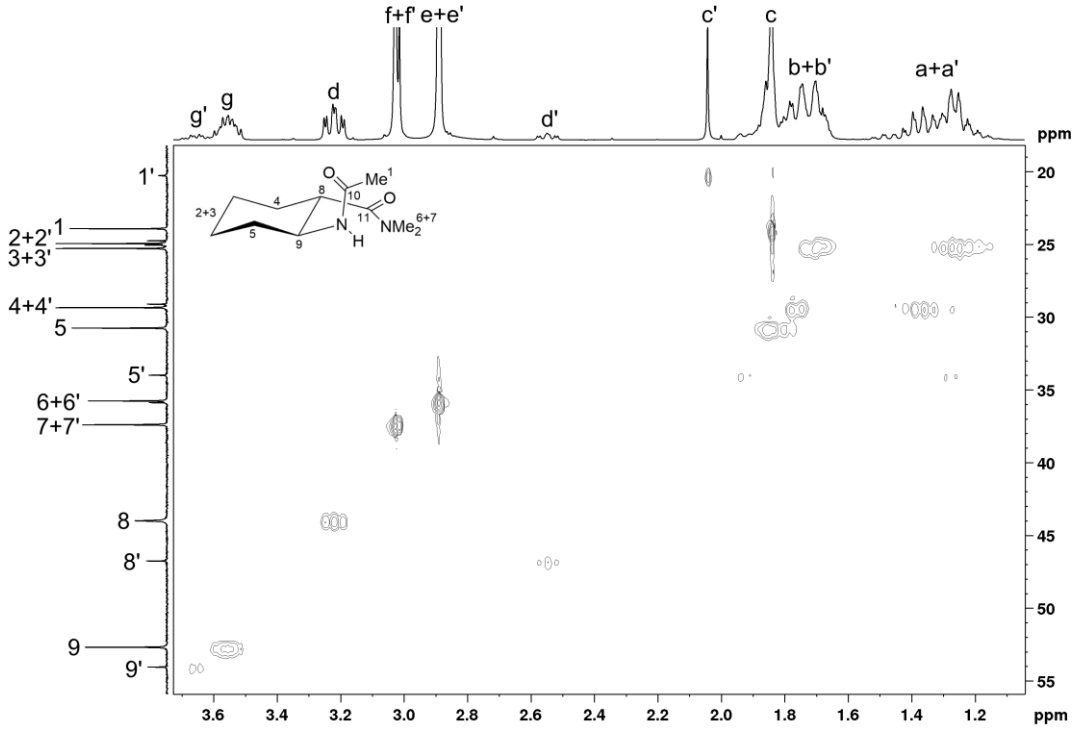

^{1}H,^{13}C-HMBC (600 MHz, $CDCl_3$)

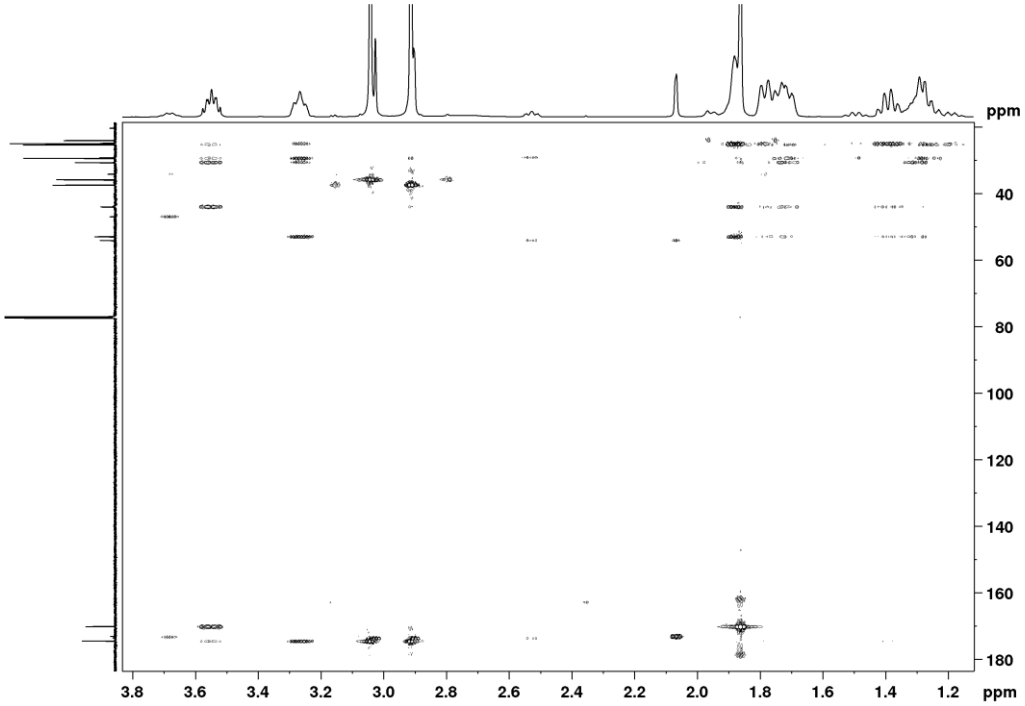

2D-NOESY (400 MHz, $CDCl_3$)

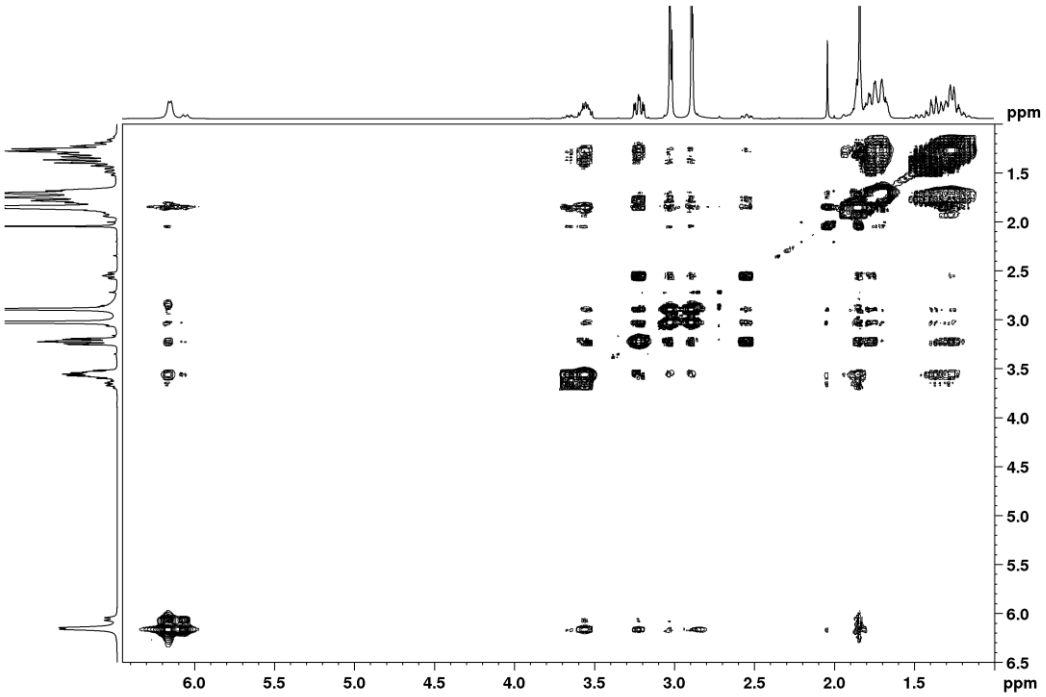

***cis*-6-(Dimethylcarbamoyl)cyclohex-3-ene-1-carboxylic acid (*cis*-96)**

^{1}H NMR (300 MHz, $CDCl_3$)

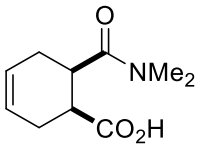

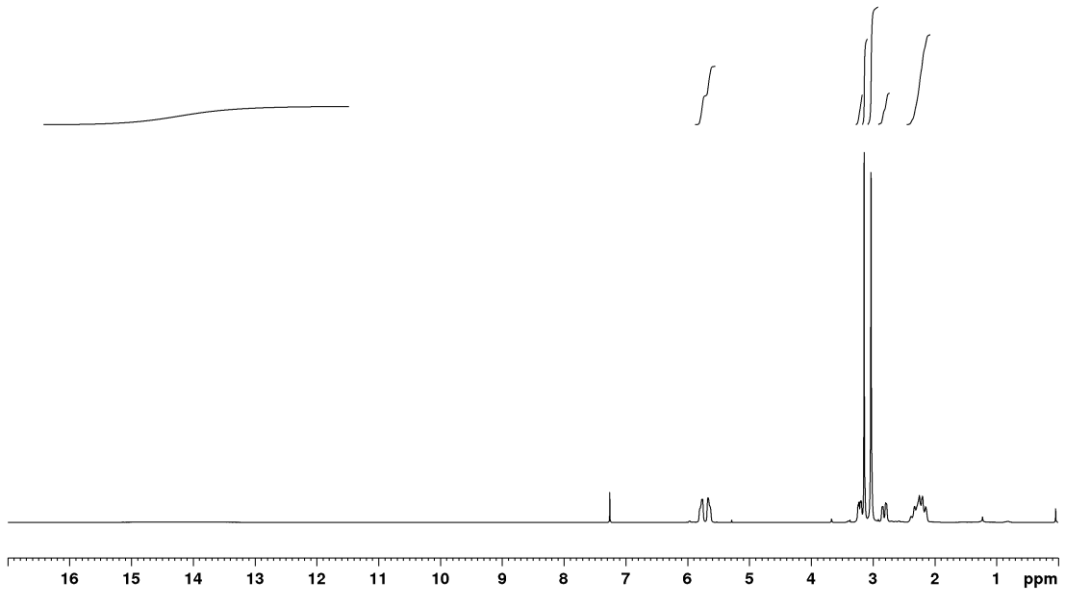

^{13}C NMR (75 MHz, $CDCl_3$)

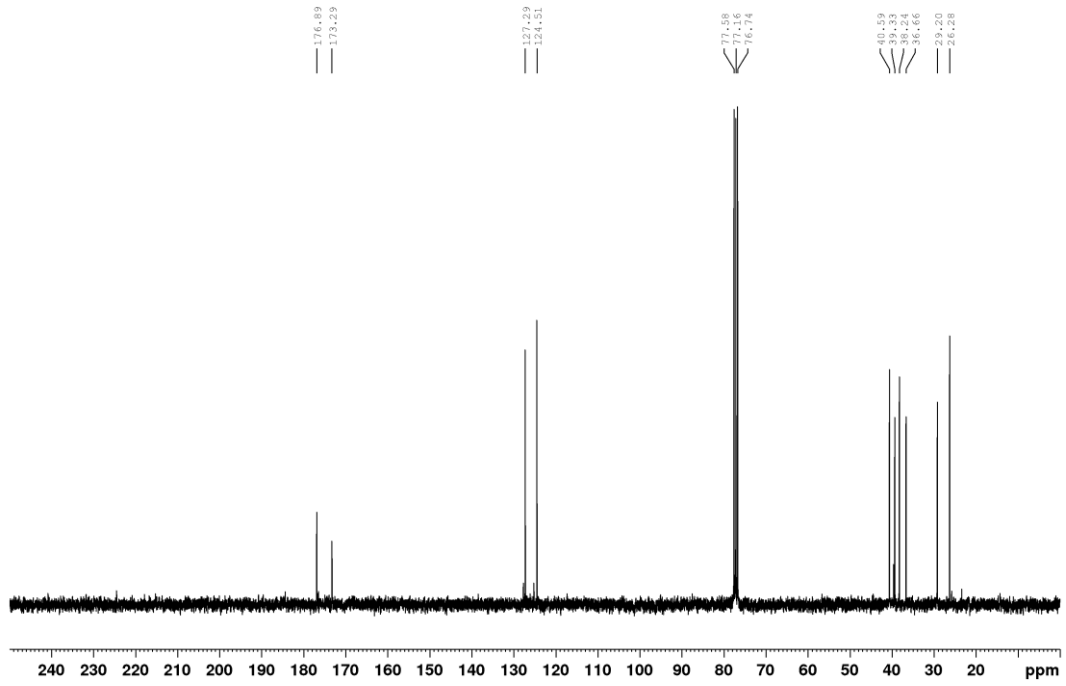

***trans*-6-(Dimethylcarbamoyl)cyclohex-3-ene-1-carboxylic acid (*trans*-96)**

^{1}H NMR (300 MHz, $CDCl_3$)

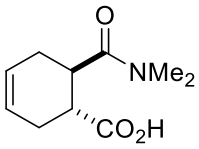

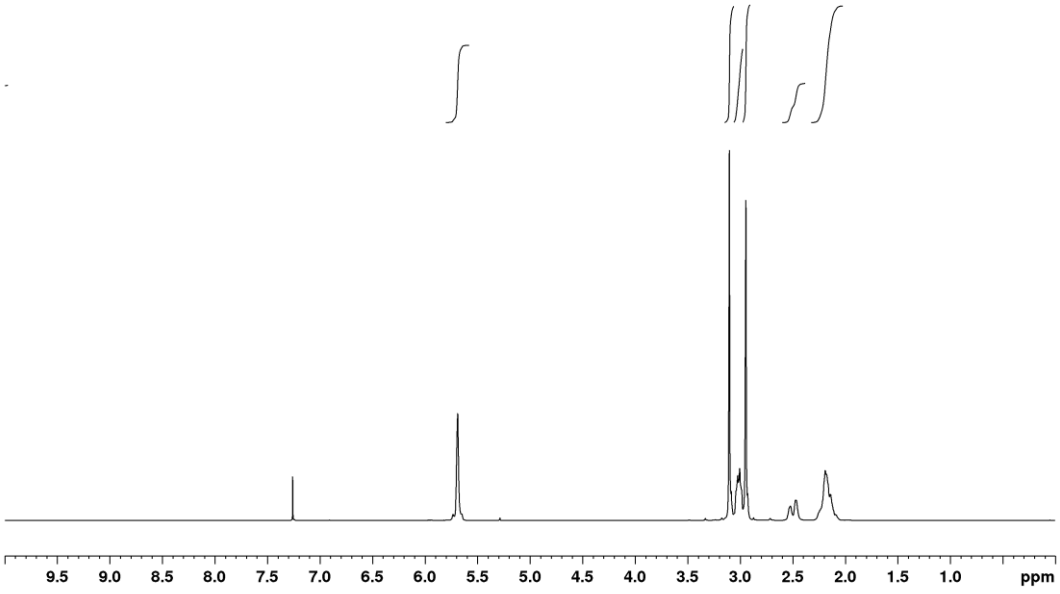

^{13}C NMR (75 MHz, $CDCl_3$)

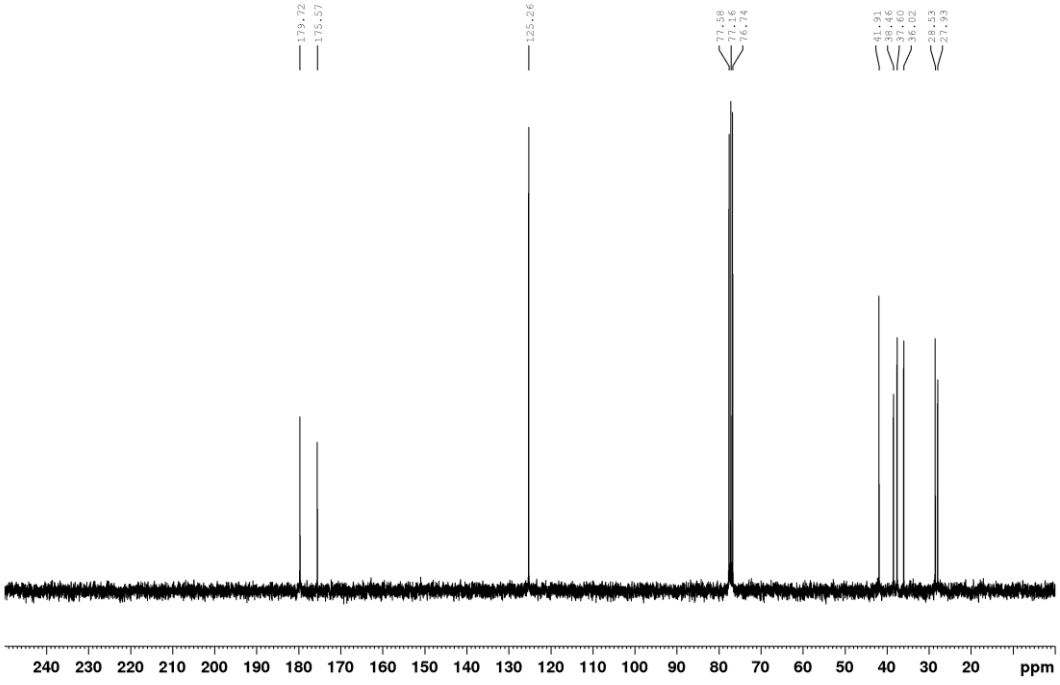

***trans*-Cyclohex-4-ene-1,2-dicarboxylic acid (*trans*-99)**

^{1}H NMR (300 MHz, $(CD_3)_2SO$)

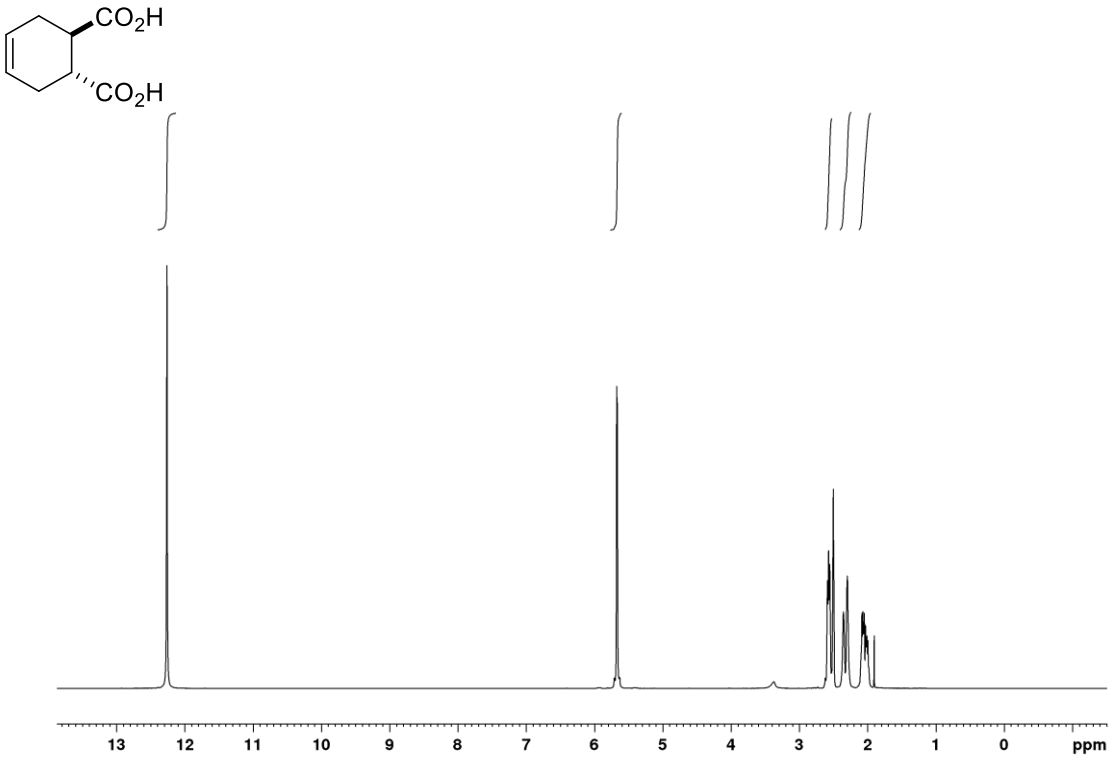

^{13}C NMR (75 MHz, $(CD_3)_2SO$)

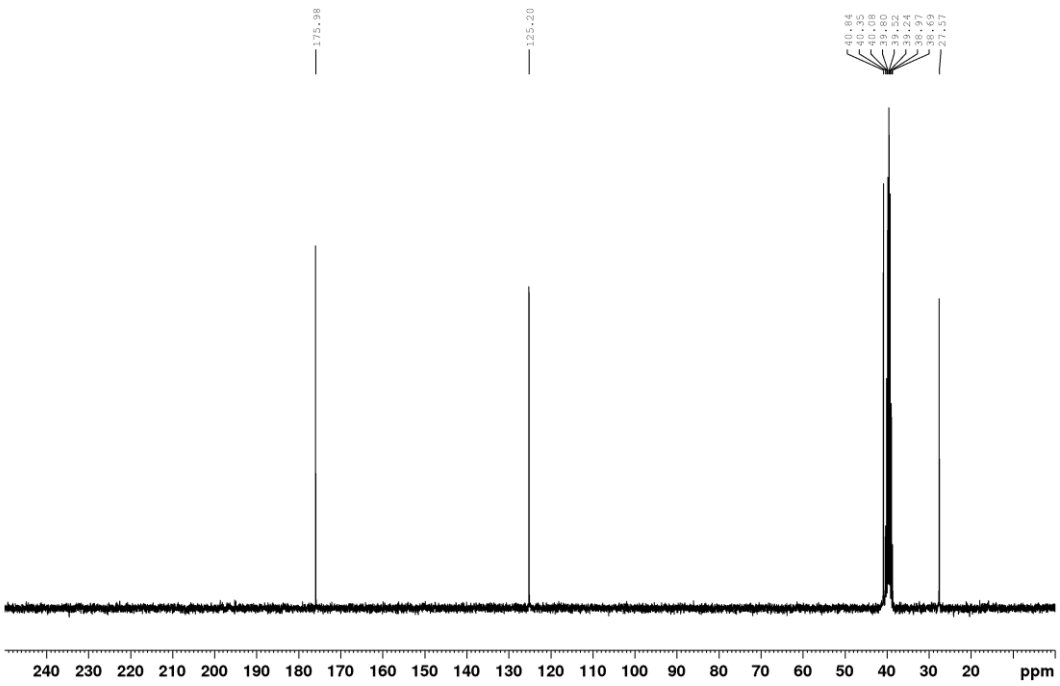

***cis*-2-(Acetylamino)cyclohexanecarboxylic acid methyl ester (*cis*-100)**

^{1}H NMR (400 MHz, $CDCl_3$)

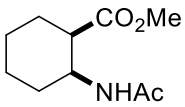

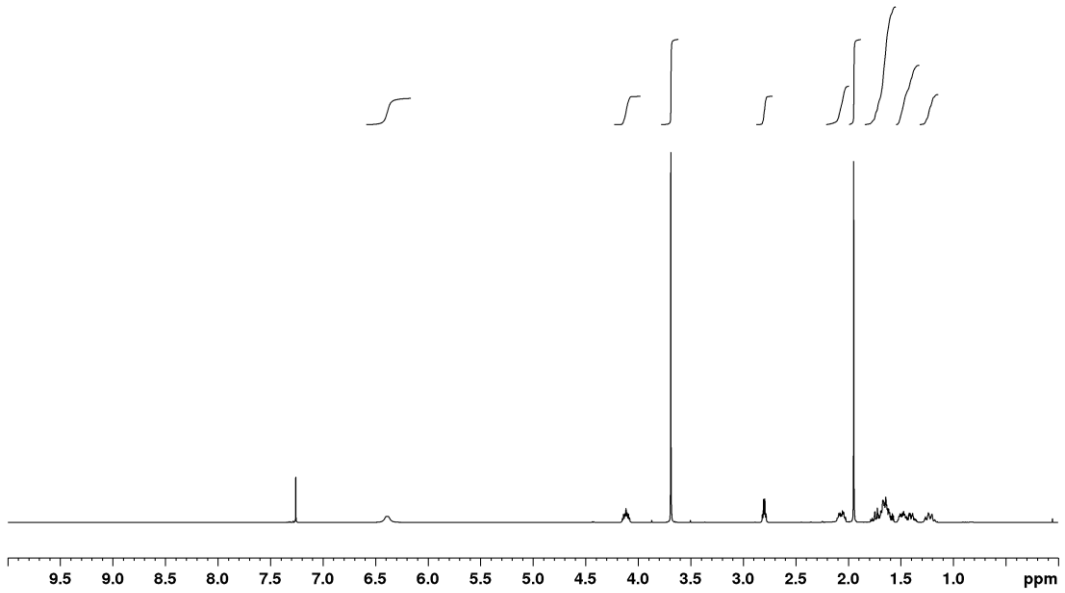

^{13}C NMR (75 MHz, $CDCl_3$)

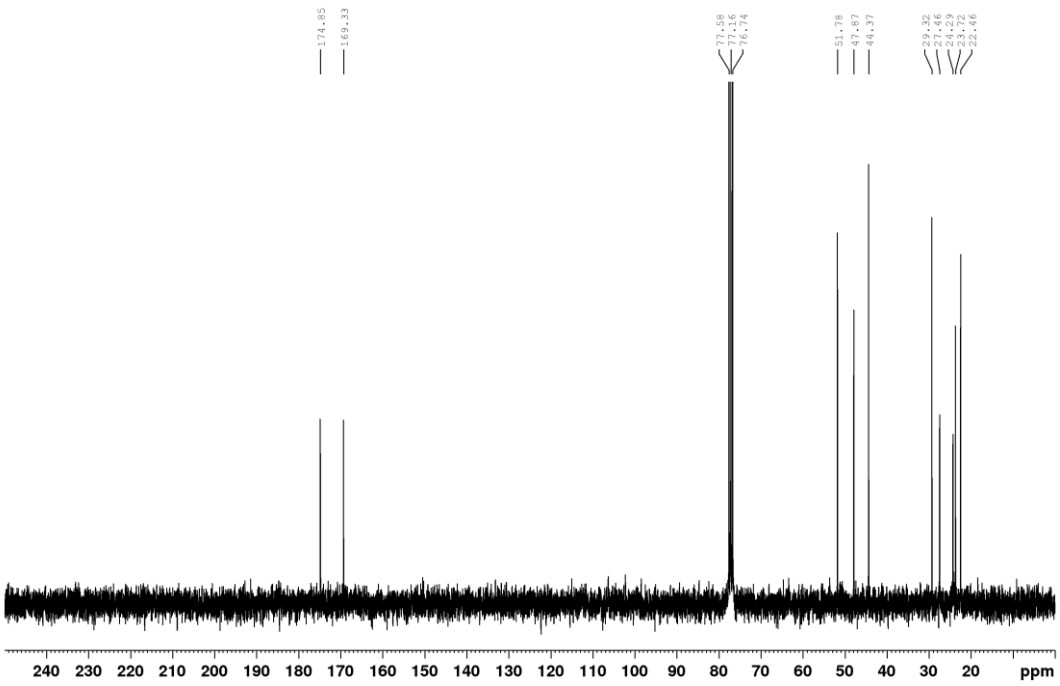

***trans*-2-(Acetylamino)cyclohexanecarboxylic acid methyl ester (*trans*-100)**

^{1}H NMR (300 MHz, $CDCl_3$)

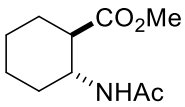

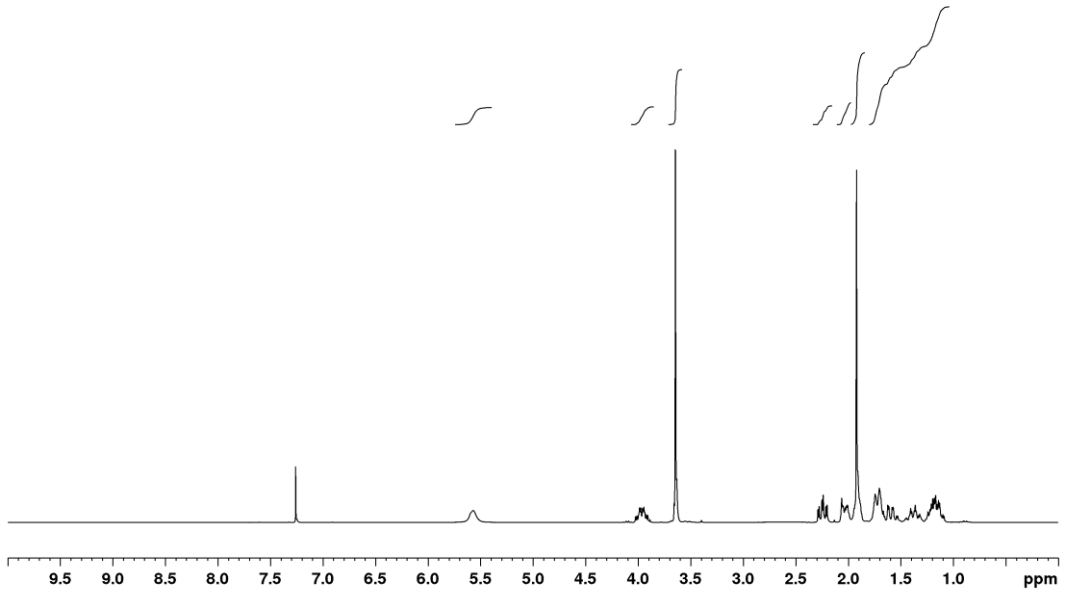

^{13}C NMR (75 MHz, $CDCl_3$)

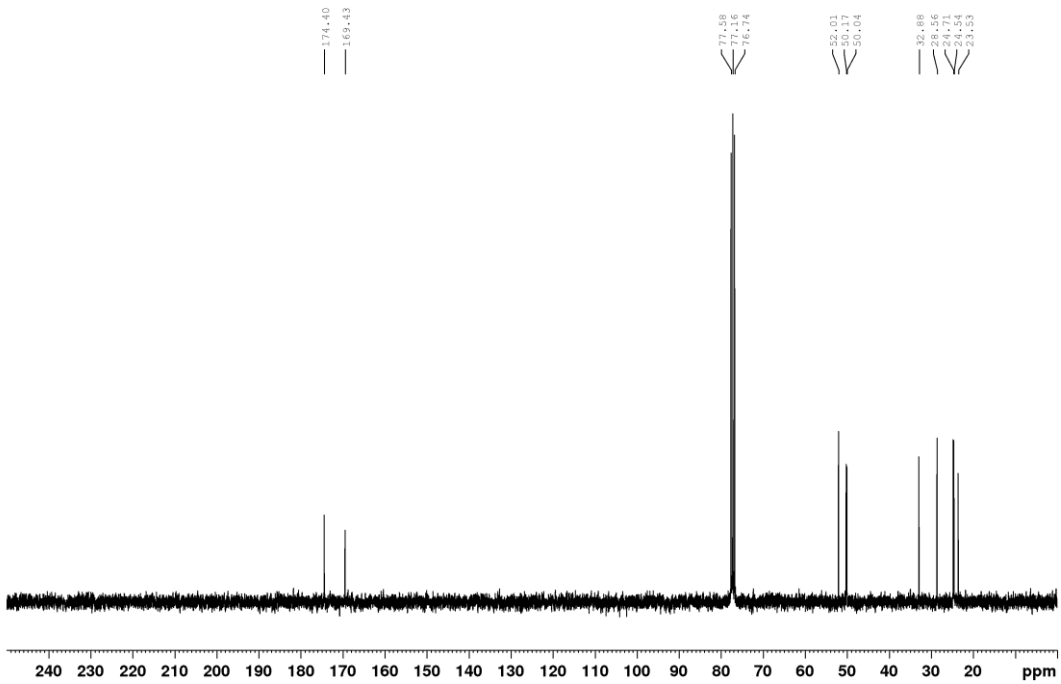

***cis*-2-Acetamidocyclohexane-1-carboxylic acid (*cis*-101)**

^{1}H NMR (300 MHz, CD_3OD)

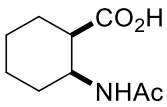

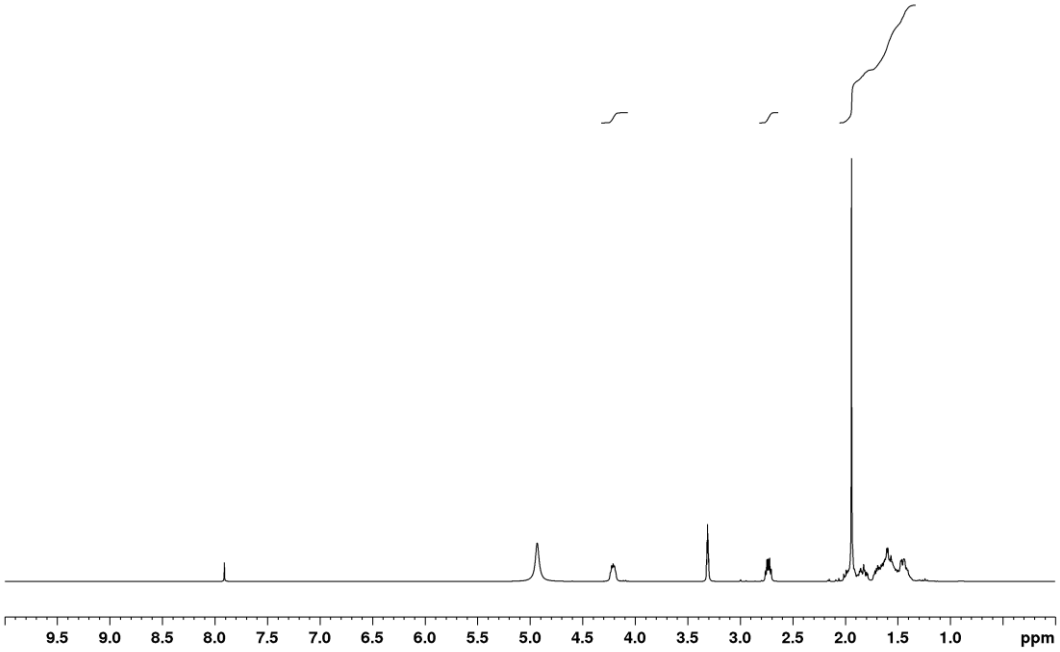

^{13}C NMR (75 MHz, CD_3OD)

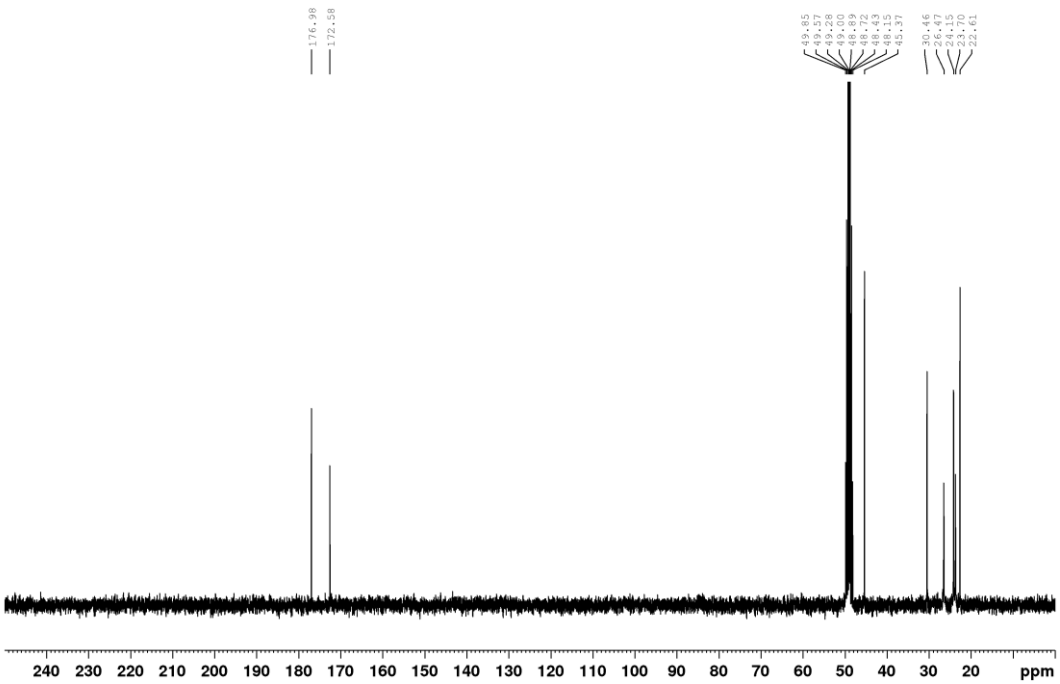

***trans*-2-Acetamidocyclohexane-1-carboxylic acid (*trans*-101)**

^{1}H NMR (300 MHz, CD_3OD)

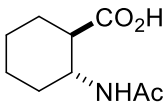

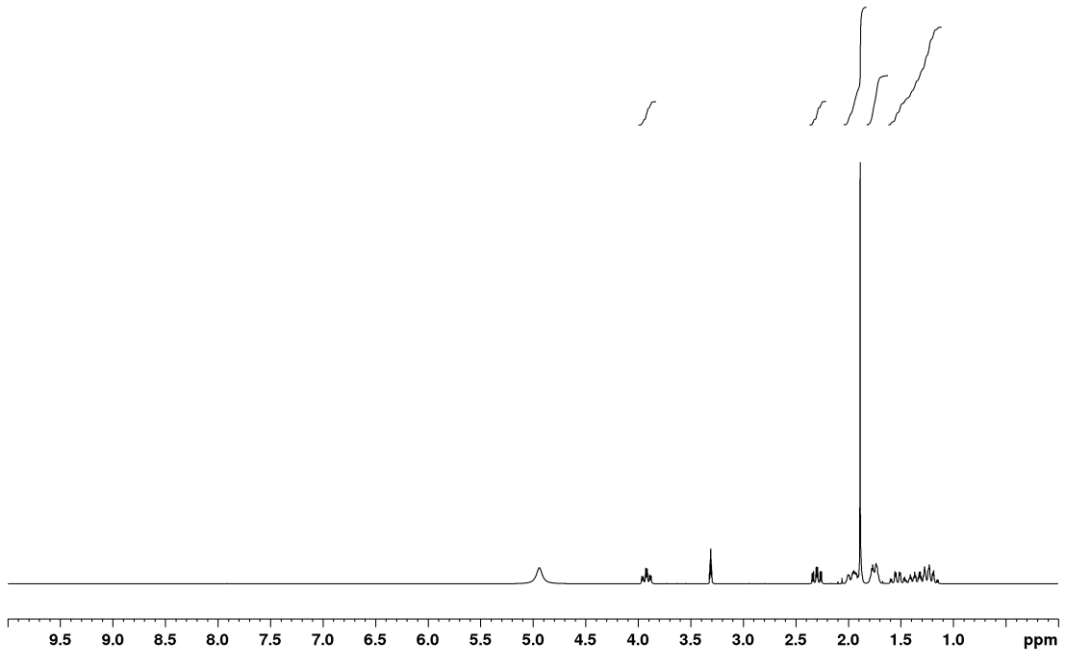

^{13}C NMR (75 MHz, CD_3OD)

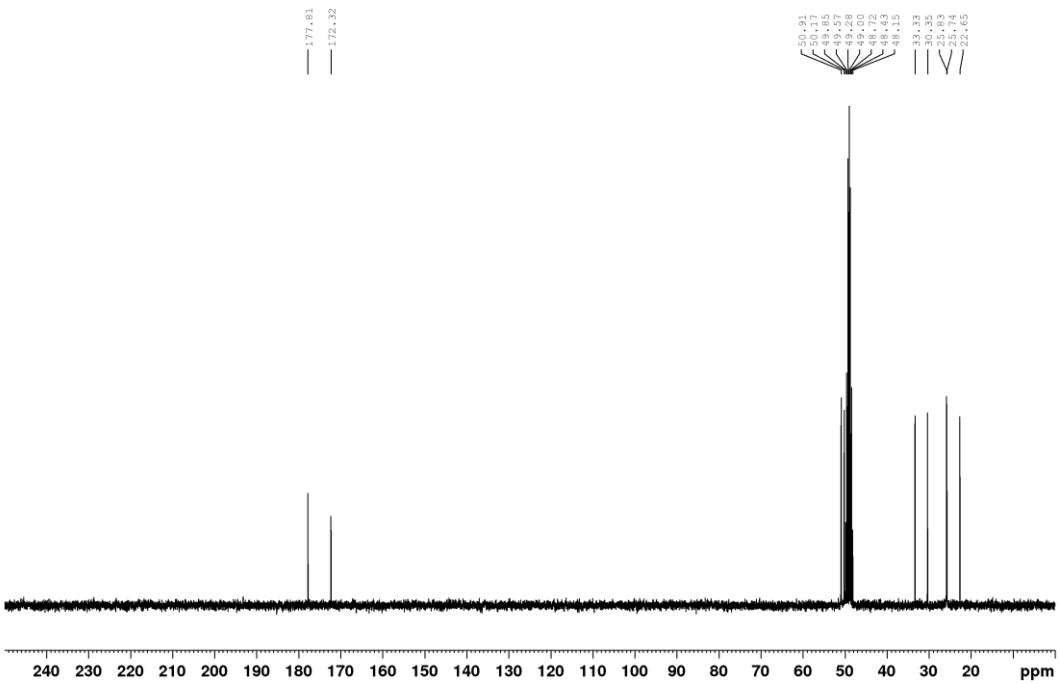

Trimethylamine ^{15}*N*-oxide dihydrate (^{15}N-102·2H$_2$O)

^{1}H NMR (400 MHz, D_2O)

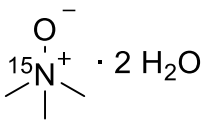

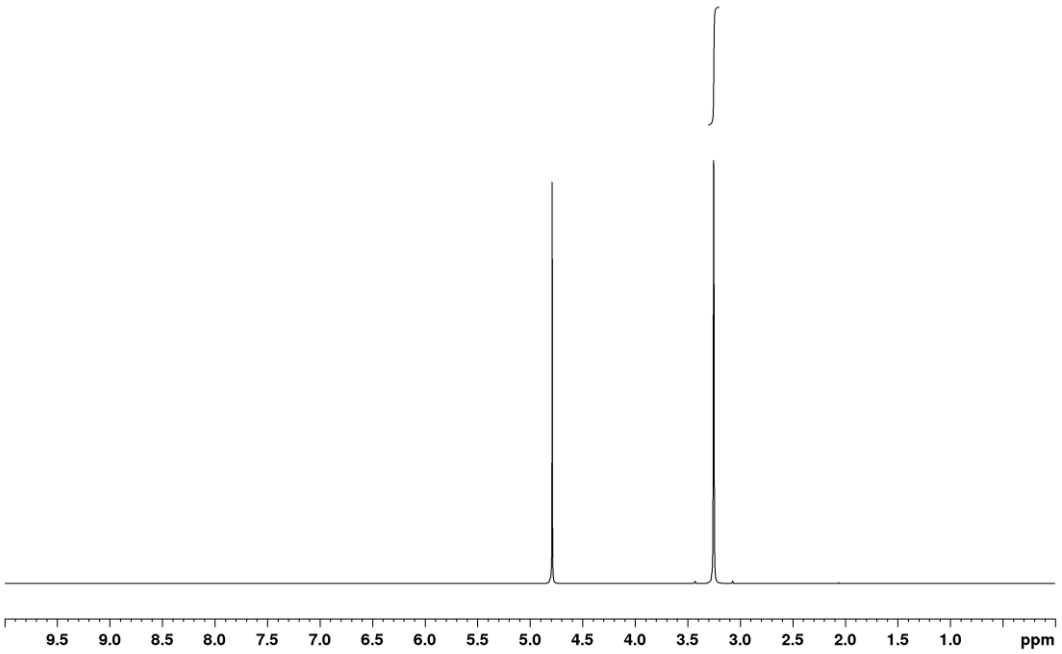

^{13}C NMR (101 MHz, D_2O)

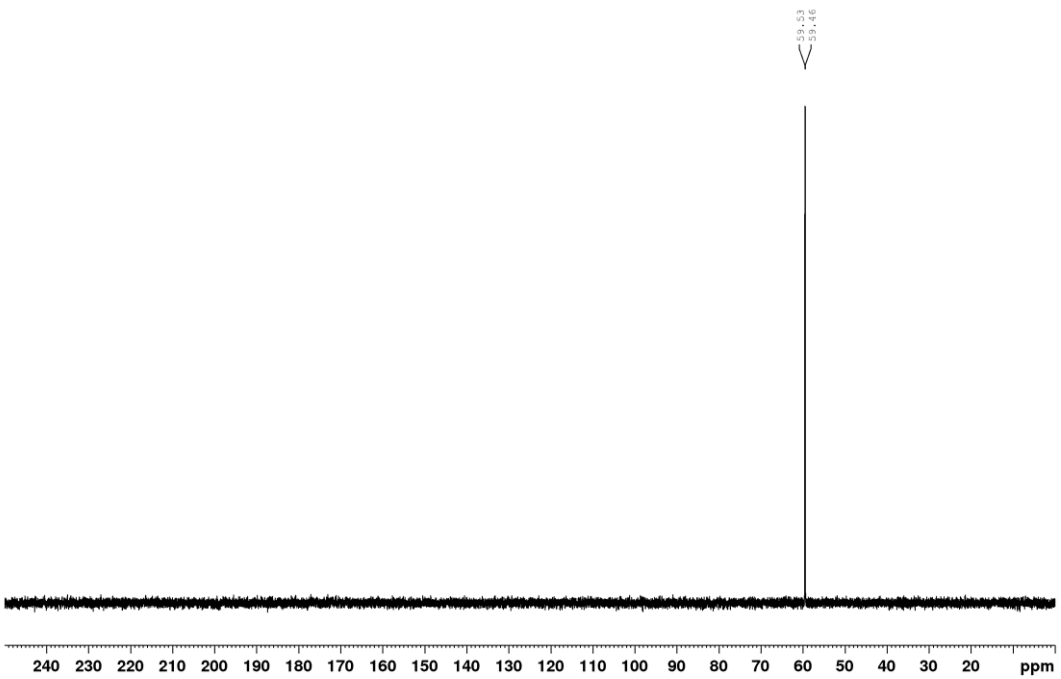

^{15}*N*-Methylacetamide (**^{15}N-103**)

^{1}H NMR (400 MHz, $CDCl_3$)

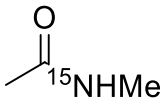

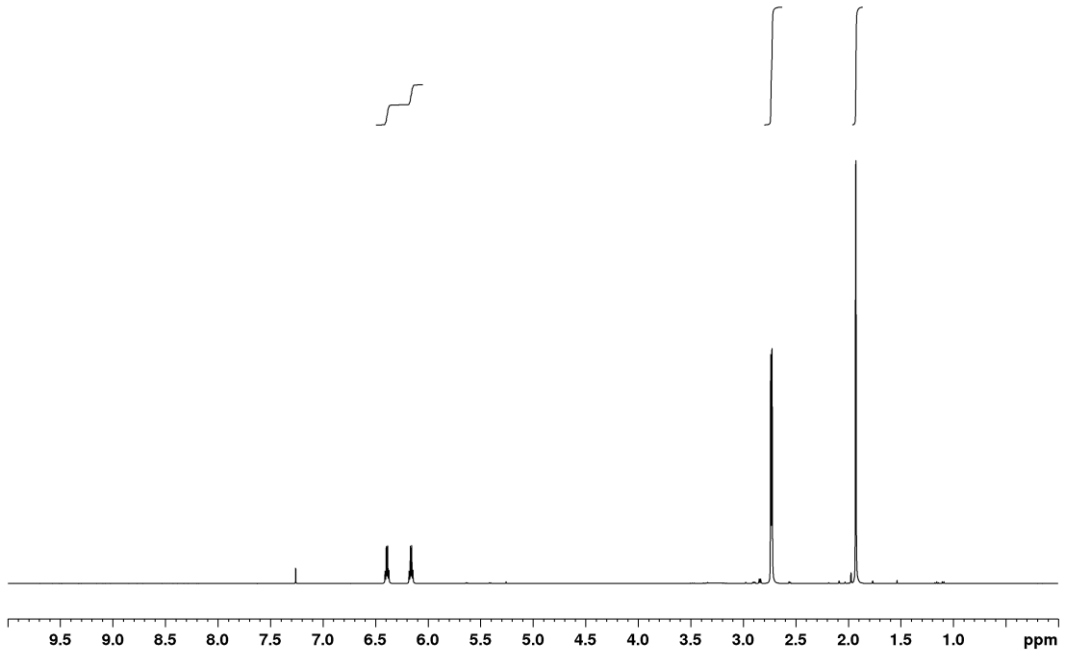

^{13}C NMR (101 MHz, $CDCl_3$)

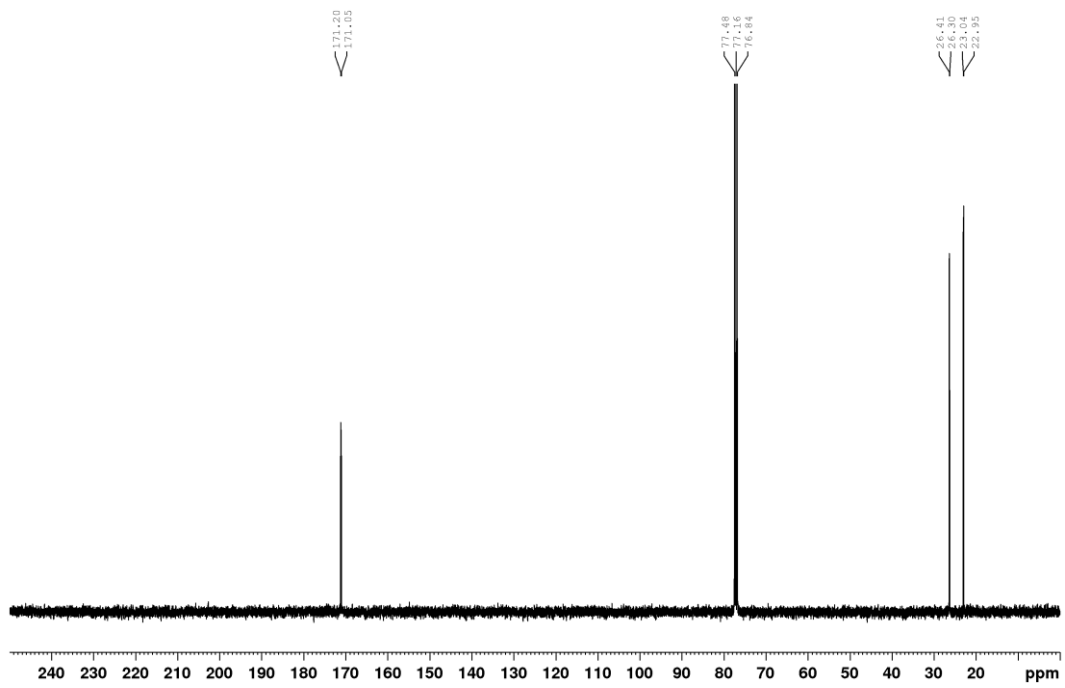

^{15}N-Acetamide (^{15}N-106)

^{1}H NMR (300 MHz, $CDCl_3$)

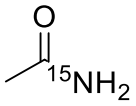

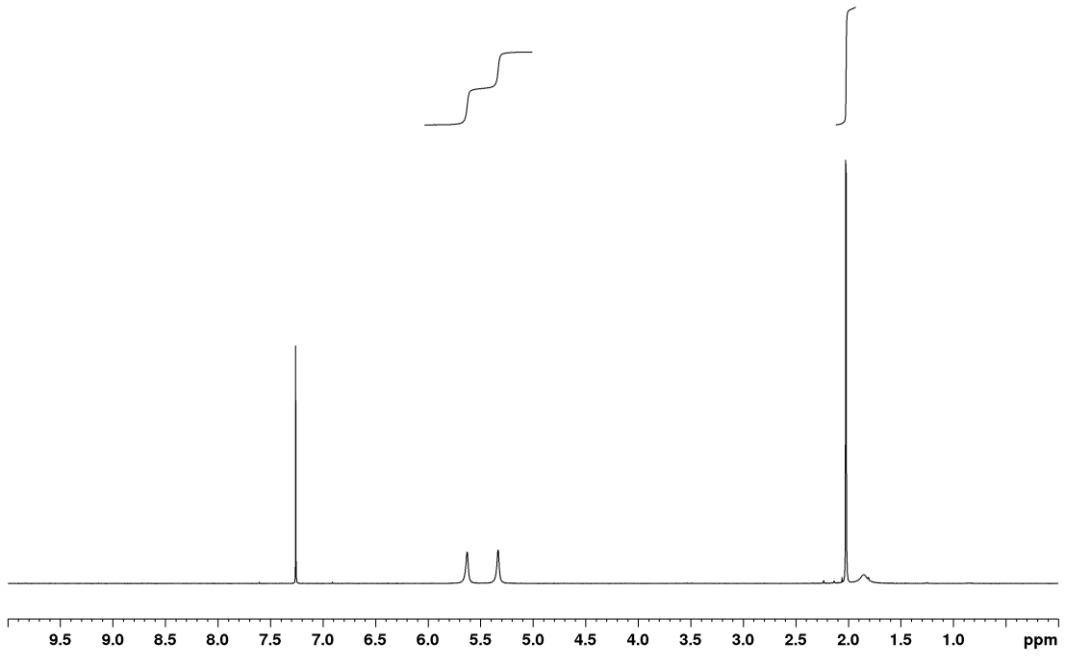

^{13}C NMR (75 MHz, $CDCl_3$)

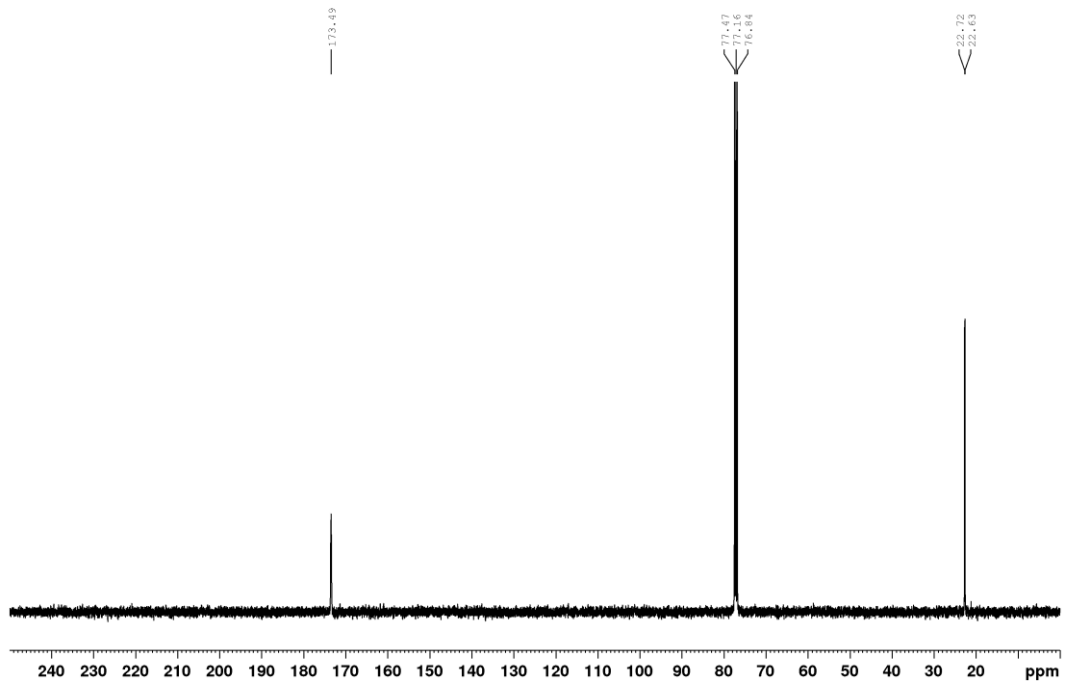

2,2,2-Trifluoroethyl acetate (107)

^{1}H NMR (300 MHz, $CDCl_3$)

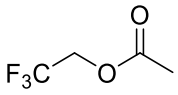

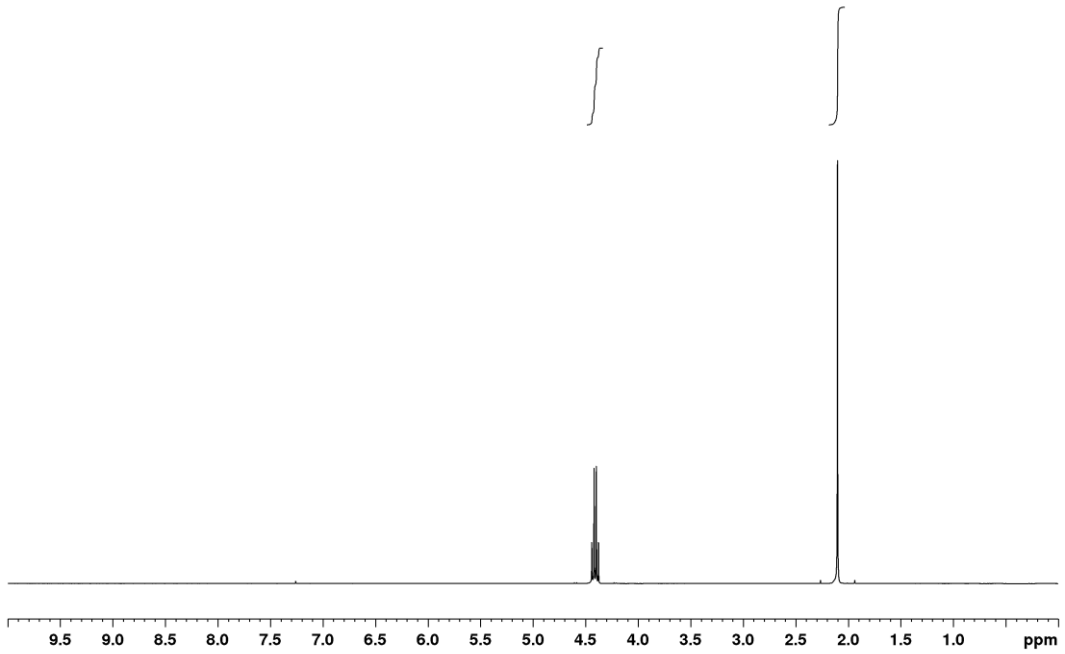

^{13}C NMR (75 MHz, $CDCl_3$)

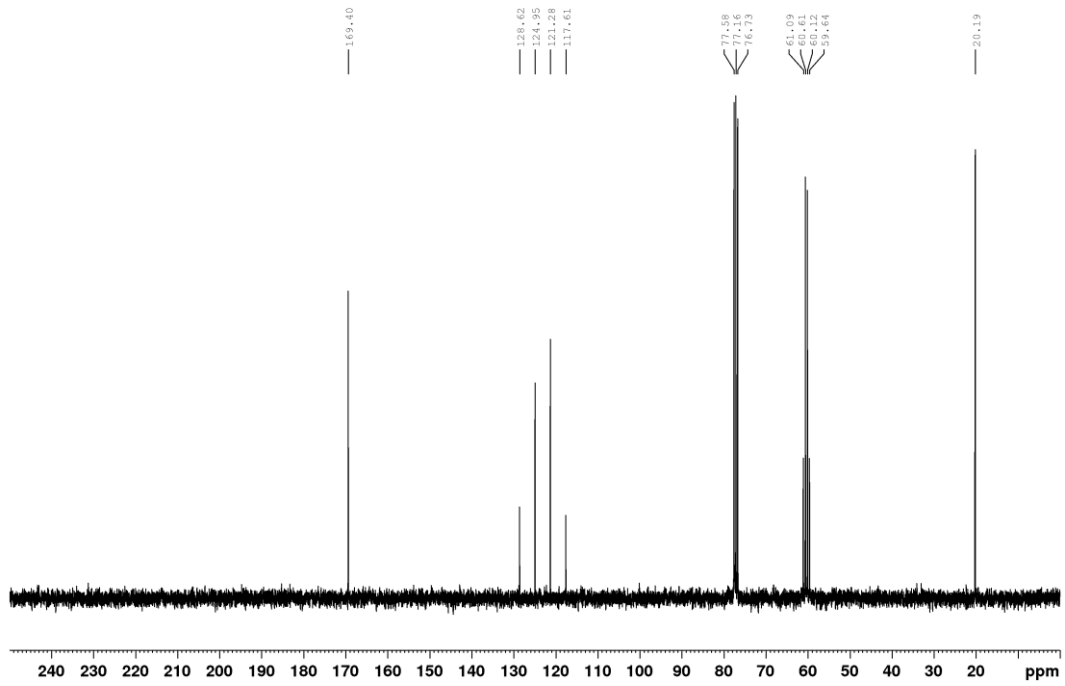

***cis*-1-(4-Bromophenyl) 2-methyl cyclohex-4-ene-1,2-dicarboxylate (108)**

^{1}H NMR (300 MHz, $CDCl_3$)

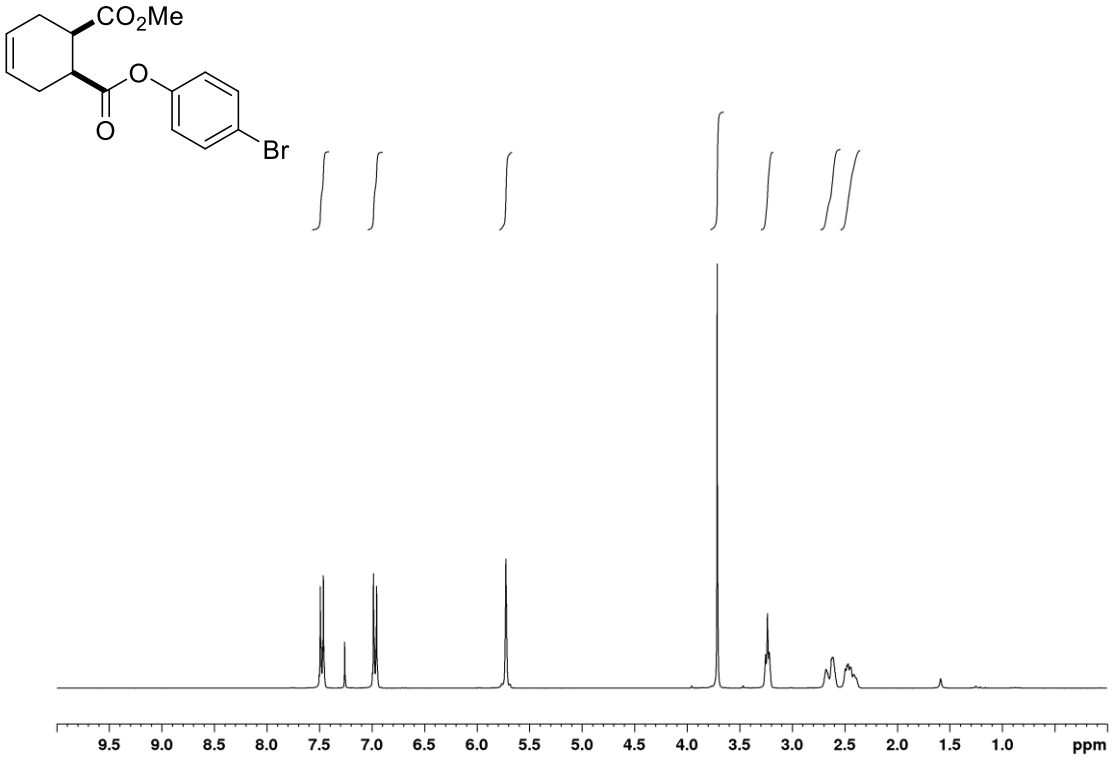

^{13}C NMR (75 MHz, $CDCl_3$)

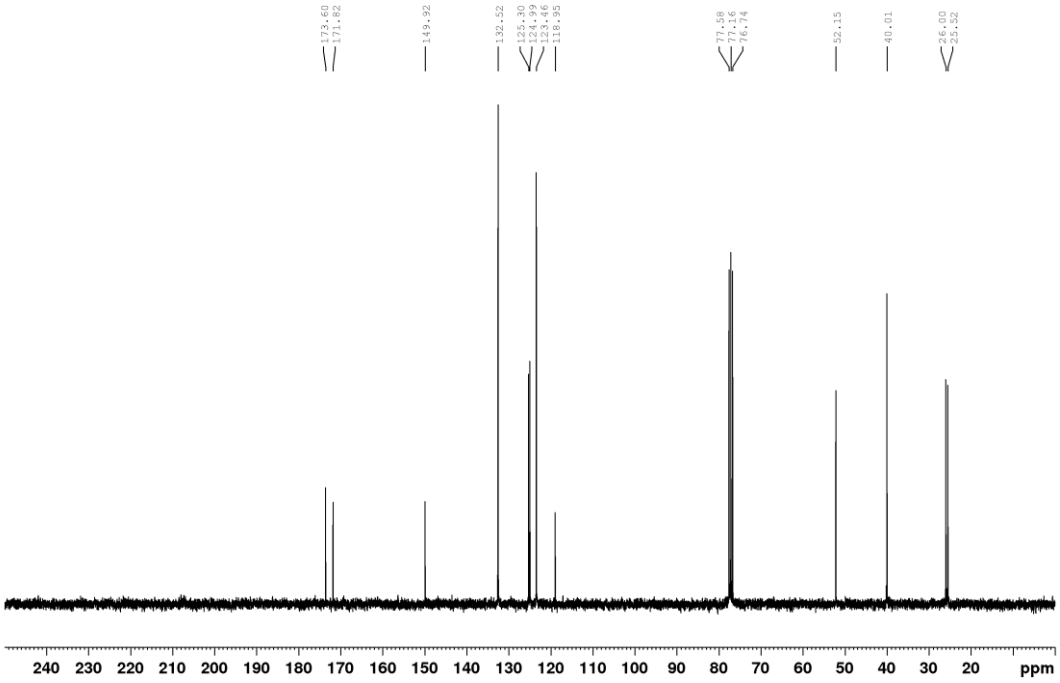

3. HPLC chromatograms

2-Ethyl-4-nitro-3-phenylbutanal (41a)

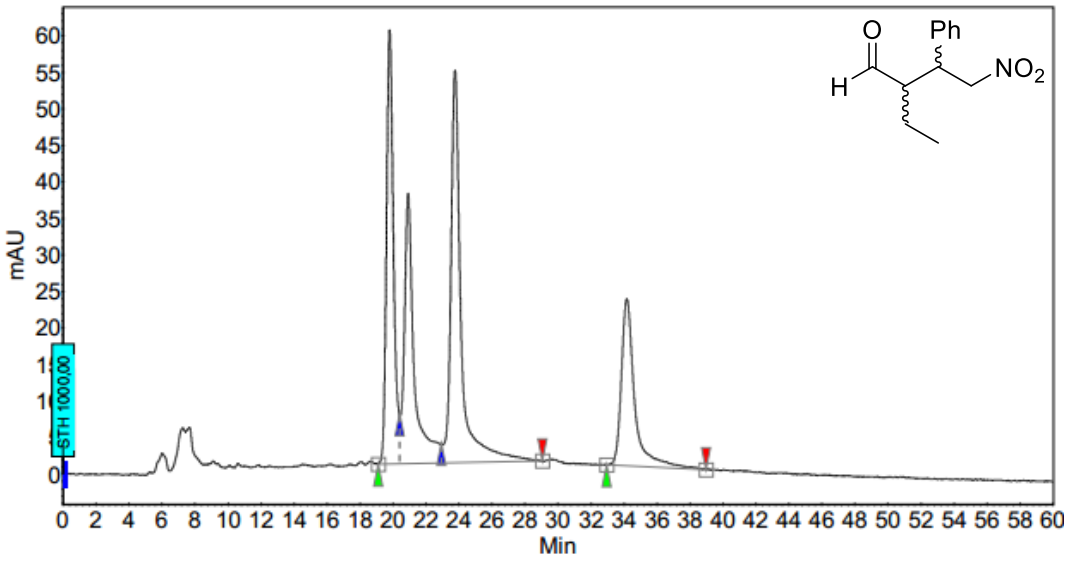

Peak Results :

Index	Name	Time [Min]	Quantity [% Area]	Height [mAU]	Area [mAU.Min]	Area % [%]
1	UNKNOWN	19,79	25,32	59,4	29,0	25,317
3	UNKNOWN	20,92	22,41	36,9	25,7	22,408
2	UNKNOWN	23,76	33,80	53,7	38,7	33,796
4	UNKNOWN	34,17	18,48	22,8	21,2	18,478
Total			100,00	172,8	114,6	100,000

(2*R*,3*S*)-2-Ethyl-4-nitro-3-phenylbutanal ((2*R*,3*S*)-41a)

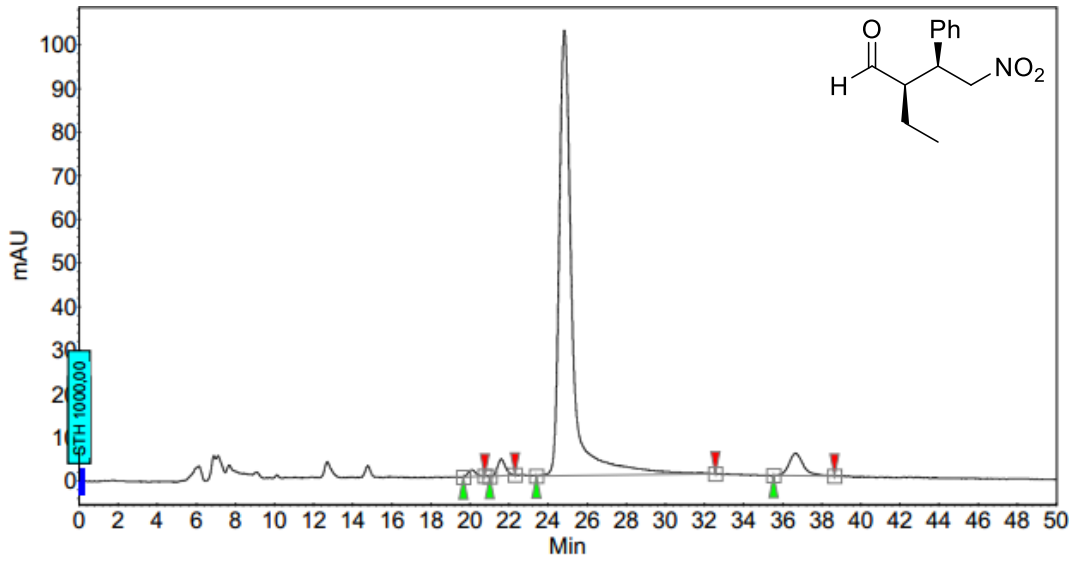

Peak Results :

Index	Name	Time [Min]	Quantity [% Area]	Height [mAU]	Area [mAU.Min]	Area % [%]
1	UNKNOWN	20,07	0,82	1,6	0,7	0,816
2	UNKNOWN	21,61	2,09	3,9	1,8	2,093
3	UNKNOWN	24,83	91,90	102,1	78,8	91,899
4	UNKNOWN	36,66	5,19	5,2	4,5	5,192
Total			100,00	112,8	85,8	100,000

2-(2-Nitro-1-phenylethyl)pentanal (41b)

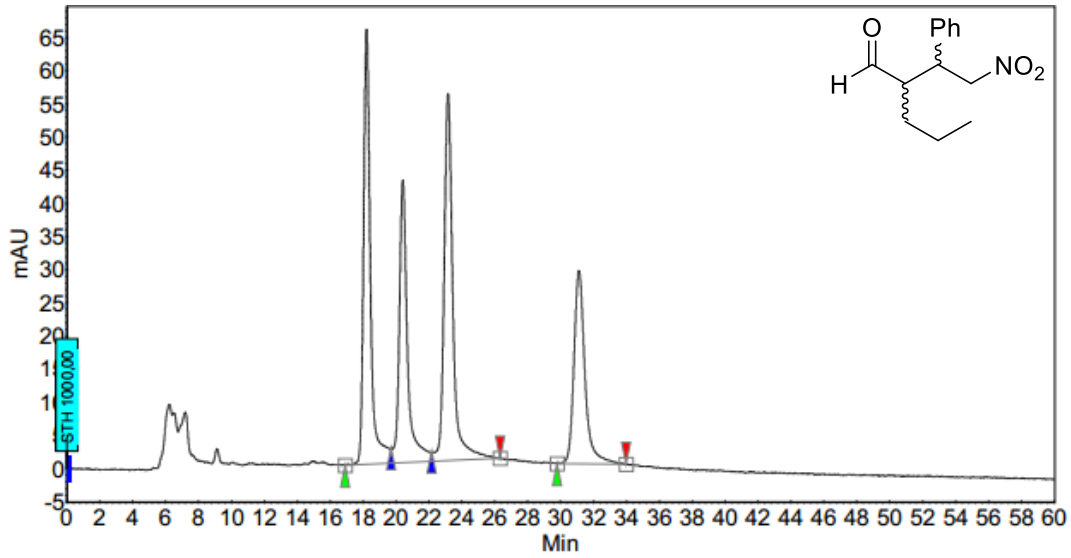

Peak Results :

Index	Name	Time [Min]	Quantity [% Area]	Height [mAU]	Area [mAU.Min]	Area % [%]
1	UNKNOWN	18,21	28,13	65,6	32,0	28,132
2	UNKNOWN	20,41	21,68	42,6	24,7	21,683
3	UNKNOWN	23,16	30,24	55,3	34,4	30,244
4	UNKNOWN	31,11	19,94	29,2	22,7	19,940
Total			100,00	192,8	113,8	100,000

(*R*)-2-((*S*)-2-Nitro-1-phenylethyl)pentanal ((*R*,2*S*)-41b)

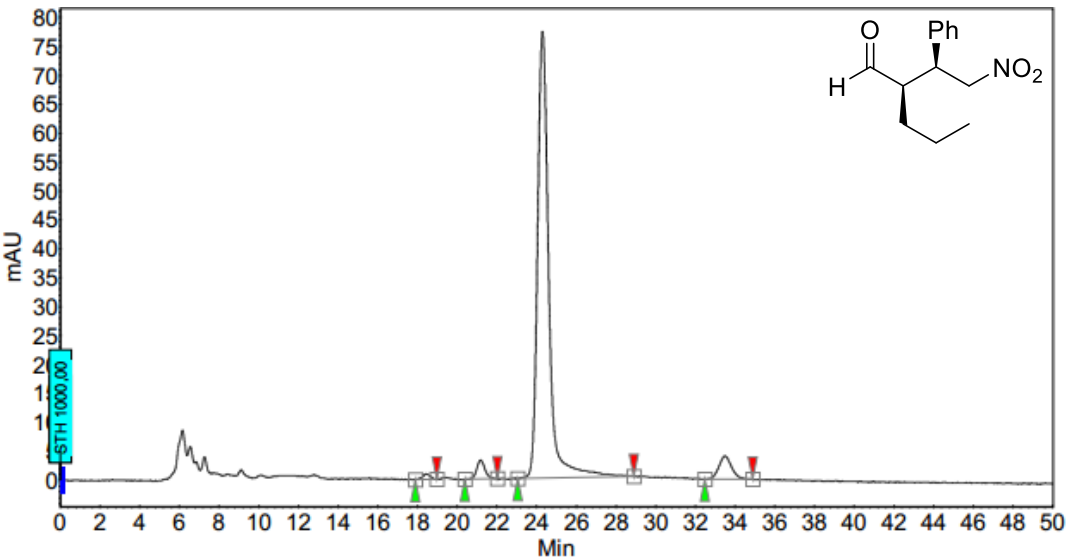

Peak Results :

Index	Name	Time [Min]	Quantity [% Area]	Height [mAU]	Area [mAU.Min]	Area % [%]
1	UNKNOWN	18,44	0,67	0,9	0,4	0,666
2	UNKNOWN	21,17	2,80	3,3	1,6	2,804
3	UNKNOWN	24,29	91,18	77,3	50,6	91,185
4	UNKNOWN	33,51	5,35	4,0	3,0	5,345
Total			100,00	85,6	55,5	100,000

2-(2-Nitro-1-phenylethyl)octanal (41c)

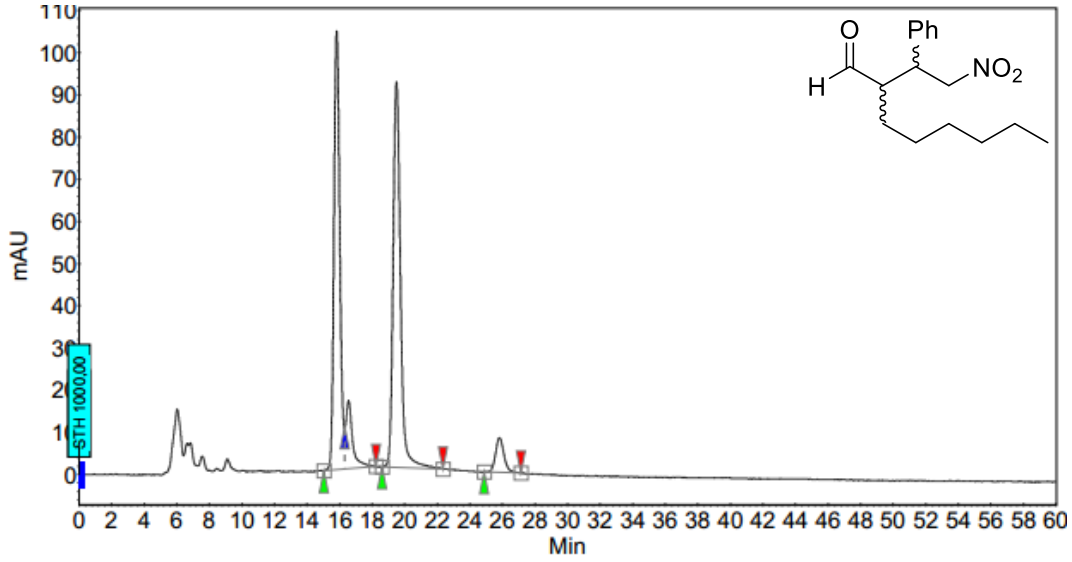

Peak Results :

Index	Name	Time [Min]	Quantity [% Area]	Height [mAU]	Area [mAU.Min]	Area % [%]
1	UNKNOWN	15,82	41,65	104,1	43,2	41,649
4	UNKNOWN	16,55	7,62	16,1	7,9	7,616
2	UNKNOWN	19,49	45,99	91,4	47,7	45,989
3	UNKNOWN	25,81	4,75	8,2	4,9	4,746
Total			100,00	219,8	103,8	100,000

(*R*)-2-((*S*)-2-Nitro-1-phenylethyl)octanal ((*R*,2*S*)-41c)

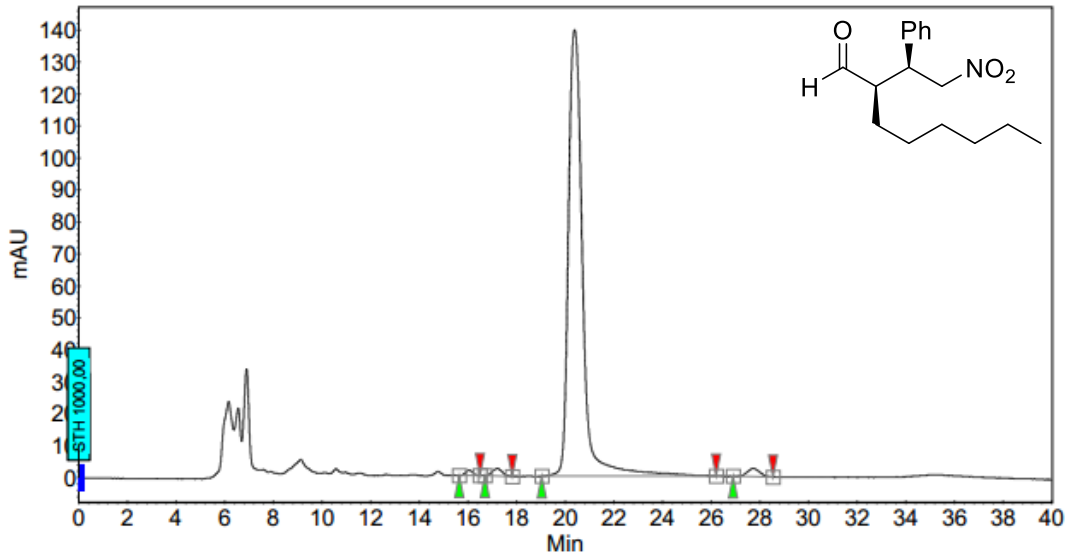

Peak Results :

Index	Name	Time [Min]	Quantity [% Area]	Height [mAU]	Area [mAU.Min]	Area % [%]
1	UNKNOWN	16,07	0,60	1,7	0,6	0,603
2	UNKNOWN	17,22	1,08	2,3	1,1	1,081
3	UNKNOWN	20,38	96,76	139,6	94,4	96,764
4	UNKNOWN	27,73	1,55	2,6	1,5	1,552
Total			100,00	146,2	97,6	100,000

2-Benzyl-4-nitro-3-phenylbutanal (41d)

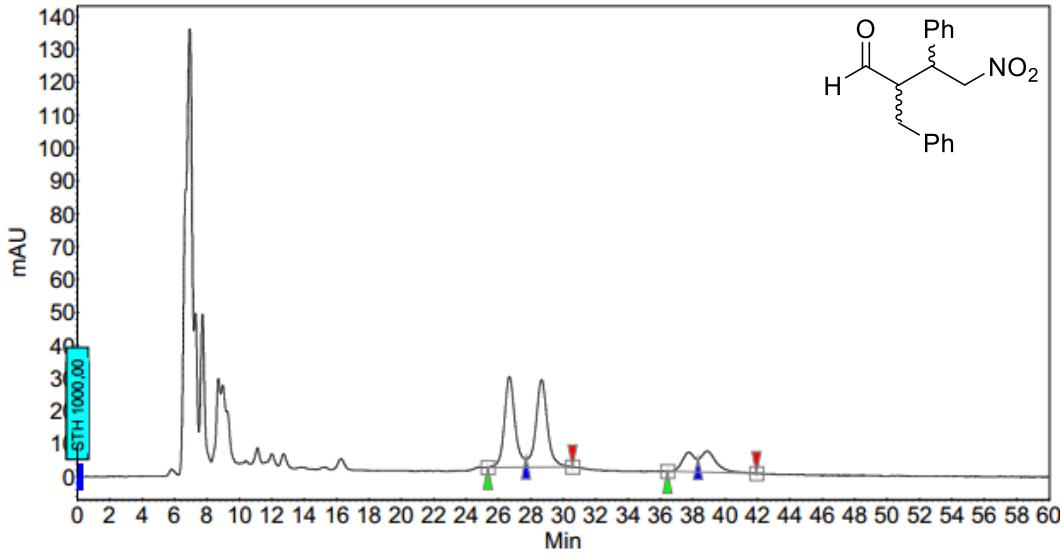

Peak Results :

Index	Name	Time [Min]	Quantity [% Area]	Height [mAU]	Area [mAU.Min]	Area % [%]
1	UNKNOWN	26,67	37,54	27,6	21,0	37,540
2	UNKNOWN	28,67	39,19	26,6	22,0	39,194
3	UNKNOWN	37,74	10,03	5,9	5,6	10,032
4	UNKNOWN	38,92	13,23	6,5	7,4	13,234
Total			100,00	66,6	56,0	100,000

(2*R*,3*S*)-2-Benzyl-4-nitro-3-phenylbutanal ((2*R*,3*S*)-41d)

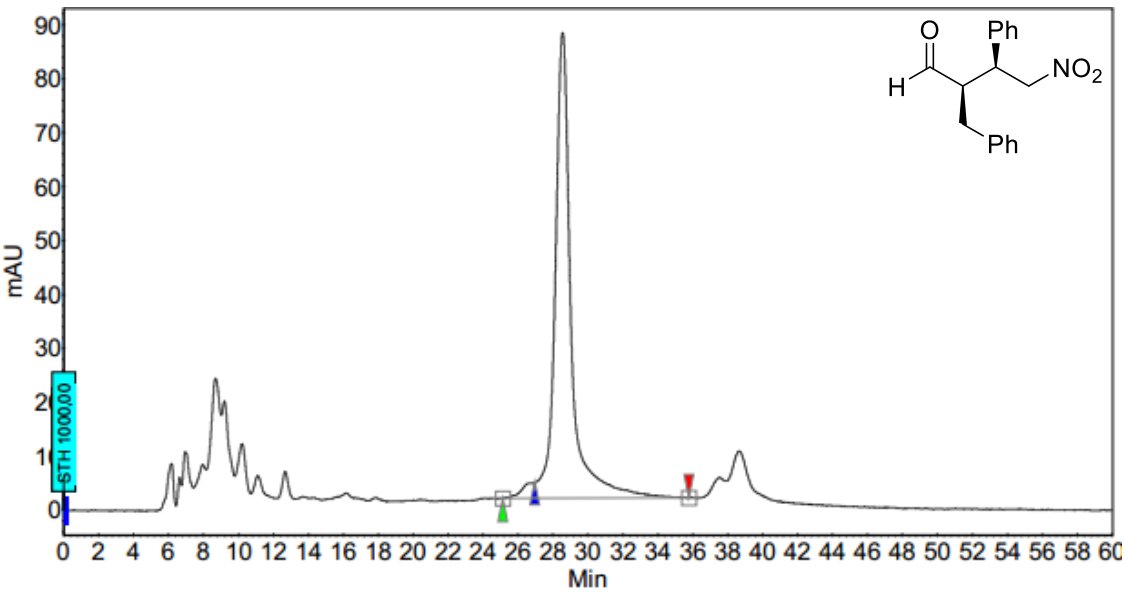

Peak Results :

Index	Name	Time [Min]	Quantity [% Area]	Height [mAU]	Area [mAU.Min]	Area % [%]
1	UNKNOWN	26,89	2,53	2,8	2,4	2,531
2	UNKNOWN	28,55	97,47	86,3	91,5	97,469
Total			100,00	89,2	93,9	100,000

2-Isopropyl-4-nitro-3-phenylbutanal (41e)

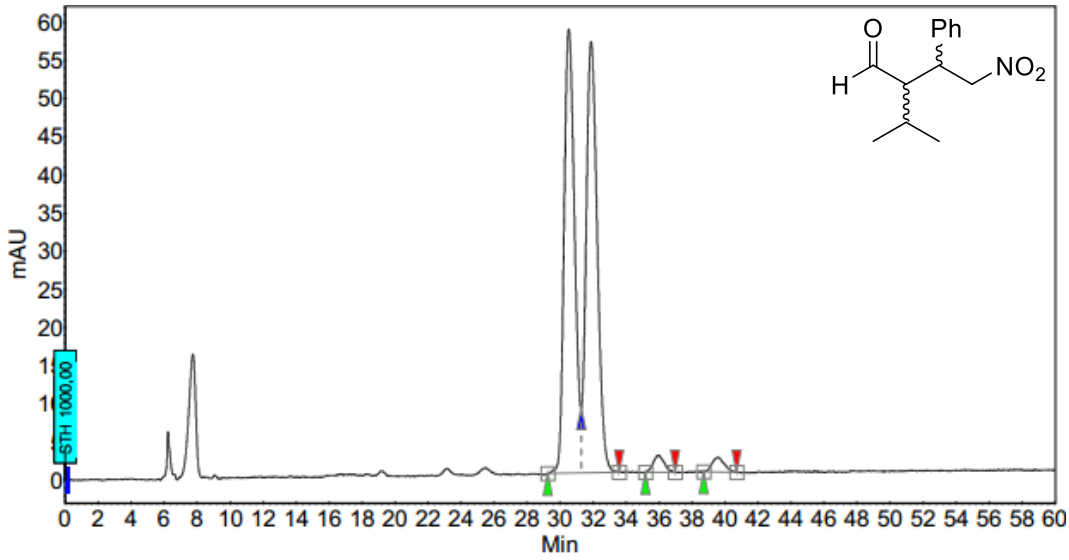

Peak Results :

Index	Name	Time [Min]	Quantity [% Area]	Height [mAU]	Area [mAU.Min]	Area % [%]
1	UNKNOWN	30,53	47,41	58,2	42,6	47,408
4	UNKNOWN	31,88	48,86	56,4	44,0	48,864
2	UNKNOWN	36,00	1,90	2,2	1,7	1,897
3	UNKNOWN	39,55	1,83	1,9	1,6	1,831
Total			100,00	118,7	90,0	100,000

(2*R*,3*S*)-2-Isopropyl-4-nitro-3-phenylbutanal ((2*R*,3*S*)-41e)

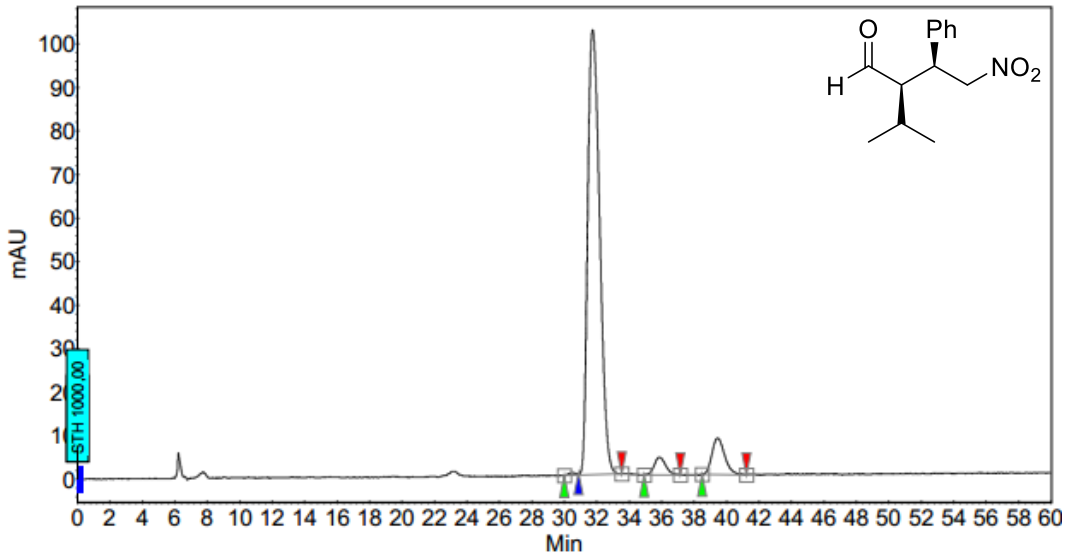

Peak Results :

Index	Name	Time [Min]	Quantity [% Area]	Height [mAU]	Area [mAU.Min]	Area % [%]
1	UNKNOWN	30,50	0,32	0,6	0,3	0,324
4	UNKNOWN	31,75	88,65	102,2	87,3	88,651
2	UNKNOWN	35,87	3,31	4,0	3,3	3,309
3	UNKNOWN	39,44	7,72	8,4	7,6	7,717
Total			100,00	115,2	98,5	100,000

2,2-Dimethyl-4-nitro-3-phenylbutanal (41f)

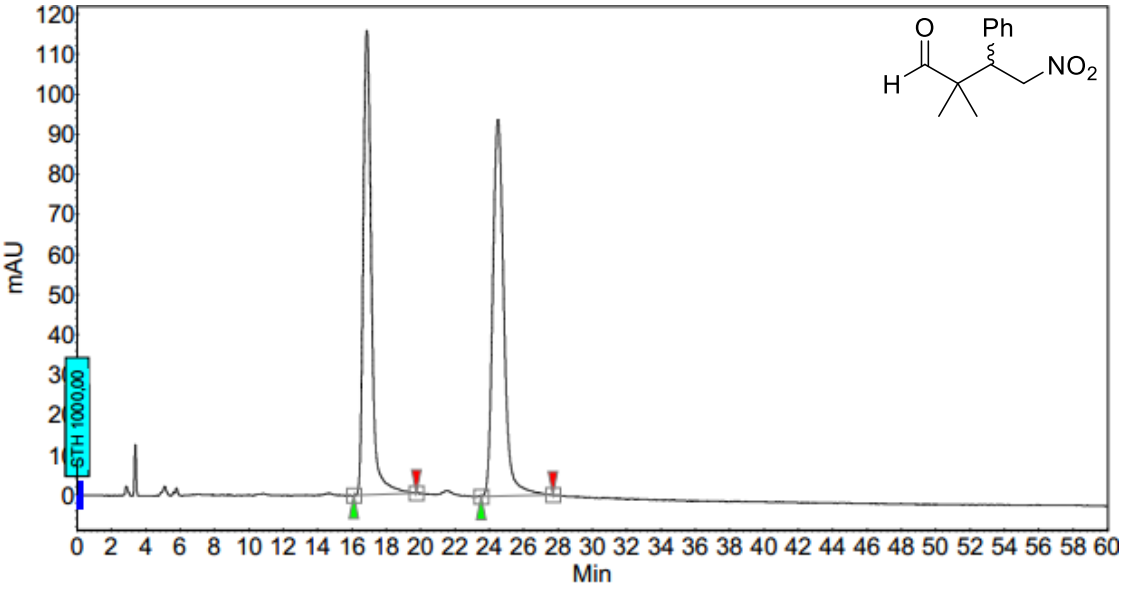

Peak Results :

Index	Name	Time [Min]	Quantity [% Area]	Height [mAU]	Area [mAU.Min]	Area % [%]
1	UNKNOWN	16,87	47,67	116,0	64,4	47,672
2	UNKNOWN	24,51	52,33	94,0	70,7	52,328
Total			100,00	210,0	135,1	100,000

(*R*)-2,2-Dimethyl-4-nitro-3-phenylbutanal ((*R*)-41f)

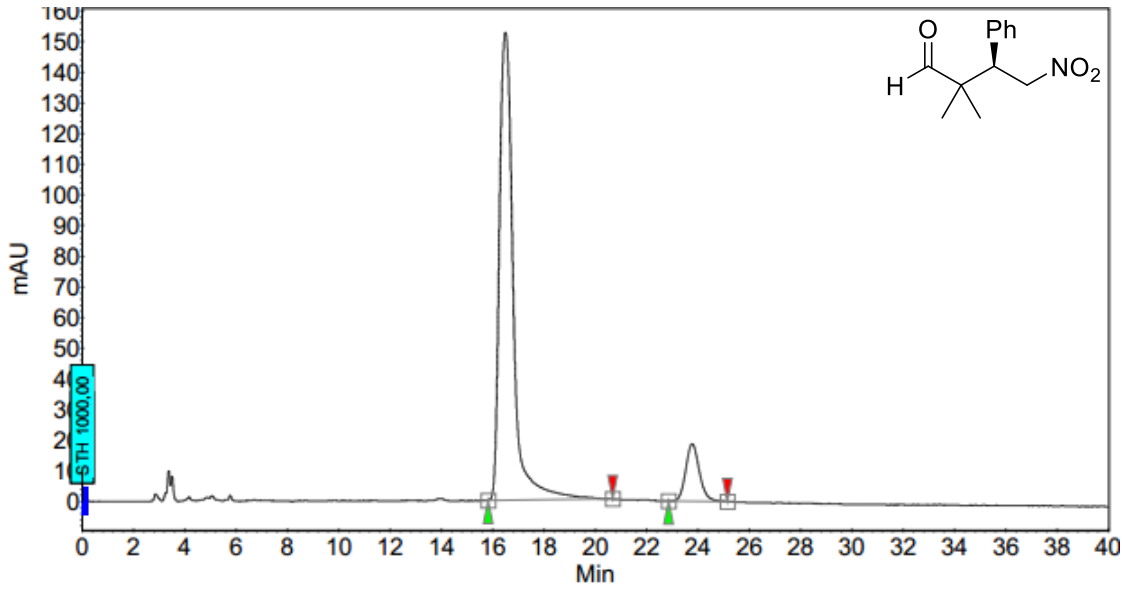

Peak Results :

Index	Name	Time [Min]	Quantity [% Area]	Height [mAU]	Area [mAU.Min]	Area % [%]
1	UNKNOWN	16,50	89,14	152,6	95,5	89,137
2	UNKNOWN	23,77	10,86	18,8	11,6	10,863
Total			100,00	171,4	107,2	100,000

1-(2-Nitro-1-phenylethyl)cyclohexane-1-carbaldehyde (41g)

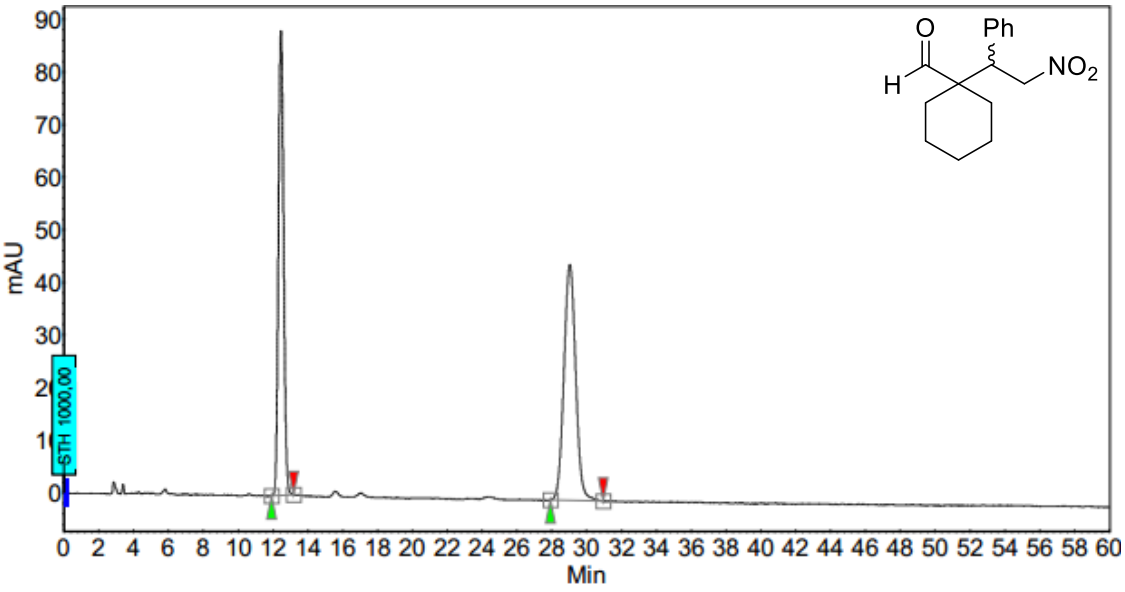

Peak Results :

Index	Name	Time [Min]	Quantity [% Area]	Height [mAU]	Area [mAU.Min]	Area % [%]
1	UNKNOWN	12,45	46,66	88,4	30,7	46,657
2	UNKNOWN	29,03	53,34	44,8	35,1	53,343
Total			100,00	133,3	65,8	100,000

(*R*)-1-(2-Nitro-1-phenylethyl)cyclohexane-1-carbaldehyde ((*R*)-41g)

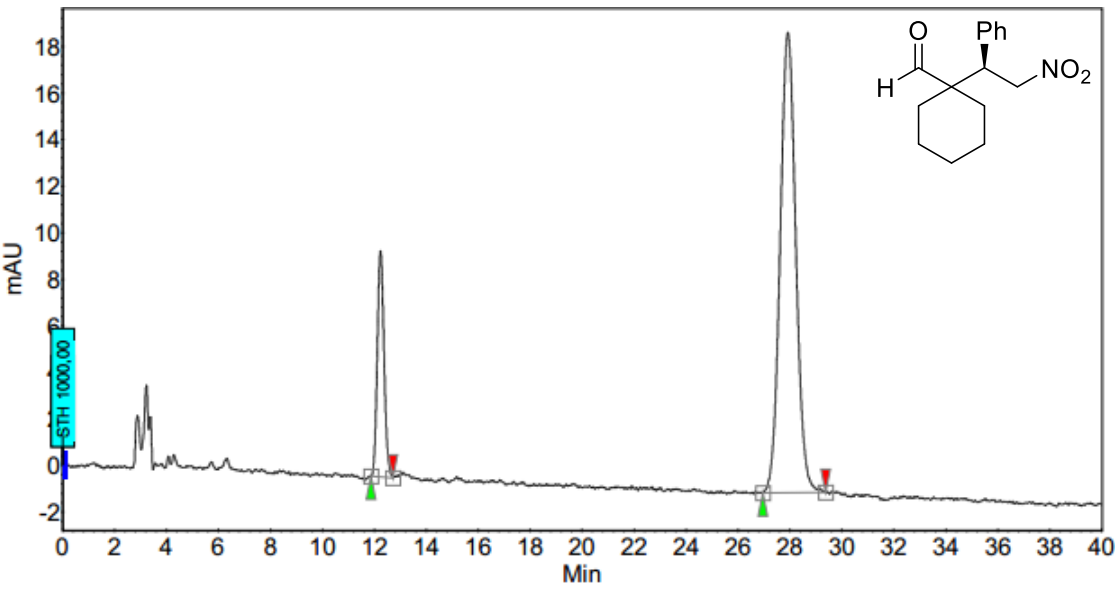

Peak Results :

Index	Name	Time [Min]	Quantity [% Area]	Height [mAU]	Area [mAU.Min]	Area % [%]
1	UNKNOWN	12,24	17,41	9,7	2,9	17,406
2	UNKNOWN	27,92	82,59	19,8	13,9	82,594
Total			100,00	29,5	16,8	100,000

Boc-Pro-(±)-⬢-OMe (*rac*-66)

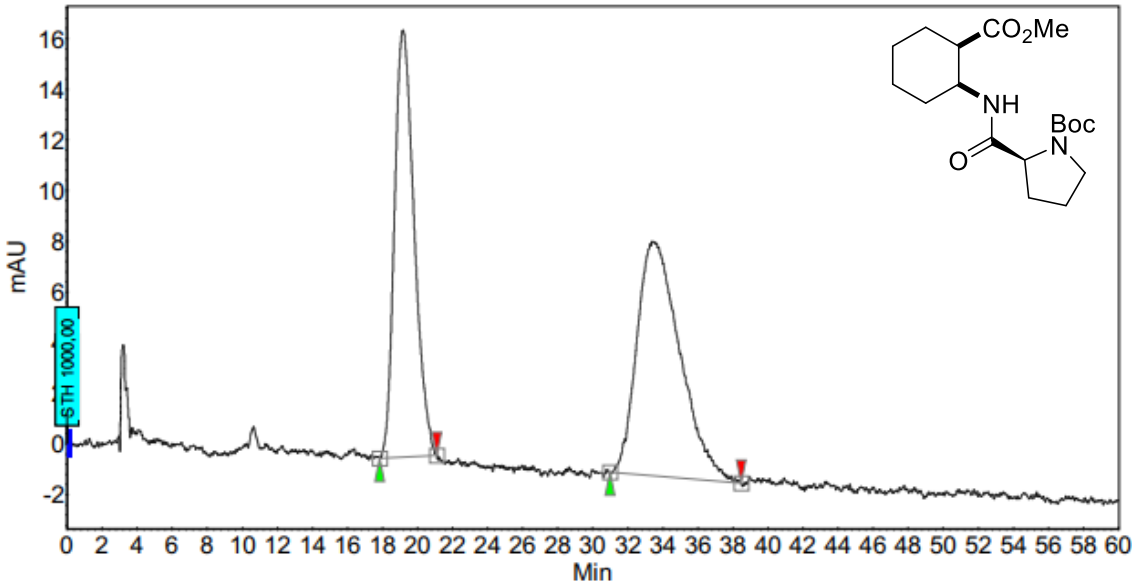

Peak Results :

Index	Name	Time [Min]	Quantity [% Area]	Height [mAU]	Area [mAU.Min]	Area % [%]
1	UNKNOWN	19,15	45,44	16,8	21,9	45,444
2	UNKNOWN	33,37	54,56	9,3	26,3	54,556
Total			100,00	26,1	48,2	100,000

Boc-Pro-(-)-⬢-OMe (66)

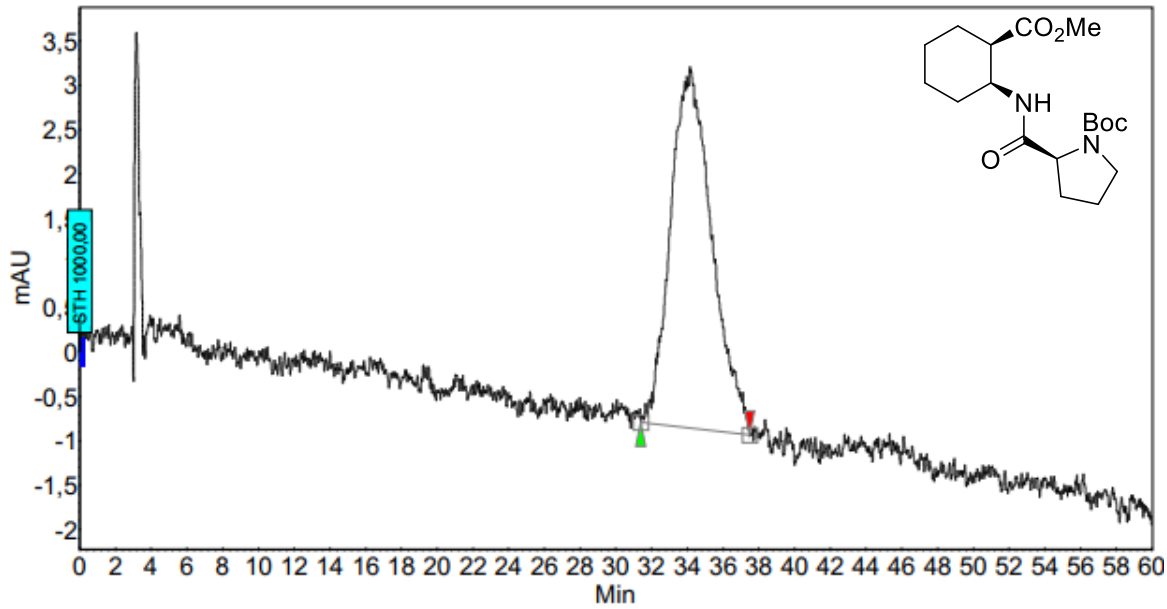

Peak Results :

Index	Name	Time [Min]	Quantity [% Area]	Height [mAU]	Area [mAU.Min]	Area % [%]
1	UNKNOWN	34,14	100,00	4,1	10,8	100,000
Total			100,00	4,1	10,8	100,000

Boc-Pro-(+)-⬢-OMe (*ent*-66)

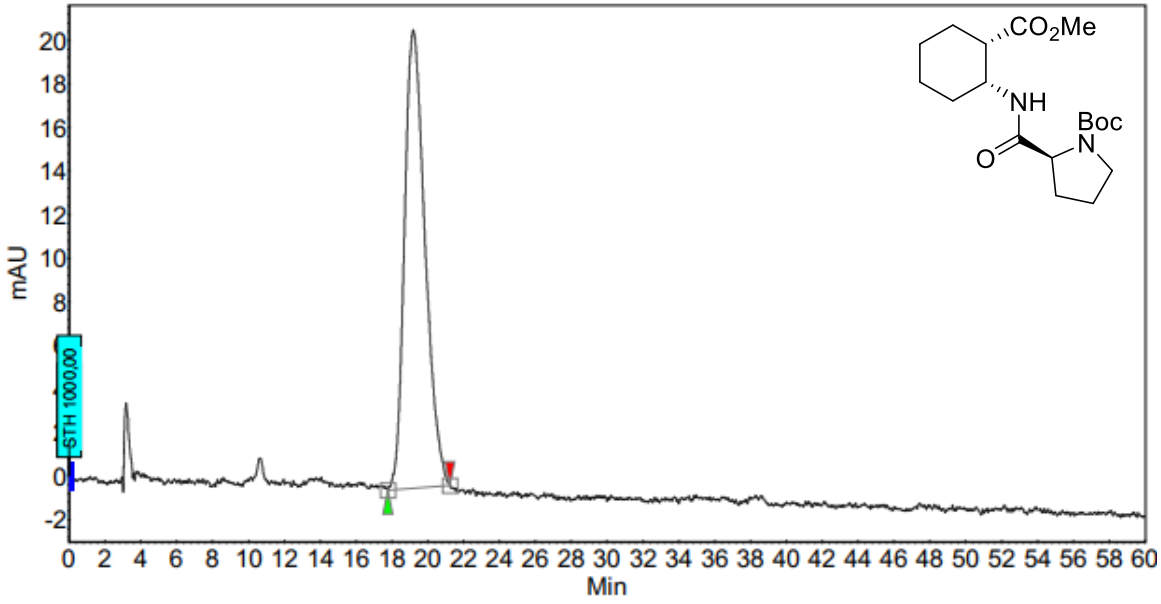

Peak Results :

Index	Name	Time [Min]	Quantity [% Area]	Height [mAU]	Area [mAU.Min]	Area % [%]
1	UNKNOWN	19,19	100,00	21,0	28,0	100,000
Total			100,00	21,0	28,0	100,000

Boc-Pro-(±)-⬢-Pro-OBn (*rac*-68)

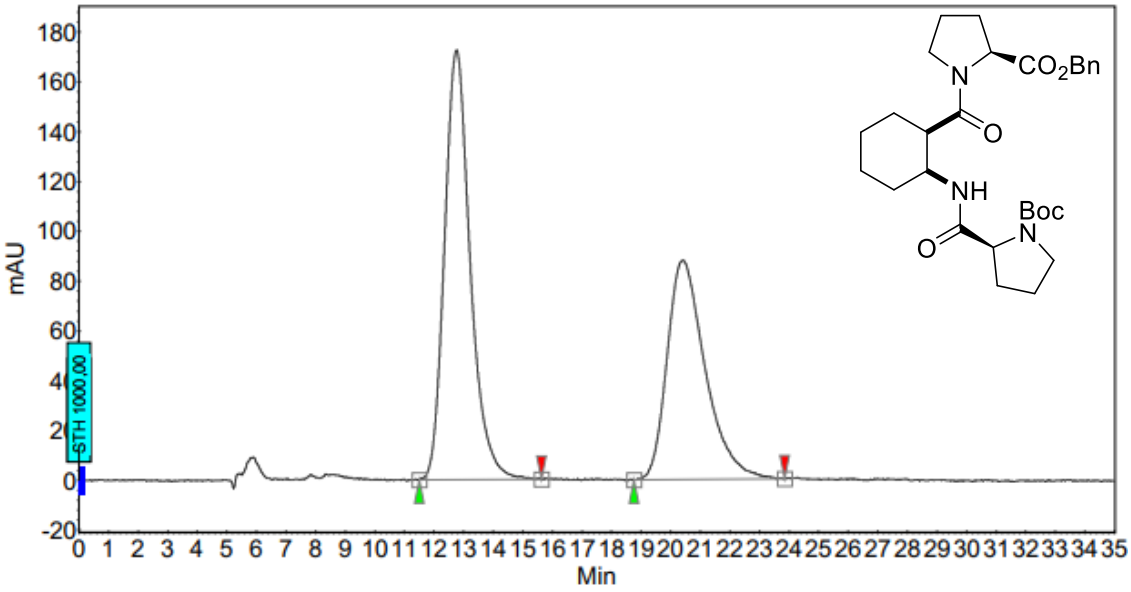

Peak Results :

Index	Name	Time [Min]	Quantity [% Area]	Height [mAU]	Area [mAU.Min]	Area % [%]
1	UNKNOWN	12,77	57,02	172,5	173,8	57,023
2	UNKNOWN	20,43	42,98	88,0	131,0	42,977
Total			100,00	260,5	304,8	100,000

Boc-Pro-(-)-⬢-Pro-OBn (68)

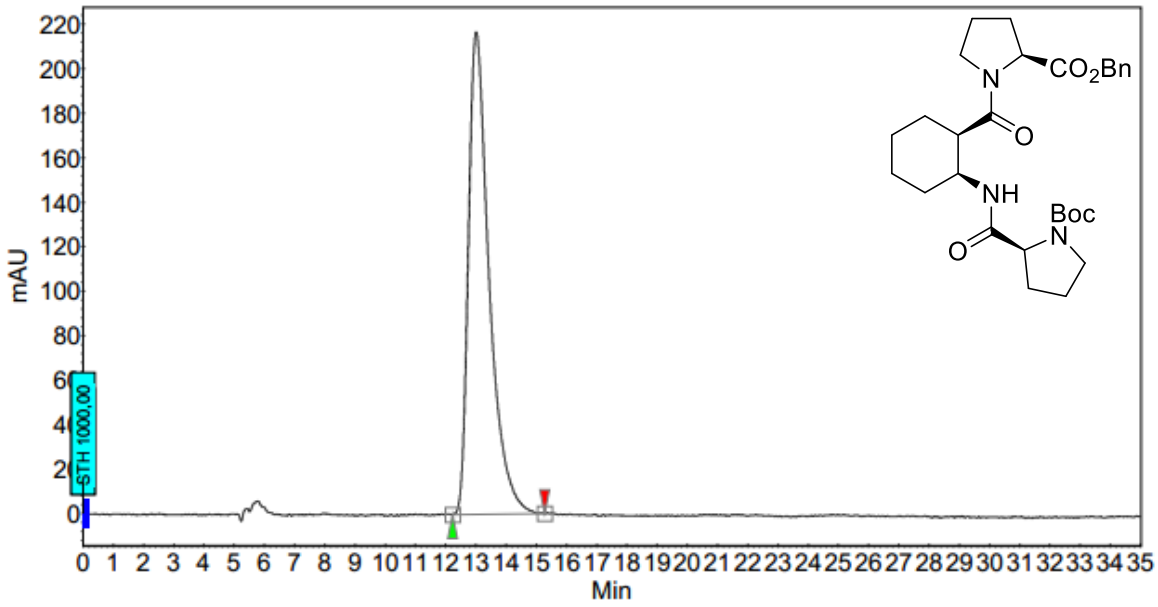

Peak Results :

Index	Name	Time [Min]	Quantity [% Area]	Height [mAU]	Area [mAU.Min]	Area % [%]
1	UNKNOWN	13,01	100,00	216,8	171,6	100,000
Total			100,00	216,8	171,6	100,000

Boc-Pro-(+)-⬢-Pro-OBn (*ent*-68)

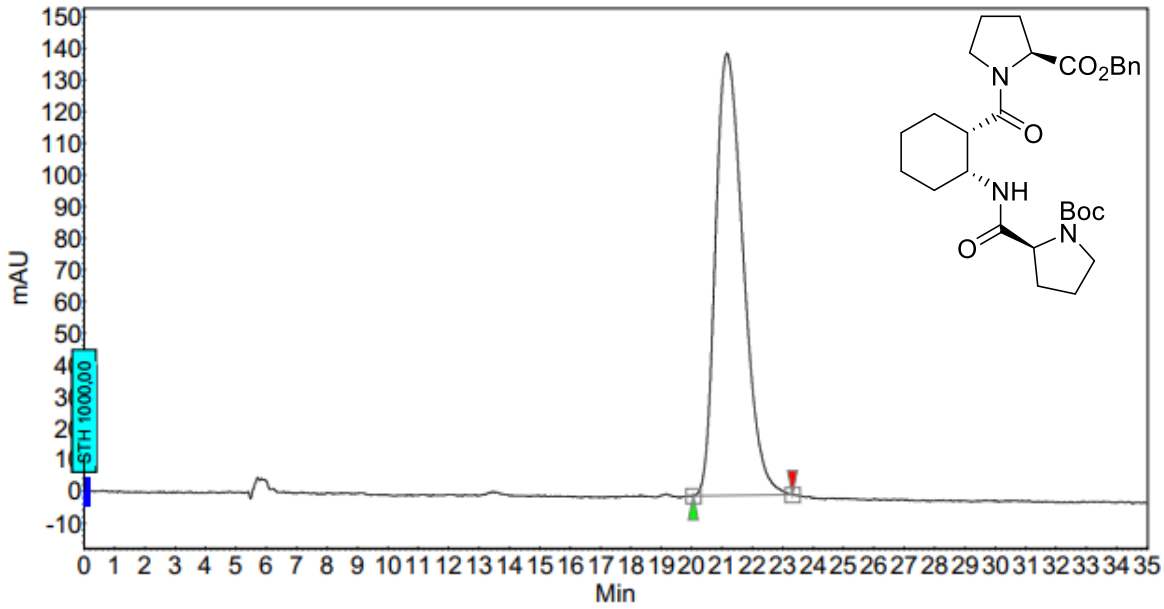

Peak Results :

Index	Name	Time [Min]	Quantity [% Area]	Height [mAU]	Area [mAU.Min]	Area % [%]
1	UNKNOWN	21,17	100,00	139,6	147,7	100,000
Total			100,00	139,6	147,7	100,000

Cbz-Pro-(±)-⬢-OMe (*rac*-71)

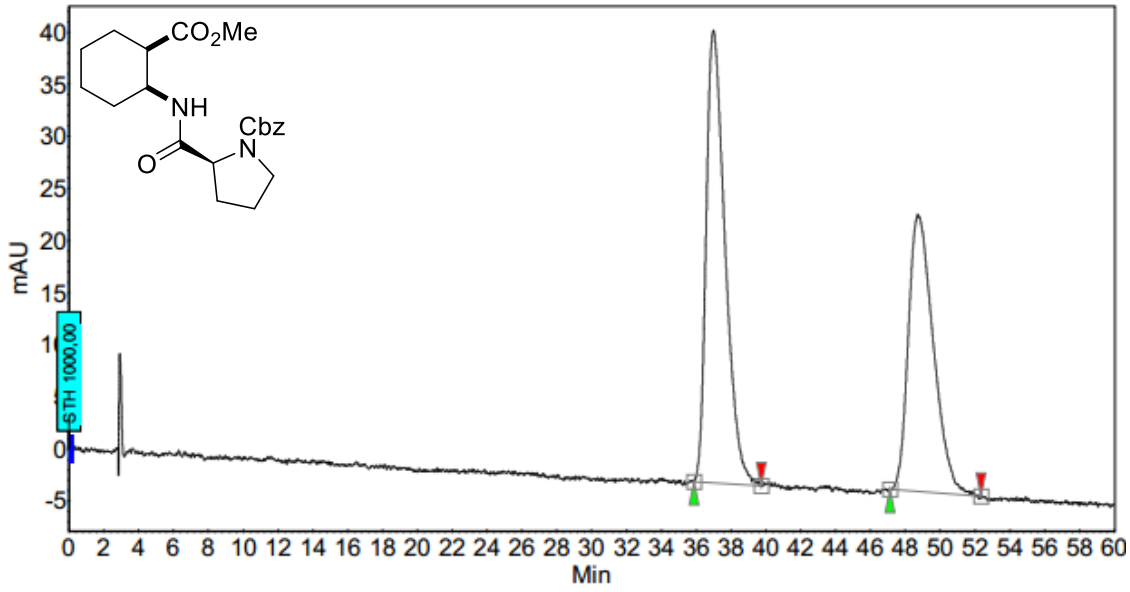

Peak Results :

Index	Name	Time [Min]	Quantity [% Area]	Height [mAU]	Area [mAU.Min]	Area % [%]
1	UNKNOWN	36,99	55,30	43,4	54,5	55,303
2	UNKNOWN	48,71	44,70	26,6	44,1	44,697
Total			100,00	70,0	98,6	100,000

Cbz-Pro-(+)-⬢-OMe (*ent*-71)

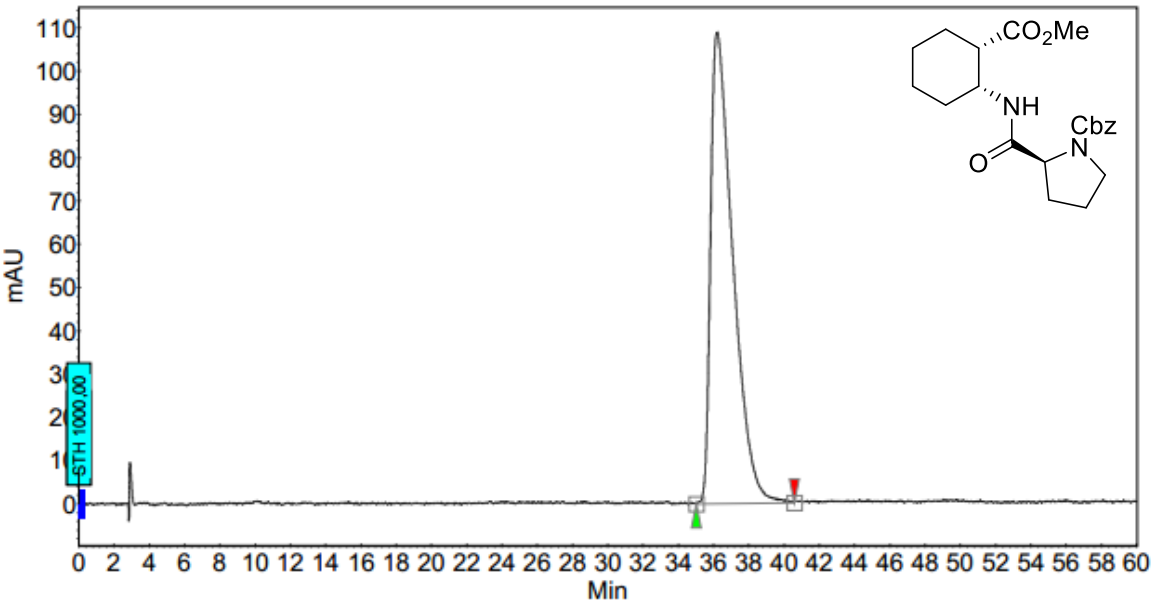

Peak Results :

Index	Name	Time [Min]	Quantity [% Area]	Height [mAU]	Area [mAU.Min]	Area % [%]
1	UNKNOWN	36,21	100,00	108,9	159,2	100,000
Total			100,00	108,9	159,2	100,000

Cbz-Pro-(±)-⬢-Pro-OBn (*rac*-72)

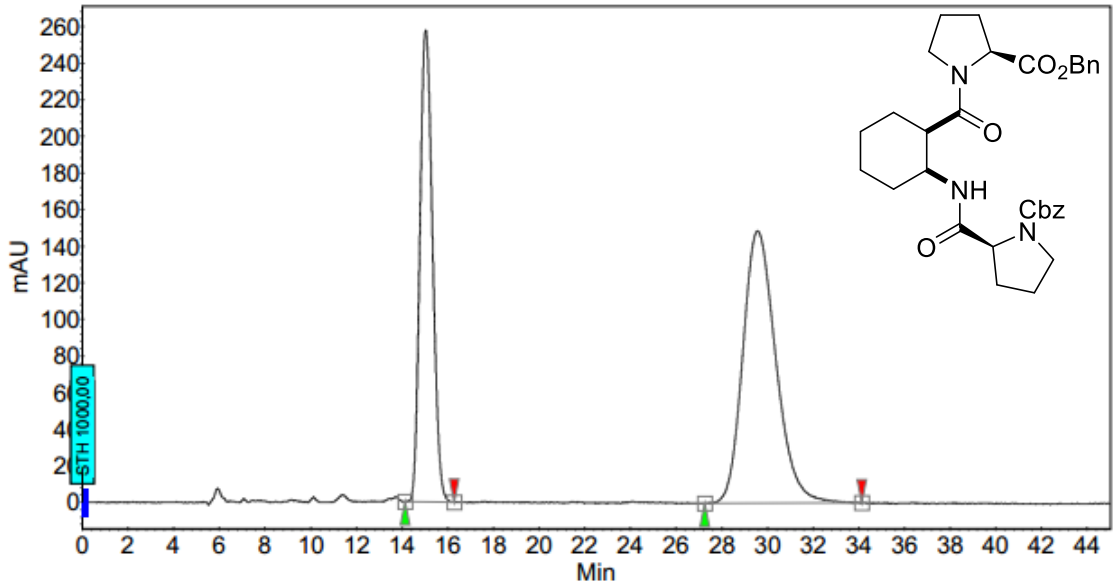

Peak Results :

Index	Name	Time [Min]	Quantity [% Area]	Height [mAU]	Area [mAU.Min]	Area % [%]
1	UNKNOWN	15,04	39,86	258,0	165,0	39,858
2	UNKNOWN	29,56	60,14	148,8	249,0	60,142
Total			100,00	406,8	414,0	100,000

Cbz-Pro-(+)-⬢-Pro-OBn (*ent*-72)

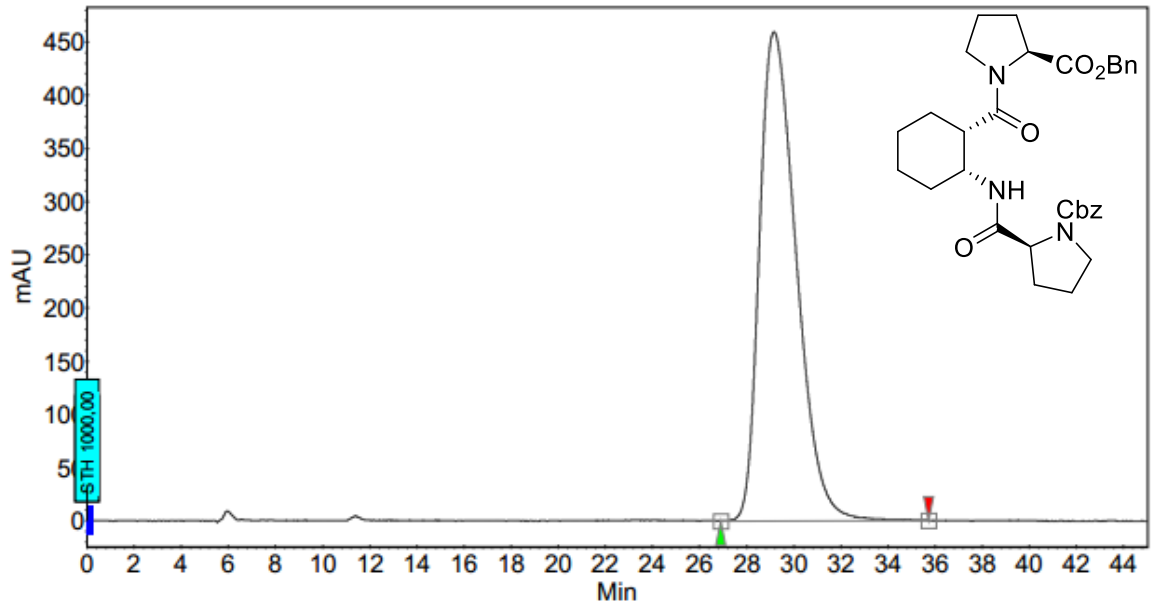

Peak Results :

Index	Name	Time [Min]	Quantity [% Area]	Height [mAU]	Area [mAU.Min]	Area % [%]
1	UNKNOWN	29,17	100,00	459,5	833,1	100,000
Total			100,00	459,5	833,1	100,000

4-Hydroxy-4-(4-nitrophenyl)butan-2-one (93)

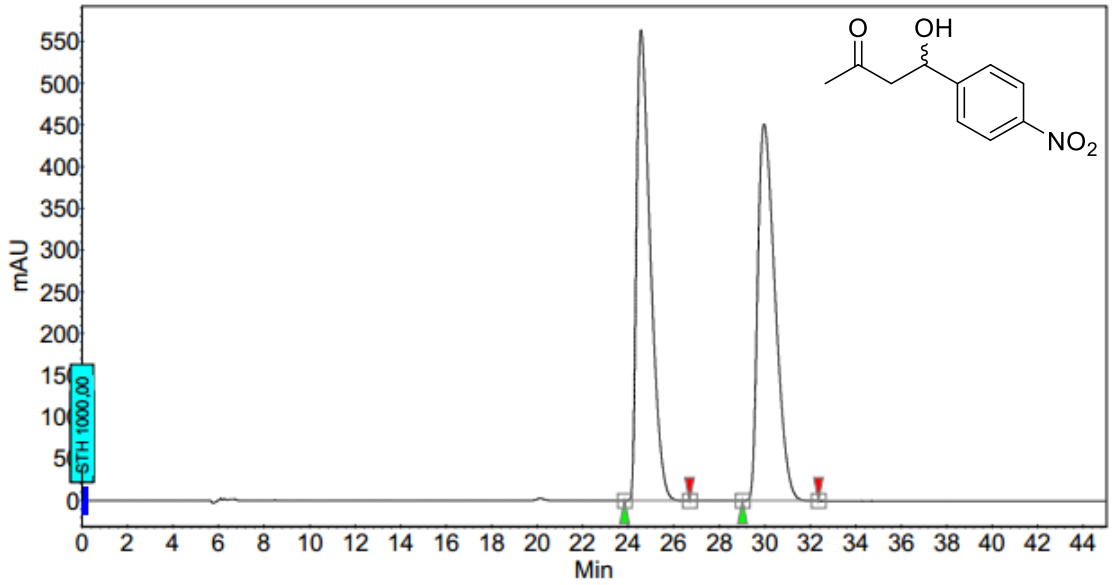

Peak Results :

Index	Name	Time [Min]	Quantity [% Area]	Height [mAU]	Area [mAU.Min]	Area % [%]
1	UNKNOWN	24,57	49,91	564,2	398,2	49,915
2	UNKNOWN	29,97	50,09	451,6	399,6	50,085
Total			100,00	1015,8	797,9	100,000

(*R*)-4-Hydroxy-4-(4-nitrophenyl)butan-2-one ((*R*)-93)

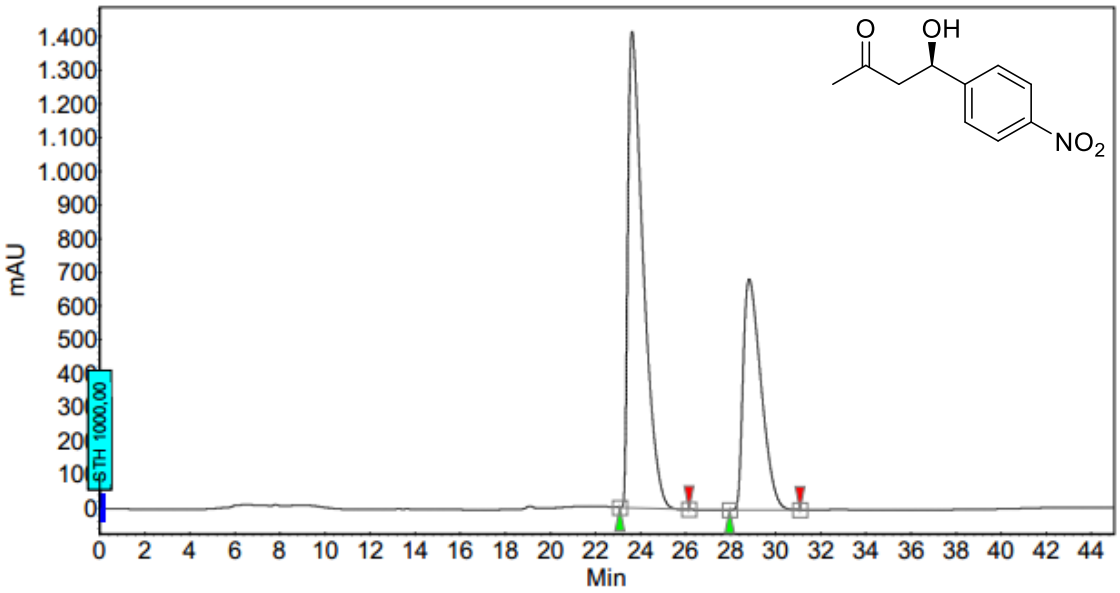

Peak Results :

Index	Name	Time [Min]	Quantity [% Area]	Height [mAU]	Area [mAU.Min]	Area % [%]
1	UNKNOWN	23,63	63,92	1413,2	1113,8	63,921
2	UNKNOWN	28,82	36,08	684,8	628,7	36,079
Total			100,00	2098,0	1742,5	100,000

5-Nitro-4-phenylpentan-2-one (94)

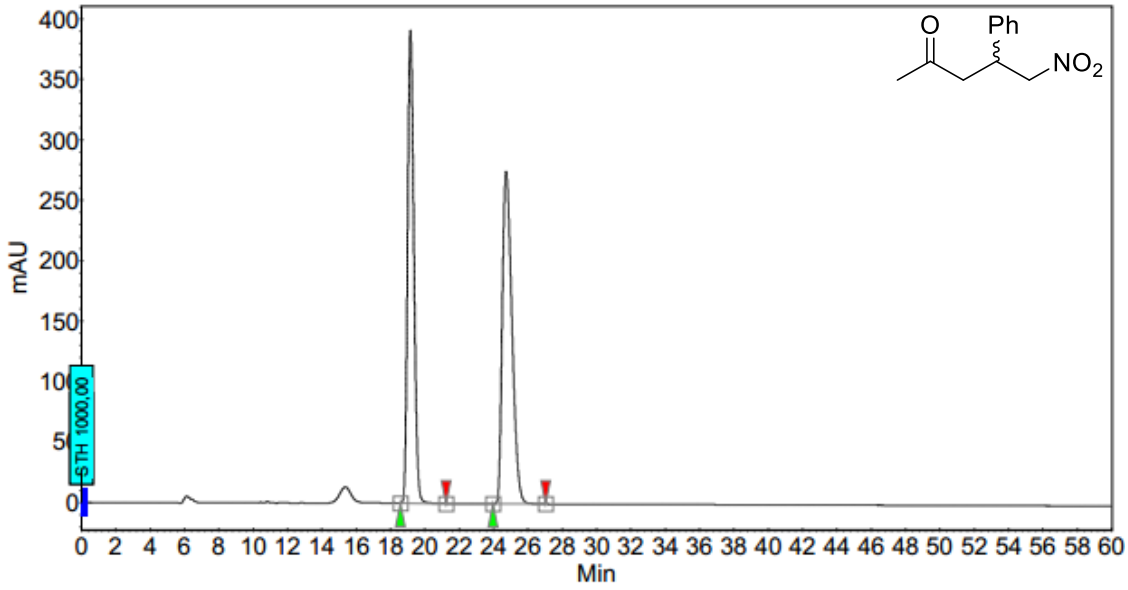

Peak Results :

Index	Name	Time [Min]	Quantity [% Area]	Height [mAU]	Area [mAU.Min]	Area % [%]
1	UNKNOWN	19,16	48,06	391,4	166,3	48,059
2	UNKNOWN	24,73	51,94	275,3	179,7	51,941
Total			100,00	666,7	346,0	100,000

(*R*)-5-Nitro-4-phenylpentan-2-one ((*R*)-94)

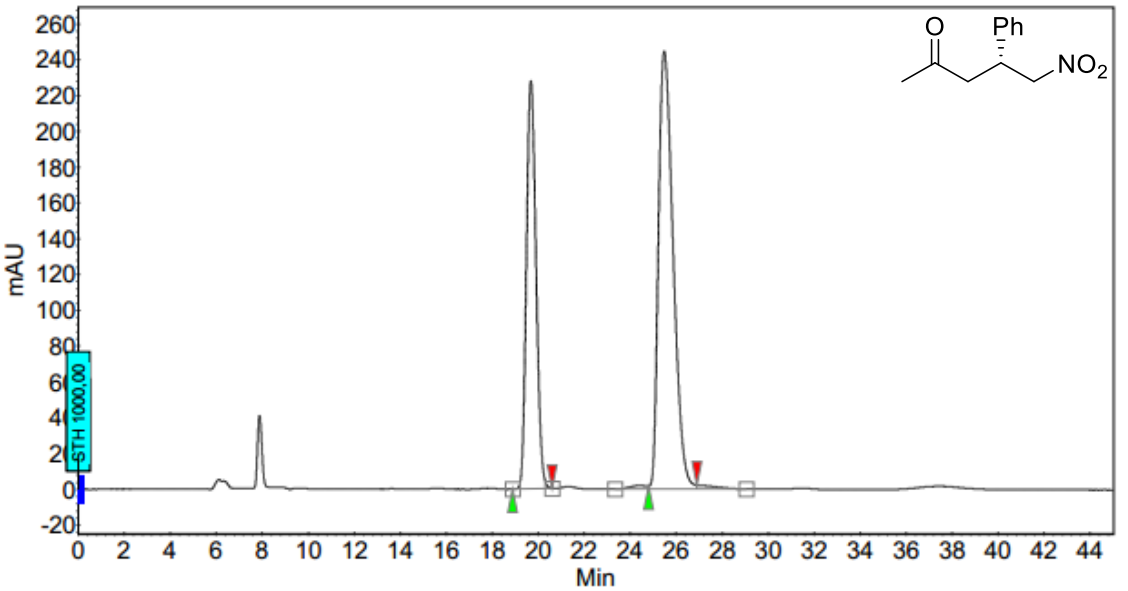

Peak Results :

Index	Name	Time [Min]	Quantity [% Area]	Height [mAU]	Area [mAU.Min]	Area % [%]
1	UNKNOWN	19,68	37,80	228,2	110,0	37,795
2	UNKNOWN	25,48	62,20	244,7	181,1	62,205
Total			100,00	472,8	291,1	100,000

***cis*-1-(4-bromophenyl) 2-methyl cyclohex-4-ene-1,2-dicarboxylate (108)**

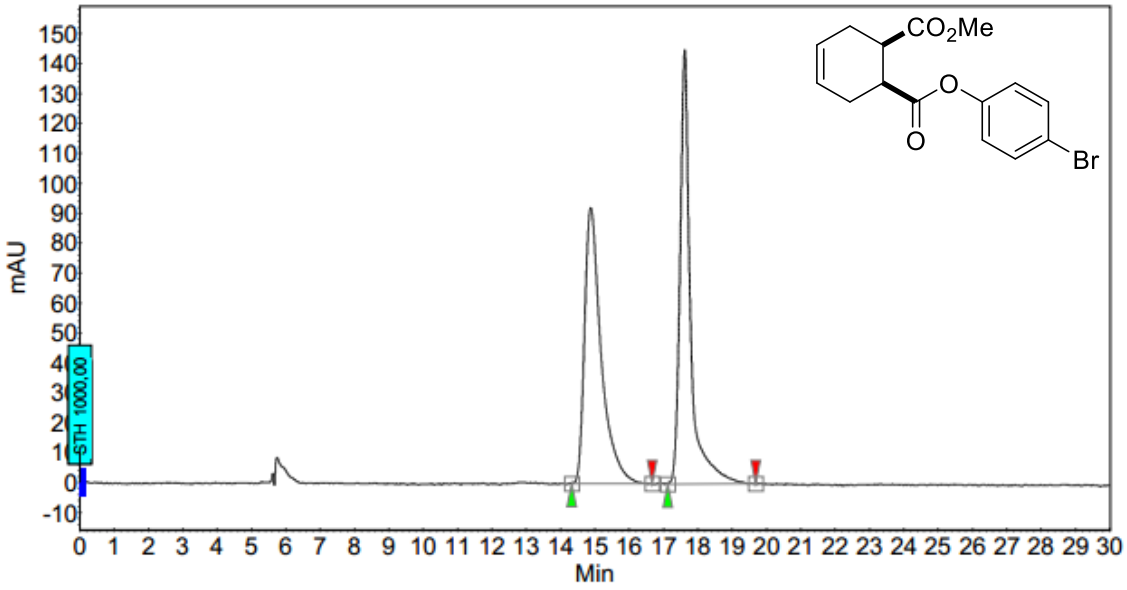

Peak Results :

Index	Name	Time [Min]	Quantity [% Area]	Height [mAU]	Area [mAU.Min]	Area % [%]
1	UNKNOWN	14,88	50,15	92,1	51,7	50,147
2	UNKNOWN	17,62	49,85	145,0	51,4	49,853
Total			100,00	237,1	103,2	100,000

1-(4-bromophenyl) 2-methyl (1*S*,2*R*)-cyclohex-4-ene-1,2-dicarboxylate (108)

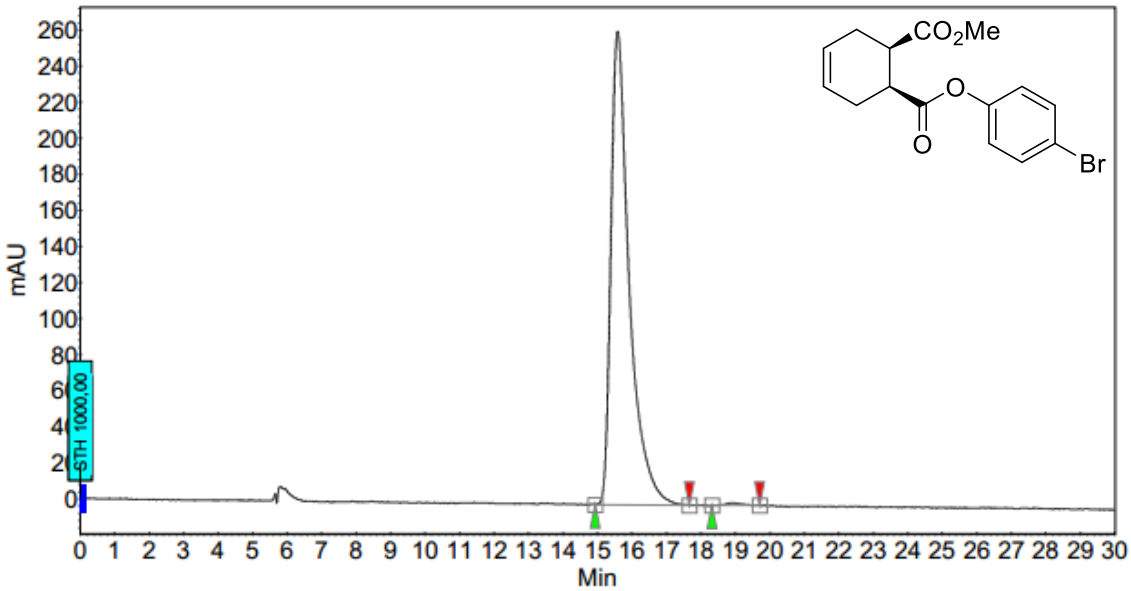

Peak Results :

Index	Name	Time [Min]	Quantity [% Area]	Height [mAU]	Area [mAU.Min]	Area % [%]
1	UNKNOWN	15,58	99,53	262,5	162,1	99,529
2	UNKNOWN	18,90	0,47	1,5	0,8	0,471
Total			100,00	264,0	162,9	100,000

1-(4-bromophenyl) 2-methyl (1*R*,2*S*)-cyclohex-4-ene-1,2-dicarboxylate (108)

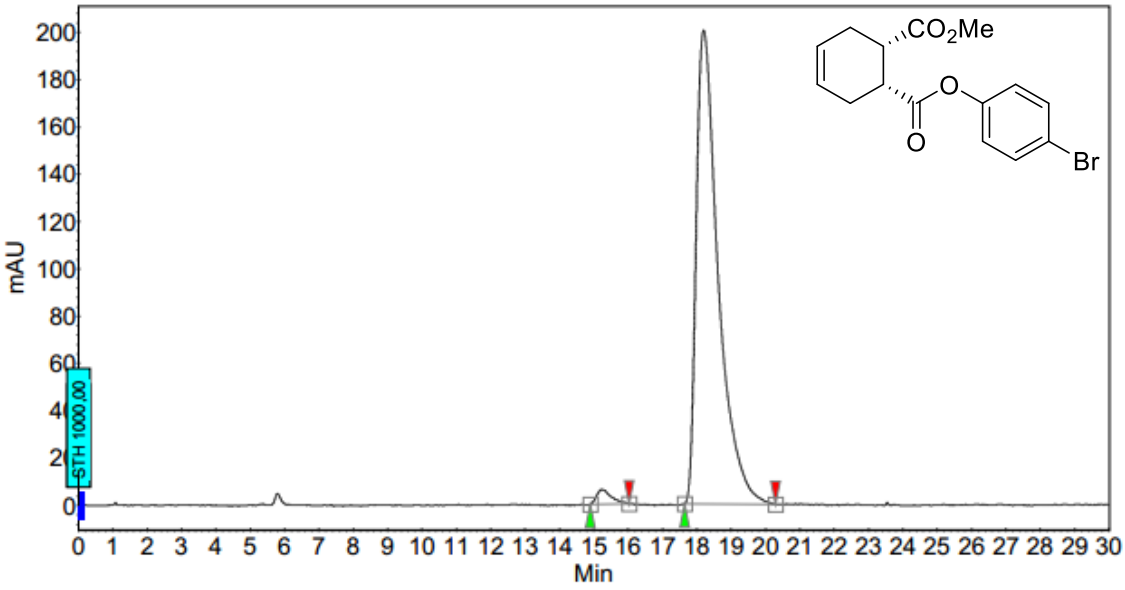

Peak Results :

Index	Name	Time [Min]	Quantity [% Area]	Height [mAU]	Area [mAU.Min]	Area % [%]
1	UNKNOWN	15,22	2,04	6,3	3,1	2,039
2	UNKNOWN	18,20	97,96	200,5	148,7	97,961
Total			100,00	206,8	151,8	100,000

4. X-ray crystallography data

((1*R*,2*S*)-2-((*S*)-Pyrrolidine-2-carboxamido)cyclohexane-1-carbonyl)-L-proline (52)

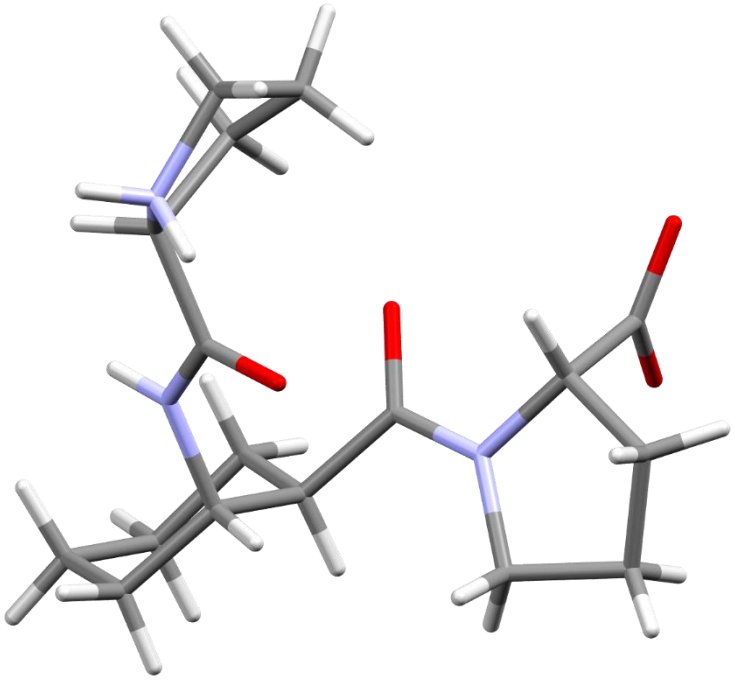

Table 1. Crystal data and structure refinement for **52**.

Empirical formula	$C_{20.83}H_{40.94}N_3O_{8.08}$
Formula weight	462.71
Temperature/K	122.98(10)
Crystal system	tetragonal
Space group	$I4_1$
a/Å	21.04247(13)
b/Å	21.04247(13)
c/Å	11.87171(15)
α/°	90
β/°	90
γ/°	90
Volume/Å^3	5256.62(9)
Z	8
ρ_{calc}g/cm^3	1.169
μ/mm^{-1}	0.742
F(000)	2012.0
Crystal size/mm^3	0.248 × 0.2025 × 0.1215
Radiation	CuKα (λ = 1.54184)
2Θ range for data collection/°	5.94 to 147.862
Index ranges	-24 ≤ h ≤ 26, -24 ≤ k ≤ 26, -14 ≤ l ≤ 14
Reflections collected	26960

Independent reflections	5251 [R_{int} = 0.0470, R_{sigma} = 0.0253]
Data/restraints/parameters	5251/8/338
Goodness-of-fit on F^2	1.058
Final R indexes [I>=2σ (I)]	R_1 = 0.0530, wR_2 = 0.1503
Final R indexes [all data]	R_1 = 0.0541, wR_2 = 0.1524
Largest diff. peak/hole / e $Å^{-3}$	0.73/-0.23
Flack parameter	-0.10(6)

Table 2. Fractional Atomic Coordinates (×10^4) and Equivalent Isotropic Displacement Parameters ($Å^2$×10^3) for **52**. U_{eq} is defined as 1/3 of of the trace of the orthogonalised U_{IJ} tensor.

Atom	*x*	*y*	*z*	U(eq)
O5AA	7216(1)	3429.8(10)	269(2)	36.4(5)
O3AA	6829.5(10)	5708(1)	511(3)	47.1(6)
N1AA	8620.7(10)	4149.1(10)	-2397(3)	28.5(5)
N2AA	10089.7(10)	4016(1)	-803(2)	27.0(5)
O4AA	9247.0(9)	4909.1(9)	-1602(2)	34.5(5)
N7	7783.4(11)	5532.6(11)	-1058(3)	34.0(5)
C8	9085.7(12)	4345.6(12)	-1728(3)	28.0(5)
C9	10185.5(18)	3994(2)	446(3)	46.8(8)
C10	8214.2(13)	4591.4(13)	-3022(3)	31.4(6)
C11	9414.7(12)	3826.5(12)	-1056(3)	31.4(6)
C12	7163.7(13)	4080.4(15)	-2464(3)	35.6(6)
C13	7384.2(16)	5652.3(15)	898(3)	42.0(7)
C14	7568.5(13)	4685.5(13)	-2423(3)	32.2(6)
C15	7679.7(12)	4909.6(13)	-1224(3)	30.9(5)
C16	7937.6(13)	5748.6(14)	81(3)	36.8(6)
C17	7751.2(19)	6054.9(15)	-1872(4)	48.8(8)
C18	7042.6(16)	3896.4(18)	-3682(4)	45.5(8)
C19	8072.0(15)	6460.5(15)	-99(4)	48.5(9)
O20	7512.1(16)	5553.4(18)	1900(3)	66.0(8)
C21	7673.6(18)	6633.4(15)	-1111(4)	50.8(9)
C22	7541.8(17)	3252.8(19)	1261(4)	48.4(8)
C23	8103.5(15)	4366.6(16)	-4225(3)	40.2(7)
C24	7669.3(17)	3784.0(17)	-4302(3)	45.0(7)
C27	9110.7(17)	3740(2)	111(4)	53.1(9)
C32	9533(4)	4110(4)	901(6)	55(2)
C33	9625(4)	3561(5)	858(7)	52(3)
O1AA	7699.1(10)	4536.8(9)	-417(2)	36.2(5)
O6AA	8766(3)	5413(4)	2403(4)	104(2)
O3	7364(4)	5749(4)	-5755(6)	67(3)

C5	7733(4)	6289(4)	-5452(7)	73(3)
C6	8835(6)	4879(6)	3078(9)	126(4)
O2AA	9421(3)	6400(3)	3274(5)	100(3)
C1	9671(3)	5806(3)	-4088(5)	73.7(13)
O2	9367(5)	6284(4)	-4246(8)	96(3)
C5A	7566(14)	6039(12)	-4734(11)	130(13)
O0AA	10023(4)	5712(4)	-5012(6)	71(2)

Table 3. Anisotropic Displacement Parameters ($Å^2 \times 10^3$) for **52**. The Anisotropic displacement factor exponent takes the form: $-2\pi^2[h^2a^{*2}U_{11}+2hka^*b^*U_{12}+\ldots]$.

Atom	**U_{11}**	**U_{22}**	**U_{33}**	**U_{23}**	**U_{13}**	**U_{12}**
O5AA	25.7(9)	30.9(10)	52.6(12)	2.8(9)	3.9(9)	0.9(7)
O3AA	26.2(10)	30.3(10)	84.8(18)	0.0(11)	19.7(11)	-1.7(8)
N1AA	23(1)	20.9(10)	41.5(11)	0.5(9)	-2.7(9)	-0.9(8)
N2AA	21.9(10)	20.3(9)	38.7(12)	-0.8(8)	-2.2(8)	-2.6(8)
O4AA	26.7(9)	19.8(9)	56.9(12)	-0.5(8)	-4.5(8)	-3.0(7)
N7	28.6(11)	22.5(11)	50.8(14)	-1.6(10)	8.2(10)	0.4(8)
C8	20.9(11)	22.7(12)	40.4(13)	-1.4(10)	2.7(10)	-2.0(9)
C9	45.7(18)	57(2)	37.6(16)	-1.5(14)	-5.9(13)	-10.3(15)
C10	26.0(12)	26.6(12)	41.7(14)	2.8(11)	-2.5(11)	1.6(10)
C11	21.4(12)	24.1(12)	48.6(15)	2.3(11)	-1.5(11)	-5.4(9)
C12	23.3(12)	34.0(14)	49.7(16)	-2.6(12)	-2.4(11)	-1.7(10)
C13	35.5(16)	28.8(13)	62(2)	-8.1(13)	15.7(14)	-4.5(11)
C14	23.4(12)	27.2(12)	46.1(15)	1.9(11)	-1.8(11)	3.6(9)
C15	22.4(11)	22.3(12)	47.8(14)	-1.6(11)	1.5(11)	0.8(9)
C16	23.3(12)	31.2(14)	55.8(17)	-10.6(13)	6.3(12)	-4.2(10)
C17	54.5(19)	25.3(14)	66(2)	5.3(14)	12.2(17)	-0.7(13)
C18	33.6(15)	48.2(18)	54.7(19)	-5.9(15)	-12.5(14)	-1.3(13)
C19	31.0(14)	31.1(14)	83(3)	-15.3(16)	22.8(16)	-9.9(11)
O20	60.4(17)	78(2)	59.6(18)	-9.3(15)	18.8(14)	-5.9(15)
C21	45.5(18)	22.6(13)	84(3)	0.7(15)	20.8(18)	-3.5(12)
C22	38.3(16)	54(2)	52.5(17)	13.6(16)	4.1(14)	-2.6(14)
C23	36.2(15)	43.2(16)	41.1(15)	3.5(12)	-2.5(12)	3.5(12)
C24	42.2(17)	46.2(18)	46.4(17)	-7.8(14)	-11.2(14)	1.7(14)
C27	34.5(16)	68(2)	57(2)	27.1(18)	9.0(15)	-4.7(15)
C32	60(4)	58(5)	46(3)	9(3)	16(3)	8(3)
C33	49(5)	61(6)	47(4)	21(4)	2(3)	-5(4)
O1AA	35.7(10)	26.2(9)	46.5(11)	-0.2(8)	0.5(9)	0.6(7)
O6AA	89(4)	160(6)	62(3)	30(3)	-6(2)	-26(4)
O3	59(5)	91(6)	49(4)	-2(3)	2(3)	-1(4)

C5	68(5)	90(6)	61(4)	-6(4)	-13(3)	-2(4)
C6	135(9)	158(10)	86(5)	56(6)	15(5)	-6(7)
O2AA	107(4)	122(5)	70(3)	33(3)	-27(3)	-55(4)
C1	94(4)	64(3)	63(3)	0(2)	13(3)	-12(3)
O2	128(8)	67(5)	94(6)	-7(4)	-46(5)	25(4)
C5A	180(30)	87(15)	130(20)	-36(14)	76(19)	-56(16)
O0AA	70(5)	79(5)	64(4)	-2(3)	-2(3)	12(3)

Table 4. Bond Lengths for **52**.

Atom	Atom	Length/Å	Atom	Atom	Length/Å
O5AA	C22	1.412(4)	C12	C18	1.518(5)
O3AA	C13	1.260(5)	C13	C16	1.529(4)
N1AA	C8	1.326(4)	C13	O20	1.238(5)
N1AA	C10	1.466(3)	C14	C15	1.517(4)
N2AA	C9	1.497(4)	C15	O1AA	1.239(4)
N2AA	C11	1.505(3)	C16	C19	1.540(4)
O4AA	C8	1.243(3)	C17	C21	1.525(5)
N7	C15	1.344(4)	C18	C24	1.529(5)
N7	C16	1.463(4)	C19	C21	1.509(7)
N7	C17	1.465(4)	C23	C24	1.532(5)
C8	C11	1.520(4)	C27	C32	1.508(10)
C9	C32	1.496(8)	C27	C33	1.448(9)
C9	C33	1.569(9)	O6AA	C6	1.387(11)
C10	C14	1.546(4)	O3	C5	1.423(12)
C10	C23	1.522(4)	O3	C5A	1.423(12)
C11	C27	1.537(5)	C1	O2	1.207(10)
C12	C14	1.533(4)	C1	O0AA	1.339(9)

Table 5. Bond Angles for **52**.

Atom	Atom	Atom	Angle/˚	Atom	Atom	Atom	Angle/˚
C8	N1AA	C10	122.4(2)	C12	C14	C10	111.5(2)
C9	N2AA	C11	108.4(2)	C15	C14	C10	109.6(2)
C15	N7	C16	118.4(3)	C15	C14	C12	112.0(2)
C15	N7	C17	128.8(3)	N7	C15	C14	117.8(3)
C16	N7	C17	112.8(3)	O1AA	C15	N7	119.9(3)
N1AA	C8	C11	115.2(2)	O1AA	C15	C14	122.3(2)
O4AA	C8	N1AA	124.8(3)	N7	C16	C13	112.1(2)
O4AA	C8	C11	119.9(2)	N7	C16	C19	102.4(3)

N2AA	C9	C33	103.0(4)	C13	C16	C19	110.9(2)
C32	C9	N2AA	103.3(4)	N7	C17	C21	102.3(3)
N1AA	C10	C14	111.2(2)	C12	C18	C24	110.7(3)
N1AA	C10	C23	111.5(2)	C21	C19	C16	104.1(3)
C23	C10	C14	109.7(2)	C19	C21	C17	102.7(3)
N2AA	C11	C8	110.1(2)	C10	C23	C24	113.4(3)
N2AA	C11	C27	104.1(2)	C18	C24	C23	111.2(3)
C8	C11	C27	111.6(3)	C32	C27	C11	104.8(3)
C18	C12	C14	109.6(3)	C33	C27	C11	105.7(4)
O3AA	C13	C16	117.5(3)	C9	C32	C27	103.4(5)
O20	C13	O3AA	124.6(3)	C27	C33	C9	102.7(5)
O20	C13	C16	117.8(3)				

Table 6. Torsion Angles for **52**.

A	**B**	**C**	**D**	**Angle/˚**	**A**	**B**	**C**	**D**	**Angle/˚**
O3AA	C13	C16	N7	-33.2(4)	C11	N2AA	C9	C33	19.2(5)
O3AA	C13	C16	C19	80.5(4)	C11	C27	C32	C9	-37.3(5)
N1AA	C8	C11	N2AA	152.2(2)	C11	C27	C33	C9	39.7(7)
N1AA	C8	C11	C27	-92.6(3)	C12	C14	C15	N7	-153.0(2)
N1AA	C10	C14	C12	-68.4(3)	C12	C14	C15	O1AA	29.5(4)
N1AA	C10	C14	C15	56.2(3)	C12	C18	C24	C23	-55.8(4)
N1AA	C10	C23	C24	71.2(3)	C13	C16	C19	C21	-91.7(3)
N2AA	C9	C32	C27	39.3(5)	C14	C10	C23	C24	-52.4(3)
N2AA	C9	C33	C27	-36.5(7)	C14	C12	C18	C24	59.0(4)
N2AA	C11	C27	C32	20.4(4)	C15	N7	C16	C13	-65.5(3)
N2AA	C11	C27	C33	-28.0(5)	C15	N7	C16	C19	175.6(2)
O4AA	C8	C11	N2AA	-29.8(4)	C15	N7	C17	C21	160.0(3)
O4AA	C8	C11	C27	85.3(3)	C16	N7	C15	C14	-175.6(2)
N7	C16	C19	C21	28.1(3)	C16	N7	C15	O1AA	1.9(4)
N7	C17	C21	C19	35.3(3)	C16	N7	C17	C21	-18.5(4)
C8	N1AA	C10	C14	-100.2(3)	C16	C19	C21	C17	-39.7(3)
C8	N1AA	C10	C23	137.0(3)	C17	N7	C15	C14	6.0(4)
C8	C11	C27	C32	-98.4(4)	C17	N7	C15	O1AA	-176.5(3)
C8	C11	C27	C33	-146.8(5)	C17	N7	C16	C13	113.2(3)
C9	N2AA	C11	C8	123.8(3)	C17	N7	C16	C19	-5.7(3)
C9	N2AA	C11	C27	4.0(3)	C18	C12	C14	C10	-59.4(3)
C10	N1AA	C8	O4AA	-3.8(4)	C18	C12	C14	C15	177.4(2)
C10	N1AA	C8	C11	174.1(2)	O20	C13	C16	N7	149.9(3)
C10	C14	C15	N7	82.6(3)	O20	C13	C16	C19	-96.3(4)
C10	C14	C15	O1AA	-94.8(3)	C23	C10	C14	C12	55.4(3)

C10	C23	C24	C18	53.3(4)	C23	C10	C14	C15	180.0(2)
C11	N2AA	C9	C32	-26.9(4)					

Table 7. Hydrogen Atom Coordinates (Å×10^4) and Isotropic Displacement Parameters (Å^2×10^3) for **52**.

Atom	***x***	***y***	***z***	**U(eq)**
H5AD	7377	3753	8	55
H1AA	8555	3748	-2466	34
H2AA	10358	3751	-1142	32
H2AB	10164	4407	-1058	32
H9AA	10345	3582	681	56
H9AB	10479	4321	691	56
H9BC	10158	4415	774	56
H9BD	10594	3808	635	56
H10	8430	5004	-3053	38
H11	9406	3425	-1473	38
H12A	7383	3738	-2080	43
H12B	6762	4153	-2084	43
H14	7337	5021	-2822	39
H16	8319	5532	359	44
H17A	7391	6007	-2374	59
H17B	8138	6082	-2315	59
H18A	6807	4232	-4054	55
H18B	6788	3513	-3706	55
H19A	7946	6706	555	58
H19B	8519	6533	-247	58
H21A	7831	7015	-1473	61
H21B	7232	6696	-903	61
H22A	7939	3058	1065	73
H22B	7288	2956	1680	73
H22C	7620	3623	1712	73
H23A	8510	4264	-4564	48
H23B	7916	4711	-4655	48
H24A	7583	3691	-5088	54
H24B	7884	3419	-3978	54
H27A	8681	3908	121	64
H27B	9098	3295	320	64
H27C	8915	4133	361	64
H27D	8788	3411	90	64
H32A	9429	4559	888	66

H32B	9495	3954	1667	66
H33A	9729	3114	778	63
H33B	9518	3648	1638	63
H6AA	8630	5708	2782	156
H3A	7398	5683	-6433	100
H3B	7608	5847	-6264	100
H5A	7918	6471	-6117	110
H5B	8065	6162	-4944	110
H5C	7466	6598	-5092	110
H6A	8580	4540	2783	189
H6B	8700	4977	3831	189
H6C	9273	4752	3087	189
H2AC	9490	6721	2871	149
H2AD	9160	6152	2945	149
H2	9581	6538	-4609	144
H5AA	8017	5984	-4648	194
H5AB	7350	5846	-4110	194
H5AC	7469	6485	-4755	194
H0AA	9869	5909	-5542	106

Table 8. Atomic Occupancy for **52**.

Atom	***Occupancy***	**Atom**	***Occupancy***	**Atom**	***Occupancy***
H9AA	0.550(14)	H9AB	0.550(14)	H9BC	0.450(14)
H9BD	0.450(14)	H27A	0.550(14)	H27B	0.550(14)
H27C	0.450(14)	H27D	0.450(14)	C32	0.550(14)
H32A	0.550(14)	H32B	0.550(14)	C33	0.450(14)
H33A	0.450(14)	H33B	0.450(14)	O6AA	0.827(12)
H6AA	0.827(12)	O3	0.439(15)	H3A	0.68(2)
H3B	0.32(2)	C5	0.68(2)	H5A	0.68(2)
H5B	0.68(2)	H5C	0.68(2)	C6	0.827(12)
H6A	0.827(12)	H6B	0.827(12)	H6C	0.827(12)
O2AA	0.814(15)	H2AC	0.814(15)	H2AD	0.814(15)
O2	0.519(12)	H2	0.519(12)	C5A	0.32(2)
H5AA	0.32(2)	H5AB	0.32(2)	H5AC	0.32(2)
O0AA	0.481(12)	H0AA	0.481(12)		

2-Methyl-4*H*-benzo[d][1,3]oxazin-4-one (89)

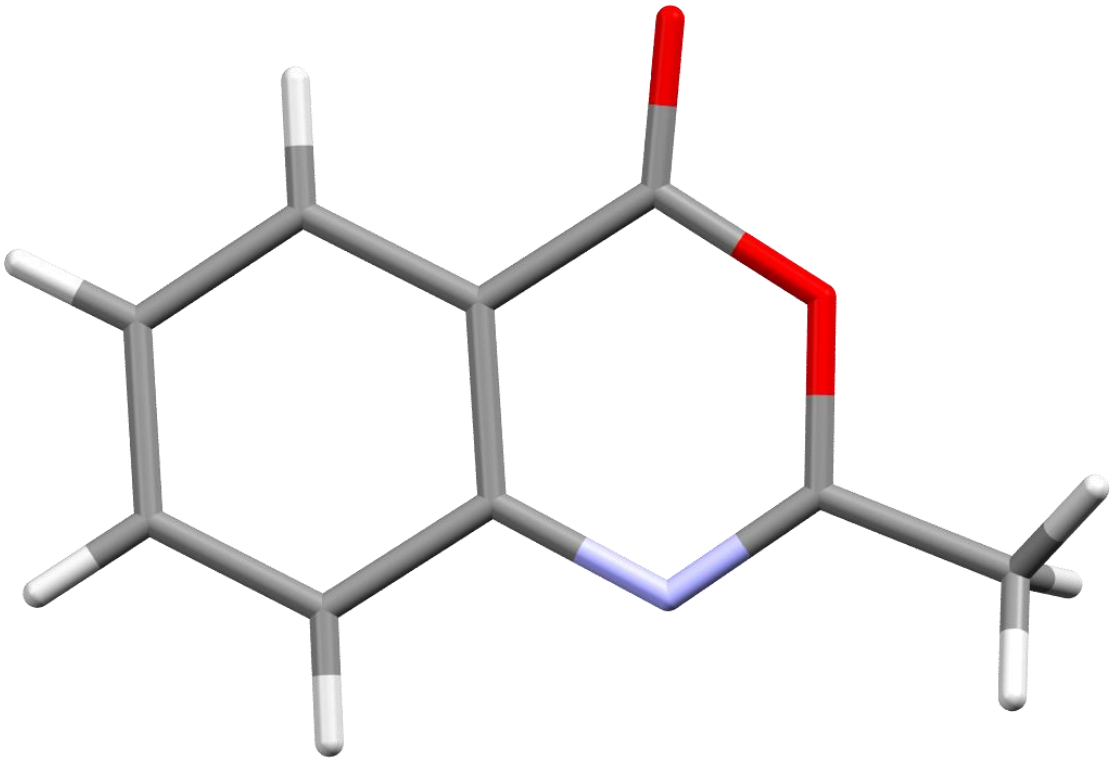

Table 1. Crystal data and structure refinement for **89**.

Empirical formula	$C_9H_7NO_2$
Formula weight	161.16
Temperature/K	123.00(10)
Crystal system	monoclinic
Space group	$P2_1/c$
a/Å	7.2435(3)
b/Å	10.3965(5)
c/Å	10.1746(6)
α/°	90
β/°	102.676(5)
γ/°	90
Volume/Å^3	747.54(7)
Z	4
ρ_{calc}g/cm^3	1.432
μ/mm^{-1}	0.853
F(000)	336.0
Crystal size/mm^3	0.141 × 0.074 × 0.056
Radiation	CuKα (λ = 1.54184)
2Θ range for data collection/°	12.328 to 147.078

Index ranges	$-7 \le h \le 8, -12 \le k \le 12, -9 \le l \le 12$
Reflections collected	3569
Independent reflections	1453 [R_{int} = 0.0224, R_{sigma} = 0.0282]
Data/restraints/parameters	1453/0/110
Goodness-of-fit on F^2	1.082
Final R indexes [I>=2σ (I)]	R_1 = 0.0373, wR_2 = 0.0911
Final R indexes [all data]	R_1 = 0.0518, wR_2 = 0.0991
Largest diff. peak/hole / e $Å^{-3}$	0.18/-0.19

Table 2. Fractional Atomic Coordinates ($\times 10^4$) and Equivalent Isotropic Displacement Parameters ($Å^2 \times 10^3$) for **89**. U_{eq} is defined as 1/3 of of the trace of the orthogonalised U_{IJ} tensor.

Atom	*x*	*y*	*z*	U(eq)
O1	6721.3(13)	3327.3(10)	3513.5(10)	27.9(3)
O2	5465.5(15)	4872.0(11)	2106.4(11)	37.4(3)
N1	8377.7(15)	3681.1(12)	5745.6(12)	27.5(3)
C1	7977.2(17)	4993.9(14)	5568.6(14)	25.0(3)
C2	6903.9(17)	5489.4(14)	4356.9(14)	23.9(3)
C3	6280.9(17)	4610.6(14)	3234.4(14)	26.0(3)
C8	7736.6(18)	2938.7(15)	4755.1(15)	27.4(3)
C7	8660.5(19)	5841.6(16)	6627.6(15)	31.4(4)
C4	6474.0(19)	6799.4(15)	4224.2(16)	29.5(3)
C5	7150(2)	7621.5(15)	5287.5(17)	34.2(4)
C6	8262(2)	7136.7(16)	6483.9(17)	35.2(4)
C9	7985(2)	1519.6(15)	4801.4(18)	37.6(4)

Table 3. Anisotropic Displacement Parameters ($Å^2 \times 10^3$) for **89**. The Anisotropic displacement factor exponent takes the form: $-2\pi^2[h^2a^{*2}U_{11}+2hka^*b^*U_{12}+\ldots]$.

Atom	U_{11}	U_{22}	U_{33}	U_{23}	U_{13}	U_{12}
O1	27.7(5)	27.9(5)	25.0(6)	0.3(4)	-0.8(4)	-2.2(4)
O2	41.7(6)	41.4(7)	24.1(6)	3.9(5)	-3.5(4)	0.9(5)
N1	24.2(5)	31.4(7)	24.8(7)	4.2(5)	0.7(5)	-3.2(5)
C1	20.8(6)	30.9(8)	23.5(7)	2.8(6)	5.4(5)	-2.7(5)
C2	20.0(6)	30.4(8)	21.8(7)	1.5(6)	5.5(5)	-2.0(5)
C3	22.0(6)	29.9(7)	25.5(8)	2.9(6)	3.7(5)	-1.5(5)
C8	21.1(6)	31.9(8)	27.1(8)	5.9(6)	1.0(5)	-2.5(5)
C7	30.6(7)	41.0(9)	22.6(8)	-1.6(6)	5.5(6)	-5.9(6)
C4	23.8(6)	33.7(8)	31.9(8)	3.6(6)	8.2(6)	0.8(5)
C5	31.8(7)	29.7(8)	44.7(10)	-3.0(7)	16.3(7)	-0.6(6)

C6	34.7(7)	40.4(9)	33.5(9)	-11.7(7)	14.1(6)	-7.7(7)
C9	33.8(7)	29.1(8)	44.8(10)	3.4(7)	-2.4(7)	-2.9(6)

Table 4. Bond Lengths for **89**.

Atom	Atom	Length/Å	Atom	Atom	Length/Å
O1	C3	1.3866(17)	C2	C3	1.455(2)
O1	C8	1.3755(17)	C2	C4	1.397(2)
O2	C3	1.2010(17)	C8	C9	1.486(2)
N1	C1	1.3988(19)	C7	C6	1.378(2)
N1	C8	1.2734(19)	C4	C5	1.381(2)
C1	C2	1.4032(19)	C5	C6	1.398(2)
C1	C7	1.396(2)			

Table 5. Bond Angles for **89**.

Atom	Atom	Atom	Angle/˚	Atom	Atom	Atom	Angle/˚
C8	O1	C3	121.55(11)	O2	C3	O1	117.14(13)
C8	N1	C1	117.40(12)	O2	C3	C2	127.66(14)
N1	C1	C2	122.05(13)	O1	C8	C9	110.94(13)
C7	C1	N1	119.23(13)	N1	C8	O1	125.27(14)
C7	C1	C2	118.73(14)	N1	C8	C9	123.79(13)
C1	C2	C3	118.41(13)	C6	C7	C1	120.29(14)
C4	C2	C1	120.77(13)	C5	C4	C2	119.63(14)
C4	C2	C3	120.81(13)	C4	C5	C6	119.76(15)
O1	C3	C2	115.19(12)	C7	C6	C5	120.80(15)

Table 6. Hydrogen Atom Coordinates (Å×10^4) and Isotropic Displacement Parameters (Å^2×10^3) for **89**.

Atom	*x*	*y*	*z*	U(eq)
H7	9388.19	5531.01	7433.65	38
H4	5736.71	7116.17	3424.62	35
H5	6867	8494.42	5207.61	41
H6	8737.42	7694.8	7191.48	42
H9A	6891.42	1123.37	5017.86	56
H9B	9087.91	1301.3	5476.94	56
H9C	8134.4	1217.16	3939.47	56

***cis*-2-Acetamido-*N*,*N*-dimethylcyclohexane-1-carboxamide (*cis*-95)**

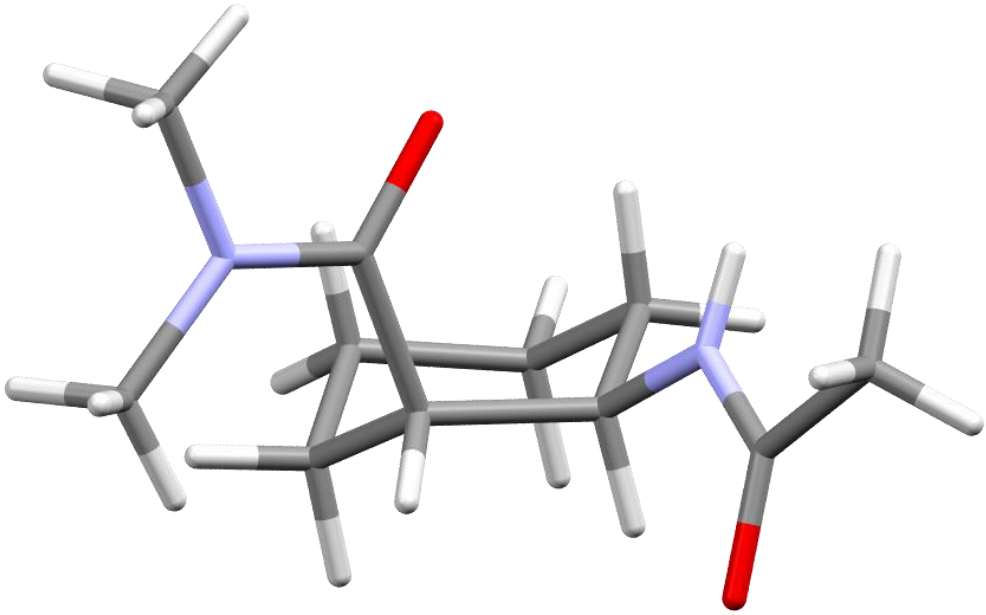

Table 1. Crystal data and structure refinement for ***cis*-95**.	
Empirical formula	$C_{11}H_{20}N_2O_2$
Formula weight	212.29
Temperature/K	294.15(10)
Crystal system	triclinic
Space group	P-1
a/Å	8.0260(4)
b/Å	8.4029(4)
c/Å	9.4537(3)
α/°	108.763(4)
β/°	95.599(4)
γ/°	102.128(4)
Volume/Å^3	580.75(5)
Z	2
ρ_{calc}g/cm^3	1.214
μ/mm^{-1}	0.674
F(000)	232.0
Crystal size/mm^3	0.59 × 0.223 × 0.107
Radiation	CuKα (λ = 1.54184)
2Θ range for data collection/°	10.042 to 147.492
Index ranges	-9 ≤ h ≤ 9, -10 ≤ k ≤ 10, -11 ≤ l ≤ 11

Reflections collected	12685
Independent reflections	2302 [R_{int} = 0.0431, R_{sigma} = 0.0234]
Data/restraints/parameters	2302/0/216
Goodness-of-fit on F^2	1.047
Final R indexes [I>=2σ (I)]	R_1 = 0.0364, wR_2 = 0.0966
Final R indexes [all data]	R_1 = 0.0404, wR_2 = 0.1026
Largest diff. peak/hole / e $Å^{-3}$	0.26/-0.22

Table 2. Fractional Atomic Coordinates (×10^4) and Equivalent Isotropic Displacement Parameters ($Å^2$×10^3) for ***cis*-95**. U_{eq} is defined as 1/3 of of the trace of the orthogonalised U_{IJ} tensor.

Atom	*x*	*y*	*z*	U(eq)
O2	5383.1(11)	4151.0(11)	6436.6(11)	32.8(2)
O1	-32.0(12)	880.5(12)	3164.0(11)	37.2(2)
N2	5254.2(13)	1628.1(13)	6820.6(12)	28.9(2)
N1	2146.5(13)	3305.8(14)	4303.6(11)	26.9(2)
C9	4514.6(14)	2866.3(14)	6629.9(12)	22.9(2)
C2	1224.2(15)	1953.3(15)	3090.7(13)	26.0(3)
C4	2588.8(14)	2632.1(14)	6669.2(12)	22.0(2)
C5	2286.1(16)	3175.9(16)	8324.4(13)	27.7(3)
C3	1756.7(15)	3653.2(15)	5830.0(13)	24.7(3)
C8	2209.5(18)	5614.4(16)	6678.7(15)	32.0(3)
C1	1842.2(18)	1827.6(19)	1609.1(15)	33.4(3)
C6	2849.5(19)	5136.0(18)	9139.9(15)	35.9(3)
C10	4416.4(19)	127.8(17)	7179.7(18)	36.0(3)
C11	7106.7(17)	1856(2)	6839.9(18)	37.7(3)
C7	1878(2)	6042.5(19)	8305.2(16)	39.6(3)

Table 3. Anisotropic Displacement Parameters ($Å^2$×10^3) for ***cis*-95**. The Anisotropic displacement factor exponent takes the form: $-2\pi^2[h^2a^{*2}U_{11}+2hka^*b^*U_{12}+\ldots]$.

Atom	U_{11}	U_{22}	U_{33}	U_{23}	U_{13}	U_{12}
O2	23.1(4)	30.9(5)	47.7(5)	21.6(4)	8.8(4)	0.1(3)
O1	31.0(5)	30.7(5)	43.6(5)	13.3(4)	7.1(4)	-5.8(4)
N2	21.5(5)	26.7(5)	40.6(6)	13.8(4)	8.1(4)	6.3(4)
N1	22.1(5)	30.1(5)	27.4(5)	14.9(4)	3.6(4)	-3.0(4)
C9	21.2(5)	23.0(5)	23.1(5)	8.3(4)	4.7(4)	2.3(4)
C2	22.9(5)	25.5(6)	31.8(6)	14.4(5)	3.4(4)	4.8(4)
C4	19.2(5)	21.8(6)	25.5(5)	10.5(4)	5.8(4)	1.9(4)
C5	25.7(6)	34.3(7)	26.8(6)	14.3(5)	8.7(5)	8.1(5)

C3	20.3(5)	28.6(6)	27.4(6)	13.8(5)	5.1(4)	4.1(4)
C8	32.7(7)	28.5(6)	38.2(7)	15.0(5)	4.4(5)	10.9(5)
C1	33.2(7)	36.2(7)	29.6(6)	12.5(5)	5.7(5)	5.0(6)
C6	40.9(8)	36.7(7)	27.7(6)	6.7(5)	6.3(5)	12.4(6)
C10	33.6(7)	29.4(7)	51.0(8)	21.4(6)	8.2(6)	8.6(6)
C11	22.8(6)	40.1(8)	49.9(8)	12.5(6)	9.2(6)	11.6(6)
C7	45.7(8)	33.3(7)	40.4(7)	8.2(6)	9.4(6)	18.4(6)

Table 4. Bond Lengths for ***cis*-95**.

Atom	Atom	Length/Å	Atom	Atom	Length/Å
O2	C9	1.2329(14)	C2	C1	1.5105(17)
O1	C2	1.2271(15)	C4	C5	1.5418(15)
N2	C9	1.3515(15)	C4	C3	1.5450(15)
N2	C10	1.4562(16)	C5	C6	1.5211(19)
N2	C11	1.4562(16)	C3	C8	1.5272(17)
N1	C2	1.3405(16)	C8	C7	1.5261(19)
N1	C3	1.4563(15)	C6	C7	1.5256(19)
C9	C4	1.5222(15)			

Table 5. Bond Angles for ***cis*-95**.

Atom	Atom	Atom	Angle/˚	Atom	Atom	Atom	Angle/˚
C9	N2	C10	126.22(10)	C9	C4	C5	110.25(9)
C9	N2	C11	119.05(11)	C9	C4	C3	112.69(9)
C10	N2	C11	114.39(11)	C5	C4	C3	109.91(9)
C2	N1	C3	123.58(10)	C6	C5	C4	112.48(10)
O2	C9	N2	120.67(10)	N1	C3	C4	111.98(9)
O2	C9	C4	121.18(10)	N1	C3	C8	109.55(10)
N2	C9	C4	118.15(10)	C8	C3	C4	114.54(10)
O1	C2	N1	122.99(11)	C7	C8	C3	111.47(11)
O1	C2	C1	121.75(11)	C5	C6	C7	110.53(11)
N1	C2	C1	115.27(11)	C6	C7	C8	110.59(11)

Table 6. Hydrogen Atom Coordinates (Å×10^4) and Isotropic Displacement Parameters (Å^2×10^3) for ***cis*-95**.

Atom	*x*	*y*	*z*	U(eq)
H3	491(19)	3160(17)	5698(15)	26(3)
H5A	2870(20)	2568(19)	8878(17)	34(4)
H5B	1030(20)	2740(19)	8292(16)	32(4)
H10A	4720(20)	-900(20)	6538(18)	42(4)
H10B	3200(20)	-100(20)	7000(18)	39(4)
H1	2950(20)	4010(20)	4172(19)	42(4)
H8A	1560(20)	6150(20)	6154(19)	46(4)
H4	1990(17)	1392(18)	6153(15)	21(3)
H6A	4120(20)	5590(20)	9213(18)	41(4)
H10C	4840(20)	310(20)	8260(20)	46(4)
H8B	3420(20)	6124(19)	6682(17)	33(4)
H6B	2630(20)	5430(20)	10180(20)	52(5)
H7A	610(20)	5630(20)	8270(20)	49(5)
H7B	2260(20)	7330(20)	8830(20)	49(5)
H11A	7730(30)	2070(20)	7880(20)	61(5)
H11B	7330(20)	800(30)	6170(20)	62(5)
H1A	900(30)	1720(30)	840(20)	65(6)
H1B	2170(30)	770(30)	1190(20)	74(6)
H1C	2760(30)	2770(30)	1680(20)	70(6)
H11C	7570(30)	2840(30)	6580(20)	71(6)

***trans*-2-Acetamido-*N*,*N*-dimethylcyclohexane-1-carboxamide (*trans*-95)**

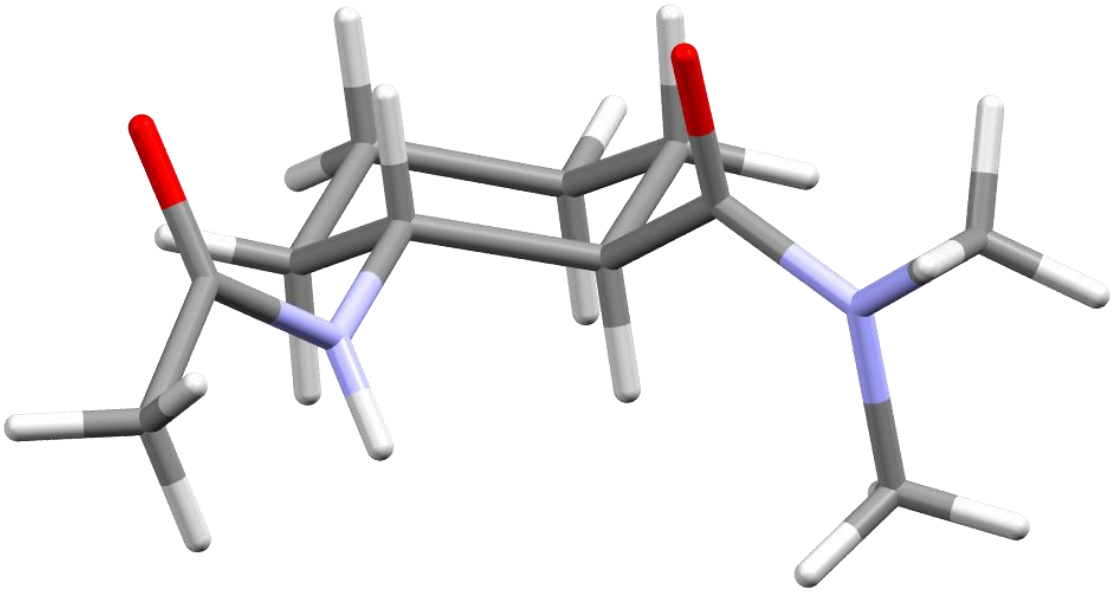

Table 1. Crystal data and structure refinement for ***trans*-95**.

Empirical formula	$C_{11}H_{20}N_2O_2$
Formula weight	212.29
Temperature/K	122.98(11)
Crystal system	monoclinic
Space group	Cc
a/Å	17.0252(4)
b/Å	8.82890(10)
c/Å	18.1222(4)
α/°	90
β/°	118.029(3)
γ/°	90
Volume/Å^3	2404.52(10)
Z	8
ρ_{calc}g/cm^3	1.173
μ/mm^{-1}	0.651
F(000)	928.0
Crystal size/mm^3	0.311 × 0.207 × 0.189
Radiation	CuKα (λ = 1.54184)
2Θ range for data collection/°	11.062 to 148.604
Index ranges	-20 ≤ h ≤ 20, -10 ≤ k ≤ 10, -22 ≤ l ≤ 22
Reflections collected	28229
Independent reflections	4725 [R_{int} = 0.0244, R_{sigma} = 0.0126]

Data/restraints/parameters	4725/2/277
Goodness-of-fit on F^2	1.075
Final R indexes [I>=2σ (I)]	R_1 = 0.0262, wR_2 = 0.0717
Final R indexes [all data]	R_1 = 0.0265, wR_2 = 0.0720
Largest diff. peak/hole / e $Å^{-3}$	0.14/-0.13
Flack parameter	0.02(4)

Table 2. Fractional Atomic Coordinates ($\times 10^4$) and Equivalent Isotropic Displacement Parameters ($Å^2 \times 10^3$) for ***trans*-95**. U_{eq} is defined as 1/3 of of the trace of the orthogonalised U_{IJ} tensor.

Atom	*x*	*y*	*z*	U(eq)
O3	4624.0(9)	5095.1(14)	5655.0(9)	41.5(3)
O2	1468.5(8)	2595.9(14)	4344.0(9)	41.5(3)
O1	2833.7(9)	714.6(18)	6621.0(8)	44.5(3)
O4	3711.7(9)	3215.8(18)	3377.9(8)	44.5(3)
N2	-16.2(10)	2662.7(15)	3778.4(9)	32.0(3)
N4	3704.8(10)	5163.0(15)	6219.6(9)	31.9(3)
N3	3123.7(9)	2789.2(17)	4247.8(8)	32.7(3)
N1	1375.3(9)	290.3(17)	5750.9(8)	32.7(3)
C9	761.5(11)	1923.9(18)	4140.5(10)	28.9(3)
C20	4119.9(10)	4424.1(18)	5858.5(10)	28.8(3)
C2	2054.1(12)	722(2)	6478.8(11)	36.3(4)
C3	1505.1(10)	-322.2(19)	5068.7(9)	29.2(3)
C14	3934.8(10)	2178.2(19)	4929.8(9)	29.2(3)
C13	3074.4(12)	3222(2)	3520(1)	36.3(4)
C15	4022.5(10)	2706.2(18)	5768.4(9)	28.0(3)
C16	4852.9(12)	2011.2(19)	6494.9(10)	34.9(4)
C4	753.7(10)	206.6(18)	4230.1(9)	28.0(3)
C21	3896.3(12)	6772(2)	6403.3(12)	39.8(4)
C17	4849.5(13)	284(2)	6437.7(11)	37.1(4)
C10	-7.4(14)	4271(2)	3595.2(12)	39.8(4)
C5	857.0(12)	-487(2)	3502.9(10)	34.8(4)
C8	1550.7(11)	-2048(2)	5111.0(11)	35.3(4)
C6	910.4(13)	-2215(2)	3560.7(11)	37.2(4)
C7	1672.0(12)	-2720(2)	4396.7(12)	38.8(4)
C19	3939.3(12)	452(2)	4887.8(11)	35.3(4)
C18	4774.4(13)	-218(2)	5601.5(12)	38.9(4)
C11	-869.8(13)	2012(2)	3618.9(16)	51.3(5)
C22	3011.9(17)	4512(2)	6380.9(16)	51.1(5)
C12	2170.5(14)	3764(3)	2875.4(14)	61.2(7)
C1	1794.4(16)	1265(3)	7123.1(14)	61.2(7)

Table 3. Anisotropic Displacement Parameters ($Å^2×10^3$) for ***trans*-95**. The Anisotropic displacement factor exponent takes the form: $-2\pi^2[h^2a^{*2}U_{11}+2hka^*b^*U_{12}+\ldots]$.

Atom	U_{11}	U_{22}	U_{33}	U_{23}	U_{13}	U_{12}
O3	36.5(7)	37.1(6)	60.3(8)	-0.8(6)	30.6(6)	-9.1(5)
O2	32.6(7)	37.6(7)	60.0(8)	0.7(6)	26.4(6)	-8.3(5)
O1	29.2(6)	63.9(9)	38.5(6)	-3.1(6)	14.3(5)	-11.2(6)
O4	37.2(7)	63.6(9)	38.7(6)	2.9(6)	22.9(6)	-8.8(6)
N2	30.7(7)	29.1(7)	35.8(7)	-1.7(5)	15.3(6)	-2.8(5)
N4	33.7(7)	28.8(7)	36.4(7)	1.7(5)	19.2(6)	-1.1(6)
N3	21.3(6)	47.1(8)	30.6(7)	1.3(6)	13.0(5)	-3.7(6)
N1	24.8(6)	46.9(8)	30.6(7)	-1.4(6)	16.5(5)	-4.7(6)
C9	30.5(8)	32.6(8)	29.1(7)	-1.7(6)	18.3(6)	-4.7(6)
C20	22.7(7)	32.3(8)	29.0(7)	1.2(6)	10.2(6)	-3.2(6)
C2	34.6(9)	44.3(9)	31.8(8)	-1.2(7)	17.2(7)	-10.2(7)
C3	22.4(7)	39.0(9)	28.4(7)	0.0(6)	13.8(6)	-2.8(6)
C14	22.5(7)	39.0(9)	28.3(7)	-0.3(6)	13.8(6)	-3.3(6)
C13	31.1(8)	44.5(9)	31.7(8)	1.2(7)	13.4(7)	-9.0(7)
C15	26.0(8)	31.5(8)	29.4(7)	-1.4(6)	15.5(6)	-4.6(6)
C16	37.7(9)	31.8(8)	30.5(8)	1.1(6)	12.1(7)	-3.2(7)
C4	24.1(7)	31.6(8)	29.2(7)	1.4(6)	13.3(6)	-3.5(6)
C21	37.3(9)	30.7(8)	44.2(9)	-1.4(7)	13.2(7)	1.1(7)
C17	41.8(10)	32.1(8)	36.3(9)	3.6(7)	17.4(7)	0.0(7)
C10	51.9(11)	30.8(8)	44.1(9)	1.2(7)	28.8(8)	2.4(7)
C5	42.2(9)	32.0(8)	30.2(8)	-1.6(6)	17.2(7)	-4.2(7)
C8	27.7(8)	41.3(9)	35.6(8)	7.3(7)	13.6(6)	3.3(7)
C6	42.2(10)	32.2(8)	36.1(9)	-3.5(7)	17.4(8)	-3.0(7)
C7	33.0(9)	36.3(9)	46.3(10)	-0.4(7)	17.9(8)	2.1(7)
C19	34.6(9)	40.8(9)	35.8(8)	-7.4(7)	20.8(7)	-4.1(7)
C18	41.4(10)	35.9(9)	46.5(10)	0.3(7)	26.5(8)	2.7(7)
C11	26.5(9)	37.4(10)	78.5(15)	-5.0(9)	15.0(9)	-1.6(7)
C22	67.5(14)	37.6(10)	78.1(14)	5.0(9)	59.1(12)	2.7(9)
C12	34.5(10)	98.5(19)	42.9(10)	24.4(11)	11.9(8)	-2.9(11)
C1	51.1(12)	98.2(19)	43.1(11)	-24.5(11)	29.4(10)	-26.8(12)

Table 4. Bond Lengths for ***trans*-95**.

Atom	Atom	Length/Å	Atom	Atom	Length/Å
O3	C20	1.233(2)	C20	C15	1.526(2)
O2	C9	1.233(2)	C2	C1	1.508(3)

O1	C2	1.227(2)	C3	C4	1.529(2)
O4	C13	1.227(2)	C3	C8	1.526(2)
N2	C9	1.339(2)	C14	C15	1.528(2)
N2	C10	1.460(2)	C14	C19	1.526(2)
N2	C11	1.460(2)	C13	C12	1.507(3)
N4	C20	1.337(2)	C15	C16	1.536(2)
N4	C21	1.460(2)	C16	C17	1.528(2)
N4	C22	1.460(2)	C4	C5	1.536(2)
N3	C14	1.457(2)	C17	C18	1.526(3)
N3	C13	1.337(2)	C5	C6	1.529(2)
N1	C2	1.337(2)	C8	C7	1.524(3)
N1	C3	1.458(2)	C6	C7	1.526(3)
C9	C4	1.526(2)	C19	C18	1.522(3)

Table 5. Bond Angles for ***trans*-95**.

Atom	**Atom**	**Atom**	**Angle/˚**	**Atom**	**Atom**	**Atom**	**Angle/˚**
C9	N2	C10	118.15(14)	N3	C14	C15	109.97(13)
C9	N2	C11	124.64(14)	N3	C14	C19	110.64(13)
C11	N2	C10	116.97(15)	C19	C14	C15	110.72(13)
C20	N4	C21	118.25(14)	O4	C13	N3	123.62(16)
C20	N4	C22	124.65(14)	O4	C13	C12	121.34(16)
C22	N4	C21	116.88(15)	N3	C13	C12	115.03(16)
C13	N3	C14	122.54(14)	C20	C15	C14	111.37(13)
C2	N1	C3	122.47(14)	C20	C15	C16	107.18(13)
O2	C9	N2	120.92(15)	C14	C15	C16	110.55(13)
O2	C9	C4	120.17(15)	C17	C16	C15	111.58(14)
N2	C9	C4	118.71(14)	C9	C4	C3	111.36(13)
O3	C20	N4	120.93(15)	C9	C4	C5	107.14(13)
O3	C20	C15	120.09(15)	C3	C4	C5	110.58(13)
N4	C20	C15	118.77(14)	C18	C17	C16	110.71(14)
O1	C2	N1	123.62(16)	C6	C5	C4	111.47(14)
O1	C2	C1	121.38(16)	C7	C8	C3	111.74(14)
N1	C2	C1	114.98(16)	C7	C6	C5	110.80(14)
N1	C3	C4	109.90(13)	C8	C7	C6	109.77(14)
N1	C3	C8	110.62(13)	C18	C19	C14	111.75(14)
C8	C3	C4	110.73(13)	C19	C18	C17	109.86(14)

Table 6. Hydrogen Atom Coordinates (Å×10^4) and Isotropic Displacement Parameters (Å^2×10^3) for ***trans*-95**.

Atom	*x*	*y*	*z*	U(eq)
H3	2658.63	2875.04	4315.81	39
H1	842.08	376.99	5682.62	39
H3A	2069.8	63.47	5123.61	35
H14	4444.69	2564.42	4875.22	35
H15	3493.3	2393.26	5811.49	34
H16A	5380.96	2404.93	6487.41	42
H16B	4875.51	2304.97	7020.32	42
H4	181.31	-106.13	4186.86	34
H21A	4512.15	6959.91	6568.43	60
H21B	3771.46	7057.74	6848.69	60
H21C	3531.1	7355.78	5913.42	60
H17A	5393.87	-115.12	6889.69	45
H17B	4352.2	-118.38	6497.31	45
H10A	124.24	4854.12	4086.93	60
H10B	-579.69	4560.4	3154.01	60
H10C	438.92	4456.28	3424.19	60
H5A	353.99	-193.01	2977.56	42
H5B	1392.69	-93.78	3510.42	42
H8A	2043.66	-2356.38	5639.73	42
H8B	1007.21	-2440.95	5087.11	42
H6A	353.33	-2616.23	3501.44	45
H6B	1001.79	-2614.93	3108.4	45
H7A	1681.41	-3816.72	4432.07	47
H7B	2234.86	-2387.05	4439.48	47
H19A	3419.74	57.92	4911.38	42
H19B	3903.79	143.88	4359.19	42
H18A	5294.32	115.67	5558.89	47
H18B	4748.94	-1315.12	5565.85	47
H11A	-936.92	1032.2	3366.18	77
H11B	-1343.17	2662.68	3248.77	77
H11C	-890.73	1912.28	4136.91	77
H22A	2470.1	4423.99	5864.4	77
H22B	2915.05	5156.81	6757.05	77
H22C	3195	3527.31	6627.28	77
H12A	2186.68	4840.22	2807.42	92
H12B	1737.88	3526.3	3056.54	92
H12C	2011.26	3271.55	2351.69	92
H1A	2159.47	773.37	7647.11	92
H1B	1180.79	1025.31	6941.98	92

H1C	1877.65	2340.99	7190.39	92

5. Curriculum Vitae

Personal data

Name	**Martin Hofmann**
Date of birth	September 21, 1988 in Tübingen
Nationality	German
Email	Martin.Hofmann@chemie.uni-regensburg.de

Education

02/2014 – current	PhD thesis in the research group of *Prof. Dr. O. Reiser* (University of Regensburg, Germany)
12/2013	Master of Science in chemistry
04/2013 – 12/2013	Master thesis in the research group of *Prof. Dr. O. Reiser* (University of Regensburg, Germany)
10/2011 – 03/2013	Advanced studies in chemistry (University of Regensburg, Germany)
10/2011	Bachelor of Science in chemistry
04/2011 – 06/2011	Bachelor thesis in the research group of *Prof. Dr. D. Díaz-Díaz* (University of Regensburg, Germany)
10/2008 – 09/2011	Studies in chemistry (University of Regensburg, Germany)
09/2005 – 06/2007	Abitur (*A-levels*), Schyren-Gymnasium (*secondary school*) Pfaffenhofen a. d. Ilm, Germany.

Publications

1. D. Kühbeck, J. Mayr, M. Häring, **M. Hofmann**, F. Quignard, D. Díaz-Díaz, *New J. Chem.* **2015**, *39*, 2306.
   "Evaluation of the nitroaldol reaction in the presence of metal ion-crosslinked alginates."
2. R. Frach, P. Kibies, S. Böttcher, T. Pongratz, S. Strohfeldt, S. Kurrmann, J. Koehler, **M. Hofmann**, W. Kremer, H. R. Kalbitzer, O. Reiser, D. Horinek, S. M. Kast, *Angew. Chem. Int. Ed.* **2016**, *55*, 8757.
   "The Chemical Shift Baseline for High-Pressure NMR Spectra of Proteins."

Conferences

6th EuCheMS Chemistry Congress – Seville (Spain), September 11–15, 2016.
"Investigation of the Effect of High Hydrostatic Pressure (HHP) on Reactivity and Selectivity of Organocatalyzed Reactions" (poster presentation).
8th International Meeting on Biomolecules under Pressure (IMBP) – Technische Universität Dortmund (Germany), February 15-17, 2016.
"Investigation of pressure effects on modular peptidic organocatalysts" (oral communication, 30 min).
GDCh-Wissenschaftsforum – Dresden (Germany), August 30 – September 02, 2015.
"High Pressure as secondary activation mode for peptidic and non-peptidic Organocatalysts" (poster presentation).
3rd FOR 1979 research group meeting – University of Regensburg (Germany), July 21–22, 2015.
"Small biologically useful molecules under high pressure" (oral communication, 25 min).
2nd FOR 1979 research group meeting – Technische Universität Dortmund (Germany), October 21, 2014.
"The influence of high pressure on peptidic and non-peptidic organocatalysts" (poster).
1st FOR 1979 research group meeting – University of Regensburg (Germany), February 11, 2014.
"Kick-off meeting FOR 1979" (short oral communication, 10 min).

Professional References

Prof. Dr. Oliver Reiser
Institut für Organische Chemie
Universität Regensburg
Universitätsstr. 31
93053 Regensburg, Germany
Phone: 0049 941 943 4631
Email: Oliver.Reiser@chemie.uni-regensburg.de

H. Acknowledgment – Danksagung

Zuallererst möchte ich Prof Dr. Oliver Reiser für die Überlassung des interessanten und anspruchsvollen Forschungsthemas, der beständigen Unterstützung sowie fachlichen Anleitung während der gesamten Promotion herzlich danken.

Mein aufrichtiger Dank gebührt Prof. Dr. Dr. Hans Robert Kalbitzer und Prof. Dr. Werner Kremer sowie ihren Mitarbeitern Dr. Sunilkumar P. Narayanan, Dr. Markus Beck Erlach und Bastian Ertinger für die Messung und gemeinsame Auswertung der NMR-Spektren unter Hochdruck.

Prof. Dr. Roland Winter und seinem Mitarbeiter Dr. Vitor D. Schuabb von der TU Dortmund danke ich für die Messung der IR-Spektren unter Hochdruck.

Des Weiteren möchte ich mich bei allen aktuellen sowie ehemaligen Mitgliedern der FOR 1979 Forschergruppe für den freundlichen Umgang und die interessanten Gespräche bedanken sowie der DFG, deren Finanzierung die Erstellung dieser Arbeit erst ermöglichte.

Mein Dank gebührt allen Mitarbeitern der Zentralen Analytik der Universität Regensburg für die zahllosen Messungen, fachlichen Diskussionen und die bereitwillige Hilfestellung bei Problemen.

Ein herzliches Dankeschön an die Mitarbeiterinnen des Sekretariats der Arbeitsgruppe, Antje Weigert und Michaela Schüle, für das Regeln aller bürokratischen und organisatorischen Anliegen und ein offenes Ohr für Probleme jeglicher Art.

Ein besonderer Dank gilt Dr. Peter Kreitmeier für die zahllosen guten Ratschläge bei chemischen als auch technischen Problemen, den lehrreichen Gesprächen sowie für das gemeinsame Durchstehen des (oft mühsamen) Prozesses der Anschaffung der neuen Hochdruckanlage.

Für die technische sowie synthetische Unterstützung am Arbeitskreis möchte ich mich bei Klaus Döring, Brigitte Eichenseher, Roxane Harteis und Helena Konkel bedanken.

Meinen Laborkollegen Dr. Andreas Bergmann, Dr. Verena Lehner, Matthias Gnahn und Carina Sonnleitner danke ich herzlichst für die stets freundschaftliche Stimmung, die gute Zusammenarbeit und gemeinsamen Aktivitäten über die letzten Jahre.

Dr. Verena Lehner danke ich für ihre Geduld und fröhliche Natur in beschwerlichen Phasen der Promotion und die vielen netten Diskussionen.

Bei Matthias Gnahn, Benjamin Kastl und Sabine Kerres möchte ich mich besonders für die vielen gemeinsamen Unternehmungen inner- und außerhalb der Universität bedanken, mit euch wird es nie langweilig!

Für seine Freundschaft und tatkräftige Unterstützung bezüglich der Peptidsynthese bedanke ich mich bei meinem Kollegen Dr. Thomas Ertl.

Auch Dr. Ludwig Pilsl danke ich für seine Freundschaft, konstante Motivation und Ratschläge auch über die Promotion hinaus.

Dr. Francesca Besostri und Dr. Soraia Fernandes danke ich für ihre Freundschaft und die spannenden Einblicke in die italienische und portugiesische Kultur.

Zudem danke ich Saerom Park, die mit ihrer fröhlichen Art und aufmunternden Worten den Büroalltag während des Schreibens aufgelockert hat.

Meine tiefe Dankbarkeit gebührt meinem langjährigen Freund Dr. Daniel Dobler, der mich seit Studienbeginn immer durch Rat und Tat unterstützt hat und mit dem ich viele lustige Stunden verbracht habe.

Ich danke allen aktuellen und ehemaligen Mitarbeitern des Arbeitskreises, insbesondere Dr. Nanaji Arisetti, Dr. Andreas Bergmann, Dr. Francesca Besostri, Dr. Daniel Dobler, Dr. Thomas Ertl, Dr. Christian Faderl, Dr. Soraia Fernandes, Dr. Quirin Kainz, Dr. Matthias Knorn, Dr. Paul Kohls, Dr. Christian Lankes, Dr. Verena Lehner, Dr. Corina Neumeister, Dr. Ludwig Pilsl, Dr. Daniel Rackl, Dr. Kathrin Ulbrich, Peter Ehrnsberger, Thomas Föll, Matthias Gnahn, Andreas Hartl, Benjamin Kastl, Sabine Kerres, Michael Leitner, Saerom Park, Carina Sonnleitner, Lisa Stadler und Thomas Weinbender.

Auch möchte ich mich bei Studienkollegen und Freunden aus anderen Arbeitskreisen bedanken, besonders bei Dr. Julian Greindl, Dr. Michal Pozník, Severin Bauer, Jens Braese, Romy Freund, Elisabeth Grünstein, Vanessa Haas, Florian Hastreiter, Marina Kaas, Anika Söldner, Moritz Modl, Bernadette Pilsl, Julian Rieder, Felix Riedlberger und Andreas Seegerer.

Zudem danke ich meinen ehemaligen Bachelorstudenten und Forschungspraktikanten Johannes Fischer, Bernhard Gregori, Christian Griesche, Andreas Hartl, Nils Jannsen und besonders Thomas Weinbender, der das Hochdruckthema hoffentlich mit Erfolg weiterführen kann.

Für das schnelle und gründliche Korrekturlesen dieser Arbeit danke ich Dr. Thomas Ertl, Dr. Verena Lehner, Dr. Ludwig Pilsl, Thomas Föll, Matthias Gnahn und Lisa Stadler.

Neben meinen Freunden und Kollegen innerhalb der Universität möchte ich mich insbesondere bei meinen Freunden Jakob Aps, Felix Geißler, Maximilian Steinfurth und Henrik Strauß bedanken, sowie bei allen Anderen. Auch wenn wir uns nicht häufig sehen, so bedeutet mir doch eure Freundschaft und Unterstützung unendlich viel.

Liebe Lisa, ohne dich hätte ich diese Arbeit wahrscheinlich nicht so zu Ende bringen können. Deine unermüdliche Unterstützung, dein Rückhalt und dein Vertrauen bringen mich jeden Tag dazu, das Beste aus mir zu machen. Dafür werde ich dir immer aus vollstem Herzen dankbar sein, vielen Dank.

Zum Abschluss möchte ich auch meiner Familie danken: meinen Eltern Barbara & Michael, meinen Geschwistern Marie und Anna, meinen Großeltern Helga & Richard und Theresia & Richard, meinen Tanten Heike und Daniela, meinen Onkeln Dietmar und Markus sowie ihren Familien und allen anderen Familienmitgliedern. Eure aufopfernde Liebe und Unterstützung hat es möglich gemacht, dass ich heute hier stehen kann. Dafür habt ihr meinen größten Respekt und meinen herzlichsten Dank.

Sollte ich noch jemanden vergessen haben, so bitte ich dies zu verzeihen und spreche auch hier meinen aufrichtigen Dank aus.

I. Declaration

Herewith I declare that this present thesis is a presentation of my original work prepared single-handed. Wherever contributions from others are involved, all of them are marked clearly, with reference to the literature, license, and acknowledgment of collaborative research.

Regensburg, May 2, 2018

_____

Martin Hofmann